Advances in High Energy Physics

Transverse Momentum Dependent Observables from Low to High Energy: Factorization, Evolution, and Global Analyses

Lead Guest Editor: Daniel Pitonyak
Guest Editors: Zhongbo Kang, Alexei Prokudin, and Alexey Vladimirov

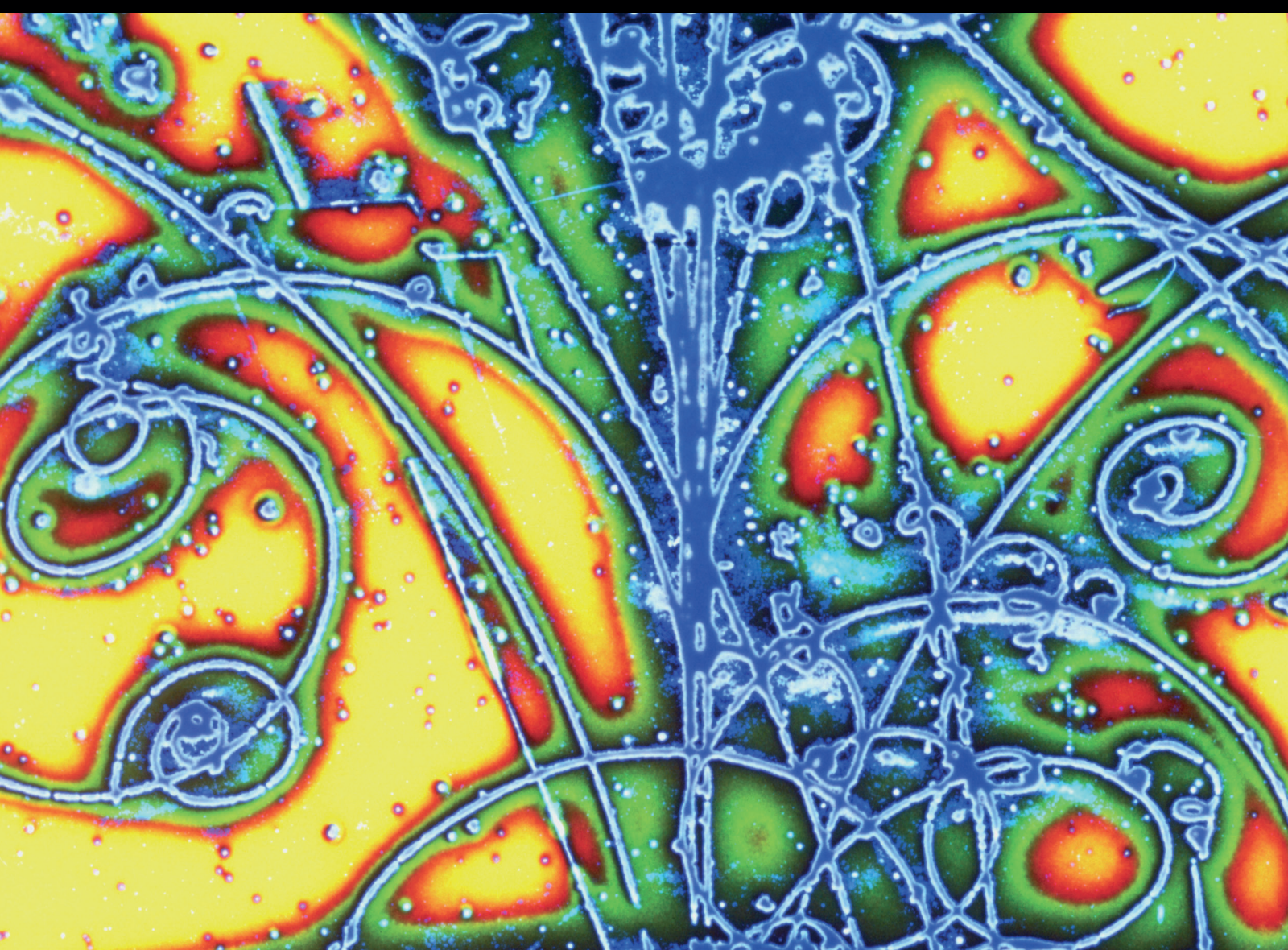

Transverse Momentum Dependent Observables from Low to High Energy: Factorization, Evolution, and Global Analyses

Advances in High Energy Physics

Transverse Momentum Dependent Observables from Low to High Energy: Factorization, Evolution, and Global Analyses

Lead Guest Editor: Daniel Pitonyak
Guest Editors: Zhongbo Kang, Alexei Prokudin, and Alexey Vladimirov

Editorial Board

Contents

Transverse Momentum Dependent Observables from Low to High Energy: Factorization, Evolution, and Global Analyses
Daniel Pitonyak, Zhong-Bo Kang, Alexei Prokudin, and Alexey Vladimirov
Editorial (2 pages), Article ID 1705263, Volume 2019 (2019)

Introduction to the Transverse-Momentum-Weighted Technique in the Twist-3 Collinear Factorization Approach
Hongxi Xing and Shinsuke Yoshida
Review Article (15 pages), Article ID 4825790, Volume 2019 (2019)

A Guide to Light-Cone PDFs from Lattice QCD: An Overview of Approaches, Techniques, and Results
Krzysztof Cichy and Martha Constantinou
Review Article (68 pages), Article ID 3036904, Volume 2019 (2019)

A Short Review on Recent Developments in TMD Factorization and Implementation
Ignazio Scimemi
Review Article (17 pages), Article ID 3142510, Volume 2019 (2019)

Nonperturbative Uncertainties on the Transverse Momentum Distribution of Electroweak Bosons and on the Determination of the W Boson Mass at the LHC
Giuseppe Bozzi and Andrea Signori
Research Article (11 pages), Article ID 2526897, Volume 2019 (2019)

Transverse Momentum Dependence in Double Parton Scattering
Jonathan R. Gaunt and Tomas Kasemets
Review Article (9 pages), Article ID 3797394, Volume 2019 (2019)

$\pi - N$ Drell-Yan Process in TMD Factorization
Xiaoyu Wang and Zhun Lu
Review Article (20 pages), Article ID 6734293, Volume 2019 (2019)

Hindawi
Advances in High Energy Physics
Volume 2019, Article ID 1705263, 2 pages
https://doi.org/10.1155/2019/1705263

Editorial

Transverse Momentum Dependent Observables from Low to High Energy: Factorization, Evolution, and Global Analyses

Daniel Pitonyak,[1] **Zhong-Bo Kang**,[2] **Alexei Prokudin**,[3,4] **and Alexey Vladimirov**[5]

[1]*Department of Physics, Lebanon Valley College, Annville, PA 17003, USA*
[2]*Department of Physics and Astronomy, University of California, Los Angeles, CA 90095, USA*
[3]*Science Division, Penn State University Berks, Reading, PA 19610, USA*
[4]*Jefferson Lab, 12000 Jefferson Avenue, Newport News, VA 23606, USA*
[5]*Institut für Theoretische Physik, Universität Regensburg, D-93040 Regensburg, Germany*

Correspondence should be addressed to Daniel Pitonyak; pitonyak@lvc.edu

Received 23 April 2019; Accepted 23 April 2019; Published 24 June 2019

Transverse momentum dependent (TMD) observables in high-energy particle collisions allow one to study the motion of hadron constituents (partons) in three dimensions. The intense theoretical, phenomenological, and experimental work over the last several decades has seen great progress in modeling and extracting TMD parton distribution functions (PDFs) and fragmentation functions (FFs) [1, 2]. The wealth of experimental data, both current and future [3–6], across various reactions and energy ranges, along with substantial progress in other approaches, such as Lattice QCD [7], has increased the demand to rigorously study the intrinsic transverse motion of hadrons. Such issues currently being addressed include factorization, evolution, and operator definitions of TMD distributions, as well as how they influence phenomenological and Lattice QCD studies.

Therefore, in this special issue we attempt to further the effort of understanding TMD structure through a series of review articles that address some of the significant areas of ongoing research.

I. Scimemi provided an overview of the tools and concepts which are behind TMD factorization and evolution. He considered both theoretical and phenomenological aspects and the importance of future collider data on further developments.

G. Bozzi and A. Signori focused on the possible flavor dependence of quark intrinsic transverse momentum. They studied the transverse momentum spectrum of electroweak gauge bosons produced in proton-proton collisions at the Large Hadron Collider and showed that flavor-dependent TMD effects are comparable in size to other nonperturbative effects.

X. Wang and Z. Lu presented the current understanding of the pion-nucleon Drell-Yan process from the point of view of TMD factorization. They studied the unpolarized cross-section, the Sivers asymmetry, and the double Boer-Mulders effects.

J. Gaunt and T. Kasemets described the status of transverse momentum dependence in double parton scattering (DPS). They emphasized the differences and similarities to TMD single parton scattering as well as the status of the factorization of double color-singlet production in DPS.

H. Xing and S. Yoshida introduced the techniques for next-to-leading order (NLO) calculations of TMD-weighted single-spin asymmetries, which can serve as a useful tool to derive the QCD evolution equations for twist-3 functions and to verify the QCD collinear factorization for twist-3 observables at NLO.

K. Cichy and M. Constantinou gave an extensive, detailed review of Lattice QCD analyses of quasi-PDFs, including theoretical and practical developments and future challenges. They also reviewed numerical results and the theoretical validation of the approach as well as alternative strategies for analyzing PDFs on the lattice.

This special issue gives a nice overview of the various avenues of research currently explored within the community. The papers do well to synthesize and elucidate the

state-of-the-art theoretical, phenomenological, and Lattice QCD frameworks of TMD distributions and TMD observables. We hope that the reader will not only gain knowledge from the breadth and depth of this work but also be motivated to engage in their own studies that are required in order to meet the demands of ongoing and future measurements.

Conflicts of Interest

The editors declare that they have no conflicts of interest regarding the publication of this special issue.

Daniel Pitonyak
Zhong-Bo Kang
Alexei Prokudin
Alexey Vladimirov

References

[1] M. Grosse Perdekamp and F. Yuan, "Transverse spin structure of the nucleon," *Annual Review of Nuclear and Particle Science*, vol. 65, artilce no. 429, 2015.

[2] A. Bacchetta, "Where do we stand with a 3-D picture of the proton?" *The European Physical Journal A*, vol. 52, no. 6, article no. 163, 2016.

[3] J. Dudek, R. Ent, R. Essig et al., "Physics opportunities with the 12 GeV upgrade at jefferson lab," *The European Physical Journal A*, vol. 48, article no. 187, 2012.

[4] D. Boer, M. Diehl, R. Milner et al., "Gluons and the quark sea at high energies: distributions, polarization, tomography," *Nuclear Theory*, 547 pages, 2011, https://arxiv.org/abs/1108.1713v2.

[5] A. Accardi, J. L. Albacete, M. Anselmino et al., "Electron ion collider: the next qcd frontier - understanding the glue that binds us all," *The European Physical Journal A*, vol. 52, no. 9, article no. 268, 164 pages, 2016.

[6] E. C. Aschenauer, C. Aidala, A. Bazilevsky et al., "The RHIC cold QCD plan for 2017 to 2023: a portal to the EIC," https://arxiv.org/abs/1602.03922.

[7] H. W. Lin, E. R. Nocera, F. Olness et al., "Parton distributions and lattice QCD calculations: a community white paper," *High Energy Physics*, vol. 100, article no. 107, 80 pages, 2018.

Hindawi
Advances in High Energy Physics
Volume 2019, Article ID 4825790, 15 pages
https://doi.org/10.1155/2019/4825790

Review Article

Introduction to the Transverse-Momentum-Weighted Technique in the Twist-3 Collinear Factorization Approach

Hongxi Xing and Shinsuke Yoshida

Institute of Quantum Matter and School of Physics and Telecommunication Engineering, South China Normal University, Guangzhou 510006, China

Correspondence should be addressed to Hongxi Xing; hxing@m.scnu.edu.cn and Shinsuke Yoshida; shinyoshida85@gmail.com

Received 21 December 2018; Accepted 31 March 2019; Published 2 June 2019

Guest Editor: Alexei Prokudin

The twist-3 collinear factorization framework has drawn much attention in recent decades as a successful approach in describing the data for single spin asymmetries (SSAs). Many SSAs data have been experimentally accumulated in a variety of energies since the first measurement was done in the late 1970s and it is expected that the future experiments like Electron-Ion-Collider will provide us with more data. In order to perform a consistent and precise description of the data taken in different kinematic regimes, the scale evolution of the collinear twist-3 functions and the perturbative higher-order hard part coefficients are mandatory. In this paper, we introduce the techniques for next-to-leading order (NLO) calculation of transverse-momentum-weighted SSAs, which can be served as a useful tool to derive the QCD evolution equation for twist-3 functions and to verify the QCD collinear factorization for twist-3 observables at NLO, as well as obtain the finite NLO hard part coefficients.

1. Introduction

The large single transverse spin asymmetries (SSAs) have been a longstanding problem over 40 years since it was turned out that the conventional perturbative calculation based on the parton model picture failed to describe the large SSAs which were experimentally observed in pion and polarized hyperon productions [1, 2]. In the recent several years, two QCD factorization frameworks have been proposed to study phenomenologically the observed SSAs: the transverse momentum dependent factorization approach [3–15] and the twist-3 collinear factorization approach [16–38]. These two frameworks are shown to be equivalent in the common applied kinematic region [39–46].

The twist-3 collinear factorization framework is a natural extension of the conventional perturbative QCD framework and it could give a reasonable description of the large SSAs. Measurements of SSAs at Relativistic-Heavy-Ion-Collider (RHIC) [47–51] have greatly motivated the theoretical work on developing the twist-3 framework, because it is a unique applicable framework for single hadron productions in proton-proton collision. A series of important works have been done in the past a few decades and the SSAs for the hadron production were completed at leading order (LO) with respect to the QCD strong coupling constant α_s [16–38]. Recent numerical simulations based on the complete LO result confirmed that the twist-3 approach gives a reasonable description of the SSA data provided by RHIC [52, 53].

Electron-Ion-Collider (EIC) is a next-generation hadron collider expected to provide more data in different kinematic regimes for SSAs. In order to extract the fundamental structure of the nucleon from the measurements at a future EIC, comprehensive and precise calculations for SSAs in transversely polarized lepton-proton collision are highly demanded. It is well known that nonperturbative functions in the perturbative QCD calculation, in general, receive logarithmic radiative corrections and the evolution equation with respect to this logarithmic scale is necessary for a systematic treatment of the cross sections in wide range of energies. Most famous example is the DGLAP evolution equation of the twist-2 parton distribution functions (PDFs). Correct description of the small scale violation of the structure function controlled by the DGLAP equation was an important success of the QCD phenomenology in

the early days. The twist-3 function is expected to have similar logarithmic dependence and its evolution equation will play an important role in global fitting of the SSA data accumulated in different energies. Consistent description of the data will be a good evidence that the twist-3 framework, one of major fundamental developments in recent QCD phenomenology, is a feasible theory to solve the 40-year mystery in high energy physics. The evolution equations for the twist-3 functions have been derived in two different methods. The first method is a calculation of the higher-order corrections to the nonperturbative function itself [54–61]. Since the nonperturbative function has the operator definition, we can investigate the infrared singularity of the operator through higher-order perturbative calculation. We can read the evolution equation from the infrared structure of the function. This is a standard technique and the evolution equations have been derived for the twist-3 distribution functions for initial state proton [54–59] and the twist-3 fragmentation functions for final state hadron [60, 61]. The second method which we will review in this paper is a transverse-momentum-weighted technique for the SSAs [62–67]. Except for deriving the QCD evolution equation for twist-3 nonperturbative functions, the transverse-momentum-weighted technique can be also used as a tool to verify the twist-3 collinear factorization at higher orders in strong coupling constant α_s. There is also phenomenological interest related to this technique. One can use the standard dimensional regularization method to derive the NLO hard part coefficient for transverse-momentum-weighted SSAs, which can be used for high precision extraction of twist-3 functions from the relevant experimental data. The recent measurement of the transverse-momentum-weighted SSAs at COMPASS [68] strongly motivates the phenomenological application of the results reviewed in this paper. We expect more data will be produced in future COMPASS and EIC measurements.

The rest of the paper is organized as follows. In Section 2 we present the notation and the calculation of transverse-momentum-weighted SSAs at leading order for semi-inclusive deep inelastic scattering (SIDIS). In Section 3 we present the detail of NLO calculation for both real and virtual corrections, we show the cancelation of soft divergence in the sum of real and virtual corrections, and the collinear divergences can be absorbed into the redefinition of twist-3 Qiu-Sterman function and unpolarized leading twist fragmentation function. In Section 4 we review the application of the transverse-momentum-weighted technique to other processes that have been done in recent years. We conclude our paper in Section 5.

2. Transverse-Momentum-Weighted SSA at Leading Order

In this paper, we take the process of SIDIS as an example to show the techniques of perturbative calculation for transverse-momentum-weighted differential cross section at twist-3. We start this section by specifying our notation and the kinematics of SIDIS and present the calculation for transverse-momentum-weighted SSA at leading order (LO).

2.1. Notation. We consider the scattering of an unpolarized lepton with momentum l on a transversely polarized proton with momentum p and transverse spin $S_\perp$ and observe the final state hadron production with momentum P_h,

$$e(l) + p^{\uparrow}(p, S_\perp) \longrightarrow e(l') + h(P_h) + X. \tag{1}$$

We focus on one-photon exchange process with the momentum of the virtual photon given by $q = l - l'$ and its invariant mass $Q^2 = -q^2$. We define all vectors in the so-called hadron frame. We define $p_c = P_h/z$ to be the momentum for the parton that fragments into the final state hadron. The conventional Lorentz invariant variables in SIDIS are defined as

$$\begin{aligned} S_{ep} &= (p + l)^2, \\ x_B &= \frac{Q^2}{2p \cdot q}, \\ z_h &= \frac{p \cdot P_h}{p \cdot q}, \\ y &= \frac{p \cdot q}{p \cdot l}. \end{aligned} \tag{2}$$

For clear understanding, we start with the $P_{h\perp}$-integrated cross section at leading twist in unpolarized lepton-proton scattering

$$\frac{d\sigma}{dx_B dy dz_h} = \int d^2 P_{h\perp} \frac{d\sigma}{dx_B dy dz_h d^2 P_{h\perp}}. \tag{3}$$

There is only one hard scale Q^2 in this case; therefore the differential cross section shown above can be reliably computed by using the standard collinear factorization formalism. The LO contribution is given by $2 \longrightarrow 1$ scattering amplitude $\gamma^* + q \longrightarrow q$. It is trivial that the LO cross section is proportional to the unpolarized PDFs and the unpolarized fragmentation functions (FFs),

$$\frac{d\sigma^{LO}}{dx_B dy dz_h} = \sigma_0 \sum_q f_{q/p}(x_B, \mu^2) D_{q \longrightarrow h}(z_h, \mu^2), \tag{4}$$

where σ_0 is the LO Born cross section $\sigma_0 = (2\pi\alpha_{em}^2/Q^2)((1 + (1 - y)^2)/y)$ with $\alpha_{em} = e^2/4\pi$ being the QED coupling constant. The bare results at $\mathcal{O}(\alpha_s)$ contain infrared divergences which represent the long-range interaction in hadronic collision process. These divergences are canceled by the renormalization of the PDFs and FFs and the DGLAP evolution equations are derived as the renormalization group equations. The final result at NLO can be written as the convolution of finite hard part coefficient H and nonperturbative functions (PDFs and FFs) [63]

$$\frac{d\sigma^{NLO}}{dx_B dy dz_h} = \sum_{i,j} f_{i/p} \otimes H^{NLO}_{\gamma^* + i \longrightarrow j + k} \otimes D_{j \longrightarrow h}. \tag{5}$$

where $\otimes$ represents convolution.

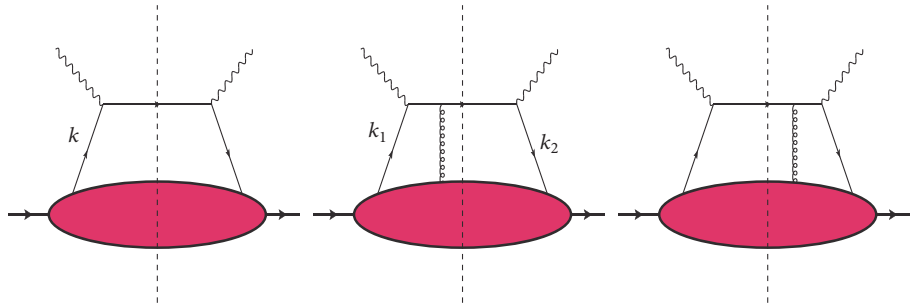

Figure 1: A series of LO diagrams in the diagrammatic method.

The concept of the transverse-momentum-weighted technique is mostly the same with the twist-2 case. Notice that direct $P_{h\perp}$-integration of the cross section for unpolarized lepton scattering off transversely polarized proton vanishes due to the linear dependence of P_h. Realize that the SSA is characterized in terms of three vectors: the momentum of the final state hadron, the momentum, and the spin of the initial state proton, which can be combined as

$$\epsilon^{\alpha\beta\rho\sigma} P_{h\alpha} S_{\perp\beta} p_\rho n_\sigma = \epsilon^{ij} P_{h\perp i} S_{\perp j} \equiv \epsilon^{P_{h\perp} S_\perp pn}, \tag{6}$$

where ϵ^{ij} is a two-dimensional antisymmetric tensor with $\epsilon^{12} = 1$; n is an arbitrary vector which satisfies $p \cdot n = 1$ and $n^2 = 0$. We introduce a weight factor $\epsilon^{P_{h\perp} S_\perp pn}$ and consider the following transverse-momentum-weighted differential cross section

$$\frac{d\left\langle P_{h\perp} \Delta\sigma \right\rangle}{dx_B dy dz_h} \equiv \int d^2 P_{h\perp} \epsilon^{P_{h\perp} S_\perp pn} \frac{d\Delta\sigma}{dx_B dy dz_h d^2 P_{h\perp}}, \tag{7}$$

which is well defined after $P_{h\perp}$-integration. Since the virtuality Q^2 is the only hard scale after the $P_{h\perp}$-integration, one can safely use the collinear twist-3 factorization formalism, and the technique in performing NLO calculation will follow those used at leading twist. Same technique has been applied to Drell-Yan dilepton production in proton-proton collisions [62, 66] and can be extended to polarized electron-positron collisions.

We recall the cross section for SIDIS presented in [64],

$$\frac{d\Delta\sigma}{dx_B dy dz_h d^2 P_{h\perp}} = \frac{\alpha_{em}^2}{128\pi^4 z_h x_B^2 S_{ep}^2 Q^2} L_{\mu\nu} W^{\mu\nu}, \tag{8}$$

where $L_{\mu\nu} = 2(l_\mu l'_\nu + l_\nu l'_\mu) - Q^2 g_{\mu\nu}$ is the leptonic tensor. We focus on the metric contribution $L_{\mu\nu} \longrightarrow -Q^2 g_{\mu\nu}$ and the SSA generated by initial state twist-3 distribution functions of the transversely polarized proton. Then we can factorize the nonperturbative part by introducing the usual twist-2 unpolarized fragmentation function

$$W^{\mu\nu} = \sum_i \int \frac{dz}{z^2} w_i^{\mu\nu} D_{i\longrightarrow h}(z). \tag{9}$$

The hadronic tensor $w_i^{\mu\nu}$ describes a scattering of the virtual photon and the transversely polarized proton. We will make the subscript i implicit in the rest part of this paper for simplicity.

2.2. Leading Order. We demonstrate how to derive the LO cross section for the transverse-momentum-weighted SSA based on the collinear twist-3 framework and show that the LO cross section is proportional to the first moment of the TMD Sivers function. The twist-3 calculation is well formulated in the diagrammatic method. We consider a set of the general diagrams shown in Figure 1 and extract twist-3 contributions from these diagrams. We start from the first diagram in Figure 1, which can be expressed as

$$\begin{aligned} w_1^{\mu\nu} = & \int d^4\xi \int \frac{d^4k}{(2\pi)^4} e^{ik\cdot\xi} \\ & \cdot \left\langle pS_\perp \left| \overline{\psi}_j(0) \psi_i(\xi) \right| pS_\perp \right\rangle \\ & \cdot H_{ji}^{\mu\nu}(k) \delta^2(k_\perp - p_{c\perp}), \end{aligned} \tag{10}$$

where k and p_c are the momenta of the parton from initial state proton and that fragments to the final state observed hadron, respectively, $p_{c\perp} = P_{h\perp}/z$. The hard part at LO is given by

$$\begin{aligned} H_{ji}^{\mu\nu}(k) = & \left[\gamma^\nu (\not{k} + \not{q}) \gamma^\mu\right]_{ji} (2\pi)^4 \delta(k^+ + q^+ - p_c^+) \\ & \cdot \delta(k^- + q^- - p_c^-). \end{aligned} \tag{11}$$

We perform $P_{h\perp}$-integration before the collinear expansion,

$$\int d^2 P_{h\perp} \epsilon^{P_{h\perp} S_\perp pn} \delta^2(k_\perp - p_{c\perp}) = z^3 \epsilon^{\alpha S_\perp pn} k_{\perp\alpha}. \tag{12}$$

Because the $P_{h\perp}$-integration gives $O(k_\perp)$ factor, we can identify the leading term in the collinear expansion as a twist-3 contribution. We perform the collinear expansion of the hard part around $k^\mu = (k\cdot n) p^\mu \equiv k_p^\mu$

$$H^{\mu\nu}(k) = H^{\mu\nu}(k_p) + O(k_\perp), \tag{13}$$

and substitute the above expansion into the hadronic tensor as shown in (10)

$$\begin{aligned} \int d^2 P_{h\perp} \epsilon^{P_{h\perp} S_\perp pn} w_1^{\mu\nu} = & z^3 \epsilon_\alpha^{S_\perp pn} \int d^4\xi \int \frac{d^4k}{(2\pi)^4} \\ & \cdot e^{ik\cdot\xi} \left\langle pS_\perp \left| \overline{\psi}_j(0) \psi_i(\xi) \right| pS_\perp \right\rangle k_\perp^\alpha H_{ji}^{\mu\nu}(k_p) \end{aligned}$$

$$= iz^3 \epsilon_\alpha^{S_\perp pn} \int dx \int \frac{d\lambda}{2\pi} \cdot e^{i\lambda x} \left\langle pS_\perp \left| \overline{\psi}_j (0) \partial^\alpha \psi_i (\lambda) \right| pS_\perp \right\rangle H_{ji}^{\mu\nu} (xp) . \tag{14}$$

where $\lambda = p^+ \xi^-$. Now we turn to the second and the third diagrams in Figure 1. These two diagrams can be expressed as

$$\begin{aligned} w_2^{\mu\nu} = & \int d^4\xi_1 \int d^4\xi_2 \int \frac{d^4k_1}{(2\pi)^4} \int \frac{d^4k_2}{(2\pi)^4} \\ & \cdot e^{ik_1\cdot\xi_1} e^{i(k_2-k_1)\cdot\xi_2} \left\langle pS_\perp \left| \overline{\psi}_j (0)\, gA^\rho (\xi_2) \psi_i (\xi_1) \right| pS_\perp \right\rangle \\ & \times \left[H_{L\rho\, ji}^{\mu\nu} (k_1, k_2) \delta^2 (k_{2\perp} - p_{c\perp}) + H_{R\rho\, ji}^{\mu\nu} (k_1, k_2) \right. \\ & \left. \cdot \delta^2 (k_{1\perp} - p_{c\perp}) \right] , \end{aligned} \tag{15}$$

where the hard parts are given by

$$\begin{aligned} H_{L\rho\, ji}^{\mu\nu} (k_1, k_2) = & - \left[\gamma^\nu (\not{k}_2 + \not{q}) \gamma_\rho (\not{k}_1 + \not{q}) \gamma^\mu \right]_{ji} \\ & \cdot \frac{1}{(q + k_1)^2 + i\epsilon} (2\pi)^4 \delta (k_2^+ + q^+ - p_c^+) \\ & \cdot \delta (k_2^- + q^- - p_c^-) , \\ H_{R\rho\, ji}^{\mu\nu} (k_1, k_2) = & - \left[\gamma^\nu (\not{k}_2 + \not{q}) \gamma_\rho (\not{k}_1 + \not{q}) \gamma^\mu \right]_{ji} \\ & \cdot \frac{1}{(q + k_2)^2 - i\epsilon} (2\pi)^4 \delta (k_1^+ + q^+ - p_c^+) \\ & \cdot \delta (k_1^- + q^- - p_c^-) . \end{aligned} \tag{16}$$

The $P_{h\perp}$-integration gives $O(k_{1,2\perp})$ and then the leading term in collinear expansion gives twist-3 contribution again,

$$H_{L(R)\rho\, ji}^{\mu\nu} (k_1, k_2) = H_{L(R)\rho\, ji}^{\mu\nu} (k_{1p}, k_{2p}) + O (k_{1,2\perp}) . \tag{17}$$

For the matrix element, we have to separate the components of the gluon field A^ρ into "longitudinal" and "transverse" part as

$$A^\rho = A^n p^\rho + (A^\rho - A^n p^\rho) . \tag{18}$$

The longitudinal part $A^n p^\rho$ gives the leading contribution. It is straightforward to derive the Ward-Takahashi identities (WTIs) for the hard parts,

$$\begin{aligned} p^\rho H_{L\rho\, ji}^{\mu\nu} (k_1, k_2) = & \left[\gamma^\nu (x_2 \not{p} + \not{q}) \gamma^\mu \right]_{ji} \\ & \cdot \frac{1}{x_2 - x_1 - i\epsilon} (2\pi)^4 \frac{2x_B}{Q^2} \delta (x_2 - x_B) \delta (1 - \widehat{z}) \\ = & \frac{1}{x_2 - x_1 - i\epsilon} H_{ji}^{\mu\nu} (x_2 p) , \\ p^\rho H_{R\rho\, ji}^{\mu\nu} (k_1, k_2) = & - \left[\gamma^\nu (x_1 \not{p} + \not{q}) \gamma^\mu \right]_{ji} \\ & \cdot \frac{1}{x_2 - x_1 - i\epsilon} (2\pi)^4 \frac{2x_B}{Q^2} \delta (x_1 - x_B) \delta (1 - \widehat{z}) \\ = & - \frac{1}{x_2 - x_1 - i\epsilon} H_{ji}^{\mu\nu} (x_1 p) . \end{aligned} \tag{19}$$

Finally the hadronic tensor shown in (15) can be expressed as

$$\begin{aligned} & \int d^2 P_{h\perp} \epsilon^{P_{h\perp} S_\perp pn} w_2^{\mu\nu} \\ & = z^3 \epsilon_\alpha^{S_\perp pn} \int d^4\xi_1 \int d^4\xi_2 \\ & \cdot \int \frac{d^4k_1}{(2\pi)^4} \int \frac{d^4k_2}{(2\pi)^4} \\ & \cdot e^{ik_1\cdot\xi_1} e^{i(k_2-k_1)\cdot\xi_2} \\ & \cdot \left\langle pS_\perp \left| \overline{\psi}_j (0)\, gA^n (\xi_2) \psi_i (\xi_1) \right| pS_\perp \right\rangle \\ & \times \frac{1}{x_2 - x_1 - i\epsilon} \\ & \cdot \left[k_{2\perp}^\alpha H_{ji}^{\mu\nu} (x_2 p) - k_{1\perp}^\alpha H_{ji}^{\mu\nu} (x_1 p) \right] \\ & = z^3 \epsilon_\alpha^{S_\perp pn} \int d^4\xi_1 \\ & \cdot \int d^4\xi_2 \int \frac{d^4k_1}{(2\pi)^4} \\ & \cdot \int \frac{d^4k_2}{(2\pi)^4} e^{ik_1\cdot\xi_1} e^{i(k_2-k_1)\cdot\xi_2} \\ & \cdot \left\langle pS_\perp \left| \overline{\psi}_j (0)\, gA^n (\xi_2) \psi_i (\xi_1) \right| pS_\perp \right\rangle \\ & \times \frac{1}{x_2 - x_1 - i\epsilon} \left[(k_{2\perp}^\alpha - k_{1\perp}^\alpha) \right. \\ & \left. \cdot H_{ji}^{\mu\nu} (x_2 p) + k_{1\perp}^\alpha \left(H_{ji}^{\mu\nu} (x_2 p) - H_{ji}^{\mu\nu} (x_1 p) \right) \right] \\ & = iz^3 \epsilon_\alpha^{S_\perp pn} \int dx \int \frac{d\lambda}{2\pi} e^{i\lambda x} \\ & \cdot \left\langle pS_\perp \left| \overline{\psi}_j (0)\, ig \int_\lambda^\infty d\lambda' \left[\partial^\alpha A^n (\lambda' n) - \partial^n A^\alpha (\lambda' n) \right] \psi_i (\lambda n) \right| pS_\perp \right\rangle \\ & \cdot H_{ji}^{\mu\nu} (xp) + iz^3 \epsilon_\alpha^{S_\perp pn} \\ & \cdot \int dx \int \frac{d\lambda}{2\pi} e^{i\lambda x} \\ & \cdot \left\langle pS_\perp \left| \overline{\psi}_j (0) \left[ig \int_\lambda^0 d\lambda' A^n (\lambda' n) \right] \partial^\alpha \psi_i (\lambda n) \right| pS_\perp \right\rangle \\ & \cdot H_{ji}^{\mu\nu} (xp) - iz^3 \epsilon_\alpha^{S_\perp pn} \\ & \cdot \int dx \int \frac{d\lambda}{2\pi} e^{i\lambda x} \\ & \cdot \left\langle pS_\perp \left| \overline{\psi}_j (0)\, igA^\alpha (\lambda n) \psi_i (\lambda n) \right| pS_\perp \right\rangle \\ & \cdot H_{ji}^{\mu\nu} (xp) . \end{aligned} \tag{20}$$

Combining (14) and (20), we can obtain the result

$$\begin{aligned} & \int d^2 P_{h\perp} \epsilon^{P_{h\perp} S_\perp pn} w^{\mu\nu} \\ & = iz^3 \epsilon_\alpha^{S_\perp pn} \\ & \cdot \int dx \int \frac{d\lambda}{2\pi} e^{i\lambda x} \end{aligned}$$

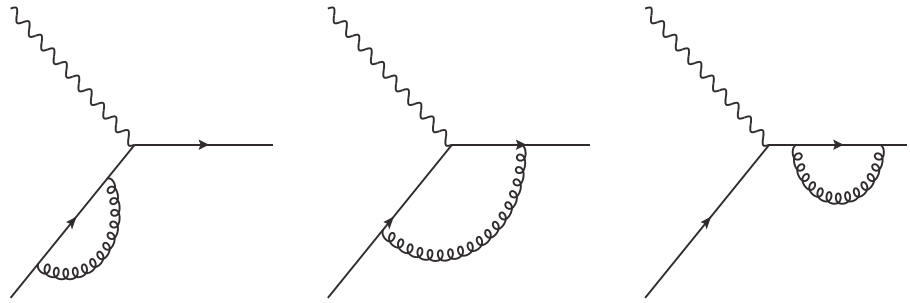

Figure 2: The NLO virtual correction diagrams in SIDIS.

$$\cdot \left\langle pS_\perp \left| \overline{\psi}_j(0) \left(D^\alpha(\lambda n)\psi_i(\lambda n) + ig\int_\lambda^0 d\lambda' A^n(\lambda' n)\partial^\alpha \psi_i(\lambda n)\right)\right| pS_\perp \right\rangle$$
$$\cdot H_{ji}^{\mu\nu}(xp) + iz^3 \epsilon_\alpha^{S_\perp pn}$$
$$\cdot \int dx \int \frac{d\lambda}{2\pi} e^{i\lambda x}$$
$$\cdot \left\langle pS_\perp \left| \overline{\psi}_j(0)\, ig\int_\lambda^\infty d\lambda' \left(\partial^\alpha A^n(\lambda' n) - \partial^n A^\alpha(\lambda' n)\right)\psi_i(\lambda n)\right| pS_\perp \right\rangle$$
$$\cdot H_{ji}^{\mu\nu}(xp). \tag{21}$$

We can find that this matrix element corresponds to $O(g)$ term in the first moment of the TMD correlator

$$\begin{aligned}
&\int d^2 p_T p_T^\alpha \left(\int \frac{d\lambda}{2\pi} \int \frac{dx_T}{2\pi} e^{i\lambda x} e^{ix_T \cdot p_T} \right.\\
&\cdot \left\langle pS_\perp \left| \overline{\psi}_j(0)\,[0,\infty n] \right.\right.\\
&\cdot [\infty n, \infty n + x_T]\,[\infty n + x_T, \lambda n + x_T]\\
&\left.\left. \cdot \psi_i(\lambda n + x_T)\right| pS_\perp \right\rangle \Big)\\
&= i\int \frac{d\lambda}{2\pi} e^{i\lambda x}\\
&\cdot \left\langle pS_\perp \left| \overline{\psi}_j(0)\,[0,\lambda n]\, D^\alpha(\lambda n)\psi_i(\lambda n)\right| pS_\perp \right\rangle\\
&+ i\int \frac{d\lambda}{2\pi} e^{i\lambda x} \int_\lambda^\infty d\lambda'\\
&\cdot \left\langle pS_\perp \left| \overline{\psi}_j(0)\left[0,\lambda' n\right] igF^{\alpha n}\left(\lambda' n\right)\left[\lambda' n, \lambda n\right]\psi_i(\lambda n)\right| pS_\perp \right\rangle\\
&= -\pi \frac{M_N}{4} \epsilon^{\alpha pnS_\perp} G_{q,F}(x,x) + \cdots,
\end{aligned} \tag{22}$$

where $[\cdots]$ represents the Wilson line, M_N is the nucleon mass, and we used the fact that the first moment of the TMD Sivers function gives the Qiu-Sterman function $G_{q,F}(x,x)$. The nonlinear term in the field strength tensor $F^{\alpha+}$ and the higher-order terms in the Wilson lines which have to be added to (21) come from the more gluon-linked diagrams in Figure 2. Finally we can derive the LO cross section formula as

$$\frac{d\left\langle P_{h\perp}\Delta\sigma\right\rangle^{\mathrm{LO}}}{dx_B dy dz_h} = \widetilde{\sigma}_0 \sum_q e_q^2 G_{q,F}(x_B, x_B)\, D_{q\longrightarrow h}(z_h). \tag{23}$$

where $\widetilde{\sigma}_0 = -\pi M_N \sigma_0$. As we demonstrated here, the LO cross section for the weighted SSA is proportional to the first moment of the TMD function (also known as the kinematical twist-3 function). We can expect the NLO contribution gives the evolution equation to the twist-3 Qiu-Sterman function, $G_{q,F}(x,x)$ in this case. This technique is quite general so that we can apply the same technique to other TMD functions. When we focus on the twist-3 fragmentation effect, we can derive the evolution equation for the first Moment of the Collins function. When we consider the double spin asymmetry A_{LT} and change the weight factor $\epsilon^{ij} P_{h\perp i} S_{\perp j} \longrightarrow (P_h \cdot S_\perp)$, we can investigate other TMD distribution functions like the Worm-Gear and the Pretzelosity.

3. Transverse-Momentum-Weighted SSA at NLO

In this section, we review the calculation for transverse-momentum-weighted SSA at NLO including both real and virtual corrections.

3.1. Virtual Correction. We first consider the NLO contribution from the virtual correction which is given by the $2 \longrightarrow 1$ scattering amplitude with one gluon loop. When we adopt the dimensional regularization scheme, the gauge-invariance of the cross section is maintained for the loop diagram. Then we can derive the same WTI as shown in (19) which is the consequence of gauge-invariance of the diagrams. Taking advantage of this fact, we just need to calculate simple diagrams shown in Figure 2 for the virtual correction. The calculation for this kind of one-loop diagrams has been well established, which is exactly the same as the vertex correction at leading twist. We follow the conventional technique here. All ultraviolet divergences can be canceled by the renormalization of the QCD Lagrangian. Then we can set the ultraviolet and infrared divergences are the same with each other in dimensions regularization approach, $\epsilon_{\mathrm{UV}} = \epsilon_{\mathrm{IR}}$, and identify all divergences as infrared. In this definition, we do not have to think about the first and the third amplitudes in Figure 2 because these are exactly zero in the mass case as we considered here. The hard partonic cross section with the second amplitude is given by

$$\left(-\frac{1}{1-\epsilon} g_{\mu\nu}\right) C_F g^2 \mu^{2\epsilon} \int \frac{d^D \ell}{(2\pi)^D i}$$
$$\cdot \mathrm{Tr}\left[x\not{p}\gamma^\nu \not{p}_c \gamma^\rho \left(\not{p}_c - \not{\ell}\right)\gamma^\mu \left(x\not{p} - \not{\ell}\right)\gamma_\rho\right]$$

$$\cdot \frac{1}{\ell^2 (p_c - \ell)^2 (xp - \ell)^2} = C_F g^2 \mu^{2\epsilon} \int \frac{d^D \ell}{(2\pi)^D i} \cdot \left[-4 \frac{1}{(p_c - \ell)^2 (xp - \ell)^2} \left(\frac{3}{2} + \epsilon \right) Q^2 + \frac{4Q^2}{\ell^2 (p_c - \ell)^2 (xp - \ell)^2} \right], \tag{24}$$

where $\epsilon = (4 - D)/2$ in D-dimension, we made a change $g_{\mu\nu} \longrightarrow (1/(1-\epsilon)) g_{\mu\nu}$ for D-dimensional calculation, and we used the fact that

$$\begin{aligned} \int \frac{d^D \ell}{(2\pi)^D i} \frac{1}{\ell^2} &= \int \frac{d^D \ell}{(2\pi)^D i} \frac{1}{(xp - \ell)^2} \\ &= \int \frac{d^D \ell}{(2\pi)^D i} \frac{1}{\ell^2 (p_c - \ell)^2} \\ &= \int \frac{d^D \ell}{(2\pi)^D i} \frac{1}{\ell^2 (xp - \ell)^2} = 0. \end{aligned} \tag{25}$$

We perform the basic D-dimensional calculation for each integration,

$$\begin{aligned} &\int \frac{d^D \ell}{(2\pi)^D i} \frac{1}{(p_c - \ell)^2 (xp - \ell)^2} = \frac{1}{16\pi^2} \left(\frac{4\pi}{Q^2} \right)^\epsilon \\ &\cdot \frac{1}{\Gamma(1-\epsilon)} \Gamma(1-\epsilon) \Gamma(\epsilon) B(1-\epsilon, 1-\epsilon) \\ &= \frac{1}{16\pi^2} \left(\frac{4\pi}{Q^2} \right)^\epsilon \frac{1}{\Gamma(1-\epsilon)} \left(\frac{1}{\epsilon} + 2 + O(\epsilon) \right), \end{aligned} \tag{26}$$

$$\begin{aligned} &\int \frac{d^D \ell}{(2\pi)^D i} \frac{1}{\ell^2 (p_c - \ell)^2 (xp - \ell)^2} = -\frac{1}{16\pi^2 Q^2} \left(\frac{4\pi}{Q^2} \right)^\epsilon \\ &\cdot \frac{1}{\Gamma(1-\epsilon)} \Gamma(1-\epsilon) \Gamma(1+\epsilon) B(1, -\epsilon) B(-\epsilon, 1-\epsilon) \\ &= -\frac{1}{16\pi^2 Q^2} \left(\frac{4\pi}{Q^2} \right)^\epsilon \frac{1}{\Gamma(1-\epsilon)} \left(\frac{1}{\epsilon^2} + O(\epsilon) \right). \end{aligned} \tag{27}$$

The complex-conjugate diagram gives the same contribution. Then we can show the cross section for the NLO virtual correction as

$$\begin{aligned} \frac{d \langle P_{h\perp} \Delta\sigma \rangle^{\text{virtual}}}{dx_B dy dz_h} &= \widetilde{\sigma}_0 \frac{\alpha_s}{2\pi} \\ &\cdot \sum_q e_q^2 G_{q,F}(x_B, x_B) D_{q \longrightarrow h}(z_h) C_F \left(\frac{4\pi\mu^2}{Q^2} \right)^\epsilon \\ &\cdot \frac{1}{\Gamma(1-\epsilon)} \left(-\frac{2}{\epsilon^2} - \frac{3}{\epsilon} - 8 \right), \end{aligned} \tag{28}$$

this is exactly the same as the virtual correction at leading twist. The strategy in the virtual correction calculation presented here is different with that shown in [63], in which the authors did not use the WTI shown in (19) and directly calculated $H^{\mu\nu}_{L(R)\rho\, ji}(k_1, k_2)$ which has one more external gluon line with the momentum $k_2 - k_1$ in Figure 2. The authors obtained a consistent result with (28), which demonstrated the validation of WTI through explicit calculation by including all virtual diagrams shown in Figures 3 and 4 in [63]. We would like to comment that the WTI reduces much calculational cost. The direct calculation of $H^{\mu\nu}_{L(R)\rho\, ji}(k_1, k_2)$ takes tremendous time as they contain significant amount of tensor reduction and integration. These two calculations should be conceptually the same with each other as long as we correctly keep track of all imaginary contributions. We confirmed in this section the consistency mathematically in $2 \longrightarrow 1$-scattering case. The consistency check in a more general way will be a future task in the collinear twist-3 factorization approach.

3.2. Real Correction. We now complete the NLO calculation by adding the real emission contribution represented by $2 \longrightarrow 2$ partonic scattering process. The calculation for $2 \longrightarrow 2$ scattering diagrams has been well studied in $P_{h\perp}$-unintegrated case. We just have to repeat the same calculation but in D-dimension. We adopt the conventional technique by separating the propagator into the principle value part and imaginary part [18–33],

$$\frac{1}{k^2 + i\epsilon} \longrightarrow P \frac{1}{k^2} - i\pi\delta\left(k^2\right), \tag{29}$$

and we focus on the pole contribution $-i\delta(k^2)$ which is required to generate the phase space for SSA. The derivation of the cross section for the pole contribution has been well developed so far based on the diagrammatic method we reviewed in Section 2. Here we recall the result derived in [23–28] as

$$\begin{aligned} w^{\mu\nu} &= i \int dx_1 \int dx_2 M^\alpha_{ij\,F}(x_1, x_2)\, p^\beta \frac{\partial}{\partial k_2^\alpha} \left(H^{\text{pole}\,\mu\nu}_{Lji\beta}(k_1, k_2) \right. \\ &\left. + H^{\text{pole}\,\mu\nu}_{Rji\beta}(k_1, k_2) \right)\Big|_{k_i = x_i p}, \end{aligned} \tag{30}$$

where the matrix element $M^\alpha_{ij\,F}$ is given by

$$\begin{aligned} &M^\alpha_{ij\,F}(x_1, x_2) \\ &= \int \frac{d\lambda}{2\pi} \int \frac{d\lambda'}{2\pi} \\ &\cdot e^{i\lambda x_1} e^{i\lambda'(x_2 - x_1)} \\ &\cdot \left\langle pS_\perp \left| \overline{\psi}_j(0)\, gF^{\alpha n}(\lambda' n) \psi_i(\lambda n) \right| pS_\perp \right\rangle \\ &= \frac{M_N}{4} \left[\epsilon^{\alpha p n S_\perp} (\not{p})_{ij} G_{q,F}(x_1, x_2) \right. \\ &\left. + i S^\alpha_\perp (\gamma_5 \not{p})_{ij} \widetilde{G}_{q,F}(x_1, x_2) \right] + \cdots. \end{aligned} \tag{31}$$

We can construct the gauge-invariant expression (30) before performing the p_h-integration. There are three types of pole

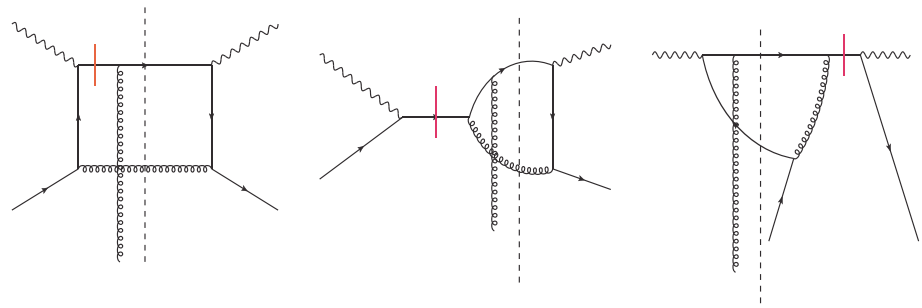

Figure 3: Typical diagrams for soft-gluon pole (left), hard pole (middle), and another hard pole (right). The red barred propagator gives the pole term.

contributions in SIDIS which are, respectively, known as soft-gluon pole contribution (SGP, $x_1 = x_2 = x$), hard pole contribution (HP, $x_1 = x$, $x_2 = x_B$ or $x_1 = x_B$, $x_2 = x$), and another hard pole contribution (HP2, $x_1 = x_B$, $x_2 = x_B - x$ or $x_2 = x_B$, $x_1 = x_B - x$) [23–28, 64], and the corresponding hard parts are given by

$$\begin{aligned}
H^{\text{pole}\,\mu\nu}_{Lji\beta} &= H^{\text{SGP}\,\mu\nu}_{Lji\beta}(k_1,k_2)\left\{-i\pi\delta\left[\left(p_c-(k_2-k_1)\right)^2\right]\right\}\\
&\cdot(2\pi)\,\delta\left[\left(k_2+q-p_c\right)^2\right] + H^{\text{HP}\,\mu\nu}_{Lji\beta}(k_1,k_2)\\
&\cdot\left\{-i\pi\delta\left[\left(k_1+q\right)^2\right]\right\}(2\pi)\,\delta\left[\left(k_2+q-p_c\right)^2\right]\\
&+ H^{\text{HP2}\,\mu\nu}_{Lji\beta}(k_1,k_2)\left\{i\pi\delta\left[\left(k_2+q\right)^2\right]\right\}(2\pi)\\
&\cdot\delta\left[\left(k_2-k_1+q-p_c\right)^2\right],\\
H^{\text{pole}\,\mu\nu}_{Rji\beta} &= H^{\text{SGP}\,\mu\nu}_{Rji\beta}(k_1,k_2)\left\{i\pi\delta\left[\left(p_c+(k_2-k_1)\right)^2\right]\right\}\\
&\cdot(2\pi)\,\delta\left[\left(k_1+q-p_c\right)^2\right] + H^{\text{HP}\,\mu\nu}_{Rji\beta}(k_1,k_2)\\
&\cdot\left\{i\pi\delta\left[\left(k_2+q\right)^2\right]\right\}(2\pi)\,\delta\left[\left(k_1+q-p_c\right)^2\right]\\
&+ H^{\text{HP2}\,\mu\nu}_{Rji\beta}(k_1,k_2)\left\{-i\pi\delta\left[\left(k_1+q\right)^2\right]\right\}(2\pi)\\
&\cdot\delta\left[\left(k_1-k_2+q-p_c\right)^2\right].
\end{aligned} \tag{32}$$

Typical diagrams for each pole contribution are shown in Figure 3 (full diagrams can be found in [64]). We write down the explicit form of each diagram in Figure 3 in order to help readers to follow our calculation,

$$\begin{aligned}
\left(H^{\text{SGP}\,\mu\nu}_{Lji\beta}(k_1,k_2)\right)_{\text{Figure 3}} &= -\left[\gamma^\sigma\left(\not{p}_c-\not{q}\right)\right.\\
&\cdot\left.\gamma^\nu\not{p}_c\gamma_\beta\left(\not{p}_c-\not{k}_2+\not{k}_1\right)\gamma^\mu\left(\not{p}_c-\not{k}_2+\not{k}_1-\not{q}\right)\gamma^\rho\right]_{ji}\\
&\cdot\frac{1}{\left(p_c-q\right)^2}\\
&\cdot\frac{1}{\left(p_c-k_2+k_1-q\right)^2}\left[-g_{\perp\rho\sigma}\left(k_2+q-p_c\right)\right],\\
\left(H^{\text{HP}\,\mu\nu}_{Lji\beta}(k_1,k_2)\right)_{\text{Figure 3}} &= -\left[\gamma^\sigma\left(\not{p}_c-\not{q}\right)\right.\\
&\cdot\left.\gamma^\nu\not{p}_c\gamma_\beta\left(\not{p}_c-\not{k}_2+\not{k}_1\right)\gamma^\rho\left(\not{k}_1+\not{q}\right)\gamma^\mu\right]_{ji}\frac{1}{\left(p_c-q\right)^2}\\
&\cdot\frac{1}{\left(p_c-k_2+k_1\right)^2}\left[-g_{\perp\rho\sigma}\left(k_2+q-p_c\right)\right],\\
\left(H^{\text{HP2}\,\mu\nu}_{Lji\beta}(k_1,k_2)\right)_{\text{Figure 3}} &= \left[\gamma^\nu\left(\not{k}_2+\not{q}\right)\right.\\
&\cdot\left.\gamma^\rho\not{p}_c\gamma_\beta\left(\not{p}_c-\not{k}_2+\not{k}_1\right)\gamma^\mu\left(\not{p}_c-\not{k}_2+\not{k}_1-\not{q}\right)\gamma_\rho\right]_{ji}\\
&\cdot\frac{1}{\left(p_c-k_2-q\right)^2}\frac{1}{\left(p_c-k_2+k_1\right)^2},
\end{aligned} \tag{33}$$

where $g_{\perp\rho\sigma}$ is the sum of the polarization vector $\sum_r \epsilon_{r\rho}(k)\epsilon_{r\sigma}(k) = -g_{\perp\rho\sigma}(k)$. We can show the WTI for the pole diagrams

$$\left(k_2-k_1\right)^\beta H^{\text{pole}\,\mu\nu}_{L(R)ji\beta}(k_1,k_2) = 0, \tag{34}$$

and it gives a useful relation

$$\begin{aligned}
&p^\beta\frac{\partial}{\partial k_2^\alpha}\,H^{\text{pole}\,\mu\nu}_{L(R)ji\beta}(k_1,k_2)\Big|_{k_i=x_ip}\\
&\quad=-\frac{1}{x_2-x_1-i\epsilon}H^{\text{pole}\,\mu\nu}_{L(R)ji\alpha}(k_1,k_2).
\end{aligned} \tag{35}$$

For HP and HP2 contributions, we can use (35) and do not have to perform k_2-derivative directly as in (30). However, we cannot use this relation for SGP contribution because it contains a delta function $\delta(x_1-x_2)$. In [69], the authors found a reduction formula for SGP contribution as

$$\begin{aligned}
&p^\beta\frac{\partial}{\partial k_2^\alpha}\left(H^{\text{SGP}\,\mu\nu}_{Lji\beta}(k_1,k_2)+H^{\text{SGP}\,\mu\nu}_{Rji\beta}(k_1,k_2)\right)\\
&=\frac{1}{2NC_F}\frac{1}{x_2-x_1-i\epsilon}\left(\frac{\partial}{\partial p_c^\alpha}-\frac{p_{c\alpha}p^\mu}{p_c\cdot p}\frac{\partial}{\partial p_c^\mu}\right)H(xp),
\end{aligned} \tag{36}$$

where $H(xp)$ is the $2 \longrightarrow 2$-scattering cross section without the external gluon line with momentum $(x_2-x_1)p$.

Substituting (31) into (30) and using ((35), (36)), we can derive the following result:

$$
\begin{aligned}
w^{\mu\nu} = {} & \frac{M_N\pi^2}{2}\int\frac{dx}{x}\delta\left[(xp+q-p_c)^2\right]\Bigg[-2\left(\left(\widehat{s}+Q^2\right)\right.\\
& \cdot\epsilon^{p_c pnS_\perp}\\
& \left.+\widehat{u}\epsilon^{qpnS_\perp}\right)\frac{d}{dx}G_{q,F}(x,x)\frac{1}{\widehat{t}\widehat{u}}\mathrm{Tr}\left[x\not{p}H(xp)\right]\\
& -2\left[\left(\widehat{s}+Q^2\right)\epsilon^{p_c pnS_\perp}+\widehat{u}\epsilon^{qpnS_\perp}\right]G_{q,F}(x,x)\\
& \cdot\frac{1}{\widehat{t}\widehat{u}}\left\{Q^2\left(\frac{\partial}{\partial\widehat{s}}-\frac{\partial}{\partial Q^2}\right)\mathrm{Tr}\left[x\not{p}H(xp)\right]\right.\\
& \left.-\mathrm{Tr}\left[x\not{p}H(xp)\right]\right\}+G_{q,F}(x,x_B)\frac{1}{\widehat{x}-1}\frac{\widehat{x}}{Q^2}\\
& \cdot\epsilon_\alpha^{pnS_\perp}\left[\mathrm{Tr}\left[x\not{p}H_L^{\mathrm{HP}\,\alpha}(x_Bp,xp)\right]\right.\\
& \left.+\mathrm{Tr}\left[x\not{p}\mathrm{H}_R^{\mathrm{HP}\,\alpha}(xp,x_Bp)\right]\right]-\widetilde{G}_{q,F}(x,x_B)\frac{1}{\widehat{x}-1}\\
& \cdot\frac{\widehat{x}}{Q^2}iS_{\perp\alpha}\left[\mathrm{Tr}\left[\gamma_5x\not{p}H_L^{\mathrm{HP}\,\alpha}(x_Bp,xp)\right]\right.\\
& \left.-\mathrm{Tr}\left[\gamma_5x\not{p}H_R^{\mathrm{HP}\,\alpha}(xp,x_Bp)\right]\right]+G_{q,F}(x_B,x_B-x)\\
& \cdot\frac{\widehat{x}}{Q^2}\epsilon_\alpha^{pnS_\perp}\left[\mathrm{Tr}\left[x\not{p}H_L^{\mathrm{HP2}\,\alpha}((x_B-x)p,x_Bp)\right]\right.\\
& \left.+\mathrm{Tr}\left[x\not{p}H_R^{\mathrm{HP2}\,\alpha}(x_Bp,(x_B-x)p)\right]\right]-\widetilde{G}_{q,F}(x_B,x_B\\
& -x)\frac{\widehat{x}}{Q^2}iS_{\perp\alpha}\left[\mathrm{Tr}\left[\gamma_5x\not{p}H_L^{\mathrm{HP2}\,\alpha}((x_B-x)p,x_Bp)\right]\right.\\
& \left.\left.-\mathrm{Tr}\left[\gamma_5x\not{p}H_R^{\mathrm{HP2}\,\alpha}(x_Bp,(x_B-x)p)\right]\right)\right],
\end{aligned}
\tag{37}
$$

where we used the Mandelstam variables

$$\widehat{s}=(xp+q)^2=\frac{1-\widehat{x}}{\widehat{x}}Q^2, \tag{38}$$

$$\widehat{t}=(p_c-q)^2=-\frac{1-\widehat{z}}{\widehat{x}}Q^2, \tag{39}$$

$$\widehat{u}=(xp-p_c)^2=-\frac{\widehat{z}}{\widehat{x}}Q^2, \tag{40}$$

with $\widehat{x}=x_B/x$, $\widehat{z}=z_h/z$. Then the cross section can be written as

$$
\begin{aligned}
\frac{d^4\left\langle P_{h\perp}\Delta\sigma\right\rangle^{\mathrm{real}}}{dx_Bdydz_h} \sim {} & \mu^{2\epsilon}\sum_q e_q^2\int dzD_{q\longrightarrow h}(z)\int\frac{d^{2-2\epsilon}p_{c\perp}}{(2\pi)^{2-2\epsilon}}\\
& \cdot\left[\int\frac{dx}{x}\delta\left(p_{c\perp}^2-\frac{(1-\widehat{x})(1-\widehat{z})\widehat{z}}{\widehat{x}}Q^2\right)\right.\\
& \times\frac{1}{1-\epsilon}\left[\frac{d}{dx}G_{q,F}(x,x)H_D+G_{q,F}(x,x)H_{ND}\right.\\
& +G_{q,F}(x,x_B)H_{HP}+\widetilde{G}_{q,F}(x,x_B)H_{HPT}\\
& +G_{q,F}(x_B,x_B-x)H_{HP2}\\
& \left.\left.+\widetilde{G}_{q,F}(x_B,x_B-x)H_{HPT2}\right],\right.
\end{aligned}
\tag{41}
$$

where we used the symmetry of the $P_{h\perp}$-integration as

$$
\begin{aligned}
& \int d^{2-2\epsilon}P_{h\perp}P_{h\perp\alpha}P_{h\perp\beta}\epsilon^{\rho\alpha pn}\epsilon^{\beta pn\sigma}\\
& \quad=-\int d^{2-2\epsilon}P_{h\perp}\frac{1}{2(1-\epsilon)}P_{h\perp}^2g_{\perp\alpha\beta}\epsilon^{\rho\alpha pn}\epsilon^{\beta pn\sigma}.
\end{aligned}
\tag{42}
$$

The authors of [63] found that the factor $1-\epsilon$ in the denominator is essential to derive the correct evolution function of $G_{q,F}(x,x)$. They calculated all SGP and HP contributions associated with $G_{q,F}$. After that, the HP2 contribution and all $\widetilde{G}_{q,F}$ contributions were calculated in [64]. The results of all hard cross sections are listed in [64]. We perform the $p_{c\perp}$-integration,

$$
\begin{aligned}
& \int\frac{d^{2-2\epsilon}p_{c\perp}}{(2\pi)^{2-2\epsilon}}\delta\left[p_{c\perp}^2-\frac{(1-\widehat{x})(1-\widehat{z})\widehat{z}}{\widehat{x}}Q^2\right]=\frac{1}{(2\pi)^{2-2\epsilon}}\\
& \cdot\int dp_{c\perp}\int d\Omega_{2-2\epsilon}\left(p_{c\perp}\right)^{1-2\epsilon}\delta\\
& \cdot\left[p_{c\perp}^2-\frac{(1-\widehat{x})(1-\widehat{z})\widehat{z}}{\widehat{x}}Q^2\right]=\frac{1}{4\pi}\left(\frac{4\pi}{Q^2}\right)^\epsilon\\
& \cdot\frac{1}{\Gamma(1-\epsilon)}\left[\frac{(1-\widehat{x})(1-\widehat{z})\widehat{z}}{\widehat{x}}\right]^{-\epsilon},
\end{aligned}
\tag{43}
$$

where $\Omega_{2-2\epsilon}$ is the solid angle and it can be integrated out as

$$\int d\Omega_{2-2\epsilon}=\frac{2\pi^{1-\epsilon}}{\Gamma(1-\epsilon)}. \tag{44}$$

We carry out the ϵ-expansion as follows:

$$\widehat{z}^{-\epsilon}\simeq 1-\epsilon\ln\widehat{z}, \tag{45}$$

$$\widehat{x}^{\epsilon}\simeq 1+\epsilon\ln\widehat{x}, \tag{46}$$

$$
\begin{aligned}
(1-\widehat{z})^{-1-\epsilon}\simeq {} & -\frac{1}{\epsilon}\delta(1-\widehat{z})+\frac{1}{(1-\widehat{z})_+}\\
& -\epsilon\left[\frac{\ln(1-\widehat{z})}{1-\widehat{z}}\right]_+,
\end{aligned}
\tag{47}
$$

$$
\begin{aligned}
(1-\widehat{x})^{-1-\epsilon}\simeq {} & -\frac{1}{\epsilon}\delta(1-\widehat{x})+\frac{1}{(1-\widehat{x})_+}\\
& -\epsilon\left[\frac{\ln(1-\widehat{x})}{1-\widehat{x}}\right]_+.
\end{aligned}
\tag{48}
$$

Then the cross section can be derived as follows:

$$\begin{aligned}
&\frac{d\left\langle P_{h\perp}\Delta\sigma\right\rangle^{\text{real}}}{dx_B dy dz_h} \\
&= \widetilde{\sigma}_0 \frac{\alpha_s}{2\pi}\left(\frac{4\pi\mu^2}{Q^2}\right)^{\epsilon}\frac{1}{\Gamma(1-\epsilon)} \\
&\cdot \sum_q e_q^2 \left[C_F \frac{2}{\epsilon^2}\, G_{q,F}(x_B,x_B)\, D_{q\longrightarrow h}(z_h)\right. \\
&+ \left(-\frac{1}{\epsilon}\right)\left\{D_{q\longrightarrow h}(z_h)\left\{\int_{x_B}^1 \frac{dx}{x}\left[C_F \frac{1+\widehat{x}^2}{(1-\widehat{x})_+}\, G_{q,F}(x,x)\right.\right.\right. \\
&+ \frac{N}{2}\left(\frac{(1+\widehat{x})\, G_{q,F}(x_B,x) - \left(1+\widehat{x}^2\right) G_{q,F}(x,x)}{(1-\widehat{x})_+}\right. \\
&\left.\left.\left.+\ \widetilde{G}_{q,F}(x_B,x)\right)\right] \\
&- N G_{q,F}(x_B,x_B) \\
&+ \frac{1}{2N}\int_{x_B}^1 \frac{dx}{x}\left((1-2\widehat{x})\, G_{q,F}(x_B,x_B-x)\right. \\
&\left.\left.+\ \widetilde{G}_{q,F}(x_B,x_B-x)\right)\right\} \\
&\left.+ G_{q,F}(x_B,x_B)\, C_F \int_{z_h}^1 \frac{dz}{z}\,\frac{1+\widehat{z}^2}{(1-\widehat{z})_+} D_{q\longrightarrow h}(z)\right\} \\
&+ \text{finite terms},
\end{aligned} \tag{49}$$

where the derivative term was converted to the nonderivative term through the partial integral,

$$\begin{aligned}
&\int_{x_B}^1 dx \frac{d}{dx} G_{q,F}(x,x)\left(1+\widehat{x}^2\right) \\
&\quad = \int_{x_B}^1 \frac{dx}{x} G_{q,F}(x,x)\left(2\widehat{x}^2 - 2\delta(1-\widehat{x})\right).
\end{aligned} \tag{50}$$

Combine the real (see (28)) and virtual corrections (see (49)), we find that the double-pole $1/\epsilon^2$ term, which represents a soft-collinear divergence, cancels out. The remaining collinear divergences, represented by the single pole $1/\epsilon$, can be eliminated by the redefinition of Qiu-Sterman function and fragmentation function,

$$\begin{aligned}
G_{q,F}(x_B,x_B) &= G_{q,F}^{(0)}(x_B,x_B) + \frac{\alpha_s}{2\pi}\left(-\frac{1}{\widehat{\epsilon}}\right)\left\{\int_{x_B}^1 \frac{dx}{x}\right. \\
&\cdot \left[P_{qq}(\widehat{x})\, G_{q,F}(x,x)\right. \\
&+ \frac{N}{2}\left(\frac{(1+\widehat{x})\, G_{q,F}(x_B,x) - \left(1+\widehat{x}^2\right) G_{q,F}(x,x)}{(1-\widehat{x})_+}\right. \\
&\left.\left.+\ \widetilde{G}_{q,F}(x_B,x)\right)\right] - N G_{q,F}(x_B,x_B) + \frac{1}{2N}\int_{x_B}^1 \frac{dx}{x} \\
&\cdot \left[(1-2\widehat{x})\, G_{q,F}(x_B,x_B-x) + \widetilde{G}_{q,F}(x_B,x_B\right. \\
&\left.\left.- x)\right]\right\},
\end{aligned} \tag{51}$$

$$\begin{aligned}
D_{q\longrightarrow h}(z_h) &= D_{q\longrightarrow h}^{(0)}(z_h) + \frac{\alpha_s}{2\pi}\left(-\frac{1}{\widehat{\epsilon}}\right)\int_{z_h}^1 \frac{dz}{z} P_{qq}(\widehat{z}) \\
&\cdot D_{q\longrightarrow h}(z),
\end{aligned} \tag{52}$$

where $P_{qq}(x)$ is well known $q \longrightarrow q$ splitting function

$$P_{qq}(x) = C_F\left[\frac{1+x^2}{(1-x)_+} + \frac{3}{2}\delta(1-x)\right], \tag{53}$$

and we adopted the $\overline{\text{MS}}$-scheme

$$\frac{1}{\widehat{\epsilon}} = \frac{1}{\epsilon} - \gamma_E + \ln 4\pi. \tag{54}$$

This collinear singularity is consistent with that of $G_{q,F}(x,x)$ explored in [54–59]. After the renormalization, the final result for the transverse-momentum-weighted SSAs at NLO is given by

$$\begin{aligned}
&\frac{d\left\langle P_{h\perp}\Delta\sigma\right\rangle^{\text{LO+NLO}}}{dx_B dy dz_h} \\
&= \widetilde{\sigma}_0 \sum_q e_q^2 \left[G_{q,F}(x_B,x_B,\mu)\, D_{q\longrightarrow h}(z_h,\mu)\right. \\
&+ \frac{\alpha_s}{2\pi}\ln\left(\frac{Q^2}{\mu^2}\right)\left\{D_{q\longrightarrow h}(z_h,\mu)\left\{\int_{x_B}^1 \frac{dx}{x}\right.\right. \\
&\cdot \left[P_{qq}(\widehat{x})\, G_{q,F}(x,x,\mu) + \frac{N}{2}\right. \\
&\cdot \left(\frac{(1+\widehat{x})\, G_{q,F}(x_B,x,\mu) - \left(1+\widehat{x}^2\right) G_{q,F} F(x,x,\mu)}{(1-\widehat{x})_+}\right. \\
&\left.\left.\left.+\ \widetilde{G}_{q,F}(x_B,x,\mu)\right)\right] \\
&- N G_{q,F}(x_B,x_B,\mu) + \frac{1}{2N} \\
&\cdot \int_{x_B}^1 \frac{dx}{x}\left((1-2\widehat{x})\, G_{q,F}(x_B,x_B-x,\mu)\right. \\
&\left.\left.+\ \widetilde{G}_{q,F}(x_B,x_B-x,\mu)\right)\right\} \\
&\left.+ G_{q,F}(x_B,x_B,\mu)\int_{z_h}^1 \frac{dz}{z} P_{qq}(\widehat{z})\, D_{q\longrightarrow h}(z,\mu)\right\}
\end{aligned}$$

$$
\begin{aligned}
&+\frac{\alpha_s}{2\pi}\int_{x_B}^{1}\frac{dx}{x}\int_{z_h}^{1}\frac{dz}{z}\\
&\cdot\left\{x\frac{dx}{x}G_{q,F}\left(x,x,\mu\right)D_{q\longrightarrow h}\left(z,\mu\right)\frac{1}{2N\widehat{z}}\right.\\
&\cdot\left[1-\widehat{z}+\frac{\left(1-\widehat{x}\right)^2+2\widehat{x}\widehat{z}}{\left(1-\widehat{z}\right)_+}-\delta\left(1-\widehat{z}\right)\right.\\
&\left.\cdot\left(\left(1+\widehat{x}^2\right)\ln\frac{\widehat{x}}{1-\widehat{x}}+2\widehat{x}\right)\right]\\
&+G_{q,F}\left(x,x,\mu\right)D_{q\longrightarrow h}\left(z,\mu\right)\frac{1}{2N\widehat{z}}\\
&\cdot\left[-2\delta\left(1-\widehat{x}\right)\delta\left(1-\widehat{z}\right)+\frac{2\widehat{x}^3-3\widehat{x}^2-1}{\left(1-\widehat{x}\right)_+\left(1-\widehat{z}\right)_+}\right.\\
&+\frac{1+\widehat{z}}{\left(1-\widehat{x}\right)_+}-2\left(1-\widehat{x}\right)+\delta\left(1-\widehat{z}\right)\\
&\cdot\left(-\left(1-\widehat{x}\right)\left(1+2\widehat{x}\right)\log\frac{\widehat{x}}{1-\widehat{x}}-2\left(\frac{\ln\left(1-\widehat{x}\right)}{1-\widehat{x}}\right)_+\right.\\
&\left.+\frac{2}{\left(1-\widehat{x}\right)_+}-2\left(1-\widehat{x}\right)+2\frac{\ln\widehat{x}}{\left(1-\widehat{x}\right)_+}\right)\\
&+\delta\left(1-\widehat{x}\right)\left(\left(1+\widehat{z}\right)\ln\widehat{z}\left(1-\widehat{z}\right)-2\frac{\ln\widehat{z}}{\left(1-\widehat{z}\right)_+}\right.\\
&\left.\left.-2\left(\frac{\ln\left(1-\widehat{z}\right)}{1-\widehat{z}}\right)_+ +\frac{2\widehat{z}}{\left(1-\widehat{z}\right)_+}\right)\right]\\
&+G_{q,F}\left(x,x_B,\mu\right)D_{q\longrightarrow h}\left(z,\mu\right)\left(C_F+\frac{1}{2N\widehat{z}}\right)\\
&\cdot\left[2\delta\left(1-\widehat{x}\right)\delta\left(1-\widehat{z}\right)+\frac{1+\widehat{x}\widehat{z}^2}{\left(1-\widehat{x}\right)_+\left(1-\widehat{z}\right)_+}\right.\\
&+\delta\left(1-\widehat{z}\right)\left(\log\frac{\widehat{x}}{1-\widehat{x}}+2\left(\frac{\ln\left(1-\widehat{x}\right)}{1-\widehat{x}}\right)_+\right.\\
&\left.-2\frac{\ln\widehat{x}}{\left(1-\widehat{x}\right)_+}-\frac{1+\widehat{x}}{\left(1-\widehat{x}\right)_+}\right)\\
&+\delta\left(1-\widehat{x}\right)\left(-\left(1+\widehat{z}\right)\ln\widehat{z}\left(1-\widehat{z}\right)+2\left(\frac{\ln\left(1-\widehat{z}\right)}{1-\widehat{z}}\right)_+\right.\\
&\left.\left.+2\frac{\ln\widehat{z}}{\left(1-\widehat{z}\right)_+}-\frac{2\widehat{z}}{\left(1-\widehat{z}\right)_+}\right)\right]\\
&+\widetilde{G}_{q,F}\left(x,x_B,\mu\right)D_{q\longrightarrow h}\left(z,\mu\right)\left(C_F+\frac{1}{2N\widehat{z}}\right)\\
&\cdot\left[-\frac{1-\widehat{x}\widehat{z}^2}{\left(1-\widehat{x}\right)_+\left(1-\widehat{z}\right)_+}\right.\\
&\left.+\delta\left(1-\widehat{z}\right)\left(\ln\frac{\widehat{x}}{1-\widehat{x}}+3\right)\right]\\
&+G_{q,F}\left(x_B,x_B-x,\mu\right)D_{q\longrightarrow h}\left(z,\mu\right)\\
&\cdot\left[\frac{1}{2N\widehat{z}}\left(\frac{\left(1-2\widehat{x}\right)\widehat{z}^2}{\left(1-\widehat{z}\right)_+}-\delta\left(1-\widehat{z}\right)\right.\right.\\
&\left.\cdot\left(1-2\widehat{x}\right)\left(\ln\frac{\widehat{x}}{1-\widehat{x}}+1\right)\right)\\
&\left.+\frac{1}{2\widehat{z}}\left(1-2\widehat{x}\right)\left\{\left(1-\widehat{z}\right)^2+\widehat{z}^2\right\}\right]\\
&+\widetilde{G}_{q,F}\left(x_B,x_B-x,\mu\right)D_{q\longrightarrow h}\left(z,\mu\right)\\
&\cdot\left[\frac{1}{2N\widehat{z}}\left(\frac{\widehat{z}^2}{\left(1-\widehat{z}\right)_+}-\delta\left(1-\widehat{z}\right)\left(\ln\frac{\widehat{x}}{1-\widehat{x}}+3\right)\right)\right.\\
&\left.-\frac{1}{2\widehat{z}}\left(1-2\widehat{x}\right)\right]\\
&\left.-8C_F\delta\left(1-\widehat{x}\right)\delta\left(1-\widehat{z}\right)\right\}\Bigg]+O\left(\alpha_s^2\right).
\end{aligned}
\tag{55}
$$

Note that the cross section above does not include the contribution from the gluon fragmentation channel. From the requirement that the physical cross section does not depend on the factorization scale μ,

$$
\frac{\partial}{\partial\ln\mu^2}\frac{d\left\langle P_{h\perp}\Delta\sigma\right\rangle^{\mathrm{LO+NLO}}}{dx_B dy dz_h}=0,
\tag{56}
$$

we can derive the LO evolution equation for $G_{q,F}(x,x)$,

$$
\begin{aligned}
&\frac{\partial}{\partial\ln\mu^2}G_{q,F}\left(x_B,x_B,\mu^2\right)\\
&=\frac{\alpha_s}{2\pi}\left\{\int_{x_B}^{1}\frac{dx}{x}\left[P_{qq}\left(\widehat{x}\right)G_{q,F}\left(x,x,\mu^2\right)+\frac{N}{2}\right.\right.\\
&\cdot\left(\frac{\left(1+\widehat{x}\right)G_{q,F}\left(x_B,x,\mu^2\right)-\left(1+\widehat{x}^2\right)G_{q,F}\left(x,x,\mu^2\right)}{\left(1-\widehat{x}\right)_+}\right.\\
&\left.\left.+\widetilde{G}_{q,F}\left(x_B,x,\mu^2\right)\right)\right]\\
&-NG_{q,F}\left(x_B,x_B,\mu^2\right)\\
&+\frac{1}{2N}\int_{x_B}^{1}\frac{dx}{x}\left(\left(1-2\widehat{x}\right)G_{q,F}\left(x_B,x_B-x,\mu^2\right)\right.\\
&\left.\left.+\widetilde{G}_{q,F}\left(x_B,x_B-x,\mu^2\right)\right)\right\}.
\end{aligned}
\tag{57}
$$

This evolution equation based on the transverse-momentum-weighted technique was first discussed in Drell-Yan process [62], in which the authors succeeded in deriving the $G_{q,F}$ terms in the parenthesis $[\cdots]$ in the evolution equation. After that, the authors of [63] pointed out that an extra term $-NG_{q,F}(x_B,x_B,\mu^2)$ also contributes to the evolution equation. The HP2 pole contribution and all $\widetilde{G}_{q,F}$ terms were obtained in [64] within the method of transverse momentum weighting.

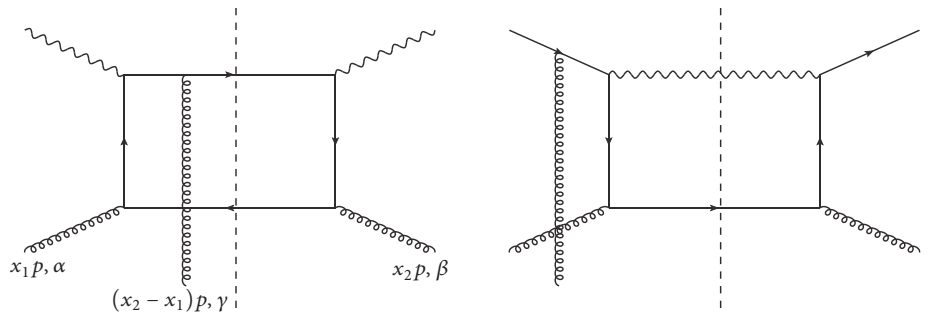

FIGURE 4: The diagrams which give the gluon mixing contribution to the evolution equation of $G_{q,F}(x, x)$ in SIDIS (left) and Drell-Yan (right).

4. Application to Other Processes

A lot of works on the transverse-momentum-weighted SSA have been done in recent years. We briefly summarize all related work in this section. The evolution equation of the Qiu-Sterman function (57) is still missing the gluon mixing contribution associated with the 3-gluon distribution functions defined by

$$\begin{aligned}
&\int \frac{d\lambda}{2\pi} \int \frac{d\lambda'}{2\pi} e^{i\lambda x_1} e^{i\lambda'(x_2 - x_1)} \left\langle pS_\perp \left| d_{bca} F_b^{\beta n}(0) \right.\right. \\
&\quad \cdot g F_c^{\gamma n}\left(\lambda' n\right) F_a^{\alpha n}(\lambda n) \left| \left. pS_\perp \right\rangle \right. = 2M_N \left[O(x_1, x_2) \right. \\
&\quad \cdot g^{\alpha\beta} \epsilon^{\gamma pnS_\perp} + O(x_2, x_2 - x_1)\, g^{\beta\gamma} \epsilon^{\alpha pnS_\perp} + O(x_1, x_1 \\
&\quad \left. - x_2)\, g^{\alpha\gamma} \epsilon^{\beta pnS_\perp} \right] + \cdots,
\end{aligned} \tag{58}$$

$$\begin{aligned}
&\int \frac{d\lambda}{2\pi} \int \frac{d\lambda'}{2\pi} e^{i\lambda x_1} e^{i\lambda'(x_2 - x_1)} \left\langle pS_\perp \left| i f_{bca} F_b^{\beta n}(0) \right.\right. \\
&\quad \cdot g F_c^{\gamma n}\left(\lambda' n\right) F_a^{\alpha n}(\lambda n) \left| \left. pS_\perp \right\rangle \right. = 2M_N \left[N(x_1, x_2) \right. \\
&\quad \cdot g^{\alpha\beta} \epsilon^{\gamma pnS_\perp} - N(x_2, x_2 - x_1)\, g^{\beta\gamma} \epsilon^{\alpha pnS_\perp} \\
&\quad \left. - N(x_1, x_1 - x_2)\, g^{\alpha\gamma} \epsilon^{\beta pnS_\perp} \right] + \cdots,
\end{aligned} \tag{59}$$

where d_{bca} and if_{bca} are the structure constants of $SU(N)$ group. Figure 4 shows typical diagrams which give the gluon mixing contribution in SIDIS and Drell-Yan.

The calculation technique for these diagrams was developed in [29–33]. There is only the soft-gluon pole ($x_1 = x_2$) contribution due to the interchange symmetry of the external gluon lines and then the cross section is expressed by four independent functions $O(x, x)$, $O(x, 0)$, $N(x, x)$, and $N(x, 0)$. The gluon mixing term in the flavor singlet evolution was discussed in both SIDIS [65, 67] and Drell-Yan [66] and the cross section up to the finite term is derived as

$$\begin{aligned}
&\left. \frac{d\left\langle P_{h\perp} \Delta\sigma \right\rangle^{\text{SIDIS}}}{dx_B dy dz_h d\phi} \right|_{\text{gluon}} \\
&\quad \sim G_{q,F}(x_B, x_B, \mu)\, D_{q \longrightarrow h}(z_h, \mu) \\
&\qquad + \frac{\alpha_s}{2\pi} \ln\left(\frac{Q^2}{\mu^2}\right) \left[D_{q \longrightarrow h}(z_h, \mu)\, \mathcal{F}_g \otimes T_{G+} \right] \\
&\qquad + \text{finite terms},
\end{aligned}$$

$$\begin{aligned}
&\left. \frac{d\left\langle q_\perp \Delta\sigma \right\rangle^{\text{DY}}}{dy dQ^2} \right|_{\text{gluon}} \\
&\quad \sim G_{q,F}(x_a, x_a, \mu)\, f_{\overline{q}/p}(x_b, \mu) \\
&\qquad + \frac{\alpha_s}{2\pi} \ln\left(\frac{Q^2}{\mu^2}\right) \left[f_{\overline{q}/p}(x_a, \mu)\, \mathcal{F}_g \otimes T_{G+} \right] \\
&\qquad + \text{finite terms},
\end{aligned} \tag{60}$$

where $x_a = (Q/\sqrt{s})e^{\eta}$, $x_b = (Q/\sqrt{s})e^{-\eta}$ with the center of mass energy $\sqrt{s}$ and the rapidity η, T_{G+} is given by a linear combination of the 3-gluon distribution functions, and $f_{\overline{q}/p}$ is the antiquark PDF. In Drell-Yan process, we use the transverse momentum of the virtual photon $q_\perp$ for the weighted cross section. Using the condition as in (56), we can derive the gluon mixing term of $G_{q,F}$. The explicit form of the evolution kernel $\mathcal{F}_g$ and the finite terms are shown in [66, 67]. Adding the mixing term to (57), the evolution equation for the Qiu-Sterman function, the first moment of the TMD Sivers function, was completed at LO with respect to QCD coupling constant α_s. As a by-product of the work on Drell-Yan, the NLO cross section related to the first momentum of the TMD Boer-Mulders function was also derived as

$$\begin{aligned}
&\left. \frac{d\left\langle q_\perp \Delta\sigma \right\rangle^{\text{DY}}}{dy dQ^2} \right|_{\text{BM}} \\
&\quad \sim T_{q,F}^{(\rho)}(x_a, x_a, \mu)\, h_1^{\overline{q}}(x_b, \mu) \\
&\qquad + \frac{\alpha_s}{2\pi} \ln\left(\frac{Q^2}{\mu^2}\right) \left[h_1^{\overline{q}}(x_a, \mu)\, \mathcal{F}_\sigma \otimes T_{q,F}^{(\rho)} \right] \\
&\qquad + \text{finite terms},
\end{aligned} \tag{61}$$

where h_1 is chiral-odd transversity distribution and the twist-3 function $T_F^{(\rho)}(x, x, \mu)$ corresponds to the first moment of

the Boer-Mulders function and its exact definition can be found in [66]. The evolution kernel $\mathscr{F}_\sigma$ and the finite terms of the cross section are shown in [66]. The authors in [67] also discussed the evolution equation for the first moment of the TMD Collins fragmentation function. The calculation of the twist-3 fragmentation contribution is different from the distribution case because the cross section only receives the nonpole contribution of the hard scattering. The calculation technique for the nonpole contribution has been well developed in [26, 34–36]. It is not difficult to extend it to the D-dimensional calculation. The NLO cross section was derived in [67] as

$$\begin{aligned}\frac{d\left\langle P_{h\perp}\Delta\sigma\right\rangle^{\text{SIDIS}}}{dx_B dy dz_h d\phi}\bigg|_{\text{Collins}} &\sim h_1^q(x_B,\mu)\,\widehat{e}_\partial^q(z_h,\mu)+\frac{\alpha}{2\pi}\\ &\cdot\ln\left(\frac{Q^2}{\mu^2}\right)h_1^q(x_B,\mu)\\ &\cdot\left[\mathscr{F}_\partial\otimes\widehat{e}_\partial^q+\mathscr{F}_F\otimes\widehat{E}_F^q+\mathscr{F}_G\otimes\widehat{E}_G^q\right]+\text{finite terms},\end{aligned}\tag{62}$$

where $\widehat{e}_\partial$, $\widehat{E}$, and $\widehat{E}_G$ are the twist-3 fragmentation functions for spin-0 hadron (different definition is shown in [70]). All evolution kernels and finite terms are shown in [67].

The NLO transverse-momentum-weighted cross section has been completed for single inclusive hadron production in SIDIS and Drell-Yan process in proton-proton collisions by a series of work presented here. These results are useful not only for the derivation of the evolution equations, but also for the verification of twist-3 collinear factorization feasibility, as well as for the global analysis of the experimental data. Measurement of the weighted SSAs just began very recently [68] and more data will be provided by future experiments. The analysis of the data based on the NLO result will lead to better understanding of the origin of the SSAs. There are still some TMD functions which have not been discussed yet; we hope the techniques presented in this paper can help extending the application of the transverse-momentum-weighted technique to resolve all these open questions.

The transverse-momentum-weighted technique has also been extended to study the transverse momentum broadening effect for semi-inclusive hadron production in lepton-nucleus scattering [71] and Drell-Yan dilepton production in proton-nucleus scattering [72]. In these studies, the QCD evolution equation for twist-4 quark-gluon correlation function was derived for the first time, and the twist-4 (double scattering) collinear factorization at NLO was confirmed through explicit calculations [73]. The finite NLO hard parts were obtained for the transverse momentum broadening effect, which can be used in global analysis of world data to extract precisely the medium properties characterized by the twist-4 matrix elements.

5. Summary

We reviewed the transverse-momentum-weighted technique as a useful tool to derive the scale evolution equation for the twist-3 collinear function which is expressed by the first moment of the TMD function. We first demonstrated the calculation of the LO cross section formula in a pedagogical way. Then we showed the basic techniques for the NLO calculation for both the virtual correction and real emission contributions. A lot of work have been done on the Qiu-Sterman function [62–65] and recently the application of this technique to other twist-3 functions was also discussed [66, 67]. There is still room of the application to many other TMD functions by considering appropriate twist-3 observables. We hope our review paper will provide basic knowledge needed to work on this subject.

In the end, we would like to point out the importance of the $P_{h\perp}$-weighted SSA from the phenomenological point of view. We introduced this observable as a tool to derive the scale evolution equation by focusing on the $1/\epsilon$-term in the cross section. However, the finite term is also important when we evaluate the cross section in order to compare it with the experimental data. The COMPASS experiment reported the data of the $P_{h\perp}$-weighted SSA very recently [68]. We expect that the data will be accumulated in the future experiments at COMPASS, JLab, and EIC and then the exact NLO cross section including the finite contribution will play an important role in the analysis of those weighted SSA data.

Conflicts of Interest

The authors declare that they have no conflicts of interest.

Acknowledgments

This research is supported by NSFC of China under Project no. 11435004 and research startup funding at SCNU.

References

[1] R. D. Klem, J. E. Bowers, H. W. Courant et al., "Measurement of asymmetries of inclusive pion production in proton-proton interactions at 6 and 11.8 GeV/c," *Physical Review Letters*, vol. 36, no. 16, pp. 929–931, 1976.

[2] G. Bunce, "Λ^0 hyperon polarization in inclusive production by 300-GeV protons on beryllium," *Physical Review Letters*, vol. 36, p. 1113, 1976.

[3] X. D. Ji, J. P. Ma, and F. Yuan, "QCD factorization for semi-inclusive deep-inelastic scattering at low transverse momentum," *Physical Review D*, vol. 71, no. 12, 2005.

[4] X. D. Jia, J. P. Maab, and F. Yuana, "QCD factorization for spin-dependent cross sections in DIS and drell-yan processes at low transverse momentum," *Physics Letters B*, vol. 597, no. 3-4, pp. 299–308, 2004.

[5] S. J. Brodsky, D. S. Hwang, and Schmidt I, "Final-state interactions and single-spin asymmetries in semi-inclusive deep inelastic scattering," *Physics Letters B*, vol. 530, pp. 99–107, 2002.

[6] S. J. Brodsky, D. S. Hwang, and I. Schmidt, "Initial-state interactions and single-spin asymmetries in Drell-Yan processes," *Nuclear Physics B*, vol. 642, no. 1-2, pp. 344–356, 2002.

[7] P. Mulders and R. Tangerman, "The complete tree-level result up to order 1/Q for polarized deep-inelastic leptoproduction," *Nuclear Physics B*, vol. 461, no. 1-2, pp. 197–237, 1996.

[8] A. Bacchetta, M. Diehl, K. Goeke, A. Metz, P. J. Mulders, and M. Schlegel, "Semi-inclusive deep inelastic scattering at small transverse momentum," *Journal of High Energy Physics*, vol. 2007, article no 093, 2007.

[9] D. Boer, P. J. Mulders, and F. Pijlman, "Universality of T-odd effects in single spin and azimuthal asymmetries," *Nuclear Physics B*, vol. 667, pp. 201–241, 2003.

[10] D. Boer and P. J. Mulders, "Time-reversal odd distribution functions in leptoproduction," *Physical Review D: Particles, Fields, Gravitation and Cosmology*, vol. 57, pp. 5780–5786, 1998.

[11] M. Anselmino, M. Boglione, U. D'Alesio, S. Melis, F. Murgia, and A. Prokudin, "Sivers effect in Drell-Yan processes," *Physical Review D: Particles, Fields, Gravitation and Cosmology*, vol. 79, Article ID 054010, 2009.

[12] M. Anselmino, M. Boglione, U. D'Alesio et al., "Sivers effect for pion and kaon production in semi-inclusive deep inelastic scattering," *The European Physical Journal A*, vol. 39, no. 1, pp. 89–100, 2009.

[13] Z. B. .Kang and J. W. Qiu, "Testing the time-reversal modified universality of the sivers function," *Physical Review Letters*, vol. 103, Article ID 172001, 2009.

[14] Z. B. Kang and J. W. Qiu, "Single transverse spin asymmetry of dilepton production near Z^0 pole," *Physical Review D: Particles, Fields, Gravitation and Cosmology*, vol. 81, Article ID 054020, 2010.

[15] J. Collins, A. Efremov, K. Goeke et al., "Sivers effect in the Drell-Yan process at BNL RHIC," *Physical Review D Covering Particles, Fields, Gravitation, and Cosmology*, vol. 73, Article ID 094023, 2006.

[16] A. V. Efremov and O. V. Teryaev, "On spin effects in quantum chromodynamics," *Soviet Journal of Nuclear Physics*, vol. 36, no. 1, pp. 242–246, 1982.

[17] A. V. Efremov and O. V. Teryaev, "QCD asymmetry and polarized hadron structure function measurement," *Physics Letters B*, vol. 150, no. 5, pp. 383–386, 1985.

[18] J.-W. Qiu and G. F. Sterman, "Single transverse spin asymmetries," *Physical Review Letters*, vol. 67, no. 17, pp. 2264–2267, 1991.

[19] J.-W. Qiu and G. F. Sterman, "Single transverse spin asymmetries in direct photon production," *Nuclear Physics B*, vol. 378, pp. 52–78, 1992.

[20] J.-W. Qiu and G. F. Sterman, "Single transverse-spin asymmetries in hadronic pion production," *Physical Review D: Particles, Fields, Gravitation and Cosmology*, vol. 59, Article ID 014004, 1999.

[21] C. Kouvaris, J. W. Qiu, W. Vogelsang, and F. Yuan, "Single transverse-spin asymmetry in high transverse momentum pion production in *pp* collisions," *Physical Review D: Particles, Fields, Gravitation and Cosmology*, vol. 74, Article ID 114013, 2006.

[22] Y. Kanazawa and Y. Koike, "Polarization in hadronic Λ hyperon production and chiral-odd twist-3 distribution," *Physical Review D Covering Particles, Fields, Gravitation, and Cosmology*, vol. 64, Article ID 034019, 2001.

[23] H. Eguchi, Y. Koike, and K. Tanaka, "Twist-3 formalism for single transverse spin asymmetry reexamined: semi-inclusive deep inelastic scattering," *Nuclear Physics B*, vol. 763, no. 1-2, pp. 198–227, 2007.

[24] Y. Koike and K. Tanaka, "Master formula for twist-3 soft-gluon-pole mechanism to single transverse-spin asymmetry," *Physics Letters B*, vol. 646, no. 5, pp. 232–241, 2007.

[25] Y. Koike and K. Tanaka, "Universal structure of twist-3 soft-gluon-pole cross sections for single transverse-spin asymmetry," *Physical Review D: Particles, Fields, Gravitation and Cosmology*, vol. 76, no. 6, Article ID 011502, 2007.

[26] Z. B. Kang, F. Yuan, and J. Zhou, "Twist-three fragmentation function contribution to the single spin asymmetry in *pp* collisions," *Physics Letters B*, vol. 691, pp. 243–248, 2010.

[27] Z. B. Kang, A. Metz, J. W. Qiu, and J. Zhou, "Exploring the structure of the proton through polarization observables in $l_p$jet X," *Physical Review D: Particles, Fields, Gravitation and Cosmology*, vol. 84, Article ID 034046, 2011.

[28] L. Gamberg and Z. B. Kang, "Single transverse spin asymmetry of prompt photon production," *Physics Letters B*, vol. 718, no. 1, pp. 181–188, 2012.

[29] H. Beppu, Y. Koike, K. Tanaka, and S. Yoshida, "Contribution of twist-3 multigluon correlation functions to single spin asymmetry in semi-inclusive deep inelastic scattering," *Physical Review D: Particles, Fields, Gravitation and Cosmology*, vol. 82, no. 5, Article ID 054005, 2010.

[30] Y. Koike and S. Yoshida, "Three-gluon contribution to the single spin asymmetry in Drell-Yan and direct-photon processes," *Physical Review D: Particles, Fields, Gravitation and Cosmology*, vol. 85, Article ID 034030, 2012.

[31] Y. Koike and S. Yoshida, "Probing the three-gluon correlation functions by the single spin asymmetry in $p\uparrow p \longrightarrow DX$," *Physical Review D: Particles, Fields, Gravitation and Cosmology*, vol. 84, Article ID 014026, 2011.

[32] Z. B. Kang and J. W. Qiu, "Single transverse-spin asymmetry for D-meson production in semi-inclusive deep inelastic scattering," *Physical Review D: Particles, Fields, Gravitation and Cosmology*, vol. 78, Article ID 034005, 2008.

[33] Z. B. Kang, J. W. Qiu, W. Vogelsang, and F. Yuan, "Accessing trigluon correlations in the nucleon via the single spin asymmetry in open charm production," *Physical Review D: Particles, Fields, Gravitation and Cosmology*, vol. 78, no. 11, Article ID 114013, 9 pages, 2008.

[34] F. Yuan and J. Zhou, "Collins function and the single transverse spin asymmetry," *Physical Review Letters*, vol. 103, Article ID 052001, 2009.

[35] A. Metz and D. Pitonyak, "Fragmentation contribution to the transverse single-spin asymmetry in proton–proton collisions," *Physics Letters B*, vol. 723, no. 4-5, pp. 365–370, 2013.

[36] K. Kanazawa and Y. Koike, "Contribution of the twist-3 fragmentation function to the single transverse-spin asymmetry in semi-inclusive deep inelastic scattering," *Physical Review D: Particles, Fields, Gravitation and Cosmology*, vol. 88, no. 7, Article ID 074022, 15 pages, 2013.

[37] Z.-T. Liang, A. Metz, D. Pitonyak, A. Schafer, Y.-K. Song, and J. Zhou, "Double spin asymmetry A_{LT} in direct photon production," *Physics Letters B*, vol. 712, no. 3, pp. 235–239, 2012.

[38] A. Metz, D. Pitonyak, A. Schaefer, and J. Zhou, "Analysis of the double-spin asymmetry A_{LT} in inelastic nucleon-nucleon collisions," *Physical Review D Covering Particles, Fields, Gravitation, and Cosmology*, vol. 86, Article ID 114020, 2012.

[39] X. Ji, J. W. Qiu, W. Vogelsang, and F. Yuan, "Unified picture for single transverse-spin asymmetries in hard-scattering processes," *Physical Review Letters*, vol. 97, Article ID 082002, 2006.

[40] X. Ji, J. W. Qiu, W. Vogelsang, and F. Yuan, "Single transverse-spin asymmetry in Drell-Yan production at large and moderate

transverse momentum," *Physical Review D Covering Particles, Fields, Gravitation, and Cosmology*, vol. 73, Article ID 094017, 2006.

[41] X. Ji, J. W. Qiu, W. Vogelsang, and F. Yuand, "Single transverse-spin asymmetry in semi-inclusive deep inelastic scattering," *Physics Letters B*, vol. 638, no. 2-3, pp. 178–186, 2006.

[42] Y. Koike, W. Vogelsang, and F. Yuan, "On the relation between mechanisms for single-transverse-spin asymmetries," *Physics Letters B*, vol. 659, no. 5, pp. 878–884, 2008.

[43] A. Bacchetta, D. Boer, M. Diehl, and P. Mulders, "Matches and mismatches in the descriptions of semi-inclusive processes at low and high transverse momentum," *Journal of High Energy Physics*, vol. 023, 2008.

[44] D. Boer, Z. Kang, W. Vogelsang, and F. Yuan, "Test of the universality of naive-time-reversal-odd fragmentation functions," *Physical Review Letters*, vol. 105, no. 20, 2010.

[45] Z.-B. Kang, J.-W. Qiu, W. Vogelsang, and F. Yuan, "Observation concerning the process dependence of the sivers functions," *Physical Review D: Particles, Fields, Gravitation and Cosmology*, vol. 83, Article ID 094001, 2011.

[46] L. Gamberg and Z.-B. Kang, "Process dependent Sivers function and implication for single spin asymmetry in inclusive hadron production," *Physics Letters B*, vol. 696, no. 1-2, pp. 109–118, 2011.

[47] J. Adams, "Cross sections and transverse single-spin asymmetries in forward neutral-pion production from proton collisions at $\sqrt{s}$=200 GeV," *Physical Review Letters*, vol. 92, Article ID 171801, 2004.

[48] B. I. Abelev, M. M. Aggarwal, Z. Ahammed et al., "Forward neutral-pion transverse single-spin asymmetries in p+p collisions at $\sqrt{s}$=200 GeV," *Physical Review Letters*, vol. 101, Article ID 222001, 2008.

[49] S. Heppelmann, "Measurement of transverse single spin asymmetry A_N in eta mass region at large feynman X_F with the star forward pion detector," *Nuclear Experiment*, 2009.

[50] S. S. Adler, S. Afanasiev, and C. Aidala, "Measurement of transverse single-spin asymmetries for midrapidity production of neutral pions and charged hadrons in polarized $p + p$ collisions at $\sqrt{s} = 200$ GeV," *Physical Review Letters*, vol. 95, Article ID 202001, 2005.

[51] I. Arsene, I. G. Bearden, D. Beavis et al., "Single-transverse-spin asymmetries of identified charged hadrons in polarized pp collisions at $\sqrt{s}$=62.4 GeV," *Physical Review Letters*, vol. 101, Article ID 042001, 2008.

[52] K. Kanazawa, Y. Koike, A. Metz, and D. Pitonyak, "Towards an explanation of transverse single-spin asymmetries in proton-proton collisions: the role of fragmentation in collinear factorization," *Physical Review D: Particles, Fields, Gravitation and Cosmology*, vol. 89, Article ID 111501, 2014.

[53] L. Gamberg, Z. Kang, D. Pitonyak, and A. Prokudin, "Phenomenological constraints on A N in p $\uparrow$ p $\longrightarrow$ π X from Lorentz invariance relations," *Physics Letters B*, vol. 770, pp. 242–251, 2017.

[54] Z. B. Kang and J. W. Qiu, "Evolution of twist-3 multiparton correlation functions relevant to single transverse-spin asymmetry," *Physical Review D Covering Particles, Fields, Gravitation, and Cosmology*, vol. 79, Article ID 016003, 2009.

[55] J. Zhou, F. Yuan, and Z. T. Liang, "QCD evolution of the transverse momentum dependent correlations," *Physical Review D Covering Particles, Fields, Gravitation, and Cosmology*, vol. 79, Article ID 114022, 2009.

[56] V. M. Braun, A. N. Manashov, and B. Pirnay, "Scale dependence of twist-three contributions to single spin asymmetries," *Physical Review D: Particles, Fields, Gravitation and Cosmology*, vol. 80, Article ID 114002, 2009.

[57] A. Schafer, J. Zhou, and D. Phys. Rev, "Note on the scale evolution of the Efremov-Teryaev-Qiu-Sterman function $T_F(x,x)$," *Physical Review D Covering Particles, Fields, Gravitation, and Cosmology*, vol. 85, Article ID 117501, 2012.

[58] J. P. Ma and Q. Wang, "Scale dependence of twist-3 quark–gluon operators for single spin asymmetries," *Physics Letters B*, vol. 715, no. 1-3, pp. 157–163, 2012.

[59] Z. B. Kang and J. W. Qiu, "QCD evolution of naive-time-reversal-odd parton distribution functions," *Physics Letters B*, vol. 713, no. 3, pp. 273–276, 2012.

[60] Z. B. Kang, "QCD evolution of naive-time-reversal-odd fragmentation functions," *Physical Review D Covering Particles, Fields, Gravitation, and Cosmology*, vol. 83, Article ID 036006, 2011.

[61] J. P. Ma and G. P. Zhang, "Evolution of chirality-odd twist-3 fragmentation functions," *Physics Letters B*, vol. 772, pp. 559–566, 2017.

[62] W. Vogelsang and F. Yuan, "Next-to-leading order calculation of the single transverse spin asymmetry in the Drell-Yan process," *Physical Review D Covering Particles, Fields, Gravitation, and Cosmology*, vol. 79, Article ID 094010, 2009.

[63] Z. B. Kang, I. Vitev, H. Xing, and D. Phys. Rev, "ransverse momentum-weighted Sivers asymmetry in semi-inclusive deep inelastic scattering at next-to-leading order," *Physical Review D: Particles, Fields, Gravitation and Cosmology*, vol. 87, Article ID 034024, 2013.

[64] S. Yoshida, "New pole contribution to $P_{h\perp}$-weighted single-transverse spin asymmetry in semi-inclusive deep inelastic scattering," *Physical Review D: Particles, Fields, Gravitation and Cosmology*, vol. 93, Article ID 054048, 2016.

[65] L. Dai, Z. Kang, A. Prokudin, and I. Vitev, "Next-to-leading order transverse momentum-weighted Sivers asymmetry in semi-inclusive deep inelastic scattering: The role of the three-gluon correlator," *Physical Review D: Particles, Fields, Gravitation and Cosmology*, vol. 92, no. 11, Article ID 114024, 2015.

[66] A. P. Chen, J. P. Ma, and G. P. Zhang, "One-loop corrections to single spin asymmetries at twist-3 in Drell-Yan processes," *Physical Review D Covering Particles, Fields, Gravitation, and Cosmology*, vol. 95, Article ID 074005, 2017.

[67] A. P. Chen, J. P. Ma, and G. P. Zhang, "One-loop corrections of single spin asymmetries in semi-inclusive DIS," *Physical Review D: Particles, Fields, Gravitation and Cosmology*, vol. 97, Article ID 054003, 2018.

[68] M. G. Alexeev, G. D. Alexeev, A. Amoroso et al., "Measurement of P_T-weighted Sivers asymmetries in leptoproduction of hadrons," *Nuclear Physics B*, vol. 940, pp. 34–53, 2019.

[69] Y. Koike and K. Tanaka, "Master formula for twist-3 soft-gluon-pole mechanism to single transverse-spin asymmetry," *Physics Letters B*, vol. 668, pp. 458-459, 2008.

[70] K. Kanazawa, Y. Koike, A. Metz, D. Pitonyak, and M. Schlegel, "Operator constraints for twist-3 functions and Lorentz invariance properties of twist-3 observables," *Physical Review D Covering Particles, Fields, Gravitation, and Cosmology*, vol. 5, Article ID 054024, 2016.

[71] Z. B. Kang, E. Wang, X. N. Wang, and H. Xing, "Transverse momentum broadening in semi-inclusive deep inelastic scattering at next-to-leading order," *Physical Review D Covering*

Particles, Fields, Gravitation, and Cosmology, vol. 94, no. 11, Article ID 114024, 2016.

[72] Z. B. Kang, J. W. Qiu, X. N. Wang, and H. Xing, "Next-to-leading order transverse momentum broadening for Drell-Yan production in $p+A$ collisions," *Physical Review D: Particles, Fields, Gravitation and Cosmology*, vol. 94, no. 7, Article ID 074038, 2016.

[73] Z. B. Kang, E. Wang, X. N. Wang, and H. Xing, "Next-to-leading order QCD factorization for semi-inclusive deep inelastic scattering at twist 4," *Physical Review Letters*, vol. 112, no. 10, Article ID 102001, 2014.

Hindawi
Advances in High Energy Physics
Volume 2019, Article ID 3036904, 68 pages
https://doi.org/10.1155/2019/3036904

Review Article

A Guide to Light-Cone PDFs from Lattice QCD: An Overview of Approaches, Techniques, and Results

Krzysztof Cichy[1] **and Martha Constantinou**[2]

[1]*Faculty of Physics, Adam Mickiewicz University, Umultowska 85, 61-614 Poznań, Poland*
[2]*Department of Physics, Temple University, Philadelphia, PA 19122 - 1801, USA*

Correspondence should be addressed to Martha Constantinou; marthac@temple.edu

Received 17 November 2018; Accepted 15 January 2019; Published 2 June 2019

Guest Editor: Alexei Prokudin

Within the theory of Quantum Chromodynamics (QCD), the rich structure of hadrons can be quantitatively characterized, among others, using a basis of universal nonperturbative functions: parton distribution functions (PDFs), generalized parton distributions (GPDs), transverse momentum dependent parton distributions (TMDs), and distribution amplitudes (DAs). For more than half a century, there has been a joint experimental and theoretical effort to obtain these partonic functions. However, the complexity of the strong interactions has placed severe limitations, and first-principle information on these distributions was extracted mostly from their moments computed in Lattice QCD. Recently, breakthrough ideas changed the landscape and several approaches were proposed to access the distributions themselves on the lattice. In this paper, we review in considerable detail approaches directly related to partonic distributions. We highlight a recent idea proposed by X. Ji on extracting quasidistributions that spawned renewed interest in the whole field and sparked the largest amount of numerical studies within Lattice QCD. We discuss theoretical and practical developments, including challenges that had to be overcome, with some yet to be handled. We also review numerical results, including a discussion based on evolving understanding of the underlying concepts and the theoretical and practical progress. Particular attention is given to important aspects that validated the quasidistribution approach, such as renormalization, matching to light-cone distributions, and lattice techniques. In addition to a thorough discussion of quasidistributions, we consider other approaches: hadronic tensor, auxiliary quark methods, pseudodistributions, OPE without OPE, and good lattice cross-sections. In the last part of the paper, we provide a summary and prospects of the field, with emphasis on the necessary conditions to obtain results with controlled uncertainties.

1. Introduction

Among the frontiers of nuclear and particle physics is the investigation of the structure of hadrons, the architecture elements of the visible matter. Hadrons consist of quarks and gluons (together called partons), which are governed by one of the four fundamental forces of nature, the strong force. The latter is described by the theory of Quantum Chromodynamics (QCD). Understanding QCD can have great impact on many aspects of science, from the subnuclear interactions to astrophysics, and, thus, a quantitative description is imperative. However, this is a very challenging task, as QCD is a highly nonlinear theory. This led to the development of phenomenological tools such as models, which have provided important input on the hadron structure. However, studies from first principles are desirable. An ideal *ab initio* formulation is Lattice QCD, a space-time discretization of the theory that allows the study of the properties of fundamental particles numerically, starting from the original QCD Lagrangian.

Despite the extensive experimental program that was developed and evolved since the first exploration of the structure of the proton [1, 2], a deep understanding of the hadrons' internal dynamics is yet to be achieved. Hadrons have immensely rich composition due to the complexity of the strong interactions that, for example, forces the partons to exist only inside the hadrons (color confinement), making the extraction of information from experiments very difficult.

Understanding internal properties of the hadrons requires the development of a set of appropriate quantities that can be accessed both experimentally and theoretically. The QCD factorization provides such formalism and can relate measurements from different processes to parton distributions. These are nonperturbative quantities describing the parton dynamics within a hadron and have the advantage of being universal, that is, do not depend on the process used for their extraction. The comprehensive study of parton distributions can provide a wealth of information on the hadrons, in terms of variables defined in the longitudinal direction (with respect to the hadron momentum) in momentum space, and two transverse directions. The latter can be defined either in position or in momentum space. These variables are as follows: (1) the longitudinal momentum fraction x carried by the parton, (2) the longitudinal momentum fraction ξ obtained via the longitudinal momentum transferred to the hadron, and (3) the momentum k_T transverse to the hadron direction of movement. Parton distributions can be classified into three categories based on their dependence on x, ξ, k_T and the momentum transferred to the hadron, t, as described below.

Parton distribution functions (PDFs) are one-dimensional objects and represent the number density of partons with longitudinal momentum fraction x while the hadron is moving with a large momentum.

Generalized parton distributions (GPDs) [3–7] depend on the longitudinal momentum fractions x and ξ and, in addition, on the momentum transferred to the parent hadron, t. They provide a partial description of the three-dimensional structure.

Transverse momentum dependent parton distribution functions (TMDs) [8–12] describe the parton distribution in terms of the longitudinal momentum fraction x and the transverse momentum k_T. They complement the three-dimensional picture of a hadron from GPDs.

As is clear from the above classification, PDFs, GPDs, and TMDs provide complementary information on parton distributions, and all of them are necessary to map out the three-dimensional structure of hadrons in spatial and momentum coordinates. Experimentally, these are accessed from different processes, with PDFs being measured in inclusive or semi-inclusive processes such as deep-inelastic scattering (DIS) and semi-inclusive DIS (SIDIS); see e.g., [13], for a review of DIS. GPDs are accessed in exclusive scattering processes such as Deeply Virtual Compton Scattering (DVCS) [14], and TMDs in hard processes in SIDIS [10, 11]. Most of the knowledge on the hadron structure is obtained from DIS and SIDIS data on PDFs, while the GPDs and TMDs are less known. More recently, data emerge from DVCS and Deeply Virtual Meson Production (DVMP) [15]. This includes measurements from HERMES, COMPASS, RHIC, Belle and Babar, E906/SeaQuest, and the 12 GeV upgrade at JLab. A future Electron-Ion Collider (EIC), that was strongly endorsed by the National Academy of Science, Engineering and Medicine [16], will be able to provide accurate data related to parton distributions and will advance dramatically our understanding on the hadron tomography. Together with the experimental efforts, theoretical advances are imperative in order to obtain a complete picture of hadrons. First, to interpret experimental data, global QCD analyses [17–26] are necessary that utilize the QCD factorization formalism and combine experimental data and theoretical calculations in perturbative QCD. Note that these are beyond the scope of this review and we refer the interested Reader to the above references and a recent community white paper [27]. Second, theoretical studies are needed to complement the experimental program and, in certain cases, provide valuable input. This is achieved using models of QCD and more importantly calculations from first principles. Model calculations have evolved and constitute an important aspect of our understanding of parton structure. An example of such a model is the diquark spectator model [28] that has been used for studies of parton distributions (for more details, see Section 4). The main focus of the models discussed in Section 4 is the one-dimensional hadron structure (x-dependence of PDFs), but more recently the interest has been extended to the development of techniques that are also applicable to GPDs and TMDs (some aspects are discussed in this review). Let us note that there have been studies related to TMDs from the lattice, and there is intense interest towards that direction (see, e.g., [29–31], and references therein).

Despite the tremendous progress in both the global analyses and the models of QCD, parton distributions are not fully known, due to several limitations: global analysis techniques are not uniquely defined [22]; certain kinematic regions are difficult to access, for instance, the very small x-region [32–34]; and models cannot capture the full QCD dynamics. Hence, an *ab initio* calculation within Lattice QCD is crucial, and synergy with global fits and model calculations can lead to progress in the extraction of distribution functions.

Lattice QCD provides an ideal formulation to study hadron structure and originates from the full QCD Lagrangian by defining the continuous equations on a discrete Euclidean four-dimensional lattice. This leads to equations with billions of degrees of freedom, and numerical simulations on supercomputers are carried out to obtain physical results. A nonperturbative tool, such as Lattice QCD, is particularly valuable at the hadronic energy scales, where perturbative methods are less reliable, or even fail altogether. Promising calculations from Lattice QCD have been reported for many years with the calculations of the low-lying hadron spectrum being such an example. More recently, Lattice QCD has provided pioneering results related to hadron structure, addressing, for instance, open questions, such as the spin decomposition [35] and the glue spin [36] of the proton. Another example of the advances of numerical simulations within Lattice QCD is the calculation of certain hadronic contributions to the muon $g-2$, for example, the connected and leading disconnected hadronic light-by-light contributions (see recent reviews of [37, 38]). Direct calculations of distribution functions on a Euclidean lattice have not been feasible due to the time dependence of these quantities. A way around this limitation is the calculation on the lattice of moments of distribution functions (historically for PDFs and GPDs) and the physical PDFs can, in principle, be obtained from operator product expansion (OPE). Realistically, only the lowest moments of PDFs and GPDs

can be computed (see, e.g., [39–44]) due to large gauge noise in high moments, and also unavoidable power-divergent mixing with lower-dimensional operators. Combination of the two prevents a reliable and accurate calculation of moments beyond the second or third, and the reconstruction of the PDFs becomes unrealistic.

Recent pioneering work of X. Ji [45] has changed the landscape of lattice calculations with a proposal to compute equal-time correlators of momentum boosted hadrons, the so-called quasidistributions. For large enough momenta, these can be related to the physical (light-cone) distributions via a matching procedure using Large Momentum Effective Theory (LaMET) (see Sections 3.1 and 8). This possibility has opened new avenues for direct calculation of distribution functions from Lattice QCD and first investigations have revealed promising results [46, 47] (see Section 3.2). Despite the encouraging calculations, many theoretical and technical challenges needed to be clarified. One concern was whether the Euclidean quasi-PDFs and Minkowski light-cone PDFs have the same collinear divergence, which underlies the matching programme. In addition, quasi-PDFs are computed from matrix elements of nonlocal operators that include a Wilson line. This results in a novel type of power divergences and the question whether these operators are multiplicatively renormalizable remained unanswered for some time. While the theoretical community was addressing such issues, the lattice groups had to overcome technical difficulties related to the calculation of matrix elements of nonlocal operators, including how to obtain reliable results for a fast moving nucleon, and how to develop a nonperturbative renormalization prescription (see Section 7). For theoretical and technical challenges, see Sections 5-6. Our current understanding on various aspects of quasi-PDFs has improved significantly, and lattice calculations of quasi-PDFs have extended to quantities that are not easily or reliably measured in experiments (see Sections 9-10), such as the transversity PDF [48, 49]. This new era of LQCD can provide high-precision input to experiments and test phenomenological models.

The first studies on Ji's proposal have appeared for the quark quasi-PDFs of the proton (see Sections 3.2 and 9). Recently, the methodology has been extended to other hadrons, in particular mesonic PDFs and distribution amplitudes (DAs). Progress towards this direction is presented in Section 10. Other recent reviews on the x-dependence of PDFs from Lattice QCD calculations can be found in [27, 50, 51]. The quasi-PDFs approach is certainly promising and can be generalized to study gluon quasi-PDFs, quasi-GPDs, and quasi-TMDs. In such investigations, technical difficulties of different nature arise and must be explored. First studies are presented here. Apart from the quasidistribution approach, we also review other approaches for obtaining the x-dependence of partonic functions, both the theoretical ideas underlying them (see Section 2) and their numerical explorations (Section 11).

The central focus of the review is the studies of the x-dependence of PDFs. We present work that appears in the literature until November 10, 2018 (published, or on the arXiv). The discussion is extended to conference proceedings for recent work that has not been published elsewhere. The presentation is based on chronological order, unless there is a need to include follow-up work by the same group on the topic under discussion. Our main priority is to report on the progress of the field, but also to comment on important aspects of the described material based on theoretical developments that appeared in later publications, or follow-up work. To keep this review at a reasonable length, we present selected aspects of each publication discussed in the main text and we encourage the interested Reader to consult the referred work. Permission for reproduction of the figures has been granted by the Authors and the scientific journals (in case of published work).

The rest of the paper is organized as follows. In Section 2, we introduce methods that have been proposed to access the x-dependence of PDFs from the lattice, which include a method based on the hadronic tensor, auxiliary quark field approaches, quasi- and pseudodistributions, a method based on OPE, and the good lattice cross-sections approach. A major part of this review is dedicated to quasi-PDFs, which are presented in more detail in Section 3, together with preliminary studies within Lattice QCD. The numerical calculations of the early studies have motivated an intense theoretical activity to develop models of quasidistributions, which are presented in Section 4. In Section 5, we focus on theoretical aspects of the approach of quasi-PDFs, that is, whether a Euclidean definition can reproduce the light-cone PDFs, as well as the renormalizability of operators entering the calculations of quark and gluon quasi-PDFs. The lattice techniques for quasi-PDFs and difficulties that one must overcome are summarized in Section 6. Recent developments on the extraction of renormalization functions related to logarithmic and/or power divergences are explained in Section 7, while Section 8 is dedicated to the matching procedure within LaMET. Lattice results on the quark quasi-PDFs for the nucleon are presented in Section 9. The quasi-PDFs approach has been extended to gluon distributions, as well as studies of mesons, as demonstrated in Section 10. In Section 11, we briefly describe results from the alternative approaches presented in Section 2. We close the review with Section 12 that gives a summary and future prospects. We discuss the x-dependence of PDFs and DAs, as well as possibilities to study other quantities, such as GPDs and TMDs. A glossary of abbreviations is given in the Appendix.

2. x-Dependence of PDFs

In this section, we briefly outline different approaches for obtaining the x-dependence of partonic distribution functions, in particular collinear PDFs. We first recall the problem by directly employing the definitions of such functions on the lattice, using the example of unpolarized PDFs. The unpolarized PDF, denoted here by $q(x)$, is defined on the light cone:

$$q(x) = \int_{-\infty}^{+\infty} \frac{d\xi^-}{4\pi} e^{-ixP^+\xi^-} \langle P| \overline{\psi}(\xi^-) \gamma^+ W(\xi^-, 0) \psi(0) |P\rangle, \quad (1)$$

where $|P\rangle$ is the hadron state with momentum P^μ, in the standard relativistic normalization[1], the light-cone vectors are taken as $v^\pm = (v^0 \pm v^3)/\sqrt{2}$, and $W(\xi^-, 0) = e^{-ig\int_0^{\xi^-} d\eta^- A^+(\eta^-)}$ is the Wilson line connecting the light-cone points 0 and ξ^-, while the factorization scale is kept implicit. Such light-cone correlations are not accessible on a Euclidean spacetime, because the light-cone directions shrink to one point at the origin. As discussed in the Introduction, this fact prevented lattice extraction of PDFs for many years, apart from their low moments, reachable via local matrix elements and the operator product expansion (OPE). However, since the number of moments that can be reliably calculated is strongly limited, alternative approaches were sought for to yield the full Bjorken-x dependence.

The common feature of all the approaches is that they rely to some extent on the factorization framework. For a lattice observable $Q(x, \mu_R)$ that is to be used to extract PDFs, one can generically write the following:[2]

$$Q(x, \mu_R) = \int_{-1}^{1} \frac{dy}{y} C\left(\frac{x}{y}, \mu_F, \mu_R\right) q(y, \mu_F), \tag{2}$$

where $C(x/y, \mu_F, \mu_R)$ is a perturbatively computable function and $q(y, \mu_F^2)$ is the desired PDF. In the above expression we distinguish between the factorization scale, μ_F, and the renormalization scale, μ_R. These scales are usually taken to be the same and, hence, from now on we will adopt this choice and take $\mu_F = \mu_R \equiv \mu$. Lattice approaches use different observables Q that fall into two classes:

(1) Observables that are generalizations of light-cone functions such that they can be accessed on the lattice; such generalized functions have direct x-dependence, but x does not have the same partonic interpretation as the Bjorken-x.

(2) Observables in terms of which hadronic tensor can be written; the hadronic tensor is then decomposed into structure functions like F_1 and g_1, which are factorizable into PDFs.

Below, we provide the general idea for several proposals that were introduced in recent years.

2.1. Hadronic Tensor. All the information about a DIS cross-section is contained in the hadronic tensor [52–56], defined by

$$W_{\mu\nu}(p, q, \lambda, \lambda') = \frac{1}{4\pi} \int d^4x e^{iqx} \left\langle p, \lambda' \right| \left[J_\mu(x), J_\nu(0) \right] \left| p, \lambda \right\rangle, \tag{3}$$

where $|p, \lambda\rangle$ is the hadron state labeled by its momentum p and polarization λ, q is virtual photon momentum, and $J_\mu(x)$ is electromagnetic current at point x. The hadronic tensor can be related to DIS structure functions and hence, in principle, PDFs can be extracted from it. $W_{\mu\nu}$ is the imaginary part of the forward Compton amplitude and can be written as the current-current correlation function

$$W_{\mu\nu}(p, q) = \left\langle p, \lambda' \right| \int \frac{d^4x}{4\pi} e^{iqx} J_\mu(x) J_\nu(0) \left| p, \lambda \right\rangle_{\overline{\lambda\lambda'}}, \tag{4}$$

where the subscript $\overline{\lambda\lambda'}$ denotes averaging over polarizations. The approach has been introduced as a possible way of investigating hadronic structure on the lattice by K.-F. Liu and S.-J. Dong already in 1993. They also proposed a decomposition of the contributions to the hadronic tensor according to different topologies of the quark paths, into valence and connected or disconnected sea ones. In this way, they addressed the origin of Gottfried sum rule violation.

A crucial aspect for the implementation in Lattice QCD is the fact that the hadronic tensor $W_{\mu\nu}$, defined in Minkowski spacetime, can be obtained from the Euclidean path-integral formalism [54–58], by considering ratios of suitable four-point and two-point functions. In the limit of the points being sufficiently away from both the source and the sink, where the hadron is created or annihilated, the matrix element receives contributions from only the ground state of the hadron. Reconstructing the Minkowski tensor from its Euclidean counterpart is formally defined by an inverse Laplace transform of the latter and can, in practice, be carried out using, e.g., the maximum entropy method or the Backus-Gilbert method. Nevertheless, this aspect is highly nontrivial and improvements thereof are looked for. As pointed out in [59], a significant role may be played by power-law finite volume effects related to the matrix elements being defined in Euclidean spacetime. A similar phenomenon was recently observed also in the context of $K - \overline{K}$ mixing [60]. Another difficulty of the hadronic tensor approach on the lattice is the necessity to calculate four-point correlation functions, which is computationally more intensive than for three-point functions, the standard tools of hadron structure investigations on the lattice. However, the theoretical appeal of the hadronic tensor approach recently sparked renewed interest in it [61–63]. We describe some exploratory results in Section 11.1.

2.2. Auxiliary Scalar Quark. In 1998, a new method was proposed to calculate light-cone wave functions (LCWFs) on the lattice [64]. This finds its motivation from the fact that LCWFs enter the description of many processes, such as electroweak decays and meson production. LCWF is the leading term of the full hadronic wave function in the $\Lambda^2_{\mathrm{QCD}}/p^2$ expansion, where p is the hadron momentum. For concreteness, we write the defining expression for the most studied LCWF, the one of the pion, $\Phi_\pi(u)$, where u is the momentum fraction:

$$\langle 0 | \overline{d}(0) W(0, x) \gamma_\mu \gamma_5 u(x) \left| \pi\left(p_\mu\right) \right\rangle_{x^2=0} = -ip_\mu f_\pi \int_0^1 du e^{-iuP_\pi x} \Phi_\pi(u), \tag{5}$$

with $|\pi(p)\rangle$ being boosted pion state, $|0\rangle$ being vacuum state, and f_π being pion decay constant. $W(0, x)$ is the Wilson line that ensures gauge invariance of the matrix element.

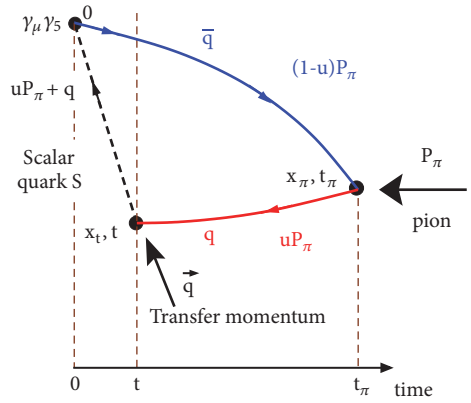

FIGURE 1: Schematic representation of the three-point function that needs to be computed to extract the pion light-cone wave function [64–66]. Source: arXiv version of [66], reprinted with permission by the Authors.

The essence of the idea is to "observe" and study on the lattice the partonic constituents of hadrons instead of the hadrons themselves [65, 66]. As shown in [64], the pion LCWF can be extracted by considering a vacuum-to-pion expectation value of the axial vector current with quark fields separated in spacetime. Gauge invariance is ensured by a scalar quark propagator with color quantum numbers of a quark, and at a large momentum transfer. The relation between the Fourier transform of this matrix element, computed on the lattice, and the pion LCWF, Φ_π, is given by the following formula:

$$\begin{aligned} F^\mu &\left(\vec{p_\pi}, \vec{q}; t, t_\pi\right) \\ &\equiv \int d^3x_\pi d^3x_t e^{-i\vec{p_\pi}\cdot\vec{x_\pi} - i\vec{q}\cdot\vec{x_t}} e^{E_\pi(t_\pi - t)} \left\langle \pi\left(p_\pi\right)\right| u\left(\vec{x_t}, t\right) \\ &\cdot S\left(\vec{x_t}, t; 0\right) \gamma_\mu\gamma_5 \overline{d}\left(0\right)\left|0\right\rangle \\ &\propto p_\pi^\mu f_\pi \sum_{u_i} \frac{e^{-(E_s + (1-u_i)E_\pi)t}}{2E_s\left(u_i\right)} \Phi_\pi\left(u_i\right), \end{aligned} \tag{6}$$

where $\vec{q}$ is momentum transfer, $S(\vec{x_t}, t; 0)$ is scalar colored propagator, and $\{u_i\}$ is discrete set of partonic momentum fractions (allowed by the discretized momenta in a finite volume). The spacetime points are explained in Figure 1, which shows the three-point function that needs to be computed. The interval $t_\pi - t$ needs to be large to have an on-shell pion. To extract the LCWF, several conditions need to be satisfied: injected pion momentum needs to be large (to have a "frozen" pion and see its partonic constituents), the scalar quark needs to carry large energy, the time t (time of momentum transfer and "transformation" of a quark to a scalar quark) has to be small (to prevent quantum decoherence and hadronization), and the lattice volume has to be large enough (to minimize effects of discretizing parton momenta). We refer to the original papers for an extensive discussion of these conditions. An exploratory study of the approach was presented in [65, 66] and later in [67], both in the quenched approximation. Naturally, the conditions outlined above are very difficult to satisfy simultaneously on the lattice, due to restrictions from the finite lattice spacing and the finite volume. However, the knowledge of the full hadronic wave function from first principles would be very much desired and further exploration of this approach may be interesting. In particular, integrals of hadronic wave functions over transverse momenta yield distribution amplitudes and PDFs.

2.3. Auxiliary Heavy Quark. In 2005, another method was proposed [58] to access hadron structure on the lattice, including PDFs. The idea relies on simulating on the lattice the Compton scattering tensor, using currents that couple physical light quarks of a hadron with a purely valence fictitious heavy quark. In the continuum limit, one can extract matrix elements of local operators in the OPE in the same renormalization scheme in which the Wilson coefficients are calculated. In this way, one gets the moments of PDFs. The crucial difference with respect to standard lattice calculations of moments is that the approach removes power divergent mixings with lower-dimensional operators, unavoidable in the lattice formulation for fourth and higher moments due to the breaking of the rotational invariance into the discrete hypercubic subgroup $H(4)$. This is derived and discussed in detail in [58]. Thus, in principle, any PDF moment can be extracted and the whole PDF can be reconstructed. Moreover, the heavy fictitious quark suppresses long-range correlations between the currents and also removes many higher-twist contaminations (twist=dimension−spin). The results are independent of the mass of the heavy quark, m_Ψ, as long as it satisfies a lattice window restriction; that is, it should be much larger than Λ_{QCD}, but much smaller than the ultraviolet cutoff a^{-1}. In practice, this means a requirement of rather small lattice spacings.

The considered heavy-light current is defined as follows:

$$J^\mu_{\Psi,\psi}\left(x\right) = \overline{\Psi}\left(x\right)\Gamma^\mu\psi\left(x\right) + \overline{\psi}\left(x\right)\Gamma^\mu\Psi\left(x\right), \tag{7}$$

with $\psi(x)$ denoting the light quark field and $\Psi(x)$ the fictitious heavy quark field. The Dirac structure Γ^μ can be general and is typically chosen according to the desired final observable. The Euclidean Compton scattering tensor is then constructed:

$$\begin{aligned} T^{\mu\nu}_{\Psi,\psi}\left(p,q\right) &\equiv \sum_S \left\langle p,S\right| t^{\mu\nu}_{\Psi,\psi}\left(q\right)\left|p,S\right\rangle \\ &= \sum_S \int d^4x e^{iq\cdot x} \left\langle p,S\right| T\left[J^\mu_{\Psi,\psi}\left(x\right) J^\nu_{\Psi,\psi}\left(0\right)\right]\left|p,S\right\rangle, \end{aligned} \tag{8}$$

where $|p,S\rangle$ are hadron states with momentum p and spin S and the spins are summed over. The momentum transfer q between the hadron and the scattered lepton in a DIS process should be smaller or at most of the order of the heavy quark mass. Furthermore, the momenta should satisfy the constraint $(p_M + q_M)^2 < (m_\Psi + \Lambda_{\mathrm{QCD}})^2$, where the momenta with subscript M are the Minkowski counterparts of the Euclidean ones. If this condition is satisfied, analytic continuation of the hadronic tensor to Euclidean spacetime

is straightforward and can be achieved by relating q_4 to iq_0. Expanding this tensor, in the continuum, using OPE, one can relate it to moments of PDFs. On the lattice, one needs to compute four-point functions to access the Compton tensor for PDFs. Analogous procedure may be applied to compute distribution amplitudes, for which the hadronic interpolating operator needs to be applied only once to the vacuum state and hence a computation of only three-point functions is required.

Numerical exploration, in the quenched approximation, is in progress [68], aimed at extracting the moments of the pion DA. Since the matching to OPE has to be performed in the continuum, at least three values of the lattice spacing need to be employed for a reliable extrapolation. Preliminary results are presented in Section 11.2 demonstrating the feasibility of this method.

2.4. Auxiliary Light Quark. Another possibility for extraction of light-cone distribution functions appeared in 2007 by V. Braun and D. Müller [69] and is based on the lattice calculation of exclusive amplitudes in coordinate space. It is similar to the fictitious heavy quark approach, but the heavy quark is replaced by an auxiliary light quark. One considers a current-current correlator:

$$T_{\mu\nu} = \langle 0| T\left\{j_\mu(z)\, j_\nu(-z)\right\}|\pi(p)\rangle, \tag{9}$$

with $j_\mu(z)$ being the electromagnetic current, but other choices of currents are also possible. For a discussion on extracting partonic distributions at light-like separations from such Euclidean correlators, we refer to Section II of [70]. On the lattice, $T_{\mu\nu}$ can be computed as an appropriate ratio of a three-point and a two-point function. If the separation between currents is small, the correlator can be computed perturbatively (using OPE) and in such a case Equation (9) yields:

$$T_{\mu\nu} = -\frac{5i}{9} f_\pi \epsilon_{\mu\nu\rho\sigma} \frac{z^\rho p^\sigma}{8\pi^2 z^4} \int_0^1 du e^{i(2u-1)p\cdot z} \phi_\pi(u,\mu), \tag{10}$$

at leading order and leading twist. Equation (10) is proportional to the Fourier transform, $\Phi_\pi(p\cdot z) = \int_0^1 du e^{i(2u-1)p\cdot x}\phi_\pi(u,\mu)$, of the pion DA, $\phi_\pi(u,\mu)$, where u is the quark momentum fraction. The perturbative expression for the correlator was also derived in [69] to NNLO, including twist-4 corrections. The LO and leading twist expression for the case of scalar-pseudoscalar densities in Equation (9) was given in [71]. It has been emphasized that the pion boost plays a different role than in some other approaches, as it does not suppress higher-twist contributions, but rather enters the Ioffe time $p\cdot z$. Thus, going to large boosts is important to have the full information on the coordinate space pion DA, $\Phi_\pi(p\cdot z)$, which can allow disentanglement between phenomenological models considered in the literature, that disagree in the regime of large Ioffe times. Advantages of the approach include the possibility of having arbitrary direction of z with respect to the boost direction, which may make it possible to minimize discretization effects. Moreover, one avoids complications related to the renormalization in the presence of a Wilson line (see Section 7); that is, one only needs renormalization of standard local operators which is at most logarithmically divergent. Finally, different possible Dirac structures may give the possibility of better control of higher-twist contamination. Obviously, the approach can also be generalized to extract PDFs, which, however, would necessitate the computation of four-point functions (see also Section 2.8).

The first numerical investigation of this approach is under way by the Regensburg group [70, 71] and is aimed at computing the pion DA, using multiple channels. The results fully prove the feasibility of this method and establish its status as a promising way of studying hadron structure; see also Section 11.3. Nevertheless, the requirement of calculation of four-point functions for extracting PDFs may prove to be a serious restriction and an exploratory study for, for example, nucleon PDFs, is not yet available.

2.5. Quasidistributions. In 2013, X. Ji proposed a new approach to extracting the x-dependence of structure functions [45]. Although historically it was not the first idea, it can be presently judged that it has been a breakthrough in the community's thinking about x-dependence from numerical simulations on a Euclidean lattice. In particular, it clearly renewed the interest also in approaches proposed earlier and described above. Ji's approach, obviously, bears similarities with the earlier methods and is also based on the factorization framework, in which a lattice computable function is factorized into a hard coefficient and a nonperturbative object like a PDF or a DA. The main difference is another type of object that is used to connect a quark and an antiquark separated by some distance and that ensures gauge invariance. In earlier proposals, different types of auxiliary quark propagators were used for this: scalar, heavy, or light quark propagators. In Ji's technique, this role is played by a Wilson line, that is, the same object that is used in definitions of PDFs and other distribution functions. Thus, in general, the quasidistribution approach is the closest transcription of a light-cone definition to Euclidean spacetime, effectively boiling down to replacing light-cone correlations by equal-time correlators along the direction of the Wilson line.

We illustrate the idea using the example of PDFs, while analogous formulations can be used to define DAs, GPDs, etc. It is instructive to see the direct correspondence between the light-cone definition (Equation (1)) and the definition of quasi-PDFs. As pointed out above, since light-cone correlations cannot be accessed on a Euclidean lattice, Ji proposed to evaluate on the lattice the following distribution, now termed the quasidistribution:

$$\tilde{q}(x,P_3) = \int_{-\infty}^{\infty} \frac{dz}{4\pi} e^{-izk_3} \langle P|\overline{\psi}(z)\gamma^0 W(z)\psi(0)|P\rangle, \tag{11}$$

where $P = (P_0, 0, 0, P_3)$, $k_3 = xP_3$ is the quark momentum in the 3-direction, and $W(z) = e^{-ig\int_0^z dz' A_3(z')}$ is the Wilson line in the boost direction[3]. The light-cone definition corresponds to the above expression at infinite momentum boost, in line with Feynman's original parton model [72, 73]. Since the momentum of the nucleon on the lattice is obviously finite,

the partonic interpretation is formally lost and some quarks can carry more momenta than the whole nucleon ($x > 1$) or move in the opposite direction to it ($x < 0$).

The quasidistribution differs from the light-cone one by higher-twist corrections suppressed with $\Lambda^2_{\rm QCD}/P_3^2$ and M_N^2/P_3^2, where M_N is the nucleon mass; see Section 3.1 for more details. A vital observation of Ji was that the difference between the two types of distributions arises only in the UV region; that is, their structure in the IR is the same. This means that the UV difference can be computed in perturbation theory and subtracted from the result, which comes under the name of matching to a light-cone distribution or Large Momentum Effective Theory (LaMET) [74]. The possibility of correcting the higher-twist effects by LaMET is an important difference with respect to previously mentioned approaches. However, explicit computation of such effects is also possible in them, as demonstrated already in the original paper for the auxiliary light quark approach [69].

The quasidistribution approach received a lot of interest in the community and sparked most of the numerical work among all the direct x-dependence methods. In further sections, we discuss in more detail its various aspects and the plethora of numerical results obtained so far.

2.6. Pseudodistributions. The approach of quasidistributions was thoroughly analyzed by A. Radyushkin [75–77] in the framework of virtuality distribution functions introduced by the same Author [78, 79] and straight-link primordial TMDs. In the process, he discovered another, but strongly related, type of distribution that is accessible on the lattice and can be related to light-cone distributions via factorization. It can be extracted from precisely the same matrix element that appears in Equation (1), $\mathscr{M}(\nu, -\xi^2) \equiv \langle P|\overline{\psi}(\xi^-)\gamma^+ W(\xi^-, 0)\psi(0)|P\rangle$, viewed as a function of two Lorentz invariants, the "Ioffe time" [52], $\nu \equiv -p\cdot\xi$ and $-\xi^2$. Thus, $\mathscr{M}(\nu, -\xi^2)$ has been termed the Ioffe time distribution (ITD). As in Ji's approach the vector ξ can be chosen to be purely spatial, $\xi = (0, 0, 0, z)$ on a Euclidean lattice. Then, one defines a pseudodistribution:

$$\mathscr{P}\left(x, z^2\right) = \frac{1}{2\pi}\int_{-\infty}^{\infty} d\nu e^{-ix\nu}\mathscr{M}\left(\nu, z^2\right). \tag{12}$$

Thus, the variation with respect to a quasi-PDF is the Fourier transform that is taken over the Ioffe time (at fixed z^2), as opposed to being over the Wilson line length z (at fixed momentum P_3). A consequence of this difference is that pseudo-PDFs have considerably distinct properties from quasi-PDFs. In particular, the distribution has the canonical support, $x \in [-1, 1]$.

We briefly mention here the issue of power divergences induced by the Wilson line, to be discussed more extensively in Sections 5.2.1 and 7. In the pseudodistribution approach, a convenient way of eliminating these (multiplicative) divergences is to take the ratio $\mathfrak{M}(\nu, z^2) = \mathscr{M}(\nu, z^2)/\mathscr{M}(0, z^2)$ [77, 80]. The reduced ITD, $\mathfrak{M}(\nu, z^2)$, can then be perturbatively matched to a light-cone Ioffe time PDF [81–86], as demonstrated in Section 8. The (inverse) length of the Wilson line plays the role of the renormalization scale and can be related to, e.g., the $\overline{\rm MS}$ scale.

Numerical investigation of the pseudodistribution approach has proceeded in parallel with the theoretical developments and promising results are being reported [81, 87–90] (see also Section 11.4).

2.7. OPE without OPE. Yet another recent proposal to compute hadronic structure functions was suggested in [91]. It is closely related to known ideas introduced around 20 years ago, dubbed "OPE without OPE" by G. Martinelli [92] and applied in, e.g., flavor physics [93]. The name originates from the fact that one directly computes the chronologically ordered product of two currents rather than matrix elements of local operators. In addition, one works in the regime of small spacetime separations between currents (to use perturbation theory to determine the expected form of the OPE), but large enough to avoid large discretization effects. The idea is also an ingredient of the proposal to compute LCWFs with the aid of a fictitious scalar quark [64].

The starting point is the forward Compton amplitude of the nucleon, defined similarly as in Equation (3). It can be decomposed in terms of DIS structure functions F_1 and F_2. With particular choice of kinematics, one can obtain the following relations between the 33-component of the Compton amplitude and F_1:

$$\begin{aligned} T_{33}(p,q) &= \sum_{n=2,4,\ldots}^{\infty} 4\omega^n \int_0^1 dx\, x^{n-1} F_1\left(x, q^2\right) \\ &= 4\omega\int_0^1 dx \frac{\omega x}{1-(\omega x)^2} F_1\left(x, q^2\right), \end{aligned} \tag{13}$$

where $\omega = 2p\cdot q/q^2$. Being able to access $T_{33}(p, q)$ for large enough number of values of ω, one can extract the moments of $F_1(x, q^2)$ or even the whole function.

Another important ingredient of the method proposed in [91] is the efficient computation of T_{33}, that is, one that avoids the computation of four-point functions. It relies on the Feynman-Hellmann relation [94]. One extends the QCD Lagrangian with a perturbation

$$\begin{aligned} \mathscr{L}(x) &\longrightarrow \mathscr{L}(x) + \lambda \mathscr{J}_3(x), \\ \mathscr{J}_3(x) &= Z_V \cos\left(\overrightarrow{q}\cdot\overrightarrow{x}\right) e_f \overline{\psi}_f(x)\gamma_3\psi_f(x), \end{aligned} \tag{14}$$

where e_f is the electric charge of the f-th flavor and λ is a parameter with dimension of mass. Evaluating the derivative of the nucleon energy with respect to λ, which requires dedicated simulations at a few λ values, leads to estimates of T_{33}:

$$T_{33}(p,q) = -2E_\lambda(p,q)\frac{\partial^2}{\partial\lambda^2}E_\lambda(p,q)\bigg|_{\lambda=0}. \tag{15}$$

The Authors also showed first results obtained in this framework and point to directions of possible improvements and to prospects of computing the entire structure function based on this method (see Section 11.5).

2.8. Good Lattice Cross Sections[4]. A novel approach to extracting PDFs or other partonic correlation functions from *ab initio* lattice calculations was proposed by Y.-Q. Ma and J.-W. Qiu [85, 86, 95]. They advocate for a global fit of "lattice cross-sections" (LCSs), i.e., appropriate lattice observables defined below, to which many of the ones described above belong. The logic is that standard phenomenological extractions of PDFs rely on an analogous fit to hadronic cross-sections (HCSs) obtained in experiments and a global fit approach can average out some of the systematics and yield ultimately good precision.

Good LCSs, i.e., ones that can be included in such a global fit, are the ones that have the following properties:

(1) They are calculable in Euclidean Lattice QCD

(2) Have a well-defined continuum limit

(3) Have the same and factorizable logarithmic collinear divergences as PDFs.

All of these properties are crucial and nontrivial. The first one excludes the direct use of observables defined on the light cone. In practice, the second one requires the observables to be renormalizable. Finally, the third property implies that the analogy with global fits to HCSs is even more appropriate; both strategies need to rely on the factorization framework: LCSs and HCSs are then written as a convolution of a perturbatively computable hard coefficient with a PDF.

Ma and Qiu constructed also a class of good LCSs in coordinate space that have the potential of being used in the proposed global fits, demonstrating that the three defining properties of LCSs are satisfied [86]. The considered class is very closely related to the one proposed by Braun and Müller (see Section 2.4), but the latter Authors concentrated on the pion DA, while the analysis of Ma and Qiu deals with the case of hadronic PDFs. In general, the relevant matrix element can be written as

$$\sigma_n\left(\omega, \xi^2, P^2, \mu\right) = \langle P| T\left\{\mathcal{O}_n\left(\xi, \mu\right)\right\}|P\rangle, \tag{16}$$

where n stands for different possible operators that can be shown to be factorizable into the desired PDF. P is the hadron momentum, and ξ is the largest separation of fields from which the n-th operator is constructed ($\xi^2 \neq 0$), $\omega \equiv P\cdot\xi$. One suggested choice for $\mathcal{O}_n$ are the current-current correlators:

$$\mathcal{O}_{J_1J_2}\left(\xi\right) \equiv \xi^{d_{J_1}+d_{J_2}-2} J_1^R\left(\xi\right) J_2^R\left(0\right), \tag{17}$$

where d_{J_i} stands for the dimension of the renormalized current $J_i^R = Z_{J_i} J_i$, with Z_{J_i} being the renormalization function of the current J_i. Different possible options for the currents were outlined and, then, factorization was demonstrated for this whole class of LCSs. Renormalizability of these objects is straightforward, as they are constructed from local currents. Also, the feasibility of a lattice calculation is easy to establish if ξ has no time component. Thus, this class of matrix elements belongs to the set of good LCSs. It was also shown in [86] that three of the observables discussed above, quasi-PDFs, pseudo-PDFs, and the Compton amplitude T_{33}, are also examples of good LCSs.

An explicit numerical investigation of the current-current correlators is in progress by the theory group of Jefferson National Laboratory (JLab) and first promising results for pion PDFs, using around 10 different currents, have been presented. For more details see Section 11.6.

3. Quasi-PDFs: More Details and Early Numerical Studies

We discuss now, in more detail, the quasidistribution approach which is the main topic of this review. The focus of this section is on the theoretical principles of this method and we closely follow the original discussion in Ji's first papers. Since these were soon followed by numerical calculation within Lattice QCD exploring the feasibility of the approach, we also summarize the progress on this side. We also identify the missing ingredients in these early studies and aspects that need significant improvement.

3.1. Theoretical Principles of Quasi-PDFs. Ji's idea of quasi-PDFs [45] relies on the intuition that if light-cone PDFs can be equivalently formulated in the infinite momentum frame (IMF), then the physics of a hadron boosted to a large but finite momentum has to have much in common with the physics of the IMF. Moreover, the difference between a large momentum frame and the IMF should vanish when the hadron momentum approaches infinity. These intuitions were formalized by Ji in his original paper and we reproduce here his arguments.

Consider a local twist-2 operator

$$O^{\mu_1\cdots\mu_n} = \overline{\psi}\gamma^{(\mu_1} iD^{\mu_2}\cdots iD^{\mu_n)}\psi - \text{traces}, \tag{18}$$

where parentheses in superscript indicate symmetrization of indices and the subtracted trace terms include operators of dimension $(n+2)$ with at most $n-2$ Lorentz indices. The matrix element of such an operator in the nucleon state reads

$$\langle P| O^{\mu_1\cdots\mu_n}\left(\mu^2\right)|P\rangle = 2a_n\left(\mu^2\right)\Pi^{\mu_1\cdots\mu_n}, \tag{19}$$

where $\Pi^{\mu_1\cdots\mu_n}$ is a symmetric rank-n tensor [96] and the coefficients a_n are moments of PDFs, i.e., $\int dx\, x^{n-1} q(x,\mu^2) = a_n(\mu^2)$ with even n. Taking all indices $\mu_1 = \cdots = \mu_n = +$, one recovers the light-cone, time-dependent correlation that defines the PDF. We now consider a different choice of indices, without any temporal component, $\mu_1 = \cdots = \mu_n = 3$:

$$O^{3\cdots3} = \overline{\psi}\gamma^3 iD^3\cdots iD^3\psi - \text{traces}, \tag{20}$$

with the trace terms containing operators with again at most $n-2$ Lorentz indices. Because of Lorentz invariance, matrix elements of the trace terms in the nucleon state are at most $(P^3)^{n-2}$ multiplied by Λ^2_{QCD}. On the other hand [96],

$$\Pi^{3\cdots3} = \sum_j^{n/2} c\left(j,n\right)\left(\left(P^3\right)^2\right)^{n/2-j}\left(M_N^2\right)^j, \tag{21}$$

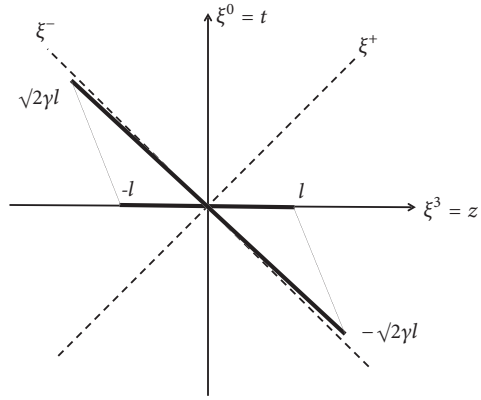

Figure 2: Schematic illustration of the relation between a finite momentum frame, with the Wilson line in a spatial direction and the light-cone frame of a hadron at rest. Due to Lorentz contraction, going to the light-cone frame increases the length by a boost factor γ, $\gamma \longrightarrow \infty$ in the IMF. Source: [74], reprinted with permission by the Author and Springer Nature.

where $c(j,n)$ is a combinatorial coefficient and M_N is the nucleon mass. As a consequence, we find that

$$\langle P|\,\overline{\psi}\gamma^3 iD^3 \cdots iD^3\psi\,|P\rangle = 2a_n\left(\mu^2\right)\left(P^3\right)^n\left(1+\mathcal{O}\left(\frac{\Lambda^2_{\mathrm{QCD}}}{\left(P^3\right)^2},\frac{M_N^2}{\left(P^3\right)^2}\right)\right). \tag{22}$$

The form of this expression implies that using an operator with the Wilson line in a spatial direction, in a nucleon state with finite momentum, leads to the light-cone PDF up to power-suppressed corrections in the inverse squared momentum. The corrections are of two kinds: generic higher-twist corrections and ones resulting from the nonzero mass of the nucleon. As we will discuss below, the latter can be calculated analytically and subtracted out. However, the former can only be overcome by simulating at a large enough nucleon boost and by using a matching procedure.

In the original paper that introduced the quasidistribution approach [45], Ji pointed out an intuitive way to understand the above result: "*(...) consider the Lorentz transformation of a line segment connecting* $(0,0,0,z)$ *with the origin of the coordinates. As the boost velocity approaches the speed of light, the space-like line segment is tilted to the light-cone direction. Of course, it cannot literally be on the light-cone because the invariant length cannot change for any amount of boost. However, this slight off-light-cone-ness only introduces power corrections which vanish asymptotically.*" This intuition is schematically represented in Figure 2.

We turn now to discussing how to match results obtained on the lattice, with a hadron momentum that is finite and relatively small, to the IMF. The subtlety of this results from the fact that regularizing the UV divergences does not commute with taking the infinite momentum limit. When defining PDFs, the latter has to be taken first, i.e., before removing the UV cutoff, whereas on the lattice one is bound to take all scales, including the momentum boost of the nucleon, much smaller than the cutoff, whose role is played by the inverse lattice spacing. To overcome this difficulty, one needs to formulate an effective field theory, termed Large Momentum Effective Theory (LaMET) [74], which takes the form of matching conditions that take the quasidistribution to the IMF, or light-cone, distribution. LaMET is an effective theory of QCD in the presence of a large momentum scale P^3, in a similar sense as Heavy Quark Effective Theory (HQET) [97] is an effective theory of QCD in the presence of a heavy quark, that can have a mass larger than the lattice UV cutoff.

The parallels of LaMET with HQET are more than superficial. We again follow Ji's discussion [74]. In HQET, a generic observable O depends on the heavy mass m_b and a cutoff Λ. The matching with an observable o defined in the effective theory, in which the heavy quark has infinite mass, can be written in the following way, due to asymptotic freedom:

$$O\left(\frac{m_b}{\Lambda}\right) = Z\left(\frac{m_b}{\Lambda},\frac{\Lambda}{\mu}\right)o\left(\mu\right) + \mathcal{O}\left(\frac{1}{m_b}\right), \tag{23}$$

where o is renormalized at a scale μ in the effective theory. Additionally, renormalization of the full theory translates the cutoff scale Λ to a renormalization scale μ. The crucial aspect is that O and o have the same infrared physics. Thus, the matching coefficient, Z, is perturbatively computable as an expansion in the strong coupling constant. Apart from the perturbative matching, there are power-suppressed corrections, which can also be calculated.

Using the same ideas, one can write the relation between an observable in the lattice theory, Q, dependent on the analogue of a heavy mass, i.e., a large momentum P^3 (and on the cutoff scale), and an observable in a theory in the IMF, q, thus corresponding to Feynman's parton model or to a light-cone correlation. This is again valid because of asymptotic freedom. The matching reads as follows:

$$Q\left(\frac{P^3}{\Lambda}\right) = C\left(\frac{P^3}{\Lambda},\frac{\Lambda}{\mu}\right)q\left(\mu\right) + \mathcal{O}\left(\frac{1}{\left(P^3\right)^2}\right). \tag{24}$$

We have, therefore, established the close analogy between HQET and the IMF parton model and the latter plays the role of an effective theory for a nucleon moving with a large momentum, just as HQET is an effective theory for QCD with a heavy mass. The infrared properties are, again, the same in both theories and the matching coefficient, C, can be computed in perturbation theory. There are power-suppressed corrections in inverse powers of $(P^3)^2$, vs. inverse powers of m_b in HQET.

To summarize, the need for LaMET when transcribing the finite boost results to light-cone parton distributions is the consequence of the importance of the order of limits. Parton physics corresponds to taking $P^3 \longrightarrow \infty$ in the observable Q first, before renormalization. On the lattice, in turn, UV regularization is necessarily taken first, before the infinite momentum limit, since no scale in the problem can be larger than the UV cutoff. However, interchanging the order of limits does not influence infrared physics and, hence, only matching in the ultraviolet has to be carried out and can be done perturbatively. The underlying factorization can be

proven order by order in perturbation theory. It is important to emphasize that any partonic observable can be accessed within this framework, with the same universal steps:

(1) Construction of a Euclidean version of the light-cone definition. The Euclidean observable needs to approach its light-cone counterpart in the limit of infinite momentum

(2) Computation of the appropriate matrix elements on the lattice and renormalizing them

(3) Calculation of the matching coefficient in perturbation theory and use of LaMET, Equation (24), to extract the light-cone distribution.

There is complete analogy also with accessing parton physics from scattering experiments, using factorization theorems and, thus, separating the nonperturbative (low-energy) and perturbative (high-energy) scales. To have similar access to partonic observables from lattice computations, LaMET plays the role of a tool for scale separation. Moreover, just as parton distributions can be extracted from a variety of different scattering processes, they can also be approached with distinct lattice operators.

We continue the discussion of LaMET by considering now the matching process in more detail. In the first paper devoted to the matching in the framework of LaMET, the nonsinglet PDF case was discussed [98]. We remind here the definition of the quasi-PDF:

$$\tilde{q}\left(x, P_3\right) = \int_{-\infty}^{\infty} \frac{dz}{4\pi} e^{-izk_3} \left\langle P\right| \overline{\psi}\left(z\right) \gamma^3 W\left(z\right) \psi\left(0\right) \left|P\right\rangle, \quad (25)$$

taking the original choice of the Dirac structure, i.e., γ^3, for the unpolarized case (see discussion about mixing for certain Dirac structures in Section 7). The matching condition should take the form

$$\tilde{q}\left(x, \mu^2, P_3\right) = \int_{-1}^{1} \frac{dy}{|y|} C\left(\frac{x}{y}, \frac{\mu}{P_3}\right) q\left(y, \mu^2\right) + \mathcal{O}\left(\frac{\Lambda_{\mathrm{QCD}}^2}{P_3^2}, \frac{M_N^2}{P_3^2}\right), \quad (26)$$

where the quasi-PDF, $\tilde{q}(x, \mu^2, P_3)$, is renormalized at a scale μ. The calculation of the matching is performed in a simple transverse momentum cutoff scheme, regulating the UV divergence, and, later in Section 8, we will consider further developments, including matching from different schemes to the $\overline{\mathrm{MS}}$ scheme. The motivation behind using the transverse momentum cutoff scheme is to take trace of the linear divergence related to the presence of the Wilson line, which would not be possible when using dimensional regularization.

The tree level of both the quasi- and the light-cone distributions is the same, i.e., a Dirac delta $\delta(1 - x)$. At one-loop level, two kinds of contributions appear: the self-energy diagram (left one in Figure 3) and the vertex diagram (right one in Figure 3). The quasidistribution receives, hence, the following one-loop correction:

$$\tilde{q}\left(x, \Lambda, P_3\right) = \left(1 + \widetilde{Z}_F^{(1)}\left(\Lambda, P_3\right)\right) \delta\left(1 - x\right) + \tilde{q}^{(1)}\left(x, \Lambda, P_3\right) + \mathcal{O}\left(\alpha_s^2\right), \quad (27)$$

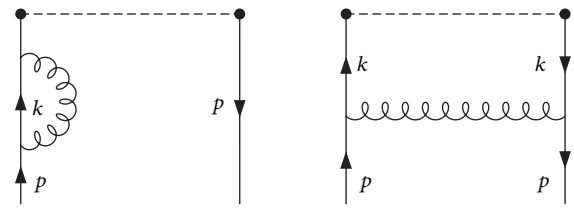

Figure 3: One-loop diagrams entering the calculation of quasidistributions: self-energy corrections (left) and vertex corrections (right). Source: [98], reprinted with permission by the Authors and the American Physical Society.

where $\widetilde{Z}_F^{(1)}$ are one-loop self-energy corrections (wave function corrections) and $\tilde{q}^{(1)}$ are the one-loop vertex corrections. Expressions for an explicit form of $\widetilde{Z}_F^{(1)}$ and $\tilde{q}^{(1)}$ are given in [98]. Their crucial aspect is that they are nonzero not only in the canonical range $x \in [0, 1]$, but also outside of it, for any positive and negative x. This corresponds to the loss of the standard partonic interpretation mentioned above. An important aspect is the particle number conservation, $\int_{-\infty}^{+\infty} dx\, \tilde{q}(x, \mu^2, P_3) = 1$. Different kinds of singularities appear:

(i) Linear (UV) divergences due to the Wilson line, taking in this scheme the form $\Lambda/(1 - x)^2 P_3$

(ii) Collinear (IR) divergences, only in $x \in (0, 1)$, expected to be the same as in the light-cone distribution

(iii) Soft (IR) divergences (singularities at $x = 1$), canceling between the vertex and the self-energy corrections ("plus prescription")

(iv) Logarithmic (UV) divergences in self-energy corrections, regulated with another cutoff[5].

We turn now to the light-cone distribution. It can be calculated in the same transverse momentum cutoff scheme by taking the limit $P_3 \longrightarrow \infty$ à la Weinberg [99]. We do not write here the final formulae, which can be found again in [98]. The result is the same as obtained from the light-cone definition. Crucially, the collinear divergence is the same as in the quasi-PDF, as anticipated based on physical arguments that the construction of quasidistributions should not modify the IR properties. Obviously, the diagrams in this case are nonzero only for $x \in [0, 1]$; i.e, x has a partonic interpretation.

Having computed the one-loop diagrams, one is ready to calculate the matching coefficient C in Equation (26). Its perturbative expansion can be written as

$$C\left(\xi, \frac{\mu}{P_3}\right) = \delta\left(1 - \xi\right) + \frac{\alpha_s}{2\pi} C_F C^{(1)}\left(\xi, \frac{\mu}{P_3}\right) + \mathcal{O}\left(\alpha_s^2\right), \quad (28)$$

with the following one-loop function:

$$C^{(1)}\left(\xi, \frac{\mu}{P_3}\right) = \begin{cases} \frac{1+\xi^2}{1-\xi}\ln\frac{\xi}{\xi-1} + 1 + \frac{1}{(1-\xi)^2}\frac{\Lambda}{P_3} & \xi > 1 \\ \frac{1+\xi^2}{1-\xi}\ln\frac{P_3^2}{\mu^2}(4\xi(1-\xi)) - \frac{2\xi}{1-\xi} + 1 + \frac{1}{(1-\xi)^2}\frac{\Lambda}{P_3} & 0 < \xi < 1 \\ -\frac{1+\xi^2}{1-\xi}\ln\frac{\xi}{\xi-1} - 1 + \frac{1}{(1-\xi)^2}\frac{\Lambda}{P_3} & \xi < 0 \end{cases} \tag{29}$$

$$+ \delta(1-\xi)\int dy \begin{cases} -\frac{1+y^2}{1-y}\ln\frac{y}{y-1} - 1 - \frac{1}{(1-y)^2}\frac{\Lambda}{P_3} & y > 1 \\ -\frac{1+y^2}{1-y}\ln\frac{P_3^2}{\mu^2}(4y(1-y)) + \frac{2y(2y-1)}{1-y} + 1 - \frac{1}{(1-y)^2}\frac{\Lambda}{P_3} & 0 < y < 1 \\ \frac{1+y^2}{1-y}\ln\frac{y}{y-1} + 1 - \frac{1}{(1-y)^2}\frac{\Lambda}{P_3} & y < 0. \end{cases}$$

Note that the matching process effectively trades the dependence on the large momentum for renormalization scale dependence (the term with the logarithm of P_3/μ), another characteristic feature of effective field theories. The antiquark distribution and the C-factor satisfy $\overline{q}(x) = -q(-x)$; hence including antiquarks is straightforward. Similar matching formulae were also derived for the case of helicity and transversity distributions [98].

The early papers of [45, 74, 98] provided the systematic framework for defining quasidistributions and matching them with their light-cone counterparts. Since then, there have been several improvements of many aspects of this programme, including renormalization, matching, target mass corrections, and other theoretical aspects, as well as developments for distributions other than the nonsinglet quark PDF of the nucleon discussed here. Before we turn to them, we report the early numerical efforts in Lattice QCD that illustrate the state-of-the-art calculations of that time.

3.2. Early Numerical Investigations. Ji's proposal for a novel approach of extracting partonic quantities on the lattice, in particular PDFs, sparked an enormous wave of interest, including numerical implementation and model investigations (see Section 4).

The first lattice results were presented in 2014 in [46] by H.-W. Lin et al. and later in [47, 100] by the ETM Collaboration[6]. Lin et al. used a mixed action setup of clover valence quarks on a HISQ sea, lattice volume $24^3 \times 64$, $a \approx 0.12$ fm, and pion mass (M_π) around 310 MeV, while ETMC used a unitary setup with maximally twisted mass quarks, lattice volume $32^3 \times 64$, $a \approx 0.082$ fm, and $M_\pi \approx 370$ MeV. Both papers implemented the bare matrix elements of the isovector unpolarized PDF ($u - d$ flavor structure, Dirac structure γ^3). The statistics for Lin et al. is 1383 measurements, while ETMC used a larger statistics of 5430 measurements. The employed nucleon boosts were in both cases the three lowest multiples of $2\pi/L$, i.e., 0.43, 0.86, and 1.29 GeV (Lin et al.) and 0.47, 0.94, and 1.42 GeV (ETMC), with noticeable increase of noise for the larger boosts, resulting in larger statistical errors. In view of the missing renormalization programme, both collaborations used HYP smearing [101] to bring the renormalization functions closer to their tree-level values (ETMC also applied the renormalization factor Z_V to correctly renormalize the local matrix element, i.e., one without the Wilson line). ETMC presented a study of the bare matrix elements dependence on the number of HYP smearing iterations, finding large sensitivity to this number especially for the imaginary part (the matrix elements are real only in the local case). Furthermore, ETMC tested the contamination by excited states by using two source-sink separations (t_s) of $8a \approx 0.66$ fm and $10a \approx 0.82$ fm, finding compatible results, but within large uncertainties. The source-sink separation in the study of Lin et al. was not reported. We note that separations below 1 fm are more susceptible to excited states contamination. However, the goal of these preliminary studies is to explore the approach of quasi-PDFs, postponing the investigation of excited states for later calculations. Having the bare matrix elements, the Fourier transform was taken to obtain the corresponding quasi-PDFs. The quasi-PDFs were matched to light-cone PDFs using the formulae of [98] and nucleon mass corrections were also applied. The obtained final PDFs are shown in Figure 4 for each study. One observes a similar picture from both setups and certain degree of qualitative agreement with phenomenological PDFs [102–104], shown for illustration purposes. Lin et al. also computed the helicity PDF (Dirac structure $\gamma^3\gamma^5$ in the matrix elements) and quoted the value of the sea quark asymmetry, but without showing the quasi- or final distributions.

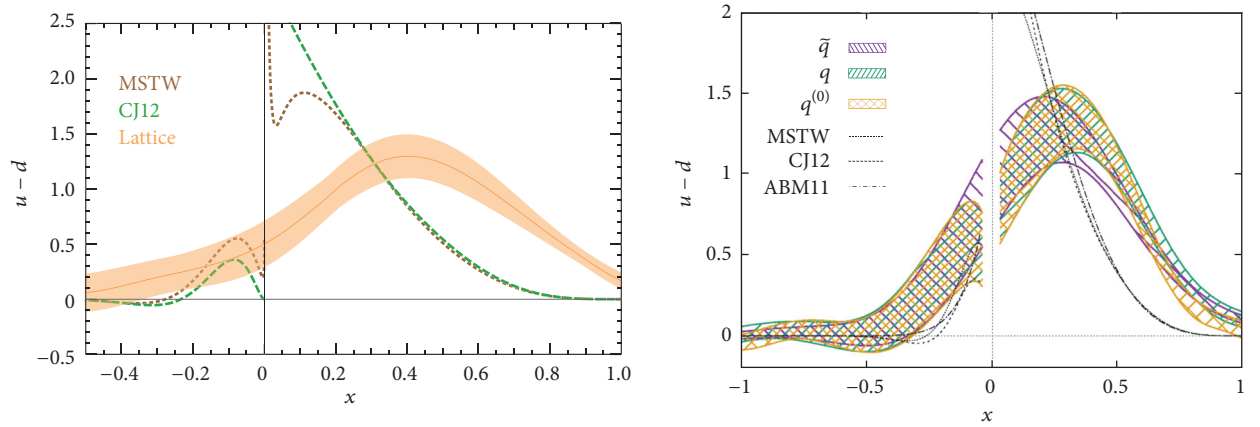

FIGURE 4: Final isovector unpolarized PDFs (shaded bands) at the largest employed nucleon boost, left: Lin et al., 1.29 GeV, right: ETMC, 1.42 GeV. The right plot also shows the quasi-PDF and the matched PDF before nucleon mass corrections. For illustration purposes, selected phenomenological parametrizations are plotted (dashed/dotted lines, no uncertainties shown) [102–104]. The errors are only statistical. Source: [46, 100], reprinted with permission by the Authors and the American Physical Society.

The two earliest numerical investigations of Ji's approach showed the feasibility of lattice extraction of PDFs. However, they also identified the challenges and difficulties. On one side, these were theoretical, like the necessity of development of the missing renormalization programme and the matching from the adopted renormalization scheme to the desired $\overline{\text{MS}}$ scheme. On the other side, it became also clear that the computation is technically challenging, in particular because of the decreasing signal-to-noise ratio when increasing the nucleon boost. The computational cost also increases with the source-sink separation, for which a large value (typically above 1 fm) is needed to suppress excited states. In addition, full control over typical lattice systematics, e.g., cutoff effects, finite volume effects, or the pion mass dependence, was also missing. At this stage, some difficulties were still unidentified, for example, the mixing between certain Dirac structures due to the chiral symmetry breaking in the used lattice discretizations, first identified by Constantinou and Panagopoulos [105, 106].

Further progress was reported in the next two papers by the same groups (with new members), early in 2016 by Chen et al. [107] and later in the same year by Alexandrou et al. (ETMC) [108]. Both groups used the same setups as in [46, 100] but implemented a number of improvements and considered all three types of collinear PDFs: unpolarized, helicity, and transversity. Chen et al. [107] considered two source-sink separations, $t_s = 8a \approx 0.96$ fm and $t_s = 10a \approx 1.2$ fm, and performed measurements on 449 gauge field configuration ensembles with 3 source positions on each configuration, using the same set of nucleon momenta as in [46], 0.43, 0.86, and 1.29 GeV. They also derived and implemented nucleon mass corrections (NMCs, also called target mass corrections, TMCs[7]) for all three cases of PDFs. The NMCs will be discussed below in Section 6. In the work of ETMC [108], a large-statistics study was performed with 30000 measurements for each of the three momenta, 0.47, 0.94, and 1.42 GeV, at an increased source-sink separation of $12a \approx 0.98$ fm. In the course of this work, the method of momentum smearing was introduced [109] (see Section 6 for details) to overcome the difficulty of reaching larger nucleon boosts. The technique was implemented by ETMC and results were presented for additional momenta, 1.89 and 2.36 GeV with small statistics of 150 and 300 measurements, respectively. Moreover, a test of compatibility between standard Gaussian smearing, applied in the earlier work of both groups, and the momentum smearing was performed at $P_3 \approx 1.42$ GeV for the unpolarized case. This revealed a spectacular property that similar statistical error as for Gaussian smearing with 30000 measurements can be obtained with only 150 measurements employing momentum smearing.

As an illustration, we show the final helicity PDFs in Figure 5. Direct visual comparison between the two results is not possible, since the plot by Chen et al. shows the PDF multiplied by x. Nevertheless, the qualitative picture is similar, revealing that no striking differences occur due to different lattice setups. The much smaller uncertainty in the plot by ETMC results predominantly from over 20 times larger statistics. Analogous plots for the unpolarized and transversity cases can be seen in [107, 108].

This concludes our discussion of the early explorations of the quasi-PDF approach. References [46, 100, 107, 108] proved its feasibility on the lattice and initiated identification of the challenges, already mentioned above. Further progress was conditioned on theoretical and practical improvements that will be described in later sections.

4. Quasidistributions: Model Investigations

Apart from theoretical analyses and numerical investigations in Lattice QCD, insights about the quasidistribution approach were obtained also from considerations in the framework of phenomenological or large-N_c models. In this section, we take a closer look at quasi-PDFs, quasi-GPDs, and quasi-DAs in such models and review the conclusions obtained in setups where direct access to analytical forms of quasi- and light-cone distributions is possible.

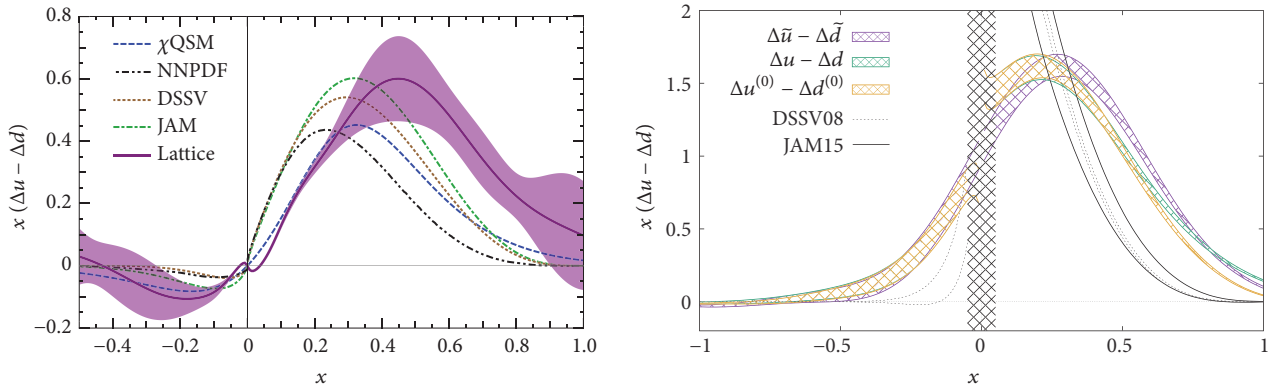

FIGURE 5: Final isovector helicity PDFs (shaded bands; $x\cdot$PDF in the left plot, PDF in the right plot) at the largest employed nucleon boost, left: Lin et al., 1.29 GeV, right: ETMC, 1.42 GeV. The right plot also shows the quasi-PDF and the matched PDF before nucleon mass corrections. For illustration purposes, also selected phenomenological parametrizations/models are plotted (left: dashed/dotted lines, no uncertainties shown, right: unfilled black bands representing uncertainties) [206–209]. The errors are only statistical. Source: left: [107], reprinted with permission by the Authors (article available under CC BY), and right: [108], reprinted with permission by the Authors and the American Physical Society.

4.1. Diquark Spectator Model. The aim of the early (2014) work of L. Gamberg et al. [110] and I. Vitev et al. [111] was to provide guidance about nucleon momenta P_3 needed for a reliable approach to the light-cone PDFs, for all collinear twist-2 distributions, i.e., unpolarized, helicity, and transversity PDFs. The Authors considered the diquark spectator model (DSM) [28], a phenomenological model that captures many of the essential features of the parton picture. The central idea of the DSM is to insert a completeness relation with intermediate states in the operator definition of PDFs (or some quark-quark correlation functions) and then truncate them to a single state with a definite mass. Such state is called the diquark spectator. This procedure boils down to making a particular ansatz for the spectral decomposition of the considered observable. The diquark spectator, in the simplest picture, can have spin-0 (scalar diquark) or spin-1 (axial-vector diquark). Finally, the nucleon is viewed as a system consisting of a constituent quark of some mass m and a scalar or axial-vector diquark. The basic object in this approximation is the nucleon-quark-diquark interaction vertex, which contains a suitably chosen form factor, taken in the so-called dipolar form in [110].

With such setup, one can derive the model expressions for all kinds of collinear quasi-PDFs, combining the expressions for scalar and axial-vector diquarks. The obtained relations can be used to study the approach to the light-cone PDFs, also calculated in the DSM. Gamberg et al. [110] got 3 couplings, fixed by normalization and 9 parameters of the model that were fixed by fitting to experimental data, with good quality of fits. Then, they considered the quasi-PDFs for different boosts from 1 to 4 GeV. It was found that the shape of quasi-PDFs approaches the PDF for $P_3 \gtrsim 2$ GeV. The agreement is especially good in the small to intermediate-x regime, while large-x needs significantly larger boost for a satisfactory agreement. The Authors also studied the Soffer inequality [112], stating that the transversity distribution should not be larger than the average of unpolarized and helicity ones. It holds for the standard PDFs. For quasi-PDFs, it was found that the inequality is always satisfied for the d quark, while it is violated for the u quark in the entire range of x for small momenta of around 0.5 GeV.

Further model study of quasi-PDFs was presented in [113] in 2016. Bacchetta et al. confirmed the conclusions of [110] and, motivated by the conclusion that the large-x region of quasi-PDFs converges much more slowly to the appropriate light-cone PDF, they proposed a procedure to aid the large-x extraction of PDFs from the quasidistribution approach. This is a relevant aspect for computations of quasi-PDFs in Lattice QCD. The main idea is to combine the result of a quasi-PDF and that of the corresponding moments of PDFs. One divides the whole x-region into two intervals, with a "matching" point x_0. For $x \leq x_0$, one assumes that the computed quasi-PDF is already a good approximation to the standard PDF. In turn, for $x \geq x_0$, a parametrization is used, with parameters fixed by conditions of smoothness at x_0 (for the value of the quasi-PDF and for its derivative) and by the available moments of PDFs. The procedure to reconstruct unpolarized and helicity PDFs was tested numerically in the DSM for two matching points, $x_0 = 0.2, 0.3$, and two nucleon momenta, $P_3 = 1.47, 2.94$ GeV. In all cases, there is significant improvement of agreement with respect to the standard PDF, especially at $x_0 = 0.2$. Excellent agreement was observed for the d quark even for the lower nucleon momentum, while the u quark seems to require a larger value of P_3, which is due to the worse agreement of the quasi-PDF and the standard PDF at the matching point. Overall, the procedure was proven to be successful in the DSM and the Authors are hopeful that it can be effectively applied also for actual Lattice QCD data.

The DSM (with scalar diquarks) was also employed as a framework for studying quasi-GPDs [114] in 2018. S. Bhattacharya, C. Cocuzza, and A. Metz calculated twist-2 unpolarized quasi-GPDs (the so-called H and E functions; for some definitions of GPDs variables and functions, see Section 8.2), using two Dirac structures, γ^0 and γ^3, motivated by the discovery of mixing for one of them [105, 106]. They verified that, in the forward limit, their expressions reduce

to the ones for the respective quasi-PDFs and, in the infinite momentum limit, their quasi-GPDs approach the appropriate GPDs. They found that all results for quasidistributions are continuous and argued that this feature should hold also at higher twist in the DSM. The Authors also checked the reliability of the cut-diagram approach, widely used in spectator models, and concluded it does not reproduce certain terms appearing from handling the calculation exactly. Thus, this approach is a simplification that should be avoided when dealing with quasidistributions. Having the final analytical expressions for quasi-GPDs and quasi-PDFs, they studied numerically the approach to infinite nucleon boost. They found that P_3 of order 2 GeV and larger yields quasifunctions within $\mathcal{O}(10\%)$ of their light-cone counterparts in a wide range of x. The problematic region, as for quasi-PDFs, is the large x regime, and the discrepancies increase for larger skewness ξ. Interestingly, the derivation of matching for GPDs [115], described shortly in Section 8.2, indicates that no matching is required for the E function (at leading order). However, in this model study, no significant differences in the convergence of the H and E functions were seen. In the ERBL region, $-\xi < x < \xi$, the agreement with standard GPDs is good, provided that ξ is not too small. The results for both Dirac structures were found to be very similar at large enough momentum ($P_3 \gtrsim 2$ GeV). To verify and strenghten the conclusions, the Authors also checked the sensitivity to parameter variations (constituent mass and spectator mass) and found no significant differences. As numerical exploration of quasi-GPDs on the lattice is still missing, the DSM results can provide very useful guidance to such attempts.

4.2. Virtuality Distribution Functions. A model investigation of quasi-PDFs was performed also by A. Radyushkin in 2016-17 [75, 76]. He used his formalism of virtuality distribution functions (VDFs) [78, 79]. In the VDF formalism, a generic diagram for a parton-hadron scattering corresponds to a double Fourier transform of the VDF, $\Phi(x, \sigma; M^2)$, where σ is related to the parton virtuality (giving the name to the VDF) and M is the hadron mass. The variables conjugates in the double Fourier transform are $x \longleftrightarrow p \cdot z$ (p is hadron momentum and z is separation of fields) and $\sigma \longleftrightarrow z^2$. The VDF representation holds for any p and z, but the case relevant for PDFs is the light-cone projection, $z^2 = 0$. Then, one can define primordial (straight-link) TMDs and derive relations between VDFs, TMDs, and quasi-PDFs. Working in a renormalizable theory, one can represent the VDF as a sum of a soft part, i.e., generating a nonperturbative evolution of PDFs, and a hard tail, vanishing with the inverse of σ.

Numerical interest in these papers was in the investigation of the nonperturbative evolution generated by the soft part of the VDF or, equivalently, the soft part of the primordial TMD. Radyushkin considers two models thereof, with a Gaussian-type dependence on the transverse momentum ("Gaussian model") and a simple non-Gaussian model ("$m = 0$ model"). These models are two extreme cases of a family of models, one with a too fast and one with a too slow fall-off in the impact parameter. In the numerical part of [75], the formalism was applied to a simple model PDF, $f(x) = (1 - x)^3\theta(x)$. Both TMD models give similar evolution patterns, implying that one observes some universal features related to the properties of quasi-PDFs. It was also observed that the approach to the limiting PDF is not uniform for different x and it can even be nonmonotonic for small nucleon momenta. These conclusions can provide very useful guidance to Lattice QCD calculations, meaning, e.g., that simple extrapolations in the inverse squared momentum might not be justifiable.

In the work of [76], Radyushkin considered target mass corrections (TMCs) in quasi-PDFs using the same framework. In both TMD models, it was found that TMCs become negligible already significantly before the quasi-PDF approaches the standard PDF. The Author suggested that, given the realistic precision of lattice simulations, TMCs can be neglected for nucleon boosts larger than around twice the nucleon mass.

4.3. Chiral Quark Models and Modeling the Relation to TMDs. Further model studies of the quasidistribution approach were performed in 2017 by W. Broniowski and E. Ruiz-Arriola [116, 117].

In the first paper [116], the pion quasi-DA and quasi-PDFs were computed in the framework of chiral quark models, namely, the Nambu-Jona-Lasinio (NJL) [118, 119] and the spectral quark model (SQM) [120–122]. The NJL model is a well-known toy model of QCD, which is a low-energy approximation to it and encompasses a mechanism of spontaneous chiral symmetry breaking from the presence of strong four-quark interactions. The SQM model, in turn, is a spectral regularization of the chiral quark model based on the introduction of the Lehmann representation of the quark propagator. The Authors derived analytical expressions for the quasi-DA and the quasi-PDF, together with their underlying unintegrated versions dependent on the transverse momentum, as well as the ITDs. They also verified the relations between different kinds of distributions found by Radyushkin [75–77]. This allowed them also to study the approach of the quasi-DA and quasi-PDF towards their light-cone counterparts and they found clear convergence for pion momenta in the range of a few GeV. Moreover, a comparison to lattice data [123] was made. For the NJL model, very good agreement was found with the lattice results at both considered pion momenta, $P_3 = 0.9, 1.3$ GeV. In the case of the SQM model, similar agreement was observed at $P_3 = 1.3$ GeV and at the smaller momentum there were some differences between the model and the lattice data, but the agreement was still satisfactory. This implies that both models are able to capture the essential physical features.

In the second paper [117], Broniowski and Ruiz-Arriola explored further the relations between nucleon quasi-PDFs, PDFs and TMDs, following the work of Radyushkin [75, 76]. They derived certain sum rules, e.g., relating the moments of quasi-PDFs, PDFs, and the width of TMDs. Furthermore, Broniowski and Ruiz-Arriola modeled the factorization separating the longitudinal and transverse parton dynamics. They applied this model to study the expected change of shape of

ITDs and reduced ITDs, for both quarks and gluons. They also considered the breakdown of the longitudinal-transverse factorization induced by the evolution equations, in the context of consequences for present-day lattice simulations, finding that the effects should be rather mild in quasi-PDFs, but could be visible in ITDs. Finally, they also performed comparisons to actual lattice data of the ETM Collaboration [108] for isovector unpolarized PDFs of the nucleon. The model quasi-PDFs, resulting from the assumed factorization, do not agree well with the ETMC data at 4 values of the nucleon boost between 0.94 and 2.36 GeV (see Section 3.2 for more details about these results). The discrepancy was attributed to the large pion mass, shifting the distributions to the right of the phenomenological ones, and to other lattice systematics (see also discussion about the role of the pion mass in Section 9.2.1 and [124]). More successful was the test of the aforementioned sum rule, predicting linearly increasing deviation of the second central moment of the quasi-PDF from that of the PDF with increasing $1/P_3^2$, with the slope giving the TMD width. Using the ETMC data, they indeed observed the linear behavior and, moreover, extrapolating to infinite momentum, they found the second central moment to be compatible with a phenomenological analysis. In the last part of the paper, the Authors offered considerations for the pion case, presenting predictions for the valence-quark quasi-PDFs and ITDs.

4.4. Quasidistributions for Mesons in NRQCD and Two-Dimensional QCD. Meson DAs were first considered in the quasidistribution formalism in 2015 by Y. Jia and X. Xiong [125]. They calculated the one-loop corrections to quasi-DAs and light-cone DAs employing the framework of nonrelativistic QCD (NRQCD). This resulted in analytical formulae for quasi- and light-cone DAs for three S-wave charmonia: the pseudoscalar η_c and both the longitudinally and the transversely polarized vector J/ψ. They checked analytically the convergence of quasi-DAs to standard DAs and performed also a numerical investigation of the rate of convergence. A function was introduced, called degree of resemblance, that quantifies the difference between the quasi- and the standard DAs. In general, momentum of around 3 times the meson mass is needed to bring the quasidistribution to within 5% of the light-cone one. The Authors also considered first inverse moments of quasi- and light-cone DAs, concluding that their rate of convergence is somewhat smaller and the difference at P_3 equal to three times the hadron mass may still be of order 20%, with 5% reached at P_3 six times larger than the meson mass.

Following the NRQCD investigation, Y. Jia and X. Xiong continued their work related to model quasidistributions of mesons. In 2018, together with S. Liang and R. Yu [126], they presented results on meson quasi-PDFs and quasi-DAs in two-dimensional QCD in its large-N_c limit, often referred to as the 't Hooft model [127]. The Authors used the Hamiltonian operator approach and Bars-Green equations in equal-time quantization [128], instead of the more standard diagrammatic approach in light-cone quantization. They performed a comprehensive study comparing the quasidistributions and their light-cone counterparts, studying the approach of the former to the latter at increasing meson momentum. Among the most interesting conclusions is the observation that the approach to the standard distributions is slower for lighter mesons than for heavier quarkonia of [125]. This observation was illustrated with numerical studies of the derived analytical equations for the different distributions. It was found that, for the pion, even momentum 8 times larger than the pion mass leads to significant discrepancies between the shapes of quasidistributions and light-cone ones. For $s\bar{s}$ ($c\bar{c}$) meson, in turn, momentum of five (two) times the meson mass already leads to the two types of distributions almost coinciding. An analogous phenomenon is also beginning to emerge in lattice studies and provides a warning that, e.g., pion PDFs might be more difficult to study than nucleon PDFs, i.e., require relatively larger momentum boosts.

Additionally, Jia et al. studied both types of distributions in perturbation theory, thus being able to consider the matching between quasi- and light-cone PDFs/DAs. The very important aspect of this part is that they were able to verify one of the crucial features underlying LaMET, that quasi- and light-cone distributions share the same infrared properties at leading order in $1/P_3$. This is interesting, because the two-dimensional model has a more severe IR divergence than standard QCD.

As such, this work in two-dimensional QCD provides a benchmark for lattice studies of quasidistributions in four-dimensional QCD. It is expected that many of the obtained conclusions regarding the 't Hooft model hold also in standard QCD. Moreover, the setup can also be used to study other proposals for obtaining the x-dependence of light-cone distributions, in particular pseudo-PDFs and LCSs.

5. Theoretical Challenges of Quasi-PDFs

In this section, we summarize the main theoretical challenges related to quasi-PDFs, that have been identified early on. Addressing and understanding these challenges was very critical in order to establish sound foundations for the quasidistribution method. We concentrate on two of them, the role of the Euclidean signature (whether an equal-time correlator in Euclidean spacetime can be related to light-cone parton physics in Minkowski) and renormalizability. The latter is not trivial due to the power-law divergence inherited from the Wilson line included in the nonlocal operator. It is clear that problems related to either challenge could lead to abandoning the whole programme for quasi-PDFs. Therefore, it was absolutely crucial to prove that both of these aspects do not hide insurmountable difficulties.

5.1. Euclidean vs. Minkowski Spacetime Signature. One of the crucial assumptions of the quasidistribution approach is that these distributions computed on the lattice with Euclidean spacetime signature are the same as their Minkowski counterparts. In particular, they should share the collinear divergences, such that the UV differences can be matched using LaMET. In [129], C. Monahan and K. Orginos considered

the Mellin moments of bare PDFs and bare quasi-PDFs in the context of smeared quasidistributions that differ from the standard ones only in the UV region, by construction (see Section 7 for more details about the smeared quasi-PDFs). They found that the Wick rotation from the bare Euclidean quasi-PDF to the light-cone PDF is simple.

However, in [130], a perturbative investigation was performed by C. Carlson and M. Freid, who discovered that there are qualitative differences between loop corrections in Euclidean and Minkowski spacetimes. In particular, it seemed that the IR divergence of the light-cone PDF is absent in the Euclidean quasi-PDF, which would be a problem at the basic root of LaMET. The complication emerged in certain diagrams, because the integration contours along real and imaginary axes of the complex loop temporal momentum plane could not be linked by smooth deformation, with physical observables being related to the integration along real k^0 and the lattice objects being extracted from integration along the imaginary k^0 axis. The Authors gave also a physical intuition justifying this finding. The IR divergence in Minkowski spacetime comes from collinear configurations of nearly on-shell quarks and gluons, with quark mass preventing exactly parallel configuration. Such a parallel situation is not possible in Euclidean spacetime and, hence, the Authors argued that no divergence can appear, invoking, thus, also mismatch of IR regions that could not be corrected for, perturbatively.

The serious doubts about the importance of spacetime signature were addressed in [131] by R. Briceño, M. Hansen, and C. Monahan. They formulated a general argument that for a certain class of matrix elements computed on the lattice, observables from the Euclidean-time dependence and from the LSZ reduction formula in Minkowski spacetime coincide. The class of (single-particle) matrix elements requires currents local in time, but not necessarily in space, and it includes the matrix elements needed to obtain quasi-PDFs. More precisely, the correlation functions depend on the spacetime signature, but matrix elements do not. The central issue was illustrated with a computation in a toy model, without the added, irrelevant from the point of view of the argument, complications of QCD. The focus was on a Feynman diagram directly analogous to the problematic one in [130]. The Authors, using the LSZ reduction formula, calculated its contribution to the quasi-PDF. They indeed found that the result depends on the contour of integration along the k^0 axis but pointed out that the contour along the imaginary axis does not coincide with what is done on the lattice. Instead, the connection can be made by computing the diagram contribution to a Euclidean correlator in a mixed time-momentum representation. At large Euclidean times, the result is dominated by a term which is exactly the same one as in the Minkowski calculation. After establishing the perturbative connection in the toy model for some specific kind of diagram, the proof was extended to all orders in perturbation theory. The Authors concluded their paper with a general statement about the proper prescription that yields the same result from Euclidean and Minkowski diagrams: the chosen contour must be an analytic deformation of the standard, Minkowski-signature definition of the diagram.

Thus, the apparent contradiction pointed out in [130] was fully resolved. As its Authors identified, the problem lied in the definition of the integration contour in the k^0 plane. However, the contour along the imaginary k^0 axis does not correspond to the perturbative contribution to Euclidean matrix elements, as shown in [131]. Even though the arguments of [130] turned out to be misplaced, they certainly discussed an interesting problem and they induced very valuable insights and a general proof in [131]. To our knowledge, the arguments were accepted by the Authors of [130] and no further arguments were given that would question the connection between Euclidean and Minkowski signatures in the context of quasidistributions.

5.2. Renormalizability of Quasi-PDFs. One of the indispensable components of the quasi-PDFs approach is the ability to match equal-time correlation functions (calculable on the lattice) to the light-cone PDFs using LaMET. For this approach to be successful, it is crucial that the quasi-PDFs can be factorized to normal PDFs to all orders in QCD perturbation theory, and this requires that quasi-PDFs can be multiplicatively renormalized [85]. However, the renormalization programme of quasi-PDFs is not straightforward due to the UV power divergences and, for quite some time, was not well understood (see Section 7 for recent progress).

One of the main concerns is whether the nonlocal operators are renormalizable. For example, the nonlocality of the operators does not guarantee that all divergences can be removed, due to the additional singularity structures compared to local operators and also the divergences with coefficients that are nonpolynomial. Due to the different UV behavior of quasi-PDFs and light-cone PDFs, the usual renormalization procedure is not ensured. Based on the work of [98], this originates from the different definition of the momentum fraction; that is $x = k^+/p^+$ (where k^+ (p^+) is plus momentum for the quark in the loop (initial quark)) for light-cone PDFs and $x = n \cdot k/n \cdot p$ (n: space-like vector) in quasi-PDFs. In addition, the momentum fraction for the light-cone PDFs is restricted to $[0, 1]$, while for the quasi-PDFs can extend to $[-\infty, +\infty]$. As a consequence of the above, the vertex correction (see diagrams in the second row of Figure 6) has different behavior. In fact, the UV divergences appear in the self-energy, while the vertex correction is UV finite. As pointed out in [132], the renormalizability of nonlocal operators has been proven up to two loops in perturbation theory by the analogy to the static heavy-light currents.

Thus, it is of utmost importance for the renormalizability to be confirmed to all orders in perturbation theory. This issue has been addressed independently by two groups [133–135], concluding that the Euclidean spacelike correlation functions leading to the quasi-PDFs are indeed renormalizable. These are based on two different approaches: the auxiliary heavy quark method [133, 135–137] and the diagrammatic expansion method [134, 138], employed for both quark and gluon quasi-PDFs. Below we highlight their main findings.

5.2.1. Renormalizability of Quark Quasi-PDFs. X. Ji and J.-H. Zhang in one of their early works [133] have studied

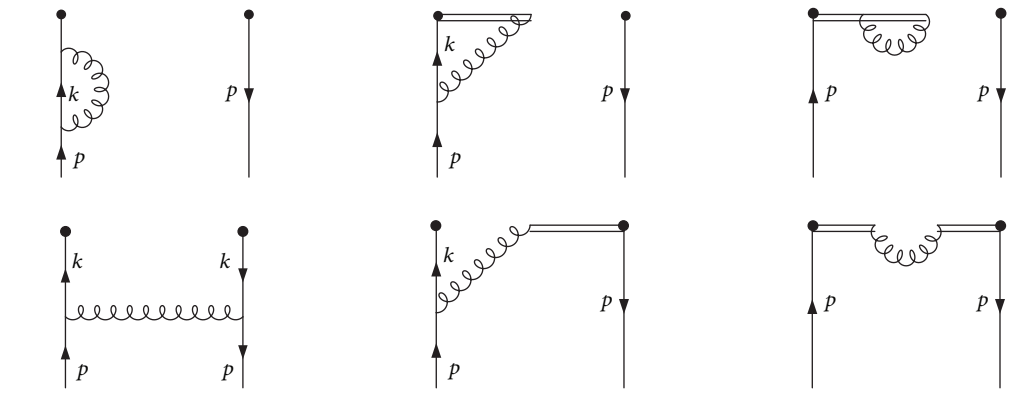

Figure 6: One-loop diagrams entering the quasiquark PDFs in Feynman gauge. Self-energy diagrams are shown in the first row and vertex correction diagrams in the second row. Source: [133], reprinted with permission by the Authors and the American Physical Society.

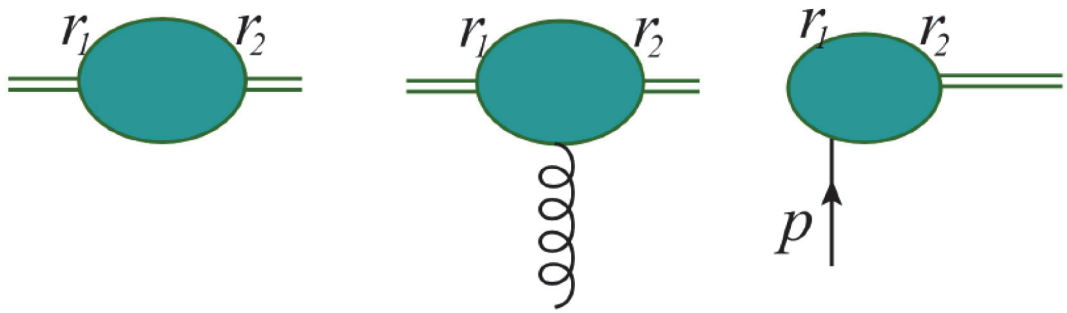

Figure 7: Topologies that may lead to UV divergent contributions to the quark quasi-PDFs. Source: [134], reprinted with permission by the Authors and the American Physical Society.

renormalization of the unpolarized nonsinglet distribution. They performed an analytic calculation in the Feynman gauge to one-loop level using dimensional regularization (DR) to extract the full contributions of the diagrams entering the calculation, as shown in Figure 6. This includes the self-energy diagrams (top row) and the vertex correction diagrams (bottom row). We point out that the self-energy diagrams require integration over all components of the loop momentum, while the vertex correction diagrams have the component of the loop momentum that is parallel to the Wilson line unintegrated. This has implications on the discussion about renormalizability. This work exhibits how in this gauge all UV divergences in the vertex correction do not alter the renormalization of the quasi-PDFs, as they are removed by counterterms for subdiagrams from the interaction. Based on this, the renormalization of the quark quasidistribution reduces to the renormalization of two quark fields in the axial gauge. This study was also extended to two loop corrections, assuming one-to-one correspondence between the two-loop diagrams, as well as equivalence between the UV divergences of the two-loop self-energy in the quasiquark PDFs and of the two-loop corrections of the heavy-light quark current. Thus, multiplicative renormalizability was proven to hold up to two loops in perturbation theory. The arguments presented in this work can be generalized to include helicity and transversity PDFs.

The renormalizability of quasi-PDFs to all orders in perturbation theory has been proven for the first time by T. Ishikawa et al. in [134]. They performed the complete one-loop calculation of the quasi-PDFs in coordinate space and in the Feynman gauge, which is convenient because the renormalization of the QCD Lagrangian is known in this gauge. The one-loop calculation shows explicitly the renormalizability (to that order) of the quasi-PDFs.

More interestingly, the Authors have studied all sources of UV divergences for the nonlocal operators that enter the quasi-PDFs calculation using a primitive basis of diagrams (see Figures 3-6 in [134]). These diagrams were used to construct all possible higher-order Feynman diagrams that are presented schematically in Figure 7, and the Authors explained in great detail the proof of both power-law and logarithmic divergences being renormalized multiplicatively to all orders. This can be summarized in the calculation of the diagrams shown in Figure 7.

Diagrams of the topology shown in Figure 7(a) can be reordered in terms of one-particle-irreducible (1PI) diagrams and, therefore, one can derive all corresponding linear UV power divergences explicitly into an exponential. The latter

may be removed by a mass renormalization of a test particle moving along the gauge link [139]. In addition, these diagrams have logarithmic UV divergences that can be removed by a "wave function" renormalization of the test particle [140]. The second type of diagrams (Figure 7(b)) has only logarithmic UV divergences, which can be absorbed by the coupling constant renormalization of QCD [140]. The last type of UV divergent diagrams is shown in Figure 7(c) that differs from types (a) and (b), because the loop momentum goes through an external quark, leading to divergences from higher-order loop corrections to the quark-gauge-link vertex. It was concluded that the UV divergent term of diagrams (c) is proportional to the tree level of the operator, and, therefore, a constant counterterm is sufficient to remove it. All the above constitute a concrete proof that all remaining perturbative UV divergences of the quark quasi-PDFs can be removed by introducing multiplicative renormalization factors. Exact calculations to one-loop level show that quasi-PDFs of different types do not mix under renormalization, which completes the proof of the renormalizability in coordinate space [134].

The study of the renormalizability of quark quasi-PDFs has been complemented with the work of Ji et al. in [135], in which the auxiliary heavy quark field formalism was employed. The approach shows renormalizability to all orders in perturbation theory and was confirmed in both the dimensional and the lattice regularizations, the latter for the first time. As in other studies, the focus was on the unpolarized PDFs and it was shown explicitly that the procedure mimics the renormalization of two heavy-light quark currents; the latter is valid to all orders in perturbation theory. We note that the conclusions hold for all types of PDFs and can be confirmed following the same procedure as the unpolarized one.

The introduction of a heavy quark auxiliary field, Q, modifies the QCD Lagrangian by including an additional term. This allows us to replace the nonlocal straight Wilson line operator by a composite operator, which is the product of two auxiliary heavy quark fields

$$O(x,y) = \overline{\psi}(x)\,\Gamma Q(x)\,\overline{Q}(y)\,\psi(y). \tag{30}$$

Thus, the question of the renormalizability of the nonlocal operator can be addressed based on the renormalization of the above operator in the extended QCD theory. This has been demonstrated in DR and we urge the interested Reader to see the proof in [135]. Here we discuss the case of the lattice regulator which is particularly interesting for the numerical simulations in Lattice QCD. Unlike the case of DR, in lattice regularization (LR) the self-energy of the auxiliary quark introduces a divergence beyond leading order in perturbation theory. This may be absorbed as an effective mass counterterm, that is [141]

$$\delta\mathscr{L}_m = -\frac{\delta}{a} m\overline{Q}Q. \tag{31}$$

Using the above, and for spacelike correlators, the linear divergence of Equation (31) can be factorized in the renormalized operator

$$O_R = Z_{\overline{j}}^{-1} Z_j^{-1} e^{\delta\overline{m}|z_2-z_1|}\overline{\psi}(z_2)\,\Gamma L(z_2,z_1)\,\psi(z_1), \tag{32}$$

where the remaining divergence is at most logarithmic and can be canceled to all orders in perturbation theory.

5.2.2. Renormalizability of Gluon Quasi-PDFs. For completeness, we also address the renormalizability of the gluon quasi-PDFs, which are more complicated to study compared to nonsinglet quark PDFs due to the presence of mixing. Their renormalizability was implied using arguments based on the quark quasi-PDFs [134, 135], but more recently there are direct studies for the renormalization of gluon quasi-PDFs [136–138].

The first investigation appeared in 2017 by W. Wang and S. Zhao [136], using the auxiliary field approach to study the renormalization of gluon nonlocal operators, and, in particular, the power divergences. The mixing under renormalization was also addressed. This follows their work on the matching between the quasi- and the normal gluon PDFs [142], as described in Section 8.2. The light-cone gluon PDFs are nonlocal matrix elements of the form

$$f_{g/H}(x,\mu) = \int \frac{d\xi^-}{2\pi x P^+} e^{-i\xi^- xP^+} \langle P|\, F^+{}_i(\xi^- n_+) \cdot W\left(\xi^- n_+, 0; L_{n_+}\right) F^{i+}(0)\,|P\rangle, \tag{33}$$

where F is the field strength tensor. Based on this, gluon quasidistribution can be defined by nonlocal spacelike matrix element

$$\widetilde{f}_{g/H}(x,\mu) = \int \frac{dz}{2\pi x P^3} e^{izxP^3} \langle P|\, F^3{}_\mu(zn_3) \cdot W\left(zn_3, 0; L_{n_3}\right) F^{\mu 3}(0)\,|P\rangle, \quad \mu = 0,1,2, \tag{34}$$

in which the sum over μ is in all directions except the direction of the Wilson line. This definition is slightly modified from the definition used in [45, 86, 142], where the sum is over the transverse directions. Despite this modification, Equation (34) is still a proper definition of a gluon quasi-PDF, as demonstrated in [136] based on the energy-momentum tensor decomposition. This is also confirmed numerically, as the one-loop matching to the light-cone PDFs coincides for the two definitions.

Reference [136] presented the complete one-loop calculation for the gluon operator of Equation (34), introducing a UV cutoff Λ on the transverse momentum. The calculation was performed in Feynman gauge and in the adjoint representation. The relevant one-loop diagrams can be separated into two categories: (1) diagrams in which the vertex from the operator does not include gluons from the Wilson line (shown in Figure 8) and diagrams that have at least one gluon from the Wilson line in the vertex of the operator, as shown in Figure 9. This calculation identified all divergences including the linear divergence, and, unlike the case of the quark quasi-PDFs, the Wilson line self-energy (right diagram of Figure 9) is not the only source of linear divergence in the gluon distributions. As a consequence, it is not possible to absorb all linear divergences in the renormalization of the Wilson line, but a more complicated renormalization is needed. However, as argued in [137], this is due to the choice of a nongauge invariant regulator.

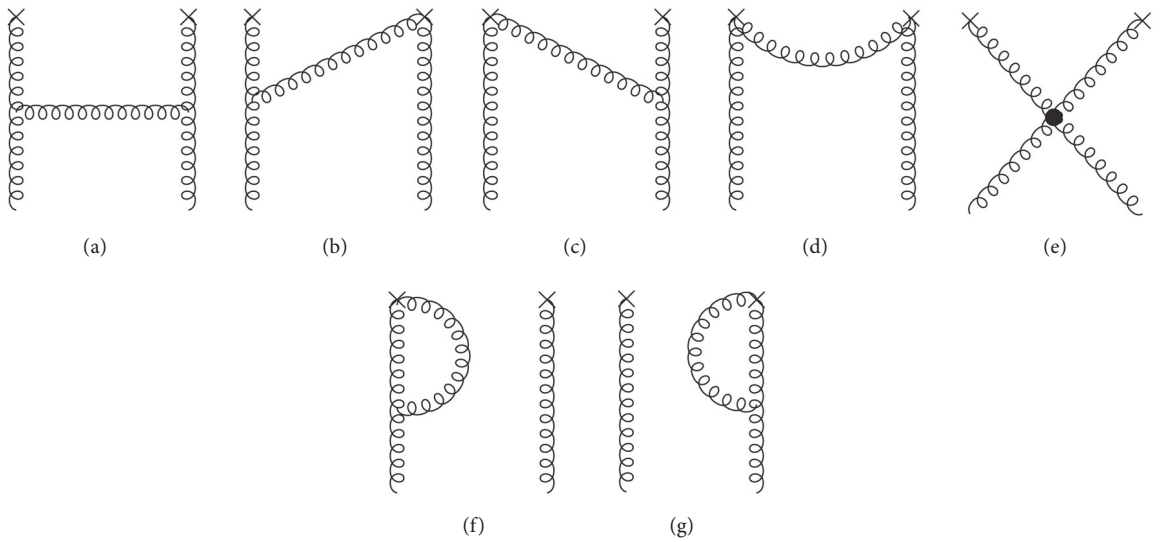

Figure 8: One-loop corrections to a gluon quasidistribution, without the Wilson line. The symbol "×" denotes the nonlocal vertex from the operator. Source: [136], reprinted with permission by the Authors (article published under an open access license).

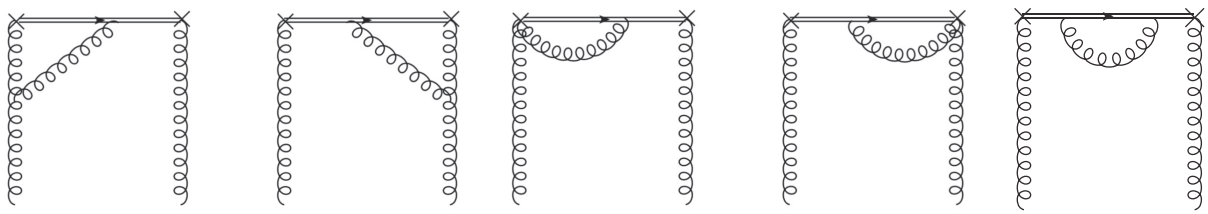

Figure 9: One-loop corrections to a gluon quasidistribution, which involve the Wilson line (double line). The symbol "×" denotes the nonlocal vertex from the operator. Source: [136], reprinted with permission by the Authors (article published under an open access license).

One approach to study the renormalization of the quasigluon PDFs is to introduce an auxiliary heavy quark field, as adopted in the renormalization of the quark distributions. This auxiliary field is in the adjoint representation of $SU(3)$ and does not have spin degrees of freedom. Therefore, this approach allows one to study local operators instead of the nonlocal operator of Equation (34). Mixing between these new operators and the gauge invariant gluon field strength tensor is permitted. In addition, it was shown at the level of one-loop corrections that the power divergence can be absorbed in the matrix elements of the local operators, which is expected to hold to all orders in perturbation theory. This work by W. Wang and S. Zhao has contributed to understanding the renormalization of the gluon quasi-PDFs, but there were a number of issues to be addressed. This included, but was not limited to, (a) the study of gauge fields in the fundamental representation and the corresponding mixing and (b) the study of the renormalization in the lattice regularization, preferably nonperturbatively. The latter is highly nontrivial and technically more complicated than in the case of quarks.

The renormalizability of both the unpolarized and the helicity gluon PDFs has been studied by J.-H. Zhang et al. in [137], including possible mixing that is permitted by the symmetries of the theory. The auxiliary field formalism was employed in a similar fashion as the studies presented above [133, 135–137]. Explicit results were given for the unpolarized quasigluon PDFs in the dimensional and gauge-invariant cutoff regularizations.

In the auxiliary field formalism, the operator presented in Equation (34) (μ summed over the transverse directions) can be replaced by a new operator; that is,

$$\mathcal{O}\left(z_2, z_1\right) = J_1^{3\mu}\left(z_2\right)\overline{J}_{1,\mu}^{3}\left(z_1\right), \tag{35}$$

where $J_1^{3\mu}(z_2) = F_a^{3\mu}(z_2)\mathcal{Q}_a(z_2)$, $\overline{J}_{1,\mu}^{3}(z_1) = \overline{\mathcal{Q}}_b(z_1)F_{b,\mu}^{3}(z_1)$. $\mathcal{Q}$ denotes the auxiliary adjoint "heavy quark" field. For a proof, see [137]. Based on symmetry properties, such a composite operator can mix with lower-dimensional operators that are gauge-invariant, BRST variations or vanish by the equations of motion. The identified mixing pattern helps to construct the proper operators for the gluon quasi-PDFs that are multiplicatively renormalizable. In particular, three (four) operators are identified for the unpolarized (helicity) gluon PDFs, that do not suffer from mixing. Here we provide the operators for the unpolarized case:

$$\mathcal{O}^1\left(z_2, z_1\right) \equiv J_1^{0i}\left(z_2\right)\overline{J}_1^{0i}\left(z_1\right), \tag{36}$$

$$\mathcal{O}^2(z_2, z_1) \equiv J_1^{3i} \overline{J}_1^{3i}, \tag{37}$$

$$\mathcal{O}^3(z_2, z_1) \equiv J_1^{0i}(z_2) \overline{J}_1^{3i}, \tag{38}$$

$$\mathcal{O}^4(z_2, z_1) \equiv J_1^{3\mu}(z_2) \overline{J}_{1,\mu}^{3}, \tag{39}$$

where the index 0 represents the temporal direction and 3 the direction of the Wilson line. In addition, i runs over all Lorentz components, while μ over the transverse components only ($\mu \neq 3$). In a similar way, it was found that three operators related to the gluon helicity distributions can be renormalized multiplicatively. For details, see Section III C of [137]. This work provides crucial guidance for numerical simulations in Lattice QCD and the development of a nonperturbative renormalization prescription. Based on the mixing pattern, the Authors provided a renormalization prescription suitable for lattice simulations, and a factorization for gluon and quark quasi-PDFs.

Z.-Y. Li, Y.-Q. Ma, and J.-W. Qiu have studied renormalizability of gluon quasi-PDFs in [138], a work that appeared simultaneously with [137]. Their work is based on diagrammatic expansion approach, as studied for the quark quasi-PDFs [134, 138]. By studying the UV divergence of gluon operators, it was demonstrated that appropriate combinations can be constructed, so that their renormalization is multiplicative to all orders in perturbation theory. Such operators are related to gluon quasi-PDFs. The demonstration is based on a quasigluon operator $\mathcal{O}_g$ that has a general form

$$\mathcal{O}_g^{\mu\nu\rho\sigma}(\xi) = F^{\mu\nu}(\xi)\, \Phi^{(a)}(\xi, 0)\, F^{\rho\sigma}(0), \tag{40}$$

where $\Phi^{(a)}(\xi, 0)$ is the Wilson line with gauge links in the adjoint representation.

The procedure followed in this work is based on a one-loop calculation of the Green's functions

$$\left\langle g(p) \right| \mathcal{O}_g^{\mu\nu\rho\sigma}(\xi) \left| g(p) \right\rangle, \tag{41}$$

which is performed in DR. It was demonstrated that the linear UV divergences of the gluon-gauge-link vertex are canceled explicitly. This was extended to all loops in perturbation theory by investigating all possible UV divergent topologies of higher-order diagrams, showing that the corresponding linear UV divergences are canceled to all orders in perturbation theory. It was also discussed in detail that the UV divergences of all 36 pure quasigluon operators (including the antisymmetry of gluon field strength) can be multiplicatively renormalized. This work, thus, constitutes a powerful proof of the renormalizability of gluon quasi-PDFs.

6. Lattice Techniques and Challenges for Quasi-PDFs

Apart from theoretical challenges of the quasidistribution approach, discussed in the previous section, also the lattice implementation and efficiency of computations are a major issue for the feasibility of the whole programme. In this section, we discuss these aspects in some detail, showing that tremendous progress has been achieved also on this side. In addition, we discuss challenges for the lattice that need to be overcome for a fully reliable extraction of PDFs.

6.1. Lattice Computation of Matrix Elements. To access quasi-PDFs of the quarks in the nucleon, one needs to compute the following matrix elements:

$$h_\Gamma(P, z) = \langle P | \overline{\psi}(0, z)\, \Gamma W(z)\, \psi(0, 0) | P \rangle, \tag{42}$$

where the Dirac structure Γ determines the type of quasi-PDF (see below), $|P\rangle$ is the boosted nucleon state with momentum $P = (P_0, 0, 0, P_3)$, and $W(z)$ is a Wilson line of length z along the spatial direction of the boost. To obtain the above matrix elements, one constructs a ratio of three-point and two-point functions:

$$h_\Gamma(P, z)^{0 \ll \tau \ll t} \mathcal{K}\left(\overrightarrow{P}\right) \frac{C^{3\text{pt}}\left(\overrightarrow{P}; t, \tau\right)}{C^{2\text{pt}}\left(\overrightarrow{P}; t\right)}, \tag{43}$$

where $\mathcal{K}(\overrightarrow{P})$ is a kinematic factor that depends on the Dirac structure, and the correlation functions are computed according to

$$C^{2\text{pt}}\left(\overrightarrow{P}; t\right) = \Gamma_{\alpha\beta} \sum_{\overrightarrow{x}} e^{-i\overrightarrow{P}\cdot\overrightarrow{x}} \langle 0 | N_\alpha\left(\overrightarrow{x}, t\right) \overline{N}_\beta\left(\overrightarrow{0}, 0\right) \cdot |0\rangle, \tag{44}$$

$$C^{3\text{pt}}\left(\overrightarrow{P}; t, \tau\right) = \Gamma'_{\alpha\beta} \sum_{\overrightarrow{x}, \overrightarrow{y}} e^{-i\overrightarrow{P}\cdot\overrightarrow{x}} \langle 0 | N_\alpha\left(\overrightarrow{x}, t\right) \cdot \mathcal{O}\left(\overrightarrow{y}, \tau; z\right) \overline{N}_\beta\left(\overrightarrow{0}, 0\right) |0\rangle, \tag{45}$$

with the proton interpolating operator, $N_\alpha(x) = \epsilon^{abc} u_\alpha^a(x)((d^b)^T(x)\mathcal{C}\gamma_5 u^c(x))$, τ the current insertion time, parity plus projector for the two-point function, $\Gamma_{\alpha\beta} = (1 + \gamma_0)/2$, and parity projector for the three-point functions, $\Gamma'_{\alpha\beta}$, dependent on the Dirac structure of the current.

The Wick contractions for the three-point function lead, in general, to a quark-connected and a quark-disconnected diagram. Since the evaluation of the latter is far more demanding than that of the former, the numerical efforts were so far restricted to connected diagrams only. One uses the fact that disconnected diagrams cancel when considering the flavor nonsinglet combination $u - d$ in the formulation of Lattice QCD with degenerate light quarks. The connected diagram that contributes to the three-point function is shown in Figure 10.

Special attention has to be paid to the Dirac structure of the insertion operator, because mixing appears among certain structures, as discovered in [106]. In particular, the originally suggested $\Gamma = \gamma_3$ for the unpolarized PDF mixes with the scalar operator; see Section 7 for details. Such mixing can be taken into account by explicitly computing a 2×2 mixing matrix of renormalization functions and matrix elements for

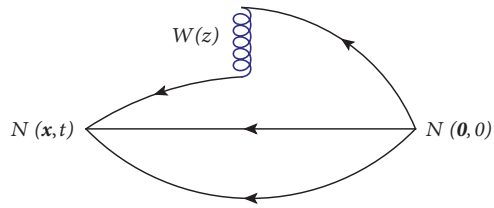

Figure 10: Diagram representing the three-point correlation function that needs to be evaluated to calculate quasi-PDFs. Source: arXiv version of [124], reprinted with permission by the Authors (article published under the terms of the Creative Commons Attribution 4.0 International license).

both Dirac structures. However, in practice, this leads to much worse signal and finally to a much less precise estimate of the PDFs. For this reason, the strongly preferred choice is $\Gamma = \gamma_0$ for the unpolarized quasi-PDF. Similar mixing occurs for the polarized cases for certain Dirac structures, with the choice of $\Gamma = \gamma_5\gamma_3$ and $\Gamma = \sigma_{13}$ or $\Gamma = \sigma_{23}$ for helicity and transversity, respectively, guaranteeing that no mixing is present [106].

We now turn to describing the lattice computation in more detail. For the two-point function, Wick contractions lead to standard point-to-all propagators that can be obtained from inversions of the Dirac operator matrix on a point source. The computation of the three-point function is more complicated. Apart from the point-to-all propagator, it requires the knowledge of the all-to-all propagator. Two main techniques exist to evaluate this object: the sequential method [143] and the stochastic method [144]. In the former, one constructs a so-called sequential source from a suitable point-to-all propagator. Inverting the Dirac matrix on this source, the sequential propagator is obtained that enters in the three-point function. The other method employs stochastic Z^4 noise sources on a single time slice, leading to a stochastic estimate of the all-to-all propagator upon inversion of the Dirac matrix. In principle, the second method is more flexible, as it allows for obtaining results for all Dirac structures and all momenta with the same inversions, the most costly part of the computation. The price to pay is the introduction of stochastic noise, but the overhead introduced by the necessity to suppress this noise is still more than compensated by the gain from flexibility, in principle. Using the sequential method or, more precisely, its fixed sink variant, implies that the momentum at the sink has to be fixed and separate inversions are needed for each nucleon boost, as well as for each Dirac structure due to different projectors.

In the early studies, both approaches were tested by ETMC [47], with the conclusion that they yield compatible results and the additional noise from the stochastic method can be suppressed by using 3-5 stochastic noise vectors. Given the flexibility of the stochastic method, ETMC decided to pursue studies with this approach in [100, 108]. In [108], the technique was changed to one involving the sequential propagator for reasons explained in the next subsection. The method for computing the all-to-all propagator was not revealed by the Authors of the other exploratory numerical study of quasi-PDFs in [46, 107].

Having computed the three-point and two-point functions, the relevant matrix elements can be obtained. The crucial issue that has to be paid special attention to is the contamination of the desired ground state matrix elements by excited states. Three major techniques are available: single-state (plateau), multistate, and summation fits. We briefly describe all of them below.

(i) *Plateau method*. The most straightforward way of obtaining the matrix element from the three-point and two-point functions is to identify a region where their ratio is independent of the insertion time τ and fitting to a constant, which is the matrix element of the ground state. As can be seen from the spectral decomposition of the three-point function, excited states manifest themselves as curvature in the ratio of Equation (88) and also in the shift of its central value. Under realistic statistical uncertainties, it is, therefore, not always clear whether an actual plateau has been reached and, thus, it is not advisable to use this method as the sole method of extracting the ground state properties.

(ii) *Summation method*. This approach [145, 146] consists in summing the ratios of three-point and two-point functions over the insertion time τ. By decomposing the correlators into sums of exponential terms, one obtains a geometric series, leading finally to

$$\mathscr{R}\left(\vec{P};t_s\right) \equiv \sum_{\tau=a}^{t_s-a} \frac{C^{3\mathrm{pt}}\left(\vec{P};t_s,\tau\right)}{C^{2\mathrm{pt}}\left(\vec{P};t_s\right)} = C + h_\Gamma\left(P,z\right)t_s + \mathcal{O}\left(e^{-(E_1-E_0)t_s}\right), \tag{46}$$

where the source and sink timeslices are excluded avoiding contact terms and C is a constant. The ground state matrix element, $h_\Gamma(P,z)$, is then extracted from a linear two-parameter fit to data at sufficiently large source-sink separations t_s. The method has the advantage that excited states are suppressed by a faster-decaying exponential with respect to the plateau fits, but the statistical uncertainties are, typically, much larger.

(iii) *Multistate fits*. A natural generalization of the plateau method is to include higher-order exponential terms in the decomposition of the two-point and three-point functions, typically the first excited state (two-state fits) or the lowest two excited states (three-state fits). In general, the two-point correlator can be written as

$$C^{2\mathrm{pt}}\left(\vec{P};t\right) = \left|A_0\right|^2 e^{-E_0 t} + \left|A_1\right|^2 e^{-E_1 t} + \cdots, \tag{47}$$

with amplitudes A_i and energies of subsequent states E_i. The three-point function reads

$$\begin{aligned} C^{3\mathrm{pt}}\left(\vec{P}; t_s, \tau\right) = {} & \left|A_0\right|^2 \langle 0|\, \mathcal{O}\, |0\rangle\, e^{-E_0 t_s} \\ & + A_0^* A_1 \langle 1|\, \mathcal{O}\, |0\rangle\, e^{-E_1 \tau} e^{-E_0 (t_s - \tau)} \\ & + A_0 A_1^* \langle 0|\, \mathcal{O}\, |1\rangle\, e^{-E_0 \tau} e^{-E_1 (t_s - \tau)} \\ & + \left|A_1\right|^2 \langle 1|\, \mathcal{O}\, |1\rangle\, e^{-E_1 t_s} + \cdots, \end{aligned} \tag{48}$$

with matrix elements of the suitable operator $\mathcal{O}$ in addition to parameters in the two-point correlator. Note that, in practice, it is difficult to consistently go beyond one or two excited states, as the number of fitting parameters is increasing faster than linearly with increased number of excited states taken into account, due to the presence of the mixed matrix elements, $\langle i|\mathcal{O}|j\rangle$, for a growing number of pairs (i, j).

In principle, the multistate method (realistically *two*-state method) allows for a better control of excited states contamination. However, in realistic lattice situations, the interpolating operators used to create the nucleon from the vacuum excite numerous states with the same quantum numbers. This contamination increases with pion mass decreasing towards the physical point; see, e.g., [39], for an illustration. Moreover, the number of excited states increases with larger nucleon boosts. All the above imply that it is unlikely to achieve a regime of source-sink separations where precisely two states play a role. Thus, also relying solely on two-state fits should not be used as the only method. Instead, ground state dominance should be established by aiming at compatibility between all three methods of extracting the ground state matrix elements. Such compatibility ensures that the probed regime of t_s values has enough suppression of excited states and excludes that many excited states mimic a single excited state. Numerically, it is hard to disentangle several excited states and the manifestation of many of them appearing would be clear incompatibility of two-state fits with plateau fits. Note also that, with exponentially decaying signal-to-noise ratio at larger source-sink separations, the danger of the two-state approach is that the fits may easily be dominated by data at the lower t_s values, heavily contaminated by excited states. Thus, we are led to conclude that the most reliable estimates of ground state matrix elements ensue from compatible results obtained using all of the three above methods (with the summation method being, in most cases, inconclusive due to large statistical uncertainty). It is still important to bear in mind that excited states are never fully eliminated, but only exponentially suppressed. This means that the ground state dominance is always established only to some level of precision. Aiming at increased statistical precision, the previously reliable source-sink separation(s) may prove to be insufficient. Obviously, when targeting larger momenta and/or smaller pion masses, conclusions for the role of excited states at a smaller boost or a larger pion mass do not apply; hence, a careful analysis is always needed at least in the setup most prone to excited states.

Having extracted the relevant matrix elements, one is finally ready to calculate the quasi-PDF. We rewrite here the definition of quasi-PDFs with a discretized form of the Fourier transform:

$$\tilde{q}\left(x, P_3\right) = \frac{2P_3}{4\pi} \sum_{z=-z_{\max}}^{z_{\max}} e^{-izP_3 x} h_\Gamma\left(P, z\right), \tag{49}$$

where the factor of P_3 ensures correct normalization for different momenta and $z_{\max}$ is to be chosen such that the matrix elements have decayed to zero both in the real and in the imaginary part (see also Section 6.3).

6.2. Optimization of the Lattice Computation. In the previous subsection, we have established the framework for the computation of quasi-PDF matrix elements on the lattice. Now, we describe some more techniques that are usually used to perform the calculation as effectively as possible.

The first technique, commonly employed in lattice hadron structure computations, serves the purpose of optimizing the overlap of the interpolating operator that creates and annihilates the nucleon with the ground state. This can be achieved by employing Gaussian smearing [147, 148] of fermionic fields, which reflects the fact that hadrons are not point-like, but are extended objects. Moreover, the smearing is further optimized by combining it with a technique for reducing short-range (UV) fluctuations of the gauge fields; gauge links used in the quark fields smearing are subjected to APE smearing [149]. The procedure involves optimizing four parameters, the parameters regulating the "strength" of the Gaussian and APE smearing, α_G and α_{APE}, respectively, and the number of Gaussian and APE smearing iterations. The typical criterion of optimization is that the root mean square (rms) radius of the proton should be around 0.5 fm.

Smearing techniques are used also to decrease UV fluctuations in gauge links entering the Wilson line in the operator insertion. In principle, any kind of smearing can be used for this purpose, with practical choices employed so far of HYP smearing [101] and stout smearing [150]. The smearing of the Wilson line has the additional effect of reducing the UV power divergence related to the Wilson line, i.e., shifting the values of renormalization factors towards their tree-level values, and thus suppressing the power-like divergence. Thus, a relatively large number of smearing iterations was used in the early works, which was necessary due to the absence of the renormalization. In principle, the renormalized matrix elements should not depend on the amount of smearing applied to the operator and it is an important consistency check to confirm this. We note that, before the advent of the full nonperturbative renormalization programme for quasi-PDFs [151], the role played by the Wilson line links smearing was somewhat different. Without explicit renormalization, the results were contaminated by the power divergence and the smearing had the task of subtracting a possibly large part of this divergence in the hope of obtaining preliminary results at not too small lattice spacings. After this premise lost its significance, this kind of smearing is applied only to reduce gauge noise to a certain extent. Alternatively, smearing of gauge links can also be applied to the whole gauge field, i.e.,

enter both the Wilson line and also the Dirac operator matrix. Note, however, that in this way it is not possible to check explicitly that the renormalized results are independent of the smearing level, at least without costly additional Dirac matrix inversions for different numbers of smearing iterations.

All the above techniques are rather standard and have been employed in the quasi-PDFs computations already in the very first exploratory studies. However, the recent progress that we review in Section 9 would not have been possible without the technique of so-called momentum smearing [109, 152]. It is a relatively simple extension of the quark fields smearing described above. The crucial observation is that a Gaussian-smeared nucleon state has maximal overlap with a nucleon at rest; i.e., it is centered around zero momentum in momentum space. It is, hence, enough to move this center to the desired momentum to obtain an improved signal for a boosted nucleon. The modification is the addition of a phase factor $\exp(i\xi \vec{P} \cdot \vec{x})$ in the position space definition of the smearing, where $\vec{P}$ is the desired nucleon momentum and ξ a tunable parameter[8]. Explicitly, the modified Gaussian momentum smearing function reads

$$\mathcal{S}_{\text{mom}} = \frac{1}{1+6\alpha_G}\left(\psi(x) + \alpha_G \sum_j U_j(x)\, e^{i\xi \vec{P}\cdot\vec{j}}\, \psi\left(x+\hat{j}\right)\right), \quad (50)$$

where U_j are gauge links in the j-direction. For optimal results, the parameter ξ should be tuned separately for every momentum and every ensemble. In the context of quasi-PDFs, momentum smearing has first been applied in the ETMC study reported in Section 3.2 [108, 153]. By now, it has become a standard technique for enhancing the signal. We note, however, that momentum smearing does not fully solve the exponentially hard problem of decaying signal at large boosts, but rather it moves it towards larger momenta. Therefore, accessing highly boosted nucleon on the lattice, necessary for reliable matching to light-cone PDFs via LaMET, remains a challenge.

To finalize this subsection, we mention one more useful technique that is applied nowadays to decrease statistical uncertainties at fixed computing time. The most expensive part of the calculation of the correlation functions is the computation of the quark propagators, i.e., the inversion of the Dirac operator matrix on specified sources. This is typically done using specialized iterative algorithms, often tailored to the used fermion discretization. The iterative algorithm is run until the residual, quantifying the distance of the current solution with respect to the true solution, falls below some tolerance level, r. The standard way is to set r to a very small number, of order $10^{-12} - 10^{-8}$. However, obviously that may need iterating the solver for a long time. To save some considerable fraction of computing time, truncated solver methods have been invented, where the precision is relaxed to $r \approx 10^{-3} - 10^{-2}$. Naturally, relaxed precision of the solver leads, in general, to a bias introduced in the solution. Hence, the second ingredient of these methods is bias correction. Below, we shortly describe one of such methods, the Covariant Approximation Averaging (CAA) [154]. One performs a certain number of low-precision (LP) inversions, N_{LP}, accompanied by a smaller number of standard, high-precision (HP) inversions, N_{HP}. The final correlation functions are defined as follows:

$$C = \frac{1}{N_{\text{LP}}}\sum_{n=1}^{N_{\text{LP}}} C_{n,\text{LP}} + \frac{1}{N_{\text{HP}}}\sum_{n=1}^{N_{\text{HP}}}\left(C_{n,\text{HP}} - C_{n,\text{LP}}\right), \quad (51)$$

where $C_{n,\text{LP}}$ and $C_{n,\text{HP}}$ denote correlation functions obtained from LP and HP inversions, respectively. To correct the bias properly, N_{HP} HP and LP inversions have to be done for the same source positions. The choice of the numbers of LP and HP inversions has to be tuned in such a way to maintain a large correlation coefficient (typically 0.99-0.999) between LP and HP correlators, which guarantees that the bias is properly subtracted.

6.3. Lattice Challenges. In this section, we discuss the challenges for lattice computations of quasi-PDFs. On the one side, this includes "standard" lattice challenges, like control over different kinds of systematic effects, some of them enhanced by the specifics of the involved observables. On the other side, the calculation of quasi-PDFs offered new challenges that had to or have to be overcome for the final reliable extraction of light-cone distributions. Below, we discuss these issues in considerable detail, starting with the "standard" ones and going towards more specific ones.

(1) *Discretization effects.*

Lattice simulations are, necessarily, performed at finite lattice spacings. Nevertheless, the goal is to extract properties or observables of continuum QCD. At finite lattice spacing, these are contaminated by discretization (cutoff) effects, which need to be subtracted in a suitable continuum limit extrapolation. Obviously, prior to taking the continuum limit, the observables need to be renormalized and we discuss this issue in Section 7. Assuming divergences have been removed in a chosen renormalization scheme, the continuum limit can be taken by simulating at three or more lattice spacings and fitting the data to an appropriate ansatz, typically linear in the leading discretization effects, of order a or a^2. In most Lattice QCD applications, $\mathcal{O}(a)$-improved fermionic discretizations or observables are used. In many cases this, however, requires calculation of observable-specific improvement coefficients (e.g., for Wilson-clover fermions). It remains to be shown how to obtain $\mathcal{O}(a)$ improvement of quasi-PDFs at least for some of the fermionic discretizations. Up to date, quasi-PDFs studies have been performed for a single lattice spacing in a given setup and, hence, discretization effects have not been reliably estimated. Going to smaller lattice spacings remains a challenge for the future. It is not a problem in principle, but obviously it requires huge computational resources, especially at the physical pion mass. However, there are indirect premises that discretization effects are not

large. Firstly, they have been relatively small in general lattice hadron structure calculations. Secondly, indirect evidence for the smallness of cutoff effects is provided by checks of the dispersion relation, i.e., the relation between energy of a boosted nucleon and its momentum (see Section 9). In the absence of large discretization effects, the continuum relativistic dispersion relation holds. Note, however, that cutoff effects can be enhanced if the nucleon boost becomes larger than the lattice UV cutoff; i.e., if $aP_3 > 1$. In principle, no energy scale on the lattice should exceed a^{-1}. Precisely for this reason, lattice calculations involving the heavy b quark need its special treatment; with typical lattice spacings, the bottom quark mass exceeds a^{-1} and a reliable computation must involve an effective theory treatment, such as the one provided by HQET or by NRQCD.

(2) *Finite volume effects*.

Apart from finite lattice spacing, also the volume of a numerical simulation is necessarily finite. Thus, another lattice systematic uncertainty may stem from finite volume effects (FVE). FVE become important if the hadron size becomes significant in comparison with the box size. The hadron size is to a large extent dictated by the inverse mass of the lightest particle in the theory. Hence, leading-order FVE are related to the pion mass of the simulation and smaller pion masses require larger lattice sizes in physical units to suppress FVE. Usually, FVE are exponentially suppressed as $\exp(-M_\pi L)$, where L is the spatial extent of the lattice. The typical rule adopted in lattice simulations is that this suppression is enough if $M_\pi L \geq 4$. At nonphysical pion masses of order 300-400 MeV, this corresponds to a box size of 2-2.5 fm, which is easy to reach with typically used lattice spacings, 0.05-0.1 fm. When simulating at the physical pion mass, the minimal box size that yields $M_\pi L \geq 4$ is 6 fm and, thus, finer lattice spacings require huge lattices. Nevertheless, lattice hadron structure calculations have usually evinced rather small FVE already with $M_\pi L \approx 3 - 3.5$. Still, an explicit check of FVE is highly advisable when aiming at a fully reliable computation.

Above, the main source of FVE that we considered was related to the size of hadrons. However, it was pointed out in [155] that, for quasi-PDFs, a relevant source of FVE may be the size of the Wilson line in the operator inserted in the matrix elements defining quasidistributions. The Authors studied perturbatively a toy scalar model with a light degree of freedom (mimicking the pion in QCD) and a heavy one (corresponding to the nucleon). The studied matrix element involved a product of two currents displaced by a vector of length ξ and they found two kinds of FVE: one decaying with $\exp(-M_\pi L)$ and the other one with $\exp(-M(L-\xi))$, where M is the mass of the heavy state. Moreover, both exponentials have prefactors scaling as $L^m/|L-\xi|^n$ (with some exponents m and n), that can further enhance FVE for larger displacements ξ. In the case of pion matrix elements, the FVE may be particularly enhanced by $\exp(-M_\pi(L-\xi))$. Even though the studied case concerned a product of two currents, not quark fields connected by a Wilson line, some enhancement of FVE may also occur for the latter case. In view of this, investigation of FVE in matrix elements for quasi-PDFs, especially ones with larger lengths of the Wilson line, is well motivated.

It is also important to mention that finite lattice extent in the direction of the boost, L/a, imposes a limit on the minimal Bjorken-x that can be reached. The parton momentum is xP_3, which determines its correlation length to be of order $1/xP_3$. This value should be smaller than the physical size of the boost direction, $1/xP_3 < L$. At the same time, the boost should be smaller than the lattice UV cutoff; i.e., $P_3 < 1/a$. Replacing "<" symbols in the above inequalities with "=" signs, one arrives at the minimal x accessible on the lattice: $L = 1/x_{\min}P_3 = a/x_{\min}$; i.e., $x_{\min} = 1/(L/a)$. Note that it is the number of sites in the boost direction that determines $x_{\min}$, not its physical size.

(3) *Pion mass dependence*.

The computational cost of Lattice QCD calculations depends on the pion mass. Hence, exploratory studies are usually performed with heavier-than-physical pions, as was also the case for quasi-PDFs (see Section 3.2). Obviously, this introduces a systematic effect. If no physical pion mass calculations are available, one can extrapolate to the physical point, if the fitting ansatz for this extrapolation is known (e.g., from chiral perturbation theory). However, the cleanest procedure is to simulate directly with pions of physical mass. Recently, quasi-PDFs computations with physical pions have become available; see Section 9 for their review including a direct comparison between ensembles with different pion mass [124].

(4) *Number of flavors, isospin breaking*.

QCD encompasses six flavors of quarks. However, due to the orders of magnitude difference between their masses, only the lightest two, three, or four flavors are included in lattice simulations. Moreover, the up and down quarks are often taken to be degenerate; i.e, one assumes exact isospin symmetry. One then speaks of a $N_f = 2$, $N_f = 2 + 1$, or $N_f = 2 + 1 + 1$ setup, respectively. Differences among these setups are observable dependent, but usually smaller than other systematic uncertainties and the statistical errors. For examples of the small dependence on the number of dynamical quarks in various observables, see, e.g., the FLAG review [156]. Hence, for most applications, all these setups can be considered to be equivalently suitable. Only when aiming at $\mathcal{O}(1\%)$ total uncertainty, well beyond the current precision of the field of lattice PDFs, it

may be necessary to include dynamical strange and charm quarks. Similar or smaller effects are expected from isospin breaking by the different up and down quark masses (QCD effect) and their different electric charges (QED effect). The order of magnitude of these effects can be deduced from the difference of proton and neutron masses, less than two per mille. Note that the setup with degenerate light quarks is very useful in lattice hadron structure calculations also for practical reasons; in such a setup, the disconnected contributions cancel in the $u - d$ flavor combination and, moreover, isovector PDFs do not mix under matching and renormalization. Thus, it is clear that all the effects discussed in this point are currently subleading but may become important in the future, when aiming at very precise extractions of PDFs.

(5) *Source-sink separation and excited states contamination*.

As already discussed in Section 6.1, a significant systematic effect may emerge in lattice matrix elements due to excited states contamination. From the correlation functions decomposition, one can see that excited states are suppressed with the source-sink separation, t_s. Hence, a careful analysis of a few separations is needed to establish ground state dominance; see Section 6.1 for more details. The issue of reaching large t_s values is nontrivial from the computational point of view, as the signal-to-noise ratio decays exponentially with increasing t_s. For this reason, a compromise is needed to keep the computational cost under control. Yet, the compromise must not affect the reliability of the results.

(6) *Momentum boost and higher-twist effects*.

Contact with the IMF via LaMET is established at large nucleon momenta. Hence, it is desirable to use large nucleon boosts on the lattice. However, this is highly nontrivial for several reasons. First, the signal-to-noise ratio decays exponentially with increasing hadron momentum, necessitating increase of statistics to keep similar statistical precision at larger boosts. Second, excited states contamination increases considerably at larger momenta, calling for an increase of the source-sink separation to maintain suppression of excited states at the same level. As argued in the previous point, the increase of t_s further decays the signal, enlarging the required statistics. Third, large hadron momenta may induce enhanced discretization effects, in particular when the boost becomes similar to or larger than the lattice UV cutoff, i.e., the inverse lattice spacing. Thus, momenta larger than the UV cutoffs of the currently employed lattice spacings, of order 2-2.5 GeV, should only be aimed at with ensembles at finer lattice spacings.

We now consider effects that may appear if the nucleon momentum is too small. Looking at the formulation of LaMET, it is clear that higher-twist effects (HTE), suppressed as $\mathcal{O}((P_3)^{-2})$, may become sizable and hinder the extraction of leading-twist PDFs. In principle, one can compute the HTE explicitly and subtract them. This would be an interesting direction of further studies, especially that HTE are of interest in their own right. Alternatively, one may compute the leading functional dependence of HTE and extrapolate them away. An example of such computation was presented in [157], based on the study of renormalons in coefficient functions within the bubble-chain approximation. The result for quasi-PDFs is an $\mathcal{O}((\Lambda^2_{\mathrm{QCD}}/P_3^2)/(x^2(1-x)))$ correction. Note, however, that the matrix elements underlying the quasi-PDFs in this analysis are normalized to unity at zero momentum, as done in the pseudo-PDF approach (see Section 2.6). This suppresses HTE at small-x at the price of enhancement for large-x. Clearly, the renormalization programme employed for quasi-PDFs, e.g., based on a variant of RI/MOM (see Section 7), can lead to different functional form of HTE. Moreover, the Authors of [157] put another warning that a perturbative analysis might not see all sources of HTE and their results should rather be considered as a minimal model that may miss nonperturbative features. Note also that knowing the functional form of leading-order HTE (with unknown prefactors) does not clarify what the range of hadron momenta is where these terms are indeed leading. At too small momenta, it may still be that higher-order HTE are sizable and even change the overall sign of the correction, rendering the extrapolation unreliable.

Another type of HTE is nucleon mass corrections (NMCs). These, in turn, can be exactly corrected by using the formulae derived by Chen et al. [107]. The calculation presented in this reference allowed us to obtain closed expressions for the mass corrections relevant for all types of quasi-PDFs. An important feature of these NMCs is that the particle number is conserved. We note that NMCs are already small at momenta not much larger than the nucleon mass, as also argued by Radyushkin [76] from a model calculation. It is important to remark that the NMCs for quasi-PDFs (also commonly referred to as TMCs) are different from TMCs in phenomenological analyses for standard PDFs (see, e.g., [158] for a review). NMCs in quasi-PDFs result from the nonzero ratio of the nucleon mass to its momentum (while this ratio is zero in the IMF), whereas TMCs in phenomenological analyses refer to corrections needed because of a nonzero mass of the target in a scattering experiment.

At the level of matrix elements, the momentum dependence is manifested, inter alia, by the physical distance at which they decay to zero. This distance, entering in the limits of summation for the discretized Fourier transform in Equation (49), becomes smaller for larger values of P_3. If it is too large, periodicity of the Fourier transform will induce nonphysical oscillations in the quasi-PDFs, especially at large x.

We note that these oscillations do not appear because of the truncation at finite $z_{\max}$, but rather because of a too large value of $z_{\max}$ at low momenta. This effect can be naturally suppressed by simulating at larger nucleon boosts and indeed, as we show in Section 9, oscillations are dampened at larger P_3. The uncertainty induced by this behavior can also result from uncertainties related to the renormalization of bare matrix elements. The large values of Z-factors amplify both the real and the imaginary part and, for complex Z-factors, also mix them with each other. The $\overline{\text{MS}}$ Z-factors should be purely real, but this feature holds only if conversion between the intermediate lattice renormalization scheme and the $\overline{\text{MS}}$ scheme is done to all orders in perturbation theory. Together with lattice artifacts appearing in the estimate of the intermediate scheme renormalization functions, this effectively induces a slower decay of matrix elements with the Wilson line length and shifts the value of z where matrix elements become zero to larger distances. Hence, the combination of too small boost and uncertainties in Z-factors manifests itself in the oscillations. Note also that the problem may be more fundamental. It is not presently clear how reliable is a distribution reconstruction procedure from a set of necessarily limited data. This issue is being investigated in the context of pseudodistributions [159]. The reconstruction techniques, mentioned in the context of the hadronic tensor in Section 2.1, may be crucial for control of this aspect. It was also speculated [51] that the Fourier transform may be a fundamental limitation of the quasi- and pseudodistribution approaches and the fundamental object may be the renormalized matrix element, or ITD.

A method to remove the nonphysical oscillations was proposed in [160] and was termed the derivative method. One rewrites the Fourier transform using integration by parts:

$$\begin{aligned}\widetilde{q}\left(x,P_3\right) = h_\Gamma\left(P,z\right)\frac{e^{izP_3x}}{2\pi i x}\Bigg|_{-z_{\max}}^{z_{\max}} \\ -\int_{-z_{\max}}^{z_{\max}}\frac{dz}{2\pi}\frac{e^{izP_3x}}{ix}\frac{\partial h_\Gamma\left(P,z\right)}{\partial z},\end{aligned} \tag{52}$$

where the derivative of the matrix elements with respect to the Wilson line length gives the name to the method. The integration by parts is exact and this definition of the Fourier transform is equivalent to the standard one if the matrix elements have decayed to zero at $z = z_{\max}$ and up to discretization effects induced by the need to lattice size the continuous derivative. Otherwise, one neglects the surface term in Equation (52), which effectively absorbs oscillations. However, it is debatable whether the procedure is safe and the neglected surface term does not hide also physical contributions at a given nucleon boost. Also, the presence of an explicit $1/x$ factor in the surface term leads to an uncontrolled approximation for small values of x. Other proposed methods to remove the oscillations are a low-pass filter [160], including a Gaussian weight in the Fourier transform [161]. However, they have not been used with real lattice data. Ideally, the nucleon momentum needs to be large enough to remove oscillations in a natural way, instead of attempting to suppress them artificially.

(7) *Other effects in the PDFs extraction procedure*.

For the sake of completeness, we mention other effects that can undermine the precision of lattice extraction of PDFs, although they are not challenges for the lattice *per se*.

In the previous point, we have already mentioned uncertainties related to renormalization. In RI/MOM-type schemes, they manifest themselves in the dependence of Z-factors on RI scales from which they were extracted, even after evolution to a common scale. This can be traced back to the breaking of continuum rotational invariance ($O(4)$) to a hypercubic subgroup $H(4)$. A way to overcome this problem is to subtract lattice artifacts computed in lattice perturbation theory, which can be done to all orders in the lattice spacing at the one-loop level; see [162] for more details about this method and an application to local Z-factors.

Another renormalization-related issue is the perturbative conversion from the intermediate lattice scheme to the $\overline{\text{MS}}$ scheme and evolution to a reference $\overline{\text{MS}}$ scale. Although not mandatory, the aim of the whole programme is to provide PDFs in the scheme of choice for phenomenological applications, i.e., the $\overline{\text{MS}}$ scheme. The conversion and evolution are currently performed using one-loop formulae and, hence, subject to perturbative truncation effects. A two-loop calculation of these steps will shed light on the magnitude of truncation effects.

Similarly, truncation effects emerge also in the matching of quasi-PDFs to light-cone PDFs, currently done to one-loop level; see Section 8 for a more thorough discussion on matching.

(8) *Finite and power-divergent mixings*. A general feature of quantum field theory is that operator mixing under renormalization is bound to appear among operators that share the same symmetry properties. On the lattice, some continuum symmetries, that otherwise prevent mixing, are broken. For operators of the same dimension, the mixing is finite. Important example of such mixing was mentioned above; for some fermionic discretizations, operator with the γ_3 Dirac structure (for unpolarized PDF) has the same symmetries as the analogous scalar operator [106] and hence mixes with it, while the γ_0 structure has different symmetry properties and avoids the mixing. This mixing is a lattice effect stemming from chiral symmetry breaking by the lattice discretization and

does not appear for lattice fermion formulations that preserve this symmetry, e.g., overlap fermions. We discuss this finite mixing in more detail in the next section.

If the dimension of the operator with the same symmetries is lower, then the mixing will be power divergent in the lattice spacing; i.e., it will contribute a term $\propto 1/a^{\Delta d}$, where Δd is the difference in the dimension. The possibility that such mixings occur for quasi-PDFs, as well as pseudo-PDFs and LCSs, was considered by G.C. Rossi and M. Testa in [163, 164]. They considered a toy model, devoid of QCD complications irrelevant in the context of their argument, and showed that moments of quasi-PDFs evince power-divergent mixings with lower-dimensional operators coming from the trace terms. They argued that, for a proper lattice extraction, such mixings would have to be computed and subtracted.

However, it was counterargued in three papers [84, 90, 165] that the problem actually does not exist. In [165], it was pointed out that indeed all moments, except for the zeroth, do not converge. However, the light-cone PDFs are extracted from the nonlocal quasidistributions that avoid the power divergence problem; i.e, moments of quasi-PDFs are never intended to be computed. They trace it back to the much simpler ultraviolet physics in the nonlocal formulation, where, apart from the Wilson-line-induced power divergence, shown to be renormalizable (see Sections 5 and 7), there are only logarithmic divergences. All of these divergences can be properly renormalized on the lattice, e.g., in a RI/MOM-type scheme.

It was also argued by Rossi and Testa that divergent moments of quasi-PDFs, $\langle \tilde{q}^n \rangle$, necessarily imply divergent moments of extracted light-cone PDFs, $\langle q^n \rangle$, since the latter are proportional to the former. However, this argument ignores the presence of moments of the matching function, $\langle C^n \rangle$:

$$\langle q^n \rangle = \langle C^n \rangle \langle \tilde{q}^n \rangle . \tag{53}$$

It is exactly the matching function that makes the moments of standard PDFs finite after the subtraction of the UV differences between the two types of distributions. In other words, the divergence in the moments $\langle \tilde{q}^n \rangle$ is exactly canceled by the divergence of moments $\langle C^n \rangle$, yielding finite moments $\langle q^n \rangle$ of light-cone PDFs.

Further explanations were provided in [84]. Radyushkin pointed out that Rossi and Testa rely on a Taylor expansion in z. This expansion may be justified in the very soft case when all derivatives with respect to z^2 exist at $z = 0$. However, in the general case, the use of the Taylor expansion for the hard logarithm $\log z^2$ "amounts to just asking for trouble." Crucially, it is the $\log z^2$ part that contributes slowly decreasing terms into the large-x part of quasi-PDFs and these terms lead to the divergence of the quasidistribution moments. These terms are not eliminated by just taking the infinite momentum limit, but they disappear upon the matching procedure. As a result, one can calculate the moments of light-cone PDFs from the quasi-PDF data.

Finally, J. Karpie, K. Orginos, and S. Zafeiropoulos demonstrated [90] explicitly that the problem does not appear for pseudo-PDFs, refuting claim thereof by Rossi and Testa. The reduced ITDs were OPE expanded in lattice-regularized twist-2 operators, which indeed have power divergences on the lattice, due to the breaking of the rotational symmetry. However, the Wilson coefficients in the OPE have exactly the same power divergences and cancel the power divergences of the matrix elements, order by order in the expansion, and the final series is finite to all orders. The Authors also provided an explicit numerical demonstration for the first two moments, obtaining compatibility within errors with an earlier lattice calculation in the same quenched setup; see Section 11.4 for more details.

With all these developments, it has been convincingly established that the problem advocated by Rossi and Testa does not hinder the lattice extraction of light-cone PDFs. Thus, power-divergent mixings only manifest themselves in certain quantities, like moments of quasi-PDFs, which are *nonphysical*. In turn, finite mixings can be avoided by a proper Dirac structure of matrix elements.

We finalize this section with a schematic flowchart (Figure 11), prepared by C. Monahan, representing the various steps on the way from bare matrix elements to final light-cone PDFs. Some of the discussed above challenges for the lattice computations are indicated. We refer also to [51] for another discussion of systematic effects.

7. Renormalization of Nonlocal Operators

The renormalization of nonlocal operators that include a Wilson line is a main component of the lattice calculation related to quasi-PDFs. Lattice results from the numerical simulations can only be related to physical quantities upon appropriate renormalization and only then comparison with experimental and phenomenological estimates becomes a real possibility. As discussed in Section 5.2, the renormalizability of the straight Wilson line bilinear operators has been investigated early on by Ji and Zhang [133] to one loop in perturbation theory, concluding that such operators are multiplicatively renormalizable. The argument was also extended to two-loop level. Ishikawa et al. showed in [132] the feasibility of the subtraction of the power divergence present in the operators under study to achieve a well-defined matching between the quasi-PDFs with the light-cone PDFs. These studies were later expanded to prove renormalizability of the operators to all orders in perturbation theory [134, 135], including the lattice regularization.

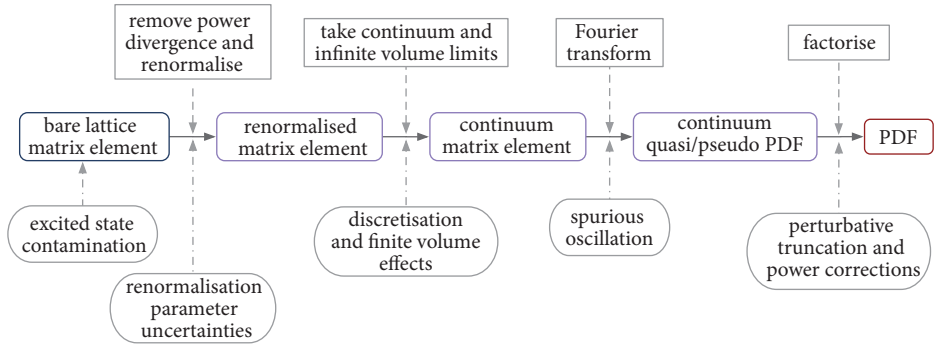

FIGURE 11: Schematic representation of different steps needed to extract light-cone PDFs from quasi-PDFs and of the challenges encountered at these steps. Source: [51] (arXiv), reprinted with permission by the Author.

Since the proposal of Ji in 2013, several aspects of quasi-PDFs have been investigated, such as the feasibility of a calculation from Lattice QCD. This includes algorithmic developments [109, 152, 154] that lead to simulations at the physical point, and the matching between the quasi- and light-cone PDFs [48, 83, 124, 142, 166]. Thus, the lattice calculations have progressed with a missing ingredient: its renormalization. It is not until 2017 that a proper renormalization prescription has been proposed, despite the theoretical developments on the renormalizability of the nonlocal operators of interest. This has proven to be a challenging and delicate process due to the presence of the Wilson line that brings in additional power divergences, the nonlocality and the complex nature of the matrix elements. As a consequence, the first studies of quasi-PDFs on the lattice were either neglecting renormalization [46] or multiplying naively the matrix elements with the renormalization function of the corresponding local operators [100, 107, 108], a procedure understood as normalization.

7.1. Power Divergence. Among the first attempts to understand the renormalization of nonlocal operators was to address the power divergence inherited from the Wilson line in the static potential approach, as described in this subsection. Eliminating the power divergence results in a well-defined matching between the quasi-PDFs and the light-cone PDFs.

The renormalization of nonlocal operators in gauge theories has been investigated long time ago [167–170], and later in the 1980's and 1990's [140, 141, 171–176]. In these seminal works, it was identified that Wilson loops along a smooth contour $\mathscr{C}$ with length $L_{\mathscr{C}}$, computed in dimensional regularization (DR), are finite functions of the renormalized coupling constant, while other regularization schemes may lead to additional renormalization functions, that is

$$Z_z e^{\delta m L_{\mathscr{C}}}. \tag{54}$$

In the above expression, the subscript z indicates the distance between the end points of the Wilson line, whereas δm is mass renormalization of a test particle that moves along $\mathscr{C}$. Also, the logarithmic divergences can be factorized within Z_z, and the power divergence is included in δm. In particular, in the lattice regularization (LR), the latter divergence manifests itself in terms of a power divergence with respect to the UV cutoff, the inverse of the lattice spacing $1/a$,

$$e^{\delta m |z|/a}, \tag{55}$$

where δm is dimensionless. This is analogous to the heavy quark approach, where similar characteristics are observed. For instance, a straight Wilson line may represent a static heavy quark propagator, and δm a corresponding mass shift. Inspired by this analogy, Chen et al. [177] and Ishikawa et al. [132] proposed a modification such that spacelike correlators do not suffer from any power divergence. In their work, the matrix element appearing in Equation (25) can be replaced by

$$e^{-\delta m |z|/a} \langle P | \overline{\psi}(0,z) \Gamma W(z) \psi(0,0) | P \rangle, \tag{56}$$

that has only logarithmic divergence in the lattice regulator. Note that, in the above expression, a general Dirac structure Γ appears, as this methodology is applicable for all types of PDFs. A necessary component of this improved matrix elements is the calculation of the mass counterterm δm. First attempts to obtain δm appear in the literature [132, 177] and are based on adopting a static potential $q\overline{q}$ [178].

Following the notation of [132], we define the static potential for separation R, via an $R \times T$ Wilson loop:

$$W_{R\times T} \propto e^{-V(R)T} \tag{57}$$

where T is large. The Wilson loop is renormalized as

$$W_{R\times T} = e^{\delta m(2R+2T)+4\nu} W^{\text{ren}}_{R\times T}, \tag{58}$$

where ν is due to the corners of the chosen rectangle. Using Equations (57)-(58), one can relate the desired mass counterterm to the static potential,

$$V^{\text{ren}}(R) = V(R) + 2\delta m. \tag{59}$$

An additional condition is necessary to determine δm, which can be fixed using

$$V^{\text{ren}}(R_0) = V_0 \longrightarrow \quad \delta m = \frac{1}{2}\left(V_0 - V(R_0)\right), \tag{60}$$

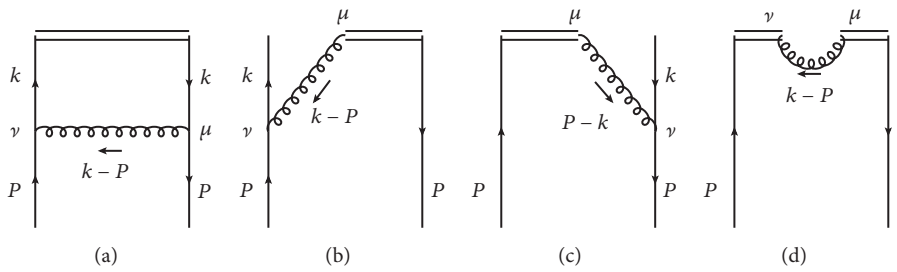

Figure 12: One-loop diagrams for the calculation of Green's function of nonlocal operators. The double line represents the gauge link in the operator. Source: [180] (arXiv), reprinted with permission by the Authors.

where the choice of R_0 depends on the scheme of choice. The appearance of an arbitrary scale is not a surprise and is in accordance with the work of R. Sommer [179], suggesting a further finite dimensionful scale that appears in the exponential of Equation (55), based on arguments from Heavy Quark Effective Theory.

A proper determination of δm requires a nonperturbative evaluation on the same ensemble used for the calculation of the quasi-PDF. This is essential in order to eliminate a source of systematic uncertainty related to the truncation of a perturbative evaluation, which is limited to typically one to two loops. Furthermore, such a quantity can be used for a purely nonperturbative matrix element. Nevertheless, this quantity has been computed to one-loop level in perturbation theory [132, 177] in an effort to qualitatively understand the structure of the power divergence. Within these works, it was demonstrated that such a mass counterterm removes the power divergence to all orders in perturbation theory.

7.2. Lattice Perturbation Theory. The promising results from the first exploratory studies of the quasi-PDFs [46, 47] have led to an interest in developing a renormalization prescription appropriate for Lattice QCD. Several features of the quasi-PDFs have been studied in continuum perturbation theory (see, e.g., Section 5.2), but more recently there appeared also calculations in lattice perturbation theory. Such development is highly desirable, as the ultimate goal is to relate quasi-PDFs extracted from numerical simulations in Euclidean spacetime to standard PDFs in continuum Minkowski space. In this subsection, we highlight three calculations that provided important insights into quasi-PDFs.

7.2.1. IR Divergence in Lattice and Continuum. X. Xiong et al. have computed in [180] the unpolarized quasi-PDF in lattice perturbation theory using clover fermions and Wilson gluons. The calculation was performed in Feynman gauge and included a nonzero quark mass. This allowed the study of the matching between lattice and continuum, and, as discussed in that work, the massless and continuum limits do not commute, leading to different IR behaviors. The calculation contained the one-loop Feynman diagrams shown in Figure 12, where the quark (P) and internal gluon (k) momenta are shown explicitly.

Here, we do not provide any technical details and focus only on the qualitative conclusions, but we encourage the interested Reader to consult [180] for further details. The one-loop results show that a correct recovery of the IR divergence of the continuum quasi-PDFs can only be achieved for $aP_3^2 \approx m$ and $m \ll P_3$; the complete continuum quasi-PDF is obtained from $aP_3^2 \ll m \ll P_3$. However, it is stressed that this is necessary only for perturbative calculations, as the nonperturbative ones do not contain collinear divergence. This is encouraging and serves as a proof of the matrix elements in Euclidean space being the same as the ones in Minkowski space. Same conclusions have been obtained from [131, 165].

7.2.2. Renormalization of Nonlocal Operators in Lattice Perturbation Theory. M. Constantinou and H. Panagopoulos have calculated in [106] the renormalization functions for the nonlocal operators in perturbation theory in lattice regularization (LR). The calculation was performed to one-loop level, in which the diagrams shown in Figure 12 were evaluated for clover fermions and a variety of Symanzik-improved gluon actions, including Iwasaki and tree-level Symanzik. Note that the schematic representation of the diagrams shown in Figure 12 appears to be the same for dimensional and lattice regularizations, but a calculation in LR is by far more complicated numerically. This is a consequence of the QCD Lagrangian discretization, coupled with the additional divergences that depend on the lattice regulator. The renormalization functions were computed for massless fermions in the $\overline{\text{MS}}$ scheme for general values of the action parameters and general gauge. The latter has served as a cross-check for gauge-independent quantities. In addition to the calculation in LR, Green's function of the nonlocal operators has been obtained in dimensional regularization (DR), which, in combination with the corresponding lattice results, gives a direct definition of the renormalization functions in the $\overline{\text{MS}}$ scheme.

The operator under study includes a straight Wilson line in the direction μ and has the general form

$$\mathcal{O}_\Gamma \equiv \overline{\psi}(x)\,\Gamma \mathscr{P} e^{ig\int_0^z A_\mu(x+\zeta\widehat{\mu})d\zeta}\psi\left(x+z\widehat{\mu}\right), \tag{61}$$

In the above operator, only $z \neq 0$ is to be considered, due to the appearance of contact terms beyond tree level, making the limit $z \longrightarrow 0$ nonanalytic. Green's functions of the above

operators are evaluated for all independent combinations of the Dirac matrices, Γ; that is,

$$\langle \psi \; \mathcal{O}_\Gamma \; \overline{\psi} \rangle \quad \text{with } \Gamma = \widehat{1},\ \gamma^5,\ \gamma^\nu,\ \gamma^5\gamma^\nu,\ \gamma^5\sigma^{\nu\rho},\ \sigma^{\nu\rho},\ \rho \neq \mu. \tag{62}$$

Note that the above includes twist-2 operators as well as higher twist. We will later see that it is important to distinguish between the cases in which the spin index is in the same direction as the Wilson line ($\nu = \mu$), or perpendicular to it ($\nu \neq \mu$).

One of the main findings of this work is the difference between the bare lattice Green's functions and the $\overline{\text{MS}}$-renormalized ones (from DR). This contributes to the renormalization of the operator in LR and was found to receive two contributions, one proportional to the tree level of the operator ($e^{iq_\mu z}\ \Gamma$), and one that has a different Dirac structure ($e^{iq_\mu z}\ \{\Gamma, \gamma_\mu\}$); that is,

$$\begin{aligned} \langle \psi\, \mathcal{O}_\Gamma\, \overline{\psi} \rangle^{DR,\overline{\text{MS}}} - \langle \psi\, \mathcal{O}_\Gamma\, \overline{\psi} \rangle^{LR} &= \frac{g^2 C_f}{16\pi^2} \\ \cdot e^{iq_\mu z} \Bigg[\Gamma \left(\alpha_1 + \alpha_2 \beta + \alpha_3 \frac{|z|}{a} + \log\left(a^2 \overline{\mu}^2\right)(4-\beta) \right) &+ \left\{ \Gamma, \gamma_\mu \right\} \left(\alpha_4 + \alpha_5 c_{\text{SW}} \right) \Bigg], \end{aligned} \tag{63}$$

where α_i are numerical coefficients that depend on the action parameters. Note that the term proportional to $|z|/a$ is the one-loop counterpart of the power divergence discussed in the previous subsection, and its numerical coefficient has been computed in [106]. Perturbation theory is not reliable in providing numerical values for mixing and power coefficients; nevertheless it provides crucial qualitative input for the quantities under study.

The conclusion from Equation (63) is that the operator with structure Γ will renormalize multiplicatively only if the anticommutator between Γ and γ^μ vanishes. This is true for the axial and tensor operators that are used for the helicity ($\gamma^5\gamma^\mu$) and transversity ($\sigma^{\mu\rho}$) PDFs, which have one index in the direction of the Wilson line. On the contrary, the vector current γ^μ turns out to mix with the scalar, a higher-twist operator. This finding impacted significantly all numerical simulations of the unpolarized PDFs, as they were using this particular operator [46, 100, 107, 108, 181], unaware of the aforementioned mixing. With this work, the Authors proposed to use a vector operator with the spin index perpendicular to the Wilson line and the ideal candidate is the temporal direction (γ^0) for reasons beyond the mixing. First, the matching procedure between the quasi-PDFs and normal-PDFs also holds for γ^0, as it belongs to the same universality class of γ^μ [182]. In addition, the temporal vector operator offers a faster convergence to the light-cone PDFs, as discussed in [75]. Note, however, that γ^3 and γ^0 do not share the same matching formula, with the latter being calculated much later. Detailed discussion on the matching to light-cone PDFs is provided in Section 8.

The work of [106] has led to a number of useful information not only on the renormalization pattern of nonlocal operators, but also on the conversion from a renormalization scheme of choice ($\mathcal{S}$) to the $\overline{\text{MS}}$ scheme. This is extracted from the ratio of renormalization functions in the two schemes computed in DR,

$$\mathcal{C}_{\mathcal{O}}^{\mathcal{S},\overline{\text{MS}}} = \frac{Z_{\mathcal{O}}^{\overline{\text{MS}}}}{Z_{\mathcal{O}}^{\mathcal{S}}}, \tag{64}$$

and multiplies nonperturbative estimates of $Z_{\mathcal{O}}^{\mathcal{S}}$ in order to obtain $Z_{\mathcal{O}}^{\overline{\text{MS}}}$. Due to the mixing found in the lattice calculation, a convenient scheme which is applicable nonperturbatively is an RI-type [183]. A well-defined prescription within RI-type schemes exists for both the multiplicative and the mixing coefficients, as described in Section 7.3. The RI′ is a natural choice for nonperturbative evaluations of renormalization functions, because it does not require to separate finite contributions with tensor structures which are distinct from those at tree level (typically denoted by $\Sigma^{(2)}$ that appears in the local vector and axial operators in the limit of zero quark mass). The conversion factor $\mathcal{C}_{\mathcal{O}}^{\text{RI}',\overline{\text{MS}}}$ has been computed and was used in the renormalization program of the ETMC [151]. The conversion factor shares certain features with the matrix elements; that is, it is complex and symmetric/antisymmetric in the real/imaginary part. A representative example is shown in Figure 13 for the vector, axial, and tensor operators that have a Dirac index in the same direction as the Wilson line.

7.2.3. Nonlocal Operators for Massive Fermions in Dimensional Regularization. G. Spanoudes and H. Panagopoulos [184] have extended the work of [106] presented in the previous paragraph, by examining the effect of nonzero quark masses on the renormalization functions and conversion factors between the RI′ and $\overline{\text{MS}}$ schemes, as obtained in DR at one-loop level. This work was motivated by the fact that lattice simulations are not performed exactly at zero renormalized mass. Of course, one expected that the correction will be very small for the light quarks, but not necessarily for the heavier quarks, which are typically used in dynamical simulations ($N_f = 2 + 1$ and $N_f = 2 + 1 + 1$). In principle, one should adopt a zeromass renormalization scheme for all quarks that requires dedicated production of ensembles with all degenerate flavors (e.g., $N_f = 3$ and $N_f = 4$), as typically done for local operators, but this entails additional complications.

Including massive quarks requires a proper modification of the RI-type renormalization conditions, as developed in [184]. Also, in addition to the fermion field renormalization function, the quark mass renormalization is required as well (see Equations (4)-(6)). More interestingly, the RI′ conditions for the nonlocal operators must be generalized to account for the more complicated structure of Green's functions. In particular, it is found that the mixing revealed in [106] extends beyond the anticommutator $\{\Gamma, \gamma^\mu\}$ (μ: direction of the Wilson line), which still holds for operators with the same flavor in the external quark fields. However, operators with a different flavor give rise to additional mixing, affecting, among other operators, γ^0 (mixes with $\sigma^{0\mu}$), $\gamma^5\gamma^\mu$ (mixes with γ^5), and $\sigma^{\mu\rho}$ (mixes with γ^ρ). Depending on the size of the

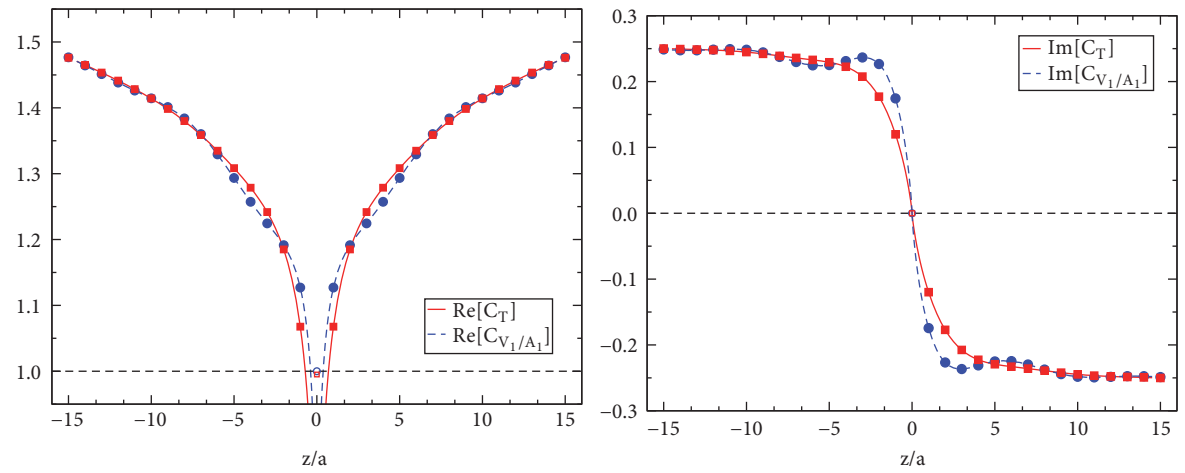

FIGURE 13: Real (left) and imaginary (right) parts of the conversion factors for the vector (V_1), axial (A_1), and tensor (T_1) operators as a function of z/a in the Landau gauge. The RI′ renormalization scale is $a\bar{q} = (2\pi/32)(4 + 1/4, 0, 0, 4)$. Source: [106], reprinted with permission by the Authors and the American Physical Society.

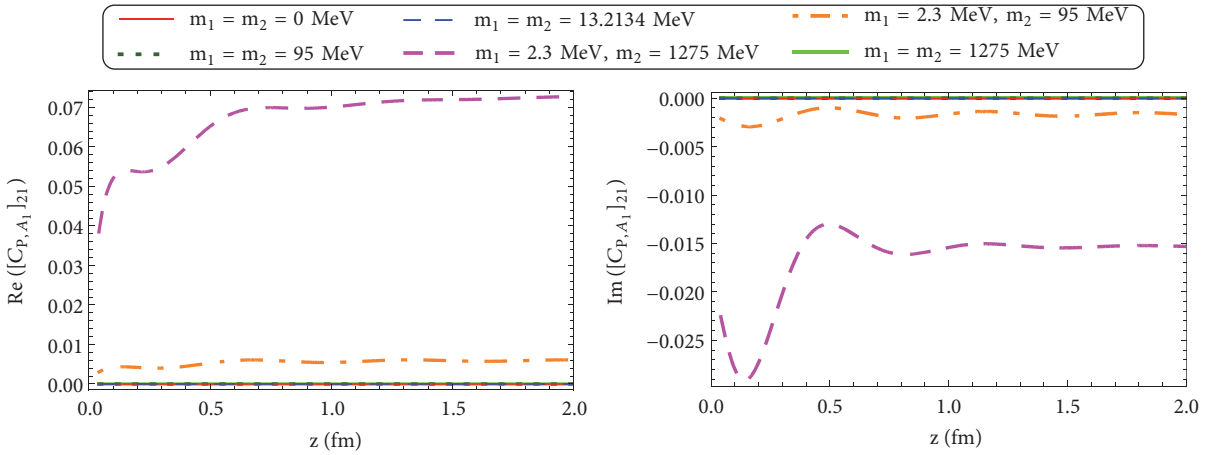

FIGURE 14: Real (left) and imaginary (right) parts of the conversion factor for the mixing coefficient for the operator pair (P, A_μ) as a function of z, for different values of quark masses. Source: [184], reprinted with permission by the Authors (article published under the terms of the Creative Commons Attribution 4.0 International license).

mixing and the simulation setup, a nonnegligible effect may occur in numerical simulations, as all these operators are used in the quasi-PDFs calculations. This is more likely to impact the results extracted using strange and charm in the sea. This includes the first studies (e.g., [46, 47]), but also the more recent work of LP^3, in which the Authors use a single $N_f = 2 + 1 + 1$ ensemble for the renormalization functions and an extrapolation to the chiral limit is not possible for the Z-factors. Unlike the case of the local operators, where quark mass dependence is negligible, the nonlocal operators exhibit quite visible mass dependence for Wilson lines of length larger than 0.8 fm [185]. However, the mixing is expected to be at most finite and thus not present in the $\overline{\text{MS}}$ scheme.

As a consequence of the additional mixing, the conversion factors are 2×2 matrices usually determined in DR, as they are regularization-independent quantities. In [184], the RI′ and $\overline{\text{MS}}$ renormalization functions were obtained by using appropriate conditions on the bare Green's functions. This is a complicated process and the results can be found in Section III of [184]. Here, we present in Figure 14 the conversion factor for the mixing coefficient between the pseudoscalar and the axial ($\gamma^5\gamma^\mu$) operators. As can be seen, the mixing is small, but nonnegligible, especially if the flavors involved have mass difference above 100 MeV. The action parameters are given in [184] and the notation is $\mu = 1$.

7.3. Nonperturbative Renormalization. The progress in the renormalization of the nonlocal operators from lattice perturbation theory has encouraged investigations of nonperturbative calculations. This was supported by theoretical developments proving the renormalizability of the operators under study to all orders in perturbation theory (see Section 5.2). The full development of a proper nonperturbative prescription has been a natural evolution of the knowledge gained from the perturbative calculations, and in particular the pattern identified in [106]. The Authors of this work have

proposed an RI-type scheme that was employed by ETMC [151] giving, for the first time, properly renormalized quasi-PDFs. The approach was also adopted by LP^3 [181] with a slight variation due to a different projection entering the renormalization prescription. The latter was motivated by the fact that the matrix elements of the vector and axial operators have additional tensor structure different than the tree level. We close the discussion on the nonperturbative renormalization with a presentation of an alternative prescription based on the auxiliary field formalism [186].

7.3.1. RI′ Scheme. C. Alexandrou et al. [151] have employed a renormalization scheme that is of similar nature as the RI′ scheme [183] that is widely used for local operators. Using the renormalization pattern of [106], the Authors developed a nonperturbative method for computing the renormalization functions of nonlocal operators that include a straight Wilson line. In this scheme, one imposes the condition that Green's functions of the operator must coincide with the corresponding tree-level values at each value of z. This approach is also applicable in the presence of mixing, via $N \times N$ matrices (N: number of operators that mix with each other). The proposed program has the advantage that it eliminates both power and logarithmic divergences at once, without the need to introduce another approach to calculate the power divergence. This is due to the fact that the vertex functions of the operator that enter the RI-type prescription have the same divergences as the matrix elements. The prescription can be summarized as follows for a pair of nonlocal operators, $\mathcal{O}_1$ and $\mathcal{O}_2$, assuming they mix under renormalization:

$$\begin{pmatrix} \mathcal{O}_1^R(z) \\ \mathcal{O}_2^R(z) \end{pmatrix} = \widehat{Z}(z) \cdot \begin{pmatrix} \mathcal{O}_1(z) \\ \mathcal{O}_2(z) \end{pmatrix}, \qquad \widehat{Z}(z) = \begin{pmatrix} Z_{11}(z) & Z_{12}(z) \\ Z_{21}(z) & Z_{22}(z) \end{pmatrix}. \tag{65}$$

According to the above mixing, the renormalized matrix element of $\mathcal{O}_1$, $h_1^R(P_3, z)$, is related to the bare matrix elements of the two operators via

$$\langle P| \mathcal{O}_1(z) |P\rangle^R = Z_{11}(z) \langle P| \mathcal{O}_1(z) |P\rangle + Z_{12}(z) \langle P| \mathcal{O}_2(z) |P\rangle, \tag{66}$$

where Z_{11} and Z_{12} are computed in the RI′ scheme and then are converted to the $\overline{\text{MS}}$ scheme, at an energy scale $\overline{\mu} = 2$ GeV. The renormalization factors can be computed following

$$Z_q^{-1} \widehat{Z}(z) \widehat{\mathcal{V}}(p, z)\big|_{p=\overline{\mu}} = \widehat{1}, \tag{67}$$

where the elements of the vertex function matrix $\widehat{\mathcal{V}}$ are given by the trace

$$\left(\widehat{\mathcal{V}}(z)\right)_{ij} = \frac{1}{12} \text{Tr}\left[\mathcal{V}_i(p, z) \left(\mathcal{V}_j^{\text{tree}}(p, z)\right)^{-1}\right], \quad i, j = 1, 2. \tag{68}$$

In the above equation, $\mathcal{V}_i^{\text{tree}}$ is the tree-level expression of the operator $\mathcal{O}_i$. Thus, all matrix elements of $\widehat{Z}$ can be extracted by a set of linear equations, which can be written in the following matrix form:

$$Z_q^{-1} \begin{pmatrix} Z_{11}(z) & Z_{12}(z) \\ Z_{21}(z) & Z_{22}(z) \end{pmatrix} \cdot \begin{pmatrix} \left(\widehat{\mathcal{V}}(z)\right)_{11} & \left(\widehat{\mathcal{V}}(z)\right)_{21} \\ \left(\widehat{\mathcal{V}}(z)\right)_{12} & \left(\widehat{\mathcal{V}}(z)\right)_{22} \end{pmatrix} = \begin{pmatrix} 1 & 0 \\ 0 & 1 \end{pmatrix}. \tag{69}$$

The complication of the mixing is not relevant for recent calculations of quasi-PDFs, as the vector operator γ^μ has become obsolete and was replaced by γ^0. In the absence of mixing, the above equations simplify significantly and reduce to

$$Z_{\mathcal{O}} = \frac{Z_q}{(1/12)\,\text{Tr}\left[\mathcal{V}(p)\left(\mathcal{V}^{\text{Born}}(p)\right)^{-1}\right]\big|_{p=\overline{\mu}}}, \tag{70}$$

where $Z_{\mathcal{O}}$ is related to the inverse of the vertex function of the operator. Let us repeat that the prescription is applied on each value of z independently.

In Figure 15, we show a representative example of the renormalization function of the axial nonlocal operator ($Z_{\Delta h}$), using an $N_f = 2 + 1 + 1$ ensemble of twisted mass fermions with a clover term ($c_{\text{SW}} = 1.57$) and lattice size $32^3 \times 64$. In the left panel of the plot, we overlay the results for the RI′ (open symbols) and the $\overline{\text{MS}}$ (filled symbols) schemes, for the real and imaginary part of the Z-factor. The momentum source technique [162, 187] was employed that offers high statistical accuracy with a small number of measurements. The RI′ scale was set to $a\overline{q} = (2\pi/32)(7 + 1/4, 3, 3, 3)$. As can be seen from the plot, the imaginary part of $Z_{\Delta h}^{\overline{\text{MS}}}$ is smaller than $Z_{\Delta h}^{\text{RI}'}$. It is worth mentioning that the perturbative renormalization function in the $\overline{\text{MS}}$, as extracted in DR, is a real function to all orders in perturbation theory. Therefore, it is expected that the imaginary part of the nonperturbative estimates should be highly suppressed.

In the aforementioned work, the Authors used several values of the RI′ renormalization scales, and each one was converted to the $\overline{\text{MS}}$ and evolved to 2GeV. Residual dependence on the initial RI′ scale was eliminated by an extrapolation to $(a\mu_0)^2 \longrightarrow 0$, and the results can be seen in the right panel of Figure 15. An investigation of systematic uncertainties was presented in [151] and upper bounds for uncertainties were estimated.

7.3.2. RI/MOM Scheme. A modification of the RI-type prescription that was first proposed by Constantinou and Panagopoulos [105] was presented by J.-W. Chen et al. in [181]. The main motivation for the modification was the intent to employ a matching procedure that relates the quasi-PDFs in RI/MOM scheme to the light-cone PDFs in $\overline{\text{MS}}$, which was developed by Stewart and Zhao [166]. However, both RI′ and RI/MOM prescriptions can be used to obtain an appropriate RI-type formula without complication.

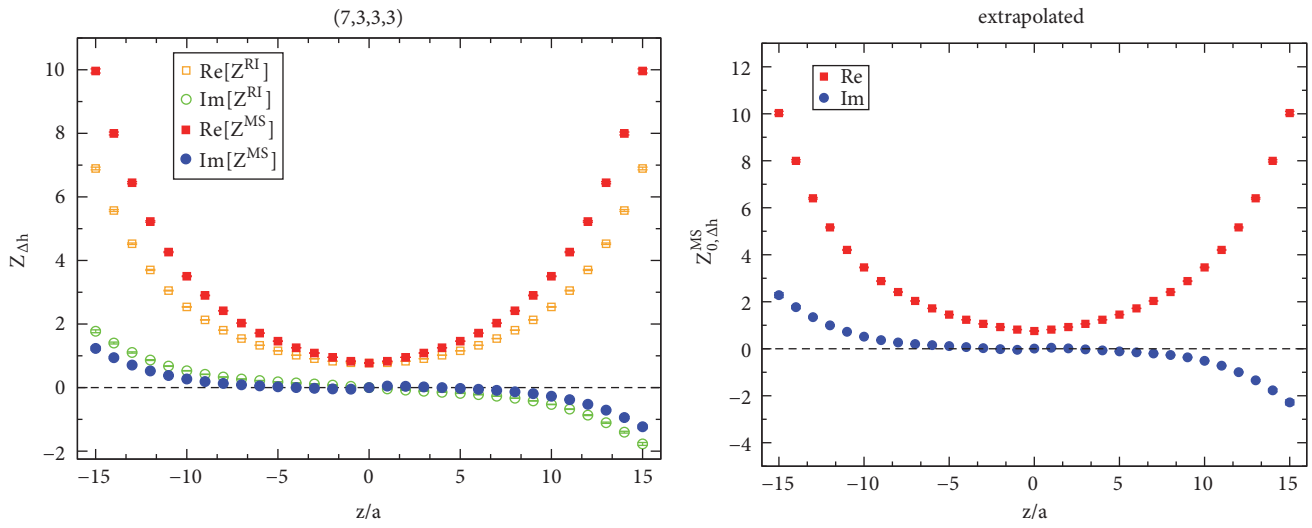

FIGURE 15: Left: the z-dependent renormalization function for the axial nonlocal operator at an RI′ scale of $(a\bar{q})^2 = 1.6$. Open (filled) symbols correspond to the RI′ ($\overline{\text{MS}}$) estimates. Right: extrapolated renormalization function using a fit range for the RI′ scale of $(a\ \mu_0)^2\ \epsilon$ [1.4–2.0]. Source: [151], reprinted with permission by the Authors (article available under CC BY).

Based on the RI/MOM prescription, the vertex function of the operator under study was projected by $\not{p}$ (instead of the tree level) in order to account for the extra tensor structure $\Sigma^{(2)}$ included in the vertex function. We note in passing that the difference between RI′ and RI/MOM is finite and should be removed by appropriate modification in the conversion factor to the $\overline{\text{MS}}$ scheme. Besides the different choice in the projector appearing in the RI/MOM prescription, the rest of the setup is equivalent to that of [151]. A minor exception is the fact that the definition of the renormalization functions of [181] is inverse to the one used in [151], which, however, has no implications in the extracted physics. For example, the RI/MOM prescription for the operator γ^μ that has mixing is given by

$$\left.\frac{\text{Tr}\left[\not{p}\Lambda\left(p,z,\gamma_\mu\right)\right]^R}{\text{Tr}\left[\not{p}\Lambda\left(p,z,\gamma_\mu\right)_{\text{tree}}\right]}\right|_{p^2=\mu_R^2,p_z=P_z} = 1, \tag{71}$$

$$\left.\frac{\text{Tr}\left[\Lambda\left(p,z,\mathcal{I}\right)\right]^R}{\text{Tr}\left[\Lambda\left(p,z,\mathcal{I}\right)_{\text{tree}}\right]}\right|_{p^2=\mu_R^2,p_z=P_z} = 1, \tag{72}$$

$$\text{Tr}\left[\left[\ \not{p}\Lambda\left(p,z,\mathcal{I}\right)\right]^R_{p^2=\mu_R^2,p_z=P_z} = 0, \tag{73}$$

$$\text{Tr}\left[\Lambda\left(p,z,\gamma_\mu\right)\right]^R_{p^2=\mu_R^2,p_z=P_z} = 0. \tag{74}$$

The renormalization matrix can be extracted via

$$\begin{aligned} Z\left(z,p_z,a,\mu_R\right) &= \widetilde{Z}^{-1}\left(z,p_z,a,\mu_R\right),\widetilde{Z}\left(z,p_z,a,\mu_R\right) \\ &\equiv \begin{pmatrix} Z_{11} & Z_{12} \\ Z_{21} & Z_{22} \end{pmatrix}\left(z,p_z,a,\mu_R\right) \\ &= \frac{1}{12e^{-ip_z z}}\begin{pmatrix} \text{Tr}\left[\widetilde{\Gamma}\Lambda\left(p,z,\gamma_z\right)\right] & \text{Tr}\left[\widetilde{\Gamma}\Lambda\left(p,z,\mathcal{I}\right)\right] \\ \text{Tr}\left[\Lambda\left(p,z,\gamma_z\right)\right] & \text{Tr}\left[\Lambda\left(p,z,\mathcal{I}\right)\right] \end{pmatrix}_{p^2=\mu_R^2,p_z=P_z}. \end{aligned} \tag{75}$$

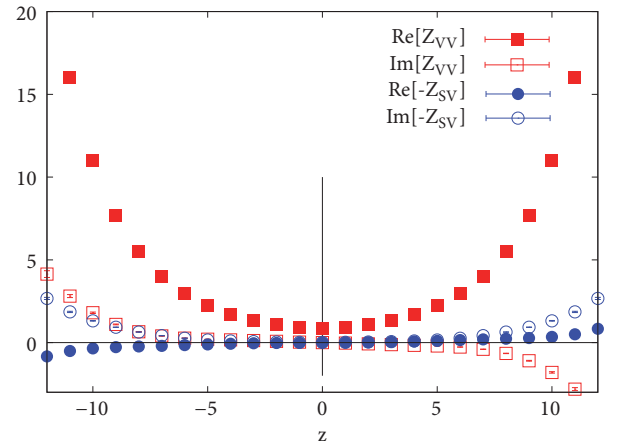

FIGURE 16: The renormalization function and mixing between vector and scalar nonlocal operators with a straight Wilson line. Source: [181], reprinted with permission by the Authors (article published under the terms of the Creative Commons Attribution 4.0 International license).

In the calculation of the renormalization factors, the Authors used an $N_f = 2 + 1 + 1$ clover on HISQ ensemble with a volume $24^3 \times 64$ [188]. The momentum source method was used that leads to high statistical accuracy, and a single RI/MOM renormalization scale (μ^0) was employed for each nucleon momentum, which corresponds to $\mu_0^2 = 5.74\text{GeV}^2$.

In Figure 16, we show the multiplicative renormalization factor of γ^μ (red squares) and the mixing coefficient (blue circles). As expected, it is found that the size of the mixing coefficient is about an order of magnitude smaller than the renormalization factor in the large-z region. However, the mixing coefficient should multiply the matrix element of the scalar operator that has very large numerical values, leading

to a nonnegligible contribution. The mixing is ignored in the rest of the analysis of [181].

Another investigation of [181] aimed at understanding the mixing discussed in [106] using symmetry properties. This was based on the invariance under parity $\mathscr{P}_\mu$, time reversal $\mathscr{T}_\mu$, and charge conjugation $\mathscr{C}$, where parity and time reversal are generalized into any Euclidean direction. The operator used was

$$O_{\Gamma\pm}(z) = \frac{1}{2}\left[\overline{\psi}(z)\,\Gamma W_z(z,0)\,\psi(0) \pm \overline{\psi}(0)\,\Gamma W_z(0,z)\,\psi(z)\right], \tag{76}$$

which has the advantage that it is either Hermitian or anti-Hermitian. Taking as an example the vector current in the direction of the Wilson line, γ^μ, one can see how the mixing arises: the "+" ("−") combination of Equation (76) is anti-Hermitian (Hermitian). In this case, the transformation properties allow mixing with the unity (scalar) operator. Unlike the case of γ^μ, the other directions of the vector operators do not suffer from mix even for formulations that break chiral symmetry. This conclusion is fully compatible with the findings of [106].

The study of the symmetries was extended to include $\mathcal{O}(a)$ nonlocal operators including a covariant derivative ($\mathcal{O}(ap)$) or a power of mass ($\mathcal{O}(am)$) [189]. It was found that operators with and without a covariant derivative may mix even if axial or chiral symmetry is preserved in the formulation under study. In addition, $\mathcal{O}(a^0)$ operators may also mix with $\mathcal{O}(am)$ operators regardless of chiral symmetry breaking. Further details on this analysis can be found in Tables 3 and 4 of [189].

In closing, let us add that a proper determination of the renormalization functions computed nonperturbatively in an RI-type scheme (e.g., the works presented in Sections 7.3.1 and 7.3.2) requires a few improvements. For once, dedicated calculations are needed on ensembles with all degenerate flavor quarks. These ensembles should correspond to the same value of the coupling constants as the ensembles used for the calculation of the hadron matrix elements. For instance, matrix elements obtained on $N_f = 2+1$ or $N_f = 2+1+1$ ensembles should be renormalized using $N_f = 3$ and $N_f = 4$, respectively. Renormalization functions should then be computed on multiple ensembles with different quark masses, so the chiral limit can be taken. Several values of the RI scale (μ_0) should be employed for each ensemble in order to take the $(a\mu_0)^2 \longrightarrow 0$ limit upon conversion to the $\overline{\text{MS}}$ and at a common scale. This will eliminate residual dependence on the initial RI scale and give more reliable estimates for the renormalization functions. We note that the extrapolation $(a\mu_0)^2 \longrightarrow 0$ has been performed in the work of [151] (see left panel of Figure 15). Potential improvements could also be a two-loop conversion factor from an RI-type to $\overline{\text{MS}}$ scheme, and also a subtraction technique of finite a effects using one-loop perturbation theory. This method was successfully employed for local operators of different lattice formulations [162, 190]. It is anticipated that both aforementioned improvements will be available in the near future.

7.4. Auxiliary Field Formalism. An alternative proposal for the renormalization of nonlocal operators is based on an auxiliary field method, a formulation also adopted to prove the renormalizability of the operators under study [135]. The use of this approach is not new but originates from other studies in the continuum [172, 173], adopting an auxiliary scalar field results to a pair of operators in an extended theory instead of the usual nonlocal operators. In this case, a renormalization prescription reduces to a three-parameter equation instead of a single equation for each z value, which characterizes the RI-type renormalization. J. Green et al. presented in [186] this nonperturbative approach and employed the twisted mass formulation on two ensembles that have pion mass of around 370 MeV and different lattice spacings ($a = 0.082, 0.064$ fm), in order to determine the three parameters of the auxiliary field renormalization scheme.

The auxiliary scalar color triplet field ($\zeta(\xi)$) is defined on the line $x + \xi n$, where ξ is the length of the Wilson line in physical units. The main component of the approach is the replacement of correlation functions with ones from the extended theory including the ζ field, which involve the local color singlet bilinear $\phi \equiv \bar{\zeta}\psi$. The introduction of the auxiliary field requires modification of the action (for details, see [186]), which yields a bare propagator in a fixed gauge background:

$$\left\langle \zeta(x+\xi n)\,\bar{\zeta}(x)\right\rangle_\zeta = \theta(\xi)\,e^{-m\xi} W(x+\xi n, x), \qquad m = a^{-1}\log(1+am_0). \tag{77}$$

In the above expression W is a straight Wilson line between points x and $x + \xi n$, and the exponent with the mass is an $O(a^{-1})$ counterterm. One obtains for the operator including the Wilson line, whose renormalization we are seeking,

$$\mathcal{O}_\Gamma(x,\xi,n) = \left\langle \overline{\phi}(x+\xi n)\,\Gamma\phi(x)\right\rangle_\zeta, \qquad \text{for } \xi > 0,\ m = 0. \tag{78}$$

Besides the counterterm m_0, the renormalization functions of the bilinear ϕ (Z_ϕ) and the operator $\mathcal{O}_\Gamma$ ($Z_{\mathcal{O}_\Gamma}$) must be calculated. Due to mixing allowed by the breaking of chiral symmetry, a proper renormalization is in this case

$$\phi_R = Z_\phi\left(\phi + r_{\text{mix}} \not{n}\phi\right), \qquad \overline{\phi}_R = Z_\phi\left(\overline{\phi} + r_{\text{mix}}\overline{\phi}\not{n}\right). \tag{79}$$

A different basis of operators may be employed to achieve diagonal renormalization in a mixing matrix; that is,

$$\mathcal{O}^R_\Gamma(x,\xi,n) = Z_\phi^2 e^{-m|\xi|}\mathcal{O}_{\Gamma'}(x,\xi,n), \qquad \Gamma' = \Gamma + r_{\text{mix}}\,\text{sgn}(\xi)\,\{\not{n},\Gamma\} + r^2_{\text{mix}}\not{n}\Gamma\not{n}. \tag{80}$$

As can be seen from the equations above, the renormalization of $\mathcal{O}_\Gamma$ requires knowledge of the linearly divergent m, the log-divergent Z_ϕ, and the finite r_{mix}. Note that r_{mix} is of similar

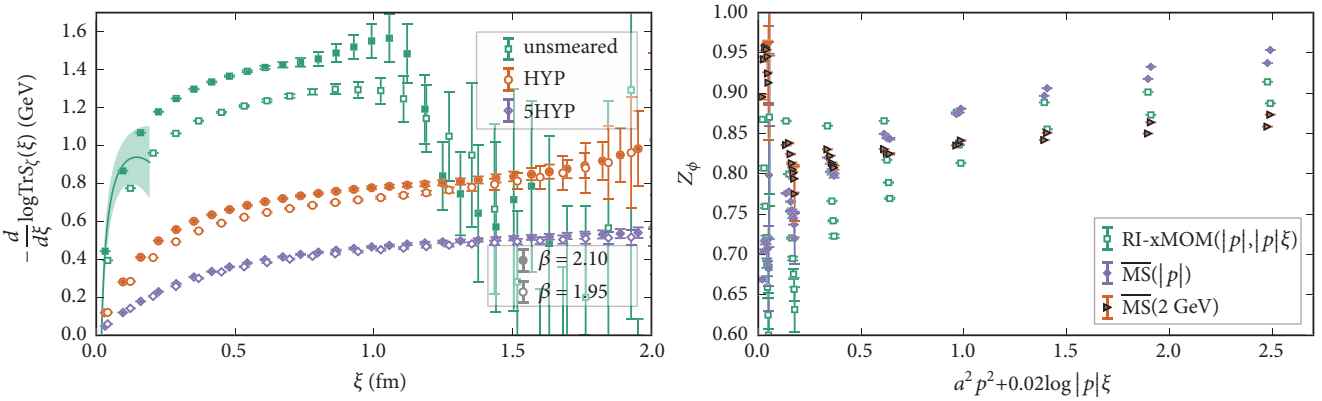

FIGURE 17: Left: Equation (81) for two lattice spacings with solid (open) symbols corresponding to the finer (coarser) lattice spacing. The curve shows the three-loop perturbative result, shifted vertically by $-m$ to match the unsmeared data on the finer lattice spacing. Right: Z_ϕ for $\beta = 2.10$, using unsmeared gauge links, for a range of p^2 and $y \equiv |p|\xi$; the horizontal axis is a^2p^2. The green open squares/ blue filled diamonds/ orange filled triangles show results in RI-xMOM / $\overline{\text{MS}}(|p|)$/ $\overline{\text{MS}}$(2GeV). Source: [186], reprinted with permission by the Authors (article published under the terms of the Creative Commons Attribution 4.0 International license).

nature as the mixing identified in [106]. In addition, this approach is not applicable for $\xi = 0$, in which case $\mathcal{O}_\Gamma$ is a local operator and its renormalization can be extracted from standard RI-type techniques.

In the work of [186], the Authors renormalized nucleon matrix elements obtained from two ensembles of $N_f = 2+1+1$ twisted mass fermions. For extracting the renormalization functions, they used ensembles of four degenerate quarks ($N_f = 4$) as expected for mass independent renormalization schemes. However, the chiral limit is yet to be taken for this approach. In summary, the three parameters and the auxiliary field renormalization, S_ζ, are determined by the RI-xMOM conditions

$$-\frac{d}{d\xi}\log \operatorname{Tr} S_\zeta(\xi)\Big|_{\xi=\xi_0} + m = 0, \tag{81}$$

$$\left[\frac{Z_\zeta}{3}\operatorname{Tr} S_\zeta(\xi_0)\right]^2 = \frac{Z_\zeta}{3}\operatorname{Tr} S_\zeta(2\xi_0), \tag{82}$$

$$\frac{1}{6}\frac{Z_\phi^\pm}{\sqrt{Z_\zeta Z_\psi}}\Re\operatorname{Tr}\left[S_\zeta^{-1}(\xi_0)\, G^\pm(\xi_0, p_0)\, S_\psi^{-1}(p_0)\right] = 1, \tag{83}$$

where S_ψ is the usual fermion field renormalization obtained from a standard RI-type prescription. As in the case of the nonperturbative schemes described in the previous paragraphs, a prescription is needed to bring the renormalized quasi-PDFs into the $\overline{\text{MS}}$ scheme and a conversion factor is necessary. This has been computed in DR to one-loop level in perturbation theory and the formula is given in [186].

Here, we present selected results from [186] and Figure 17 showing the quantity in Equation (81) (left panel) for the two ensembles discussed above with $a = 0.082$ fm ($\beta = 1.95$) and $a = 0.064$ fm ($\beta = 2.10$). As can be seen, smearing of the gauge links reduces the statistical noise but more importantly reduces the difference between the two ensembles. This is an evidence of reduction of the linear divergence. In case of no mixing (axial operator $\gamma^5\gamma^\mu$), r_{mix} is not relevant and only m_0 and Z_ϕ need to be determined. Z_ϕ is shown in the right panel of Figure 17 upon conversion to the $\overline{\text{MS}}$ scheme and evolution to the scale 2 GeV. The one-loop conversion factor removes the bulk of the dependence on the scheme parameter $|p|\xi$, and the two-loop evolution removes most of the dependence on the scale $|p|$.

7.5. Other Developments. In this subsection, we review some other developments related to the renormalization of PDF-related operators, in particular the Wilson-line-induced power divergence.

In 2016, the idea of removing such divergence by smearing was proposed by C. Monahan and K. Orginos [129]. It takes advantage of the properties of the gradient flow (GF), introduced by M. Lüscher a few years ago [191, 192] and applied to many problems in Lattice QCD [193]. As shown by Lüscher and P. Weisz in [194], it defines a 4+1-dimensional field theory, wherein the extra dimension is the flow time. The crucial property of GF, proven to all orders in perturbation theory, is that the correlation functions defined at nonzero flow time are finite after usual renormalization of the 4-dimensional theory. As such, GF defines a renormalization scheme with the flow time, τ, being the renormalization scale. Thus, using GF, one can define smeared quasidistributions, which are finite, in particular devoid of the power divergence from the presence of the Wilson line. Note that GF only regulates the UV behavior, leaving the IR structure intact, which is a prerequisite for factorization. The quasi-PDF results in the GF scheme can be converted perturbatively to other renormalization schemes or directly matched to light-cone PDFs, e.g., in the $\overline{\text{MS}}$ scheme. The Authors of [129] demonstrated a simple relation between the moments of the smeared quasi-PDF and the renormalized moments of the light-cone PDF. For this relation to be valid and to allow matching to light-cone PDFs, the scales in the problem have to satisfy $M_N \ll P_3 \ll \tau^{-1/2}$. Apart from usual higher-twist corrections, $\mathcal{O}(\Lambda^2_{\text{QCD}}/P_3^2)$, there are also

corrections of $\mathcal{O}(\Lambda^2_{\rm QCD}\tau)$. The explicit one-loop perturbative analysis of smeared quasi-PDFs was performed, in 2017, by C. Monahan [195]. It was shown that indeed the IR divergences of smeared quasi- and light-cone PDFs are the same. The perturbative computation led in the end to establishing the matching equation that could be used to extract light-cone PDFs from a lattice computation. An interesting aspect also shown by Monahan is that the smeared matrix element satisfies a relation akin to a usual renormalization group equation. This could, in principle, allow a nonperturbative step-scaling procedure to be defined, which would connect lattice-extracted matrix elements to high scales at which matching could be performed with much reduced truncation effects.

Smeared operators are the fundament of another method, introduced in 2012 by Z. Davoudi and M. Savage [196]. It aims at calculations of arbitrarily many moments of PDFs or other structure functions, that could, in principle, allow us to reconstruct the full distributions. The main idea is to avoid the power-divergent mixings with lower-dimensional operators in higher moments by removing their source, the breaking of rotational invariance by the lattice. The paper considers a mechanism for the restoration of this symmetry in the continuum limit of lattice field theories, in particular the $\lambda\phi^4$ theory and QCD. In general, the interpolating operators that are used to excite a hadron do not have definite angular momentum; i.e., it is not possible to assign a well-defined angular momentum to a lattice state and the latter is a linear combination of infinitely many different angular momentum states. The essence of the approach of [196] is to construct appropriate operators on the hypercubic lattice with maximum overlap with states with definite angular momentum in the continuum. Such operators are constructed on multiple lattice sites using smearing that renders the contributions of both lower- and higher-dimensional operators subleading and totally suppressed in the continuum limit. The Authors performed detailed calculations in the $\lambda\phi^4$ theory demonstrating the mechanism. For the QCD case, things are complicated by the gauge symmetry. However, Davoudi and Savage showed that the idea can also be applied for this case, relevant for moments of partonic functions. Apart from smearing of the operators, the essential ingredient is tadpole improvement. Recently, this approach has been revisited and exploratory numerical results were recently presented [197].

We finalize by shortly discussing one more method of dealing with the power divergence related to the Wilson line in quasidistributions. In 2016, H.-n. Li proposed [198] to modify the definition of such distributions by using "nondipolar" gauge links, i.e., two pieces of links oriented in orthogonal directions. He showed with an explicit calculation of one-loop corrections that the linear divergence of the standard quasiapproach (with dipolar links) is absent in such a case and the IR region is untouched. In general, the hadron boost direction needs to differ from the direction of the Wilson line links to avoid the linear divergence. However, due to developments in the renormalization of the power divergence (and other divergences present in quasidistributions), in particular the full nonperturbative renormalization, this interesting idea of Li has not been implemented in numerical calculations. Clearly, the implementation itself is possible, but much less practical than with straight links for the standard definition. It is also worth mentioning that [198] discussed also a potential problem with two-loop factorization of standard quasi-PDFs (but absent in the nondipolar ones). The power divergence in such setup induces an additional collinear divergence at the two-loop order, rendering the matching kernel IR divergent and breaking the factorization. However, the problem does not appear if the power divergence is properly renormalized [165].

8. Matching of Quasi-PDFs to Light-Cone PDFs

In this section, we focus on the matching from quasi-PDFs to light-cone PDFs. Since the inception of LaMET, there has been a lot of effort devoted to understanding many aspects of this procedure. In particular, the first matching paper [98], discussed in Section 3, considered the nonsinglet quark quasi- and light-cone PDFs in a simple transverse momentum cutoff scheme. Later work concentrated on matching from different renormalization schemes to the $\overline{\rm MS}$ scheme, on the issue of particle number conservation and on observables different than nonsinglet quark PDFs, in particular gluon PDFs, singlet quark PDFs, GPDs, TMDs, and meson DAs. We review all of the below and we also include a discussion on the matching of pseudo-PDFs/ITDs.

For convenience, we repeat here the general factorization formula for the matching:

$$\tilde{q}\left(x, \frac{\mu}{P_3}\right) = \int_{-1}^{1} \frac{dy}{|y|} C\left(\frac{x}{y}, \frac{\mu}{|y|\,P_3}\right) q\left(y, \mu^2\right) + \mathcal{O}\left(\frac{\Lambda^2_{\rm QCD}}{P_3^2}, \frac{M_N^2}{P_3^2}\right), \tag{84}$$

where μ is the common factorization and renormalization scale, and the second argument of the matching kernel C emphasizes that the relevant momentum is that of a parton.

Let us first briefly revisit the early attempt to remove the Wilson-line-related power divergence, discussed in Section 7, from the point of view of the matching process. We will then move to the presentation of the matching of $\overline{\rm MS}$-renormalized and RI-renormalized quasi-PDFs. T. Ishikawa et al. discussed in [132] that the counterterm that subtracts this divergence to all orders in the coupling can be provided by an independent lattice observable that shares the same power divergence as the nonlocal operator defining the quasi-PDF. It was noted that a natural and simple choice for such an observable is the static $q\bar{q}$ potential. The Authors calculated the matching (to PDFs in the UV cutoff scheme) in one-loop lattice perturbation theory for the case of naive fermions. The idea was also followed in [177], where J.-W. Chen, X. Ji, and J.-H. Zhang defined improved quasi-PDFs with the power divergence, calculated from, e.g., the static potential, subtracted. The modification amounts to multiplication of bare matrix elements by an exponential factor, $\exp(-\delta m|z|)$.

The matching formulae of [98] are then modified by ignoring the terms containing the cutoff Λ.

8.1. Matching of Nonsinglet Quark Quasi-PDFs to the $\overline{MS}$ Scheme PDFs. One of the possibilities of renormalizing the quasi-PDF is to obtain it in the $\overline{\text{MS}}$ scheme. Obviously, this scheme cannot be directly applied on the lattice and, hence, nonperturbative renormalization of lattice matrix elements proceeds via an intermediate scheme, like a variant of RI (see Section 7). Having renormalization functions in such an intermediate scheme, one then converts them perturbatively to the $\overline{\text{MS}}$ scheme and evolves to some reference scale, like 2 GeV. The last step is the Fourier transform that yields the quasi-PDF in the $\overline{\text{MS}}$ scheme.

The first paper that considered the matching from $\overline{\text{MS}}$ quasi-PDF was [142] by W. Wang, S. Zhao, and R. Zhu. The Authors presented complete matching for quarks and gluons, that we discuss more below in Section 8.2. For the case of nonsinglet quark PDFs (with $\Gamma = \gamma_3$ or $\Gamma = \gamma_5\gamma_3$ Dirac structure), it was found that the change with respect to [98] is simple; the terms with the transverse momentum cutoff Λ do not appear and there is a modified polynomial dependence in the physical region of quasi-PDFs. Explicitly, the matching kernel reads

$$C^{\overline{\text{MS}}}_{\text{Ref.}[142]}\left(\xi, \frac{\mu}{|y|\,P_3}\right) = \delta(1-\xi) + \frac{\alpha_s C_F}{2\pi}\begin{cases}\left(\dfrac{1+\xi^2}{1-\xi}\ln\dfrac{\xi}{\xi-1}+1\right)_{+(1)} & \xi > 1\\ \left(\dfrac{1+\xi^2}{1-\xi}\ln\dfrac{y^2P_3^2}{\mu^2}(4\xi(1-\xi)) + \dfrac{\xi^2-5\xi+2}{1-\xi}\right)_{+(1)} & 0<\xi<1\\ \left(-\dfrac{1+\xi^2}{1-\xi}\ln\dfrac{-\xi}{1-\xi}-1\right)_{+(1)} & \xi<0,\end{cases} \tag{85}$$

where we now use the notation with plus functions at $x = x_0$ over some domain of integration D, defined as

$$\int_D dx\,[f(x)]_{+(x_0)}\,g(x) = \int_D dx\,f(x)\,[g(x)-g(x_0)]. \tag{86}$$

However, one more issue remained unresolved for the $\overline{\text{MS}}$ to $\overline{\text{MS}}$ matching. Namely, the self-energy corrections have a UV divergence in the limit $\xi \longrightarrow \pm\infty$ (cf. Equation (85)). Thus, the form of the matching kernel in [142] still needs a cutoff for the ξ-integration. The issue was addressed by T. Izubuchi et al. in [83]. The aforementioned divergence can be canceled by adding a term $3/2\xi$ (for $\xi > 1$) or $3/2(1-\xi)$ (for $\xi < 0$) to the self-energy corrections. In the $\overline{\text{MS}}$ scheme, another term arises from this modification, outside of the integral sign, and finally the matching kernel reads

$$C^{\overline{\text{MS}}}_{\text{Ref.}[83]}\left(\xi, \frac{\mu}{|y|\,P_3}\right) = \delta(1-\xi) + \frac{\alpha_s C_F}{2\pi}\begin{cases}\left(\dfrac{1+\xi^2}{1-\xi}\ln\dfrac{\xi}{\xi-1}+1+\dfrac{3}{2\xi}\right)_{+(1)} - \dfrac{3}{2\xi} & \xi > 1\\ \left(\dfrac{1+\xi^2}{1-\xi}\ln\dfrac{y^2P_3^2}{\mu^2}(4\xi(1-\xi)) - \dfrac{\xi(1+\xi)}{1-\xi} + 2\iota(1-\xi)\right)_{+(1)} & 0<\xi<1\\ \left(-\dfrac{1+\xi^2}{1-\xi}\ln\dfrac{-\xi}{1-\xi}-1+\dfrac{3}{2(1-\xi)}\right)_{+(1)} - \dfrac{3}{2(1-\xi)} & \xi<0,\end{cases} \tag{87}$$
$$+\frac{\alpha_s C_F}{2\pi}\delta(1-\xi)\left(\frac{3}{2}\ln\frac{\mu^2}{4y^2P_3^2}+\frac{5}{2}\right),$$

where $\iota = 0$ for $\Gamma = \gamma_0$ and $\iota = 1$ for $\Gamma = \gamma_3$ or $\Gamma = \gamma_5\gamma_3$. Note that the polynomial term in the physical interval agrees with the one of [142] when $\iota = 1$. Equation (87) is the pure $\overline{\text{MS}}$ expression for the matching kernel. However, it violates particle number conservation; i.e., $\int_{-\infty}^{+\infty} dx\,\widetilde{q}(x,\mu/P_3) \neq \int_{-1}^{+1} dx\,q(x,\mu^2)$ after the matching process. Moreover, the violation grows for increasing P_3. To satisfy particle number conservation, the Authors proposed a modified scheme, the so-called "ratio scheme." It is a modification of the $\overline{\text{MS}}$ scheme, in which the problem is avoided by using pure plus functions:

$$C^{\mathrm{r}}\left(\xi, \frac{\mu}{|y|\,P_3}\right) = \delta(1-\xi) + \frac{\alpha_s C_F}{2\pi}\begin{cases}\left(\dfrac{1+\xi^2}{1-\xi}\ln\dfrac{\xi}{\xi-1} + 1 - \dfrac{3}{2(1-\xi)}\right)_{+(1)} & \xi > 1\\ \left(\dfrac{1+\xi^2}{1-\xi}\left[\ln\dfrac{y^2P_3^2}{\mu^2}(4\xi(1-\xi)) - 1\right] + 1 + 2\imath(1-\xi) + \dfrac{3}{2(1-\xi)}\right)_{+(1)} & 0 < \xi < 1\\ \left(-\dfrac{1+\xi^2}{1-\xi}\ln\dfrac{-\xi}{1-\xi} - 1 + \dfrac{3}{2(1-\xi)}\right)_{+(1)} & \xi < 0.\end{cases} \tag{88}$$

In this scheme, all regions in the ξ-integration of the plus functions contain the same $3/2(1-\xi)$ term and no additional term appears. Formally, this is a different renormalization scheme and, hence, the quasi-PDF used in the matching procedure needs to be renormalized in this scheme. This requires a relatively simple modification of the perturbative conversion from the intermediate renormalization scheme to $\overline{\mathrm{MS}}$:

$$C_0\left(\mu^2 z^2\right) = 1 + \frac{\alpha_s C_F}{2\pi}\left[\frac{3}{2}\ln\left(\frac{\mu^2 z^2 e^{2\gamma_E}}{4}\right) + \frac{5}{2}\right]. \tag{89}$$

This factor simply multiplies the conversion factor or the Z-factors.

Alternative procedure was used in [124] by ETMC. Similarly to the ratio scheme, the matching kernel contains only pure plus functions:

$$C^{\mathrm{M}\overline{\mathrm{MS}}}_{\mathrm{Ref.[124]}}\left(\xi, \frac{\mu}{|y|\,P_3}\right) = \delta(1-\xi) + \frac{\alpha_s}{2\pi}C_F\begin{cases}\left[\dfrac{1+\xi^2}{1-\xi}\ln\dfrac{\xi}{\xi-1} + 1 + \dfrac{3}{2\xi}\right]_{+(1)} & \xi > 1\\ \left[\dfrac{1+\xi^2}{1-\xi}\ln\dfrac{y^2P_3^2}{\mu^2}(4\xi(1-\xi)) - \dfrac{\xi(1+\xi)}{1-\xi} + 2\imath(1-\xi)\right]_{+(1)} & 0 < \xi < 1\\ \left[-\dfrac{1+\xi^2}{1-\xi}\ln\dfrac{\xi}{\xi-1} - 1 + \dfrac{3}{2(1-\xi)}\right]_{+(1)} & \xi < 0.\end{cases} \tag{90}$$

It amounts to the kernel of Equation (87) but without the terms outside the plus functions and without the additional P_3-dependent term outside of the integral and, thus, satisfies the particle number conservation requirement by construction. Similarly to the ratio scheme, it is a modification of the $\overline{\mathrm{MS}}$ scheme (that we denote by $\mathrm{M}\overline{\mathrm{MS}}$ in the superscript), thus requiring modification of conversion. In the procedure used by ETMC [124], this conversion modification was not taken into account, on grounds that the modification of $\overline{\mathrm{MS}}$ is done only in the unphysical region and it disappears in the infinite momentum limit. After the publication of [124], ETMC has calculated the required conversion modification that was presented in the results of [51]. More details can be found in [185]. As anticipated, the effect is numerically very small and the ensuing light-cone PDFs are compatible with the ones obtained from the simplified procedure. This is in contrast with the ratio scheme, wherein the modification of the physical region in the matching kernel, combined with the C_0 factor of Equation (89), brings about large modification of the quasi-PDF and the final $\overline{\mathrm{MS}}$ light-cone PDF [185].

The matching kernel for transversity PDFs ($\Gamma = \sigma_{31}, \sigma_{32}$) for the $\overline{\mathrm{MS}} \longrightarrow \overline{\mathrm{MS}}$ matching has been calculated by ETMC in [48], following the same method to preserve particle number. Thus, it also needs the conversion modification that will be shown in [185]. Explicitly, it reads

$$\delta C^{\mathrm{M}\overline{\mathrm{MS}}}\left(\xi, \frac{\mu}{|y|\,P_3}\right) = \delta(1-\xi) + \frac{\alpha_s}{2\pi} \cdot C_F\begin{cases}\left[\dfrac{2\xi}{1-\xi}\ln\dfrac{\xi}{\xi-1} + \dfrac{2}{\xi}\right]_{+(1)} & \xi > 1\\ \left[\dfrac{2\xi}{1-\xi}\ln\dfrac{y^2P_3^2}{\mu^2}(4\xi(1-\xi)) - \dfrac{2\xi}{1-\xi}\right]_{+(1)} & 0 < \xi < 1\\ \left[-\dfrac{2\xi}{1-\xi}\ln\dfrac{\xi}{\xi-1} + \dfrac{2}{1-\xi}\right]_{+(1)} & \xi < 0.\end{cases} \tag{91}$$

The formula for the transversity case is not the same as the unpolarized and helicity distributions due to the different splitting function, different polynomial dependence in the physical region, and different term added in the nonphysical regions to renormalize the UV divergence in the self-energy corrections.

An alternative way of bringing the results from the intermediate RI renormalization scheme to the $\overline{\mathrm{MS}}$ scheme is to match directly the RI-renormalized quasi-PDFs onto the $\overline{\mathrm{MS}}$ light-cone PDFs. This way was advocated by I. Stewart and Y. Zhao [166], including the derivation of the relevant formulae. Such one-step procedure can be used as the sole means of obtaining light-cone PDFs or compared to the two-step procedure (first conversion to $\overline{\mathrm{MS}}$ and evolution to a reference scale and matching as the second step), with differences in the final PDFs taken as a measure of systematic

uncertainty. Both procedures have been derived to one-loop order in perturbation theory, but clearly they can differ in the magnitude of neglected higher-order contributions. The derivation of the RI$\longrightarrow$ $\overline{\text{MS}}$ matching is somewhat more complicated than that for the $\overline{\text{MS}} \longrightarrow \overline{\text{MS}}$ case. Stewart and Zhao presented it (for the $\Gamma = \gamma_3$ or $\Gamma = \gamma_5\gamma_3$ Dirac structures) in the general covariant gauge, including the practically relevant case of the Landau gauge, typically implemented on the lattice. They also showed a detailed numerical study of the dependence on the choice of the gauge and on the initial and final scales. While the $\overline{\text{MS}} \longrightarrow \overline{\text{MS}}$ matching has only one scale involved, the RI$\longrightarrow$ $\overline{\text{MS}}$ case depends on three scales: the final $\overline{\text{MS}}$ scale and the two scales of the RI scheme: the overall scale and the scale defined by the momentum in the 3-direction. Explicit checks showed that, when aiming at a result at some reference $\overline{\text{MS}}$ scale, the dependence on the intermediate RI scales is rather small. It is important to note that the RI$\longrightarrow$ $\overline{\text{MS}}$ conserves the particle number and also that the problem with the UV divergence in self-energy corrections does not appear, since the RI scheme introduces a counterterm to the quasi-PDF that cancels this divergence. Results for the $\Gamma = \gamma_0$ case and for transversity PDFs matching were presented in [49, 199] by Y.-S. Liu et al. For final RI$\longrightarrow$ $\overline{\text{MS}}$ matching formulae, we refer to the original publications.

8.2. Matching of Other Quasidistributions and Pseudodistributions. In this section, we review other developments in the matching of quasidistributions to their light-cone counterparts. We also shortly discuss the matching process for the pseudo-PDFs/ITDs.

GPDs. Apart from PDFs, also other kinds of parton distributions can be accessed on the lattice via LaMET. Already in 2015, matching was worked out for GPDs, for (nonsinglet) unpolarized and helicity in [115] and for transversity in [200]. In both papers, the transverse momentum cutoff was used, as in the first paper for the matching of PDFs. The lattice matrix elements are extracted in a similar way as for quasi-PDFs, but there is momentum transfer in the boost direction between the source and the sink, Δ^3. The obtained quasi-GPD can be decomposed into two functions, $\mathscr{H}(x,\xi,t,P_3)$ and $\mathscr{E}(x,\xi,t,P_3)$, for the unpolarized case, and $\widetilde{\mathscr{H}}$, $\widetilde{\mathscr{E}}$, for helicity (chiral-even), and four functions $\mathscr{H}_T$, $\widetilde{\mathscr{H}}_T$, $\mathscr{E}_T$, $\widetilde{\mathscr{E}}_T$, for transversity (chiral-odd), where the additional variables with respect to standard PDFs are $\xi = \Delta^3/2P_3$ and $t = \Delta^2$. For $\xi = t = 0$, the $\mathscr{H}(x,0,0)$, $\widetilde{\mathscr{H}}(x,0,0)$, and $\mathscr{H}_T(x,0,0)$ quasifunctions become the standard quasi-PDFs and all the $\mathscr{E}$ functions and $\widetilde{\mathscr{H}}_T$ have no quasi-PDF counterparts. After matching, the x-integrals of unpolarized H and E give the Dirac and Pauli form factors $F_1(t)$ and $F_2(t)$, respectively. The x-integrals of helicity $\widetilde{H}$ and $\widetilde{E}$ give the generalized axial and pseudoscalar form factors $G_A(t)$ and $G_P(t)$. Finally, the first moments of transversity GPDs give the generalized tensor form factors $G_T(t)$, $\widetilde{A}_{T10}(t)$, $B_{T10}(t)$, and $\widetilde{B}_{T10}(t) = 0$, for H_T, $\widetilde{H}_T$, E_T, and $\widetilde{E}_T$, respectively. In the papers [115, 200], it was shown that the matching is nontrivial for the functions $\mathscr{H}$, $\widetilde{\mathscr{H}}$, and $\mathscr{H}_T$ and reduces to the matching for the corresponding quasi-PDFs in the forward limit, as expected. In turn, the matching kernel for all the $\mathscr{E}$ functions is a trivial δ-function at leading order in the coupling. The fourth transversity quasi-GPD, $\widetilde{\mathscr{H}}_T$, is power suppressed by the hadron momentum and omitted at leading power accuracy. We refer to the original publications for the final matching formulae. It is worth mentioning that, for quasi-PDFs, the formulae decompose into three intervals in x, the physical one and two nonphysical ones outside of the partonic support for x, whereas for quasi-GPDs there are, in general, four intervals with different matching functions for the physical ERBL ($-\xi < x < \xi$) and DGLAP ($-1 < x < -\xi$ and $\xi < x < 1$) regions.

Complete Matching for Quark and Gluon PDFs. In 2017, the first calculation of the matching of gluon quasi-PDFs to light-cone PDFs was done by W. Wang, S. Zhao, and R. Zhu [142]. This paper was already discussed in the previous subsection in the context of $\overline{\text{MS}} \longrightarrow \overline{\text{MS}}$ matching for nonsinglet quark PDFs. However, the aim of the paper was more broad, to consider the complete matching for quark and gluon quasi-PDFs. The Authors used two ways to regulate UV divergences: the UV cutoff scheme and DR, and also two ways for IR divergences: finite gluon mass and offshellness. The gluon quasi-PDF was defined as the Fourier transform of a boosted nucleon matrix element of two gluon field strength tensors $F_{\mu\nu}$ displaced by length z and connected with a Wilson line in the adjoint representation, $\langle P|F_{i3}(z)\widetilde{W}(z)F_{i3}(0)|P\rangle$, with a sum over transverse directions, $i = 1,2$. The Authors calculated the one-loop expressions for gluon quasi-PDFs and light-cone PDFs in the UV cutoff scheme and confirmed they have the same infrared structure, with IR divergences present only in the physical x region, as expected. They also noted the presence of a linear divergence in the quasidistribution, however, related in the gluon case not only to the presence of the Wilson line. Having performed the calculation in the UV cutoff scheme, they pointed to a difficulty in the self-energy diagram, coming from the breaking of gauge invariance by this scheme. This motivated further computations in DR, performed for both quark and gluon quasi- and light-cone PDFs. They considered all possible cases of quark-in-quark, gluon-in-gluon, gluon-in-quark, and quark-in-gluon distribution functions, required for the complete matching. The quark-in-quark matching, the only one relevant for the nonsinglet quark distributions, has already been described above; see Equation (85). Together with the derived equations for the other cases, one is ready to write the final matching formula:

$$\widetilde{f}_{i|H}(x,P_3) = \int_{-1}^{1} \frac{dy}{|y|} Z_{ij}\left(\frac{x}{y}, \frac{\mu}{P_3}\right) f_{j|H}(y,\mu), \tag{92}$$

where f ($\widetilde{f}$) denotes the light-cone (quasi-) distribution. The indices $i, j = q, g$ and the four cases mentioned above correspond to matching kernels Z_{qq}, Z_{gg}, Z_{gq}, and Z_{qg}, respectively. The matching equation implies mixing under matching between quark and gluon distributions, which can only be avoided in nonsinglet quark distributions. Finally, the

Authors derived P_3 evolution formulae for quasidistributions that turned out to be the DGLAP evolution equations of light-cone PDFs.

In a follow-up work [136], W. Wang and S. Zhao considered in more detail the issue of the power divergence in quasigluon PDFs; see Section 5.2.2 for more details from the point of view of renormalizability. As remarked above, linear divergences exist also in one-loop diagrams without a Wilson line, which means that the divergence cannot be absorbed into the renormalization of the Wilson line. The adopted definition of the gluon quasi-PDF was slightly modified with respect to [142] by extending the sum in $\langle P|F_{\mu 3}(z)\widetilde{W}(z)F_{\mu 3}(0)|P\rangle$ from the transverse directions to all directions except the direction of the boost; i.e., $\mu = 0, 1, 2$. The calculation of one-loop corrections to quasigluon distributions was performed in a UV cutoff scheme, with the cutoff interpreted as the lattice cutoff. The Authors included diagrams arising in lattice perturbation theory (counterterm from the measure in the path integral and quark and ghost tadpoles) that preserve the gauge invariance, broken in the naive cutoff scheme. The main result of the paper, derived in the auxiliary field formalism, is that the linear divergences can be renormalized by considering the contribution from operator mixing (only with certain gluonic operators, i.e., no mixing with quark quasi-PDFs occurs) and the mass counterterm of the Wilson line. This allowed the Authors to define an improved quasigluon PDF with matrix elements multiplied by $\exp(-\delta m|z|)$, where the mass counterterm can be determined nonperturbatively, and with a subtraction of the mixing calculated in perturbation theory. In addition to the one-loop calculation, they discussed two-loop corrections and conjectured that they hold to all orders. Finally, they provided the formula for the one-loop matching of the improved gluon quasi-PDF, which is IR finite and free from the linear UV divergence.

The proof of renormalizability to all orders was indeed provided a few months later by the same Authors, together with J.-H. Zhang, X. Ji, and A. Schäfer [137] (see Section 5.2 for more details on this paper and another proof of renormalizability of gluon quasi-PDFs [138]). From the point of view of matching, the important contribution of this paper was to confirm that the conclusions of [136] hold when using gauge-invariant DR instead of the UV cutoff scheme. Moreover, it was pointed out that one can construct gluonic operators that are multiplicatively renormalizable; i.e., they evince no mixing under renormalization. However, mixing still occurs at the level of matching, as in Equation (92). The Authors wrote schematic matching equations for the proposed nonperturbatively renormalized gluon quasi-PDFs in the RI/MOM scheme, postponing the calculation of the matching kernels RI$\longrightarrow \overline{\text{MS}}$ to a forthcoming publication. The latter computation, as well as the alternative possibility of RI$\longrightarrow \overline{\text{MS}}$ conversion and $\overline{\text{MS}} \longrightarrow \overline{\text{MS}}$ matching, will open the prospect of obtaining light-cone gluon PDFs in the $\overline{\text{MS}}$ scheme from the lattice.

TMDs. Yet another important class of partonic distributions that can, in principle, be accessed on a Euclidean lattice is TMDs. The quasi-TMDs were considered already in 2014 by X. Ji and collaborators in [201]. They performed a one-loop perturbative calculation of quasi-TMDs in the Drell-Yan process. The crucial subtlety that makes the TMD case much more cumbersome than the PDF case is the subtraction of the soft term. It needs to be constructed in such a way to make it computable on the lattice. It is related to the presence of a light-cone singularity in TMDs. The unsubtracted matrix element for quasi-TMDs, $q(x, k_T)$, is defined as the correlation between a quark and an antiquark in a boosted nucleon, with the quark fields spatially separated by a distance z and connected by two gauge links: one going from the quark field to infinity (for Drell-Yan) and the second one from infinity to the antiquark (in the covariant gauge; in the axial gauge an explicit link at infinity is additionally needed). The TMD depends on the longitudinal momentum fraction, x, and the transverse momentum, k_T, where the latter is often exchanged for the impact parameter, b_T, via a two-dimensional Fourier transform. Having defined the quasi-TMD, the Authors proposed a lattice-calculable subtraction of the soft factor. The latter was conjectured to also play an important role in the two-loop matching for quasi-PDFs, where it could be handled similarly. Further, they proceeded with the derivation of the one-loop formulae and demonstrated the one-loop factorization. Finally, they also considered the TMD evolution (Collins-Soper evolution) in the scale ζ related to the hadron momentum or the hard scale of the scattering process.

Early in 2018, X. Ji et al. reinvestigated quasi-TMDs [202]. They considered gauge links of finite lengths (staples), instead of infinite ones. Moreover, they redefined the subtraction of the soft factor, since the one defined in [201] could have practical implementation difficulties on the lattice. With this modified subtraction and finite-link TMDs, the Authors could show that the so-called pinch pole singularities are regulated. The new subtraction leads to an additional term in the one-loop computation of the quasi-TMD. Before establishing the matching formula, resummation of large logarithms needed to be performed to avoid scheme dependence in regulating light-cone singularities. This could be done using the Collins-Soper evolution derived in [201]. Finally, the matching equation was given to the TMDs in the standard TMD scheme.

Very recently, a third paper considering quasi-TMDs appeared by M. Ebert, I.W. Stewart, and Y. Zhao [203]. TMDs depend on two scales, the virtuality scale μ and the scale ζ introduced above. Evolution in the former can usually be done fully perturbatively, á la DGLAP. For the latter, the (Collins-Soper) evolution involves the impact parameter dependent anomalous dimension, $\gamma_\zeta^q(\mu, b_T)$ (q – parton flavor index), and becomes nonperturbative for transverse momenta of the order of Λ_{QCD}, even for $\mu \gg \Lambda_{\text{QCD}}$. The focus of this paper was on this aspect. The Authors proposed a method of a first-principle nonperturbative determination of γ_ζ^i, using the quasi-TMD formalism. They defined the quasibeam function (unsubtracted quasi-TMD) with finite-length (L) gauge links that can be related to the corresponding light-cone beam function. However, for the soft function that provides the subtraction of the soft term, they argued that a straightforward definition of a quasianalogue is not

possible, since the Wilson lines of the soft function involve both light-cone directions and would require opposite boosts to be recovered from Wilson lines in the spatial directions. A detailed study of this aspect was postponed to a forthcoming publication. For this paper, the Authors introduced a function that describes the missing IR physics and b_T-dependence, $\Delta_S^q(b_T, a, L)$. This function removes the L/a linear divergences in the Wilson line self-energy and an explicit form that cancels all divergences in L may be used in the form proposed in [202]. The crucial aspect for the extraction of γ_ζ^i is that the Δ_S^q factor cancels in the ratios of quasi-TMDs defined at different nucleon boosts. The matching between quasi-TMDs and light-cone TMDs can be spoiled by the issue in the soft function and the Authors introduced a function g_q^S expressing the mismatch between quasi- and light-cone soft functions and allowed it to be nonperturbative. They expressed the quasi-TMD in terms of the light-cone TMD for the nonsinglet case via the perturbative kernel (matching between quasi- and light-cone beam functions), the unknown g_q^S and the Collins-Soper anomalous dimension. Knowing the Δ_S^q that matches the IR physics of the light-cone soft function, the g_q^S could also be calculated perturbatively. The interpretation of the matching equation differs from the analogous one in [202], wherein the analogue of g_q^S is assumed to be fully perturbative, which is claimed to be incorrect due to missing the nonperturbative physics when b_T is of order $\Lambda_{\mathrm{QCD}}^{-1}$. Taking the ratio of two matching equations, the P_3-independent factor g_q^S drops out and one can extract the anomalous dimension based on the perturbative matching relation between the quasi- and the standard beam functions. The method was illustrated by an explicit one-loop computation. It was also remarked that it is restricted to the nonsinglet quark channel, because of mixings between singlet quarks and gluons under matching (see the previous paragraph).

Meson DAs. Another type of observables that can be considered in the framework of LaMET is meson DAs. They are defined as vacuum-to-meson matrix elements of the same operator as for PDFs, quark, and antiquark connected with a Wilson line, with Γ-structure of, e.g., $\gamma^5\gamma^3$, for pseudoscalar mesons. They are easier to calculate, since they require only two-point functions, as the pion is not annihilated in the matrix element. The matching can be extracted as a limit of the matching formula for GPDs by crossing the initial quark to the final state and it was extracted for the first time (for the pseudoscalar case) in the paper [115] commented on above. We refer to this paper for explicit matching formulae in the transverse momentum cutoff scheme.

Further, (pseudoscalar) meson mass corrections were calculated analytically in [123], yielding an infinite series in which the few first terms are enough to take into account for practical application.

The heavy quarkonium case was considered in [125] by Y. Jia and X. Xiong, with the one-loop corrections to both quasi- and light-cone DAs computed in the framework of NRQCD factorization. The matching for meson DAs and PDFs was also analyzed by Jia et al. within two-dimensional QCD [126]. In both papers, the UV divergences were regulated with a transverse momentum cutoff, interpreted as a renormalization scale. For more details about these two papers, see Section 4.4.

The matching for vector meson DAs was also considered [204], by J. Xu, Q.-A. Zhang, and S. Zhao. They derived the formulae in the UV cutoff scheme and in DR (with $\overline{\mathrm{MS}}$ subtraction), both for longitudinally and transversely polarized mesons.

Recently, the matching for meson DAs was also obtained for the case of RI-renormalized quasi-DAs to bring them into $\overline{\mathrm{MS}}$-renormalized light-cone DAs [205], by Y.-S. Liu et al. They considered the cases of pseudoscalar, as well as longitudinally and transversely polarized vector mesons. The quasi-DA can be renormalized with the same renormalization factors as the corresponding quasi-PDF, in a variant of the RI/MOM scheme. The one-loop calculation of the matching relation proceeded along the lines of analogous computations for quasi-PDFs, first done in [166], and we refer to the original paper for the final formulae.

Pseudo-PDFs. The one-loop corrections to pseudo-PDFs were first considered in [87] by K. Orginos et al., in the leading logarithmic approximation (LLA), appropriate to study the $\ln z^2$ dependence. In the LLA, pseudo-PDFs are simply related to the $\overline{\mathrm{MS}}$ PDFs at the scale μ: $\mu^2 = 4\exp(-2\gamma_E)/z^2$, where $1/z$ plays the role of the renormalization scale for the pseudodistribution. The full one-loop corrections to pseudo-PDFs were calculated by X. Ji, J.-H. Zhang, and Y. Zhao [165] and also by A. Radyushkin [80]. Further insights into the structure of these corrections were given in [81] of Radyushkin, which also contains the explicit matching between reduced ITDs and standard light-cone PDFs in the $\overline{\mathrm{MS}}$ scheme. The matching was also simultaneously computed by two other independent studies: J.-H. Zhang, J.-W. Chen, C. Monahan [82], and T. Izubuchi et al. [83], and the preprints were made available for all three papers almost simultaneously. After initial discrepancies due to finite terms, all three results agree with one another.

The matching of pseudo-PDFs is, to some extent, simpler than that for quasi-PDFs, since there are no complications related to the nonperturbative renormalization of the pseudo-PDF when taking the ratio of matrix elements to construct the reduced ITD. Crucially, taking the ratio does not alter the IR properties and the factorization framework can be applied, as in the case of matching quasidistributions. We write here the final matching formula in the notation of [81]:

$$\mathcal{I}\left(\nu,\mu^2\right) = \mathfrak{M}\left(\nu,z^2\right) + \frac{\alpha_s}{2\pi}C_F\int_0^1 dw\,\mathfrak{M}\left(w\nu,z^2\right) \cdot\left\{B(w)\left[\ln\left(z^2\mu^2\frac{e^{2\gamma_E}}{4}\right)+1\right] + \left[4\frac{\ln(1-w)}{1-w} - 2(1-w)\right]_+\right\}, \tag{93}$$

where $\mathcal{I}(\nu,\mu^2)$ is the light-cone ITD, at Ioffe time $\nu = P_3 z$ and renormalized at the scale μ in the $\overline{\mathrm{MS}}$ scheme, $\mathfrak{M}(\nu,z^2)$ is the

pseudo-ITD at the scale $1/z^2$, and $B(w) = [(1+w^2)/(1-w)]_+$ is the Altarelli-Parisi kernel. The first term under the integral corresponds to the LLA result used in [87], i.e., the invoked above multiplicative difference between the pseudo-ITD and $\overline{\text{MS}}$ scales. The term containing $\ln(1-w)/(1-w)$ leads to a large negative contribution and causes that the z-dependence of vertex diagrams involving the gauge link is generated by an effective scale smaller than z. This can be seen by rewriting the matching equation in such a way that the logarithmic term has an argument $(1-w)z\mu e^{\gamma_E+1/2}/2$; i.e., it involves $(1-w)z$ instead of z. In this way, the evolution is governed by this combined logarithm instead of simple $\ln(z^2)$, which leads to $\mu \sim k/z_3$ rescaling with a coefficient k, numerically found to be relatively large, around 4 for the setup of [87] (cf. its LLA value of approximately 1.12).

In [83], the relation between quasi-PDFs, pseudo-PDFs, and ITDs was emphasized. This relation implies that their matching involves a unique factorization formula that involves small distances and large nucleon boosts. For these reasons, Izubuchi et al. claim that LaMET and pseudo-/Ioffe-time distribution approaches are, in principle, equivalent. However, it should be noted that the structure of one-loop corrections is different between them and, obviously, the lattice systematics are not equivalent. Because of this, in the absence of all-order (or nonperturbative) matching formulae and under realistic lattice situations, it seems more proper to view them as complementary approaches that aim at the same physical observables.

9. Quark Quasi-PDFs of the Nucleon

The preliminary studies presented in Section 3.2 have evolved based on the progress on various aspects of PDFs, including simulations with improved parameters, renormalization, and choice for the matching procedure. It is the goal of this section to present the advances in the numerical simulations, including a critical discussion on the systematic uncertainties outlined in Section 6. We first present results on ensembles with the quark masses tuned to produce a pion mass larger than its physical value, and we extend the discussion for the simulations with physical values for the quark masses (*physical point*). To avoid repetition, let us point out that all the works presented here correspond to the isovector flavor combination $u-d$, which receives contributions only from the connected diagram (up to cutoff effects).

9.1. Simulations at Unphysical Quark Masses. Once the nonperturbative renormalization of the nonlocal operators with straight Wilson line has been developed and presented to the community [105] (see Section 7.3), the first implementation for the quasi-PDFs appeared in the literature in 2017, by ETMC [151] in the RI′ scheme, and a modification of the proposal in the RI/MOM scheme by the LP^3 collaboration [181].

In the original proposal for the nonperturbative renormalization [151], Alexandrou et al. (ETMC) applied the renormalization prescription on their previous work of [108] for an ensemble with $M_\pi \approx 370$ MeV (see Section 3.2 for a discussion on the simulations). This employed large-statistics results for nucleon momentum 1.42 GeV and source-sink separation of about 0.98 fm, to demonstrate the effect of the renormalization for the helicity PDFs, which has a multiplicative renormalization, $Z_{\Delta h}$ [9]. The renormalization function was extracted in the $\overline{\text{MS}}$ scheme at a scale of 2 GeV, and the remaining dependence on the RI scale ($\overline{\mu}_0$) was reduced by an extrapolation:

$$Z_{\Delta h}^{\overline{\text{MS}}} = Z_{0,\Delta h}^{\overline{\text{MS}}} + Z_{1,\Delta h}^{\overline{\text{MS}}} \left(a\,\overline{\mu}_0\right)^2, \tag{94}$$

where $Z_{0,\Delta h}^{\overline{\text{MS}}}$ is the desired quantity. In the work of [151], the fit was performed in the range $(a\,\overline{\mu}_0)^2 \in [1.4, 2.0]$. One technical consequence of the renormalization is the behavior of the renormalized matrix element in the large-z region: while the real (imaginary) part of the bare matrix element decays to zero for $z/a > 10$ ($z/a > 13$), the renormalization function grows exponentially due to the power divergence. This leads to the unwanted effect of enhanced values for the matrix elements that are almost compatible with zero within uncertainties. This effect is propagated to the quasi-PDF (with the truncation of the integration limits of the Fourier transform), as well as the final extraction of the PDFs. Let us also add that, in the RI-type renormalization prescription, each value of z/a is renormalized independently. More discussion on this systematic effect can be found in Section 6.3.

A Fourier transform is applied on renormalized matrix elements leading to x-dependent quasi-PDFs, followed by the matching procedure and target mass correction to finally extract the light-cone PDFs. The obtained helicity PDF from the aforementioned work is shown in Figure 18. To demonstrate the effect of a proper renormalization, we compare the PDF computed with either fully renormalized matrix elements (blue band) or matrix elements renormalized with the local axial vector current renormalization function Z_A for all z values (magenta band) that was previously used in [108].

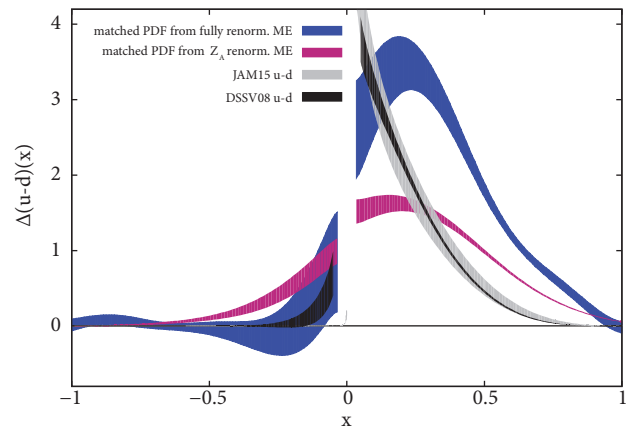

Figure 18: Comparison of lattice estimates of the ETMC's helicity PDF, properly renormalized (blue band) or renormalized using the local axial current renormalization factor Z_A (magenta band). For qualitative comparison, phenomenological PDFs (DSSV08 [206] and JAM15 [208]) are also plotted. Source: [151], reprinted with permission by the Authors (article available under CC BY).

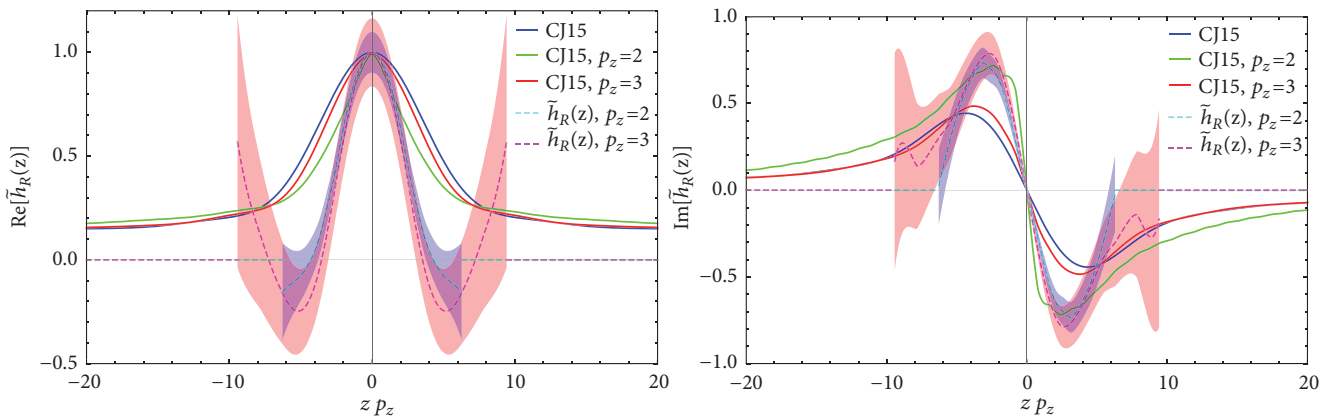

FIGURE 19: Real (left) and imaginary (right) part of LP^3's renormalized unpolarized matrix elements (dashed lines) and phenomenological PDFs compared in coordinate space as a function of zP_3. Data are presented for the scale of 5.76 GeV^2 in the $\overline{\text{MS}}$ scheme. The solid lines are the Fourier transforms of the corresponding CJ15 PDF (blue), after matching and mass corrections (green and red). Source: [181], reprinted with permission by the Authors (article published under the terms of the Creative Commons Attribution 4.0 International license).

As can be seen from the figure, the blue band has a form that is closer to the phenomenological PDFs, as compared to the magenta band. There is also a visual improvement for the antiquark region ($x < 0$), which, however, should not be considered conclusive, as this region is, to date, unreliably extracted.

Despite the improvement from previous works on quasi-PDFs, a number of further improvements were still necessary at this point, as described in Section 6.3. Let us also add that [151] employed the matching formula of Xiong et al. [98] that was obtained in the transverse momentum cutoff scheme and was later replaced by matching formulae calculated in dimensional regularization (see Section 8).

In the work of J.-W. Chen et al. (LP^3) presented in [181], a nonperturbative renormalization was also applied, using the RI/MOM scheme. They focused on results for the unpolarized PDF, which however uses the "γ^3" vector operator. The mixing present in this operator was ignored under the assumption that it is small. Indeed, the mixing coefficient is smaller than the multiplicative factor (see Figure 16), but the scalar operator (that mixes with "γ^3") is expected to be sizable. This can also be seen from the extraction of the scalar charge using the same ensemble, which has the bare value $g_S^{u-d} = 0.96(5)$ [232]. The RI/MOM renormalization scale is fixed to the nucleon momentum, P_3, which also appears in the matching and, thus, cancels to leading order. Even so, residual dependence on this scale can be nonnegligible (estimated to up to 10% based on studies with ultralocal operators ($z = 0$)) and an extrapolation would be desirable; otherwise this systematic uncertainty cannot be assessed.

The renormalization function of this work was used on the results obtained in [107] (for an ensemble with $M_\pi \approx 310$ MeV) for the unpolarized PDF, together with the matching obtained by I. Stewart and Y. Zhao [166] (see also Section 8.1). The matching formula of the latter work was the first one obtained for renormalized quasi-PDFs in the RI scheme matched to the light-cone PDFs in the $\overline{\text{MS}}$ scheme. A different kind of comparison between lattice and phenomenological data is presented in Figure 19. The renormalized matrix elements for the unpolarized case are compared to phenomenological data [214] on which an inverse Fourier transform and matching have been applied to bring them to coordinate space. This procedure was applied on the central values and, thus, statistical and systematic uncertainties are absent. It is found that the lattice data have a narrower peak around $zP_3 = 0$ (real part) and are not compatible with the CJ15 data for large values of the Ioffe time, zP_3. Note, however, that the lattice data carry very large uncertainties for the large-z region that prevents proper comparison. In addition, there are concerns on whether such a comparison is meaningful due to higher-twist effects.

A recent effort to quantify systematic uncertainties was presented by Y.-S. Liu et al. (LP^3) in [199], using an ensemble with pion mass value of about 310 MeV [188]. Clover valence fermions were employed on an $N_f = 2 + 1 + 1$ HISQ ensemble [233]. The lattice spacing is $a \approx 0.06$ fm, and the volume has a spatial extent $L \approx 2.9$ fm. In this work, Liu et al. computed the unpolarized PDF with nucleon momentum 1.7, 2.15, and 2.6 GeV, and source-sink separations that correspond to 0.60, 0.72, 0.84, 0.96, and 1.08 fm. The main goal of this work was to study uncertainties related to excited states, the nonperturbative renormalization, and the matching to light-cone PDFs. For the Fourier transform to momentum (x) space, the Authors used the derivative method [160], which is based on an integration by parts, instead of the standard Fourier transform. In this procedure, the corresponding surface term is neglected (see Section 6.3 for details), which carries systematic uncertainties; the latter is not addressed in this work.

Possibly the largest systematic effect comes from the excited states contamination, which is sensitive to the pion mass (worsens for simulations at the physical point) [39], an issue that also appears in matrix elements of local operators. In fact, the situation for the nonlocal operators entering the quasi-PDFs calculation is more severe, as the number of excited states increases with an increase of the nucleon momentum. The effect of excited states can be understood

using different analysis methods, as presented in Section 6.1, with the single- and two-state fits being crucial for identifying the ground state of the nucleon. This is particularly important for nonlocal operators that are limitedly studied and are less understood than other hadron structure quantities. Ideally, one should perform a combined analysis with source-sink separations higher than 1 fm. The need for two different analysis techniques is to ensure that the dominant excited states are eliminated by achieving convergence between different techniques. In addition, a single-state fit (applied on each source-sink separation separately) gives important information on the statistical uncertainties of the lattice data. Such information is not to be underestimated, as multistate fits will be driven by the most accurate data. Since statistical noise increases exponentially with the source-sink separation, the most accurate data typically correspond to small separations, which are severely affected by excited states contamination. In the work of Liu et al., the analysis is exclusively based on two-state fits using either all five separations, or four/three largest ones. The Authors did not provide any details on the statistics used in this work, nor the statistical accuracy of the data on each separation, leading to an inadequacy in the quality of their analysis procedure.

The work of [199] addressed systematic uncertainties related to a convenient choice of an RI-type scheme, by examining two possible projectors in the renormalization prescription. This was motivated by the fact that Green's function, $\Lambda_{\gamma^t}(p,z)$, of the unpolarized operator has additional tensor structures; that is,

$$\Lambda_{\gamma^t}(p,z) = \widetilde{F}_t(p,z)\,\gamma^t + \widetilde{F}_z(p,z)\,\frac{p_t\gamma^z}{p_z} + \widetilde{F}_p(p,z)\,\frac{p_t\not{p}}{p^2}, \tag{95}$$

where $\widetilde{F}_i$'s are form factors. The minimal projection only projects out $\widetilde{F}_t$, while an alternative choice for the projection is $\not{p}/(4p^t)$ [166], which we call the $\not{p}$ projection, leading to the conditions

$$Z_{mp}\left(z, p_z^R, a^{-1}, \mu_R\right) \equiv \widetilde{F}_t(p,z)\Big|_{\substack{p^2=-\mu_R^2 \\ p_z=p_z^R}}, \tag{96}$$

$$Z_{\not{p}}\left(z, p_z^R, a^{-1}, \mu_R\right) \equiv \left[\widetilde{F}_t(p,z) + \widetilde{F}_z(p,z) + \widetilde{F}_p(p,z)\right]\Big|_{\substack{p^2=-\mu_R^2 \\ p_z=p_z^R}}. \tag{97}$$

An appropriate matching formula to the $\overline{\text{MS}}$ scheme had been also derived for each RI scheme, and it was concluded that the minimal projector leads to better controlled final estimates, shown in Figure 20, compared with global analysis PDFs [210–212]. The Authors reported reasonable agreement with global analyses in small- and large-x regions, while the slope of the lattice data at intermediate x-values is different, possibly due to uncertainties in the derivative method for the Fourier transform. The pion mass of the ensemble used for the data is 310 MeV, making the comparison only qualitative.

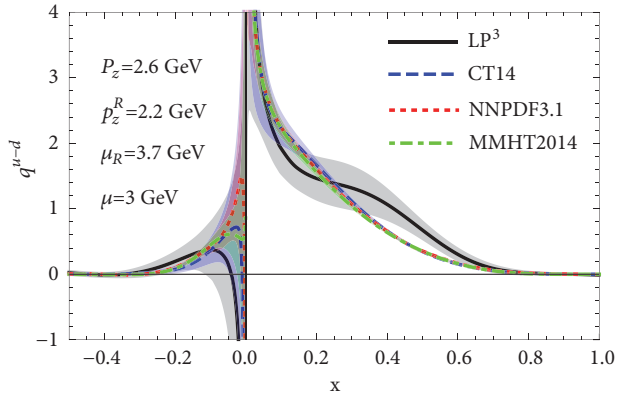

FIGURE 20: LP^3's final unpolarized PDF at $\mu = 3$ GeV calculated from RI/MOM quasi-PDF at nucleon momentum $P_z = 2.6$ GeV, compared with CT14nnlo (90CL) [210], NNPDF3.1 (68CL) [211], and MMHT2014 (68CL) [212]. Source: [199] (arXiv), reprinted with permission by the Authors.

9.2. Simulations at Physical Quark Masses. One of the highlights of the current year is the appearance of lattice results on quasi-PDFs using simulations at the physical point [10] by ETMC [48, 124] and LP^3 [49, 218, 219]. Unlike previous studies, these results include proper nonperturbative renormalization and an appropriate matching procedure, for the unpolarized, helicity, and transversity PDFs. We note that, in these works, the use of the Dirac structure parallel to the Wilson line, γ^μ, has been abandoned due to the mixing discussed in Section 7.2.2 and is replaced by the vector operator with the Dirac structure in the temporal direction, γ^0. Here we outline the most important results from each work.

9.2.1. Unpolarized and Helicity PDFs. The work by C. Alexandrou et al. (ETMC) presented in [124] is the first complete calculation of ETMC with several of the systematic uncertainties under control: simulations at the physical point, nonperturbative renormalization, matching to light-cone PDFs computed in dimensional regularization in the $\overline{\text{MS}}$ scheme. The ensemble corresponds to $N_f = 2$ twisted mass fermions (at maximal twist) with a clover improvement [234]. The ensemble has a lattice spacing of 0.093 fm, lattice spatial extent of 4.5 fm ($48^3 \times 96$), and a pion mass of 130 MeV. The nucleon matrix elements of the nonlocal vector and axial operator were computed for three values of the momentum, 0.83, 1.11, and 1.38 GeV, and employ momentum smearing on the nucleon interpolating field [109], that leads to a better signal for the high momenta at a reasonable computational cost (see also Section 6.2 for more details about optimization of the lattice setup). In addition, stout smearing [150] was applied to the links of the Wilson line entering the operator, that reduces the power divergence, and it was checked that different numbers of steps for the stout smearing lead to compatible (almost equivalent) renormalized matrix elements.

A large number of configurations is necessary to keep the statistical uncertainties under control, in particular, as

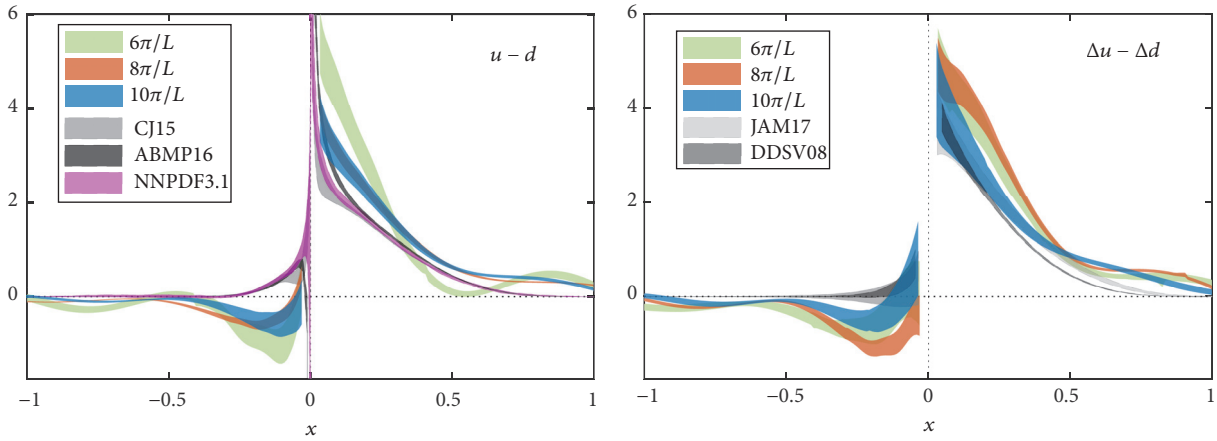

FIGURE 21: Comparison of ETMC's unpolarized (left) and helicity (right) PDF for momenta 0.83 GeV (green band), 1.11 GeV (orange band), and 1.38 GeV (blue band). The results from the phenomenological analysis of ABMP16 [213] (NNLO), NNPDF [211] (NNLO), CJ15 [214] (NLO), DSSV08 [206], NNPDF1.1pol [207], and JAM17 NLO phenomenological data [215] are displayed for illustrative purposes. Source: [124], reprinted with permission by the Authors (article published under the terms of the Creative Commons Attribution 4.0 International license).

the nucleon momentum increases. The work of [124] analyzed 9600, 38250 and 58950 independent correlators for the momenta 0.83, 1.11, and 1.38 GeV, respectively, so that statistical uncertainties are at the same level. A first study of excited states contamination was presented using only two values of the source-sink separation, 0.93 and 1.12 fm, and demonstrating that within statistical uncertainties the matrix elements are compatible. Nevertheless, a dedicated study of excited states is missing from the presentation and was recently completed [216], concluding that the separation 1.12 fm is sufficient for a nucleon momentum of about 1.5 GeV. We will discuss this investigation below.

The renormalization was performed according to the procedure outlined in Section 7.3.1 and the quasi-PDFs were extracted by the standard Fourier transform. The matching formula used in the work of ETMC was a modified expression with respect to the one suggested in [83] (see discussion is Section 8.1), that preserves the normalization of the distribution functions. However, there is a small mismatch in the renormalization procedure and the matching process, as the conversion factor brings the quasi-PDFs to the $\overline{\text{MS}}$ scheme, while the matching assumes that the quasi-PDFs are given in the M$\overline{\text{MS}}$ scheme. Preliminary investigation showed a small effect, but this mismatch adds to the overall systematic uncertainties. A follow-up work by ETMC eliminated this uncertainty by computing the quasi-PDFs in the proper M$\overline{\text{MS}}$ scheme [51, 185]. Nucleon mass corrections were applied according to the formulae of [107].

In Figure 21, we show the final results for the unpolarized (left) and helicity (right) distributions for the three values of the nucleon boost. For qualitative comparison, we also include the phenomenological determinations: CJ15 [214], ABMP16 [213], NNPDF3.1 [211], DSSV08 [206], NNPDF1.1pol [207], and JAM17 [215]. The Authors reported that the increase of the nucleon momentum shifts the lattice data towards the phenomenological results. For the unpolarized PDF, the two largest momenta give compatible result, while it is not the case for the helicity PDF. For the latter, there is better agreement with phenomenology, compared to the unpolarized case. As seen from the plots, the large-x region suffers from the so-called oscillations that are unphysical. This result from the fact that the bare matrix element does not decay to zero fast enough for large z (due to finite momentum), while the renormalization grows exponentially. It is worth mentioning that the oscillations become milder as the momentum increases from 0.83 GeV to 1.38 GeV. It is clear that there are several aspects of the current studies to be improved and the removal of the oscillations is one of them. For this to be achieved while systematic uncertainties are under control, different directions must be pursued, for instance, new techniques that can contribute to a reduction of the gauge noise in the correlators.

An interesting discussion presented in [124] is the comparison between results at the physical point and results from an ensemble with pion mass of about 370 MeV [108] (labeled as B55), as shown in Figure 22. The nucleon momentum is the same for both ensembles (≈1.4 GeV) and a clear pion mass dependence is observed. This is not surprising, as similar pion mass dependence is found in the first moment, $\langle x \rangle_{u-d}$, computed with other techniques in Lattice QCD.

A follow-up study by ETMC was presented recently [216] and focused on understanding systematic uncertainties originating from excited states contamination. This study used a high-statistics analysis for the physical point ensemble used in [124]. Four (three) source-sink separations (t_s) were used for the unpolarized (helicity and transversity) case, corresponding to 0.75, 0.84, 0.93, and 1.12 fm (0.75, 0.93, and 1.12 fm) in physical units. All three analysis techniques described in Section 6.1, that is a single-state fit for each separation t_s, a two-state fit, and the summation method, were used. For a reliable analysis, it is absolutely critical to keep the statistical uncertainties at the same level for all separations, and this is achieved with 4320, 8820, 9000, and 72990 measurements for the unpolarized PDFs at the

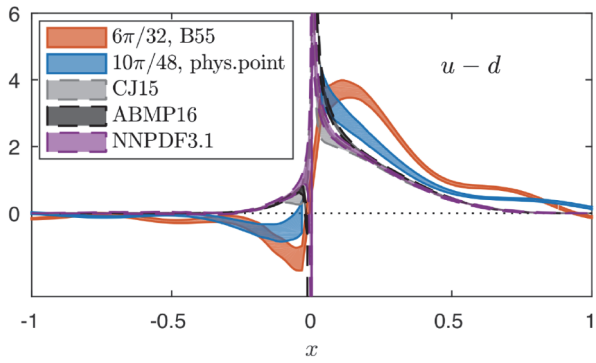

FIGURE 22: Comparison of ETMC's unpolarized PDF using the ensemble at the physical point [124] (blue) and the B55 ensemble (pion mass 370 MeV) [108] (orange) at momentum ≈1.4 GeV. Source: [124], reprinted with permission by the Authors (article published under the terms of the Creative Commons Attribution 4.0 International license).

four separations. For the helicity and transversity PDFs, the number of measurements is 3240, 7920, and 72990 for the separations $t_s = 8a, 10a, 12a$, respectively.

A comparison of the three methods for the helicity is presented in Figure 23, where one clearly observes the discrepancy between separations 0.75 and 1.12 fm for both the real and the imaginary parts. In addition, the real part (left plot) obtained for 0.93 fm is compatible with both 0.75 and 1.12 fm. The most striking effect of excited states for this particular study can be seen in the imaginary part (right plot), where separations 0.75 and 0.93 fm are compatible, but in huge disagreement with $t_s = 1.12$ fm, indicating that excited states are severe and one should focus on separations above 1 fm. The two-state fit is compatible with the results from the largest separation $t_s = 12a$, but not with the two lower separations in the imaginary part. The summation method has large statistical uncertainties and is not providing any useful information. Based on these findings, the Authors concluded that a source-sink separation of 1.12 fm for nucleon momentum up to ~1.5 GeV is sufficient for isolating the ground state dominance within statistical uncertainties. We would like to stress the importance of having raw lattice data with similar statistical precision to avoid bias in the various analysis techniques.

We now continue the discussion with a presentation of the work of LP^3 for the unpolarized distribution of [218]. The calculation was carried out using a mixed action setup of clover fermions in the valence sector on a HISQ $N_f = 2 + 1 + 1$ ensemble that has lattice spacing $a = 0.09$ fm, with spatial lattice extent $L \approx 5.8$ fm and a pion mass ≈135 MeV [188]. A single step of hypercubic smearing (HYP) was employed to improve discretization effects, but also to possibly address a delicate issue: the mixed action setup of clover on HISQ is nonunitary and suffers from exceptional configurations as the quark masses approach their physical value for a fixed lattice spacing [235, 236]. As a consequence, the results would be biased in the presence of exceptional configurations. Based on the empirical evidence of [235, 236] for local operators, it is expected that, for physical value of the pion mass, the ensembles with lattice spacing above 0.09 fm could be vulnerable to exceptional configurations. However, this problem is not addressed in the work of LP^3 for the quasi-PDFs, and a more concrete investigation is imperative to eliminate possible bias in the results.

In this work, the Gaussian momentum smearing [109] was employed, and the nucleon was boosted with momenta 2.2, 2.6, and 3 GeV. As pointed out by the Authors, one should be particularly cautious in the investigation of excited states contamination, which are expected to worsen with momentum boost, as the energy states come closer to each other. Thus, four variations of two-state fits were tested using source-sink separation of 0.72, 0.81, 0.90, and 1.08 fm giving compatible results. Despite the effort to employ different analysis techniques with the intention to eliminate excited states contamination, we believe that it is unlikely for this procedure to be conclusive, as the two-state fit alone does not guarantee reliability and the different variations used in the work of [218] are correlated. In addition, the success of the fits relies on having all correlators with similar accuracy; otherwise the fit is biased by the accurate data (typically at small values of the separation). Note that [218] does not report any measurements for the nucleon matrix elements. We stress that the statistical accuracy for the data should be verified from plots of the ratio on each separation that enters the fit.

The lattice data were properly renormalized using an RI-type scheme [181], as described in Section 7.3.2, and the quasi-PDFs were obtained using the "derivative" method. Finally, a matching appropriate for the choice of renormalization was applied [166, 181] to bring the final estimates in the $\overline{\text{MS}}$ scheme. This is an alternative to the procedure of ETMC in which a two-step process is used in order to bring the renormalized quasi-PDFs in the $\overline{\text{MS}}$ and then match using a proper matching formula. Both processes are equivalent to a one-loop correction, which is currently the level at which both the conversion and the matching formula are available. It is yet to be identified which process brings the final results closer to a two-loop correction; this will be possible once the two-loop expressions are extracted.

The final result for the unpolarized PDF is shown in the left plot of Figure 24, together with global fit data from CT14 [210], with agreement between the two within uncertainties. The same setup was applied for the helicity PDF presented in [219], where two values for the source-sink separations were added, giving $t_s = 0.54, 0.72, 0.81, 0.90, 0.99, 1.08$ fm. The number of measurements for each separation is 16000, 32000, 32000, 64000, 64000, and 128000, respectively; these data are used exclusively for a two-state fit, but it would certainly be critical to compare with plateau values and the summation method. The renormalization program includes various choices for the scales appearing in the RI and $\overline{\text{MS}}$ schemes, and we refer the Reader to [219] for details. The final estimates are given in the $\overline{\text{MS}}$ scheme at 3 GeV and are shown in the right plot of Figure 24 (red curve with grey band for reported systematics). The lattice data have similar behavior as the phenomenological estimates [207, 215, 217].

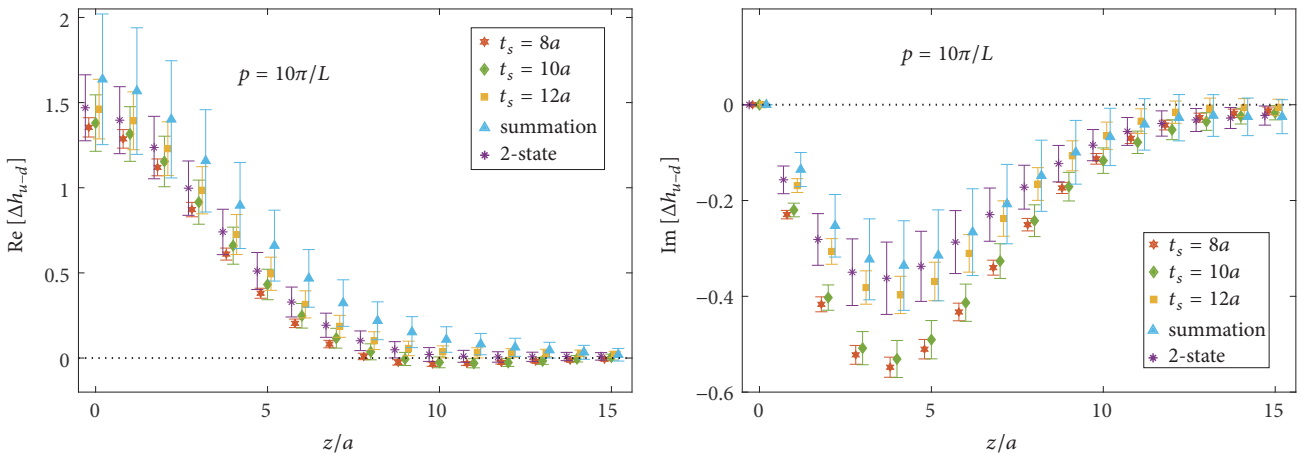

FIGURE 23: Real (left) and imaginary (right) part of the matrix element for the ETMC's helicity PDF from the plateau method (t_s value given in label), the two-state fits (using all t_s values), and the summation method. Nucleon momentum is $10\pi/L \simeq 1.38$ GeV. Source: [216], reprinted with permission by the Authors.

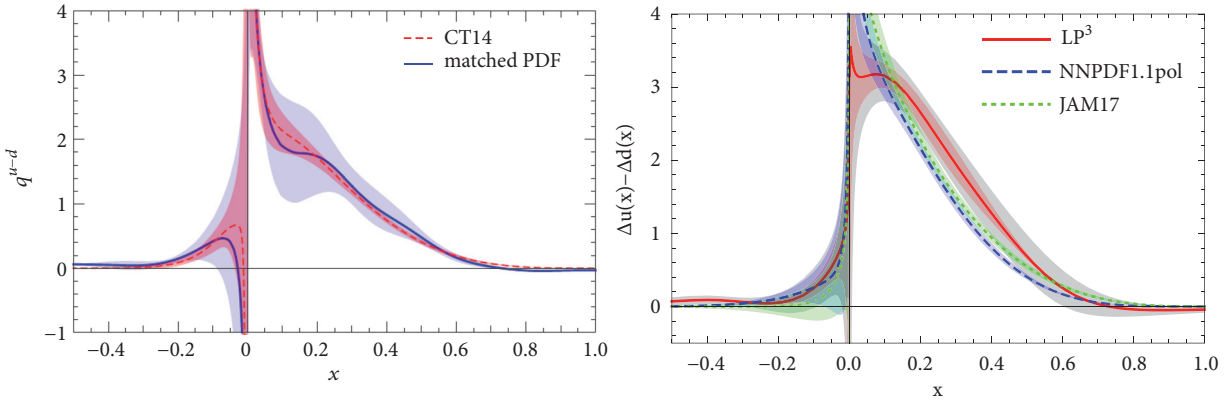

FIGURE 24: Left: LP^3's final estimate of unpolarized PDF at 3 GeV (blue curve) plotted together with the phenomenological distribution CT14 [210] (dashed red line). Right: LP^3's helicity PDF at 3 GeV (red curve) and global fits data from NNPDFpol1.1 [207] DSSV [217], JAM [215]. Source: [218, 219] (arXiv), reprinted with permission by the Authors.

9.2.2. Transversity PDF. Extracting the transversity PDF is a powerful demonstration of the advances in the quasi-PDFs approach using Lattice QCD simulations. Preliminary studies can be found in the literature already in 2016 [107, 108]. However, these lack two major components that prevent comparison with global analysis fits: proper renormalization and matching procedures. Complete studies of the transversity quasi-PDFs appeared this year by ETMC [48] and by LP^3 [49] using the same lattice setup as their work for the unpolarized and helicity PDFs described above.

The main motivation for first-principle calculations of the transversity PDF is the fact that it is less known experimentally [220, 237–241], because it is chirally odd, and totally inclusive processes cannot be used. In particular, one may extract information on the transversity PDF from e^+e^- annihilation into dihadrons with transverse momentum [242–244] and semi-inclusive deep-inelastic scattering (SIDIS) TMD data for single hadron production [245–247]. This method requires disentanglement of the dependence on the momentum fraction from the transverse momentum on TMD form factors and TMD PDFs. Alternatively, dihadron SIDIS cross-section data can be analyzed to obtain the transversity distribution directly from the measured asymmetry [248–250]. However, this analysis leads to large uncertainties, as the available data are less precise, and the collinear factorization at large x is problematic [251].

The ETM Collaboration presented the first computation of the x-dependence for the transversity PDF in [48] in Lattice QCD which includes a nonperturbative renormalization in lattice regularization (RI′), and a matching procedure similar to the $\overline{\text{MMS}}$ scheme of [124]. The latter was recalculated using the appropriate tensor nonlocal operator. We remind the Reader of the parameters for the $N_f = 2$ ensemble at a pion mass of 130 MeV [234], which has the lattice spacing $a = 0.093$ and the volume of $48^3 \times 96$. As in the case of the unpolarized and helicity PDFs, the nucleon was boosted with momenta 0.83, 1.11, and 1.38 GeV, while the source-sink separation was fixed to $t_s = 12a \sim 1.12$ fm for the final results. This value has been chosen after a thorough investigation of excited states [216]. The statistics increases with the nucleon

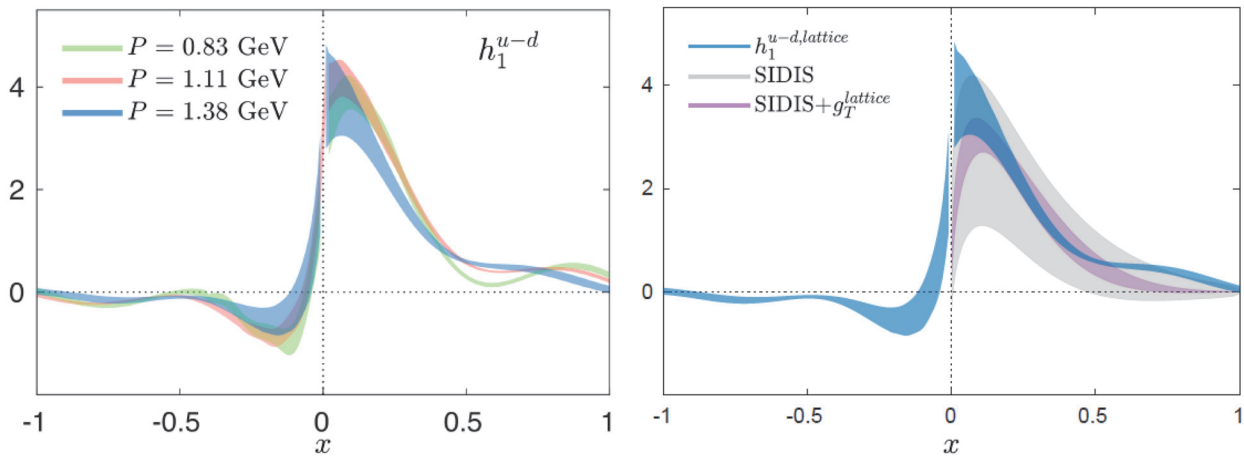

FIGURE 25: ETMC's transversity PDF with momentum 1.38 GeV (blue) as a function of Bjorken-x, at renormalization scale of $\sqrt{2}$ GeV. The phenomenological fits have been obtained using SIDIS data (grey) [220] and SIDIS data constrained using g_T^{lattice} (purple) [220]. Source: [48], reprinted with permission by the Authors (article published under the terms of the Creative Commons Attribution 4.0 International license).

momentum, that is, 9600, 38250, and 72990 measurements for momenta 0.83, 1.11, and 1.38 GeV, respectively.

The final lattice data for the transversity isovector PDF, $h_1^{u-d,\text{lattice}}$, are shown in Figure 25 in the $\overline{\text{MS}}$ scheme and at a scale of $\sqrt{2}$ GeV, so that they can be compared to phenomenological fits extracted at the same scale. In the left plot, we show the dependence on the nucleon momentum, which is found to be small for most values of x, with the highest momentum having milder oscillatory behavior. In the right panel, we present the lattice data for the highest momentum $P = 10\pi/L$ and compare with phenomenological fits on SIDIS data without [220] or with [220] constraints from lattice estimates of the tensor charge g_T ("SIDIS+lattice"). The difference in the statistical accuracy between the global fit and the lattice data is impressive, with the data of [48] being more accurate than both the constrained and the unconstrained SIDIS results. One way to check for systematic uncertainties is to compare the tensor charge as extracted: (a) directly from the local tensor operator, and (b) by integrating over x within the interval $[-1, 1]$ of PDFs. This consistency check reveals that both results are well compatible within uncertainties and both give a value of $g_T = 1.09(11)$ (the exact matching of the two numbers is to some degree accidental). Even though the agreement is nontrivial, as the steps leading to both values are different, it is, obviously, not sufficient for a complete quantitative understanding of systematic effects.

The latest work of LP^3 on the quasi-PDFs was very recently extended to the transversity distribution [49], using the same $N_f = 2 + 1 + 1$ ensemble with clover valence quarks on a HISQ sea [188], physical pion mass, the lattice spacing $a \approx 0.09$ fm, and the volume of $64^3 \times 96$. For the lattice setup, we refer the Reader to Section 9.2.1 and [218, 219]. Six source-sink separations were used with the highest at 1.08 fm and the same statistics as in [219]. These were analyzed based on different variations of a two-state fit, and the extracted matrix elements are shown in Figure 26 for the three momenta employed in this work, that is 2.2, 2.6, and 3 GeV. It is observed that the dependence on the nucleon momentum is weak within the uncertainties, which also holds for the matched PDFs. This can be seen in Figure 3 of [49], with the exception of the very small-x region. However, this is not conclusive, as lattice calculations have limitations on the reliability for this region. The observed convergence could be partly due to limitations in the matching formula, which is available to one-loop level only. Given the latter, a convergence can be possibly achieved at smaller nucleon momentum, which has the advantage that excited states can be better controlled. Evidence of nonnegligible excited states

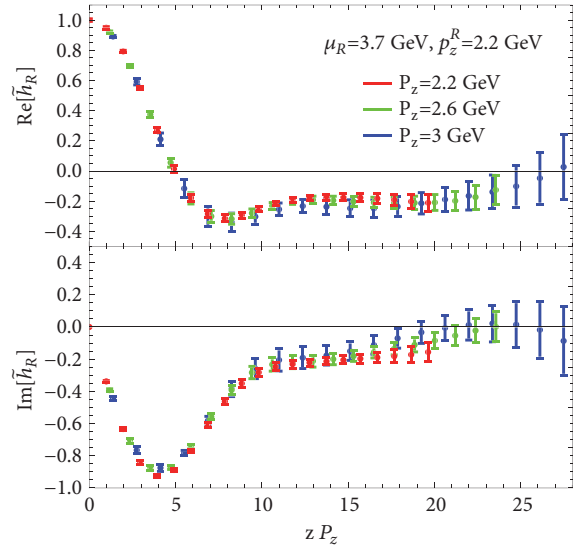

FIGURE 26: The real (top panel) and imaginary (bottom panel) parts of the matrix elements extracted from a two-state fit at momentum 3 GeV. The data are renormalized in the RI scheme and normalized with the matrix element of the local operator at same momentum. Source: [49] (arXiv), reprinted with permission by the Authors.

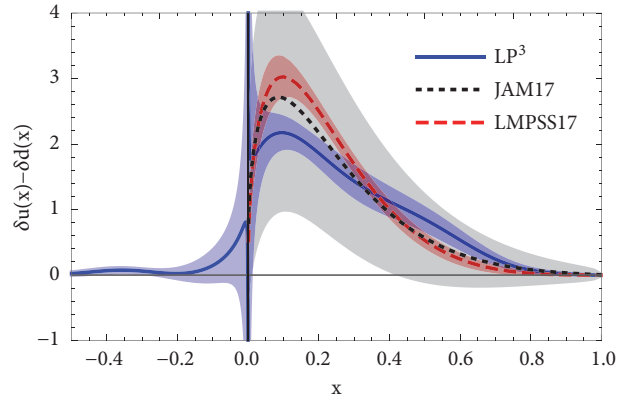

Figure 27: LP^3's final proton isovector transversity PDF at the renormalization scale $\mu = \sqrt{2}$ GeV ($\overline{\text{MS}}$ scheme), extracted from Lattice QCD and LaMET at $P_z = 3$ GeV, compared with global fits by JAM17 and LMPSS17 [220]. The blue error band includes statistical errors and some of the systematic uncertainties. Source: [49] (arXiv), reprinted with permission by the Authors.

contamination for momenta as high as 3 GeV can be seen in Figure 26, particularly in the real part where the matrix element becomes negative for large values of z. The latter is a clear evidence of excited states and it has been observed in other works that increasing source-sink separation (thus decreasing the contamination) brings the real part of large-z bare matrix elements to values compatible with zero; see, e.g., the upper left plot of Figure 1 in [216] and, to a lesser extent, the left panel of Figure 23.

Final estimates for the transversity PDF are given in Figure 27, where the lattice results (blue curve) underestimate the global fits from LMPSS17 [220] for $x < 0.4$ and are slightly higher in the region $x > 0.4$. Note that the results of ETMC shown in Figure 25 overlap with the fit from LMPSS17 ("SIDIS+lattice" in Figure 25) [220] for $x > 0.5$ and overestimate it for $x > 0.5$, possibly due to the oscillatory behavior. We believe that the difference in the behavior of the data from ETMC and LP^3 has its origin in the employment of the derivative method by LP^3 instead of the standard Fourier transform, which, as argued in Section 6.3, may lead to uncontrolled systematic uncertainties.

10. Other Results from the Quasidistribution Approach

In the previous section, we have concentrated on numerical results for the isovector quark PDFs in the nucleon. Now, we review other results obtained with the quasidistribution method, for mesonic DAs and PDFs, as well as first exploratory results for gluon PDFs.

10.1. Meson DAs. Arguably the simplest partonic functions are distribution amplitudes (DAs) of mesons. The interest in them is at least for two reasons. First, being very simple, they can be used for investigating and comparing different techniques. Many exploratory studies were or are performed focusing on the pion DA. Second, mesonic DAs are of considerable physical interest as well. They represent probability amplitudes of finding a $q\bar{q}$ configuration in the final meson state, with the quark carrying fraction x of the total momentum and the antiquark fraction $1 - x$. In phenomenology, they serve as nonperturbative inputs in analyses of hard exclusive processes with mesons, most notably the pion, in the final state. The shape of the pion DA is well known at large momentum transfers, where it follows an asymptotic form $\phi_\pi(x) = 6x(1-x)$. However, for smaller momentum transfers, different models lead to different functional forms and, hence, a first-principle investigation on the lattice could shed light on this issue and eliminate the theoretical uncertainty in analyses requiring DA as an input.

The first lattice computation of the pion quasi-DA was presented early in 2017 by J.-H. Zhang et al. [123]. They used a setup of clover valence quarks on an $N_f = 2 + 1 + 1$ HISQ sea with pion mass of 310 MeV, lattice spacing $a \approx 0.12$ fm, and lattice volume $24^3 \times 64$ that yields $M_\pi L \approx 4.5$. The measurements were done on 986 gauge field configurations with 3 source positions, averaging over two directions of boost. The employed pion momenta were $4\pi/L$ and $6\pi/L$, which corresponds to around 0.86 and 1.32 GeV, respectively. The matrix elements defining the quasi-DA can be accessed with two-point correlation functions and, after taking the Fourier transform, the distribution can be matched to its light-cone counterpart. At this stage, only matching formulae in the transverse momentum cutoff scheme were available from [115]. The Authors calculated the pion mass correction of $\mathcal{O}(M_\pi^2/P_3^2)$ along the lines of their earlier derivation of NMCs for nucleon quasi-PDFs [107]. They also parametrized the higher-twist corrections by extrapolating linearly in $1/P_3^2$ to zero after employing the matching and the mass correction. The results were presented, first, without any renormalization of the Wilson-line-related power divergence and, next, with the latter being subtracted by multiplication of the matrix elements by $\exp(-\delta m|z|)$ ("improved" pion DA), with δm extracted from the static potential. The latter computation was performed only on one lattice spacing and, hence, the obtained value, $\delta m \approx -260$ MeV, was attributed a large uncertainty of 200 MeV.

The final result for the improved DA, after matching and mass corrections, is shown in Figure 28. In the left panel, the curves correspond to $\Lambda = \mu_R = 2$ GeV for the transverse momentum cutoff and the central value of δm without uncertainty (error bands correspond to statistical uncertainties). One can see significant dependence on the pion momentum and the nonphysical nonzero values outside of $x \in [0, 1]$. In the right panel, the uncertainty in the determination of δm is included and dominates the total error. Within this large uncertainty, there is reasonable agreement with various models and parametrizations. However, the precision is clearly not enough to disentangle between different possibilities suggested from phenomenology. Naturally, that was not the aim of an exploratory study, where several systematic uncertainties are yet to be addressed (see Section 6.3 for a general discussion of such systematics). The main result of the paper is, thus, establishing the feasibility of the computation

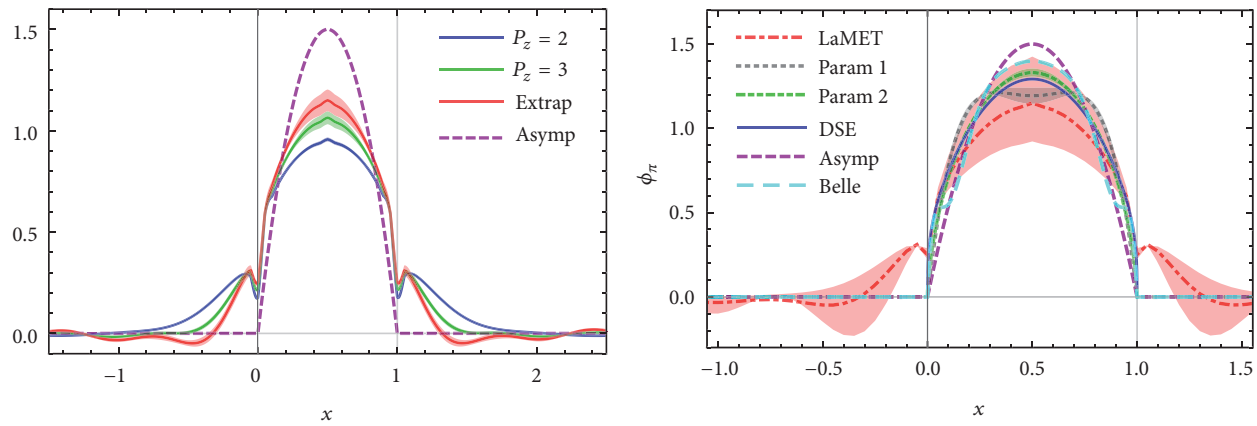

FIGURE 28: Improved pion DA obtained in the first lattice study [123] employing the quasidistribution approach. Left: $\delta m = -260$ MeV, momenta 0.86 GeV (blue), and 1.32 GeV (green), and extrapolated to $1/P_3^2 = 0$ (red), along with the asymptotic form $6x(1-x)$ (dashed line). Right: $\delta m = -260 \pm 200$ MeV, extrapolated to $1/P_3^2 = 0$ ("LaMET," red band), together with models and parametrizations: from Dyson-Schwinger equation ("DSE," blue) [221], fit to Belle data ("Belle," cyan) [222], parametrized fits to lattice moments ("Param 1," gray and "Param 2," green) [223] and the asymptotic form ("Asymp," purple). Source: [123], reprinted with permission by the Authors and the American Physical Society.

and the qualitative agreement with phenomenology can certainly be considered as reassuring.

The above study was extended by the LP^3 Collaboration [224] to include also the kaon and η mesons, with the view of studying the $SU(3)$ flavor symmetry breaking and testing predictions of chiral perturbation theory (χPT). Further extension with respect to [123] was to include momentum smearing to improve the signal for the boosted meson and access one more unit of lattice momentum, i.e., $8\pi/L$, corresponding to around 1.74 GeV. The used gauge field configurations ensemble was the same as in [123]

Technically, the computation of the kaon DA amounts to changing the mass of one valence quark to represent the strange quark mass. For the η meson, things are more subtle, because of the ensuing quark-disconnected diagrams and mixing with the $SU(3)$ singlet state. The Authors argued that the mixing is small and can be safely neglected, while the effect from using only connected diagrams (corresponding to the unphysical η_s meson) can be taken into account and the final result for ϕ_η can be approximated as $(\phi_\pi + 2\phi_{\eta_s})/3$. They again used the "improved" pion DA definition but employed three additional ensembles, with $a \approx 0.06, 0.09, 0.12$ fm, all at the physical pion mass, to determine precisely the mass counterterm δm, the dominating source of uncertainty in their previous work. The computation yielded the value -253(3) MeV. The final DAs show that the data at the two largest momenta are compatible with each other in most regions of x, while there are also regions where the behavior is nonmonotonic in P_3. Hence, the Authors did not attempt the extrapolation to $1/P_3^2 = 0$. The data for ϕ_{η_s} are rather close to the ones for ϕ_π; hence the result for ϕ_η is also close to the two.

A comparison of the pion and kaon DAs (at the largest meson boost) with models and parametrizations is shown in Figure 29. At the attained meson momenta, there are still sizable contributions outside of the physical region. Since the distributions are normalized to 1, the central regions of the LaMET DAs are significantly below all other results. The Authors concluded that larger momenta are needed, together with higher-order matching. Moreover, most of the standard lattice systematics is yet to be addressed (see Section 6.3). The Authors also converted their results on ϕ_π to the data for the pseudoscalar-scalar current correlator, to compare to the auxiliary light quark approach of [71], and found compatible behavior (see also Section 11.3). Finally, first attempt at testing the $SU(3)$ flavor symmetry breaking was made, with indications of agreement with χPT. The effect manifests itself mostly as the difference between the DAs of K^- and K^+, predicted to be $\mathcal{O}(m_q)$ by χPT. For a more complete study, simulations at additional light quark masses are needed.

10.2. Meson PDFs. Apart from DAs of mesons, the interest is, obviously, also in their PDFs, particularly for the pion. Phenomenological extraction of the pion PDF uses predominantly experimental data from the Drell-Yan process in the pion-nucleon scattering. This established that the large-x behavior of the pion PDF is $(1-x)^2$ [228], corroborated by certain models. However, other models indicate rather a $(1-x)$ decay. A first-principle computation could solve this discrepancy.

The first lattice extraction of the pion PDF based on LaMET was shown in [226] by the LP^3 Collaboration. They used again the same ensemble as for the pion DA (see previous subsection) and applied boosts of 0.86, 1.32, and 1.74 GeV to the pion. The (isovector) quasi-PDF is defined analogously to the nucleon case and the Dirac structure was chosen to be $\Gamma = \gamma_0$ to avoid the mixing discovered in [106]. The Authors used four source-sink separations, ranging from $6a$ to $9a$ (0.72 to 1.08 fm), to investigate excited states contamination. They demonstrated that different two-state fits lead to consistent results in the real part of the matrix

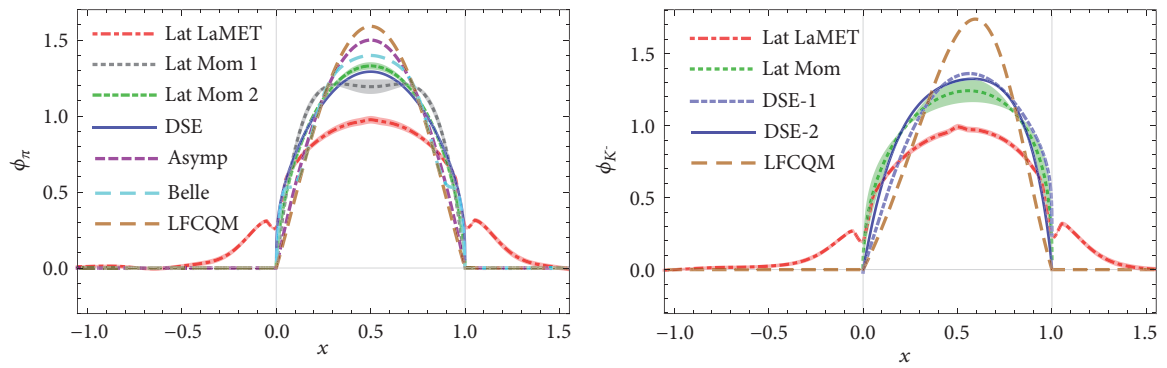

FIGURE 29: Improved pion (left) and kaon (right) DAs obtained in [224] employing the quasidistribution approach with $P_3 \approx 1.74$ GeV ("LaMET"), together with models and parametrizations: from Dyson-Schwinger equation ("DSE") [221], fit to Belle data ("Belle") [222], parametrized fits to lattice moments ("Lat Mom") [223], light-front constituent quark model ("LFCQM") [225], and the asymptotic form ("Asymp"). Source: [224] (arXiv), reprinted with permission by the Authors.

elements, at their intermediate pion momentum. The effects in the imaginary part were, unfortunately, not shown. As we argued in Section 6.1, the two-state method is, by itself, not enough to check excited states effects. Much stronger conclusions can be drawn from comparison of two-state fits with the plateau method. Else, the danger is that two-state fits are dominated by the lowest source-sink separations and/or many excited states mimic one excited state. Moreover, it is not clear what happens in this study at the largest pion boost, where the excited states contamination is bound to be larger.

For renormalization, LP^3 followed two procedures. They used a variant of RI/MOM but also decided to apply the procedure of removing the power divergence by the mass counterterm determined from the static potential for comparison. The RI-renormalized quasi-PDF results were matched directly to the $\overline{\text{MS}}$ scheme using the kernel of [199] and mass corrections were applied [107]. To reduce the oscillations in the large-x region, the Authors used the derivative method. They investigated the momentum dependence of the final results and for RI results they also varied the renormalization scale p_3^R. Comparison between the RI and Wilson line renormalizations revealed large differences, attributed by the Authors to possibly large higher-order corrections in the matching.

The final results for the $\overline{\text{MS}}$-renormalized pion PDF, taken from lattice quasi-PDFs renormalized in the RI scheme and matched to $\overline{\text{MS}}$ at $\mu = 4$ GeV, are shown in Figure 30. The LP^3 result is contrasted with a model calculation based on Dyson-Schwinger equations (DSE at a different scale of $\mu = 5.2$ GeV) [227] and with the ASV fit to experimental Drell-Yan data [228]. Within the reported uncertainty, coming from statistical errors and comparing results for two values of the RI intermediate scale, the Authors observed compatibility with the ASV fit for small $x \lesssim 0.4$, where the ASV fit disagrees with the Dyson-Schwinger analysis. For large x, the phenomenological fit agrees with DSE, but the LP^3 extraction lies significantly above the two. The reliability of the computation (in particular the large-x region) is expected to increase when using larger pion boosts and decreasing the pion mass towards its physical value, as well as when taking higher-order matching into account. Obviously, other systematics, such as cutoff effects and FVE, need to be addressed too; see Section 6.3.

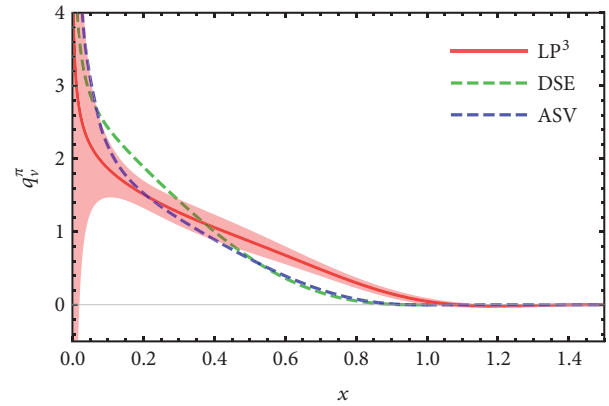

FIGURE 30: Pion PDF obtained in [226] from the quasidistribution approach with $P_3 \approx 1.74$ GeV, $\mu = 4$ GeV ("LP^3"), together with model calculation from Dyson-Schwinger equations at $\mu = 5.2$ GeV ("DSE") [227] and a fit to Drell-Yan data at $\mu = 4$ GeV ("ASV" [228]). Source: [226] (arXiv), reprinted with permission by the Authors.

10.3. Gluon PDFs. Very recently, the first investigation of quasi-gluon PDFs appeared [229], by Z.-Y. Fan et al. Needless to say, gluon PDFs are relevant for many analyses, especially in the small-x region, where they become the dominating partons. Phenomenologically, they are determined from DIS and jet-production cross-sections. The employed lattice setup consisted of valence overlap quarks on an $N_f = 2 + 1$ domain-wall sea with lattice spacing $a \approx 0.11$ fm, lattice volume $24^3 \times 64$, and pion mass of 330 MeV. The Authors used two valence pion masses, one slightly larger than the sea quark mass (340 MeV) and one corresponding to light quarks having the strange quark mass (pion mass 678 MeV). The computations were performed on 203 gauge field configurations with many smeared point sources, yielding $\mathcal{O}(200000)$ total measurements for the two-point functions.

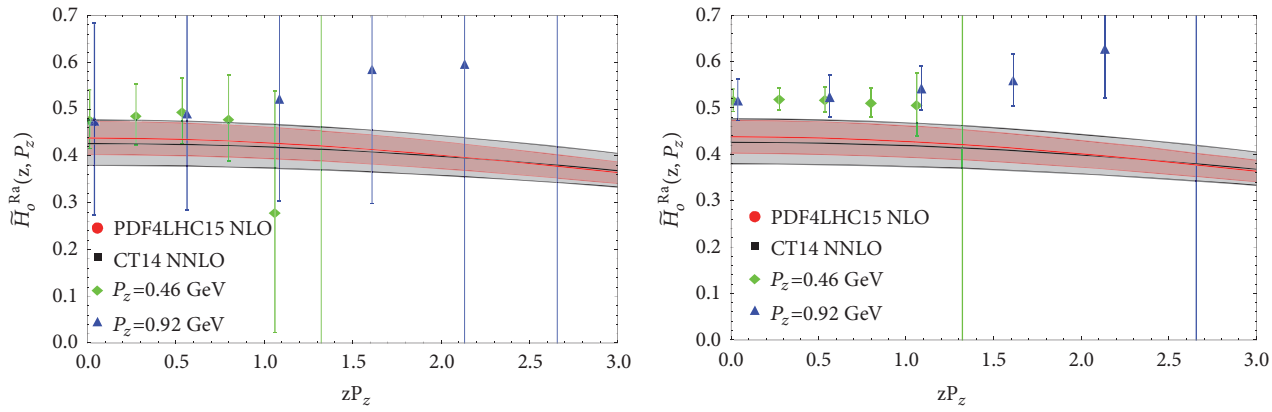

FIGURE 31: "Ratio-renormalized" matrix elements of the operator $\mathcal{O}_0$ defining gluon quasi-PDFs in the study of [229]. Nucleon momenta are 0.46 and 0.92 GeV. Valence pion mass of 340 MeV (left) and 678 MeV (right). Also plotted are inverse Fourier transforms of two phenomenological fits to experimental data: CT14 [210] and PDF4LHC15 [24]. Source: [229] (arXiv), reprinted with permission by the Authors.

The bare matrix elements were extracted using the method proposed in [252], based on the derivative of the summed ratio of three-point and two-point functions, grounded on the Feynman-Hellmann theorem.

Fan et al. employed the following definition of gluon quasi-PDF:

$$\tilde{g}\left(x, P_3^2, \mu\right) = \int \frac{dz}{\pi x} e^{-ixzP_3} \widetilde{H}_0^R\left(z, P_3, \mu\right), \tag{98}$$

with the bare matrix element $\widetilde{H}_0(z, P_3)$ being the boosted proton state expectation value of the Euclidean operator:

$$\mathcal{O}_0 = -\frac{P_0\left(\mathcal{O}\left(F_{0\mu}, F_{\mu 0}; z\right) - (1/4)\,\mathcal{O}\left(F_{\mu\nu}, F_{\nu\mu}; z\right)\right)}{(3/4)\,P_0^2 + (1/4)\,P_z^2}, \tag{99}$$

where $\mathcal{O}(F_{\rho\mu}, F_{\mu\tau}; z) = 2\mathrm{Tr}[F_{\rho\mu}(z)W(z,0)F_{\mu\tau}(0)W(0,z)]$ and the gluon operator is subject to HYP smearing to improve the signal. This operator was shown not to be multiplicatively renormalizable by the Authors of [137] (see also discussion in Section 5.2.1 about the renormalizability of gluon quasi-PDFs). However, in this exploratory study, the Authors did not perform a rigorous renormalization procedure, but only tried to eliminate the power divergence by taking the ratio

$$\widetilde{H}_0^{Ra}\left(z, P_3, \mu\right) = \frac{\widetilde{H}_0^{\overline{\mathrm{MS}}}\left(0, 0, \mu\right)}{\widetilde{H}_0\left(z, 0\right)} \widetilde{H}_0\left(z, P_3\right), \tag{100}$$

with $\widetilde{H}_0^{Ra}(0,0,\mu)$ equal to $\langle x\rangle_g^{\overline{\mathrm{MS}}}(\mu)$. This was justified by an empirical observation from unpolarized quark quasi-PDFs, where an analogous ratio reproduces the RI-renormalized matrix elements with $\mathcal{O}(10\%)$ deviation.

In their numerical investigation, Fan et al. compared the z-dependence of bare and ratio-renormalized matrix elements for different levels of HYP smearing, using nucleon momenta of 0, 0.46 and 0.92 GeV (without momentum smearing). At this level of precision, not much sensitivity to P_3 could be seen. The bare matrix elements are significantly enhanced by the removal of the power divergence. Since the lattice computation is very noisy in the gluon sector, the signal extends only to $z = 4a \approx 0.44$ fm. The Authors also compared results from the operator $\mathcal{O}_0$ to three other operators that can be used to define gluon quasi-PDFs, finding that the other ones either suffer from large mixing with higher-twist operators or provide a worse signal. They also plotted the results for the ratio-renormalized matrix elements $\mathcal{O}_0$ together with two phenomenological gluon PDFs inverse Fourier transformed to coordinate space, observing compatibility within large uncertainties for their smaller valence pion mass; see Figure 31. Finally, matrix elements were shown also for gluon quasi-PDF in the pion.

The Authors concluded that, at the present level of precision, their study could not constrain gluon PDFs, which would require taking the Fourier transform and performing the matching to the light-cone PDF. Due to the fact that the magnitude of the gluon PDF is significant predominantly for small x, the distribution in coordinate space is very broad, necessitating reaching large values of zP_3 (while in the current study only $zP_3 \approx 2$ could be reached). Thus, significant improvements are needed to obtain a reliable gluon PDF from the quasidistribution approach. The challenge is further extended by the mixing between the gluon quasi-PDF and the singlet quark quasi-PDFs (see Section 8.2), which have not been yet explored on the lattice and would require calculations involving quark-disconnected diagrams.

11. Results from Other Approaches

The last two sections were devoted to reviewing results obtained for the x-dependence of nonsinglet quark PDFs, gluon PDFs, and meson DAs/PDFs from the quasidistribution method. In the present one, we discuss some other results obtained in the last few years from alternative approaches, shortly described in Section 2. We review them in the order of discussion in Section 2.

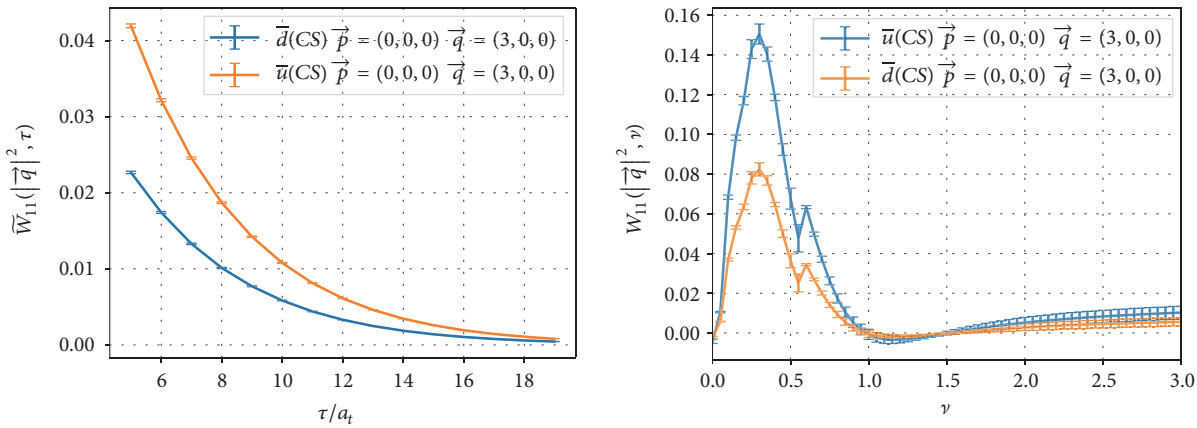

FIGURE 32: Euclidean (left) and Minkowski (right) hadronic tensor obtained in the study of [63]. Source: [63], reprinted with permission by the Authors (article published under the terms of the Creative Commons Attribution 4.0 International license).

11.1. Hadronic Tensor. Despite being proposed in the early 1990s, the hadronic tensor approach [54–56] (see also Section 2.1) has not led to many numerical applications, because it requires the computation of difficult four-point correlators and faces the inverse Laplace transform problem. However, recently there is renewed interest in it, due to hugely increased computational powers and new reconstruction techniques to tackle the inverse problem. In [63], J. Liang, K.-F. Liu, and Y.-B. Yang presented preliminary results obtained using the classical Backus-Gilbert technique [253]. They used an ensemble of clover fermions on an anisotropic $12^3 \times 128$ lattice with pion mass 640 MeV and lattice spacing of 0.1785 fm, performing measurements on 500 gauge field configurations.

The preliminary results are shown in Figure 32. The Euclidean hadronic tensor $\widetilde{W}_{11}(\vec{p}, \vec{q}, \tau)$ (left plot) vs. the current separation τ is shown for nucleon at rest ($\vec{p} = 0$) with momentum transfer $\vec{q} = (3,0,0)$ and corresponds to connected sea antiup and antidown partons. The reconstructed Minkowski tensor $W_{11}(q^2, \nu)$, where ν is conjugate to τ in the inverse Laplace transform, is shown in the right plot. The first peaks are elastic and correspond to the energy transfer invoked by the momentum transfer. The less pronounced second peaks are quasielastic and are related to nucleon excitations. Unfortunately, with these kinematics, the DIS region is inaccessible, as it would require both $\nu < |\vec{q}|$ ($|\vec{q}| \approx$ 1.7 GeV in this case) and at the same time ν much larger than the one corresponding to the quasielastic peaks (extending to $\nu \approx 1$, which yields 5.5 GeV). This could be achieved on lattices with much smaller lattice spacings. The Authors, nevertheless, concluded that the observation of both elastic and quasielastic peaks is encouraging.

The investigations are continued and further results were presented in the Lattice 2018 Symposium, using other reconstruction methods and an ensemble with much finer lattice spacing, $a_t \approx 0.035$ fm (in the temporal direction), lattice size $24^3 \times 128$, and lower pion mass of 380 MeV; see upcoming proceedings [254] for more details.

11.2. Auxiliary Heavy Quark. The approach with auxiliary heavy quark [58] (see also Section 2.3) was also recently revived by its Authors, W. Detmold and C.-J. D. Lin, in collaboration with I. Kanamori, S. Mondal, and Y. Zhao [68]. Their study is aimed at extracting the pion DA and the current investigations employed three quenched ensembles (Wilson plaquette action discretization), with lattice spacings of 0.05 fm, 0.06 fm, and 0.075 fm and fixed physical spatial extent of $L \approx 2.4$ fm, $T = 2L$. The valence pion mass is 450 MeV, and the auxiliary heavy quark mass 1.3 or 2 GeV.

The calculation proceeds via evaluating the vacuum-to-pion matrix elements of the product of two heavy-light currents separated in spacetime. The spatial Fourier transform of such matrix elements, for large enough temporal separation of the three points in the correlator, gives a quantity called $R_3^{\mu\nu}(\vec{p}, \vec{q}, \tau)$, where $\vec{p}$ is the pion momentum, $\vec{q}$ the momentum transfer, and τ the separation of currents. $R_3^{\mu\nu}(\vec{p}, \vec{q}, \tau)$ is then an input to a temporal Fourier transform yielding the Euclidean hadronic tensor $U_A^{[\mu\nu]}(q, p) = \int_{\tau_{\min}}^{\tau_{\max}} d\tau e^{iq_4\tau} R_3^{[\mu\nu]}(\tau, \vec{q}, \vec{p})$, which, in the continuum limit, gives access to moments of the structure function by varying q_4. As an illustration, the integrand of this Fourier transform is shown in Figure 33 (left), for $\mu\nu = 12$, pion at rest, and with minimal spatial momentum transfer of $2\pi/L$ in the 3-direction. The heavy quark mass is 1.3 GeV and two lattice spacings and two values of q_4 are shown. The signal is clear, but lattice cutoff effects are not negligible, as also evidenced in the right plot of Figure 33, showing the full quantity $U_A^{[12]}(q, p)$ for three lattice spacings and three choices of q_4. Since the extraction of moments requires reliable extrapolation to the continuum limit, the Authors prefer first to analyze smaller lattice spacings. To this end, they already have quenched ensembles with lattice spacings down to 0.025 fm. Furthermore, the momentum smearing technique will be employed to enhance the signal for a moving pion. Preliminary investigation of this case was also shown in [68].

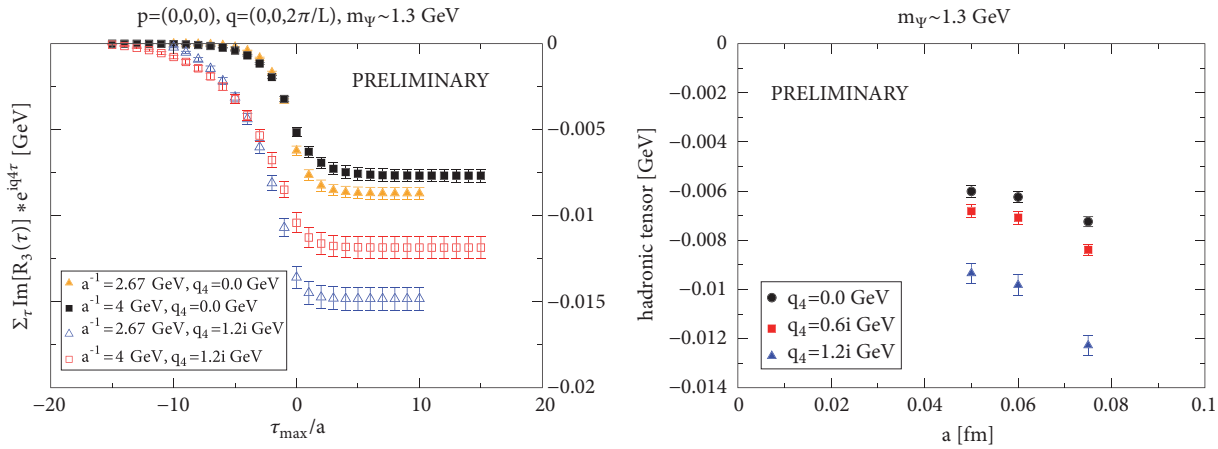

FIGURE 33: Left: integrand of $U_A^{[12]}(q, p)$ for a pion at rest, momentum transfer $(0, 0, 2\pi/L)$, heavy quark mass of 1.3 GeV. Different sets of data points correspond to two lattice spacings and two values of q_4. Right: imaginary part of $U_A^{[12]}(q, p)$ for three lattice spacings and three values of q_4, other parameters the same as in the left plot. Source: [68] (arXiv), reprinted with permission by the Authors.

11.3. Auxiliary Light Quark. Instead of an auxiliary heavy quark, one can also use an auxiliary light quark [69] (see also Section 2.4). The wave of renewed interest in light-cone distribution functions on the lattice in recent years sparked also revival of numerical studies of this approach, by the Regensburg group [70, 71]. Their aim is to extract the pion DA. In their exploratory study, they employed one gauge field ensemble of $N_f = 2$ clover fermions, with lattice spacing $a \approx 0.071$ fm, lattice volume $32^3 \times 64$, and pion mass 295 MeV. The auxiliary light quark has the same mass as the physical quarks. Relatively large momenta were reached, up to around 2 GeV, thanks to the momentum smearing technique introduced by the same group. It is clear that going much beyond 2 GeV is currently impossible on the lattice, if aiming at a reliable analysis, in particular large enough temporal separations between points in the three-point correlator.

As in the auxiliary heavy quark approach, the lattice part consists in calculating the vacuum-to-pion matrix element of two currents, separated spatially by $\vec{z}$. In [71], the pion DA was extracted from the scalar-pseudoscalar channel. The Authors paid particular attention to discretization effects from the breaking of rotational invariance that leads to very different behavior of points with the same $|\vec{z}|$, but different choices of its components. In particular, the "democratic" points, like (1,1,1), tend to behave better than "nondemocratic" ones, e.g. (1,0,0). This is a well-known effect in coordinate space and it can be seen already in the free theory (cf., e.g., [255]). To improve the behavior, one can discard points that are too "nondemocratic" and also define a tree-level improvement coefficient. Renormalization (involving only local operators) was performed in the RI/MOM scheme, with a three-loop conversion to the $\overline{\text{MS}}$ scheme. The data at different renormalization scales $\mu = 1/|\vec{z}|$ and different Ioffe times were compared to continuum perturbation theory predictions for three different phenomenological models, at leading twist and with twist-4 corrections. The Authors concluded that there are indications of deviating from the asymptotic form of the pion DA, $6x(1 - x)$, in the large Ioffe time region; however, for reliable conclusions one needs to access this region at larger pion boosts, to keep $|\vec{z}|$ in the perturbative region. Larger pion boosts should be accompanied by computations at smaller lattice spacings, to keep the momenta sufficiently away from the cutoff. At small Ioffe times, one would need significantly larger statistics to disentangle between the three models.

The follow-up work of [70], by the same group and using the same lattice ensemble, concentrated on exploring higher-twist effects (HTE) and comparing results from six channels: vector-vector (VV), axial-axial (AA), vector-axial (VA), axial-vector (AV), scalar-pseudoscalar (SP), and pseudoscalar-scalar (PS). Other channels, like scalar-vector, although possible in principle, may suffer from enhanced HTE. For the employed channels, the Authors calculated the leading HTE in the framework of three phenomenological models. Results from some channels can be combined to eliminate certain effects; e.g., imaginary parts cancel in SP+PS. In the end, three linear combinations were formed: VV+AA, VA+AV, and SP+PS. On the lattice side, the Regensburg group also tested another technique to calculate the all-to-all propagator, using stochastic estimators instead of the sequential source method. This technique allowed them to take a volume average at a smaller computational cost and hence it was considered superior to the previously employed one. They chose six momentum vector choices at five different boost magnitudes and $|\vec{z}| > 3a$ to avoid enhanced lattice artifacts observed at very small distances.

Example results for the Ioffe-time dependence of the pion DA are shown in Figure 34 (left). They correspond to two of the linear combinations, VV+AA and SP+PS, and one spatial distance of $|\vec{z}| \approx 0.33$ fm. The lattice data are compared to tree-level and one-loop-corrected continuum perturbative results, with and without leading HTE. The Authors observed that the sign and magnitude of the predicted splitting are in good agreement with the data, but quantitative differences emerge. Obviously, no quantitative agreement was expected, since lattice data have their systematics and the

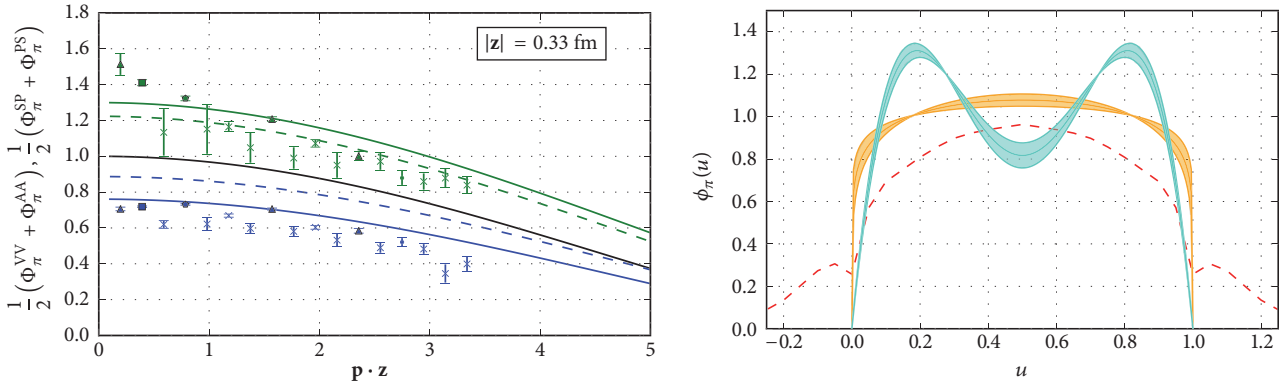

FIGURE 34: Left: Ioffe-time dependence of the pion DA extracted from two linear combinations: VV+AA (blue) and SP+PS (green), at $|\vec{z}| \approx 0.33$ fm. The black solid line is the channel-independent tree-level result at leading twist. The colored dashed (solid) lines correspond to including one-loop corrections for both channels without (with) twist-4 contribution. Right: pion DA from a global fit to all data, using two parametrizations for the leading-twist DA and a selected fitting range (colored bands). The errors are only statistical. For comparison, also result from the quasidistribution approach is shown (dashed line), from [224]. Source: [70] (arXiv), reprinted with permission by the Authors.

phenomenological models may not be correct and/or are subject to unknown higher-order corrections. To investigate the final shape of DA, Bali et al. performed a global fit to all channels and all data at different separations and momenta, using three different parametrizations of the leading-twist DA and different fitting ranges. An example result (with only statistical errors), for two parametrizations and one selected fitting range, is shown in Figure 34 (right). Both DAs describe the lattice data equally well, having similar second Gegenbauer coefficients a_2^π, which is the only relevant parameter for the description of available data. With data extending to larger Ioffe times, the next Gegenbauer coefficient should become accessible and allow us to disentangle between the two parametrizations. The Authors concluded that these results are very promising and the dominating uncertainty is the systematic one, which can be reliably improved, in particular, by using smaller lattice spacings, larger pion boosts, and higher-order perturbative corrections and HTE.

11.4. Pseudodistributions. The first numerical investigation of the pseudodistribution approach [75–77] (see also Section 2.6) was performed by J. Karpie, K. Orginos, A. Radyushkin, and S. Zafeiropoulos in 2017. The computation proceeded using a quenched ensemble with lattice spacing $a \approx 0.093$ fm, lattice volume $32^3 \times 64$, and clover fermions in the valence sector, with pion mass around 600 MeV. The employed momenta for the nucleon boost reached up to $12\pi/L$, i.e., approximately 2.5 GeV. The matrix elements (lattice ITDs) were obtained using the methodology of [252]. From these, reduced matrix elements, $\mathfrak{M}(\nu, z_3^2)$, were formed and they require no further renormalization. After plotting $\mathfrak{M}(\nu, z_3^2)$ vs. the Ioffe time, the Authors noticed a significant z-dependence of the results and applied the one-loop LLA evolution for all points with $z \leq 4a$, i.e., $1/z \geq 500$ MeV. When using $\alpha_s/\pi = 0.1$ and evolving to $z = 2a$, this led to all points collapsing close to a universal line, for both the real part and the imaginary part. Clearly, it is difficult to imagine one-loop perturbative formula to work rigorously at scales down to 500 MeV. Hence, the LLA evolution should rather be treated as a model of evolution. The model was further extended to check the behavior of data under LLA for even lower scales $1/z$. Around $z = 6a$, the evolution was observed to stop. Hence, points for $6a < z \leq 10a$ were treated as if they corresponded to the scale $6a$. The result of this procedure is shown in the left panel of Figure 35. The evolved data were fitted to cosine Fourier transforms of $N(a,b)x^a(1-x)^b$-type functions ($N(a,b)$ – normalization, $a = 0.36(6)$, $b = 3.95(22)$), which yielded the blue band in the plot. The corresponding PDFs at two scales are shown in Figure 35 (right) and compared to three sets of phenomenological PDFs. Obviously, no quantitative agreement was expected, but the general shape of the ensuing PDF evinces features of the experimental distributions and the evolution from the original scale of $1/z = 1/2a \approx 1$ GeV to 2 GeV moves the lattice-extracted PDFs closer to phenomenology.

As argued by Radyushkin in [80, 81] (see Section 8.2), the LLA is only an approximation appropriate for studying the $\ln z^2$ dependence. To obtain the full PDF, one should perform the matching procedure based on factorization [81–83, 85, 86], taking into account all one-loop corrections. The matching equation (93) has the outcome of effectively changing the relation between the $1/z$ lattice scale and the $\overline{\text{MS}}$ scale, as discussed in Section 8.2. Radyushkin [81] applied the matching to the data of [87] and found that the matched ITD, denoted by $\mathcal{I}_R(\nu, \mu^2)$, is approximately equal to the reduced ITD $\mathfrak{R}(\nu, (4/\mu)^2)$ and thus the rescaling factor is close to 4, as opposed to the LLA value of about 1.12. The matched ITD is shown in the left plot of Figure 36 and the resulting PDF is in its right panel. Both plots also contain, for comparison, data from phenomenological parametrizations, inverse Fourier transformed for the ITD plot. As could be expected, the matched ITDs lie close to a universal curve and the curve corresponds to a fit to the same model as in [87], with parameters $a = 0.35$ and $b = 3$. The fitted curve lies significantly below the phenomenological ITD.

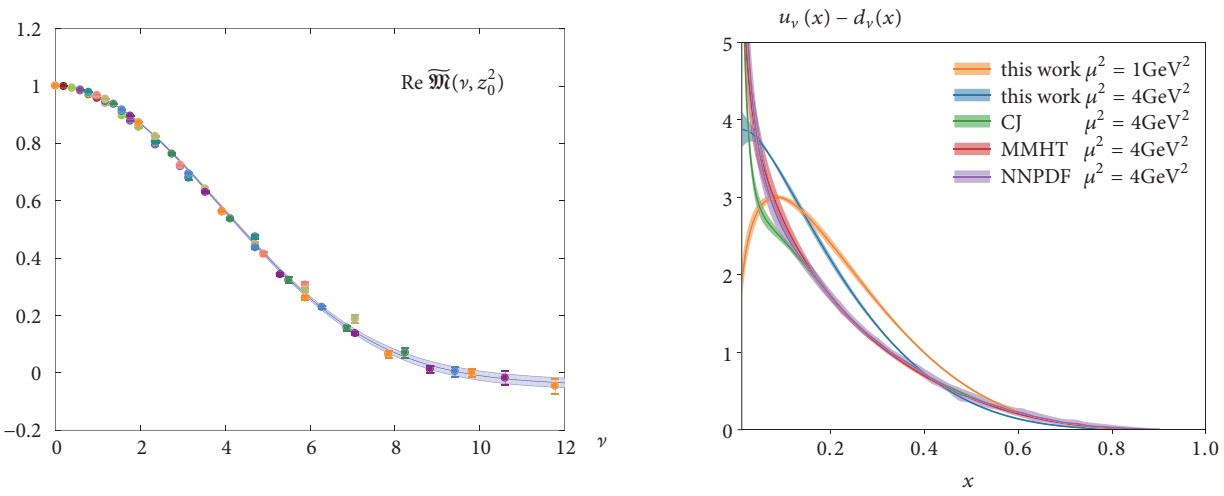

FIGURE 35: Left: real part of reduced matrix elements with all points evolved to $z = 2a \approx 1$ GeV^{-1}. The points with $6a < z \leq 10a$ were evolved as if they corresponded to $z = 6a$. The blue band is a fit explained in the text. Right: final PDF resulting from the rescaled data in the left plot and comparison with CJ15 [214], MMHT [212], and NNPDF [211] phenomenological data. Source: [87], reprinted with permission by the Authors and the American Physical Society.

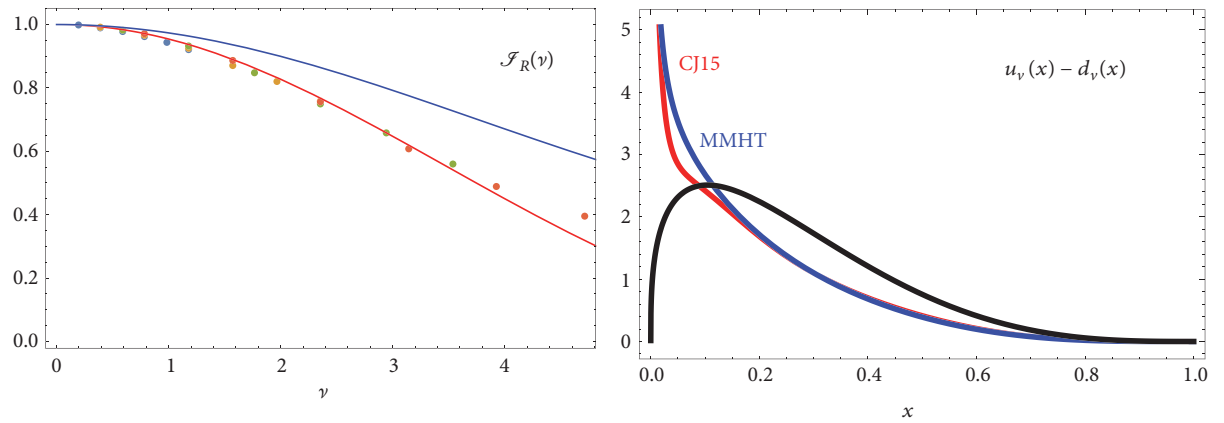

FIGURE 36: Left: real part of light-cone ITD (real part), matched from pseudo-ITD via Equation (93). The matched ITD was fitted to a model ITD. For comparison, the ITD corresponding to the CJ15 phenomenological set is also shown. Right: final PDF resulting from the data in the left plot, together with two phenomenological PDFs: CJ15 [214] and MMHT [212]. Source: arXiv version of [81], reprinted with permission by the Author (article published under the terms of the Creative Commons Attribution 4.0 International license).

Correspondingly, the final PDF deviates from phenomenology, especially for small and intermediate x. The Author pointed out that alternative fitting ansatzes lead to a similar curve as in the left panel, but the final PDF may significantly differ. The reason for this is that the ITD is unknown in the whole region $0 \leq \nu < \infty$ and, having a limited set of Ioffe times, one needs to add assumptions about the behavior of the ITD outside the region or about the functional form of the PDF. Radyushkin also compared the present result to the one from LLA in [87]. The final PDF is changed to a large extent and is further away from phenomenology. He pointed out that this is because the LLA analysis assumes that the final $\overline{\text{MS}}$ scale differs from $1/z$ by only the factor 1.12, while the full one-loop formula implies that the true $\overline{\text{MS}}$ scale is in fact around $4/z$, i.e., about 4 GeV. Thus, the evolution to the reference scale of phenomenological PDFs, 2 GeV, should proceed downwards from 4 GeV to 2 GeV and not upwards from 1 GeV to 2 GeV.

The final result that we report from the pseudodistribution approach is the computation of the two lowest moments of the isovector unpolarized PDF, erroneously claimed to be impossible due to fatal flaws in the approach in [164]. We refer to Section 6.3 for more details about this argument and its refutation. In [90], J. Karpie, K. Orginos, and S. Zafeiropoulos used the same quenched ensemble as in [87] and demonstrated that the two lowest moments agree with an earlier explicit computations thereof by the QCDSF collaboration [230]; see Figure 37.

Further progress was reported in the Lattice 2018 Symposium, including first calculations with dynamical flavors [256] and the issue of reconstruction of distributions from a limited set of data [11].

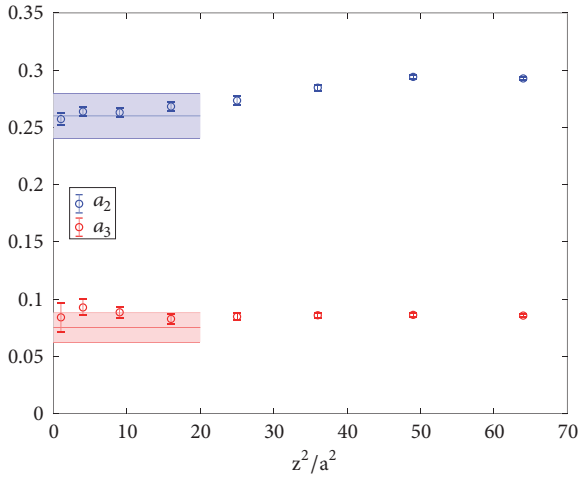

FIGURE 37: The first (blue) and second (red) lowest moments of the isovector unpolarized PDF obtained from a quenched ensemble with $a \approx 0.093$ fm and valence pion mass of approximately 600 MeV. The data points come from the pseudodistribution approach at different values of z^2 and the shaded bands correspond to an earlier explicit computation by the QCDSF collaboration [230]. Source: [90] (arXiv), reprinted with permission by the Authors.

11.5. OPE without OPE. The approach dubbed "OPE without OPE" was first investigated numerically in [91] (see also Section 2.7) by the QCDSF collaboration. The Authors took an exemplary parametrization of a nonsinglet PDF and applied the proposed method. They showed that the parametrized PDF can be reconstructed from computed moments with very promising agreement already using a very limited set of data points; see Figure 38 (left). Moreover, they performed an exploratory study with real lattice data, employing an ensemble of $N_f = 3$ clover fermions, with lattice spacing $a \approx 0.074$ fm and lattice volume $32^3 \times 64$. They computed the Compton amplitude $T_{33}(p, q)$ for 10 spatial momenta $\vec{p}$ and one momentum transfer $\vec{q}$. The result is shown in the right plot of Figure 38. For low momenta, the precision was found to be already very good and for larger ones the usage of the momentum smearing technique is planned. Further exploration is in progress, at three lattice spacings and a pion mass of 470 MeV, and results were reported in the Lattice 2018 Symposium; see upcoming proceedings [257].

11.6. Good Lattice Cross-Sections. This approach, suggested in [85, 86, 95] (see Section 2.8) and closely related to the auxiliary light quark method, is being pursued by the theory group at JLab, aiming at meson PDFs [231]. They use clover fermions with lattice spacing $a \approx 0.127$ fm, pion mass of 430 MeV, and the largest momentum employed is about 1.5 GeV. Preliminary results are illustrated in Figure 39 [12]. It shows the vector-vector $(\gamma_1 - \gamma_1)$ current-current matrix element for the pion PDF calculation vs. the Ioffe time $p \cdot \xi$, where p is the pion boost and ξ the separation of currents. Different colors correspond to different separations ξ^2 (in lattice units). The higher-twist effects are visible at large separations and the Authors are calculating the NLO perturbative kernel that will give a correction in ξ^2. For more results, see [231].

12. Summary and Future Prospects

In this paper, we give an overview of several approaches to obtain the Bjorken-x dependence of partonic distribution functions from *ab initio* calculations in Lattice QCD. A major part of this review is dedicated to a discussion on the state-of-the-art of the field, demonstrated with modern numerical simulations. We considered different theoretical ideas that were proposed over the last years to access parton distribution functions (PDFs) and parton distribution amplitudes (DAs), as well as more complex generalized parton distributions (GPDs) and transverse momentum dependent PDFs (TMDs). Even though their x-dependence was believed to be practically impossible to calculate on the lattice, breakthrough ideas were conceived and sparked renewed interest in these difficult observables. Arguably, the single most seminal idea was the one of X. Ji, who developed a general framework for accessing light-cone quantities on a Euclidean lattice, the quasidistribution approach. This framework itself has been heavily studied and has led to very encouraging results, but, moreover, it has prompted also the rediscovery of previously proposed ideas, like the hadronic tensor, and approaches with auxiliary heavy/light quarks. It has spawned also new or related concepts, such as pseudodistributions, OPE without OPE, and good lattice cross-sections.

As a summary, we would like to offer the Reader a flowchart (Figure 40) with an overview of how progress of the different approaches has been evolving. For all these new methods, we distinguish four general stages in the evolution of our understanding.

(i) Starting with the proposed theoretical idea (e.g., quasidistributions, good lattice cross-sections, pseudodistributions, etc.), several challenges (theoretical and technical) must be studied and overcome to achieve a successful implementation of the method. Theoretical analyses of the idea may lead to additional challenges on the lattice.

(ii) The second stage is exploratory studies aiming at a demonstration of the feasibility of the method. During this stage, further technical difficulties can be revealed, as well as possible additional theoretical challenges.

(iii) The next stage consists of more advanced studies focusing on a more thorough investigation of the method and first estimation of certain systematic effects. Before precision calculations can be carried out with full systematics taken into account, usually further technical difficulties must be overcome. During this evolution of knowledge, additional theoretical challenges may arise, as well as subleading systematic uncertainties.

(iv) The final desired outcome is an accurate and reliable Lattice QCD estimate of the observable of interest. For this to be achieved, the various sources of uncertainties must be quantified and brought under control.

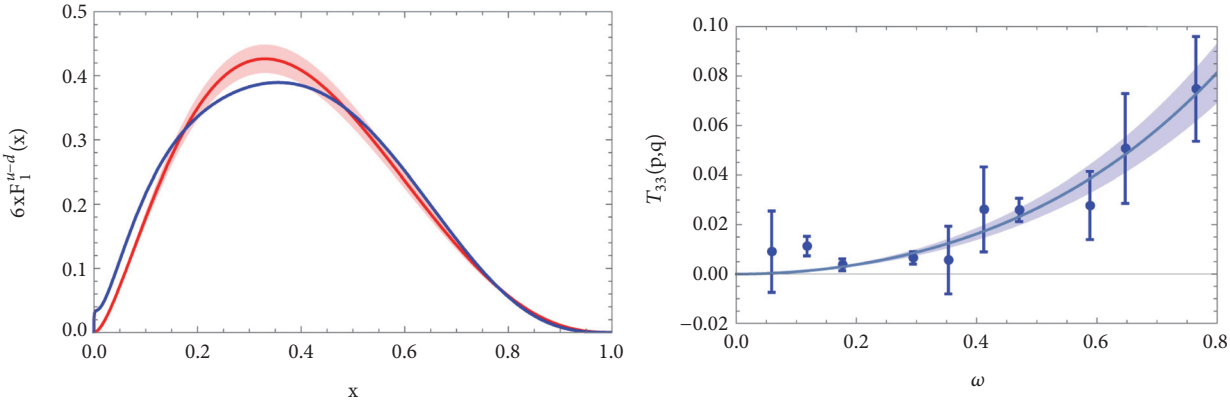

Figure 38: Left: exemplary parametrized PDF (blue) and its reconstruction (red) using the method proposed in [91]. Right: Compton amplitude obtained in an exploratory lattice computation. The solid line is a fit to a sixth order polynomial. Source: arXiv version of [91], reprinted with permission by the Authors (article published under the terms of the Creative Commons Attribution 4.0 International license).

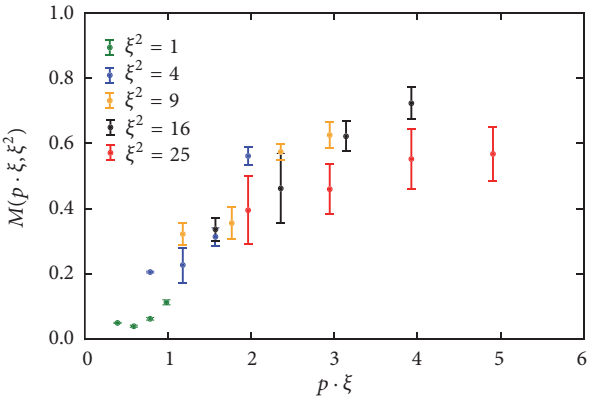

Figure 39: The vector-vector ($\gamma_1 - \gamma_1$) current-current matrix element in a boosted pion state vs. the Ioffe time $p \cdot \xi$ (p is pion momentum and ξ is separation of currents). Colors correspond to different separations ξ^2 in lattice units. These matrix elements can be factorized into the pion PDF. Source: [231], reprinted with permission by the Authors.

Based on Figure 40, we comment on the status of the different approaches presented in this paper. Most of the methods are still at an exploratory stage, or toward the third phase of advanced studies. Notable exceptions are, in our view, the isovector quark quasi-PDFs, as the numerical exploration began immediately after Ji's proposal. As we argued, the exploratory studies of 2014-2016 (see Section 3.2) showed the feasibility of the method and identified theoretical and lattice challenges. Among the former, we discussed the role of the spacetime signature and renormalizability (Section 5), renormalization studies (Section 7), and matching onto light-cone PDFs (Sections 3.1 and 8). The lattice challenges were of various origins and we described them in detail (Section 6). The most recent results of 2018 are, undoubtedly, in the advanced stage, using ensembles at physical pion masses and optimized lattice techniques, as well as reliable renormalization and matching procedures (Section 9). However, reaching into the precision era is still extremely demanding and will require overcoming further challenges, most of them classifiable as lattice ones. Careful investigation of systematic uncertainties is imperative and this will necessitate additional simulations employing ensembles with finer lattice spacings, larger volumes, accessing larger nucleon boosts, etc., as thoroughly reviewed in Section 6.3. This will require tremendous amount of computing time but is, in principle, possible. The difficult part of this programme is to reliably access large nucleon momenta and the main obstacle is the exponential signal-to-noise problem when increasing the boost and, at the same time, increasing the source-sink separation to avoid excited states contamination. We have highlighted the latter, since, in our view, this is an essential feature, if quasi-PDFs are to give reliable results. The present results are highly encouraging and steady increase of convergence towards phenomenologically extracted PDFs is being observed, even with partial agreement within uncertainties in some Bjorken-x regions. However, fully reliable results are still to be obtained. Nevertheless, it is highly conceivable that these lattice-extracted results may have extensive phenomenological impact, in particular the transversity PDF, which is much less constrained experimentally.

The quasidistribution approach has also been applied to other kinds of distributions (besides the isovector flavor combination) and notable progress has recently been achieved. We discussed the exploratory studies concerning quark DAs/PDFs for mesons and gluonic PDFs (Section 10). These results are promising for prospective reliable calculations that will also have an impact on phenomenological studies. However, as Figure 40 indicates, there are already challenges to go to the advanced stage, especially in the gluonic sector, which is characterized by noisy signal and mixings under matching with singlet quark PDFs, the latter requiring computation of noisy quark-disconnected diagrams. Yet other quasidistributions that are accessible, in principle, are quasi-GPDs and quasi-TMDs (Section 8.2). These are, obviously, much more difficult to compute, given the fact that they involve additional variables such as momentum transfer or transverse momentum. Both are receiving considerable

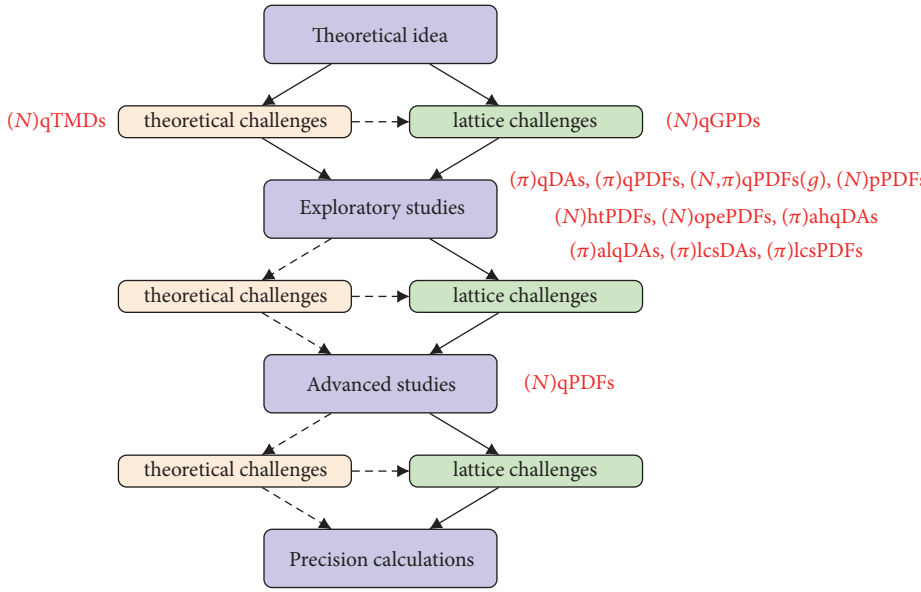

FIGURE 40: Flowchart of different methods of accessing partonic distributions considered in this review. Four main stages of every calculation are presented in blue boxes, connected with red/green boxes representing the theoretical and lattice challenges that need to be overcome to go to the next stage. Solid arrows indicate that given types of challenges emerge as a general rule, while dashed arrows signify that a given type of challenge does not have to appear for every method. The red text corresponds to different approaches and their current status. The symbol in parentheses indicates the hadron to which a given type of distribution pertains (N is nucleon and π is pion (also other mesons in certain cases)). The considered distributions are PDFs/DAs/GPDs/TMDs, in general for quarks (with an explicit counterexample of gluonic PDFs indicated with parentheses at the end (g)). The approach is indicated with small letters before the distribution name: q is quasidistributions, p is pseudodistributions, ht is hadronic tensor, ope is OPE without OPE, ahq is auxiliary heavy quark, alq is auxiliary light quark, and lcs is good lattice cross-sections. Example: (N)qPDFs: quark PDFs of the nucleon accessed with the quasidistribution method.

theoretical attention and continuous progress, but numerical explorations are still absent and, in the case of quasi-TMDs, important theoretical challenges are yet to be overcome.

Even though quasidistributions are currently the most explored, other approaches are beginning to yield very interesting results as well. Several exploratory studies have been reported for quark PDFs and DAs of nucleons and pions (Section 11). These methods are in different phases of exploratory studies, but steadily pushing towards more advanced investigations. Theoretical and lattice challenges are beginning to be clear. We note that many of them are common to all approaches, such as cutoff effects, other typical lattice systematics, or the need for precise signal extraction for highly boosted hadrons. However, some of them are more specific to certain approaches, such as the renormalization of nonlocal operators for quasidistributions. The level of numerical difficulty may also vary. For example, some approaches require the computation of three-/two-point functions for PDFs/DAs (e.g., quasidistributions), while other ones necessitate the use of four-/three-point correlators (e.g., hadronic tensor, auxiliary quark methods). It is also clear that all these approaches, even though aiming at the same physical observables, may have very different systematics in practice. Hence, it can be expected that a global fitting strategy, combining results from various methods, can prove in the end to be the optimal one. Thus, all the efforts of the lattice community, with the aid of experts in phenomenology, can contribute to obtaining reliable first-principle determinations of partonic distributions.

Appendix

Abbreviations

1PI: 1-Particle irreducible
APE: Array processor experiment
CAA: Covariant Approximation Averaging
χPT: Chiral perturbation theory
DA: Distribution amplitude
DIS: Deep-inelastic scattering
DR: Dimensional regularization
DSM: Diquark spectator model
DVCS: Deeply Virtual Compton Scattering
DVMP: Deeply Virtual Meson Production
EIC: Electron-Ion Collider
ETMC: Extended Twisted Mass Collaboration[13]
FVE: Finite volume effects
GPD: Generalized parton distribution
HCS: Hadronic cross-section
HISQ: Highly improved staggered quarks
HP: High precision
HQET: Heavy Quark Effective Theory
HYP: Hypercubic
HTE: Higher-twist effects

IMF: Infinite momentum frame
IR: Infrared
ITD: Ioffe-time distribution
JLab: Jefferson Laboratory
LaMET: Large Momentum Effective Theory
LCS: Lattice cross-section
LCWF: Light-cone wave function
LLA: Leading logarithmic approximation
LP: Low precision
LP^3: Lattice Parton Physics Project
LR: Lattice regularization
NJL: Nambu-Jona-Lasinio
NLO: Next-to-leading order
NMC: Nucleon mass correction
NRQCD: Nonrelativistic Quantum Chromodynamics
OPE: Operator product expansion
PDF: Parton distribution function
RI: Regularization independent
RI/MOM: Regularization-independent momentum subtraction
rms: Root mean square
QCD: Quantum Chromodynamics
QED: Quantum Electrodynamics
SIDIS: Semi-inclusive deep-inelastic scattering
SQM: Spectral quark model
TMC: Target mass correction
TMD: Transverse momentum dependent parton distribution function
UV: Ultraviolet
VDF: Virtuality distribution function.

Conflicts of Interest

The authors declare that they have no conflicts of interest.

Acknowledgments

We first want to thank the editors of the special issue "Transverse Momentum Dependent Observables from Low to High Energy: Factorization, Evolution, and Global Analyses" for the invitation to prepare this review and the guidance they provided throughout the process. We are also grateful to all Authors for giving permission for the figures we used to illustrate the progress of the field. We are indebted to several people with whom we had discussions over the years and who helped to shape our view on different aspects discussed in this review. Their names are, in alphabetical order, C. Alexandrou, G. Bali, R. Briceño, W. Broniowski, J.-W. Chen, I. C. Cloet, W. Detmold, V. Drach, M. Engelhardt, L. Gamberg, E. García-Ramos, K. Golec-Biernat, J. Green, K. Hadjiyiannakou, K. Jansen, X. Ji, P. Korcyl, G. Koutsou, P. Kotko, K. Kutak, C.-J.D. Lin, K.-F. Liu, S. Liuti, W. Melnitchouk, A. Metz, Z.-E. Meziani, C. Monahan, K. Orginos, H. Panagopoulos, A. Prokudin, J.-W. Qiu, A. Radyushkin, G. C. Rossi, N. Sato, M. Savage, A. Scapellato, R. Sommer, F. Steffens, I. W. Stewart, R. Sufian, J. Wagner, Ch. Wiese, J. Wosiek, Y.-B. Yang, F. Yuan, S. Zafeiropoulos, J.-H. Zhang, and Y. Zhao. We also thank all members of the TMD Topical Collaboration for enlightening discussions. Krzysztof Cichy is supported by the National Science Centre (Poland) Grant SONATA BIS no. 2016/22/E/ST2/00013. Martha Constantinou acknowledges financial support by the U.S. Department of Energy, Office of Nuclear Physics, within the framework of the TMD Topical Collaboration, as well as by the National Science Foundation under Grant no. PHY-1714407.

Endnotes

1. In the remainder of the paper, the standard relativistic normalization is always assumed and the states are labeled with the hadron momentum and other labels, if necessary.
2. For simplicity, we neglect possible mixings under factorization.
3. The Dirac structure was, in the original papers, also in the same direction, i.e. γ^3 was used. However, it became clear that γ^0 is a better choice that leads to the same PDF, as described in Section 7.
4. The term "factorizable matrix elements" is also employed [51] to better represent the properties of such matrix elements.
5. For proper treatment thereof, see Section 8
6. Effective from this year, the European Twisted Mass Collaboration has officially changed its name to Extended Twisted Mass Collaboration, as it comprises now members also from non-European institutions. Along with the name change, there is a new logo.
7. Note that the same abbreviation is used in phenomenological analyses for the corrections due to a non-zero mass of the target in scattering experiments.
8. not to be confused with the symbol ξ used in other sections which denotes the length of the Wilson line in physical units.
9. We remind the Reader that prior to 2018 all available lattice data in the literature corresponded to the "γ^3" operator for the unpolarized PDFs, which has a finite mixing in lattice regularization due to chiral symmetry breaking.
10. Preliminary results have been presented last year [160, 258]
11. After the submission of this manuscript, a complete calculation was presented in Ref. [159].
12. The complete work appeared after the submission of this manuscript, in Ref. [231].
13. Effective from this year, the European Twisted Mass Collaboration has officially changed its name to Extended Twisted Mass Collaboration, as it comprises now members also from non-European institutions. Along with the name change, there is a new logo.

References

[1] M. Breidenbach, J. I. Friedman, H. W. Kendall et al., "Observed behavior of highly inelastic electron-proton scattering," *Physical Review Letters*, vol. 23, no. 16, pp. 935–939, 1969.

[2] E. D. Bloom, D. H. Coward, H. DeStaebler et al., "High-energy inelastic e p scattering at 6-degrees and 10-degrees," *Physical Review Letters*, vol. 23, pp. 930–934, 1969.

[3] X. Ji, "Gauge-invariant decomposition of nucleon spin," *Physical Review Letters*, vol. 78, no. 4, pp. 610–613, 1997.

[4] A. V. Radyushkin, "Scaling limit of deeply virtual compton scattering," *Physics Letters B*, vol. 380, no. 3-4, pp. 417–425, 1996.

[5] M. Diehl, "Generalized parton distributions," *Physics Reports*, vol. 388, no. 2–4, pp. 41–277, 2003.

[6] X. Ji, "Generalized parton distributions," *Annual Review of Nuclear and Particle Science*, vol. 54, no. 1, pp. 413–450, 2004.

[7] A. V. Belitsky and A. V. Radyushkin, "Unraveling hadron structure with generalized parton distributions," *Physics Reports*, vol. 418, no. 1–6, pp. 1–387, 2005.

[8] J. C. Collins and D. E. Soper, "Back-to-back jets in QCD," *Nuclear Physics B*, vol. 193, no. 2, pp. 381–443, 1981, [Erratum: Nuclear Physics B, vol. 213,p. 545, 1983].

[9] J. C. Collins and D. E. Soper, "Parton distribution and decay functions," *Nuclear Physics B*, vol. 194, no. 3, pp. 445–492, 1982.

[10] D. Boer, R. Venugopalan, M. Diehl, R. Milner, W. Vogelsang et al., "Gluons and the quark sea at high energies: distributions, polarization, tomography," 2011, https://arxiv.org/abs/1108.1713.

[11] A. Accardi, J. L. Albacete, M. Anselmino et al., "Electron Ion Collider: The Next QCD Frontier - Understanding the glue that binds us all," *The European Physical Journal A*, vol. 52, p. 268, 2016.

[12] R. Angeles-Martinez, A. Bacchetta, I. Balitsky et al., "Transverse momentum dependent (TMD) parton distribution functions: status and prospects," *Acta Physica Polonica B*, vol. 46, no. 12, p. 2501, 2015.

[13] R. Devenish and A. Cooper-Sarkar, *Deep Inelastic Scattering*, Oxford University Press, 2003.

[14] X. Ji, "Deeply virtual Compton scattering," *Physical Review D: Particles, Fields, Gravitation and Cosmology*, vol. 55, no. 11, pp. 7114–7125, 1997.

[15] L. Favart, M. Guidal, T. Horn, and P. Kroll, "Deeply virtual meson production on the nucleon," *The European Physical Journal A*, vol. 52, no. 6, p. 158, 2016.

[16] National Academies of Sciences Engineering Medicine, *An Assessment of U.S.-Based Electron-Ion Collider Science*, National Academies Press, Washington, DC, USA, 2018.

[17] E. Perez and E. Rizvi, "The quark and gluon structure of the proton," *Reports on Progress in Physics*, vol. 76, no. 4, Article ID 046201, 2013.

[18] A. De Roeck and R. Thorne, "Structure functions," *Progress in Particle and Nuclear Physics*, vol. 66, no. 4, pp. 727–781, 2011.

[19] S. Alekhin, S. Alioli, R. D. Ball et al., "The PDF4LHC working group interim report," 2011, https://arxiv.org/abs/1101.0536.

[20] R. D. Ball, S. Carrazza, L. Del Debbio et al., "Parton distribution benchmarking with LHC data," *Journal of High Energy Physics*, vol. 2013, no. 4, 2013.

[21] S. Forte and G. Watt, "Progress in the determination of the partonic structure of the proton," *Annual Review of Nuclear and Particle Science*, vol. 63, no. 1, pp. 291–328, 2013.

[22] P. Jimenez-Delgado, W. Melnitchouk, and J. F. Owens, "Parton momentum and helicity distributions in the nucleon," *Journal of Physics G: Nuclear and Particle Physics*, vol. 40, no. 9, Article ID 093102, 2013.

[23] J. Rojo, A. Accardi, R. D. Ball et al., "The PDF4LHC report on PDFs and LHC data: results from Run I and preparation for Run II," *Journal of Physics G: Nuclear and Particle Physics*, vol. 42, no. 10, Article ID 103103, 2015.

[24] J. Butterworth, S. Carrazza, and A. Cooper-Sarkar, "PDF4LHC recommendations for LHC Run II," *Journal of Physics G: Nuclear and Particle Physics*, vol. 43, no. 2, Article ID 023001, 2016.

[25] A. Accardi, S. Alekhin, J. Blümlein et al., "A critical appraisal and evaluation of modern PDFs," *The European Physical Journal C*, vol. 76, no. 8, 2016.

[26] J. Gao, L. Harland-Lang, and J. Rojo, "The structure of the proton in the LHC precision era," *Physics Reports*, vol. 742, pp. 1–121, 2018.

[27] H.-W. Lin, E. R. Nocera, F. Olness et al., "Parton distributions and lattice QCD calculations: a community white paper," *Progress in Particle and Nuclear Physics*, vol. 100, pp. 107–160, 2017.

[28] R. Jakob, P. Mulders, and J. Rodrigues, "Modelling quark distribution and fragmentation functions," *Nuclear Physics A*, vol. 626, no. 4, pp. 937–965, 1997.

[29] M. Engelhardt, B. Musch, P. Hagler, J. Negele, and A. Schäfer, "Lattice study of the Boer-Mulders transverse momentum distribution in the pion," *Physical Review D: Covering Particles, Fields, Gravitation, and Cosmology*, vol. 93, no. 5, Article ID 054501, 2016.

[30] M. Engelhardt, "Quark orbital dynamics in the proton from Lattice QCD – from Ji to Jae-Manohar orbital angular momentum," *Physical Review D*, vol. 95, Article ID 094505, 2017.

[31] B. Yoon, M. Engelhardt, R. Gupta et al., "Nucleon transverse momentumdependent parton distributions in lattice QCD: renormalization patterns and discretization effects," *Physical Review D*, vol. 96, Article ID 094508, 2017.

[32] L. V. Gribov, E. M. Levin, and M. G. Ryskin, "Semihard processes in QCD," *Physics Reports*, vol. 100, no. 1-2, pp. 1–150, 1983.

[33] A. Mueller and J.-W. Qiu, "Gluon recombination and shadowing at small values of x," *Nuclear Physics B*, vol. 268, no. 2, pp. 427–452, 1986.

[34] L. McLerran and R. Venugopalan, "Computing quark and gluon distribution functions for very large nuclei," *Physical Review D: Particles, Fields, Gravitation and Cosmology*, vol. 49, no. 5, pp. 2233–2241, 1994.

[35] C. Alexandrou, M. Constantinou, K. Hadjiyiannakou et al., "Nucleon Spin and Momentum Decomposition Using Lattice QCD Simulations," *Physical Review Letters*, vol. 119, no. 14, Article ID 142002, 2017.

[36] Y.-B. Yang, R. S. Sufian, A. Alexandru et al., "Glue spin and helicity in the proton from lattice QCD," *Physical Review Letters*, vol. 118, no. 10, Article ID 102001, 2017.

[37] L. Jin, "Review of lattice muon g-2 HLbL calculation," *PoS(LATTICE2018)011, PoS LATTICE2018*, vol. 011, 2018.

[38] M. Marinkovic, "Leading hadronic contribution to muon g-2 from lattice QCD and the MUonE experiment," *PoS(LATTICE2018)012, PoS LATTICE2018*, vol. 012, 2018.

[39] J. Green, "Systematics in nucleon matrix element calculations," in *Proceedings of the 36th International Symposium on Lattice Field Theory (Lattice '18)*, East Lansing, MI, USA, 2018.

[40] M. Constantinou, "Hadron Structure," in *Proceedings of the 32nd International Symposium on Lattice Field Theory (Lattice '14)*, Brookhaven, New York, NY, USA, June 2014.

[41] M. Constantinou, "Recent progress in hadron structure from Lattice QCD," in *Proceedings of the 8th International Workshop on Chiral Dynamics (CD '15)*, Pisa, Italy, June 2015.

[42] C. Alexandrou and K. Jansen, "Hadron structure from lattice QCD," *Nuclear and Particle Physics Proceedings*, vol. 261-262, pp. 202–217, 2015.

[43] C. Alexandrou, "Selected results on hadron structure using state-of-the-art lattice QCD simulations," in *Proceedings of the 45th International Symposium on Multiparticle Dynamics (ISMD '15)*, Kreuth, Germany, October 2015.

[44] S. Syritsyn, "Review of hadron structure calculations on a lattice," in *Proceedings of the 31st International Symposium on Lattice Field Theory (LATTICE '13)*, p. 009, Mainz, Germany, July 2013.

[45] X. Ji, "Parton physics on a euclidean lattice," *Physical Review Letters*, vol. 110, no. 26, Article ID 262002, 2013.

[46] H.-W. Lin, J.-W. Chen, S. D. Cohen, and X. Ji, "Flavor structure of the nucleon sea from lattice QCD," *Physical Review D: Particles, Fields, Gravitation and Cosmology*, vol. 91, no. 5, Article ID 054510, 2015.

[47] C. Alexandrou, K. Cichy, V. Drach et al., "First results with twisted mass fermions towards the computation of parton distribution functions on the lattice," in *Proceedings of the 32nd International Symposium on Lattice Field Theory (Lattice '14)*, Brookhaven, New York, NY, USA, June 2014.

[48] C. Alexandrou, K. Cichy, M. Constantinou et al., "Transversity parton distribution functions from lattice QCD," *Physical Review D: Particles, Fields, Gravitation, and Cosmology*, vol. 98, no. 9, Article ID 091503, 2018.

[49] Y.-S. Liu, J.-W. Chen, L. Jin et al., "Nucleon transversity distribution at the physical pion mass from lattice QCD," 2018, https://arxiv.org/abs/1810.05043.

[50] H.-W. Lin, "From C to parton sea: bjorken-x dependence of the PDFs," in *Proceedings of the 34th International Symposium on Lattice Field Theory (Lattice '16)*, Southampton, UK, July 2016.

[51] C. Monahan, "Recent developments in x-dependent structure calculations," in *Proceedings of the 36th International Symposium on Lattice Field Theory (Lattice '18)*, East Lansing, MI, USA, July 2018.

[52] B. L. Ioffe, "Space-time picture of photon and neutrino scattering and electroproduction cross section asymptotics," *Physics Letters B*, vol. 30, no. 2, pp. 123–125, 1969.

[53] Y. Frishman, "Scale invariance and current commutators near the light cone," *Physical Review Letters*, vol. 25, no. 14, pp. 966–969, 1970.

[54] K.-F. Liu and S. Dong, "Origin of difference between anti-d and anti-u partons in the nucleon," *Physical Review Letters*, vol. 72, no. 12, pp. 1790–1793, 1994.

[55] K. F. Liu, S. J. Dong, T. Draper et al., "Valence QCD: Connecting QCD to the quark model," *Physical Review D: Particles, Fields, Gravitation and Cosmology*, vol. 59, no. 11, Article ID 112001, 1999.

[56] K.-F. Liu, "Parton degrees of freedom from the path-integral formalism," *Physical Review D: Particles, Fields, Gravitation and Cosmology*, vol. 62, no. 7, Article ID 074501, 2000.

[57] U. Aglietti, M. Ciuchini, G. Corbò, E. Franco, G. Martinelli, and L. Silvestrini, "Model independent determination of the shape function for inclusive b decays and of the structure functions in DIS," *Physics Letters B*, vol. 432, no. 3-4, pp. 411–420, 1998.

[58] W. Detmold and C.-J. D. Lin, "Deep-inelastic scattering and the operator product expansion in lattice QCD," *Physical Review D: Particles, Fields, Gravitation and Cosmology*, vol. 73, no. 1, Article ID 014501, 2006.

[59] M. T. Hansen, H. B. Meyer, and D. Robaina, "From deep inelastic scattering to heavy-flavor semileptonic decays: Total rates into multihadron final states from lattice QCD," *Physical Review D: Particles, Fields, Gravitation and Cosmology*, vol. 96, no. 9, Article ID 094513, 2017.

[60] N. Christ, X. Feng, G. Martinelli, and C. T. Sachrajda, "Effects of finite volume on the $K_L - K_S$ mass difference," *Physical Review D: Particles, Fields, Gravitation, and Cosmology*, vol. 91, no. 11, Article ID 114510, 2015.

[61] K.-F. Liu, "Parton distribution function from the hadronic tensor on the lattice," in *Proceedings of the 33rd International Symposium on Lattice Field Theory (Lattice '15)*, Kobe, Japan, July 2015.

[62] K.-F. Liu, "Evolution equations for connected and disconnected sea parton distributions," *Physical Review D: Particles, Fields, Gravitation and Cosmology*, vol. 96, no. 3, Article ID 033001, 2017.

[63] J. Liang, K.-F. Liu, Y.-B. Yang et al., "Lattice calculation of hadronic tensor of the nucleon," in *Proceedings of the 35th International Symposium on Lattice Field Theory (Lattice '17) & EPJ Web Conference*, vol. 175, Granada, Spain, June 2017.

[64] U. Aglietti, M. Ciuchini, G. Corbò, E. Franco, G. Martinelli, and L. Silvestrini, "Model independent determination of the light-cone wave functions for exclusive processes," *Physics Letters B*, vol. 441, no. 1–4, pp. 371–375, 1998.

[65] A. Abada, P. Boucaud, G. Herdoiza et al., "Preliminaries on a lattice analysis of the pion light-cone wave function: A partonic signal?" *Physical Review D: Particles, Fields, Gravitation and Cosmology*, vol. 64, no. 7, Article ID 074511, 2001.

[66] A. Abada, P. Boucaud, G. Herdoiza et al., "The pion light-cone wave function $\Phi\pi$ on the lattice: a partonic signal?" *Nuclear Physics B—Proceedings Supplements*, vol. 106-107, pp. 338–340, 2002.

[67] W. Broniowski, S. Prelovsek, L. Šantelj, and E. Ruiz Arriola, "Pion wave function from lattice QCD vs. chiral quark models," *Physics Letters B*, vol. 686, no. 4-5, pp. 313–318, 2010.

[68] W. Detmold, I. Kanamori, C. J. D. Lin, S. Mondal, and Y. Zhao, "Moments of pion distribution amplitude using operator product expansion on the lattice," 2018, https://arxiv.org/abs/1810.12194.

[69] V. Braun and D. Müller, "Exclusive processes in position space and the pion distribution amplitude," *The European Physical Journal C*, vol. 55, no. 3, pp. 349–361, 2008.

[70] G. S. Bali, V. M. Braun, B. Gläßle et al., "Pion distribution amplitude from Euclidean correlation functions: Exploring universality and higher twist effects," *Physical Review D: Particles, Fields, Gravitation, and Cosmology*, vol. 78, no. 3, Article ID 094507, 2018.

[71] G. S. Bali, V. M. Braun, B. Gläßle et al., "Pion distribution amplitude from Euclidean correlation functions," *The European Physical Journal C: Proceedings of the 35th Interna-tional Symposium on Lattice Field Theory (Lattice 2017): Granada, Spain*, vol. 78, 2018.

[72] R. P. Feynman, "Very high-energy collisions of hadrons," *Physical Review Letters*, vol. 23, no. 24, pp. 1415–1417, 1969.

[73] R. P. Feynman, *Photon-Hadron Interactions*, Frontiers in Physics, Benjamin, Reading, MA, USA, 1972.

[74] X. Ji, "Parton physics from large-momentum effective field theory," *Science China Physics, Mechanics & Astronomy*, vol. 57, no. 7, pp. 1407–1412, 2014.

[75] A. V. Radyushkin, "Nonperturbative evolution of parton quasi-distributions," *Physics Letters. B. Particle Physics, Nuclear Physics and Cosmology*, vol. 767, pp. 314–320, 2017.

[76] A. Radyushkin, "Target mass effects in parton quasi-distributions," *Physics Letters B*, vol. 770, pp. 514–522, 2017.

[77] A. Radyushkin, "Quasi-parton distribution functions, momentum distributions, and pseudo-parton distribution functions," *Physical Review D: Particles, Fields, Gravitation and Cosmology*, vol. 96, no. 3, Article ID 034025, 2017.

[78] A. V. Radyushkin, "Virtuality distributions in application to $\gamma\gamma^* \longrightarrow \pi^0$ transition form factor at handbag level," *Physics Letters B*, vol. 735, pp. 417–425, 2014.

[79] A. V. Radyushkin, "Virtuality and transverse momentum dependence of the pion distribution amplitude," *Physical Review D: Particles, Fields, Gravitation and Cosmology*, vol. 93, no. 5, Article ID 056002, 2016.

[80] A. V. Radyushkin, "Quark pseudodistributions at short distances," *Physics Letters B*, vol. 781, pp. 433–442, 2018.

[81] A. Radyushkin, "One-loop evolution of parton pseudo-distribution functions on the lattice," *Physical Review D: Particles, Fields, Gravitation and Cosmology*, vol. 98, Article ID 014019, 2018.

[82] J.-H. Zhang, J.-W. Chen, and C. Monahan, "Patron distribution functions from reduced Ioffe-time distributions," *Physical Review D: Particles, Fields, Gravitation and Cosmology*, vol. 97, no. 7, Article ID 074508, 2018.

[83] T. Izubuchi, X. Ji, L. Jin, I. W. Stewart, and Y. Zhao, "Factorization theorem relating Euclidean and light-cone parton distributions," *Physical Review D: Particles, Fields, Gravitation and Cosmology*, vol. 98, no. 5, Article ID 056004, 2018.

[84] A. V. Radyushkin, "Structure of parton quasi-distributions and their moments," *Physics Letters B*, vol. 788, pp. 380–387, 2019.

[85] Y.-Q. Ma and J.-W. Qiu, "Extracting parton distribution functions from lattice QCD calculations," *Physical Review D: Particles, Fields, Gravitation and Cosmology*, vol. 98, no. 7, Article ID 074021, 2018.

[86] Y.-Q. Ma and J.-W. Qiu, "Exploring partonic structure of hadrons using ab initio lattice QCD calculations," *Physical Review Letters*, vol. 120, no. 2, Article ID 022003, 2018.

[87] K. Orginos, A. Radyushkin, J. Karpie, and S. Zafeiropoulos, "Lattice QCD exploration of parton pseudo-distribution functions," *Physical Review D: Particles, Fields, Gravitation and Cosmology*, vol. 96, no. 9, Article ID 094503, 2017.

[88] A. Radyushkin, "Quasi-PDFs and pseudo-PDFs," in *Proceedings of the QCD Evolution Workshop (QCD '17)*, Newport News, VA, USA, May 2017.

[89] J. Karpie, K. Orginos, A. Radyushkin et al., "Parton distribution functions on the lattice and in the continuum," in *Proceedings of the 35th International Symposium on Lattice Field Theory (Lattice '17) & EPJ Web Conference*, vol. 175, Granada, Spain, June 2017.

[90] J. Karpie, K. Orginos, and S. Zafeiropoulos, "Moments of Ioffe time parton distribution functions from non-local matrix elements," *Journal of High Energy Physics*, vol. 2018, no. 11, 2018.

[91] A. Chambers, R. Horsley, Y. Nakamura et al., "Nucleon structure functions from operator product expansion on the lattice," *Physical Review Letters*, vol. 118, no. 24, Article ID 242001, 2017.

[92] G. Martinelli, "Hadronic weak interactions of light quarks," *Nuclear Physics B—Proceedings Supplements*, vol. 73, no. 1–3, pp. 58–71, 1999.

[93] C. Dawson, G. Martinelli, G. Rossi et al., "New lattice approaches to the delta I = 1/2 rule," *Nuclear Physics B*, vol. 514, no. 1-2, pp. 313–335, 1998.

[94] R. Horsley, R. Millo, Y. Nakamura et al., "A lattice study of the glue in the nucleon," *Physics Letters B*, vol. 714, no. 2–5, pp. 312–316, 2012.

[95] Y.-Q. Ma and J.-W. Qiu, "QCD factorization and PDFs from lattice QCD calculation," *International Journal of Modern Physics: Conference Series*, vol. 37, Article ID 1560041, 2015.

[96] H. Georgi and H. D. Politzer, "Freedom at moderate energies: Masses in color dynamics," *Physical Review D: Particles, Fields, Gravitation and Cosmology*, vol. 14, no. 7, pp. 1829–1848, 1976.

[97] A. V. Manohar and M. B. Wise, "Heavy quark physics," *Cambridge Monographs on Particle Physics, Nuclear Physics, and Cosmology*, vol. 10, pp. 1–191, 2000.

[98] X. Xiong, X. Ji, J. Zhang, and Y. Zhao, "One-loop matching for parton distributions: Nonsinglet case," *Physical Review D: Particles, Fields, Gravitation and Cosmology*, vol. 90, no. 1, Article ID 014051, 2014.

[99] S. Weinberg, "Dynamics at infinite momentum," *Physical Review A: Atomic, Molecular and Optical Physics*, vol. 150, no. 4, pp. 1313–1318, 1966.

[100] C. Alexandrou, K. Cichy, V. Drach et al., "Lattice calculation of parton distributions," *Physical Review D: Particles, Fields, Gravitation and Cosmology*, vol. 92, Article ID 014502, 2015.

[101] A. Hasenfratz, R. Hoffmann, and S. Schaefer, "Hypercubic smeared links for dynamical fermions," *Journal of High Energy Physics*, vol. 2007, no. 05, Article ID 029, 2007.

[102] A. D. Martin, W. J. Stirling, and G. Watt, "Parton distributions for the LHC," *The European Physical Journal C*, vol. 63, no. 2, pp. 189–285, 2009.

[103] J. F. Owens, A. Accardi, and W. Melnitchouk, "Global parton distributions with nuclear and finite-Q^2 corrections," *Physical Review D: Particles, Fields, Gravitation and Cosmology*, vol. 87, no. 9, Article ID 094012, 2013.

[104] S. Alekhin, J. Blümlein, and S. Moch, "Parton distribution functions and benchmark cross sections at next-to-next-to-leading order," *Physical Review D: Particles, Fields, Gravitation and Cosmology*, vol. 86, no. 5, Article ID 054009, 2012.

[105] M. Constantinou, "Renormalization issues on long-link operators," in *Proceedings of the 7th Workshop of the APS Topical Group on Hadronic Physics*, February 2017.

[106] M. Constantinou and H. Panagopoulos, "Perturbative renormalization of quasi-parton distribution functions," *Physical Review D: Particles, Fields, Gravitation and Cosmology*, vol. 96, no. 5, Article ID 054506, 2017.

[107] J.-W. Chen, S. D. Cohen, X. Ji, H.-W. Lin, and J.-H. Zhang, "Nucleon helicity and transversity parton distributions from lattice QCD," *Nuclear Physics B*, vol. 911, pp. 246–273, 2016.

[108] C. Alexandrou, K. Cichy, M. Constantinou et al., "Updated lattice results for parton distributions," *Physical Review D: Particles, Fields, Gravitation and Cosmology*, vol. 96, Article ID 014513, 2017.

[109] G. S. Bali, B. Lang, B. U. Musch, and A. Schäfer, "Novel quark smearing for hadrons with high momenta in lattice QCD," *Physical Review D: Particles, Fields, Gravitation and Cosmology*, vol. 93, no. 9, Article ID 094515, 2016.

[110] L. Gamberg, Z.-B. Kang, I. Vitev, and X. Hongxi, "Quasi-parton distribution functions: a study in the diquark spectator model," *Physics Letters B*, vol. 743, Article ID 112120, pp. 112–120, 2015.

[111] I. Vitev, L. Gamberg, Z. Kang, and H. Xing, "A study of quasi-parton distribution functions in the diquark spectator model," in *Proceedings of the QCD Evolution Workshop (QCD '15)*, Newport News, VA, USA, May 2015.

[112] J. Soffer, "Positivity constraints for spin-dependent parton distributions," *Physical Review Letters*, vol. 74, no. 8, pp. 1292–1294, 1995.

[113] A. Bacchetta, M. Radici, B. Pasquini, and X. Xiong, "Reconstructing parton densities at large fractional momenta," *Physical Review D: Particles, Fields, Gravitation and Cosmology*, vol. 95, no. 1, Article ID 014036, 2017.

[114] S. Bhattacharya, C. Cocuzza, and A. Metz, "Generalized quasi parton distributions in a diquark spectator model," *Physics Letters B*, vol. 788, pp. 453–463, 2019.

[115] X. Ji, A. Schäfer, X. Xiong, and J. Zhang, "One-loop matching for generalized parton distributions," *Physical Review D: Particles, Fields, Gravitation and Cosmology*, vol. 92, no. 1, Article ID 014039, 2015.

[116] W. Broniowski and E. Ruiz Arriola, "Nonperturbative partonic quasidistributions of the pion from chiral quark models," *Physics Letters B*, vol. 773, pp. 385–390, 2017.

[117] W. Broniowski and E. Ruiz Arriola, "Partonic quasidistributions of the proton and pion from transversemomentum distributions," *Physical Review D: Particles, Fields, Gravitation and Cosmology*, vol. 97, Article ID 034031, 2018.

[118] Y. Nambu and G. Jona-Lasinio, "Dynamical model of elementary particles based on an analogy with superconductivity. 1," *Physical Review Journals Archive*, vol. 122, pp. 345–358, 1961.

[119] Y. Nambu and G. Jona-Lasinio, "Dynamical model of elementary particles based on an analogy with superconductivity. II," *Physical Review A: Atomic, Molecular and Optical Physics*, vol. 124, no. 1, pp. 246–254, 1961.

[120] E. Ruiz Arriola, "Parton distributions for the pion in a chiral quark model," in *Proceedings of the Workshop on Lepton Scattering, Hadrons and QCD*, pp. 37–44, Adelaide, Australia, March 2001.

[121] E. Ruiz Arriola and W. Broniowski, "Spectral quark model and low-energy hadron phenomenology," *Physical Review D: Particles, Fields, Gravitation and Cosmology*, vol. 67, no. 7, Article ID 074021, 2003.

[122] E. Ruiz Arriola and W. Broniowski, "The spectral quark model and light cone phenomenology," in *Proceedings of the Light Cone Physics: Hadrons and beyond*, University of Durham, August 2003.

[123] J. Zhang, J. Chen, X. Ji, L. Jin, and H. Lin, "Pion distribution amplitude from lattice QCD," *Physical Review D: Particles, Fields, Gravitation and Cosmology*, vol. 95, no. 9, Article ID 094514, 2017.

[124] C. Alexandrou, K. Cichy, M. Constantinou, K. Jansen, A. Scapellato, and F. Steffens, "Light-cone parton distribution functions from lattice QCD," *Physical Review Letters*, vol. 121, no. 11, Article ID 112001, 2018.

[125] Y. Jia and X. Xiong, "Quasidistribution amplitude of heavy quarkonia," *Physical Review D: Particles, Fields, Gravitation and Cosmology*, vol. 94, no. 9, Article ID 094005, 2016.

[126] Y. Jia, S. Liang, X. Xiong, and R. Yu, "Partonic quasidistributions in two-dimensional QCD," *Physical Review D: Particles, Fields, Gravitation and Cosmology*, vol. 98, no. 5, Article ID 054011, 2018.

[127] G. Hooft, "A two-dimensional model for mesons," *Nuclear Physics B*, vol. 75, no. 3, pp. 461–470, 1974.

[128] I. Bars and M. B. Green, "Poincaré- and gauge-invariant two-dimensional quantum chromodynamics," *Physical Review D: Particles, Fields, Gravitation and Cosmology*, vol. 17, no. 2, pp. 537–545, 1978.

[129] C. Monahan and K. Orginos, "Quasi parton distributions and the gradient flow," *Journal of High Energy Physics*, vol. 2017, p. 116, 2017.

[130] C. E. Carlson and M. Freid, "Lattice corrections to the quark quasidistribution at one loop," *Physical Review D: Particles, Fields, Gravitation and Cosmology*, vol. 95, no. 9, Article ID 094504, 2017.

[131] R. A. Briceño, M. T. Hansen, and C. J. Monahan, "Role of the Euclidean signature in lattice calculations of quasidistributions and other nonlocal matrix elements," *Physical Review D: Particles, Fields, Gravitation and Cosmology*, vol. 96, no. 1, Article ID 014502, 2017.

[132] T. Ishikawa, Y.-Q. Ma, J.-W. Qiu, and S. Yoshida, "Practical quasi parton distribution functions," 2016, https://arxiv.org/abs/1609.02018.

[133] X. Ji and J. Zhang, "Renormalization of quasiparton distribution," *Physical Review D: Particles, Fields, Gravitation and Cosmology*, vol. 92, no. 3, Article ID 034006, 2015.

[134] T. Ishikawa, Y. Ma, J. Qiu, and S. Yoshida, "Renormalizability of quasiparton distribution functions," *Physical Review D: Particles, Fields, Gravitation and Cosmology*, vol. 96, no. 9, Article ID 094019, 2017.

[135] X. Ji, J. Zhang, and Y. Zhao, "Renormalization in large momentum effective theory of parton physics," *Physical Review Letters*, vol. 120, no. 11, Article ID 112001, 2018.

[136] W. Wang and S. Zhao, "On the power divergence in quasi gluon distribution function," *Journal of High Energy Physics*, vol. 05, Article ID 142, 2018.

[137] J.-H. Zhang, X. Ji, A. Schäfer, W. Wang, and S. Zhao, "Accessing gluon parton distributions in large momentum effective theory," *Physical Review Letters*, vol. 122, no. 14, Article ID 142001, 2019.

[138] Z.-Y. Li, Y.-Q. Ma, and J.-W. Qiu, "Multiplicative renormalizability of quasi-parton distributions," *Physical Review Letters*, vol. 122, no. 6, Article ID 062002, 2019.

[139] A. M. Polyakov, "Gauge fields as rings of glue," *Nuclear Physics B*, vol. 164, no. 1, pp. 171–188, 1980.

[140] V. S. Dotsenko and S. N. Vergeles, "Renormalizability of phase factors in nonabelian gauge theory," *Nuclear Physics B*, vol. 169, no. 5-6, pp. 527–546, 1980.

[141] T. Mannel, W. Roberts, and Z. Ryzak, "A derivation of the heavy quark effective lagrangian from QCD," *Nuclear Physics B*, vol. 368, pp. 204–217, 1992.

[142] W. Wang, S. Zhao, and R. Zhu, "Gluon quasidistribution function at one loop," *The European Physical Journal C*, vol. 78, no. 2, 2018.

[143] G. Martinelli and C. T. Sachrajda, "A lattice study of nucleon structure," *Nuclear Physics B*, vol. 316, no. 2, pp. 355–372, 1989.

[144] C. Alexandrou, M. Constantinou, S. Dinter et al., "A stochastic method for computing hadronic matrix elements," *The European Physical Journal C*, vol. 74, no. 1, Article ID 2692, 2014.

[145] S. Capitani, B. Knippschild, M. Della Morte, and H. Wittig, "Systematic errors in extracting nucleon properties from lattice QCD," in *Proceedings of the 28th International Symposium on Lattice eld theory (Lattice '10)*, Villasimius, Italy, June 2010.

[146] J. Bulava, M. A. Donnellan, and R. Sommer, "The B*Bpi coupling in the static limit," in *Proceedings of the XXVIII International Symposium on Lattice Field Theory (Lattice '10)*, Villasimius, Italy, June 2010.

[147] S. Güsken, "A study of smearing techniques for hadron correlation functions," *Nuclear Physics B—Proceedings Supplements*, vol. 17, pp. 361–364, 1990.

[148] C. Alexandrou, S. Güsken, F. Jegerlehner, K. Schilling, and R. Sommer, "The static approximation of heavy-light quark systems. A detailed lattice study," *Nuclear Physics B*, vol. 414, no. 3, pp. 815–855, 1994.

[149] M. Albanese, F. Costantini, G. Fiorentini et al., "Glueball masses and string tension in lattice QCD," *Physics Letters B*, vol. 192, no. 1-2, pp. 163–169, 1987.

[150] C. Morningstar and M. Peardon, "Analytic smearing of SU(3) link variables in lattice QCD," *Physical Review D: Particles, Fields, Gravitation and Cosmology*, vol. 69, no. 5, Article ID 054501, 2004.

[151] C. Alexandrou, K. Cichy, M. Constantinou et al., "A complete non-perturbative renormalization prescription for quasi-PDFs," *Nuclear Physics B*, vol. 923, pp. 394–415, 2017.

[152] G. Bali, V. Braun, M. Göckeler et al., "Second moment of the pion distribution amplitude with the momentum smearing technique," *Physics Letters B*, vol. 774, pp. 91–97, 2017.

[153] C. Alexandrou, K. Cichy, K. Hadjiyiannakou, K. Jansen, F. Steffens, and C. Wiese, "A lattice calculation of parton distributions," in *Proceedings of the 24th International Workshop on Deep-Inelastic Scattering and Related Subjects (DIS '16)*, Hamburg, Germany, April 2016.

[154] T. Blum, T. Izubuchi, and E. Shintani, "New class of variance-reduction techniques using lattice symmetries," *Physical Review D: Particles, Fields, Gravitation and Cosmology*, vol. 88, no. 9, Article ID 094503, 2013.

[155] R. A. Briceño, J. V. Guerrero, M. T. Hansen, and C. J. Monahan, "Finite-volume effects due to spatially nonlocal operators," *Physical Review D: Particles, Fields, Gravitation and Cosmology*, vol. 98, no. 1, Article ID 014511, 2018.

[156] S. Aoki, Y. Aoki, D. Becirevic et al., "Review of lattice results concerning low-energy particle physics," *The European Physical Journal C*, vol. 77, 2017.

[157] V. M. Braun, A. Vladimirov, and J. Zhang, "Power corrections and renormalons in parton quasidistributions," *Physical Review D: Particles, Fields, Gravitation and Cosmology*, vol. 99, no. 1, 2019.

[158] I. Schienbein, V. A. Radescu, G. P. Zeller et al., "Target mass corrections," *Journal of Physics G: Nuclear and Particle Physics*, vol. 35, no. 5, Article ID 053101, 2008.

[159] J. Karpie, K. Orginos, A. Rothkopf, and S. Zafeiropoulos, "Reconstructing parton distribution functions from one time data: from Bayesian methods to Neural Networks," *Journal of High Energy Physics*, vol. 1904, 57 pages, 2019.

[160] H.-W. Lin, J.-W. Chen, T. Ishikawa, and J.-H. Zhang, "Improved parton distribution functions at the physical pion mass," *Physical Review D: Particles, Fields, Gravitation and Cosmology*, vol. 98, no. 5, Article ID 054504, 2018.

[161] J.-W. Chen, T. Ishikawa, L. Jin et al., "Gaussian-weighted Parton Quasi-distribution," 2017, https://arxiv.org/abs/1711.07858.

[162] C. Alexandrou, M. Constantinou, and H. Panagopoulos, "Renormalization functions for Nf=2 and Nf=4 twisted mass fermions," *Physical Review D: Particles, Fields, Gravitation and Cosmology*, vol. 95, no. 3, Article ID 034505, 2017.

[163] G. C. Rossi and M. Testa, "Note on lattice regularization and equal-time correlators for parton distribution functions," *Physical Review D: Particles, Fields, Gravitation and Cosmology*, vol. 96, no. 1, Article ID 014507, 2017.

[164] G. Rossi and M. Testa, "Euclidean versus Minkowski short distance," *Physical Review D: Particles, Fields, Gravitation and Cosmology*, vol. 98, no. 5, 2018.

[165] X. Ji, J.-H. Zhang, and Y. Zhao, "More on large-momentum eective theory approach to parton physics," *Nuclear Physics B*, vol. 924, pp. 366–376, 2017.

[166] I. W. Stewart and Y. Zhao, "Matching the quasiparton distribution in a momentum subtraction scheme," *Physical Review D: Particles, Fields, Gravitation and Cosmology*, vol. 97, no. 5, Article ID 054512, 2018.

[167] S. Mandelstam, "Feynman rules for electromagnetic and Yang-Mills fields from the gauge-independent field-theoretic formalism," *Physical Review A: Atomic, Molecular and Optical Physics*, vol. 175, no. 5, pp. 1580–1603, 1968.

[168] A. M. Polyakov, "String representations and hidden symmetries for gauge fields," *Physics Letters B*, vol. 82, no. 2, pp. 247–250, 1979.

[169] Y. M. Makeenko and A. A. Migdal, "Exact equation for the loop average in multicolor QCD," *Physics Letters B*, vol. 88, no. 1-2, pp. 135–137, 1979, [Erratum: Physics Letters B, vol. 89B, no. 437, 1980].

[170] E. Witten, "Gauge theories and integrable lattice models," *Nuclear Physics. B. Theoretical, Phenomenological, and Experimental High Energy Physics. Quantum Field Theory and Statistical Systems*, vol. 322, no. 3, pp. 629–697, 1989.

[171] I. Aref'eva, "Quantum contour field equations," *Physics Letters B: Developments in the Theory of Fun-Damental Interactions. Proceedings of the 17th Winter School, Karpacz, Poland*, vol. 93, no. 3, pp. 347–353, 1980.

[172] N. Craigie and H. Dorn, "On the renormalization and short-distance properties of hadronic operators in QCD," *Nuclear Physics B*, vol. 185, no. 1, pp. 204–220, 1981.

[173] H. Dorn, "Renormalization of path ordered phase factors and related hadron operators in gauge field theories," *Fortschritte der Physik/Progress of Physics*, vol. 34, no. 1, pp. 11–56, 1986.

[174] P. Boucaud, C. L. Lin, and O. Pène, "B meson decay constant on the lattice and renormalization," *Physical Review D: Particles, Fields, Gravitation and Cosmology*, vol. 40, no. 5, pp. 1529–1545, 1989.

[175] E. Eichten and B. Hill, "Renormalization of heavy-light bilinears and F(B) for Wilson fermions," *Physics Letters B*, vol. 240, no. 1-2, pp. 193–199, 1990.

[176] G. Martinelli and C. Sachrajda, "Computation of the b-quark mass with perturbative matching at the next-to-next-to-leading order," *Nuclear Physics B*, vol. 559, no. 1-2, pp. 429–452, 1999.

[177] J.-W. Chen, X. Ji, and J.-H. Zhang, "Improved quasi parton distribution through Wilson line renormalization," *Nuclear Physics B*, vol. 915, pp. 1–9, 2017.

[178] B. U. Musch, P. Hägler, J. W. Negele, and A. Schäfer, "Exploring quark transverse momentum distributions with lattice QCD," *Physical Review D: Particles, Fields, Gravitation and Cosmology*, vol. 83, no. 9, Article ID 094507, 2011.

[179] R. Sommer, "Non-perturbative heavy quark effective theory: introduction and status," *Nuclear and Particle Physics Proceedings*, vol. 261-262, pp. 338–367, 2015.

[180] X. Xiong, T. Luu, and U.-G. Meißner, "Quasi-parton distribution function in lattice perturbation theory," 2017, https://arxiv.org/abs/1705.00246.

[181] J. Chen, T. Ishikawa, L. Jin et al., "Parton distribution function with nonperturbative renormalization from lattice QCD," *Physical Review D: Particles, Fields, Gravitation and Cosmology*, vol. 97, no. 1, Article ID 014505, 2018.

[182] Y. Hatta, X. Ji, and Y. Zhao, "Gluon helicity ΔG from a universality class of operators on a lattice," *Physical Review D: Particles, Fields, Gravitation and Cosmology*, vol. 89, no. 8, Article ID 085030, 2014.

[183] G. Martinelli, C. Pittori, C. Sachrajda, M. Testa, and A. Vladikas, "A general method for non-perturbative renormalization of lattice operators," *Nuclear Physics B*, vol. 445, no. 1, pp. 81–105, 1995.

[184] G. Spanoudes and H. Panagopoulos, "Renormalization of Wilson-line operators in the presence of nonzero quark masses," *Physical Review D: Particles, Fields, Gravitation and Cosmology*, vol. 98, no. 1, Article ID 014509, 2018.

[185] C. Alexandrou, K. Cichy, M. Constantinou, K. Hadjiyiannakou, K. Jansen, and F. Steffens, "Systematic uncertainties in parton distribution functions from lattice QCD simulations at the physical point," 2019, https://arxiv.org/abs/1902.00587.

[186] J. Green, K. Jansen, and F. Steffens, "Nonperturbative renormalization of nonlocal quark bilinears for parton quasidistribution functions on the lattice using an auxiliary field," *Physical Review Letters*, vol. 121, no. 2, Article ID 022004, 2018.

[187] M. Göckeler, R. Horsley, H. Oelrich et al., "Non-perturbative renormalisation of composite operators in lattice QCD," *Nuclear Physics B*, vol. 544, no. 3, pp. 699–733, 1999.

[188] A. Bazavov, C. Bernard, J. Komijani et al., "Lattice QCD ensembles with four flavors of highly improved staggered quarks," *Physical Review D: Particles, Fields, Gravitation and Cosmology*, vol. 87, no. 5, Article ID 054505, 2013.

[189] J.-W. Chen, T. Ishikawa, L. Jin et al., "Symmetry properties of nonlocal quark bilinear operators on a lattice," 2017, https://arxiv.org/abs/1710.01089.

[190] M. Constantinou, R. Horsley, H. Panagopoulos et al., "Renormalization of local quark-bilinear operators for Nf=3 flavors of stout link nonperturbative clover fermions," *Physical Review D: Particles, Fields, Gravitation and Cosmology*, vol. 91, no. 1, Article ID 014502, 2015.

[191] M. Lüscher, "Trivializing maps, the Wilson flow and the HMC algorithm," *Communications in Mathematical Physics*, vol. 293, no. 3, pp. 899–919, 2010.

[192] M. Lüscher, "Properties and uses of the Wilson flow in lattice QCD," *Journal of High Energy Physics*, vol. 2010, Article ID 071, 2010.

[193] M. Lüscher, "Future applications of the Yang-Mills gradient flow in lattice QCD," in *Proceedings of the 31st International Symposium on Lattice Field Theory (Lattice '13)*, Mainz, Germany, July 2013.

[194] M. Lüscher and P. Weisz, "Perturbative analysis of the gradient flow in non-abelian gauge theories," *Journal of High Energy Physics*, vol. 2011, no. 02, Article ID 051, 2011.

[195] C. Monahan, "Smeared quasidistributions in perturbation theory," *Physical Review D: Particles, Fields, Gravitation and Cosmology*, vol. 97, no. 5, Article ID 054507, 2018.

[196] Z. Davoudi and M. J. Savage, "Restoration of rotational symmetry in the continuum limit of lattice field theories," *Physical Review D: Particles, Fields, Gravitation and Cosmology*, vol. 86, no. 5, Article ID 054505, 2012.

[197] Z. Davoudi, "The path from nite to innite volume: Hadronic observables from lattice QCD," in *Proceedings of the 36th Interna-tional Symposium on Lattice Field Theory (Lattice '18)*, East Lansing, MI, USA, July 2018.

[198] H.-n. Li, "Nondipolar Wilson links for quasiparton distribution functions," *Physical Review D: Particles, Fields, Gravitation and Cosmology*, vol. 94, no. 7, Article ID 074036, 2016.

[199] Y.-S. Liu, J.-W. Chen, L. Jin et al., "Unpolarized quark distribution from lattice QCD: A systematic analysis of renormalization and matching," 2018, https://arxiv.org/abs/1807.06566.

[200] X. Xiong and J. Zhang, "One-loop matching for transversity generalized parton distribution," *Physical Review D: Particles, Fields, Gravitation and Cosmology*, vol. 92, no. 5, Article ID 054037, 2015.

[201] X. Ji, P. Sun, X. Xiong, and F. Yuan, "Soft factor subtraction and transverse momentum dependent parton distributions on the lattice," *Physical Review D: Particles, Fields, Gravitation and Cosmology*, vol. 91, no. 7, Article ID 074009, 2015.

[202] X. Ji, L.-C. Jin, F. Yuan, J.-H. Zhang, and Y. Zhao, "Transverse momentum dependent quasi-parton-distributions," https://arxiv.org/abs/1801.05930.

[203] M. A. Ebert, I. W. Stewart, and Y. Zhao, "Determining the nonperturbative collins-soper kernel from lattice QCD," https://arxiv.org/abs/1811.00026.

[204] J. Xu, Q. Zhang, and S. Zhao, "Light-cone distribution amplitudes of vector meson in a large momentum effective theory," *Physical Review D: Particles, Fields, Gravitation and Cosmology*, vol. 97, no. 11, Article ID 114026, 2018.

[205] Y.-S. Liu, W. Wang, J. Xu, Q.-A. Zhang, S. Zhao, and Y. Zhao, "Matching the quasi meson distribution amplitude in RI/MOM scheme," 2018, https://arxiv.org/abs/1810.10879.

[206] D. de Florian, R. Sassot, M. Stratmann, and W. Vogelsang, "Extraction of spin-dependent parton densities and their uncertainties," *Physical Review D: Particles, Fields, Gravitation and Cosmology*, vol. 80, no. 3, Article ID 034030, 2009.

[207] E. R. Nocera, R. D. Balla, S. Forteb, G. Ridolfic, and J. Rojo, "A first unbiased global determination of polarized PDFs and their uncertainties," *Nuclear Physics B*, vol. 887, pp. 276–308, 2014.

[208] N. Sato, W. Melnitchouk, S. Kuhn, J. Ethier, and A. Accardi, "Iterative Monte Carlo analysis of spin-dependent parton distributions," *Physical Review D: Particles, Fields, Gravitation and Cosmology*, vol. 93, no. 7, Article ID 074005, 2016.

[209] P. Schweitzer, D. Urbano, M. V. Polyakov, C. Weiss, P. V. Pobylitsa, and K. Goeke, "Transversity distributions in the nucleon in the large N(c) limit," *Physical Review D: Particles, Fields, Gravitation and Cosmology*, vol. 64, no. 3, Article ID 034013, 2001.

[210] S. Dulat, T.-J. Hou, J. Gao et al., "New parton distribution functions from a global analysis of quantum chromodynamics," *Physical Review D: Particles, Fields, Gravitation and Cosmology*, vol. 93, no. 3, Article ID 033006, 2016.

[211] R. D. Ball, V. Bertone, S. Carrazza et al., "Parton distributions from high-precision collider data," *The European Physical Journal C*, vol. 77, p. 663, 2017.

[212] L. A. Harland-Lang, A. D. Martin, P. Motylinski, and R. S. Thorne, "Parton distributions in the LHC era: MMHT 2014 PDFs," *The European Physical Journal C*, vol. 75, article 204, 2015.

[213] S. Alekhin, J. Blümlein, S. Moch, and R. Plačakytė, "Parton distribution functions, α_s, and heavy-quark masses for LHC Run II," *Physical Review D: Particles, Fields, Gravitation and Cosmology*, vol. 96, no. 1, Article ID 014011, 2017.

[214] A. Accardi, L. Brady, W. Melnitchouk, J. Owens, and N. Sato, "Constraints on large-x parton distributions from new weak boson production and deep-inelastic scattering data," *Physical Review D: Particles, Fields, Gravitation and Cosmology*, vol. 93, no. 11, Article ID 114017, 2016.

[215] J. Ethier, N. Sato, and W. Melnitchouk, "First simultaneous extraction of spin-dependent parton distributions and fragmentation functions from a global QCD analysis," *Physical Review Letters*, vol. 119, no. 13, Article ID 132001, 2017.

[216] C. Alexandrou, K. Cichy, M. Constantinou, K. Hadjiyiannakou, K. Jansen, and F. Steffens, "Light-cone PDFs from Lattice QCD," 2018, https://arxiv.org/abs/1811.01588.

[217] D. de Florian, R. Sassot, M. Stratmann, and W. Vogelsang, "Evidence for polarization of gluons in the proton," *Physical Review Letters*, vol. 113, no. 1, Article ID 012001, 2014.

[218] J.-W. Chen, L. Jin, H.-W. Lin et al., "Lattice calculation of parton distribution function from LaMET at physical pion mass with large nucleon momentum," 2018, https://arxiv.org/abs/1803.04393.

[219] H.-W. Lin, J.-W. Chen, L. Jin et al., "Proton isovector helicity distribution on the lattice at physical pion mass," *Physical Review Letters*, vol. 121, no. 24, Article ID 242003, 2018.

[220] H. Lin, W. Melnitchouk, A. Prokudin, N. Sato, and H. Shows, "First monte carlo global analysis of nucleon transversity with lattice QCD constraints," *Physical Review Letters*, vol. 120, no. 15, Article ID 152502, 2018.

[221] L. Chang, I. C. Cloët, J. J. Cobos-Martinez, C. D. Roberts, S. M. Schmidt, and P. C. Tandy, "Imaging dynamical chiral-symmetry breaking: pion wave function on the light front," *Physical Review Letters*, vol. 110, no. 13, Article ID 132001, 2013.

[222] S. S. Agaev, V. M. Braun, N. Offen, and F. A. Porkert, "Belle data on the $\pi^0\gamma^*\gamma$ form factor: A game changer?" *Physical Review D: Particles, Fields, Gravitation and Cosmology*, vol. 86, no. 7, Article ID 077504, 2012.

[223] V. Braun, S. Collins, M. Göckeler et al., "Second moment of the pion light-cone distribution amplitude from lattice QCD," *Physical Review D: Particles, Fields, Gravitation and Cosmology*, vol. 92, no. 1, Article ID 014504, 2015.

[224] J.-W. Chen, L. Jin, H.-W. Lin et al., "Kaon distribution amplitude from lattice QCD and the flavor SU(3) symmetry," *Nuclear Physics B*, vol. 939, pp. 429–446, 2019.

[225] J. P. de Melo, I. Ahmed, and K. Tsushima, "Parton distribution in pseudoscalar mesons with a light-front constituent quark model," in *Proceedings of the 16th International Conference on Hadron Spectroscopy (Hadron '15), AIP Conference Proceedings*, vol. 1735, Newport News, VA, USA, 2016.

[226] J.-W. Chen, L. Jin, H.-W. Lin et al., "First direct lattice-QCD calculation of the x-dependence of the pion parton distribution function," 2018, https://arxiv.org/abs/1804.01483.

[227] C. Chen, L. Chang, C. D. Roberts, S. Wan, and H. Zong, "Valence-quark distribution functions in the kaon and pion," *Physical Review D: Particles, Fields, Gravitation and Cosmology*, vol. 93, no. 7, Article ID 074021, 2016.

[228] M. Aicher, A. Schäfer, and W. Vogelsang, "Soft-gluon resummation and the valence parton distribution function of the pion," *Physical Review Letters*, vol. 105, no. 25, Article ID 252003, 2010.

[229] Z. Fan, Y. Yang, A. Anthony, H. Lin, and K. Liu, "Gluon quasi-parton-distribution functions from lattice QCD," *Physical Review Letters*, vol. 121, no. 24, 2018.

[230] M. Göckeler, R. Horsley, E.-M. Ilgenfritz et al., "Polarized and unpolarized nucleon structure functions from lattice QCD," *Physical Review D: Particles, Fields, Gravitation and Cosmology*, vol. 53, no. 5, pp. 2317–2325, 1996.

[231] R. S. Sufian, J. Karpie, C. Egerer, K. Orginos, J.-W. Qiu, and D. G. Richards, "Pion valence quark distribution from matrix element calculated in lattice QCD," *Physical Review D*, vol. 99, no. 7, Article ID 074507, 2019.

[232] R. Gupta, Y.-C. Jang, B. Yoon, H.-W. Lin, V. Cirigliano, and T. Bhattacharya, "Isovector charges of the nucleon from 2+1+1 -flavor lattice QCD," *Physical Review D: Particles, Fields, Gravitation and Cosmology*, vol. 98, no. 3, 2018.

[233] E. Follana, Q. Mason, C. Davies et al., "Highly improved staggered quarks on the lattice with applications to charm physics," *Physical Review D: Particles, Fields, Gravitation and Cosmology*, vol. 75, no. 5, Article ID 054502, 2007.

[234] A. Abdel-Rehim, C. Alexandrou, F. Burger et al., "First physics results at the physical pion mass from Nf = 2 Wilson twisted mass fermions at maximal twist," *Physical Review D: Particles, Fields, Gravitation and Cosmology*, vol. 95, no. 9, Article ID 094515, 2017.

[235] T. Bhattacharya, S. D. Cohen, R. Gupta, A. Joseph, H. Lin, and B. Yoon, "Nucleon charges and electromagnetic form factors from 2+1+1-flavor lattice QCD," *Physical Review D: Particles, Fields, Gravitation and Cosmology*, vol. 89, no. 9, Article ID 094502, 2014.

[236] T. Bhattacharya, V. Cirigliano, S. D. Cohen et al., "Isovector and isoscalar tensor charges of the nucleon from lattice QCD," *Physical Review D: Particles, Fields, Gravitation and Cosmology*, vol. 92, no. 9, Article ID 094511, 2015.

[237] M. Anselmino, M. Boglione, and U. D'Alesio, "Transversity and Collins functions from SIDIS and e^+e^- data," *Physical Review D: Particles, Fields, Gravitation and Cosmology*, vol. 75, Article ID 054032, 2007.

[238] M. Anselmino, M. Boglione, U. D'Alesio et al., "Collins functions for pions from SIDIS and new e^+e^- data: a rst glance at their transverse momentum dependence," *Physical Review D: Particles, Fields, Gravitation and Cosmology*, vol. 92, no. 11, Article ID 114023, 2015.

[239] M. Radici, A. Courtoy, A. Bacchetta, and M. Guagnelli, "Improved extraction of valence transversity distributions from inclusive dihadron production," *Journal of High Energy Physics*, vol. 2015, no. 5, 2015.

[240] Z. Kang, A. Prokudin, P. Sun, and F. Yuan, "Extraction of quark transversity distribution and Collins fragmentation functions with QCD evolution," *Physical Review D: Particles, Fields, Gravitation and Cosmology*, vol. 93, no. 1, Article ID 014009, 2016.

[241] M. Radici and A. Bacchetta, "First extraction of transversity from a global analysis of electron-proton and proton-proton data," *Physical Review Letters*, vol. 120, no. 19, Article ID 192001, 2018.

[242] R. Seidl et al., "Measurement of azimuthal asymmetries in inclusive production of hadron pairs in e^+e^- annihilation at Belle," *Physical Review Letters*, vol. 96, no. 23, Article ID 232002, 2006.

[243] R. Seidl et al., "Measurement of Azimuthal Asymmetries in Inclusive Production of Hadron Pairs in e+e- Annihilation at $s^{**}(1/2)$ = 10.58-GeV," *Physical Review D: Particles, Fields, Gravitation and Cosmology*, vol. 78, Article ID 032011, 2008, [Erratum: Physical Review D, vol. 86, Article ID 039905, 2012].

[244] I. Garzia, "Measurement of Collins asymmetries in inclusive production of pion pairs in e^+e^- collisions at BABAR," in

Proceedings of the 36th International Conference on High Energy Physics (ICHEP '12), Melbourne, Australia, July 2012.

[245] A. Airapetian et al., "Effects of transversity in deep-inelastic scattering by polarized protons," *Physics Letters B*, vol. 693, no. 1, pp. 11–16, 2010.

[246] M. Alekseev et al., "Collins and Sivers asymmetries for pions and kaons in muon-deuteron DIS," *Physics Letters B*, vol. 673, no. 2, pp. 127–135, 2009.

[247] C. Adolph et al., "Collins and Sivers asymmetries in muonproduction of pions and kaons off transversely polarised protons," *Physics Letters B*, vol. 744, pp. 250–259, 2015.

[248] J. C. Collins, S. F. Heppelmann, and G. A. Ladinsky, "Measuring transversity densities in singly polarized hadron-hadron and lepton-hadron collisions," *Nuclear Physics B*, vol. 420, no. 3, pp. 565–582, 1994.

[249] R. L. Jaffe, X. Jin, and J. Tang, "Interference fragmentation functions and the nucleon's transversity," *Physical Review Letters*, vol. 80, no. 6, pp. 1166–1169, 1998.

[250] A. Bacchetta, A. Courtoy, and M. Radici, "First glances at the transversity parton distribution through dihadron fragmentation functions," *Physical Review Letters*, vol. 107, no. 1, Article ID 012001, 2011.

[251] E. Moat, W. Melnitchouk, T. C. Rogers, and N. Sato, "What are the low-Q and large-x boundaries of collinear QCD factorization theorems?" *Physical Review D: Particles, Fields, Gravitation and Cosmology*, vol. 95, Article ID 096008, 2017.

[252] C. Bouchard, C. C. Chang, T. Kurth, K. Orginos, and A. Walker-Loud, "On the Feynman-Hellmann theorem in quantum field theory and the calculation of matrix elements," *Physical Review D: Particles, Fields, Gravitation and Cosmology*, vol. 96, no. 1, Article ID 014504, 2017.

[253] G. Backus and F. Gilbert, "The resolving power of gross earth data," *The Geophysical Journal of the Royal Astronomical Society*, vol. 16, no. 2, pp. 169–205, 1968.

[254] J. Liang, T. Draper, K.-F. Liu, and Y.-B. Yang, "Lattice QCD calculation of the nucleon hadronic tensor," in *Proceedings of the 36th Annual International Symposium on Lattice Field Theory, LATTICE 2018*, vol. 101.

[255] K. Cichy, K. Jansen, and P. Korcyl, "Non-perturbative renormalization in coordinate space for N f=2 maximally twisted mass fermions with tree-level Symanzik improved gauge action," *Nuclear Physics B*, vol. 865, no. 2, pp. 268–290, 2012.

[256] J. Karpie et al., "Progress on parton pseudo distributions," in *Proceedings of the 36th Annual International Symposium on Lattice Field Theory, LATTICE 2018*, vol. 100.

[257] K. Somfleth et al., "Nucleon Structure Functions from the Feynman-Hellmann Theorem," in *Proceedings of the 36th Annual International Symposium on Lattice Field Theory, LATTICE 2018*, vol. 102.

[258] C. Alexandrou, S. Bacchio, K. Cichy et al., "Computation of parton distributions from the quasi-PDF approach at the physical point," in *Proceedings of the 35th International Symposium on Lattice Field Theory (Lattice '17) & EPJ Web Conference*, vol. 175, Granada, Spain, June 2017.

Hindawi
Advances in High Energy Physics
Volume 2019, Article ID 3142510, 17 pages
https://doi.org/10.1155/2019/3142510

Review Article

A Short Review on Recent Developments in TMD Factorization and Implementation

Ignazio Scimemi

Departamento de Física Teórica and IPARCOS, Universidad Complutense de Madrid, Ciudad Universitaria, 28040 Madrid, Spain

Correspondence should be addressed to Ignazio Scimemi; ignazios@ucm.es

Received 20 December 2018; Accepted 7 April 2019; Published 13 May 2019

Guest Editor: Zhongbo Kang

In the latest years the theoretical and phenomenological advances in the factorization of several collider processes using the transverse momentum dependent distributions (TMD) have greatly increased. I attempt here a short resume of the newest developments discussing also the most recent perturbative QCD calculations. The work is not strictly directed to experts in the field and it wants to offer an overview of the tools and concepts which are behind the TMD factorization and evolution. I consider both theoretical and phenomenological aspects, some of which have still to be fully explored. It is expected that actual colliders and the Electron Ion Collider (EIC) will provide important information in this respect.

1. Introduction

The knowledge of the structure of hadrons is a leitmotiv for the study of quantum chromodynamics (QCD) for decades. Apart from the notions of quarks and gluons (we call them generically "partons" in the following), the natural question is how the momenta of these particles are distributed inside the hadrons and how the spin of hadrons is generated. Phenomenologically it is possible to access at this problem only in some particular kinematical conditions, as provided, for instance, in experiments like (semi-inclusive) deep inelastic scattering, vector and scalar boson production, $\ell^+\ell^- \longrightarrow$ hadrons, or jets. I review the basic principle which supports this investigation. Let us consider, to start with, the cross section for di-lepton production in a typical Drell-Yan process $pp \longrightarrow \ell^+\ell^- + X$ where X includes all particles which are not directly measured. The cross section for this process can be written formally as

$$\frac{d\sigma}{dQ^2} \simeq \sum_{i,j=q,g} \int_0^1 dx_1 dx_2 \mathscr{H}_{ij}\left(Q^2,\mu^2\right) f_{i\longleftarrow h}\left(x_1,\mu^2\right) \cdot f_{j\longleftarrow h}\left(x_2,\mu^2\right) \tag{1}$$

where Q^2 is the virtual di-lepton invariant mass, x_i are the parton momenta fraction along a light-cone direction or Bjorken variables, and f are the parton distribution functions (PDF). The r.h.s. of (1) assumes several notions which, nowadays, can be found in textbooks. In fact a central hypothesis is a clear energy separation between the di-lepton invariant mass and the scale at which QCD cannot be treated perturbatively any more (we call it the hadronization scale $\Lambda \sim \mathcal{O}(1)$ GeV), that is, $Q^2 \gg \Lambda^2$. Given this, one can factorize the cross section in a perturbatively calculable part $\mathscr{H}$ and the rest. Formula (1) represents just a first term of an "operator product expansion" of the cross section. The price to pay for this separation is the introduction of a factorization scale μ which can be used to resume logarithms in combination with renormalization group equations [1–3]. Another aspect, which is remarkable, is that the nonperturbative part of the cross section can be also expressed as the product of two parton distribution functions. This fact has two main consequences: on the one hand, all the nonperturbative information of the process is included in the PDFs; on the other hand, the partons belonging to different hadrons are completely disentangled. In these conditions so the longitudinal momenta of quarks and gluons can be reconstructed nonperturbatively and this fact has given rise to a large investigation whose review goes beyond the purpose of this writing.

The ideal description of the process in (1) however becomes more involved in the case of more differential cross sections [32–34]. So, for instance, one can wonder whether a formula like

$$\frac{d\sigma}{dQ^2 dq_T^2 dy} \stackrel{?}{=} \sum_{i,j=q,g} \int d^2\boldsymbol{b}_T e^{-i\boldsymbol{b}_T\cdot\boldsymbol{q}_T} \cdot \int_0^1 dx_1 dx_2 \mathscr{H}_{ij}\left(Q^2,\mu^2\right) F_{i\longleftarrow h}\left(x_1,\boldsymbol{b}_T,\mu^2\right) \cdot F_{j\longleftarrow h}\left(x_2,\boldsymbol{b}_T,\mu^2\right) \tag{2}$$

has any physical consistency. (I use the notation $\boldsymbol{b}_T$ for 2-dimensional impact parameter, $-b_T^2 = \boldsymbol{b}_T{}^2 \geq 0$, s is the center of mass energy of the process, $x_1 = (\sqrt{Q^2+q_T^2}/\sqrt{s})e^{y}, x_2 = (\sqrt{Q^2+q_T^2}/\sqrt{s})e^{-y}$.) The answer to this question is necessarily more complex than in the case of (1) for the simple fact that a new kinematic scale, q_T, the transverse momentum of the di-lepton pair, has now appeared. In this article I will concentrate on the description of the case

$$q_T \ll Q, \tag{3}$$

which is interesting for a number of observables. The restriction to this kinematical regime represents also a limitation of the present approach which should be overcome with further studies.

The study of factorization [25, 27, 29, 30, 35, 36] has lead finally to the conclusion that actually (2) in not completely correct because the cross section for these kind of processes should instead be of the form

$$\frac{d\sigma}{dQ^2 dq_T^2 dy} = \sum_{i,j=q,g} \int d^2\boldsymbol{b}_T e^{-i\boldsymbol{b}_T\cdot\boldsymbol{q}_T} \cdot \int_0^1 dx_1 dx_2 \mathscr{H}_{ij}\left(Q^2,\mu^2\right) F_{i\longleftarrow h}\left(x_1,\boldsymbol{b}_T,\zeta_1,\mu^2\right) \cdot F_{j\longleftarrow h}\left(x_2,\boldsymbol{b}_T,\zeta_2,\mu^2\right) \tag{4}$$

with $\zeta_1\zeta_2 = Q^4$ and ζ_i being the rapidity scales. Formula (4) shows explicitly that the TMD functions F contain nonperturbative QCD information different from the usual PDF, while they still allow completing disentangle QCD effects coming from different hadrons. These new nonperturbative QCD inputs can be written in terms of well-defined matrix elements of field operators which can be extracted from experiments or evaluated with appropriate theoretical tools. These objectives require some discussion, which I partially provide in this text.

The scale ζ is the authentic key stone of the TMD factorization. Its origin is different from the usual factorization scale μ and because of this it is allowed to perform a special resummation for this scale. This leads to the fact that a consistent and efficient implementation of the (μ,ζ) evolution is crucial for the prediction and extraction of TMDs from data. A possible implementation of the TMD evolution is historically provided by Collins-Soper-Sterman (CSS) [32–34]. However a complete discussion of more efficient alternatives has started more recently [21–23, 26, 37]. The point is that the rapidity scale evolution has both a perturbative and nonperturbative input, as it is actually provided by (derivatives of) an operator matrix element (the so called soft function). An efficient implementation and scale choice so should separate as much as possible the nonperturbative inputs with different origin inside the cross sections. This target is not completely realized with the CSS implementation, while it can be achieved with the ζ-prescription discussed in the text. This discussion is also relevant for multiple reasons. In fact various orders in perturbation theory are available already for unpolarized and polarized distribution and, in the future, one expects more results in this respect for many polarized distributions. When dealing with several perturbative orders, the convergence of the perturbative series can be seriously undermined by an inappropriate choice of scales, and this is a well-known problem that can affect the theoretical error of any result. A more subtle issue comes from the fact that the evolution corrections can also be of nonperturbative nature. It would be certainly clarifying a scheme in which the nonperturbative effects of the evolution are clearly separated from the intrinsic nonperturbative TMD effects. Such a request results to be important when several extraction of TMD from data are compared and also when a complete nonperturbative evaluation of TMD can be provided.

In the rest of this review I will try to give an idea on how all these problems can be consistently treated, which can be useful also to explore new and more efficient solutions. Several parts of this review use material that can be originally found in [4, 23, 38].

2. Factorization

The factorization of the cross sections into TMD matrix elements has been provided by several authors and it has been object of many discussions [25, 27, 29, 30, 32–36]. We briefly review the main ideas here for the case of Drell-Yan. The process is characterized by two initial hadrons which come from opposite collinear directions and produce two leptons in the final state plus unmeasured radiation. We identify collinear (anticollinear) light-cone directions n ($\overline{n}$) and $n^2 = \overline{n}^2 = 0$, $n\cdot\overline{n} = 1$ for the momentum of colliding particles. The momentum of collinear particles is $p = (p^+, p^-, p_\perp)$ with $n\cdot p = p^-$, $\overline{n}\cdot p = p^+$ and $p_\perp = p - (n\cdot p)\overline{n} - (\overline{n}\cdot p)n$ and $p^+ \gg p_\perp \gg p_-$. The momenta of collinear particles are characterized by the scaling $p \simeq Q(1,\lambda^2,\lambda)$ where Q is the di-lepton invariant mass and λ is a small parameter $\lambda \sim \Lambda_{QCD}/Q$ being Λ_{QCD} the hadronization scale. A reversed scaling of momentum is valid for anticollinear particles, say $p \simeq Q(\lambda^2,1,\lambda)$. The soft radiation which entangles collinear and anticollinear particles is homogeneous in momentum distribution (its momentum scales as $p \sim Q(\lambda,\lambda,\lambda)$) and can be distinguished from the collinear radiation only for a different scaling of the components of the momenta. Given this, it is natural to divide the hadronic phase space in regions as in Figure 1. In this picture, the collinear and soft regions are

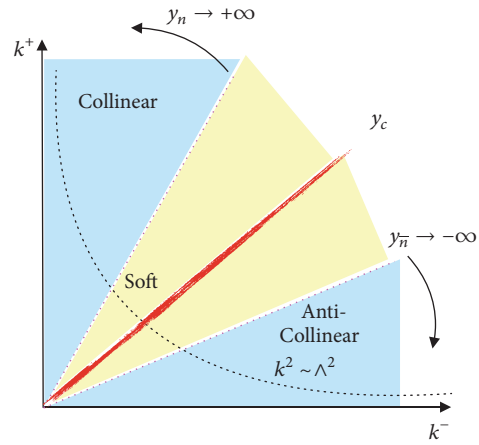

FIGURE 1: Diagrams of regions for TMD factorization (original figure in [30]).

necessarily separated by rapidity and they all share the same energy $p^2 \sim \Lambda^2$.

2.1. Soft Interactions and Soft Factor. Because the soft radiation is not finally measured, its interactions should be included (and resumed) in the collinear parts, which become sensitive to a rapidity scale which acts in a way similar to the usual factorization scale. It is possible to define the soft radiation through a "soft factor"; that is, by an operator matrix element,

$$S(\boldsymbol{k}) = \int \frac{d^2\boldsymbol{b}_T}{(2\pi)^2} e^{i\boldsymbol{b}_T\cdot\boldsymbol{k}} \frac{\mathrm{Tr}_c}{N_c} \langle 0| \left[S_n^{T\dagger}\widetilde{S}_{\overline{n}}^{T}\right](0^+,0^-,\boldsymbol{b}_T) \cdot \left[\widetilde{S}_{\overline{n}}^{T\dagger}S_n^T\right](0)\,|0\rangle\,, \tag{5}$$

where we have used the Wilson line definitions [39–41] appropriate for a Drell-Yan process,

$$S_n^T = T_{n(\overline{n})}S_n,$$

$$\widetilde{S}_{\overline{n}}^T = \widetilde{T}_{n(\overline{n})}\widetilde{S}_{\overline{n}},$$

$$S_n(x) = P\exp\left[ig\int_{-\infty}^{0} ds n\cdot A(x+sn)\right],$$

$$T_n(x_T) = P\exp\left[ig\int_{-\infty}^{0} d\tau \boldsymbol{l}_\perp\cdot\boldsymbol{A}_\perp(\infty^+,0^-,\boldsymbol{x}_T+\boldsymbol{l}_\perp\tau)\right],$$

$$T_{\overline{n}}(x_T) = P\exp\left[ig\int_{-\infty}^{0} d\tau \boldsymbol{l}_\perp\cdot\boldsymbol{A}_\perp(0^+,\infty^-,\boldsymbol{x}_T+\boldsymbol{l}_\perp\tau)\right],$$

$$\widetilde{S}_{\overline{n}}(x) = P\exp\left[-ig\int_{0}^{\infty} ds\overline{n}\cdot A(x+\overline{n}s)\right],$$

$$\widetilde{T}_n(x_T) = P\exp\left[-ig\int_{0}^{\infty} d\tau \boldsymbol{l}_\perp\cdot\boldsymbol{A}_\perp(\infty^+,0^-,\boldsymbol{x}_T+\boldsymbol{l}_\perp\tau)\right],$$

$$\widetilde{T}_{\overline{n}}(x_T) = P\exp\left[-ig\int_{0}^{\infty} d\tau \boldsymbol{l}_\perp\cdot\boldsymbol{A}_\perp(0^+,\infty^-,\boldsymbol{x}_T+\boldsymbol{l}_\perp\tau)\right]. \tag{6}$$

The direct calculation of the soft factor is all but trivial and the way the calculation is performed can influence directly the final formal definition of the transverse momentum dependent distribution used by different authors. In fact a simple perturbative calculation shows that in the soft factor there are divergences which cannot be regularized dimensionally (say, they are not explicitly ultraviolet (UV) or infrared (IR)) which occur when the integration momenta are big and aligned on the light-cone directions. The divergences that arise in this configuration of momenta are generically called rapidity divergences and regulated by a rapidity regulator. One can understand the necessity of a specific regulator observing that the light-like Wilson lines are invariant under the coordinate rescaling in their own light-like directions. This invariance leads to an ambiguity in the definition of rapidity divergences. Indeed, the boost of the collinear components of momenta $k^+ \longrightarrow ak^+$, $k^- \longrightarrow k^-/a$ (with a an arbitrary number) leaves the soft function invariant, while in the limit $a \longrightarrow \infty$ one obtains the rapidity divergent configuration. Therefore the soft function cannot be explicitly calculated without a regularization which breaks its boost invariance. The coordinate space description of rapidity divergences as well as the counting rules for them have been derived in [42, 43]. The nature of the divergences in the soft factor has been studied explicitly in [44] at one loop and in [45] at NNLO, which conclude that, once all contributions are included, the soft factor depends only on ultraviolet and rapidity divergences (and IR divergences are present only in the intermediate steps of the calculations, but not in the final result). Different regulators have also been shown to be more or less efficient within different approaches to the calculations of transverse momentum dependent distributions. For instance, NNLO perturbative calculations for unpolarized distributions, transversity, and pretzelosity have been performed using de δ-regulator of

[4, 15, 19] while for the recent attempts of lattice calculations off-the-light-cone Wilson lines are preferred [46–56]. The discussion of the type of regulator involves usually another issue, which is also important for the complete definition of TMDs. While collinear and soft sectors can be distinguished by rapidity, the choice of a rapidity regulator forces a certain overlap of the two regions which should be removed, in order to arrive to a consistent formulation of the factorized cross section. This is called "zero-bin" problem in Soft Collinear Effective Theory (SCET) [57]) and its solution is usually provided in any formulation of the factorization theorem. The amount of the zero-bin overlap is usually fixed by the same soft function in some particular limit although it is generally impossible to define this subtraction in a unique (in the sense of regulator independent) form. Because of this overlap one can find in the literature that the soft function is used in a different way in different formulations of the factorization theorem. The evolution properties of TMDs however are independent of these subtleties and they are the same in all formulations. A possible rapidity renormalization scheme-dependence is traditionally fixed by requiring $R^{-1}SR^{-1} = 1$ (for this notation see discussion on Section 2.2).

The factorization theorem to all orders in perturbation theory relies on the peculiar property of soft function of being at most linear in the logarithms generated by the rapidity divergences. Then it comes natural to factorize it in two pieces [30], and in turn this feature allows to define the individual TMDs. Using the δ-regulator one can write to all orders in perturbation theory, as well as to all orders in the ϵ-expansion (the UV divergences are regulated in dimensional regularization $d = 4 - 2\epsilon$)[45].

$$\widetilde{S}\left(\mathbf{L}_{\mu}, \mathbf{L}_{\sqrt{\delta^{+}\delta^{-}}}\right) = \widetilde{S}^{1/2}\left(\mathbf{L}_{\mu}, \mathbf{L}_{\delta^{+}/\nu}\right)\widetilde{S}^{1/2}\left(\mathbf{L}_{\mu}, \mathbf{L}_{\nu\delta^{-}}\right), \quad (7)$$

where tildes mark quantities calculated in coordinate space, ν is an arbitrary and positive real number that transforms as p^{+} under boosts, and we introduce the convenient notation

$$\boldsymbol{L}_{X} \equiv \ln\left(\frac{X^{2}\boldsymbol{b}_{\boldsymbol{T}}^{2}e^{2\gamma_{E}}}{4}\right). \quad (8)$$

Despite the fact that the soft function is not measurable *per se*, its derivative provides the so-called *rapidity anomalous dimension*,

$$\mathscr{D} = \frac{1}{2}\frac{d\ln\widetilde{S}}{d\mathbf{l}_{\delta}}\bigg|_{\epsilon\text{-finite}}. \quad (9)$$

with $\mathbf{l}_{\delta} = \ln(\mu^{2}/|\delta_{+}\delta_{-}|)$. Because of its definition the rapidity anomalous dimension $\mathscr{D}$ has both a perturbative (finite; calculable) part and a nonperturbative part. This fact should be always taken into account despite the fact that many experimental data are actually marginally sensitive to the nonperturbative nature of the rapidity anomalous dimension. A nonperturbative estimation of the evolution kernel with lattice has been recently proposed in [58] and I expect a deep discussion on this issue in the future. A renormalon based calculation has also provided some approximate value for this nonperturbative contribution [59].

2.2. TMD Operators. Another fundamental ingredient in the formulation of the factorization theorem is represented by the definition of the TMD operators that are involved. We use here the notation of [4]. The TMDs which appear in a Drell-Yan process can be rewritten starting from the bare operators (here I consider only the quark case, for simplicity)

$$O_{q}^{bare}(x, \boldsymbol{b}_{T}) = \frac{1}{2}\sum_{X}\int\frac{d\xi^{-}}{2\pi}e^{-ixp^{+}\xi^{-}}\left\{T\left[\overline{q}_{i}\widetilde{W}_{n}^{T}\right]_{a}\left(\frac{\xi}{2}\right)\right.$$
$$\left.\cdot|X\rangle\,\Gamma_{ij}\,\langle X|\,\overline{T}\left[\widetilde{W}_{n}^{T\dagger}q_{j}\right]_{a}\left(-\frac{\xi}{2}\right)\right\}, \quad (10)$$

where $\xi = \{0^{+}, \xi^{-}, \boldsymbol{b}_{T}\}$, n and $\overline{n}$ are light-cone vectors ($n^{2} = \overline{n}^{2} = 0, n\cdot\overline{n} = 1$), and Γ is some Dirac matrix; the repeated color indices a ($a = 1, \ldots, N_{c}$) are summed up. The representations of the color SU(3) generators inside the Wilson lines are the same as the representation of the corresponding partons. The collinear Wilson lines $W_{n}, \widetilde{W}_{n}^{T}$ are defined in the same way as in $S_{n}, \widetilde{S}_{n}^{T}(x)$ in (6). The collinear and soft Wilson line should be distinguished because the gluons which define them have a different scaling in effective field theories and also because they should be regularized differently with respect to rapidity divergences (see the definition of δ-regulator in [45] for soft and collinear matrix elements). The hadronic matrix elements,

$$\Phi_{f\longleftarrow N}(x, \boldsymbol{b}_{T}) = \langle N|\,O_{f}^{bare}(x, \boldsymbol{b}_{T})\,|N\rangle\,, \quad (11)$$

define the *bare* or unsubtracted TMDs. These bare operators do not include for the moment any soft radiation and they are just collinear object (one can refer to them as "beam functions") and because of boost invariance they can be calculated in principle in any frame. A renormalization issue however appears because of rapidity divergences and overlap with the soft radiation (this problem is usually referred to as zero-bin problem in effective field theory [57]). The soft interactions can be incorporated in the definition of the TMD through an appropriate "rapidity renormalization factor". The final form of the rapidity renormalization factor (R in the following) is dictated by the factorization theorem. The renormalized operators and the TMD are defined, respectively, as

$$O_{q}(x, \boldsymbol{b}_{T}, \mu, \zeta) = Z_{q}(\zeta, \mu)\,R_{q}(\zeta, \mu)\,O_{q}^{bare}(x, \boldsymbol{b}_{T}) \quad (12)$$

$$F_{f\longleftarrow N}(x, \boldsymbol{b}_{T}; \mu, \zeta) = \langle N|\,O_{f}(x, \boldsymbol{b}_{T}; \mu, \zeta)\,|N\rangle$$
$$= Z_{q}(\zeta, \mu)\,R_{q}(\zeta, \mu)\,\Phi_{f\longleftarrow N}(x, \boldsymbol{b}_{T}) \quad (13)$$

and Z_{q} is the UV renormalization constant for TMD operators and R_{q} is the rapidity renormalization factor. Both these factors are the same for particle and antiparticle; however they are different for quarks and gluons. These factors also occur in the same way in parton distribution functions and fragmentation functions. The scales μ and ζ are the scales of UV and rapidity subtractions, respectively. The way these factors are ordered corresponds to first removing rapidity divergences and then the rest of UV divergences from the bare matrix elements as in [4]. It is possible to proceed

also in a different way (for instance, in [29, 60, 61] they cancel the rapidity divergences from the beam functions and soft factors independently); however finally one achieves an equivalent resummation of rapidity logarithms. In [5, 27, 62] for TMDPDFs the soft function is hidden in the product of two TMDs.

Some comments finally are necessary for the zero-bin overlap problem. In principle an overlap factor affects the rapidity renormalization factor as

$$R_f(\zeta,\mu) = \frac{\sqrt{S_f(\boldsymbol{b}_T)}}{\mathbf{Zb}_f} \quad f = q, g, \tag{14}$$

where $S_f(\boldsymbol{b}_T)$ is the soft function and $\mathbf{Zb}_f$ is the zero-bin contribution [25, 30, 36, 57, 63] and both are different in the quark and gluon cases. The zero-bin part assumes a particular form depending on the regulator for rapidity divergences. For instance, the modified δ-regularization [45] has been constructed such that the zero-bin subtraction is literally equal to the soft function: $\mathbf{Zb}_f = S_f(\boldsymbol{b}_T)$. The definition is nontrivial because it implies a different regularized form for collinear Wilson lines $W_{n(\overline{n})}(x)$ and for soft Wilson lines $S_{n(\overline{n})}(x)$. In the modified δ-regularization, the expression for the rapidity renormalization factor is

$$R_f(\zeta,\mu)\big|_{\delta\text{-reg.}} = \frac{1}{\sqrt{S_f(\boldsymbol{b}_T;\zeta)}}, \tag{15}$$

and this relation has been tested at NNLO in [4, 24, 45]. In the formulation of TMDs by Collins in [25] the rapidity divergences are handled by tilting the Wilson lines off-the-light-cone. Then the contribution of the overlapping regions and soft factors can be recombined into individual TMDs by the proper combination of different soft functions with a partially removed regulator. This combination gives the factor R_f,

$$R_f(\zeta,\mu)\big|_{JCC} = \sqrt{\frac{\widetilde{S}(y_n, y_c)}{\widetilde{S}(y_c, y_{\overline{n}})\,\widetilde{S}(y_n, y_{\overline{n}})}}. \tag{16}$$

The rest of logical steps remain the same as with the δ-regulator. Notice that, due to the process independence of the soft function [25, 30, 36, 63, 64], the factor R_f is also process independent.

An important aspect of factorization is finally represented by the cancellation of unphysical modes, the Glauber gluons. A check of this cancellation has been provided in [25, 65–67] and I do not review it here.

3. Matching at Large q_T (or Small-b)

The practical implementation of the TMD for data analysis benefits from asymptotic limits of the distribution. These limits allow defining the TMDs at different scale and constraining the nonperturbative behavior of the TMDs. Commonly one starts with the large transverse momentum limit of the TMD. In this case one can refactorize the TMDs in terms of Wilson coefficient and collinear parton distribution functions (PDF), following the usual rules for operator product expansion (OPE). At operator level one finds

$$O_f(x,\boldsymbol{b}_T;\mu,\zeta) = \sum_{f'} C_{f\leftarrow f'}(x,\boldsymbol{b}_T;\mu,\zeta,\mu_b) \otimes O_{f'}(x,\mu_b) + \mathcal{O}\left(\frac{\boldsymbol{b}_T}{B_T}\right), \tag{17}$$

and the symbol $\otimes$ is the Mellin convolution in variable x or z, and f, f' enumerate the flavors of partons. The running on the scales μ, μ_b, and ζ is independent of the regularization scheme and it is dictated by the renormalization group equations which we discuss later. In the case of initial states (17) reduces to

$$F_{f\leftarrow N}(x,\boldsymbol{b}_T;\mu,\zeta) = \sum_{f'} C_{f\leftarrow f'}(x,\boldsymbol{b}_T;\mu,\zeta,\mu_b) \otimes f_{f'\leftarrow N}(x,\mu_b) + \mathcal{O}\left(\frac{\boldsymbol{b}_T}{B_T}\right), \tag{18}$$

where $f_{f'\leftarrow N}$ are the integrated collinear distributions, that is, the parton distribution functions (PDF) which depend only on the Bjorken variables (x for PDFs) and the renormalization scale μ. All dependence on the transverse coordinate $\boldsymbol{b}_T$ and rapidity scale is contained in the matching coefficient and can be calculated perturbatively. I report the definition of the PDFs for completeness

$$f_{q\leftarrow N}(x) = \frac{1}{2}\sum_X \int \frac{d\xi^-}{2\pi} e^{-ixp^+\xi^-} \langle N| \left\{ T\left[\overline{q}_i \widetilde{W}_n^T\right]_a \cdot \left(\frac{\xi^-}{2}\right) |X\rangle \gamma_{ij}^+ \langle X| \overline{T}\left[\widetilde{W}_n^{T\dagger} q_j\right]_a \left(-\frac{\xi^-}{2}\right)\right\} |N\rangle . \tag{19}$$

The calculation of the Wilson coefficients in (17) uses the standard methods of the operator product expansion which profit of the fact that the coefficients do not depend on the infrared limit of the matrix elements. The current status of these calculations for quark distributions is resumed in Table 1. Less information is generally available in the case of gluon TMDs. Basically the matching coefficients for unpolarized gluons are known at NNLO [6] and linearly polarized gluons at NLO [15]. In general the TMDs which match onto collinear twist-3 functions are much less known, which reflects the difficulty of the computations. It would be very useful to have a better knowledge of all these less known functions at higher perturbative order before the advent of Electron Ion Collider (EIC). In the rest of this Section 1 focuses on unpolarized quark distributions which offer also an important understanding on the power of the TMD factorization. The necessity of a complete NLO estimation of all TMDs is both theoretical and phenomenological. Actually a difficulty of the TMD extraction from data is due to the fact that it is a nontrivial function of two variables (Bjorken x and transverse momentum) so that a complete mapping on a plane is necessary. This target is achievable

Table 1: Summary of available perturbative calculations of quark TMD distributions and their leading matching at small-b.

Name	Function	Leading matching function	Twist of leading matching	Maximum known order of coef. function	Ref.	Mix with gluon
unpolarized	$f_1(x, \boldsymbol{b})$	f_1	tw-2	NNLO (a_s^2)	[4, 5]	yes
Sivers	$f_{1T}^{\perp}(x, \boldsymbol{b})$	T	tw-3	NLO (a_s^1)	[6–14]$***$	yes
helicity	$g_{1L}(x, \boldsymbol{b})$	g_1	tw-2	NLO (a_s^1)	[6, 15–17]	yes
worm-gear T	$g_{1T}(x, \boldsymbol{b})$	$g_1, T, \Delta T$	tw-2/3	LO (a_s^0)	[18]$*$ [6]	yes
transversity	$h_1(x, \boldsymbol{b})$	h_1	tw-2	NNLO(a_s^2)	[19]	no
Boer-Mulders	$h_1^{\perp}(x, \boldsymbol{b})$	δT_ϵ	tw-3	LO (a_s^0)	[6]	no
worm-gear L	$h_{1L}^{\perp}(x, \boldsymbol{b})$	$h_1, \delta T_g$	tw-2/3	LO (a_s^0)	[18]$*$ [6]	no
pretzelosity$**$	$h_{1T}^{\perp}(x, \boldsymbol{b})$	–	tw-4	–	–	–

$*$The calculation is done in the momentum space. The result is given for the moments of distribution.

$**$The pretzelosity can in principle be a twist-2 observable; however its twist-2 matching coefficient has been found to be zero up to NNLO [19]. Therefore one can conjecture that pretzelosity is actually a twist-4 observable. Some arguments in favor of this can also be found in [20].

$***$The quark Sivers function at NLO has a long story [8–13]. A complete calculation is now available in [14].

Table 2: Notation for TMD anomalous dimensions used in the literature.

	rapidity evolution scale	TMD anomalous dimension	cusp anomalous dimension	vector form factor anomalous dimensions	rapidity anomalous dimension
[21–24]	ζ	γ_F	Γ	γ_V	$\mathscr{D}$
[25, 26]	ζ	γ_F $(=\gamma_D)$	$\frac{1}{2}\gamma_K$	$-\gamma_F(g(\mu);1)$	$-\frac{1}{2}\widetilde{K}$
[5, 27, 28]	–	–	Γ_{cusp}	$2\gamma^q$	$\frac{1}{2}F_{f\overline{f}}$
[29]	ν^2	$\gamma_\mu^{f_\perp}$	Γ_{cusp}	–	$-\frac{1}{2}\gamma_\nu^{f_\perp}$

thanks to the factorization of the cross section and the consequent extraction of the TMD evolution part, which is process independent. A second important information comes from the asymptotic limit of the TMD for large transverse momentum, which is perturbatively calculable. The simple LO expressions for the TMD in general do not provide much information (they are just constants), so that in order to achieve a wise modeling a NLO calculation is always necessary. The higher order calculations allow also testing the stability with respect to the scales that match the TMD perturbative and nonperturbative parts. For the unpolarized case a study in this sense can be found in [22] both for high energy and low-energy data. Using a LO calculations one cannot even quantify this error. Finally, another lesson that comes from the analysis of the unpolarized case is that a good portion of the TMD is tractable starting from their asymptotic expansion for large transverse momenta. In any case even a 10% average precision of the SIDIS cross section at EIC will need a NLO theoretical input.

4. Evolution

The evolution of the TMDs in the factorization, μ, scale is derived from their defining operators and from (15),

$$\begin{aligned}
&\mu^2\frac{d}{d\mu^2}O_f\left(x,\boldsymbol{b}_T\right)=\frac{1}{2}\gamma^f\left(\mu,\zeta\right)O_f\left(x,\boldsymbol{b}_T\right)\hookrightarrow\\
&\mu^2\frac{d}{d\mu^2}F_{f\longleftarrow h}\left(x,\boldsymbol{b}_T;\mu,\zeta\right)\\
&\quad=\frac{\gamma_F^f\left(\mu,\zeta\right)}{2}F_{f\longleftarrow h}\left(x,\boldsymbol{b}_T;\mu,\zeta\right),
\end{aligned}\tag{20}$$

in an usual way. Equation (20) is a standard renormalization group equation (which comes from the renormalization of the ultraviolet divergences), the function $\gamma_F(\mu,\zeta)$ is called the TMD anomalous dimension, and it contains both single and double logarithms. The same (13) can be used to write the running with respect to the rapidity scale, ζ. Because the rapidity scale evolution comes from soft interactions and more specifically from the soft factor (see discussion in [45, 61] and, e.g., [24, 42, 43]) which is the same for initial and final states, the rapidity scale evolution is the same for TMD parton distribution functions and TMD fragmentation functions, and it is also spin-independent (so it is the same also for TMDs at higher twist),

$$\begin{aligned}
&\zeta\frac{d}{d\zeta}O_f\left(x,\boldsymbol{b}_T\right)=-\mathscr{D}^f\left(\mu,\boldsymbol{b}_T\right)O_f\left(x,\boldsymbol{b}_T\right).\hookrightarrow\\
&\zeta\frac{d}{d\zeta}F_{f\longleftarrow h}\left(x,\boldsymbol{b}_T;\mu,\zeta\right)\\
&\quad=-\mathscr{D}^f\left(\mu,\boldsymbol{b}_T\right)F_{f\longleftarrow h}\left(x,\boldsymbol{b}_T;\mu,\zeta\right),
\end{aligned}\tag{21}$$

The function $\mathscr{D}(\mu,\boldsymbol{b}_T)$ is called the rapidity anomalous dimension and actually one has $\mathscr{D}(\mu,\boldsymbol{b}_T)\equiv\mathscr{D}(\mu,|\boldsymbol{b}_T|)$. The anomalous dimensions for these pair of evolution have been addressed with several names in the literature as it is shown in Table 2.

Quark and gluon rapidity anomalous dimensions are related up to three loops by the Casimir scaling (see [45]), $\mathscr{D}^q/\mathscr{D}^g=C_F/C_A=(N_c^2-1)/2N_c^2$.

The consistency of the differential equations ((20)-(21)) implies that the cross-derivatives of the anomalous dimension are equal to each other ([45, 61]),

$$\begin{aligned}
&\mu^2\frac{d}{d\mu^2}\left(-\mathscr{D}^f\left(\mu^2,\boldsymbol{b}_T\right)\right)=\zeta\frac{d}{d\zeta}\left(\frac{\gamma^f\left(\mu,\zeta\right)}{2}\right)\\
&\quad=-\frac{\Gamma_{cusp}^f}{2}.
\end{aligned}\tag{22}$$

From (22) one finds that the anomalous dimension γ is

$$\gamma^f=\Gamma_{cusp}^f\mathbf{l}_\zeta-\gamma_V^f,\tag{23}$$

where we introduce the notation

$$\mathbf{l}_X\equiv\ln\left(\frac{\mu^2}{X}\right).\tag{24}$$

The large-q_T expansion of the TMD introduces also another evolution scale, which is needed for in the matching of Wilson coefficients with the collinear operators. In the case of the unpolarized TMDs this is provided by the DGLAP (DGLAP is an acronym for Dokshitzer, Gribov, Lipatov, Altarelli, Parisi [1–3]) equations

$$\mu_b^2\frac{d}{d\mu_b^2}O_f\left(x,\mu_b\right)=\sum_{f\prime}P_{f\longleftarrow f'}\left(x\right)O_{f'}\left(x,\mu_b\right),\tag{25}$$

where P are the DGLAP kernels for the PDF. Similar equations hold for unpolarized TMD fragmentation functions. It

is useful to recall also the running of the matching coefficient with respect to the rapidity scale (we set $\mu_b = \mu$)

$$\zeta \frac{d}{d\zeta} C_{f\leftarrow f'}(x, \boldsymbol{b}_T; \mu, \zeta) = -\mathscr{D}^f(\mu, \boldsymbol{b}_T)\, C_{f\leftarrow f'}(x, \boldsymbol{b}_T; \mu, \zeta), \tag{26}$$

The solutions of these differential equations are

$$C_{f\leftarrow f'}(x, \boldsymbol{b}_T; \mu, \zeta) = \exp\left(-\mathscr{D}^f(\mu, \boldsymbol{b}_T)\, \mathbf{L}_{\sqrt{\zeta}}\right) \widehat{C}_{f\leftarrow f'}\left(x, \mathbf{L}_\mu\right). \tag{27}$$

This defines the reduced matching coefficients $\widehat{C}$ whose renormalization group evolution equations are

$$\mu^2 \frac{d}{d\mu^2} \widehat{C}_{f\leftarrow f'}\left(x, \mathbf{L}_\mu\right) = \sum_r \widehat{C}_{f\leftarrow r}\left(x, \mathbf{L}_\mu\right) \otimes K^f_{r\leftarrow f'}\left(x, \mathbf{L}_\mu\right), \tag{28}$$

with the kernel K

$$K^f_{r\leftarrow f'}\left(x, \mathbf{L}_\mu\right) = \frac{\delta_{rf'}}{2}\left(\Gamma^f_{cusp} \mathbf{L}_\mu - \gamma^f_V\right) - P_{r\leftarrow f'}(x). \tag{29}$$

The perturbative expansion of all these functions provides consistency requirements for the logarithmic terms at a given order. Using the notation for the n-th perturbative order,

$$\widehat{C}^{[n]}_{f\leftarrow f'}\left(x, \mathbf{L}_\mu\right) = \sum_{k=0}^{2n} C^{(n;k)}_{f\leftarrow f'}(x)\, \mathbf{L}^k_\mu. \tag{30}$$

one finds that the knowledge of the coefficient at order $n-1$ provides all the terms with $k \neq 0$ at order n in this series. So finally any higher order calculation provides new information on terms $C^{(n;0)}_{f\leftarrow f'}$. A resume of the present status of available calculations is provided in Table 1.

5. Implementation of TMD Formalism and TMD Extraction from Data

As an example of application of the TMD formalism I review the study of unpolarized TMD parton distribution functions in Drell-Yan and Z-boson production following [23].

Namely, I consider the process $h_1 + h_2 \longrightarrow G(\longrightarrow ll') + X$, where G is the electroweak neutral gauge boson, γ^* or Z. The incoming hadrons h_i have momenta p_1 and p_2 with $(p_1 + p_2)^2 = s$. The gauge boson decays to the lepton pair with momenta k_1 and k_2. The momentum of the gauge boson or equivalently the invariant mass of lepton pair is $Q^2 = q^2 = (k_1 + k_2)^2$. The differential cross section for the Drell-Yan process can be written in the form [68, 69]

$$d\sigma = \frac{d^4q}{2s} \sum_{G,G'=\gamma,Z} L^{\mu\nu}_{GG'} W^{GG'}_{\mu\nu}\, \Delta_G(q)\, \Delta_{G'}(q), \tag{31}$$

where $1/2s$ is the flux factor; Δ_G is the (Feynman) propagator for the gauge boson G. The hadron and lepton tensors are, respectively,

$$W^{GG'}_{\mu\nu} = \int \frac{d^4z}{(2\pi)^4} e^{-iqz} \langle h_1(p_1)\, h_2(p_2)|\, J^G_\mu(z)\, J^{G'}_\nu(0) \cdot |h_1(p_1)\, h_2(p_2)\rangle, \tag{32}$$

$$L^{GG'}_{\mu\nu} = \int \frac{d^3k_1}{(2\pi)^3\, 2E_1} \frac{d^3k_2}{(2\pi)^3\, 2E_2} (2\pi)^4\, \delta^4(k_1 + k_2 - q) \cdot \langle l_1(k_1)\, l_2(k_2)|\, J^G_\nu(0)\, |0\rangle\, \langle 0|\, J^{G'}_\mu(0)\, |l_1(k_1)\, l_2(k_2)\rangle, \tag{33}$$

where J^G_μ is the electroweak current. Within the TMD factorization, the unpolarized hadron tensor (see, e.g., [70]) is

$$W^{GG'}_{\mu\nu} = \frac{-g_{T\mu\nu}}{\pi N_c} |C_V(q_T, \mu)|^2 \sum_{f,f'} z^{GG'}_{ff'} \int \frac{d^2\boldsymbol{b}_T}{4\pi} e^{i(\boldsymbol{b}_T \cdot \boldsymbol{q}_T)} \cdot F_{f\leftarrow h_1}(x_1, \boldsymbol{b}_T; \mu, \zeta_1)\, F_{f'\leftarrow h_2}(x_2, \boldsymbol{b}_T; \mu, \zeta_2) \tag{34}$$

where g_T is the transverse part of the metric tensor and the summation runs over the active quark flavors. The variable μ is the hard factorization scale. The variables $\zeta_{1,2}$ are the scales of soft-gluons factorization, and they fulfill the relation $\zeta_1\zeta_2 = Q^4$. In the following, we consider the symmetric point $\zeta_1 = \zeta_2 = \zeta = Q^2$. The factors $z^{GG'}_{ff'}$ are the electro-weak charges and they are given explicitly in [23]. The factor C_V is the matching coefficient of the QCD neutral current to the same current expressed in terms of collinear quark fields. The explicit expressions for C_V can be found in [71–73].

In (34) I have not included power corrections to the TMD factorization (to be distinguished from the power corrections to the TMD operator product expansion). It is difficult to establish the amount of these corrections but a phenomenological study in [23] and a more formal study in the large-N_c limit (that is, the limit of large number of colors) in [74] have found a reasonable upper value $(q_T/Q)_{max} \sim 0.2$. A study which takes into account the structure of operators in the type of corrections has been started in [75]. In general the power corrections should be included when the di-lepton invariant mass is of order a few GeV (this is the case, for instance, of HERMES experiment and, perhaps to a possibly less extent, COMPASS) or when the experimental precision is extreme (as it possibly happens with ATLAS experiment). This is issue is important phenomenologically and involves the study of cross sections with the inclusion of factorization breaking contributions. Some recent suggestion have appeared in [76, 77] which have still to be tested phenomenologically. One should remark however that the implementation of these factorization breaking corrections strongly depends on the fact that the factorized part of the cross section is correctly realized and phenomenologically tested. More studies on this issue are necessary in the future.

Evaluating the lepton tensor and combining together all factors one obtains the cross section for the unpolarized

Drell-Yan process at leading order of TMD factorization, in the form [25, 27, 34, 36, 78, 79]

$$\begin{aligned}\frac{d\sigma}{dQ^2 dy d\left(q_T^2\right)} &= \frac{4\pi}{3N_c}\frac{\mathscr{P}}{sQ^2}\sum_{GG'} z_{ll'}^{GG'}(Q)\\ &\cdot \sum_{ff'} z_{ff'}^{GG'}\left|C_V(Q,\mu)\right|^2\\ &\cdot \int \frac{d^2\boldsymbol{b}_T}{4\pi} e^{i(\boldsymbol{b}_T\boldsymbol{q}_T)} F_{f\leftarrow h_1}(x_1,\boldsymbol{b}_T;\mu,\zeta)\\ &\cdot F_{f'\leftarrow h_2}(x_2,\boldsymbol{b}_T;\mu,\zeta),\end{aligned} \tag{35}$$

where y is the rapidity of the produced gauge boson. The factor $\mathscr{P}$ is a part of the lepton tensor and contains information on the fiducial cuts. This factor provides important information on the actual measured leptons and should be always included when the relative experimental information is provided.

The evolution of the TMDs play a special role in (35) and we collect of evolution equations here:

$$\begin{aligned}&\mu^2\frac{d}{d\mu^2}F_{f\leftarrow h}(x,\boldsymbol{b}_T;\mu,\zeta)\\ &\quad=\frac{\gamma_F(\mu,\zeta)}{2}F_{f\leftarrow h}(x,\boldsymbol{b}_T;\mu,\zeta),\\ &\zeta\frac{d}{d\zeta}F_{f\leftarrow h}(x,\boldsymbol{b}_T;\mu,\zeta)\\ &\quad=-\mathscr{D}(\mu,\boldsymbol{b}_T)F_{f\leftarrow h}(x,\boldsymbol{b}_T;\mu,\zeta).\\ &\mu\frac{d}{d\mu}\mathscr{D}(\mu,\boldsymbol{b}_T)=\Gamma(\mu),\\ &\zeta\frac{d}{d\zeta}\gamma_F(\mu,\zeta)=-\Gamma(\mu),\\ &\gamma_F(\mu,\zeta)=\Gamma(\mu)\ln\left(\frac{\mu^2}{\zeta}\right)-\gamma_V(\mu),\end{aligned} \tag{36}$$

and on the right hand side of these equation we have omitted the reference to flavor f for simplicity. The main features of these anomalous dimensions that have been discussed in previous sections are the following: The TMD anomalous dimension $\gamma_F(\mu,\zeta)$ contains both single and double logarithms and the anomalous dimension γ_V refers to the finite part of the renormalization of the vector form factor; see Table 2. Equation (36) cannot fix the logarithmic part of $\mathscr{D}$ entirely, but only order by order in perturbation theory, because the parameter μ is also responsible for the running of the coupling constant. The rapidity anomalous dimension $\mathscr{D}$ is a nonperturbative function (see the discussion about the renormalon in the perturbative series of this function in [32, 59, 80]), although it can be perturbatively expanded for small $|\boldsymbol{b}_T|$.

The double-evolution equation of the TMDs can be formulated as in [23] using a two-dimensional vector field notation, that i reproduces here. The procedure consists in introducing a convenient two-dimensional variable which treats scales μ and ζ equally,

$$\boldsymbol{\nu} = \left(\ln\left(\frac{\mu^2}{(1\ \mathrm{GeV}^2)}\right), \ln\left(\frac{\zeta}{(1\ \mathrm{GeV}^2)}\right)\right), \tag{37}$$

where the dimension of the scale parameters is explicitly indicated and the bold font means the two-dimensional vectors. Then one defines the standard vector differential operations in the plane $\boldsymbol{\nu}$, namely, the gradient and the curl

$$\begin{aligned}\boldsymbol{\nabla} &= \frac{d}{d\boldsymbol{\nu}} = \left(\mu^2\frac{d}{d\mu^2}, \zeta\frac{d}{d\zeta}\right),\\ \mathbf{curl} &= \left(-\zeta\frac{d}{d\zeta}, \mu^2\frac{d}{d\mu^2}\right).\end{aligned} \tag{38}$$

The TMD anomalous dimensions can be all included in a vector evolution field $\mathbf{E}(\boldsymbol{\nu},\boldsymbol{b}_T)$,

$$\mathbf{E}(\boldsymbol{\nu},\boldsymbol{b}_T) = \frac{1}{2}\left(\gamma_F(\boldsymbol{\nu}), -2\mathscr{D}(\boldsymbol{\nu},\boldsymbol{b}_T)\right). \tag{39}$$

Here and in the following, we use the vectors $\boldsymbol{\nu}$ as the argument of the anomalous dimensions for brevity, keeping in mind that $\mathscr{D}(\boldsymbol{\nu},\boldsymbol{b}_T) = \mathscr{D}(\mu,\boldsymbol{b}_T)$, $\gamma_F(\boldsymbol{\nu}) = \gamma_F(\mu,\zeta)$, etc. In other words, the anomalous dimensions are to be evaluated on the corresponding values of μ and ζ defined by value of $\boldsymbol{\nu}$ in (37). The TMD evolution equations (36) and the evolution factor R in this notation have the form

$$\begin{aligned}\boldsymbol{\nabla}F(x,\boldsymbol{b}_T;\boldsymbol{\nu}) &= \mathbf{E}(\boldsymbol{\nu},\boldsymbol{b}_T)F(x,\boldsymbol{b}_T;\boldsymbol{\nu}),\\ \ln R\left[b,\boldsymbol{\nu}_f\longrightarrow\boldsymbol{\nu}_i\right] &= \int_P \mathbf{E}\cdot d\boldsymbol{\nu}.\end{aligned} \tag{40}$$

Using this formalism, (36) are equivalent to the statement that the evolution flow is *irrotational*,

$$\begin{aligned}\boldsymbol{\nabla}\times\mathbf{E} &= 0,\\ \mathbf{E}(\boldsymbol{\nu},\boldsymbol{b}_T) &= \boldsymbol{\nabla}U(\boldsymbol{\nu},\boldsymbol{b}_T),\end{aligned} \tag{41}$$

and U is the evolution scalar potential for TMD. According to the gradient theorem any line integral of the field $\mathbf{E}$ is path-independent and equals the difference of values of potential at end-points. Therefore, the solution for the R factor in (40) is

$$\ln R\left[b;\boldsymbol{\nu}_f\longrightarrow\boldsymbol{\nu}_i\right] = U\left(\boldsymbol{\nu}_f,\boldsymbol{b}_T\right) - U\left(\boldsymbol{\nu}_i,\boldsymbol{b}_T\right), \tag{42}$$

$$\begin{aligned}U(\boldsymbol{\nu},\boldsymbol{b}_T) &= \int^{\nu_1}\frac{\Gamma(s)\,s-\gamma_V(s)}{2}ds\\ &\quad-\mathscr{D}(\boldsymbol{\nu},\boldsymbol{b}_T)\,\nu_2 + \mathrm{const.}(\boldsymbol{b}_T),\end{aligned} \tag{43}$$

and $\nu_{1,2}$ are the first and second components of the vector $\boldsymbol{\nu}$ in (37), and the last term is an arbitrary b-dependent function.

The evolution field presented in the previous section is conservative only when the full perturbative expansion of the evolution equations is known. In practice only a few terms of the evolution are calculated, so that it is

important to understand in which sense the evolution field remains conservative. Using the Helmholtz decomposition, the evolution field is split into two parts

$$\mathbf{E}\left(\boldsymbol{\nu}, \boldsymbol{b}_T\right) = \widetilde{\mathbf{E}}\left(\boldsymbol{\nu}, \boldsymbol{b}_T\right) + \boldsymbol{\Theta}\left(\boldsymbol{\nu}, \boldsymbol{b}_T\right). \tag{44}$$

The field $\widetilde{\mathbf{E}}$ is irrotational, the field $\boldsymbol{\Theta}$ is divergence-free, and they are orthogonal to each other

$$\begin{aligned} \operatorname{curl} \widetilde{\mathbf{E}} &= 0, \\ \boldsymbol{\nabla} \cdot \boldsymbol{\Theta} &= 0, \\ \widetilde{\mathbf{E}} \cdot \boldsymbol{\Theta} &= 0, \end{aligned} \tag{45}$$

with the notation curl(**curl**) $= \nabla^2$. Then, one can write the irrotational field $\widetilde{\mathbf{E}}$, which is conservative, as the gradient of a scalar potential

$$\widetilde{\mathbf{E}}\left(\boldsymbol{\nu}, \boldsymbol{b}_T\right) = \boldsymbol{\nabla}\widetilde{U}\left(\boldsymbol{\nu}, \boldsymbol{b}_T\right), \tag{46}$$

and the divergence-free part as the vector curl (see (38)) of another scalar potential $\boldsymbol{\Theta}(\boldsymbol{\nu}, \boldsymbol{b}_T) = \mathbf{curl} V(\boldsymbol{\nu}, \boldsymbol{b}_T)$. The curl of the evolution field can be calculated using the definitions (36),

$$\begin{aligned} \operatorname{curl}\mathbf{E} = \operatorname{curl}\boldsymbol{\Theta} &= \frac{\delta\Gamma\left(\boldsymbol{\nu}, \boldsymbol{b}_T\right)}{2}, \\ \text{with } \delta\Gamma\left(\mu, \boldsymbol{b}_T\right) &= \Gamma\left(\mu\right) - \mu\frac{d\mathscr{D}\left(\mu, \boldsymbol{b}_T\right)}{d\mu}. \end{aligned} \tag{47}$$

The function $\delta\Gamma$ can be calculated order by order in perturbation theory. For instance, at order N one finds

$$\begin{aligned} \delta\Gamma^{(N)} &= 2\sum_{n=1}^{N}\sum_{k=0}^{n} n\overline{\beta}_{n-1}\left(a_s\right) a_s^{n-1} d^{(n,k)} \mathbf{L}_\mu^k, \\ \text{where } \overline{\beta}_n\left(a_s\right) &= \beta\left(a_s\right) - \sum_{k=0}^{n-1}\beta_k a_s^{k+2}, \end{aligned} \tag{48}$$

is the β-function with first n terms removed. For instance, we have

$$\delta\Gamma^{(1)} = \Gamma_0\beta\left(a_s\right)\mathbf{L}_\mu \sim \mathcal{O}\left(a_s^2\mathbf{L}_\mu\right), \tag{49}$$

$$\begin{aligned} \delta\Gamma^{(2)} &= \Gamma_0\overline{\beta}_1\left(a_s\right)\mathbf{L}_\mu \\ &\quad + \beta\left(a_s\right)a_s\left(\Gamma_0\beta_0\mathbf{L}_\mu^2 + 2\Gamma_1\mathbf{L}_\mu + 4d^{(2,0)}\right) \\ &\sim \mathcal{O}\left(a_s^3\mathbf{L}_\mu^2\right). \end{aligned} \tag{50}$$

In these expressions the β-function is not expanded because in applications one can find a different perturbative order with respect to the rest of the anomalous dimensions.

The immediate consequence of the fact that the evolution field $\mathbf{E}$ is no more conservative is that the evolution factor $R[\boldsymbol{b}_T; \boldsymbol{\nu}_f \longrightarrow \boldsymbol{\nu}_i]$ is dependent on the path chosen to join the initial and final points $\boldsymbol{\nu}_i, \boldsymbol{\nu}_f$ and this fact introduces a theoretical error which can be dominant in certain implementation of the evolution kernels. The difference between two solutions evaluated on different paths is

$$\begin{aligned} \ln\frac{R\left[\boldsymbol{b}_T; \{\mu_1, \zeta_1\} \xrightarrow{P_1} \{\mu_2, \zeta_2\}\right]}{R\left[\boldsymbol{b}_T; \{\mu_1, \zeta_1\} \xrightarrow{P_2} \{\mu_2, \zeta_2\}\right]} &= \oint_{P_1 \cup P_2} \mathbf{E}\cdot d\boldsymbol{\nu} \\ &= \frac{1}{2}\int_{\Omega(P_1\cup P_2)} d^2\nu\,\delta\Gamma\left(\boldsymbol{\nu}, \boldsymbol{b}_T\right), \end{aligned} \tag{51}$$

where $P_1 \cup P_2$ is the closed path built from paths P_1 and P_2 and $\Omega(P_1 \cup P_2)$ is the area surrounded by these paths. Using the independence of $\delta\Gamma$ on the variable ζ, (51) becomes

$$\begin{aligned} &\ln\frac{R\left[\boldsymbol{b}_T; \{\mu_1, \zeta_1\} \xrightarrow{P_1} \{\mu_2, \zeta_2\}\right]}{R\left[\boldsymbol{b}_T; \{\mu_1, \zeta_1\} \xrightarrow{P_2} \{\mu_2, \zeta_2\}\right]} \\ &\quad = \int_{\mu_2}^{\mu_1}\frac{d\mu}{\mu}\delta\Gamma\left(\mu, \boldsymbol{b}_T\right)\ln\left(\frac{\zeta_1\left(\mu\right)}{\zeta_2\left(\mu\right)}\right), \end{aligned} \tag{52}$$

where $\zeta_{1,2}(\mu)$ is the ζ-component of the path $P_{1,2}$ at the scale μ. This equation shows that the difference between paths becomes bigger with largely separated rapidity scales ζ_i.

The path independence of the evolution is crucial for the implementation of the perturbative formalism, as its absence can derive into uninterpretable extractions of TMDs or big theoretical errors. The path independence can be achieved observing that

$$\mu\frac{d\mathscr{D}\left(\mu, \boldsymbol{b}_T\right)}{d\mu} = -\zeta\frac{d\gamma\left(\mu, \zeta\right)}{d\zeta} \tag{53}$$

should hold order by order in perturbation theory. Once this is realized it is possible to define null-evolution lines in the (μ, ζ) plane, which coincide with equipotential lines, and the evolution of TMD takes place only between two different lines. I resume here two possible solutions to this problem, following [23].

In the literature one can find a typical way to implement the evolution that one can call the improved $\mathscr{D}$ scenario which includes the Collins-Soper-Sterman formalism [21, 22, 25, 26, 29, 81, 82]. In this scenario one chooses a scale μ_0 such that

$$\delta\Gamma\left(\mu_0, \boldsymbol{b}_T\right) = 0. \tag{54}$$

In this way one obtains

$$\mathscr{D}\left(\mu, \boldsymbol{b}_T\right) = \int_{\mu_0}^{\mu}\frac{d\mu'}{\mu'}\Gamma\left(\mu'\right) + \mathscr{D}\left(\mu_0, \boldsymbol{b}_T\right), \tag{55}$$

and the TMD evolution factor R depends on μ_0

$$\begin{aligned} &\text{improved } \mathscr{D} \text{ solution: } \ln R\left[\boldsymbol{b}_T; \left(\mu_f, \zeta_f\right)\right. \\ &\left.\longrightarrow \left(\mu_i, \zeta_i\right); \mu_0\right] = \int_{\mu_i}^{\mu_f}\frac{d\mu}{\mu}\left(\Gamma\left(\mu\right)\ln\left(\frac{\mu^2}{\zeta_f}\right)\right. \end{aligned}$$

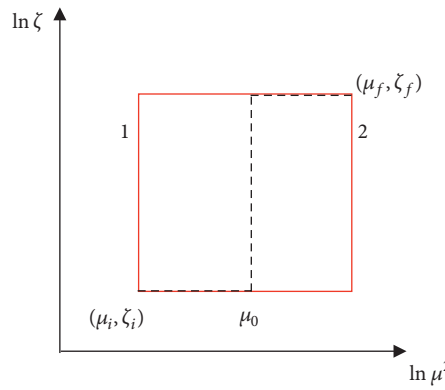

FIGURE 2: Paths for the improved $\mathscr{D}$ solution which depend on the choice of the reference scale μ_0.

$$- \gamma_V(\mu)\Big) - \int_{\mu_0}^{\mu_i} \frac{d\mu}{\mu}\Gamma(\mu) \ln\left(\frac{\zeta_f}{\zeta_i}\right) - \mathscr{D}(\mu_0, \boldsymbol{b}_T) \cdot \ln\left(\frac{\zeta_f}{\zeta_i}\right). \tag{56}$$

The situation in this scenario can be visualized in Figure 2. Any choice of μ_0 corresponds to a different scheme as μ_0 is the point where evolution flips from path 1 and path 2 in Figure 2. The differences that can appear in the extraction of TMDs which depend on the choice of μ_0 can be numerically large, so that the selection of this scale can cause also some problems when a sufficient precision is required.

The presence of the intermediate scale μ_0 is not unavoidable in the implementation of the TMD evolution. In fact the integrability condition (53) can be restored by changing the anomalous dimension γ_F to a modified value γ_M such that

$$\gamma_M(\mu, \zeta, \boldsymbol{b}_T) = (\Gamma(\mu) - \delta\Gamma(\mu, \boldsymbol{b}_T)) \ln\left(\frac{\mu^2}{\zeta}\right) - \gamma_V(\mu). \tag{57}$$

and the corresponding solution for the evolution factor reads

$$\text{improved } \gamma \text{ solution: } \ln R\left[\boldsymbol{b}_T; (\mu_f, \zeta_f) \longrightarrow (\mu_i, \zeta_i)\right] = -\int_{\mu_i}^{\mu_f} \frac{d\mu}{\mu}\left(2\mathscr{D}(\mu, \boldsymbol{b}_T) + \gamma_V(\mu)\right) + \mathscr{D}\left(\mu_f, \boldsymbol{b}_T\right) \ln\left(\frac{\mu_f^2}{\zeta_f}\right) - \mathscr{D}(\mu_i, \boldsymbol{b}_T) \ln\left(\frac{\mu_i^2}{\zeta_i}\right). \tag{58}$$

These expressions should be completed with the resummation of $\mathscr{D}$ by means of renormalization group equation (55) as it is not implicitly included in this scenario.

5.1. ζ Prescription and Optimal TMDs. Because we have a double scale running of the TMD one can find lines of null evolution in the (μ, ζ) plane. These lines are by default the equipotential lines, that we call $\boldsymbol{\omega}(\boldsymbol{\nu}_B, b)$. In formulas this can be written as

$$F(x, \boldsymbol{b}_T; \boldsymbol{\nu}_B) = F\left(x, \boldsymbol{b}_T; \boldsymbol{\nu}_B'\right), \quad \boldsymbol{\nu}_B' \in \boldsymbol{\omega}(\boldsymbol{\nu}_B, \boldsymbol{b}_T), \tag{59}$$

when the scales $\boldsymbol{\nu}_B$ and $\boldsymbol{\nu}_B'$ belong to the same null-evolution curve. Any point of the line $\boldsymbol{\nu}_B$ in the (ζ, μ) plane does not change the value of the TMDs. When two TMDs do not belong to the same equipotential curve one finds

$$F\left(x, \boldsymbol{b}_T; \mu_f, \zeta_f\right) = R\left[\boldsymbol{b}_T; \left(\mu_f, \zeta_f\right) \longrightarrow \left(\mu_i, \zeta_{\mu_i}(\boldsymbol{\nu}_B, \boldsymbol{b}_T)\right)\right] \cdot F(x, \boldsymbol{b}_T; \boldsymbol{\nu}_B), \tag{60}$$

where ζ_μ is defined such that $(\mu_i, \zeta_{\mu_i}(\boldsymbol{\nu}_B, \mathbf{b}_T)) \in \omega(\boldsymbol{\nu}_B, b_T)$ and $(\mu_f, \zeta_f) \notin \omega(\boldsymbol{\nu}_B, \boldsymbol{b}_T)$. In order to minimize the evolution effect and so to have a more stable prediction/extraction of TMDs the initial and final evolution curves should be selected with care. Once this is settled, it remains to find an appropriate set of initial and final line which is sufficiently stable for all relevant processes. The final point of the rapidity evolution, ζ_f, is as usual dictated by the hard subprocess. Concerning the starting line it is convenient to take into account also the matching of the TMD on the respective integrated distributions, which formally is

$$F_{f \leftarrow k}(x, \boldsymbol{b}_T; \mu_i, \zeta_i) = \sum_n \sum_{f'} C^{(n)}_{f \leftarrow f'}\left(x, \mathbf{L}_{\mu_i}, \mathbf{L}_{\sqrt{\zeta_i}}\right) \otimes f^{(n)}_{f' \leftarrow h}(x, \mu_i), \tag{61}$$

where f is PDF or FF and C is the Wilson coefficient function. The coefficient function includes the dependence on $\boldsymbol{b}_T$ within the logarithms $\mathbf{L}_\mu$ and $\mathbf{L}_{\sqrt{\zeta}}$. The traditional choice, see, e.g., [25, 26, 83], $\zeta_i = \mu_i^2$ leaves uncanceled logarithmic factors in the coefficient function which explode at small $\boldsymbol{b}_T$. The damage caused by this choice is partially cured inserting more prescriptions like the b^* prescription [25], which however

bias the modeling of the nonperturbative part of the TMD. In fact, among the others, this prescription correlated the nonperturbative part of the evolution factor with the intrinsic nonperturbative part of the TMD. Although this prescription may work for some initial studies it results to have serious drawbacks for more precise analysis.

The ζ-prescription suggested in [22, 23] provides an attempt to improve the stability of the perturbative series and keep separate the truly nonperturbative TMD distribution from the nonperturbative part of the evolution kernel. The advantage of this separation is that one can always use all known perturbative information for the evolution factor, even if the knowledge of the collinear matching is not at the same perturbative order. This reduces drastically the perturbative uncertainty in the extractions of TMDs from data and also facilitates the understanding of direct calculations of the TMD through nonperturbative QCD methods like lattice.

I provide here some description of the ζ-prescription following [22, 23]. A TMD distribution in the ζ-prescription reads

$$\begin{aligned} &F\left(x, \boldsymbol{b}_T; \mu_f, \zeta_f\right) \\ &\quad = R\left[b; \left(\mu_f, \zeta_f\right) \longrightarrow \left(\mu_i, \zeta_{\mu_i}\left(\boldsymbol{\nu}_B, \boldsymbol{b}_T\right)\right)\right] F\left(x, b_T; \boldsymbol{\nu}_B\right), \end{aligned} \tag{62}$$

where ζ_μ is defined such that $(\mu_i, \zeta_{\mu_i}(\boldsymbol{\nu}_B, \boldsymbol{b}_T)) \in \omega(\boldsymbol{\nu}_B, \boldsymbol{b}_T)$, that is, the value of ζ_i is such that the initial scales of the TMD distribution (μ_i, ζ_{μ_i}) belong to the null-evolution curve $\omega(\boldsymbol{\nu}_B, \boldsymbol{b}_T)$. At this stage let me rewrite (61) specifying the scales,

$$\begin{aligned} F_{f \longleftarrow k}\left(x, \boldsymbol{b}_T; \boldsymbol{\nu}_B\right) &= \sum_n \sum_{f'} C^{(n)}_{f \longleftarrow f'}\left(x, \boldsymbol{b}_T, \boldsymbol{\nu}_B, \mu_{\mathrm{OPE}}\right) \\ &\quad \otimes f^{(n)}_{f' \longleftarrow h}\left(x, \mu_{\mathrm{OPE}}\right), \end{aligned} \tag{63}$$

where μ_{OPE} is an intrinsic scale for the expansion of the TMD in terms of Wilson coefficients and PDFs and it is a free parameter. In general the values of μ_{OPE} are restricted by the values of μ,

$$\begin{aligned} &\text{if } \nu_{B,1} < \ln \mu^2_{\mathrm{saddle}} \Longrightarrow \mu_{\mathrm{OPE}} < \mu_{\mathrm{saddle}}, \\ &\text{if } \nu_{B,1} > \ln \mu^2_{\mathrm{saddle}} \Longrightarrow \mu_{\mathrm{OPE}} > \mu_{\mathrm{saddle}}, \end{aligned} \tag{64}$$

except

$$\text{if } \boldsymbol{\nu}_B = \left(\ln \mu^2_{\mathrm{saddle}}, \ln \zeta_{\mathrm{saddle}}\right) \Longrightarrow \mu_{\mathrm{OPE}} \text{ unrestricted.} \tag{65}$$

The last choice give us much more freedom to model the nonperturbative part of the TMD and the definition of the initial scale is unique and nonperturbatively defined. The choice of μ_{saddle} as the initial point is so *optimal* and consistent with the reexpression of TMDs using PDFs. This scheme fixes the optimal-TMD-distribution; that is, it fixes the initial special null-evolution curve. As a summery any initial point in the saddle curve is defined nonperturbatively and it is unique and performing this choice it is consistent to write optimal TMD simply as $F(x, \boldsymbol{b}_T)$.

A plot for the R-factor is given in Figure 3. At large-b the shape of the rapidity anomalous dimension is nonperturbative as renormalon studies confirm [59, 80] (see also [84]). So, at large-b the expression for $\mathscr{D}$ should be extracted from data fitting, while at small-b it should match the perturbative expression. We recall that the ζ-prescription has, among its benefit, the one of separating the modeling of the nonperturbative part of the evolution factor from the rest of nonperturbative parts of the TMD. This implies that it always recommendable to use the highest nonperturbative order in the evolution factor, even if the matching coefficients of the TMD with the collinear functions are known to a lesser precision perturbatively.

The nonperturbative part of the evolution kernel can be modeled in different ways. For instance, one can introduce a simple ansatz like a the modification

$$\begin{aligned} \mathscr{D}_{\mathrm{NP}}\left(\mu, b\right) &= \mathscr{D}\left(\mu, b^*\right), \\ b^*\left(b\right) &= \begin{cases} b, & b \ll \overline{b}, \\ b_{\max}, & b \gg \overline{b}, \end{cases} \end{aligned} \tag{66}$$

where $b = |\boldsymbol{b}_T|$ and $b_{\max}$ is a parameter, such that $b_{\max} < \overline{b}$ as suggested a long ago in [33],

$$b^*\left(b\right) = b\left(1 + \frac{b^2}{b^2_{\max}}\right)^{-1/2}, \tag{67}$$

as part of the b^* prescription [25]. Let us stress that the choice of a b^* can be admissible separately for the evolution factor and that (66) does not imply b^*-prescription for the whole TMD distribution. With the choice $b_{\max} < \overline{b}$ the saddle point is always in the observable region, which allows determining the optimal TMD. In this case the evolution factor reads

$$\begin{aligned} &R^f\left[b; \left(\mu_f, \zeta_f\right)\right] \\ &\quad = \exp\left\{-\int_{\mu_{\mathrm{saddle}}}^{\mu_f} \frac{d\mu}{\mu}\left(2\mathscr{D}^f_{\mathrm{NP}}\left(\mu, b\right) + \gamma^f_V\left(\mu\right)\right)\right. \\ &\quad \left. + \mathscr{D}^f_{\mathrm{NP}}\left(\mu_f, b\right) \ln\left(\frac{\mu^2_f}{\zeta_f}\right)\right\} \\ &\quad = \exp\left\{-\mathscr{D}^f_{\mathrm{NP}}\left(\mu_f, b\right) \ln\left(\frac{\zeta_f}{\zeta_{\mu_f}\left(b\right)}\right)\right\}. \end{aligned} \tag{68}$$

and the resumed expression for the TMD anomalous dimension as in [21] is understood in the last line. In (68), the scale μ_{saddle} is b-dependent and defined by the equation

$$\mathscr{D}^f_{\mathrm{NP}}\left(\mu_{\mathrm{saddle}}, b\right) = 0. \tag{69}$$

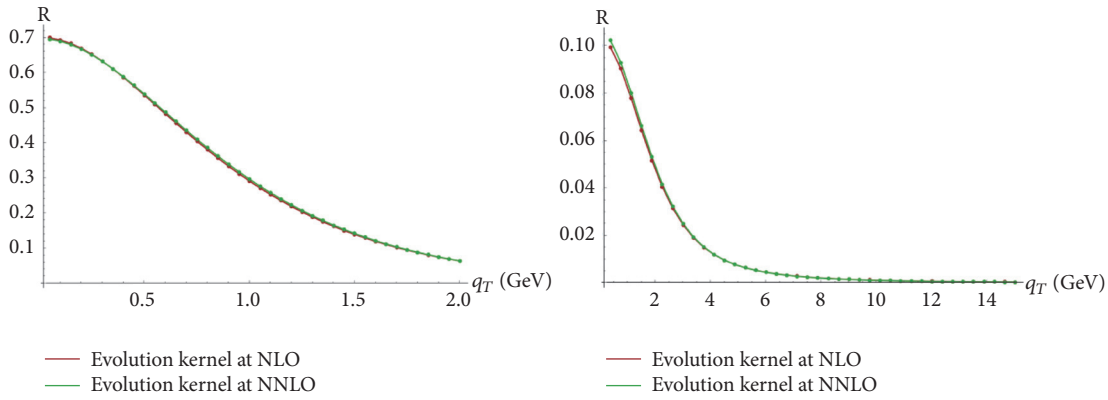

FIGURE 3: R evolution factor using the optimal TMD prescriptions when the high scale is fixed at the Z-boson mass (right side) and at BELLE center of mass energy 10.52 GeV (left side). In this figure one has chosen $b_{max} = 2.5\ \text{GeV}^{-1}$ and $\mathcal{D}_{NP} = \exp(-g_K \boldsymbol{b}_T{}^2)$ with $g_K = 0.1\ \text{GeV}^2$.

The expression for the cross section with the optimal TMD definition is particularly compact and reads

$$\begin{aligned}\frac{d\sigma}{dX} = \sigma_0 \sum_f \int \frac{d^2b}{4\pi} e^{i(b\cdot q_T)} H_{ff'}\left(Q, \mu_f\right) \\ \cdot \left\{R^f\left[b; \left(\mu_f, \zeta_f\right)\right]\right\}^2 F_{f\leftarrow h}\left(x_1, b\right) \\ \cdot F_{f'\leftarrow h}\left(x_2, b\right).\end{aligned} \tag{70}$$

The derivation of the saddle point using formula (69) is in practice done numerically, so that an efficient method to extract it or to approximate this point should be discussed as in [23]. A technical discussion of this issue is beyond the point of this paper.

Let me conclude this section discussing a comparison of the optimal TMD construction with a more traditional implementation on data following the recent fits in [22, 85]. The absence of an intermediate scale μ_0 removes one (scheme dependent) source of error and at the same time it allows the path independence of the final result. In this way it is possible to directly compare $\mathcal{D}_{\text{NP}}$ from different extractions and models. In the definition of the optimal TMD the low-energy normalization is defined "nonperturbatively" and uniquely by (69) which implies that the perturbative order of the evolution is completely unrelated to the perturbative order of matching of the TMD on the respective collinear functions. Because the evolution factor is known often at higher orders with respect to the Wilson coefficient matching factors, it is always possible to fully use all the available perturbative information. The theoretical uncertainty of TMDs is estimated with the variation of μ_f and μ_{OPE}. The fact that the number of varied scales is different from more standard analysis does not necessarily imply a reduction of theoretical errors. The error in fact reshuffles in μ_f and μ_{OPE}, but the description is now more coherent. One can appreciate this effect in Figure 4 taken from [22]. In this figure one compares for the ATLAS experiment a standard method to test the dependence on the scales and thus the stability of the perturbation theory prediction, multiplying each scale by a parameter [22, 37, 86, 87], and varying the parameters nearby their central value. For example, in the notation of [22], one changes scales as

$$\begin{aligned}\mu_0 &\longrightarrow c_1\mu_0, \\ \mu_f &\longrightarrow c_2\mu_f, \\ \mu_i &\longrightarrow c_3\mu_i, \\ \mu_{\text{OPE}} &\longrightarrow c_4\mu_{\text{OPE}},\end{aligned} \tag{71}$$

and checks the variations of $c_i \in (1/2, 2)$. The variation of all these four parameters is consistent with a nonoptimal definition of TMDs, while in the optimal case only the variation of c_2 and c_4 is necessary.

6. Conclusions

The formulation of factorization theorems in terms of TMDs is a first fundamental step for the study of the structure of hadrons and the origin of spin. The use of the effective field theory appears essential to correctly order the QCD contributions. Properties of TMDs like evolution and their asymptotic limit at large values of transverse momentum can be systematically calculated starting from the definition of correct operators and the evaluation of the interesting matrix elements. A key point for the renormalization of TMDs is represented by the so-called soft matrix element which is common in the definition of all spin dependent leading twist TMD.

Still, all this is just a starting point for the study of TMDs. In fact a correct implementation of evolution requires a control of all renormalization scales that appear in the factorization theorem. I have described here some of these possibility putting the accent on some recent interesting developments which, at least theoretically, allow a better control of the resumed QCD series. The understanding of factorization allows also precisely defining the range of ideal experimental conditions where this formalism can be applied. A full analysis of present data using all the theoretical information collected so far is still missing and it will certainly be an object of research in the forthcoming years. The formalism

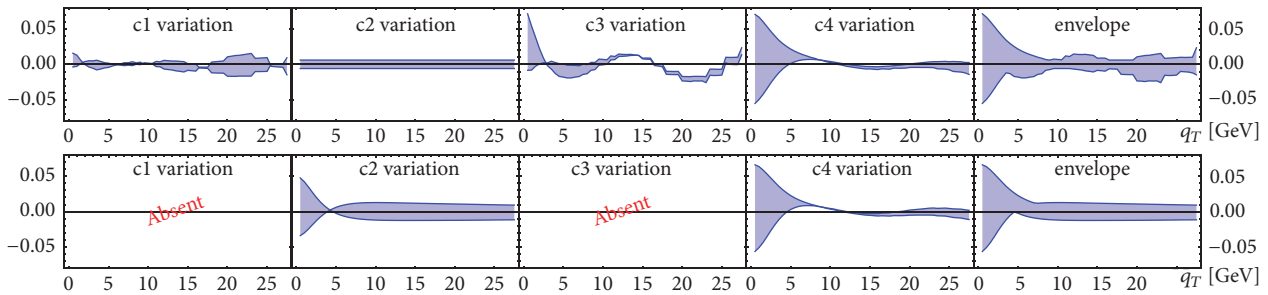

Figure 4: Comparison of error bands obtained by the scale-variations for cross sections at NNLO in traditional (upper figure) and optimal (lower figure) TMD implementation. Here, the kinematics bin-integration, etc., is for the Z-boson production measure at ATLAS at 8 TeV [31].

described in this work is the one developed for unpolarized distributions. However the evolution factors are universal; that is, they are the same for polarized and unpolarized leading twist TMDs and they are valid in Drell-Yan, SIDIS experiments, and e^+e^- colliders, where the factorization theorem applies. All this formalism is expected to be tested on data in the near future. Nevertheless a lot of perturbative and nonperturbative information is still missing. Giving a look at Table 1 one can see that for many TMD one has only a lowest order perturbative calculation which should be improved in order to have a reliable description of data. While the information on the nonperturbative structure of TMD is still poor and still driven by phenomenological models, it is important to implement the TMD formalism in such a way that perturbative and nonperturbative effects are well separated. And among the nonperturbative effects, one should be able to distinguish the ones of the evolution kernel from the rest. In the text I have discussed a possible solution to this problem. Some prominent research lines which possibly will deserve more attention in the future include the cases where hadrons are measured inside the jets, see, for instance, [88–90] or outside a jet (say, hadron-jet interactions) [91–93] and lattice.

Conflicts of Interest

The authors declare that they have no conflicts of interest.

Acknowledgments

I would like to thank Alexey Vladimirov and Daniel Gutierrez Reyes for discussing this paper. Ignazio Scimemi is supported by the Spanish MECD grant FPA2016-75654-C2-2-P.

References

[1] V. N. Gribov and L. N. Lipatov, "Deep inelastic e p scattering in perturbation theory," *Soviet Journal of Nuclear Physics*, vol. 15, pp. 438–450, 1972, [Yad. Fiz.15,781(1972)].

[2] Y. L. Dokshitzer and Sov. Phys. JETP, "Calculation of structure functions of deep-inelastic scattering and e+e- annihilation by perturbation theory in quantum chromodynamics," *Journal of Experimental and Theoretical Physics*, vol. 46, p. 641, 1977.

[3] G. Altarelli and G. Parisi, "Asymptotic freedom in parton language," *Nuclear Physics B*, vol. 126, pp. 298–318, 1977.

[4] M. G. Echevarria, I. Scimemi, and A. Vladimirov, "Unpolarized Transverse Momentum Dependent Parton Distribution and Fragmentation Functions at next-to-next-to-leading order," *Journal of High Energy Physics*, vol. 2016, p. 4, 2016.

[5] T. Gehrmann, T. Luebbert, and L. L. Yang, "Calculation of the transverse parton distribution functions at next-to-next-to-leading order," *Journal of High Energy Physics*, vol. 2014, no. 6, p. 155, 2014.

[6] I. Scimemi and A. Vladimirov, "Matching of transverse momentum dependent distributions at twist-3," *High Energy Physics - Phenomenology*, vol. 78, p. 802, 2018.

[7] D. Boer, P. J. Mulders, and F. Pijlman, "Universality of T-odd effects in single spin and azimuthal asymmetries," *High Energy Physics - Phenomenology*, vol. 667, no. 1-2, Article ID 0303034, pp. 201–241, 2003.

[8] X. Ji, J. W. Qiu, W. Vogelsang, and F. Yuan, "Unified picture for single transverse-spin asymmetries in hard-scattering processes," *Physical Review Letters*, vol. 97, Article ID 082002, 2006.

[9] X. Ji, J. W. Qiu, W. Vogelsang, and F. Yuan, "Single transverse-spin asymmetry in Drell-Yan production at large and moderate transverse momentum," *Physical Review D: Particles, Fields, Gravitation and Cosmology*, vol. 73, Article ID 094017, 2006.

[10] Y. Koike, W. Vogelsang, and F. Yuan, "On the relation between mechanisms for single-transverse-spin asymmetries," *High Energy Physics - Phenomenology*, vol. 659, no. 5, pp. 878–884, 2008.

[11] Z. B. Kang, B. W. Xiao, and F. Yuan, "QCD resummation for single spin asymmetries," *Physical Review Letters*, vol. 107, Article ID 152002, 2011.

[12] P. Sun and F. Yuan, "Energy evolution for the Sivers asymmetries in hard processes," *Physical Review D: Particles, Fields, Gravitation and Cosmology*, vol. 88, Article ID 114012, 2013.

[13] L.-Y. Dai, Z.-B. Kang, A. Prokudin, and I. Vitev, "Next-to-leading order transverse momentum-weighted Sivers asymmetry in semi-inclusive deep inelastic scattering: the role of the three-gluon correlator," *Physical Review D: Covering Particles, Fields, Gravitation, and Cosmology*, vol. 92, Article ID 114024, 2015.

[14] I. Scimemi, A. Tarasov, and A. Vladimirov, "Collinear matching for Sivers function at next-to-leading order," *High Energy Physics - Phenomenology*, 2019.

[15] D. Gutierrez-Reyes, I. Scimemi, and A. A. Vladimirov, "Twist-2 matching of transverse momentum dependent distributions," *Physics Letters B*, vol. 769, pp. 84–89, 2017.

[16] A. Bacchetta and A. Prokudin, "Evolution of the helicity and transversity Transverse-Momentum-Dependent parton distributions," *Nuclear Physics B*, vol. 875, p. 536, 2013.

[17] M. G. A. Bu_ng, M. Diehl, T. Kasemets, and JHEP., "Transverse momentum in double parton scattering: factorisation, evolution and matching," *Journal of High Energy Physics*, vol. 2018, p. 044, 2018.

[18] K. Kanazawa, Y. Koike, A. Metz, D. Pitonyak, and M. Schlegel, "Operator constraints for twist-3 functions and lorentz invariance properties of twist-3 observables," *Physical Review D: Covering Particles, Fields, Gravitation, And Cosmology*, vol. 93, Article ID 054024, 2016.

[19] D. Gutierrez-Reyes, I. Scimemi, and A. Vladimirov, "Transverse momentum dependent transversely polarized distributions at next-to-next-to-leading-order," *Journal of High Energy Physics*, vol. 2018, no. 172, 2018.

[20] X. P. Chai, K. B. Chen, and J. P. Ma, "A note on Pretzelosity TMD parton distribution," *Physics Letters B*, vol. 789, pp. 360–365, 2018.

[21] M. G. Echevarría, A. Idilbi, A. Schäfer, and I. Scimemi, "Model-independent evolution of transverse momentum dependent distribution functions (TMDs) at NNLL," *The European Physical Journal C*, vol. 73, article 2636, 2013.

[22] I. Scimemi, A. Vladimirov, and Eur., "Analysis of vector boson production within TMD factorization," *The European Physical Journal C*, vol. 78, p. 89, 2018.

[23] I. Scimemi and A. Vladimirov, "Systematic analysis of double-scale evolution," *Journal of High Energy Physics*, vol. 2018, p. 3, 2018.

[24] M. G. Echevarria, I. Scimemi, and A. Vladimirov, "Erratum: transverse momentum dependent fragmentation function at next-to–next-to–leading order," *Physical Review D: Particles, Fields, Gravitation and Cosmology*, vol. 94, no. 9, 2016.

[25] J. Collins, *Foundations of Perturbative QCD*, Cambridge University Press, 2013.

[26] S. M. Aybat and T. C. Rogers, "Transverse momentum dependent parton distribution and fragmentation functions with QCD evolution," *Physical Review D: Particles, Fields, Gravitation and Cosmology*, vol. 83, no. 11, Article ID 114042, 2011.

[27] T. Becher and M. Neubert, "Drell-Yan production at small q_T, transverse parton distributions and the collinear anomaly," *The European Physical Journal C*, vol. 71, p. 1665, 2011.

[28] T. Becher, M. Neubert, and D. Wilhelm, "Electroweak gauge-boson production at small q_T: Infrared safety from the collinear anomaly," *Journal of High Energy Physics*, vol. 2012, p. 124, 2012.

[29] J.-Y. Chiu, A. Jain, D. Neill, and I. Z. Rothstein, "A formalism for the systematic treatment of rapidity logarithms in Quantum Field Theory," *Journal of High Energy Physics*, vol. 2012, p. 84, 2012.

[30] M. G. Echevarría, A. Idilbi, A. Schäfer, and I. Scimemi, "Soft and collinear factorization and transverse momentum dependent parton distribution functions," *The European Physical Journal C*, vol. 726, pp. 795–801, 2013.

[31] G. Aad et al., "Measurement of the transverse momentum and ϕ_η^* distributions of Drell-Yan lepton pairs in proton-proton collisions at $\sqrt{s}$=8 TeV with the ATLAS detector," *The European Physical Journal C*, vol. 76, p. 291, 2016.

[32] G. Parisi and R. Petronzio, "Small transverse momentum distributions in hard processes," *Nuclear Physics B*, vol. 154, no. 3, pp. 427–440, 1979.

[33] J. C. Collins and D. E. Soper, "Back-to-back jets: Fourier transform from b to k_T," *Nuclear Physics B*, vol. 197, p. 446, 1982.

[34] J. C. Collins, D. E. Soper, G. F. Sterman, and B. Nucl. Phys, "Transverse momentum distribution in Drell-Yan pair and W and Z boson production," *Nuclear Physics B*, vol. 250, pp. 199–244, 1985.

[35] X. D. Ji, J. Ma, and F. Yuan, "QCD factorization for semi-inclusive deep-inelastic scattering at low transverse momentum," *Physical Review D: Particles, Fields, Gravitation and Cosmology*, vol. 71, no. 3, Article ID 034005, 2005.

[36] M. G. Echevarria, A. Idilbi, and I. Scimemi, "Factorization theorem for Drell-Yan at low q_T and transverse-momentum distributions on-the-light-cone," *Journal of High Energy Physics*, vol. 2012, no. 2, 2012.

[37] M. F. Ghajari, M. V. Golpayegani, M. Bargrizan, G. Ansari, and S. Shayeghi, "Non-perturbative QCD effects in q_T spectra of Drell-Yan and Z-boson production," *Journal of High Energy Physics*, vol. 11, p. 98, 2014.

[38] A. Bacchetta, "Electron-ion collider: the next QCD frontier," *The European Physical Journal A*, vol. 2016, p. 163, 2016.

[39] A. Idilbi and I. Scimemi, "Singular and regular gauges in soft–collinear effective theory: The introduction of the new Wilson line T," *Physics Letters B*, vol. 695, p. 463, 2011.

[40] A. Idilbi and I. Scimemi, "The T-Wilson Line," in *Proceedings of the Publisher Logo Conference*, vol. 1343, p. 320, 2011.

[41] M. García-Echevarría, A. Idilbi, and I. Scimemi, "Soft-collinear effective theory, light-cone gauge, and the T-Wilson lines," *Physical review D*, vol. 84, no. 1, Article ID 011502, 2011.

[42] A. Vladimirov and JHEP., "Soft factors for double parton scattering at NNLO," *Journal of High Energy Physics*, vol. 2016, p. 38, 2016.

[43] A. Vladimirov, "Structure of rapidity divergences in soft factors," *High Energy Physics - Phenomenology*, vol. 4, no. 045, 2018.

[44] M. G. Echevarria, A. Idilbi, and I. Scimemi, "On rapidity divergences in the soft and collinear limits of QCD," *International Journal of Modern Physics: Conference Series*, vol. 25, Article ID 1460005, 2014.

[45] M. G. Echevarria, I. Scimemi, and A. Vladimirov, "Universal transverse momentum dependent soft function at NNLO," *Physical Review D: Particles, Fields, Gravitation and Cosmology*, vol. 93, Article ID 054004, 2016.

[46] P. Hagler, B. U. Musch, J. W. Negele, and A. Schafer, "Intrinsic quark transverse momentum in the nucleon from lattice QCD," *High Energy Physics - Lattice*, vol. 88, no. 6, Article ID 61001, 2009.

[47] B. U. Musch, P. Hägler, J. W. Negele, and A. Schäfer, "Exploring quark transverse momentum distributions with lattice QCD," *Physical Review D: Particles, Fields, Gravitation and Cosmology*, vol. 83, no. 9, Article ID 094507, 2011.

[48] B. U. Musch, P. Hägler, M. Engelhardt, J. W. Negele, and A. Schäfer, "Sivers and Boer-Mulders observables from lattice QCD," *Physical Review D: Particles, Fields, Gravitation and Cosmology*, vol. 85, Article ID 094510, 2012.

[49] X. Ji, "Parton Physics on a Euclidean Lattice," *Physical Review Letters*, vol. 110, Article ID 262002, 2013.

[50] X. Ji, "Parton physics from large-momentum effective field theory," *Science China Physics, Mechanics & Astronomy*, vol. 57, p. 1407, 2014.

[51] M. Engelhardt, P. Haegler, B. Musch, J. Negele, and A. Schfer, "Lattice QCD study of the Boer-Mulders effect in a pion," *Physical Review D*, vol. 93, Article ID 054501, 2016.

[52] B. Yoon, T. Bhattacharya, M. Engelhardt et al., "Lattice QCD calculations of nucleon transverse momentum-dependent parton distributions using clover and domain wall fermions," in *Proceedings of the 33rd International Symposium on Lattice Field Theory (LATTICE2015)*, pp. 14–18, SISSA, Kobe, Japan, 2015.

[53] B. Yoon, M. Engelhardt, R. Gupta et al., "Lattice QCD calculations of nucleon transverse momentum-dependent parton distributions using clover and domain wall fermions," *High Energy Physics - Lattice*, vol. 96, Article ID 094508, 2017.

[54] A. V. Radyushkin, "Quasi-parton distribution functions, momentum distributions, and pseudo-parton distribution functions," *Physical Review D: Particles, Fields, Gravitation and Cosmology*, vol. 96, Article ID 034025, 2017.

[55] K. Orginos, A. Radyushkin, J. Karpie, and S. Zafeiropoulos, "Lattice QCD exploration of parton pseudo-distribution functions," *Physical Review D: Particles, Fields, Gravitation and Cosmology*, vol. 96, no. 9, Article ID 094503, 2017.

[56] X. Ji, L.-C. Jin, F. Yuan, J.-H. Zhang, and Y. Zhao, "Transverse momentum dependent quasi-parton-distributions," *High Energy Physics - Phenomenology*, 2018.

[57] A. V. Manohar and I. W. Stewart, "The zero-bin and mode factorization in quantum field theory," *High Energy Physics - Phenomenology*, vol. 76, Article ID 074002, 2007.

[58] M. A. Ebert, I. W. Stewart, and Y. Zhao, "Determining the nonperturbative Collins-Soper kernel from lattice QCD," *Physical Review D: covering particles, fields, gravitation, and cosmology*, vol. 99, Article ID 034505, 2018.

[59] I. Scimemi and A. Vladimirov, "Power corrections and renormalons in transverse momentum distributions," *Journal of High Energy Physics*, vol. 2017, no. 2, 2017.

[60] T. Luebbert, J. Oredsson, and M. Stahlhofen, "Rapidity renormalized TMD soft and beam functions at two loops," *High Energy Physics - Phenomenology*, vol. 2016, no. 3, p. 168, 2016.

[61] J.-y. Chiu, A. Jain, D. Neill, and I. Z. Rothstein, "The rapidity renormalization group," *Physical Review Letters*, vol. 108, Article ID 151601, 2012.

[62] T. Gehrmann, T. Luebbert, and L. L. Yang, "Transverse parton distribution functions at next-to-next-to-leading order: the quark-to-quark case," *Physical Review Letters*, vol. 109, Article ID 242003, 2012.

[63] M. G. Echevarria, A. Idilbi, and I. Scimemi, "Unified treatment of the QCD evolution of all (un-)polarized transverse momentum dependent functions: Collins function as a study case," *Physical Review D: Particles, Fields, Gravitation and Cosmology*, vol. 90, no. 1, Article ID 014003, 2014.

[64] J. C. Collins and A. Metz, "Universality of soft and collinear factors in hard-scattering factorization," *Physical Review Letters*, vol. 93, no. 25, Article ID 252001, 2004.

[65] J. R. Gaunt, "Glauber gluons and multiple parton interactions," *Journal of High Energy Physics*, vol. 2014, p. 110, 2014.

[66] M. Diehl, J. R. Gaunt, D. Ostermeier, P. Pll, and A. Schfer, "Cancellation of Glauber gluon exchange in the double Drell-Yan process," *Journal of High Energy Physics*, vol. 2016, p. 076, 2016.

[67] D. Boer, T. van Daal, J. R. Gaunt, T. Kasemets, and P. J. Mulders, "Colour unwound - disentangling colours for azimuthal asymmetries in Drell-Yan scattering," *High Energy Physics - Phenomenology*, vol. 3, p. 040, 2017.

[68] S. D. Drell and T.-M. Yan, "Massive lepton-pair production in hadron-hadron collisions at high energies," *Physical Review Letters*, vol. 25, p. 316, 1970.

[69] G. Altarelli, R. Ellis, and G. Martinelli, "Leptoproduction and drell-yan processes beyond the leading approximation in chromodynamics," *Nuclear Physics B*, vol. 143, no. 3, pp. 521–545, 1978.

[70] R. D. Tangerman and P. J. Mulders, "Intrinsic transverse momentum and the polarized Drell-Yan process," *Physical Review D: Particles, Fields, Gravitation and Cosmology*, vol. 51, no. 7, pp. 3357–3372, 1995.

[71] G. Kramer and B. Lampe, "Two Jet Cross-Section in e+ e-Annihilation," *Zeitschrift für Physik C Particles and Fields*, vol. 34, no. 4, pp. 497–522, 1989.

[72] T. Matsuura, S. C. van der Marck, and W. L. van Neerven, "The calculation of the second order soft and virtual contributions to the Drell-Yan cross section," *Nuclear Physics B*, vol. 319, no. 3, pp. 570–622, 1989.

[73] A. Idilbi, X.-d. Ji, and F. Yuan, "Resummation of threshold logarithms in effective field theory for DIS, Drell–Yan and Higgs production," *Nuclear Physics B*, vol. 753, no. 1-2, Article ID 0605068, pp. 42–68, 2006.

[74] I. Balitsky and A. Tarasov, "Power corrections to TMD factorization for Z-boson production," *High Energy Physics - Phenomenology*, vol. 2018, p. 150, 2018.

[75] M. A. Ebert, I. Moult, I. W. Stewart, F. J. Tackmann, G. Vita, and H. X. Zhu, "Power corrections for N-jettiness subtractions at $\mathcal{O}(\alpha_s)$," *Journal of High Energy Physics*, vol. 84, 2018.

[76] J. Collins, L. Gamberg, A. Prokudin, T. Rogers, N. Sato, and B. Wang, "Relating transverse-momentum-dependent and collinear factorization theorems in a generalized formalism," *Physical Review D: Particles, Fields, Gravitation and Cosmology*, vol. 94, no. 3, Article ID 034014, 2016.

[77] D. Pitonyak, L. Gamberg, A. Metz, and A. Prokudin, "Connections between collinear and transverse-momentum-dependent polarized observables within the Collins-Soper-Sterman formalism," *Physics Letters B*, vol. 781, pp. 443–454, 2018.

[78] C. T. H. Davies, B. R. Webber, and W. J. Stirling, "Nucl. Phys," B256, 413 (1985).

[79] R. K. Ellis and S. Veseli, "W and Z transverse momentum distributions: resummation in q_T-space," *Nuclear Physics B*, vol. 511, p. 649, 1998.

[80] G. P. Korchemsky and G. F. Sterman, "Nonperturbative corrections in resummed cross sections," *Nuclear Physics B*, vol. 437, no. 2, pp. 415–432, 1995.

[81] J. C. Collins and D. E. Soper, "Back-to-back jets in QCD," *Nuclear Physics B*, vol. 193, no. 2, pp. 381–443, 1981.

[82] Y. Li, D. Neill, and H. X. Zhu, "An exponential regulator for rapidity divergences," *Physical Review D: Particles, Fields, Gravitation and Cosmology*, 2016.

[83] A. Bacchetta, F. Delcarro, C. Pisano, M. Radici, and A. Signori, "Extraction of partonic transverse momentum distributions from semi-inclusive deep-inelastic scattering, Drell-Yan and Z-boson production," *Journal of High Energy Physics*, vol. 2017, p. 81, 2017.

[84] T. Becher and G. Bell, "Enhanced Nonperturbative Effects through the Collinear Anomaly," *Physical Review Letters*, vol. 112, no. 18, 2014.

[85] V. Bertone, I. Scimemi, and A. Vladimirov, "Extraction of unpolarized quark transverse momentum dependent parton distributions from Drell-Yan/Z-boson production," *High Energy Physics - Phenomenology*, 2019.

[86] P. M. Nadolsky, D. R. Stump, and C. P. Yuan, "Phenomenology of multiple parton radiation in semi-inclusive deep-inelastic

scattering," *Physical Review D: Covering Particles, Fields, Gravitation, and Cosmology*, vol. 64, Article ID 114011, 2001.

[87] G. Bozzi, S. Catani, G. Ferrera, D. de Florian, and M. Grazzini, "Production of Drell–Yan lepton pairs in hadron collisions: Transverse-momentum resummation at next-to-next-to-leading logarithmic accuracy," *Nuclear Physics B*, vol. 696, no. 207, pp. 207–2013, 2011.

[88] Z.-B. Kang, J.-W. Qiu, X.-N. Wang, and H. Xing, "Next-to-leading order transverse momentum broadening for Drell-Yan production in P + A collisions," *Physical Review D: Covering Particles, Fields, Gravitation, and Cosmology*, vol. 94, Article ID 074038, 2016.

[89] Z.-B. Kang, X. Liu, F. Ringer, H. Xing, and JHEP., "The transverse momentum distribution of hadrons within jets," *Journal of High Energy Physics*, vol. 2017, p. 68, 2017.

[90] Z.-B. Kang, A. Prokudin, F. Ringer, and F. Yuan, "Collins azimuthal asymmetries of hadron production inside jets," *Physics Letters B*, vol. 2017, pp. 635–642, 2017.

[91] D. Gutierrez-Reyes, I. Scimemi, W. J. Waalewijn, and L. Zoppi, "Transverse-momentum-dependent distributions with jets," *Physical Review Letters*, vol. 121, no. 16, 2018.

[92] X. Liu, F. Ringer, W. Vogelsang, and F. Yuan, "Lepton-jet correlations in deep inelastic scattering at the electron-ion collider," *High Energy Physics - Phenomenology*, 2018.

[93] M. G. A. Bu_ng, Z.-B. Kang, K. Lee, and X. Liu, "A transverse momentum dependent framework for back-to-back photon+jet production," *High Energy Physics - Phenomenology*, 2018.

Hindawi
Advances in High Energy Physics
Volume 2019, Article ID 2526897, 11 pages
https://doi.org/10.1155/2019/2526897

Research Article

Nonperturbative Uncertainties on the Transverse Momentum Distribution of Electroweak Bosons and on the Determination of the W Boson Mass at the LHC

Giuseppe Bozzi [1,2] **and Andrea Signori** [3]

[1] *Dipartimento di Fisica, Università di Pavia, Via Bassi 6, I-27100 Pavia, Italy*
[2] *INFN, Sezione di Pavia, Via Bassi 6, I-27100 Pavia, Italy*
[3] *Physics Division, Argonne National Laboratory, 9700 S. Cass Avenue, Lemont, IL 60439, USA*

Correspondence should be addressed to Andrea Signori; asignori@anl.gov

Received 10 December 2018; Accepted 14 February 2019; Published 17 March 2019

Guest Editor: Daniel Pitonyak

In this contribution we present an overview of recent results concerning the impact of a possible flavour dependence of the intrinsic quark transverse momentum on electroweak observables. In particular, we focus on the q_T spectrum of electroweak gauge bosons produced in proton-proton collisions at the LHC and on the direct determination of the W boson mass. We show that these effects are comparable in size to other nonperturbative effects commonly included in phenomenological analyses and should thus be included in precise theoretical predictions for present and future hadron colliders.

1. Introduction

Electroweak precision observables are interesting benchmarks to test the limits of the Standard Model and to discriminate between different scenarios for new physics. The mass of the W boson, m_W, is an example of such an observable.

The Standard Model prediction for the W boson mass from the global fit of the electroweak parameters ($m_W = 80.356 \pm 0.008$ GeV) [1] has a very small uncertainty that represents a natural target for the precision of the experimental measurements of m_W at hadron colliders.

Direct measurements of m_W at hadronic colliders have been performed at the Tevatron $p\overline{p}$ collider with the D0 [2] and CDF [3] experiments and at the LHC pp collider with the ATLAS [4] experiment, with a total uncertainty of 23 MeV, 19 MeV, and 19 MeV, respectively. The current world average, based on these measurements and the ones performed at LEP, is $m_W = 80.379 \pm 0.012$ GeV [5]. Figure 1 presents an overview of these measurements compared to the electroweak global fit. The CPT theorem [6, 7] implies that the mass and lifetime of a particle and its antiparticle are the same. The ATLAS measurement of the W^+ and W^- mass difference yields $m_{W^+} - m_{W^-} = -29 \pm 28$ MeV [4]. The experimental determinations are based on a template-fit procedure applied to differential distributions of the W decay products: in particular, the transverse momentum of the final lepton, p_T^ℓ, the transverse momentum of the neutrino p_T^ν (only at the Tevatron), and the transverse mass m_T of the lepton pair (where $m_T = \sqrt{2p_T^\ell p_T^\nu \ (1 - \cos(\phi_\ell - \phi_\nu))}$, with $\phi_{\ell,\nu}$ being the azimuthal angles of the lepton and the neutrino, respectively). The transverse momentum of the lepton pair, though not directly used in the template-fit procedure, is relevant for reweighing purposes (see, for instance, Sec. 6 of Ref. [4]).

At leading order the W boson is produced with zero transverse momentum (q_T^W), but perturbative and nonperturbative corrections give rise to nonvanishing values of q_T^W. While perturbative and flavour-independent nonperturbative corrections have received much attention and reached a high level of accuracy (see, for instance, Ref. [8, 9] and references therein), a possible flavour dependence of the intrinsic

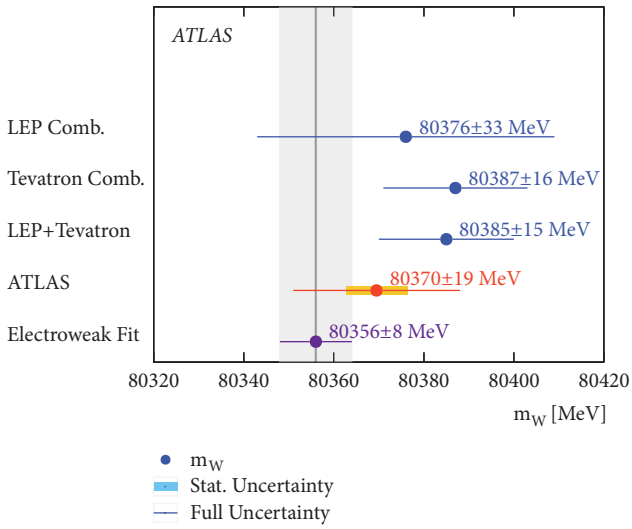

FIGURE 1: Overview of the measurements of the W boson mass. The indirect determination via the electroweak fit sets the precision for the measurements via direct determinations. Figure from Ref. [4].

transverse momentum (k_T) of the initial state partons has been less investigated.

In Figure 2, we examine the decomposition in flavour channels of the cross section for Z and $W^{\pm}$ production differential with respect to q_T^V, $V = Z, W^{\pm}$. A nontrivial interplay among the different flavours and the gluon is observed. The role of the gluon becomes increasingly important at larger values of the transverse momentum. In the region of the peak, instead, the dominant channels involve combinations of u_{val}, d_{val}, $\overline{u}$, and $\overline{d}$ (where $a = a_{val} + a_{sea}$ and $\overline{a} = a_{sea}$). For this reason, we consider it important to study the impact of flavour-dependent effects on the production of electroweak bosons and on the determination of m_W.

In this contribution we give an overview of selected studies related to flavour-dependent effects, focusing in particular on the results obtained in [10, 11], showing that they can be nonnegligible compared to other sources of theoretical uncertainty and should thus be included in precision physics programs at hadron colliders.

2. Formalism

In processes with a hard scale Q and a measured transverse momentum q_T, for instance, the mass and the transverse momentum of an electroweak boson produced in hadronic collisions, we can distinguish three regions: a small q_T region ($q_T \ll Q$), where large logarithms of q_T/Q have to be properly resummed; a large q_T region ($q_T \gtrsim Q$), where fixed-order perturbation theory provides reliable results; and an intermediate region, where a proper matching procedure between all-order resummed and fixed-order contributions is necessary. For a concise discussion (and for additional relevant references) on the development of the different frameworks available to resum the logs of q_T/Q and on their matching to fixed-order perturbative calculations, we refer the reader to [18–25].

In the Transverse-Momentum-Dependent (TMD) factorisation framework [26], the unpolarized TMD Parton Distribution Function (TMD PDF) for a parton with flavour a, carrying a fraction x of longitudinal momentum at a certain scale Q^2, can be written in b_T-space (where b_T is the variable Fourier-conjugated to the partonic transverse momentum k_T) as

$$\tilde{f}_1^a\left(x, b_T; Q^2\right) = \sum_{i=q,\overline{q},g} \left(C_{a/i} \otimes f_1^i\right)\left(x, b_T, \mu_b^2\right) \cdot e^{S\left(\mu_b^2, Q^2\right)} e^{g_K\left(b_T, \boldsymbol{\lambda}\right) \ln\left(Q^2/Q_0^2\right)} \tilde{f}_{\mathrm{NP}}^a\left(b_T, \boldsymbol{\lambda}'\right), \tag{1}$$

where μ_b is the b_T-dependent scale at which the collinear parton distribution functions are computed and Q_0 is a hadronic mass scale. Equation (1) is a generic schematic implementation of the perturbative and nonperturbative components of a renormalized TMD PDF. Depending on the chosen perturbative accuracy, S includes the UV-anomalous dimension of the TMD PDF and the Collins-Soper kernel. Also, in principle the TMD PDF depends on two kinds of renormalization scales, related to the renormalization of UV and light-cone divergences. Here we specify their initial and final values as μ_b and Q, respectively. Moreover, the perturbative scales can be chosen in position or momentum space [12, 14, 27–30]. For the implementation of all these details, we refer the reader to the description of the public codes that we are going to discuss.

The C coefficients in (1), also called Wilson coefficients for the TMD distribution, are calculable in perturbation theory and are presently known at order α_s^2 in the unpolarized case [21, 31, 32]. They are convoluted with the corresponding collinear parton distribution functions f_1^i according to

$$\left(C_{a/i} \otimes f_1^i\right)\left(x, b_T, \mu_b^2\right) = \int_x^1 \frac{du}{u} C_{a/i}\left(\frac{x}{u}, b_T, \alpha_s\left(\mu_b^2\right)\right) f_1^i\left(u; \mu_b^2\right), \tag{2}$$

The perturbative part of the evolution, the S factor in (1), can be written as

$$S\left(\mu_b^2, Q^2\right) = \int_{\mu_b^2}^{Q^2} \frac{d\mu^2}{\mu^2} \gamma_F\left[\alpha_s\left(\mu^2\right), \frac{Q^2}{\mu^2}\right] - K\left(b_T; \mu_b^2\right) \log \frac{Q^2}{\mu_b^2}. \tag{3}$$

It involves, in principle, the UV-anomalous dimension γ_F and the Collins-Soper kernel K, which can be decomposed as

$$\gamma_F\left[\alpha_s\left(\mu^2\right), \frac{Q^2}{\mu^2}\right] = -\left[\sum_{k=1}^{\infty} A_k \left(\frac{\alpha_s\left(\mu^2\right)}{4\pi}\right)^k\right] \ln\left(\frac{Q^2}{\mu^2}\right) + \sum_{k=1}^{\infty} B_k \left(\frac{\alpha_s\left(\mu^2\right)}{4\pi}\right)^k,$$

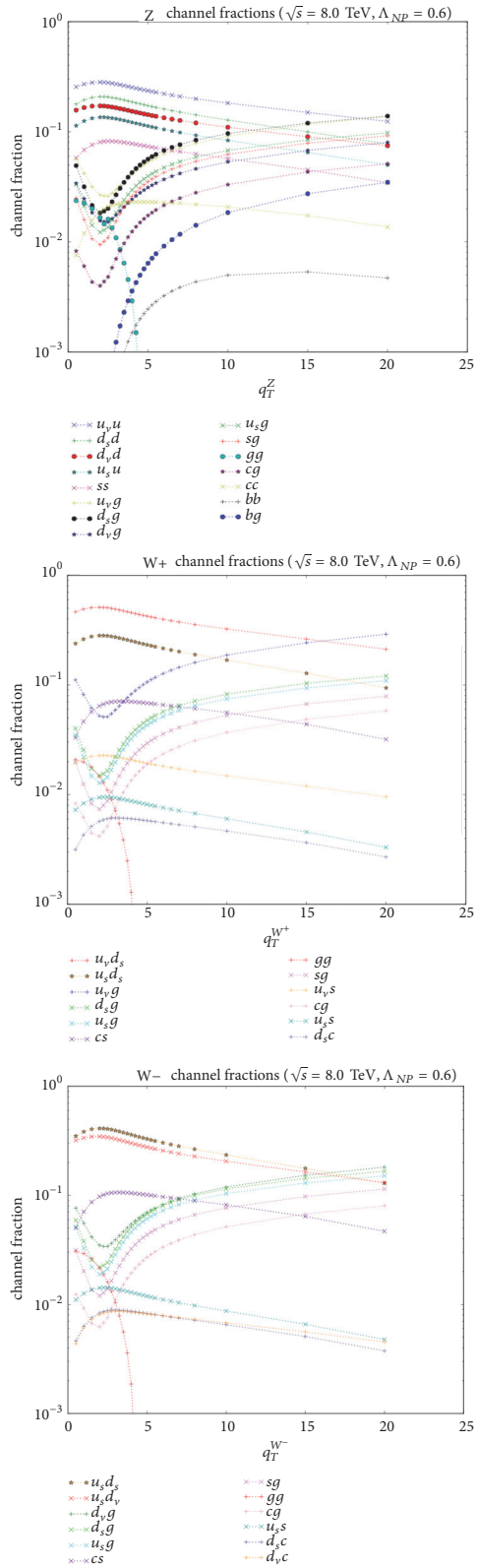

FIGURE 2: From top to bottom: the decomposition in flavour channels of the cross section $d\sigma/dq_T$ for Z, W^+, W^- production differential with respect to the transverse momentum of the produced electroweak boson q_T^V, $V = Z, W^+, W^-$. The rapidity and the collinear momentum fractions have been integrated over the kinematically allowed ranges. The cross section is calculated by means of `CuTe` [12] at LHC $\sqrt{s} = 8$ TeV. The nonperturbative correction is implemented as a flavour-independent Gaussian smearing, governed by the parameter Λ_{NP} (see [12] and the Appendix). The channels add to one.

$$K\left(b_T, \mu_b^2\right) = \sum_{k=1}^{\infty} d_k \left(\frac{\alpha_s\left(\mu^2\right)}{4\pi}\right)^k. \tag{4}$$

The A_k and B_k coefficients are known up to NNNLL (at least, their numerical value) and the integration of the Sudakov exponent in (4) can be done analytically up to NNNLL (for the complete expressions see, e.g., [33–35]). The perturbative coefficients of the kernel K are also known analytically up to NNNLL.

A well-known problem in the implementation of the QCD evolution of transverse-momentum-dependent distributions (TMDs) is the divergent behaviour at large b_T caused by the QCD Landau pole. Two common prescriptions to deal with this divergence consist in replacing b_T with a variable that saturates at a certain $b_{T\max}$, as suggested by the CSS formalism [26, 36], or perform the b_T integration on the complex plane in such a way that the Landau pole is never reached [37]. On the other hand, also the small b_T region needs to be regularized, in order to eliminate unjustified contributions from the evolution of TMDs in the intermediate and large q_T regions and to recover the expression for the cross section in collinear factorisation upon integration over q_T. Several prescriptions exist [14, 20, 33, 38, 39] also in this case. In `CuTe` the cross section is calculated integrating b_T on the real axis and the initial value for the renormalization scale is $\mu_b \equiv \mu_c \doteq q_T + q_\star$, where the scale $q_\star$ screens the cross section from receiving long-distance contributions. The definition of $q_\star$ is given analytically in (3.2) in [12] and its numerical value is $\sim$ 1.88 GeV. Also in `DyRes` the cross section is calculated integrating b_T on the real axis. The initial scale is defined as $\mu_b = 2e^{-\gamma_E}/b_\star$ [28] and a freezing prescription is given for $b_\star$ in order to avoid the Landau pole; see (2.18) in [28]. The value of the cutoff parameter $b_{T\max}$ in b_T space is a function of the renormalization scale μ_R and the resummation scale Q: $b_{max}\ Q \sim 1.2 \cdot 10^3\ \mu_R/m_Z$. In our case, $\mu_R = Q = m_W$. In `DyqT`, instead, the integration over b_T is performed using the complex-b prescription [37]; thus no freezing parameter is needed and μ_b is just defined as $2e^{-\gamma_E}/b_T$ [27].

Two intrinsically nonperturbative factors are introduced in (1) in order to account for the large b_T behavior. The first one is named $g_K(b_T; \boldsymbol{\lambda})$ in the TMD/CSS literature [26]. It embodies the nonperturbative part of the evolution, which is flavour-independent. The second one, $\widetilde{f}^a_{\mathrm{NP}}(b_T; \boldsymbol{\lambda}')$, accounts for a flavour-(in)dependent intrinsic transverse momentum of the parton with flavour a. We note that, in principle, this contribution can be also x-dependent (see, e.g., [15]), but in this treatment we choose to neglect this feature. The $\boldsymbol{\lambda}$ and $\boldsymbol{\lambda}'$ are (vectors of) nonperturbative parameters that can be fit to data. The $\boldsymbol{\lambda}'$ parameters are related to the quantity $\langle \boldsymbol{k}_T^2 \rangle_a$. For example, in case of a simple Gaussian functional form, $e^{-\lambda' b_T^2}$, we have $\lambda' = \langle \boldsymbol{k}_\star^2 \rangle_a / 4$. For both the nonperturbative factors g_K and $\widetilde{f}^a_{\mathrm{NP}}$, several implementations have been discussed; see, e.g., [14, 23] and references therein. In particular, a kinematic- and flavour-dependent Gaussian parametrisation has been proposed in [15, 29].

The studies that we discuss make use of three different computational tools: `CuTe` [12], `DyqT` [27], and `DYRes` [28]. `CuTe` is based on resummed expressions calculated using soft-collinear effective theory (SCET). It gives the transverse momentum spectrum of on-shell electroweak bosons up to NLO ($\mathcal{O}(\alpha_s)$) accuracy in the C Wilson coefficients and up to NNLL in the Sudakov exponent (`CuTe` is labelled NNLL in the SCET language but NNLL$'$ in standard pQCD language. The accuracy of NNLL$'$ is considered lower than that of the full NNLL, in which Wilson coefficients are computed at NNLO).

`DyqT` and `DYRes` are based on [27, 28] and perform soft gluon resummation in b_T-space. The first computes the q_T spectrum of an electroweak boson produced in hadronic collisions. The second also provides the full kinematics of the vector boson and of its decay products, allowing for the application of arbitrary cuts on the final-state kinematical variables and giving differential distributions in form of bin histograms. The accuracy of both codes is up to NNLL in the resummed part and up to NLO ($\mathcal{O}(\alpha_s^2)$) at large q_T.

A simple Gaussian parametrisation of the nonperturbative effects is present in these codes, as in most of the computational tools used to analyse the electroweak observables relevant for the determination of the W boson mass. A single nonperturbative parameter, g_{NP}, usually encodes both the (flavour-independent) effect of g_K and the distribution in the (potentially flavour-dependent) intrinsic transverse momentum (`ResBos` [40] is a counter-example, but it does not account for the flavour dependence of the intrinsic transverse momentum):

$$e^{-g_{NP} b_T^2} \equiv e^{2 g_K(b_T;\boldsymbol{\lambda}) \ln(Q^2/Q_0^2)}\, \widetilde{f}^a_{\mathrm{NP}}\left(b_T; \boldsymbol{\lambda}'\right) \widetilde{f}^{a'}_{\mathrm{NP}}\left(b_T; \boldsymbol{\lambda}'\right). \tag{5}$$

The values of the nonperturbative parameters used in fitting the W boson mass are usually obtained through fits on Z production data [40], for which the relevant partonic channels are of the type $q_i \overline{q}_i$, and then used to predict $W^\pm$ production, despite the process being sensitive to different partonic channels, $q_i \overline{q_j}$ ($i \neq j$). This procedure essentially neglects any possible flavour dependence of the intrinsic partonic transverse momentum.

In order to introduce the flavour dependence, one can simply decompose g_{NP} in the LHS of (5) into the sum $g^a_{NP} + g^{a'}_{NP}$, where the flavour indices span the range $a, a' = u_v, u_s, d_v, d_s, s, c, b, g$ (the subscripts referring to the valence and sea components, respectively), additionally disentangling the nonperturbative contribution to the evolution and the intrinsic transverse momentum distribution. Thus, for each parton with flavour a, the nonperturbative contributions $\widetilde{f}^a_{\mathrm{NP}}$ and g_K in (1) and (5) are included in the corresponding term in the flavour sum of the TMD factorisation formula. More details regarding the nonperturbative parameters in the codes under consideration have been collected in the Appendix.

3. Effects on the q_T Spectrum of the W

The impact of a flavour-dependent intrinsic $\langle \boldsymbol{k}_T^2 \rangle$ on the q_T spectrum of the electroweak bosons has been first studied in

Table 1: Summary of the shifts in GeV induced on the peak position in q_T spectra of $W^{\pm}/Z$, generated by different effects. "f.i." stands for flavour-independent, whereas "f.d." for flavour-dependent. "Max $W^{\pm}$" effect indicates the maximum shift induced on the peak position of the $W^{\pm}$ q_T spectrum by flavour-dependent variations of $\langle \boldsymbol{k}_T^2 \rangle$ that keep the peak of the Z q_T spectrum unchanged. For the values of the flavour-dependent non-perturbative parameters we refer the reader to [10].

	W^+		W^-		Z	
$\mu_R = \mu_c/2, 2\mu_c$	+0.30	−0.09	+0.29	−0.06	+0.23	−0.05
pdf (68% cl)	+0.03	+0.03	+0.04	+0.00	+0.03	−0.02
pdf (90% cl)	+0.03	−0.05	+0.06	−0.02	+0.05	−0.02
$\alpha_s = 0.118 \pm 0.003$	+0.14	−0.12	+0.14	−0.14	+0.15	−0.15
f.i. $\langle \boldsymbol{k}_T^2 \rangle = 1.0, 1.96$	+0.16	−0.16	+0.16	−0.14	+0.16	−0.15
f.d. $\langle \boldsymbol{k}_T^2 \rangle$ (max W^+ effect)	+0.09			−0.06	±0	
f.d. $\langle \boldsymbol{k}_T^2 \rangle$ (max W^- effect)		−0.03	+0.05		±0	

[10] and here we partly summarize the findings therein. Part of the analysis is devoted to the shifts induced in the position of the peak for the distribution in q_T^V, $V = W^+, W^-$ and Z. Flavour-independent (f.i.) and flavour-dependent (f.d.) variations of the average intrinsic transverse momentum squared are considered, together with the uncertainties associated to other nonperturbative factors, such as the collinear PDFs, the renormalisation scale, and the value of the strong coupling constant. As justified in Section 1 and Figure 2, it is assumed that the intrinsic transverse-momentum depends on five flavours only: u_v, d_v, u_s, d_s, s, where s collectively refers to the strange, charm, and bottom quarks and to the gluon.

The numerical results are obtained by means of a modified (i.e., flavour-dependent) version of `CuTe` [12]. Namely, the nonperturbative parameter $2\Lambda_{NP}^2$ (see the Appendix), which corrects the whole cross section at large b_T, is split into a sum of two flavour-dependent nonperturbative contributions, $\Lambda_{i,j}$, such that $\Lambda_i^2 + \Lambda_j^2 = 2\Lambda_{NP}^2$. This decomposition reabsorbs the nonperturbative contribution to QCD radiation into $\Lambda_{i,j}$. The flavour dependence of $\Lambda_{i,j}$ is compatible with the ratios fitted in [15]. The goal is to combine flavour dependent parameters in such a way to respect the values of Λ_{NP} fitted on the Z data, generating at the same time different values $\Lambda_{i,j}$ to be used in the calculation of the differential cross section for $W^{\pm}$ (we refer the reader to [10] for the precise values of $\Lambda_{i,j}$ used in the study).

The shifts (quantified in GeV) induced by different perturbative and nonperturbative contributions are summarized in Table 1. The renormalisation scale is varied between $1/2\mu_c$ and $2\mu_c$, with $\mu_c = q_T + q^*$, where q^* is the cutoff introduced in the Cute to avoid the Landau pole [12]. The scale in the hard part has not been varied. Regarding the impact of the collinear PDFs, the result shown in the table is the smallest interval which contains 68% or 90% of peak positions, computed for every member of the NNPDF3.0 set [41]. The strong coupling is varied by ±0.003 from the central value of 0.118.

The shift induced in the peak position from flavour-dependent $\langle \boldsymbol{k}_T^2 \rangle$ is smaller than that induced by scale variation, α_s variation, and flavour-independent $\langle \boldsymbol{k}_T^2 \rangle$, but comparable in magnitude. It is also bigger than the uncertainty from the PDF set, which is the only other uncertainty where the shifts are not almost perfectly correlated between the three vector bosons. With flavour-dependent variations of $\langle \boldsymbol{k}_T^2 \rangle$, the peaks of the W^+ and W^- distributions shift in different directions. Since the $\langle \boldsymbol{k}_T^2 \rangle$ parameters are selected under the constraint that the Z q_T-distribution is left unchanged (see Table 1), the channels for W^+ and W^- move in different directions. The anticorrelation of the shifts between W^+ and W^- is a peculiarity of the uncertainty generated by flavour-dependent variations of the intrinsic k_T. This means that the uncertainty stemming from the nonperturbative hadron structure in the transverse plane can affect the determination of m_{W^+} and m_{W^-} in different ways. Indeed, this feature nicely emerges in the analysis summarized in Section 4.

The analysis in [10] thus shows that the uncertainty on the peak position for $W^{\pm}$ bosons arising from the flavour dependence of the intrinsic transverse momentum is not negligible with respect to the other sources of theoretical uncertainties and comparable in magnitude with the uncertainties due to the collinear PDFs.

We now analyse the ratios of the q_T-differential cross section calculated with a flavour-independent set of nonperturbative parameters in $\widetilde{f}_{\mathrm{NP}}^a(b_T; \boldsymbol{\lambda}')$ over the same cross section calculated with flavour-dependent parameters. The results are presented in Figure 3 for Z, W^+, W^-. The calculation has been performed by means of a flavour-dependent modification of `DyqT`, where the nonperturbative contributions in (1) have been coded as

$$\exp\{-g_{NP}^a\} = \exp\left\{-\left[g_{evo}\ln\left(\frac{Q^2}{Q_0^2}\right) + g_a\right] b_T^2\right\}. \quad (6)$$

The values for g_{evo}, Q_0, g_a are taken from [14] and the flavour-dependence in g_a is inspired to the flavour ratios in [15]. The curves in Figure 3 correspond to 50 sets of flavour-dependent nonperturbative parameters built according to these criteria. The chosen perturbative accuracy is NLL [11, 13] and the collinear PDF set used is NNPDF3.1 [42].

As predicted by the TMD formalism, the effect induced by the non-perturbative corrections is more evident at low q_T. In particular, it is stronger for $q_T < 5$ GeV but sizable up to $q_T = 10$ GeV. The flavour dependence of the intrinsic transverse momentum can modify the shape of $d\sigma/dq_T$ by $\sim 5 - 10\%$ at very low transverse momentum. This observable affects the cross section differential with respect to the kinematics of the final state particles, namely, the distributions in p_T^{ℓ}, p_T^{γ}, m_T,

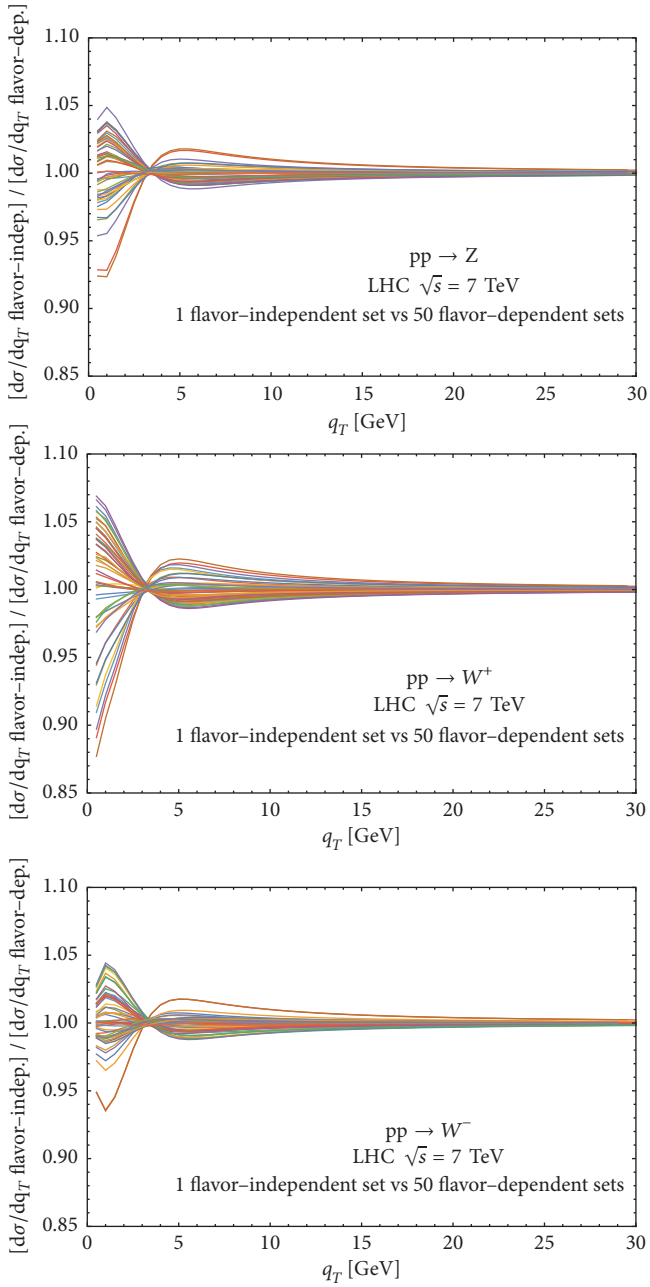

FIGURE 3: In these figures the ratio $(d\sigma^V/dq_T)(f.i.)/(d\sigma^V/dq_T)(f.d.)$ is plotted for the three different electroweak bosons ($V = Z, W^+, W^-$, respectively), with a single set of flavour-independent (f.i.) nonperturbative parameters in the transverse part of the TMD PDFs and 50 different flavour-dependent (f.d.) sets of the same parameters. The analysis has been performed at NLL [11, 13]. The values of the nonperturbative parameters have been chosen from the results in [14, 15].

and thus has an impact also on the determination of the W boson mass.

4. Impact on the Determination of the W Boson Mass

As previously mentioned, the measurements of m_W at hadron colliders rely on a template-fit procedure performed on selected observables, i.e., the distributions in the transverse mass of the lepton pair and the lepton/neutrino transverse momentum. Both CDF and D0 experiments at Tevatron use data from all the three observables. In the ATLAS case, however, the transverse momentum of the (anti)neutrino is used for consistency checks only, since it is affected by larger uncertainties with respect to m_T and p_T^ℓ.

In this section we consider selected results concerning the estimate of the uncertainties of nonperturbative origin on the determination of m_W. In particular, we focus on shifts of the $W^\pm$ mass induced by possible configurations for the flavour dependence of the intrinsic transverse momentum, and we

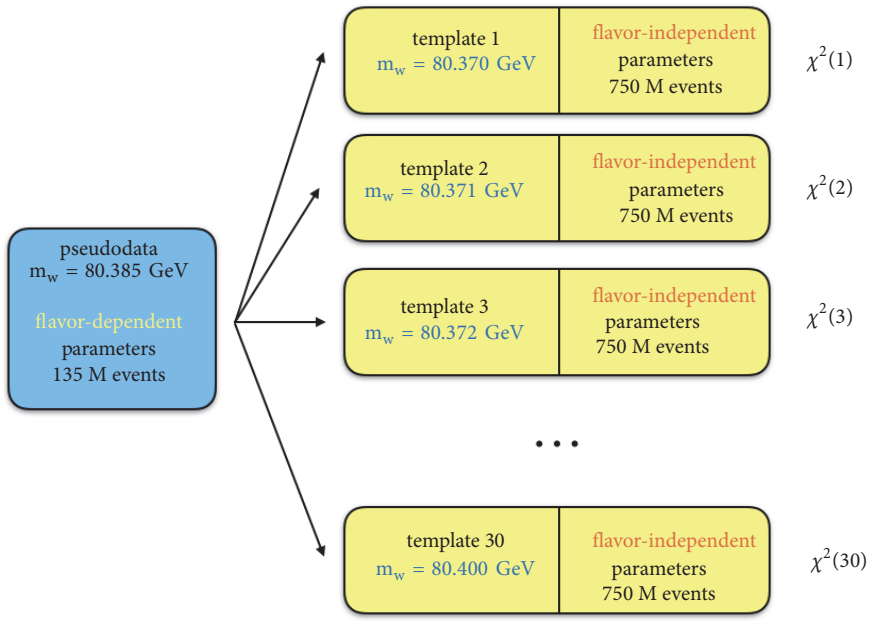

FIGURE 4: Flowchart for a template-fit procedure to estimate shifts in m_W induced by the flavour dependence of the intrinsic quark transverse momentum.

will compare them with the corresponding shifts generated by the uncertainties in the collinear PDFs.

In the template-fit procedure, several histograms are generated with a specific theoretical accuracy and description of detector effects, letting the fit parameter(s) (only m_W, in this case) vary in a range: the histogram best describing the experimental data selects the measured value for m_W. The details of the theoretical calculations used to compute the templates (the choice of the scales, of the collinear PDFs, of the perturbative order, the resummation of logarithmically enhanced contributions, the nonperturbative effects, etc.) affect the result of the fit and define the theoretical systematics.

This procedure can also be used to estimate the effect of each *single* theoretical uncertainty, by generating sets of pseudodata (with the same event generator used for the templates, but at a lower statistics) differing by the value of the parameter(s) controlling that uncertainty [43, 44]. Figure 4 contains a graphical illustration of the flowchart for the template-fit procedure, specified to the comparison of one set of pseudodata generated with flavour-dependent parameters with 30 templates generated with one set of flavour-independent parameters and 30 values of m_W (80385 ± 15 MeV with steps of 1 MeV). This method has been also used to estimate the shift in m_W induced by the variation of the collinear PDF set in fitting the transverse mass [16, 45] and the lepton p_T [17, 45] both at Tevatron and at the LHC in the central rapidity region of the produced electroweak boson ($|\eta| < 1.0$ for Tevatron and $|\eta| < 2.5$ for the LHC). A similar study dedicated to LHCb and its forward acceptance $2 < \eta < 4.5$ has been performed in [46].

In the transverse mass case, the total error (envelope) induced by three different PDF sets (CTEQ6.6 [47], MSTW2008 [48], and NNPDF2.1 [49]) is less than 10 MeV both at the Tevatron and at the LHC [16]. The results are shown in the left plot of Figure 5. The analysis has been performed at fixed-order NLO QCD ($\mathcal{O}(\alpha_s)$), thus without all-order resummation, since the m_T-shape is mildly sensitive to soft gluon emission from the initial state. The key factor in reducing the PDF uncertainty is the use of normalised differential distributions in the fitting procedure, in such a way to eliminate normalisation effects which are irrelevant for m_W.

A similar analysis applied to the lepton p_T observable reveals a much larger error due to PDF variations (CT10 [50], MSTW2008CPdeut [48], MMHT2014 [51], NNPDF2.3 [52], and NNPDF3.0 [41]), as shown in the right plot of Figure 5. While the individual sets provide nonpessimistic estimates ($\mathcal{O}(10\,\text{MeV})$), the distance between the best predictions of the various sets ranges between 8 and 15 MeV, and the total envelope ranges between 16 and 32 MeV (depending on the collider, the energy, and the final state) [16]. While soft gluon emission already provides a nonvanishing transverse momentum, additional contributions may come from the intrinsic transverse momentum of the colliding partons. The study of the impact of a possible flavour-dependent intrinsic k_T on the determination of m_W has been first performed in [11], using the same template-fit procedure described above and sketched in Figure 4, performed with modified versions of the `DYqT` [27] and `DYRes` [28] codes. In this case, the pseudodata are built with the Gaussian widths g_a associated with the different flavours in (6).

In order to estimate the impact of the flavour dependence, it is necessary to first identify those sets of flavor-dependent parameters which perform equally well in describing the Z boson q_T-spectrum, despite having potentially a very different flavor structure. This is motivated physically by the fact that the Z boson is produced from a $q_i\overline{q}_i$ pair whereas

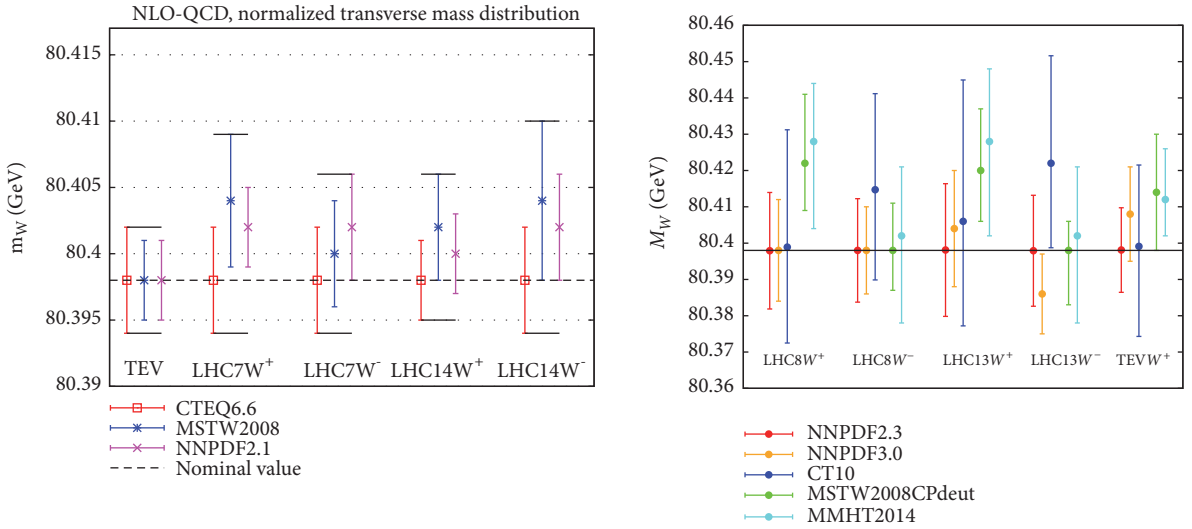

FIGURE 5: Shifts induced on m_W by the choice of different PDF sets, obtained through a template-fit performed on the transverse mass m_T (left) and the lepton p_T (right) observables (left figure from [16], right figure from [17]).

the $W^{\pm}$ bosons are produced from $q_i\overline{q}_j$ pairs, with $i \neq j$. For this reason, the Z is less sensitive to the flavor structure with respect to the $W^{\pm}$, and there might be flavor combinations that perform equally well in describing the q_T-spectrum of the Z but produce very different results when applied to the case of $W^{\pm}$. We identify as "Z-equivalent" those sets of flavor-dependent parameters in agreement with the Z transverse momentum distribution measured at hadron colliders [11]. To this extent

(i) a single flavour-independent (*i.e.*, using a version of Eq. (6) without a-dependence) q_T-spectrum for the Z boson is produced based on the parameters presented in Ref. [14];

(ii) each bin of this flavour-independent spectrum is assigned an uncertainty equal to the one quoted by the CDF and ATLAS experiments, which includes statistical and systematic components, neglecting the correlations;

(iii) several flavour-dependent sets for g_a in Eq. (6) are generated randomly within a variation range consistent with the information obtained in previous TMD fits (in particular, taking into account the estimate for the flavour-independent contribution to the non-perturbative part of the evolution obtained in Ref. [14]);

(iv) a flavour-dependent set is defined "Z-equivalent" if the associated q_T spectrum for the Z has a $\Delta\chi^2 \leq 1$ with respect to one generated by the flavour-independent set.

We note that the Z boson data alone are not able to discriminate between flavor-independent and flavor-dependent sets of nonperturbative parameters. Data from flavor-sensitive processes are needed, in particular from SIDIS.

The flavour-dependent sets for CDF and ATLAS who pass this filter are treated as the pseudodata of the template-fit procedure, while the flavour-independent one is used for the generation of the templates at high statistics. The number of events corresponds to 135M for the pseudodata and 750M for the templates. Only 9 sets out of the 30 ones which are "Z-equivalent" both with respect to CDF and ATLAS uncertainties have been investigated. The values of the flavour-dependent parameters for each set are given in Table 2. A summary of the shifts obtained through this procedure is given in Table 3.

TABLE 2: Values of the g^a_{NP} parameter in (6) for the flavours $a = u_v, d_v, u_s, d_s, s = c = b = g$. Units are GeV^2.

Set	u_v	d_v	u_s	d_s	s
1	0.34	0.26	0.46	0.59	0.32
2	0.34	0.46	0.56	0.32	0.51
3	0.55	0.34	0.33	0.55	0.30
4	0.53	0.49	0.37	0.22	0.52
5	0.42	0.38	0.29	0.57	0.27
6	0.40	0.52	0.46	0.54	0.21
7	0.22	0.21	0.40	0.46	0.49
8	0.53	0.31	0.59	0.54	0.33
9	0.46	0.46	0.58	0.40	0.28

The statistical uncertainty of the template-fit procedure has been estimated by considering statistically equivalent those templates for which $\Delta\chi^2 = \chi^2 - \chi^2_{min} \leq 1$. Overall, the quoted statistical uncertainty on the results in Table 3 is ±2.5 MeV.

Being the transverse mass mildly sensitive to the modeling of the $W^{\pm}$ transverse momentum, the corresponding shifts are compatible with zero considering the statistical uncertainty of the template-fit procedure. On the contrary, in the p_T^{ℓ} case the shifts can be incompatible with statistical fluctuations and are comparable to the ones induced by collinear PDFs, with an envelope of 15 MeV in the case of W^+ production and 11 MeV for W^- production. We also notice a

Table 3: Shifts in $m_{W^\pm}$ (in MeV) induced by the corresponding sets of flavour-dependent intrinsic transverse momenta outlined in Table 2 (statistical uncertainty: 2.5 MeV).

	Δm_{W^+}		Δm_{W^-}	
Set	m_T	p_T^ℓ	m_T	p_T^ℓ
1	0	-1	-2	3
2	0	-6	-2	0
3	-1	9	-2	-4
4	0	0	-2	-4
5	0	4	-1	-3
6	1	0	-1	4
7	2	-1	-1	0
8	0	2	1	7
9	0	4	-1	0

hint of a possible anti-correlation between the shifts in the W^+ and W^- cases, as it was also noticed in Section 3.

Along this line, we also stress that ATLAS measured $m_{W^+} - m_{W^-} = -29 \pm 28$ MeV [4]. From Table 3, we can infer that part of the discrepancy between the mass of the W^+ and the W^- can be artificially induced by not considering the flavour structure in transverse momentum. For example, the sets 1 and 2 in Table 2 feature $\delta m_{W^-} > \delta m_{W^+}$ (induced by p_T^ℓ). This implies that for templates built with sets 1 and 2, instead of flavour-independent values, the difference between the two masses would be reduced. An opposite result would be obtained if building templates with flavour-dependent sets for which $\delta m_{W^-} < \delta m_{W^+}$ (e.g., sets 3 and 5, for the p_T^ℓ case).

5. Outlook and Future Developments

The selected results presented in this contribution point out that the impact of a possible flavour dependence of the intrinsic partonic transverse momentum should not be neglected, even in the kinematic region where nonperturbative effects are expected to be small [53–55], such as for electroweak boson production at the LHC.

This kind of uncertainty directly affects the electroweak observables relevant for the measurement of m_W: the transverse momentum distribution for the W and the decay lepton and the transverse mass distribution of the lepton pair. The numerical results presented in Sections 3 and 4 indicate that flavour-dependent effects are comparable in size to other uncertainties of (non-)perturbative origin (for example, the choice of collinear PDF set). Thus, a flavour-blind analysis is not a sufficiently accurate option for a program of precision electroweak measurements at the LHC and at future colliders.

Moreover, in hadron colliders at a lower energy such as RHIC and a possible fixed-target experiment at the LHC, the non-perturbative effects can play an even more significant role (due to the larger x-values probed) and affect the study of polarised TMDs [56] and the structure of the light sea quarks [57].

A detailed knowledge of TMD distributions is thus important, not only for nucleon tomography beyond the collinear picture [58–66], but also to constrain fundamental parameters of the Standard Model, thus providing a direct connection between hadron physics and the high-energy phenomenology.

In light of these results, we call for improved investigations of the impact of nonperturbative effects linked to the hadron structure at hadron colliders and for the inclusion of these effects in the event generators employed in experimental and theoretical investigations of high-energy physics.

Appendix

Conventions for Nonperturbative Parameters

For convenience, we collect in this Appendix the naive translation of the nonperturbative parameters used in the numerical codes cited in the text. In the conventions of [15, 29], the nonperturbative parameters appear as

$$\mathrm{d}\sigma \propto \exp\left(-\frac{1}{4}\left(\left\langle k_T^2\right\rangle_{q_1} + \left\langle k_T^2\right\rangle_{q_2}\right) b_T^2\right). \tag{A.1}$$

In CuTe [12] there is a single nonperturbative parameter entering the cross section:

$$\mathrm{d}\sigma \propto \exp\left(-2\Lambda_{NP}^2 b_T^2\right). \tag{A.2}$$

The same happens in DyqT [27] and DYRes [28], in terms of the nonperturbative parameter g_{NP}:

$$\mathrm{d}\sigma \propto \exp\left(-g_{NP} b_T^2\right). \tag{A.3}$$

We obtain the parameter employed in CuTe as

$$\begin{aligned} \Lambda_{NP} &= \sqrt{\frac{1}{8}\left(\left\langle k_T^2\right\rangle_{q_1} + \left\langle k_T^2\right\rangle_{q_2}\right)}, \\ \Lambda_{NP} &= \sqrt{\frac{g_{NP}}{2}}. \end{aligned} \tag{A.4}$$

and similarly for the DYqT parameter:

$$\begin{aligned} g_{NP} &= \frac{1}{4}\left(\left\langle k_T^2\right\rangle_{q_1} + \left\langle k_T^2\right\rangle_{q_2}\right), \\ g_{NP} &= 2\Lambda_{NP}^2. \end{aligned} \tag{A.5}$$

The default value for Λ_{NP} discussed in [12] is $0.60\,\mathrm{GeV}^2$, whereas the conservative value for g_{NP} discussed in [27] is $0.8\,\mathrm{GeV}^2$ and in [28] is $1.2\,\mathrm{GeV}^2$.

Data Availability

The data used to support the findings presented in this study (authors: G. Bozzi, A. Signori) have been produced by means of the following public codes: (1) CuTe: https://cute.hepforge.org/ (2) DyqT: http://pcteserver.mi.infn.it/~ferrera/dyqt.html (3) DyRes: http://pcteserver.mi.infn.it/~ferrera/dyres.html. The data are available from the corresponding author upon request.

Conflicts of Interest

The authors declare that they have no conflicts of interest.

Acknowledgments

We thank Alessandro Bacchetta and Marco Radici for the fruitful collaboration on this topic, Alessandro Vicini for many suggestions and discussions, Chao Shi for carefully reading the manuscript, and Piet Mulders and Mathias Ritzmann for contributing to the investigations summarized in this article. Andrea Signori acknowledges support from the U.S. Department of Energy, Office of Science, Office of Nuclear Physics, Contract no. DE-AC02-06CH11357. Giuseppe Bozzi acknowledges support from the European Research Council (ERC) under the European Union's Horizon 2020 research and innovation program (Grant Agreement no. 647981, 3DSPIN).

References

[1] Gfitter Group collaboration, M. Baak, J. Cth et al., "The global electroweak fit at NNLO and prospects for the LHC and ILC," *The European Physical Journal C*, vol. 74, article 3046, 2014.

[2] V. M. Abazov, B. K. Abbott, B. S. Acharya et al., "Measurement of the W boson mass with the D0 detector," *Physical Review D*, vol. 89, article 012005, 2014.

[3] D. Ayres, H. Akimoto, A. Akopian et al., "Precise measurement of the W -boson mass with the collider detector at fermilab," *Physical Review D*, vol. 89, article 072003, 2014.

[4] M. Aaboud, G. Aad, B. Abbott et al., "Measurement of the W-boson mass in pp collisions at $\sqrt{s}$=7 TeV with the ATLAS detector," *The European Physical Journal C*, vol. 78, article 110, 2018.

[5] M. Tanabashi, K. Hagiwara, and K. Hikasa, "Review of Particle Physics," *Physical Review D*, vol. 98, article 030001, 1973.

[6] S. Weinberg, "The quantum theory of fields," in *Foundations*, vol. 1, Cambridge University Press, 2005.

[7] M. E. Peskin and D. V. Schroeder, *An Introduction to Quantum Field Theory*, Addison-Wesley, Massachusetts, Mass, USA, 1995.

[8] S. Alioli, A. B. Arbuzov, D. Y. Bardin et al., "Precision studies of observables in $pp \longrightarrow W \longrightarrow l\nu_l$ and $pp \longrightarrow \gamma, Z \longrightarrow l^+l^-$ processes at the LHC," *The European Physical Journal C*, vol. 77, article 280, 2017.

[9] C. M. Carloni Calame, M. Chiesa, H. Martinez et al., "Precision measurement of the W-boson mass: theoretical contributions and uncertainties," *Physical Review D*, vol. 96, article, 2017.

[10] A. Signori, *Flavor and evolution effects in TMD phenomenology [Ph.D. thesis]*, Vrije U, Amsterdam, Netherlands, 2016, https://userweb.jlab.org/~asignori/research/PhD_thesis_Andrea.pdf.

[11] A. Bacchetta, G. Bozzi, M. Radici, M. Ritzmann, and A. Signori, "Effect of flavor-dependent partonic transverse momentum on the determination of the W boson mass in hadronic collisions," *Physics Letters B*, vol. 788, pp. 542–545, 2019.

[12] T. Becher, M. Neubert, and D. Wilhelm, "Electroweak gauge-boson production at small q T: Infrared safety from the collinear anomaly," *Journal of High Energy Physics*, vol. 2012, no. 2, 2012.

[13] The ATLAS Collaboration, "Studies of theoretical uncertainties on the measurement of the mass of the W boson at the LHC," Tech. Rep. ATL-PHYS-PUB-2014-015, CERN, Geneva, Switzerland, 2014.

[14] A. Bacchetta, F. Delcarro, C. Pisano, M. Radici, and A. Signori, "Extraction of partonic transverse momentum distributions from semi-inclusive deep-inelastic scattering, Drell-Yan and Z-boson production," *Journal of High Energy Physics*, vol. 6, article 81, 2017.

[15] A. Signori, A. Bacchetta, M. Radici, and G. Schnell, "Investigations into the flavor dependence of partonic transverse momentum," *Journal of High Energy Physics*, vol. 11, article 194, 2013.

[16] G. Bozzi, J. Rojo, and A. Vicini, "The Impact of PDF uncertainties on the measurement of the W boson mass at the Tevatron and the LHC," *Physical Review D*, vol. 83, article 113008, 2011.

[17] G. Bozzi, L. Citelli, and A. Vicini, "Parton density function uncertainties on the W boson mass measurement from the lepton transverse momentum distribution," *Physical Review D*, vol. 91, article 113005, 2015.

[18] S. Catani, L. Cieri, D. de Florian, G. Ferrera, and M. Grazzini, "Universality of transverse-momentum resummation and hard factors at the NNLO," *Nuclear Physics. B. Theoretical, Phenomenological, and Experimental High Energy Physics. Quantum Field Theory and Statistical Systems*, vol. 881, pp. 414–443, 2014.

[19] M. Boglione, J. O. G. Hernandez, S. Melis, and A. Prokudin, "A study on the interplay between perturbative QCD and CSS/TMD formalism in SIDIS processes," *Journal of High Energy Physics*, vol. 2, article 95, 2015.

[20] J. Collins, L. Gamberg, A. Prokudin, T. Rogers, N. Sato, and B. Wang, "Relating transverse-momentum-dependent and collinear factorization theorems in a generalized formalism," *Physical Review D*, vol. 94, article 034014, 2016.

[21] J. Collins and T. C. Rogers, "Connecting different TMD factorization formalisms in QCD," *Physical Review D*, vol. 96, article 054011, 2017.

[22] M. G. Echevarria, T. Kasemets, J. Lansberg, C. Pisano, and A. Signori, "Matching factorization theorems with an inverse-error weighting," *Physics Letters B*, vol. 781, pp. 161–168, 2018.

[23] I. Scimemi and A. Vladimirov, "Analysis of vector boson production within TMD factorization," *The European Physical Journal C*, vol. 78, article 89, 2018.

[24] M. A. Ebert, I. Moult, I. W. Stewart et al., "Subleading power rapidity divergences and power corrections for q_T," 2018, https://arxiv.org/abs/1812.08189.

[25] I. Balitsky and A. Tarasov, "Power corrections to TMD factorization for Z-boson production," *Journal of High Energy Physics*, vol. 5, article 150, 2018.

[26] J. Collins, *Foundations of Perturbative QCD*, vol. 32 of *Cambridge Monographs on Particle Physics, Nuclear Physics and Cosmology*, Cambridge University Press, Cambridge, UK, 2011.

[27] G. Bozzi, S. Catani, G. Ferrera, D. de Florian, and M. Grazzini, "Production of Drell-Yan lepton pairs in hadron collisions: transverse-momentum resummation at next-to-next-to-leading logarithmic accuracy," *Physics Letters B*, vol. 696, pp. 207–213, 2011.

[28] S. Catani, D. de Florian, G. Ferrera, and M. Grazzini, "Vector boson production at hadron colliders: transverse-momentum resummation and leptonic decay," *Journal of High Energy Physics*, vol. 2015, no. 12, pp. 1–47, 2015.

[29] A. Bacchetta, M. G. Echevarria, P. J. Mulders, M. Radici, and A. Signori, "Effects of TMD evolution and partonic flavor on e^+ e^- annihilation into hadrons," *Journal of High Energy Physics*, vol. 11, article 76, 2015.

[30] D. Kang, C. Lee, and V. Vaidya, "A fast and accurate method for perturbative resummation of transverse momentum-dependent observables," *Journal of High Energy Physics*, vol. 4, article 149, 2018.

[31] S. Catani, L. Cieri, D. de Florian, G. Ferrera, and M. Grazzini, "Vector boson production at hadron colliders: hard-collinear coefficients at the NNLO," *The European Physical Journal C*, vol. 72, article 2195, 2012.

[32] M. G. Echevarria, I. Scimemi, and A. Vladimirov, "Unpolarized transverse momentum dependent parton distribution and fragmentation functions at next-to-next-to-leading order," *Journal of High Energy Physics*, vol. 9, article 4, 2016.

[33] G. Bozzi, S. Catani, D. de Florian, and M. Grazzini, "Transverse-momentum resummation and the spectrum of the Higgs boson at the LHC," *Nuclear Physics B*, vol. 737, no. 1-2, pp. 73–120, 2006.

[34] M. G. Echevarría, A. Idilbi, A. Schäfer, and I. Scimemi, "Model-independent evolution of transverse momentum dependent distribution functions (TMDs) at NNLL," *The European Physical Journal C*, vol. 73, article 2636, 2013.

[35] W. Bizoń, X. Chen, A. Gehrmann-De Ridder et al., "Fiducial distributions in Higgs and Drell-Yan production at $N^3LL+NNLO$," *Journal of High Energy Physics*, vol. 2018, article 132, 2018.

[36] S. M. Aybat and T. C. Rogers, "TMD parton distribution and fragmentation functions with QCD evolution," *Physical Review D*, vol. 83, article 114042, 2011.

[37] E. Laenen, G. Sterman, and W. Vogelsang, "Higher order QCD corrections in prompt photon production," *Physical Review Letters*, vol. 84, no. 19, pp. 4296–4299, 2000.

[38] D. Boer and W. J. den Dunnen, "TMD evolution and the Higgs transverse momentum distribution," *Nuclear Physics B*, vol. 886, pp. 421–435, 2014.

[39] D. Boer, "Linearly polarized gluon effects in unpolarized collisions," in *Proceedings of the QCD Evolution '15*, p. 23, October 2015.

[40] F. Landry, R. Brock, P. M. Nadolsky, and C. Yuan, "Tevatron Run-1 Z boson data and Collins-Soper-Sterman resummation formalism," *Physical Review D*, vol. 67, article 073016, 2003.

[41] R. D. Ball, V. Bertone, S. Carrazza et al., "Parton distributions for the LHC Run II," *Journal of High Energy Physics*, vol. 4, article 40, 2015.

[42] R. D. Ball, V. Bertone, S. Carrazza et al., "Parton distributions from high-precision collider data," *European Physical Journal C*, vol. 77, article 663, 2017.

[43] C. M. Carloni Calame, G. Montagna, O. Nicrosini, and M. Treccani, "Higher-order QED corrections to W-boson mass determination at hadron colliders," *Physical Review D*, vol. 69, article 037301, 2004.

[44] C. M. Carloni Calame, G. Montagna, O. Nicrosini, and M. Treccani, "Multiple photon corrections to the neutral-current Drell-Yan process," *Journal of High Energy Physics*, vol. 5, article 19, 2005.

[45] S. Quackenbush and Z. Sullivan, "Parton distributions and the W mass measurement," *Physical Review D*, vol. 92, article 033008, 2015.

[46] G. Bozzi, L. Citelli, M. Vesterinen, and A. Vicini, "Prospects for improving the LHC W boson mass measurement with forward muons," *The European Physical Journal C*, vol. 75, article 601, 2015.

[47] P. M. Nadolsky, H.-L. Lai, Q.-H. Cao et al., "Implications of CTEQ global analysis for collider observables," *Physical Review D*, vol. 78, article 013004, 2008.

[48] A. D. Martin, W. J. Stirling, R. S. Thorne, and G. Watt, "Parton distributions for the LHC," *The European Physical Journal C*, vol. 63, pp. 189–285, 2009.

[49] R. D. Ball, V. Bertone, F. Cerutti et al., "Impact of heavy quark masses on parton distributions and LHC phenomenology," *Nuclear Physics B*, vol. 849, no. 2, pp. 296–363, 2011.

[50] J. Gao, M. Guzzi, J. Huston et al., "CT10 next-to-next-to-leading order global analysis of QCD," *Physical Review D*, vol. 89, article 033009, 2014.

[51] L. A. Harland-Lang, A. D. Martin, P. Motylinski, and R. S. Thorne, "Parton distributions in the LHC era: MMHT 2014 PDFs," *The European Physical Journal C*, vol. 75, article 204, 2015.

[52] R. D. Ball, V. Bertone, S. Carrazza et al., "Parton distributions with LHC data," *Nuclear Physics B*, vol. 867, pp. 244–289, 2013.

[53] E. L. Berger and J. Qiu, "Differential cross section for Higgs boson production including all-orders soft gluon resummation," *Physical Review D*, vol. 67, article 034026, 2003.

[54] E. L. Berger and J. Qiu, "Differential cross-sections for Higgs boson production at Tevatron collider energies," *Physical Review Letters*, vol. 91, article 222003, 2003.

[55] E. L. Berger, J. Qiu, and Y. Wang, "Transverse momentum distribution of Υ production in hadronic collisions," *Physical Review D*, vol. 71, article 034007, 2005.

[56] E. C. Aschenauer, U. D'Alesio, and F. Murgia, "TMDs and SSAs in hadronic interactions," *The European Physical Journal A*, vol. 52, no. 6, 2016.

[57] C. Hadjidakis, D. Kikoła, J. P. Lansberg et al., "A fixed-target programme at the LHC: physics case and projected performances for heavy-ion, hadron, spin and astroparticle studies," 2018, https://arxiv.org/abs/1807.00603.

[58] D. Boer, M. Diehl, R. Milner et al., "Gluons and the quark sea at high energies: distributions, polarization, tomography," 547 pages, 2011, https://arxiv.org/abs/1108.1713.

[59] J. Dudek, R. Ent, R. Essig et al., "Physics opportunities with the 12 GeV upgrade at jefferson lab," *European Physical Journal A*, vol. 48, article 187, 2012.

[60] A. Accardi, J. L. Albacete, M. Anselmino et al., "Electron ion collider: the next QCD frontier," *The European Physical Journal A*, vol. 52, article 268, 2016.

[61] R. Angeles-Martinez, A. Bacchetta, I. Balitsky et al., "Transverse momentum dependent (TMD) parton distribution functions: status and prospects," *Acta Physica Polonica B*, vol. 46, no. 12, pp. 2501–2534, 2015.

[62] M. Diehl, "Introduction to GPDs and TMDs," *The European Physical Journal A*, vol. 52, article 149, 2016.

[63] M. Boglione and A. Prokudin, "Phenomenology of transverse spin: past, present and future," *The European Physical Journal A*, vol. 52, article 154, 2016.

[64] A. Bacchetta, "Where do we stand with a 3-D picture of the proton?" *The European Physical Journal A*, vol. 52, article 163, 2016.

[65] D. Boer, S. Cotogno, T. van Daal et al., "Gluon and Wilson loop TMDs for hadrons of spin ≤ 1," *Journal of High Energy Physics*, vol. 10, article 13, 2016.

[66] A. Metz and A. Vossen, "Parton fragmentation functions," *Progress in Particle and Nuclear Physics*, vol. 91, pp. 136–202, 2016.

Hindawi
Advances in High Energy Physics
Volume 2019, Article ID 3797394, 9 pages
https://doi.org/10.1155/2019/3797394

Review Article

Transverse Momentum Dependence in Double Parton Scattering

Jonathan R. Gaunt[1] **and Tomas Kasemets**[2]

[1]*CERN Theory Division, 1211 Geneva 23, Switzerland*
[2]*PRISMA Cluster of Excellence & Mainz Institute for Theoretical Physics Johannes Gutenberg University, 55099 Mainz, Germany*

Correspondence should be addressed to Jonathan R. Gaunt; jonathan.richard.gaunt@cern.ch

Received 21 December 2018; Accepted 14 February 2019; Published 12 March 2019

Guest Editor: Alexey Vladimirov

In this review, we describe the status of transverse momentum dependence (TMD) in double parton scattering (DPS). The different regions of TMD DPS are discussed, and expressions are given for the DPS cross section contributions that make use of as much perturbative information as possible. The regions are then combined with each other as well as single parton scattering to obtain a complete expression for the cross section. Particular emphasis is put on the differences and similarities to transverse momentum dependence in single parton scattering. We further discuss the status of the factorisation proof for double colour singlet production in DPS, which is now on a similar footing to the proofs for TMD factorisation in single Drell-Yan, discuss parton correlations, and give an outlook on possible research on DPS in the near future.

1. Introduction

Double parton scattering (DPS) is the process in which one has two hard scatterings, producing two sets of particles that we can label as '1' and '2', in an individual proton-proton collision (one allows any possibility for the final-state particles accompanying '1' and '2'; these are often denoted by the symbol X and are typically the products of additional soft scatterings and soft/collinear radiation from the partons active in the hard processes. The proof of factorisation for double colour-singlet production in DPS relies on this inclusive definition [1].). The region in which the transverse momenta of systems 1 and 2, $\boldsymbol{q}_1$ and $\boldsymbol{q}_2$, are small is particularly important in studies of DPS, since DPS is especially prominent in this region compared to the usual single parton scattering (SPS) mechanism [2, 3] (note that here we use boldface symbols to denote transverse momentum vectors). Indeed, many experimental extractions of DPS use variables sensitive to this 'double back-to-back' configuration, for example, the $\Delta_{ij}^{p_T}$ variable in [4]. In the small $\boldsymbol{q}_1$, $\boldsymbol{q}_2$ region a description in terms of double parton transverse momentum dependent (TMD) distributions is appropriate. There are many parallels between the treatment of TMD cross sections in single parton scattering (SPS) and double parton scattering (DPS). There are however also clear differences, with direct physical consequences. In this review, we aim to highlight these differences and similarities in order to facilitate researchers interested in spin and TMD physics to make important contributions to the field of DPS.

While TMD factorisation in SPS has been rigorously proven for colour singlet production (see, e.g., [5]), it runs into problems for hadron collisions producing coloured final states [6–8]. These issues are expected to be important also for DPS, and we will therefore restrict ourselves to double colour-singlet production, i.e., where each of the two hard collisions separately produces a colour singlet final state.

In the production of two colour singlets, such as two vector bosons, the TMD SPS factorisation theorem can be applied as usual to study the region where the sum of the two transverse momenta is small. If, however, the transverse momenta of both bosons are measured to be much smaller than the hard scale, standard TMD factorisation alone is no longer sufficient. For these observables, DPS contributes at the same power as SPS, and no leading-power factorisation theorem can be derived without simultaneously taking care of SPS and DPS, including their interference. An overview of the different factorisation theorems in hadron collisions and the treatment of the initial state in different regions of

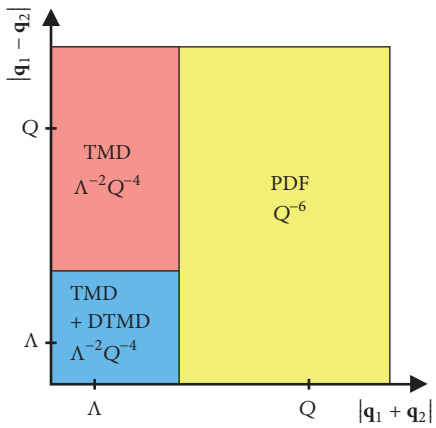

Figure 1: Transverse momentum regions and descriptions of the initial state in the leading power factorisation theorems. The power counting behaviour of the differential cross section in each region is indicated on the figure.

the sum and difference of the transverse momenta of the two colour singlets is shown in Figure 1. Once we integrate over the transverse momentum difference $\boldsymbol{q}_1 - \boldsymbol{q}_2$ DPS is degraded to a power correction to the SPS cross section. Nonetheless, there are several processes in high energy collisions where DPS can compete with or surpass the SPS contribution even for the total cross section. This is usually due to enhancements caused by the large increase in parton densities at small momentum fractions and/or that the SPS cross section is suppressed by additional small coupling constants.

An important issue to address when describing processes which can receive significant contributions from DPS is the consistent combination of SPS and DPS, avoiding double counting. First approaches to this problem are described in [3, 9–12], but these approaches suffer from the drawback that the process does not factorise in the usual sense into hard cross sections and parton densities for each hadron. A new approach which maintains the usual factorisation (and has certain other advantages) was put forward in [13].

A description of the transverse momentum dependent DPS cross section was pursued at the leading logarithmic (LL) level in [3], which uses a generalisation of the Dokshitzer-Diakonov-Troian (DDT) formula [14] to DPS and takes the former approach to handling DPS/SPS double counting. It is known from the SPS case that beyond-LL corrections are in practice important; for example, the DDT formula anticipates a dip in $d\sigma/d|\boldsymbol{q}^2|$ as the transverse momentum of the final-state colour singlet system $\boldsymbol{q}$ approaches 0, which is not observed in practice (see, e.g., [15]). In [16] a framework was developed that holds beyond LL and uses the approach of [13] for handling DPS/SPS double counting. In this paper the ingredients required for an NLL description of transverse momentum distributions were also computed. In this review we will focus on the latter approach.

We note in passing that double parton distributions depending on transverse momentum arguments, sometimes referred to as 'unintegrated' double parton distributions (UDPDFs), appear in approaches designed to describe the DPS cross section at small x (see, e.g., [17–20]). We will not discuss further such approaches, nor the associated UDPDFs, here.

The TMD distributions in DPS (DTMDs) depend on the longitudinal momentum fractions x_i carried by the interacting partons and two transverse distances $\boldsymbol{z}_i$ which are the DPS analogs of the single TMD 'impact parameter' $\boldsymbol{b}$. In addition to these, the distributions depend on the average transverse distance $\boldsymbol{y}$ between the partons. This distance must be equal in the two DTMDs to ensure the two partons are in the same transverse region in each set of colliding partons. In the cross section, the DTMDs are integrated over this common $\boldsymbol{y}$ value.

In the rest of this review, we will take a closer look at the current status of TMD and spin physics in DPS. In Section 2 we give the factorisation theorem for the TMD DPS cross section, discuss the different ingredients and their scale evolution. The different regions of TMD DPS, matching calculations in these regions and the combination of regions including both DPS and SPS are discussed in Section 3. The status of factorisation proofs for DTMDs is reviewed in Section 4. We discuss interparton correlations in Section 5, before outlining a few promising future research directions in Section 6.

2. Factorisation Theorem and Evolution Equations

The TMD DPS cross section formula can be written in terms of two hard coefficients and two DTMDs as [16]

$$\begin{aligned}\frac{d\sigma_{\mathrm{DPS}}}{dx_1\,dx_2\,d\overline{x}_1\,d\overline{x}_2\,d^2\boldsymbol{q}_1\,d^2\boldsymbol{q}_2} &= \frac{1}{C}\\ &\cdot \sum_{a_1,a_2,b_1,b_2} \widehat{\sigma}_{a_1b_1}\left(Q_1,\mu_1\right)\widehat{\sigma}_{a_2b_2}\left(Q_2,\mu_2\right)\\ &\times \int \frac{d^2\boldsymbol{z}_1}{(2\pi)^2}\frac{d^2\boldsymbol{z}_2}{(2\pi)^2}d^2\boldsymbol{y}\\ &\cdot e^{-i\boldsymbol{q}_1\boldsymbol{z}_1 - i\boldsymbol{q}_2\boldsymbol{z}_2} W_{a_1a_2b_1b_2}\left(\overline{x}_i, x_i, \boldsymbol{z}_i, \boldsymbol{y}; \mu_i, \nu\right),\end{aligned} \tag{1}$$

with

$$\begin{aligned}W_{a_1a_2b_1b_2}\left(\overline{x}_i, x_i, \boldsymbol{z}_i, \boldsymbol{y}; \mu_i, \nu\right) &= \Phi\left(\nu\boldsymbol{y}_+\right)\Phi\left(\nu\boldsymbol{y}_-\right)\\ &\times \sum_R \eta_{a_1a_2}(R)\,{}^R F_{b_1b_2}\left(\overline{x}_i, \boldsymbol{z}_i, \boldsymbol{y}; \mu_i, \overline{\zeta}\right)\\ &\cdot {}^R F_{a_1a_2}\left(x_i, \boldsymbol{z}_i, \boldsymbol{y}; \mu_i, \zeta\right).\end{aligned} \tag{2}$$

We use light-cone coordinates $w^{\pm} = (w^0 \pm w^3)/\sqrt{2}$ and the transverse component $\boldsymbol{w} = (w^1, w^2)$ for any four-vector w. For the production of two electroweak gauge bosons $pp \longrightarrow V_1 + V_2 + X$ with $V_i = \gamma^*, Z, W$, Q_i^2 is the squared invariant

mass of V_i, and $x_i, \overline{x}_i$ are related to the Q_i^2 and the rapidities of the produced vector bosons Y_i as follows:

$$x_i = \sqrt{\frac{Q_i^2}{s}} e^{Y_i}$$
$$\overline{x}_i = \sqrt{\frac{Q_i^2}{s}} e^{-Y_i} \tag{3}$$

Although the structure of this formula is very similar to the TMD factorisation for SPS, there are several interesting differences as we will see as we have a closer look at the different ingredients. ${}^R F_{a_1 a_2}(x_i, \boldsymbol{z}_i, \boldsymbol{y}; \mu_i, \zeta)$ is the TMD for partons a_1 and a_2 to be found inside the proton, with longitudinal momentum fractions x_1 and x_2, respectively, and at transverse positions $\boldsymbol{y} \pm \boldsymbol{z}_1/2$ and $\pm \boldsymbol{z}_2/2$ (where the plus sign corresponds to the position in the amplitude, and the minus sign corresponds to the position in the conjugate). R labels the colour representation of a a parton in the amplitude coupled to its partner in the conjugate amplitude. The motivation for this choice of colour decomposition (instead of coupling the two partons in the amplitude) is the separation of the colour singlet $R = 1$ as the representation that is free from any colour correlations between the two hard interactions. The DTMD depends on three scales, two separate renormalization scales μ_1 and μ_2, and a rapidity scale ζ, as will be shown in more detail when we discuss their definitions and evolution equations. The two functions $\Phi(\nu \boldsymbol{y}_\pm)$ with

$$\boldsymbol{y}_\pm = \boldsymbol{y} \pm \frac{1}{2}(\boldsymbol{z}_1 - \boldsymbol{z}_2) \tag{4}$$

regulate the UV-region where SPS and DPS overlap as will be discussed further when we return to the consistent combination of SPS and DPS in Section 3.5. The factor $\eta_{a_1 a_2}(R)$ is equal to 1 except for very specific combinations of parton flavours and colour representations (see [16]). The subprocess cross sections are denoted by $\widehat{\sigma}_{a_i b_i}(Q_i^2, \mu_i^2)$. The sum over a_1, a_2, b_1, b_2 in (1) runs over both parton species and polarisations. C is a combinatorial factor equal to 2 if the final states of the two hard processes are indistinguishable and 1 otherwise.

2.1. Definitions of Double Parton Distributions. In TMD measurements in SPS, it is well known that the collinear and soft momentum regions individually contain rapidity divergences. To tame these divergences and obtain one function describing each of the hadrons, the soft function is split up and combined with the collinear regions. There are several techniques for this procedure depending on the choice of regulator used for the rapidity divergences, but in essence it boils down to separating soft radiation on each side of a rapidity parameter [5, 21]. This procedure generates another scale in which the TMDs evolve. The story for DTMDs is in many aspects equivalent, with a number of complications due to the more complicated colour structure leading in particular to soft factors which are matrices in colour space. For two partons a_1 and a_2, the unsubtracted (i.e., before cancellations of rapidity divergences) DTMDs for a right moving proton ($p^3 > 0$) are defined in terms of matrix elements as [2, 22]

$$\begin{aligned} F_{\mathrm{us},a_1 a_2}(x_1, x_2, \boldsymbol{z}_1, \boldsymbol{z}_2, \boldsymbol{y}) &= 2p^+ (x_1 p^+)^{-n_1} (x_2 p^+)^{-n_2} \\ &\cdot \int \frac{dz_1^-}{2\pi} \frac{dz_2^-}{2\pi} dy^- e^{i(x_1 z_1^- + x_2 z_2^-)p^+} \\ &\times \left\langle p \left| \mathcal{O}_{a_1}(y, z_1)\, \mathcal{O}_{a_2}(0, z_2) \right| p \right\rangle, \end{aligned} \tag{5}$$

where $n_i = 1$ if parton number i is a gluon and $n_i = 0$ otherwise. It is understood that $\boldsymbol{p} = \boldsymbol{0}$ and that the proton polarisation are averaged over. The operators for quarks (see, e.g., [2] for the gluon equivalent) in a right moving proton read

$$\begin{aligned} \mathcal{O}_a(y, z) &= \overline{q}\left(y - \frac{1}{2}z\right) W^\dagger\left(y - \frac{1}{2}z, v_L\right) \\ &\cdot \Gamma_a W\left(y + \frac{1}{2}z, v_L\right) q\left(y + \frac{1}{2}z\right)\Big|_{z^+ = y^+ = 0} \end{aligned} \tag{6}$$

with spin projections $\Gamma_q = (1/2)\gamma^+$ for an unpolarised quark. The field with argument $y + (1/2)z$ in $\mathcal{O}_q(y, z)$ is associated with a quark in the amplitude of a double scattering process and the field with argument $y - (1/2)z$ with a quark in the complex conjugate amplitude. $W(y, v)$ is a past-pointing Wilson line in the direction v originating at the point y. The vector v_L is a spacelike, purely longitudinal vector that is nearly aligned with the minus light-cone direction; this vector is tilted slightly off the lightcone to regulate the rapidity divergences. For the left-moving proton one uses a vector v_R nearly aligned with the plus light-cone direction.

In processes producing colourless particles, one needs the soft factor

$$\begin{aligned} &S_{qq}(\boldsymbol{z}_1, \boldsymbol{z}_2, \boldsymbol{y}; v_L, v_R) \\ &\quad = \left\langle 0 \left| O_{S,q}(\boldsymbol{y}, \boldsymbol{z}_1; v_L, v_R)\, O_{S,q}(\boldsymbol{0}, \boldsymbol{z}_2; v_L, v_R) \right| 0 \right\rangle \end{aligned} \tag{7}$$

with

$$\begin{aligned} &O_{S,q}(\boldsymbol{y}, \boldsymbol{z}; v_L, v_R) \\ &\quad = \left[W\left(\boldsymbol{y} + \frac{1}{2}\boldsymbol{z}, v_L\right) W^\dagger\left(\boldsymbol{y} + \frac{1}{2}\boldsymbol{z}, v_R\right) \right] \\ &\quad \cdot \left[W\left(\boldsymbol{y} - \frac{1}{2}\boldsymbol{z}, v_R\right) W^\dagger\left(\boldsymbol{y} - \frac{1}{2}\boldsymbol{z}, v_L\right) \right]. \end{aligned} \tag{8}$$

The soft matrix S in (7) depends on v_L and v_R only via the difference of the Wilson line rapidities $Y \equiv Y_R - Y_L$: that is, $S(v_L, v_R) = S(Y)$. The matrix $S(Y)$ can be divided into two pieces at some rapidity Y_0 according to [16, 23]

$$S(Y) = s(Y - Y_0)\, s^\dagger(Y_0) \qquad \text{for } Y \gg 1 \text{ and arbitrary } Y_0. \tag{9}$$

We have kept the colour indices implicit in these equations, where the colour indices of the soft factor can be projected

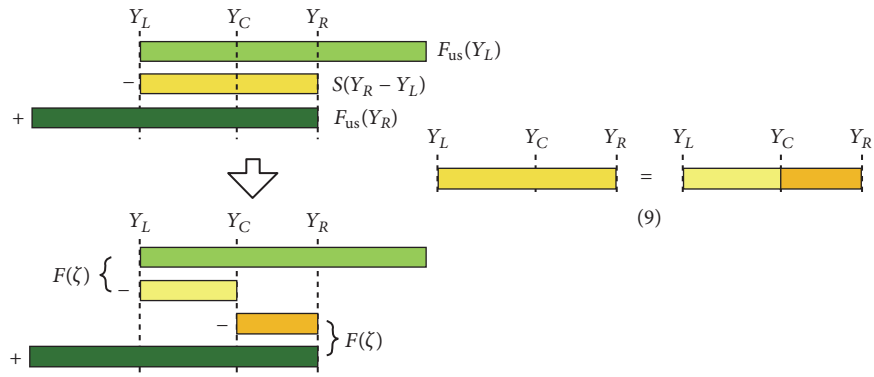

Figure 2: Rapidity subtractions and definition of right and left moving DTMDs.

into a colour matrix in RR', and the unsubtracted DTMDs are vectors in this colour space.

The subtracted DTMDs, i.e., with the rapidity divergences subtracted through the combination with the soft factor as illustrated in Figure 2, are defined as [16]

$$
\begin{aligned}
&{}^{R}F_{a_1a_2}(\zeta) \\
&\quad = \lim_{Y_L \longrightarrow -\infty} \sum_{R'}^{RR'} s^{-1}_{a_1a_2}(Y_C - Y_L)\, {}^{R'}F_{\mathrm{us},a_1a_2}(Y_L),
\end{aligned}
\tag{10}
$$

for the distributions in a right-moving proton. Y_C is a central rapidity (typically chosen to be close to zero), used to separate left- from right-moving soft radiation, $Y_L \ll Y_C \ll Y_R$. The rapidity scales ζ and $\overline{\zeta}$ in (2) are related to this central rapidity parameter through

$$
\zeta = 2x_1x_2\left(p^+\right)^2 e^{-2Y_C}, \tag{11}
$$

$$
\overline{\zeta} = 2\overline{x}_1\overline{x}_2\left(\overline{p}^-\right)^2 e^{2Y_C}. \tag{12}
$$

where p^+ ($\overline{p}^-$) is the plus (minus) momentum of the right- (left-) moving proton.

It can be useful to compare this result to the definition of the subtracted (single parton scattering) TMD; see, e.g., chapter 13 in [5] and section 3.4 of [16].

$$
f_a(\zeta) = \lim_{Y_L \longrightarrow -\infty} s_a^{-1}(Y_C - Y_L)\, f_{\mathrm{us},a}(Y_L), \tag{13}
$$

where the colour matrix s is now reduced to a single function and the product x_1x_2 in ζ has been replaced by the square of the single parton momentum fraction, x^2.

2.2. RGE Evolution and Resummation. The DTMD evolves two renormalisation scales, related to the two partons and one rapidity scale [16]. The renormalisation group equation for the DTMDs reads

$$
\begin{aligned}
&\frac{\partial}{\partial \log \mu_1} {}^{R}F_{a_1a_2}(x_i, \boldsymbol{z}_i, \boldsymbol{y}; \mu_i, \zeta) \\
&\quad = \gamma_{F,a_1}\left(\mu_1, \frac{x_1\zeta}{x_2}\right) {}^{R}F_{a_1a_2}(x_i, \boldsymbol{z}_i, \boldsymbol{y}; \mu_i, \zeta)
\end{aligned}
\tag{14}
$$

for the scale μ_1, and in analogy for μ_2. The rapidity scale evolution (Collins-Soper equation) is given by

$$
\begin{aligned}
&\frac{\partial}{\partial \log \zeta} {}^{R}F_{a_1a_2}(x_i, \boldsymbol{z}_i, \boldsymbol{y}; \mu_i, \zeta) \\
&\quad = \frac{1}{2}\sum_{R'}^{RR'} K_{a_1a_2}(\boldsymbol{z}_i, \boldsymbol{y}; \mu_i)\, {}^{R'}F_{a_1a_2}(x_i, \boldsymbol{z}_i, \boldsymbol{y}; \mu_i, \zeta).
\end{aligned}
\tag{15}
$$

The one-loop results for these kernels are all available in [16]. The scale dependence of the Collins-Soper kernel is given by the cusp anomalous dimension

$$
\frac{\partial}{\partial \log \mu_1} {}^{RR'}K_{a_1a_2}(\boldsymbol{z}_i, \boldsymbol{y}; \mu_i) = -\gamma_{K,a_1}(\mu_1)\,\delta_{RR'} \tag{16}
$$

and correspondingly for μ_2. All UV divergences and dependence on the renormalisation scales are contained in the diagonal elements of ${}^{RR'}K$. The kernel $K_{a_1a_2}$ and the anomalous dimensions $\gamma_{F,a}$ and $\gamma_{K,a}$ depend on the colour representation of the parton (quarks or antiquarks versus gluons) but not on their flavour or polarisation. The solution to the rapidity and renormalisation evolution equations, relating the DTMDs at different scales, reads

$$
\begin{aligned}
&{}^{R}F_{a_1a_2}(x_i, \boldsymbol{z}_i, \boldsymbol{y}; \mu_i, \zeta) \\
&\quad = \exp\left\{\int_{\mu_{01}}^{\mu_1} \frac{d\mu}{\mu}\left[\gamma_{a_1}(\mu) - \gamma_{K,a_1}(\mu)\log\frac{\sqrt{x_1\zeta/x_2}}{\mu}\right]\right. \\
&\qquad + {}^{1}K_{a_1}(\boldsymbol{z}_1; \mu_{01})\log\frac{\sqrt{\zeta}}{\sqrt{\zeta_0}} \\
&\qquad + \int_{\mu_{02}}^{\mu_2} \frac{d\mu}{\mu}\left[\gamma_{a_2}(\mu) - \gamma_{K,a_2}(\mu)\log\frac{\sqrt{x_2\zeta/x_1}}{\mu}\right] \\
&\qquad \left. + {}^{1}K_{a_2}(\boldsymbol{z}_2; \mu_{02})\log\frac{\sqrt{\zeta}}{\sqrt{\zeta_0}}\right\} \\
&\qquad \times \sum_{R'}^{RR'} \exp\left[M_{a_1a_2}(\boldsymbol{z}_i, \boldsymbol{y})\log\frac{\sqrt{\zeta}}{\sqrt{\zeta_0}}\right] \\
&\qquad \cdot {}^{R'}F_{a_1a_2}(x_i, \boldsymbol{z}_i, \boldsymbol{y}; \mu_{01}, \mu_{02}, \zeta_0).
\end{aligned}
\tag{17}
$$

Table 1: Regions of $\boldsymbol{y}$ discussed in the text.

region	approximations
DPS, large $\boldsymbol{y}$	$\lvert\boldsymbol{z}_i\rvert \ll \lvert\boldsymbol{y}\rvert,\ 1/\Lambda$
DPS, small $\boldsymbol{y}$	$\lvert\boldsymbol{z}_i\rvert, \lvert\boldsymbol{y}\rvert \ll 1/\Lambda$
SPS	$\lvert\boldsymbol{y}_+\rvert, \lvert\boldsymbol{y}_-\rvert \ll \lvert\boldsymbol{z}_i\rvert \ll 1/\Lambda$

The exponential in the second and third lines is the generalisation to two partons of the evolution factor for a single parton TMD. It resums both double and single logarithms. The last line in (17) describes the mixing between different colour representations R under rapidity evolution and involves a single logarithm. The double logarithms in the evolution of ${}^{R}F_{a_1a_2}(x_i, \boldsymbol{z}_i, \boldsymbol{y}; \mu_i, \zeta)$ are thus the same as those for a product of two single TMDs.

3. Regions and Matching

3.1. Regions. Similar to the small impact parameter expansion possible in TMD SPS, the small $\boldsymbol{z}_i$ region of TMD DPS enables additional perturbative calculations and matching. This is relevant when the transverse momenta of the vector bosons obey $\Lambda << q_T << Q$, and Fourier oscillations suppress contributions to the cross section from the nonperturbative region of z_i (care must be taken if $|\boldsymbol{q}_1 \pm \boldsymbol{q}_2|$ is of order Λ, as this can spoil the cancellations from the Fourier oscillations; see, e.g., section 6.1 of [16].). The presence of, in particular, the distance scale $\boldsymbol{y}$, leads to different regions of DPS which all contribute to the DTMD cross section. In order to make maximal use of the predictive power of perturbation theory, we will consider three different regions as summarised in Table 1. The first is the large-$\boldsymbol{y}$ region, where the distance within the pairs of partons inside the protons is of hadronic size. The second region is for small-$\boldsymbol{y}$ where the distance is of the same order as $\boldsymbol{z}_i$, i.e., $1/q_T$, and finally there is the SPS region where $\boldsymbol{y}$ is of the order of the inverse of the hard scale.

3.2. Large-$\boldsymbol{y}$. The large-$\boldsymbol{y}$ region is perhaps the most natural region for DPS. When a perturbative scale inside the DTMDs is provided by $\boldsymbol{z}_i$, the large distance between the two partons allows for separate matching calculations for each of the two partons. This connects the DTMDs with the collinear DPDFs as

$$\begin{aligned} {}^{R}F_{a_1a_2}(x_i, \boldsymbol{z}_i, \boldsymbol{y}; \mu_i, \zeta) = \sum_{b_1,b_2} {}^{R}C_{a_1b_1}\left(x_1', \boldsymbol{z}_1; \mu_1, \frac{x_1\zeta}{x_2}\right) \\ \otimes_{x_1} {}^{R}C_{a_2b_2}\left(x_2', \boldsymbol{z}_2; \mu_2, \frac{x_2\zeta}{x_1}\right) \\ \otimes_{x_2} {}^{R}F_{b_1b_2}\left(x_i', \boldsymbol{y}; \mu_i, \zeta\right), \end{aligned} \tag{18}$$

with $\otimes_x$ denoting a convolution in momentum fraction x. This matching is very similar to that of the standard TMD matching onto PDFs, with the same matching coefficients ${}^{R}C_{a_2b_2}$ for the colour singlet contribution, $R = 1$. To avoid large logarithms in the coefficients ${}^{R}C_{a_1b_1}$ this matching should be conducted with $\mu_i \sim \sqrt{\zeta} \sim b_0/|\boldsymbol{z}_i|$; the DTMDs can then be evolved to other scales using (17), whose form simplifies in the $|\boldsymbol{z}_1||\boldsymbol{z}_2| \ll |y|$ limit to

$$\begin{aligned} {}^{R}F_{a_1a_2}(x_i, \boldsymbol{z}_i, \boldsymbol{y}; \mu_i, \zeta) = \exp\Bigg\{ \int_{\mu_{01}}^{\mu_1} \frac{d\mu}{\mu} \\ \cdot \left[\gamma_{a_1}(\mu) - \gamma_{K,a_1}(\mu) \log\frac{\sqrt{x_1\zeta/x_2}}{\mu}\right] + \int_{\mu_{02}}^{\mu_2} \frac{d\mu}{\mu} \\ \cdot \left[\gamma_{a_2}(\mu) - \gamma_{K,a_2}(\mu) \log\frac{\sqrt{x_2\zeta/x_1}}{\mu}\right] \\ + \left[{}^{R}K_{a_1}(\boldsymbol{z}_1; \mu_{01}) + {}^{R}K_{a_2}(\boldsymbol{z}_2; \mu_{02}) + {}^{R}J(\boldsymbol{y}; \mu_{0i})\right] \\ \cdot \log\frac{\sqrt{\zeta}}{\sqrt{\zeta_0}}\Bigg\} {}^{R}F_{a_1a_2}(x_i, \boldsymbol{z}_i, \boldsymbol{y}; \mu_{0i}, \zeta_0), \end{aligned} \tag{19}$$

where, in particular, the different colour channels no longer mix with each other. The hadronic distance between the two partons does not allow the perturbative evolution to connect the two partons and therefore can not change their colour representation. The matching in this region can in principle be extrapolated into the region of nonperturbative z_i, by extending methods such as the b^* method from TMDs in single parton scattering [24, 25], although this has not been extensively explored.

3.3. Small-$\boldsymbol{y}$. When $\boldsymbol{y}$ becomes small, i.e., $y \sim z_i \sim 1/q_T$, one no longer has a separate matching for each of the two partons. Following the discussion in [13], we write

$${}^{R}F = {}^{R}F_{\text{spl}} + {}^{R}F_{\text{int}}, \tag{20}$$

where the short-distance expansion of the terms on the r.h.s. involves proton matrix elements of operators with twist two and twist four.

The splitting contribution F_{spl} describes the case where a single parton splits into partons a_1 and a_2:

$$\begin{aligned} {}^{R}F_{a_1a_2,\text{spl}}(x_i, \boldsymbol{z}_i, \boldsymbol{y}; \mu, \mu, \zeta) = \frac{\boldsymbol{y}_+^l \boldsymbol{y}_-^{l'}}{\boldsymbol{y}_+^2 \boldsymbol{y}_-^2} \frac{\alpha_s(\mu)}{2\pi^2} \\ \cdot {}^{R}T^{ll'}_{a_0 \longrightarrow a_1a_2}\left(\frac{x_1}{x_1+x_2}\right) \frac{f_{a_0}(x_1+x_2; \mu)}{x_1+x_2} + \mathcal{O}\left(\alpha_s^2\right), \end{aligned} \tag{21}$$

with the one loop coefficients given in [16, 26]. A ζ dependence appears only at order α_s^2.

The term F_{int} in (20) is referred to as the "intrinsic" contribution to the DPD and may be thought of as describing parton pairs a_1, a_2 in the "intrinsic" proton wave function. Unlike F_{spl}, it starts at order α_s^0 and reads

$$\begin{aligned} {}^{R}F_{a_1a_2,\text{int}}(x_i, \boldsymbol{z}_i, \boldsymbol{y}; \mu, \mu, \zeta) \\ = {}^{R}G_{a_1a_2}(x_1, x_2, x_2, x_1; \mu) + \mathcal{O}(\alpha_s), \end{aligned} \tag{22}$$

where ${}^{R}G$ denotes a collinear twist-four distribution. Since the corresponding expansion for the intrinsic part of the

DPDFs is the same up to $\mathcal{O}(\alpha_s^0)$, one may replace the twist-four functions by the intrinsic part of the DPDFs at leading-order accuracy:

$$\begin{aligned} &{}^{R}F_{\mathrm{int},a_1a_2}\left(x_i, \boldsymbol{z}_i, \boldsymbol{y}; \mu, \mu, \zeta\right) \\ &\quad = {}^{R}F_{\mathrm{int},a_1a_2}\left(x_i, \boldsymbol{y}; \mu, \mu, \zeta\right) + \mathcal{O}\left(\alpha_s\right), \end{aligned} \tag{23}$$

To avoid large logarithms in the matching coefficients, one should perform this matching at the scale $\mu_i \sim \sqrt{\zeta} \sim b_0/|\boldsymbol{z}_i| \sim b_0/|\boldsymbol{y}|$; the DTMDs can then be evolved to other scales using (17).

3.4. Combination of DPS Regions. The full DPS cross section can be obtained from the combination of the large- and small-$\boldsymbol{y}$ regions through

$$W_{\mathrm{DPS}}(\nu) = W_{\mathrm{large}\,y}\left(\nu'\right) - W_{\mathrm{sub}}\left(\nu'\right) + W_{\mathrm{small}\,y}(\nu), \tag{24}$$

where we make explicit the choice of cutoff parameters for the $\boldsymbol{y}$ integration, taking $\nu' \sim q_T$ and $\nu \sim Q$. The W terms in the different regions are obtained by replacing the DTMDs in (2) by their approximations in the corresponding regions. The double counting subtraction term is defined as

$$W_{\mathrm{sub}} = W_{\mathrm{small}\,y}\Big|_{\text{approx. for } |\boldsymbol{z}_i| \ll |\boldsymbol{y}|} \tag{25}$$

with the small-$\boldsymbol{y}$ expression for W. The limit $|\boldsymbol{z}_1|, |\boldsymbol{z}_2| \ll |\boldsymbol{y}|$ should be taken in all parts of the expression.

In the region $|\boldsymbol{y}| \gg |\boldsymbol{z}_1|, |\boldsymbol{z}_2|$ the last two terms of (24) are cancelled by virtue of (25), and one is left with the first term, which is designed to give a correct approximation of the cross section there. For $|\boldsymbol{y}| \sim |\boldsymbol{z}_1|, |\boldsymbol{z}_2|$, the first and second terms are cancelled, and the third term gives a correct approximation of the cross section. In this way, W_{DPS} leads to a correct approximation of the DPS cross section for $|\boldsymbol{y}|$ of order $1/q_T$ and larger.

3.5. Combination with SPS. The DPS cross section discussed in the last section can be combined with SPS in a consistent manner following [13]. In essence, the functions Φ of (2) cut off the DPS cross section where it enters the SPS region. In order to avoid double counting in the DPS region, the part of DPS which is already included in the SPS contributions (i.e., part of the splitting) must be subtracted. However, this is not the end of the story, as one has to consistently include the interference between double and single parton scattering (which we shall denote as $\sigma_{\mathrm{DPS/SPS}}$ or $\sigma_{\mathrm{SPS/DPS}}$, depending on which process is in the amplitude/conjugate). This leads to the master formula

$$\begin{aligned} \sigma = \sigma_{\mathrm{DPS}} &+ \left[\sigma_{\mathrm{DPS/SPS}} - \sigma_{\mathrm{DPS},y_-\longrightarrow 0} + \sigma_{\mathrm{SPS/DPS}}\right. \\ &\left. - \sigma_{\mathrm{DPS},y_+\longrightarrow 0}\right] + \left[\sigma_{\mathrm{SPS}} - \sigma_{\mathrm{DPS/SPS},y_+\longrightarrow 0}\right. \\ &\left. - \sigma_{\mathrm{SPS/DPS},y_-\longrightarrow 0} + \sigma_{\mathrm{DPS},y_\pm\longrightarrow 0}\right], \end{aligned} \tag{26}$$

describing the nested subtraction structure of the full combination. For further details on the different terms, scale setting, etc., see, in particular, section 4.2 of [13] and section 6.5 of [16].

A discussion of the perturbative order at which the ingredients in the SPS as well as DPS cross sections and logarithmic accuracy are achievable is given in section 6.6 of [16]. For the colour singlet representation, the ingredients are to a large extent recyclable from resummation for single parton scattering and therefore allow for very high logarithmic accuracy.

4. Status of Factorisation

Essentially all the steps towards a proof of factorisation for TMD DPS producing two uncoloured systems have now been completed [1, 2, 16, 23]. Many of the steps have been achieved by adapting the methodology for the corresponding steps in the proof of factorisation for TMD SPS producing an uncoloured system [5, 27–29] (for a brief review of these steps, see [30] or [1]).

In derivations of factorisation theorems the most difficult momentum region to treat is the Glauber region; this region is characterised by the momentum of the particle being mainly transverse (technically, a Glauber momentum r satisfies $|r^+r^-| \ll \boldsymbol{r}^2$). For attachments of Glauber gluons into the two collinear sectors, one cannot apply the so-called Grammer-Yennie approximations [5, 31] that one uses for the (central) soft and collinear momenta to separate lines with these momenta into separate functions. A proof of Glauber gluon cancellation for TMD DPS was presented in [1]. The argument is based on unitarity and can be cast into a form where it is rather similar to the corresponding cancellation argument for single scattering found in [5, 29].

A further important step of the proof is to show that the central soft gluon attachments into the collinear factors can ultimately be disentangled into attachments into the soft Wilson lines given in (8), via nonabelian Ward identities. This step was achieved recently in [32].

To achieve a description of the TMD cross section in which the soft factor is absorbed into the separate TMDs, it is necessary that the soft factor has the property described in (9). An all-order proof of this property has been put forward in [23], albeit using a different rapidity regulator from that used in [16]. In [16] it was demonstrated that, provided the soft factor can be decomposed in this way, the 'splitting' of the soft function into DTMD distributions free from rapidity divergences can be achieved; in particular, the more complicated colour structure compared to SPS does not spoil the factorisation procedure. The systematic combination of SPS and DPS, avoiding any double counting, discussed in the previous section was another important step to obtain a fully consistent DTMD factorisation theorem including both types of scatterings [13].

At this point the factorisation status for TMD DPS is essentially at the same level as that for TMD SPS. One remaining technical issue relates to Wilson line self-interactions; see section 9 of [33] for more information.

5. Correlations in DPS

One of the most exciting aspects of DPS is the access it provides to the correlations between two partons bound inside the proton. The study of these correlations actually dates back all the way to the 80s [34, 35], but recent years have seen a revival of activity in this area. The two partons can be correlated either kinematically or through their quantum numbers, for recent reviews we refer to [36, 37] and references therein. Model calculations of DPDFs suggest that such correlations can be large, at least at large values of x [38–45]; however, evolution to large scales tends to decrease their importance, especially at low x [26, 46]. It was recently demonstrated that spin correlations can have a measurable impact on differential distributions in at least one process (same-sign WW production) at the LHC [47].

The description of spin correlations in DPS has many parallels and similarities to the spin correlations in TMD physics. The main difference is actually in the physical interpretation, where the correlations between the hadron spin and the spin of a parton is replaced by parton-parton spin correlations. The correlations between the transverse momenta and spin of a parton and/or proton in SPS TMDs are in DTMDs replaced by correlations involving (one or two) parton spins, their two transverse momenta, and the transverse distance between them. The physical difference means that intuition on the size of the correlations built up from SPS can not be applied, but the similarities in the calculations means that large parts of calculations for TMDs can be recycled for DTMDs or DPDFs.

Colour correlations in DPS do not have a simple analogy in QCD TMD studies; however, certain similarities may be found in recent work on resumming electroweak (EW) logarithms (i.e., logarithms of the hard scale Q over the electroweak scale M when $Q \gg M$); see [48–52]. An important difference in resumming electroweak logarithms, compared to QCD, is that the initial state carries $SU(2)$ charge. This means that there can be correlations between the proton EW charge and the charge of the partons probed, which is analogous to correlations between the (colour) charge of two partons inside the proton in DPS.

6. Forecast

The recent progress in DPS in general and for DTMD factorisation in particular has made the different ingredients necessary for a lot of interesting phenomenology available. What has never been done is taking the theoretical framework, producing all the ingredients, and applying them to a particular process such as same-sign W-boson production or double Drell-Yan. This, however, is a rather daunting task if one aims to directly treat all possible correlations, all momentum regions, interferences, etc. A more approachable way might be to start the development towards this goal, step by step. It would, for example, be very interesting to see the results of the RGE and rapidity evolution on the DPDs, in particular for the different colour channels. While it is known that the colour correlations decrease with evolution scale, this has never been investigated taking the full evolution equations into account, and simplified studies only explicitly treated the quark nonsinglet DPDF [46]. A different, interesting and complementary path would be to study the contribution only from the colour singlet DTMDs, and the effect the combination of the regions of y in the DPS cross section has on the transverse momentum distribution of the two vector bosons. On the fixed order computational side, single parton scattering calculations could, with mere changes of colour factors, produce important input for DPS. The, by far, largest uncertainty on the transverse momentum dependent DPS cross section comes from the DTMDs themselves. Recent work enables us to make use of as much perturbative information as possible, but there is a lot of potential in model calculations, lattice, evolution studies, and extrapolations of the DTMDs into the region of large z_i. The latter region is challenging from the modelling perspective, as it requires the treatment of nonperturbative functions depending on three different transverse directions (z_1, z_2, and y). With the LHC ultimately able to reach the integrated luminosity required for detailed studies of the most clean DPS processes, it is envisaged that experimental efforts will be able to put important constraints on the DPDFS, DTMDs, and the correlations between two partons inside a proton.

Conflicts of Interest

The authors declare that they have no conflicts of interest.

Acknowledgments

Tomas Kasemets acknowledges support from the Alexander von Humboldt Foundation.

References

[1] M. Diehl, J. R. Gaunt, D. Ostermeier, P. Plößl, and A. Schäfer, "Cancellation of Glauber gluon exchange in the double Drell-Yan process," *Journal of High Energy Physics*, vol. 2016, no. 1, article no. 76, 2016.

[2] M. Diehl, D. Ostermeier, and A. Schäfer, "Elements of a theory for multiparton interactions in QCD," *Journal of High Energy Physics*, vol. 2012, no. 3, article no. 89, 2012.

[3] B. Blok, Y. Dokshitzer, L. Frankfurt, and M. Strikman, "pQCD physics of multiparton interactions," *European Physical Journal*, vol. 72, no. 4, article no. 1963, 2012.

[4] ATLAS Collaboration, M. Aaboud et al., "Study of hard double-parton scattering in four-jet events in pp collisions at $\sqrt{s}$=7 TeV with the ATLAS experiment," *Journal of High Energy Physics*, vol. 2016, no. 11, 2016.

[5] J. Collins, "Foundations of Perturbative QCD," *Cambridge Monographs on Particle Physics, Nuclear Physics and Cosmology*, vol. 32, pp. 1–624, 2011.

[6] T. C. Rogers and P. J. Mulders, "No generalized transverse momentum dependent factorization in the hadroproduction of high transverse momentum hadrons," *Physical Review D*, vol. 81, no. 9, article no. 094006, 2010.

[7] J. Collins and J. Qiu, "kT factorization is violated in production of high-transverse-momentum particles in hadron-hadron collisions," *Physical Review D*, vol. 75, no. 11, article no. 114014, 2007.

[8] J. Collins, "2-soft-gluon exchange and factorization breaking," https://arxiv.org/abs/0708.4410.

[9] B. Blok, Y. Dokshitzer, L. Frankfurt, and M. Strikman, "Perturbative QCD correlations in multi-parton collisions," *European Physical Journal C*, vol. 74, no. 6, article no. 2926, 2014.

[10] J. R. Gaunt and W. J. Stirling, "Double parton scattering singularity in one-loop integrals," *Journal of High Energy Physics*, vol. 2011, no. 6, article no. 048, 2011.

[11] J. R. Gaunt, "Single perturbative splitting diagrams in double parton scattering," *Journal of High Energy Physics*, vol. 2013, no. 1, article no. 042, 2013.

[12] A. V. Manohar and W. J. Waalewijn, "What is double parton scattering?" *Physics Letters B*, vol. 713, no. 3, pp. 196–201, 2012.

[13] M. Diehl, J. R. Gaunt, and K. Schönwald, "Double hard scattering without double counting," *Journal of High Energy Physics*, vol. 2017, no. 6, article no. 083, 2017.

[14] Y. L. Dokshitzer, D. I. Dyakonov, and S. I. Troyan, "Hard processes in quantum chromodynamics," *Physics Reports*, vol. 58, no. 5, pp. 269–395, 1980.

[15] R. K. Ellis, W. J. Stirling, and B. R. Webber, "QCD and collider physics," *Cambridge Monographs on Particle Physics, Nuclear Physics and Cosmology*, vol. 8, pp. 1–435, 1996.

[16] M. G. Buffing, M. Diehl, and T. Kasemets, "Transverse momentum in double parton scattering: factorisation, evolution and matching," *Journal of High Energy Physics*, vol. 2018, no. 1, article no. 044, 2018.

[17] R. Maciuła and A. Szczurek, "Double-parton scattering effects in D^0B^+ and B^+B^+ meson-meson pair production in proton-proton collisions at the LHC," *Physical Review D*, vol. 97, no. 9, article no. 094010, 2018.

[18] K. Kutak, R. Maciuła, M. Serino, A. Szczurek, and A. van Hameren, "Search for optimal conditions for exploring double-parton scattering in four-jet production: kt-factorization approach," *Physical Review D*, vol. 94, no. 1, article no. 014019, 2016.

[19] K. Golec-Biernat and A. Staśto, "Unintegrated double parton distributions," *Physical Review D*, vol. 95, no. 3, article no. 034033, 2017.

[20] E. Elias, K. Golec-Biernat, and A. M. Staśto, "Numerical analysis of the unintegrated double gluon distribution," *Journal of High Energy Physics*, vol. 2018, no. 1, article no. 141, 2018.

[21] M. G. Echevarria, I. Scimemi, and A. Vladimirov, "Unpolarized transverse momentum dependent parton distribution and fragmentation functions at next-to-next-to-leading order," *Journal of High Energy Physics*, vol. 2016, no. 9, article no. 4, 2016.

[22] M. Diehl and A. Schäfer, "Theoretical considerations on multiparton interactions in QCD," *Physics Letters B*, vol. 698, no. 5, pp. 389–402, 2011.

[23] A. Vladimirov, "Structure of rapidity divergencies in multiparton scattering soft factors," *Journal of High Energy Physics*, vol. 2018, no. 4, article no. 45, 2018.

[24] J. C. Collins and D. E. Soper, "Back-to-back jets: fourier transform from B to K-transverse," *Nuclear Physics B*, vol. 197, no. 3, pp. 446–476, 1982.

[25] J. C. Collins, D. E. Soper, and G. F. Sterman, "Transverse momentum distribution in Drell-Yan pair and W and Z boson production," *Nuclear Physics B*, vol. 250, no. 1–4, pp. 199–224, 1985.

[26] M. Diehl, T. Kasemets, and S. Keane, "Correlations in double parton distributions: effects of evolution," *Journal of High Energy Physics*, vol. 2014, no. 5, article no. 118, 2014.

[27] G. T. Bodwin, "Erratum: Factorization of the Drell-yan cross section in perturbation theory," *Physical Review D*, vol. 31, no. 10, article no. 2616, 1985.

[28] J. C. Collins, D. E. Soper, and G. Sterman, "Factorization for short distance hadron-hadron scattering," *Nuclear Physics B*, vol. 261, pp. 104–142, 1985.

[29] J. C. Collins, D. E. Soper, and G. Sterman, "Soft gluons and factorization," *Nuclear Physics B*, vol. 308, no. 4, pp. 833–856, 1988.

[30] D. Boer, T. van Daal, J. Gaunt, T. Kasemets, and P. Mulders, "Colour unwound - disentangling colours for azimuthal asymmetries in Drell-Yan scattering," *SciPost Physics*, vol. 3, no. 6, article no. 40, 2017.

[31] G. Grammer Jr. and D. R. Yennie, "Improved treatment for the infrared-divergence problem in quantum electrodynamics," *Physical Review D*, vol. 8, no. 12, pp. 4332–4344, 1973.

[32] M. Diehl and R. Nagar, "Factorisation of soft gluons in multiparton scattering," https://arxiv.org/abs/1812.09509.

[33] M. Diehl and J. R. Gaunt, "Double parton scattering theory overview," in *Multiple Parton Interactions at the LHC*, P. Bartalini and J. R. Gaunt, Eds., vol. 29 of *Advanced Series on Directions in High Energy Physics*, pp. 7–28, 2018.

[34] M. Mekhfi, "Correlations in color and spin in multiparton processes," *Physical Review D: Particles, Fields, Gravitation and Cosmology*, vol. 32, no. 9, pp. 2380–2384, 1985.

[35] M. Mekhfi and X. Artru, "Sudakov suppression of color correlations in multiparton scattering," *Physical Review D: Particles, Fields, Gravitation and Cosmology*, vol. 37, no. 9, pp. 2618–2622, 1988.

[36] B. Blok and M. Strikman, "Multiparton pp and pA collisions: from geometry to Parton–Parton correlations," in *Multiple Parton Interactions at the LHC*, P. Bartalini and J. R. Gaunt, Eds., vol. 29 of *Advanced Series on Directions in High Energy Physics*, pp. 63–99, 2018.

[37] T. Kasemets and S. Scopetta, "Parton correlations in double parton scattering," in *Multiple Parton Interactions at the LHC*, P. Bartalini and J. R. Gaunt, Eds., vol. 29 of *Advanced Series on Directions in High Energy Physics*, pp. 49–62, 2018.

[38] T. Kasemets and A. Mukherjee, "Quark-gluon double parton distributions in the light-front dressed quark model," *Physical Review D*, vol. 94, no. 7, article no. 074029, 2016.

[39] M. Rinaldi, S. Scopetta, M. Traini, and V. Vento, "A model calculation of double parton distribution functions of the pion," *The European Physical Journal C*, vol. 78, no. 9, article no. 781, 2018.

[40] M. Rinaldi and F. A. Ceccopieri, "Relativistic effects in model calculations of double parton distribution functions," *Physical Review D*, vol. 95, no. 3, article no. 034040, 2017.

[41] W. Broniowski, E. Ruiz Arriola, and K. Golec-Biernat, "Generalized valon model for double parton distributions," *Few-Body Systems*, vol. 57, no. 6, pp. 405–410, 2016.

[42] W. Broniowski and E. Ruiz Arriola, "Valence double parton distributions of the nucleon in a simple model," *Few-Body Systems*, vol. 55, no. 5-7, pp. 381–387, 2014.

[43] M. Rinaldi, S. Scopetta, M. Traini, and V. Vento, "Double parton correlations and constituent quark models: a light front approach to the valence sector," *Journal of High Energy Physics*, vol. 2014, no. 12, article no. 28, pp. 1–23, 2014.

[44] M. Rinaldi, S. Scopetta, and V. Vento, "Double parton correlations in constituent quark models," *Physical Review D*, vol. 87, no. 11, article no. 114021, 2013.

[45] H. Chang, A. V. Manohar, and W. J. Waalewijn, "Double parton correlations in the bag model," *Physical Review D*, vol. 87, no. 3, article no. 034009, 2013.

[46] A. V. Manohar and W. J. Waalewijn, "QCD analysis of double parton scattering: Spin and color correlations, interference effects, and evolution," *Physical Review D*, vol. 85, no. 11, article no. 114009, 2012.

[47] S. Cotogno, T. Kasemets, and M. Myska, "A spin on same-sign W-boson pair production," https://arxiv.org/abs/1809.09024.

[48] M. Ciafaloni, P. Ciafaloni, and D. Comelli, "Towards collinear evolution equations in electroweak theory," *Physical Review Letters*, vol. 88, no. 10, article no. 102001, 2002.

[49] P. Ciafaloni and D. Comelli, "Electroweak evolution equations," *Journal of High Energy Physics*, vol. 2005, no. 11, article no. 22, 2005.

[50] C. W. Bauer, N. Ferland, and B. R. Webber, "Standard model parton distributions at very high energies," *Journal of High Energy Physics*, vol. 2017, no. 8, article no. 36, 2017.

[51] B. Fornal, A. V. Manohar, and W. J. Waalewijn, "Electroweak gauge boson parton distribution functions," *Journal of High Energy Physics*, vol. 2018, no. 5, article no. 106, 2018.

[52] A. V. Manohar and W. J. Waalewijn, "Electroweak logarithms in inclusive cross sections," *Journal of High Energy Physics*, vol. 2018, no. 8, article no. 137, 2018.

Hindawi
Advances in High Energy Physics
Volume 2019, Article ID 6734293, 20 pages
https://doi.org/10.1155/2019/6734293

Review Article

$\pi - N$ Drell-Yan Process in TMD Factorization

Xiaoyu Wang [1] **and Zhun Lu** [2]

[1] *School of Physics and Engineering, Zhengzhou University, Zhengzhou, Henan 450001, China*
[2] *School of Physics, Southeast University, Nanjing 211189, China*

Correspondence should be addressed to Zhun Lu; zhunlu@seu.edu.cn

Received 16 November 2018; Accepted 9 January 2019; Published 22 January 2019

Guest Editor: Zhongbo Kang

This article presents the review of the current understanding on the pion-nucleon Drell-Yan process from the point of view of the TMD factorization. Using the evolution formalism for the unpolarized and polarized TMD distributions developed recently, we provide the theoretical expression of the relevant physical observables, namely, the unpolarized cross section, the Sivers asymmetry, and the $\cos 2\phi$ asymmetry contributed by the double Boer-Mulders effects. The corresponding phenomenology, particularly at the kinematical configuration of the COMPASS πN Drell-Yan facility, is displayed numerically.

1. Introduction

After the first observation of the $\mu^+\mu^-$ lepton pairs produced in pN collisions [1], the process was interpreted that a quark and an antiquark from each initial hadron annihilate into a virtual photon, which in turn decays into a lepton pair [2]. This explanation makes the process an ideal tool to explore the internal structure of both the beam and target hadrons. Since then, a wide range of studies on this (Drell-Yan) process have been carried out. In particular, the πN Drell-Yan process has the unique capability to pin down the partonic structure of the pion, which is an unstable particle and therefore cannot serve as a target in deep inelastic scattering processes. Several pion-induced experiments have been carried out, such as the NA10 experiment at CERN [3–6], the E615 [7], E444 [8], and E537 [9] experiments at Fermilab three decades ago. These experimental measurements have provided plenty of data, which have been used to considerably constrain the distribution function of the pion meson. Recently, a new pion-induced Drell-Yan program with polarized target was also proposed [10] at the COMPASS of CERN, and the first data using a high-intensity π beam of 190 GeV colliding on a NH_3 target has already come out [11].

Bulk of the events in the Drell-Yan reaction are from the region where the transverse momentum of the dilepton $q_\perp$ is much smaller than the mass Q of the virtual vector boson; thus the intrinsic transverse momenta of initial partons become relevant. It is also the most interesting regime where a lot of intriguing physics arises. Moreover, in the small $q_\perp$ region ($q_\perp \sim \Lambda_{QCD}$), the fixed-order calculations of the cross sections in the collinear picture fail, leading to large double logarithms of the type $\alpha \ln^2(q_\perp^2/Q^2)$. It is necessary to resum such logarithmic contributions to all orders in the strong coupling α_s to obtain a reliable result. The standard approach for such resummation is the Collins-Soper-Sterman (CSS) formalism [12], originated from previous work on the Drell-Yan process and the e^+e^- annihilation three decades ago. In recent years the CSS formalism has been successfully applied to develop a factorization theorem [13–15] in which the gauge-invariant [16–19] transverse momentum dependent (TMD) parton distribution functions or fragmentation functions (collectively called TMDs) [20, 21] play a central role. From the point of view of TMD factorization [12, 13, 15, 22], physical observables can be written as convolutions of a factor related to hard scattering and well-defined TMDs. After solving the evolution equations, the TMDs at fixed energy scale can be expressed as a convolution of their collinear counterparts and perturbatively calculable coefficients in the perturbative region, and the evolution from one energy scale to another energy scale is included in the exponential factor of the so-called Sudakov-like form factors [12, 15, 23, 24]. The TMD factorization has been widely applied to various high

energy processes, such as the semi-inclusive deep inelastic scattering (SIDIS) [14, 15, 22, 23, 25, 26], e^+e^- annihilation [15, 27, 28], Drell-Yan [15, 29], and W/Z production in hadron collision [12, 15, 30]. The TMD factorization can be also extended to the moderate $q_\perp$ region where an equivalence [31, 32] between the TMD factorization and the twist-3 collinear factorization is found.

One of the most important observables in the polarized Drell-Yan process is the Sivers asymmetry. It is contributed by the so-called Sivers function [33], a time-reversal-odd (T-odd) distribution describing the asymmetric distribution of unpolarized quarks inside a transversely polarized nucleon through the correlation between the quark transverse momentum and the nucleon transverse spin. Remarkably, QCD predicts that the sign of the Sivers function changes in SIDIS with respect to the Drell-Yan process [16, 34, 35]. The verification of this sign change [36–41] is one of the most fundamental tests of our understanding of the QCD dynamics and the factorization schemes, and it is also the main pursue of the existing and future Drell-Yan facilities [10, 11, 42–45]. The advantage of the πN Drell-Yan measurement at COMPASS is that almost the same setup [11, 46] is used in SIDIS and Drell-Yan processes, which may reduce the uncertainty in the extraction of the Sivers function. In particular, the COMPASS Collaboration measured for the first time the transverse-spin-dependent azimuthal asymmetries [11] in the $\pi^- N$ Drell-Yan process.

Another important observable in the Drell-Yan process is the $\cos 2\phi$ angular asymmetry, where ϕ corresponds to the azimuthal angle of the dilepton. The fixed-target measurements from the NA10 and E615 collaborations showed that the unpolarized cross section possesses large $\cos 2\phi$ asymmetry, which violates the Lam-Tung relation [47]. Similar violation has also been observed in the pp colliders at Tevatron [48] and LHC [49]. It has been explained from the viewpoints of higher-twist effect [50–53], the noncoplanarity effect [30, 54], and the QCD radiative effects at higher order [55, 56]. Another promising origin [57] for the violation of the Lam-Tung relation at low transverse momentum is the convolution of the two Boer-Mulders functions [58] from each hadron. The Boer-Mulders function is also a TMD distribution. As the chiral-odd partner of the Sivers function, it describes the transverse-polarization asymmetry of quarks inside an unpolarized hadron [57, 58], thereby allowing the probe of the transverse spin physics from unpolarized reaction.

This article aims at a review on the current status of our understanding on the Drell-Yan dilepton production at low transverse momentum, especially from the πN collision, based on the recent development of the TMD factorization. We will mainly focus on the phenomenology of the Sivers asymmetry as well as the $\cos 2\phi$ asymmetry from the double Boer-Mulders effect. In order to quantitatively understand various spin/azimuthal asymmetries in the πN Drell-Yan process, a particularly important step is to know in high accuracy the spin-averaged differential cross section of the same process with azimuthal angles integrated out, since it always appears in the denominator of the asymmetries' definition. Thus, the spin-averaged cross section will be also discussed in great details.

The remained content of the article is organised as follows. In Section 2, we will review the TMD evolution formalism of the TMDs, mostly following the approach established in [15]. Particularly, we will discuss in detail the extraction of the nonperturbative Sudakov form factor for the unpolarized TMD distribution of the proton/pion as well as that for the Sivers function. In Section 3, putting the evolved result of the TMD distributions into the TMD factorization formulae, we will present the theoretical expression of the physical observables, such as the unpolarized differential cross section, the Sivers asymmetry, and the $\cos 2\phi$ asymmetry contributed by the double Boer-Mulders effect. In Section 4, we present the numerical evolution results of the unpolarized TMD distributions and the Boer-Mulders function of the pion meson, as well as that of the Sivers function of the proton. In Section 5, we display the phenomenology of the physical observables (unpolarized differential cross section, the Sivers asymmetry, and the $\cos 2\phi$ asymmetry) in the πN Drell-Yan with TMD factorization at the kinematical configuration of the COMPASS experiments. We summarize the paper in Section 6.

2. The TMD Evolution of the Distribution Functions

In this section, we present a review on the TMD evolution of the distribution functions. Particularly, we provide the evolution formalism for the unpolarized distribution function f_1, transversity h_1, Sivers function $f_1^\perp$, and the Boer-Mulders function $h_1^\perp$ of the proton, as well as f_1 and $h_1^\perp$ of the pion meson, within the Collins-11 TMD factorization scheme [15].

In general, it is more convenient to solve the evolution equations for the TMD distributions in the coordinate space ($\mathbf{b}$ space) other than that in the transverse momentum $\mathbf{k}_\perp$ space, with $\mathbf{b}$ conjugate to $\mathbf{k}_\perp$ via Fourier transformation [12, 15]. The TMD distributions $\widetilde{F}(x, b; \mu, \zeta_F)$ in $\mathbf{b}$ space have two kinds of energy dependence, namely, μ is the renormalization scale related to the corresponding collinear PDFs, and ζ_F is the energy scale serving as a cutoff to regularize the light-cone singularity in the operator definition of the TMD distributions. Here, F is a shorthand for any TMD distribution function and the tilde denotes that the distribution is the one in $\mathbf{b}$ space. If we perform the inverse Fourier transformation on $\widetilde{F}(x, b; \mu, \zeta_F)$, we recover the distribution function in the transverse momentum space $F_{q/H}(x, k_\perp; \mu, \zeta_F)$, which contains the information about the probability of finding a quark with specific polarization, collinear momentum fraction x, and transverse momentum $k_\perp$ in a specifically polarized hadron H.

2.1. TMD Evolution Equations. The energy evolution for the ζ_F dependence of the TMD distributions is encoded in the Collins-Soper (CS) [12, 15, 63] equation:

$$\frac{\partial \ln \widetilde{F}(x, b; \mu, \zeta_F)}{\partial \sqrt{\zeta_F}} = \widetilde{K}(b; \mu), \tag{1}$$

while the μ dependence is driven by the renormalization group equation as

$$\frac{d\widetilde{K}}{d\ln\mu} = -\gamma_K\left(\alpha_s\left(\mu\right)\right), \tag{2}$$

$$\frac{d\ln\widetilde{F}\left(x,b;\mu,\zeta_F\right)}{d\ln\mu} = \gamma_F\left(\alpha_s\left(\mu\right);\frac{\zeta_F^2}{\mu^2}\right), \tag{3}$$

with α_s being the strong coupling at the energy scale μ, $\widetilde{K}$ being the CS evolution kernel, and γ_K, γ_F being the anomalous dimensions. The solutions of these evolution equations were studied in detail in [15, 63, 64]. Here, we will only discuss the final result. The overall structure of the solution for $\widetilde{F}(x,b;\mu,\zeta_F)$ is similar to that for the Sudakov form factor. More specifically, the energy evolution of TMD distributions from an initial energy μ to another energy Q is encoded in the Sudakov-like form factor S by the exponential form $\exp(-S)$

$$\widetilde{F}\left(x,b,Q\right) = \mathscr{F}\times e^{-S}\times\widetilde{F}\left(x,b,\mu\right), \tag{4}$$

where $\mathscr{F}$ is the factor related to the hard scattering. Hereafter, we will set $\mu = \sqrt{\zeta_F} = Q$ and express $\widetilde{F}(x,b;\mu = Q,\zeta_F = Q^2)$ as $\widetilde{F}(x,b;Q)$.

As the b-dependence of the TMDs can provide very useful information regarding the transverse momentum dependence of the hadronic 3D structure through Fourier transformation, it is of fundamental importance to study the TMDs in b space. In the small b region, the b dependence is perturbatively calculable, while in the large b region, the dependence turns to be nonperturbative and may be obtained from the experimental data. To combine the perturbative information at small b with the nonperturbative part at large b, a matching procedure must be introduced with a parameter $b_{\max}$ serving as the boundary between the two regions. The prescription also allows for a smooth transition from perturbative to nonperturbative regions and avoids the Landau pole singularity in $\alpha_s(\mu_b)$. A b-dependent function b_* is defined to have the property $b_* \approx b$ at low values of b and $b_* \approx b_{\max}$ at large b values. In this paper, we adopt the original CSS prescription [12]:

$$b_* = \frac{b}{\sqrt{1+b^2/b_{\max}^2}}, \quad b_{\max} < \frac{1}{\Lambda_{\mathrm{QCD}}}. \tag{5}$$

The typical value of $b_{\max}$ is chosen around 1 GeV^{-1} to guarantee that b_* is always in the perturbative region. Besides the CSS prescription, there were several different prescriptions in literature. In [65, 66] a function $b_{\min}(b)$ decreasing with increasing $1/Q$ was also introduced to match the TMD factorization with the fixed-order collinear calculations in the very small b region.

In the small b region $1/Q \ll b \ll 1/\Lambda_{\mathrm{QCD}}$, the TMD distributions at fixed energy μ can be expressed as the convolution of the perturbatively calculable coefficients and the corresponding collinear PDFs or the multiparton correlation functions [22, 67]

$$\widetilde{F}_{q/H}\left(x,b;\mu\right) = \sum_i C_{q\leftarrow i}\otimes F_{i/H}\left(x,\mu\right). \tag{6}$$

Here, $\otimes$ stands for the convolution in the momentum fraction x

$$\begin{aligned} &C_{q\leftarrow i}\otimes f_1^{i/H}\left(x,\mu\right)\\ &\quad\equiv\int_x^1\frac{d\xi}{\xi}C_{q\leftarrow i}\left(\frac{x}{\xi},b;\mu\right)f_1^{i/H}\left(\xi,\mu\right)\end{aligned} \tag{7}$$

and $f^{i/H}(x,\mu)$ is the corresponding collinear counterpart of flavor i in hadron H at the energy scale μ. The latter one could be a dynamic scale related to b_* by $\mu_b = c_0/b_*$, with $c_0 = 2e^{-\gamma_E}$ and the Euler Constant $\gamma_E \approx 0.577$ [22]. The perturbative hard coefficients $C_{q\leftarrow i}$, independent of the initial hadron type, have been calculated for the parton-target case [23, 68] as the series of (α_s/π) and the results have been presented in [67] (see also Appendix A of [23]).

2.2. Sudakov Form Factors for the Proton and the Pion. The Sudakov-like form factor S in (4) can be separated into the perturbatively calculable part S_{P} and the nonperturbative part S_{NP}

$$S = S_{\mathrm{P}} + S_{\mathrm{NP}}. \tag{8}$$

According to the studies in [26, 39, 69–71], the perturbative part of the Sudakov form factor S_P has the same result among different kinds of distribution functions, i.e., S_P is spin-independent. It has the general form

$$\begin{aligned} &S_{\mathrm{P}}\left(Q,b_*\right)\\ &\quad=\int_{\mu_b^2}^{Q^2}\frac{d\overline{\mu}^2}{\overline{\mu}^2}\left[A\left(\alpha_s\left(\overline{\mu}\right)\right)\ln\frac{Q^2}{\overline{\mu}^2}+B\left(\alpha_s\left(\overline{\mu}\right)\right)\right].\end{aligned} \tag{9}$$

The coefficients A and B in(9) can be expanded as the series of α_s/π:

$$A = \sum_{n=1}^{\infty}A^{(n)}\left(\frac{\alpha_s}{\pi}\right)^n, \tag{10}$$

$$B = \sum_{n=1}^{\infty}B^{(n)}\left(\frac{\alpha_s}{\pi}\right)^n. \tag{11}$$

Here, we list $A^{(n)}$ to $A^{(2)}$ and $B^{(n)}$ to $B^{(1)}$ up to the accuracy of next-to-leading-logarithmic (NLL) order [12, 23, 26, 69, 72, 73]:

$$A^{(1)} = C_F \tag{12}$$

$$A^{(2)} = \frac{C_F}{2}\left[C_A\left(\frac{67}{18}-\frac{\pi^2}{6}\right)-\frac{10}{9}T_R n_f\right] \tag{13}$$

$$B^{(1)} = -\frac{3}{2}C_F. \tag{14}$$

For the nonperturbative form factor S_{NP}, it can not be analytically calculated by the perturbative method, which means it has to be parameterized to obtain the evolution information in the nonperturbative region.

The general form of $S_{\mathrm{NP}}(Q;b)$ was suggested as [12]

$$S_{\mathrm{NP}}\left(Q;b\right) = g_2\left(b\right)\ln\frac{Q}{Q_0}+g_1\left(b\right). \tag{15}$$

The nonperturbative functions $g_1(b)$ and $g_2(b)$ are functions of the impact parameter b and depend on the choice of $b_{\max}$.

To be more specific, $g_2(b)$ contains the information on the large b behavior of the evolution kernel $\widetilde{K}$. Also, according to the power counting analysis in [74], $g_2(b)$ shall follow the power behavior as b^2 at small-b region, which can be an essential constraint for the parameterization of $g_2(b)$. The well-known Brock-Landry-Nadolsky-Yuan (BLNY) fit parameterizes $g_2(b)$ as $g_2 b^2$ with g_2 a free parameter [72]. We note that $g_2(b)$ is universal for different types of TMDs and does not depend on the particular process, which is an important prediction of QCD factorization theorems involving TMDs [15, 23, 39, 75]. The nonperturbative function $g_1(b)$ contains information on the intrinsic nonperturbative transverse motion of bound partons, namely, it should depend on the type of hadron and the quark flavor as well as x for TMD distributions. As for the TMD fragmentation functions, it may depend on z_h, the type of the produced hadron, and the quark flavor. In other words, $g_1(b)$ depends on the specific TMDs.

There are several extractions for S_{NP} in literature, we review some often-used forms below.

The original BLNY fit parameterized S_{NP} as [72]

$$\left(g_1 + g_2 \ln\left(\frac{Q}{2Q_0}\right) + g_1 g_3 \ln\left(100 x_1 x_2\right)\right) b^2, \tag{16}$$

where x_1 and x_2 are the longitudinal momentum fractions of the incoming hadrons carried by the initial state quark and antiquark. The BLNY parameterization proved to be very reliable to describe Drell-Yan data and $W^{\pm}, Z$ boson production [72]. However, when the parameterization is extrapolated to the typical SIDIS kinematics in HERMES and COMPASS, the transverse momentum distribution of hadron can not be described by the BLNY-type fit [76, 77].

Inspired by [72, 78], a widely used parameterization of S_{NP} for TMD distributions or fragmentation functions was proposed [39, 67, 72, 78–80]

$$S_{\mathrm{NP}}^{\mathrm{pdf/ff}} = b^2 \left(g_1^{\mathrm{pdf/ff}} + \frac{g_2}{2} \ln\frac{Q}{Q_0}\right), \tag{17}$$

where the factor 1/2 in front of g_2 comes from the fact that only one hadron is involved for the parameterization of $S_{\mathrm{NP}}^{\mathrm{pdf/ff}}$, while the parameter in [78] is for pp collisions. The parameter $g_1^{\mathrm{pdf/ff}}$ in (17) depends on the type of TMDs, which can be regarded as the width of intrinsic transverse momentum for the relevant TMDs at the initial energy scale Q_0 [23, 73, 81]. Assuming a Gaussian form, one can obtain

$$\begin{aligned} g_1^{\mathrm{pdf}} &= \frac{\left\langle k_\perp^2 \right\rangle_{Q_0}}{4}, \\ g_1^{\mathrm{ff}} &= \frac{\left\langle p_T^2 \right\rangle_{Q_0}}{4z^2}, \end{aligned} \tag{18}$$

where $\langle k_\perp^2 \rangle_{Q_0}$ and $\langle p_T^2 \rangle_{Q_0}$ represent the relevant averaged intrinsic transverse momenta squared for TMD distributions and TMD fragmentation functions at the initial scale Q_0, respectively.

Since the original BLNY fit fails to simultaneously describe Drell-Yan process and SIDIS process, in [77] the authors proposed a new form for S_{NP} which releases the tension between the BLNY fit to the Drell-Yan (such as W, Z and low energy Drell-Yan pair productions) data and the fit to the SIDIS data from HERMES/COMPASS in the CSS resummation formalism. In addition, the x-dependence in (16) was separated with a power law behavior assumption: $(x_0/x)^{\lambda}$, where x_0 and λ are the fixed parameters as $x_0 = 0.01$ and $\lambda = 0.2$. The two different behaviors (logarithmic in (16) and power law) will differ in the intermediate x regime. Reference [76] showed that a direct integration of the evolution kernel from low Q to high Q led to the form of $\ln(Q)$ term as $\ln(b/b_*)\ln(Q)$ and could describe the SIDIS and Drell-Yan data with Q values ranging from a few GeV to 10 GeV. Thus, the $g_2(b)$ term was modified to the form of $\ln(b/b_*)$ and the functional form of S_{NP} extracted in [77] turned to the form

$$\begin{aligned} &g_1 b^2 + g_2 \ln\left(\frac{b}{b_*}\right) \ln\left(\frac{Q}{Q_0}\right) \\ &\quad + g_3 b^2 \left(\left(\frac{x_0}{x_1}\right)^{\lambda} + \left(\frac{x_0}{x_2}\right)^{\lambda}\right). \end{aligned} \tag{19}$$

At small b region (b is much smaller than $b_{\max}$), the parameterization of the $g_2(b)$ term $g_2 \ln(b/b_*)$ can be approximated as $b^2/(2b_{\max}^2)$, which satisfied the constraint of the b^2 behavior for $g_2(b)$. However, at large b region, the logarithmic behavior will lead to different predictions on the Q^2 dependence, since the Gaussian-type parameterization suggests that it is strongly suppressed [82]. This form has been suggested in an early research by Collins and Soper [83], but has not yet been adopted in any phenomenological study until the study in [77]. The comparison between the original BLNY parameterization and this form with the experimental data of Drell-Yan type process has shown that the new form of S_{NP} can fit with the data as equally well as the original BLNY parameterization.

In [66], the $g_2(b)$ function was parameterized as $g_2 b^2$, following the BLNY convention. Furthermore, in the function $g_1(b)$, the Gaussian width also depends on x. The authors simultaneously fit the experimental data of SIDIS process from HERMES and COMPASS Collaborations, the Drell-Yan events at low energy, and the Z boson production with totally 8059 data points. The extraction can describe the data well in the regions where TMD factorization is supposed to hold.

To study the pion-nucleon Drell-Yan data, it is also necessary to know the nonperturbative Sudakov form factor for the pion meson. In [59], we extended the functional form for the proton TMDs [77] to the case of the pion TMDs:

$$S_{\mathrm{NP}}^{f_1^{q/\pi}} = g_1^{q/\pi} b^2 + g_2^{q/\pi} \ln\frac{b}{b_*} \ln\frac{Q}{Q_0}, \tag{20}$$

with $g_1^{q/\pi}$ and $g_2^{q/\pi}$ the free parameters. Adopting the functional form of S_{NP} in (20), for the first time, we performed the extraction [59] of the nonperturbative Sudakov form factor for the unpolarized TMD PDF of pion meson using

the experimental data in the $\pi^- p$ Drell-Yan process collected by the E615 Collaboration at Fermilab [7, 84]. The data fitting was performed by the package MINUIT [85, 86], through a least-squares fit:

$$\chi^2(\boldsymbol{\alpha}) = \sum_{i=1}^{M}\sum_{j=1}^{N_i} \frac{\left(\text{theo}\left(q_{\perp ij}, \boldsymbol{\alpha}\right) - \text{data}_{ij}\right)^2}{\text{err}_{ij}^2}. \tag{21}$$

The total number of data in our fit is $N = \sum_i^8 N_i = 96$. Since the TMD formalism is valid in the region $q_\perp \ll Q$, we did a simple data selection by removing the data in the region $q_\perp > 3$ GeV. We performed the fit by minimizing the chi-square in (21), and we obtained the following values for the two parameters:

$$\begin{aligned} g_1^{q/\pi} &= 0.082 \pm 0.022, \\ g_2^{q/\pi} &= 0.394 \pm 0.103, \end{aligned} \tag{22}$$

with $\chi^2/\text{d.o.f} = 1.64$.

Figure 1 plots the $q_\perp$-dependent differential cross section (solid line) calculated from the fitted values for $g_1^{q/\pi}$ and $g_2^{q/\pi}$ in (22) at the kinematics of E615 at different x_F bins. The full squares with error bars denote the E615 data for comparison. As Figure 1 demonstrates, a good fit is obtained in the region $x_F < 0.8$.

From the fitted result, we find that the value of the parameter $g_1^{q/\pi}$ is smaller than the parameter $g_1^{q/p}$ extracted in [77] which used the same parameterized form. For the parameter $g_2^{q/\pi}$ we find that its value is very close to that of the parameter $g_2^{q/p}$ for the proton [77] (here $g_2^{q/p} = g_2/2 = 0.42$). This may confirm that g_2 should be universal, e.g., g_2 is independent on the hadron type. Similar to the case of the proton, for the pion meson g_2^π is several times larger than g_1^π. We note that a form of $S_{\text{NP}}^{f_{1,q/\pi}}$ motivated by the NJL model was given in [87].

2.3. Solutions for Different TMDs. After solving the evolution equations and incorporating the Sudakov form factor, the scale-dependent TMD distribution function $\widetilde{F}$ of the proton and the pion in b space can be rewritten as

$$\begin{aligned} &\widetilde{F}_{q/p}(x, b; Q) \\ &\quad = e^{-(1/2)S_{\text{p}}(Q,b_*) - S_{\text{NP}}^{F_{q/p}}(Q,b)} \mathscr{F}\left(\alpha_s(Q)\right) \sum_i C_{q\longleftarrow i} \\ &\qquad \otimes F_{i/p}(x, \mu_b), \end{aligned} \tag{23}$$

$$\begin{aligned} &\widetilde{F}_{q/\pi}(x, b; Q) \\ &\quad = e^{-(1/2)S_{\text{p}}(Q,b_*) - S_{\text{NP}}^{F_{q/\pi}}(Q,b)} \mathscr{F}\left(\alpha_s(Q)\right) \sum_i C_{q\longleftarrow i} \\ &\qquad \otimes F_{i/\pi}(x, \mu_b). \end{aligned} \tag{24}$$

Here, $F_{i/H}(x, \mu_b)$ is the corresponding collinear distributions at the initial energy scale μ_b. To be more specific, for the unpolarized distribution function $f_{1,q/H}$ and transversity distribution function $h_{1,q/H}$, the collinear distributions $F_{i/H}(x, \mu_b)$ are the integrated distribution functions $f_{1,q/H}(x, \mu_b)$ and $h_{1,q/H}(x, \mu_b)$. As for the Boer-Mulders function and Sivers function, the collinear distributions are the corresponding multiparton correlation functions. Thus, the unpolarized distribution function of the proton and pion in b space can be written as

$$\begin{aligned} &\widetilde{f}_{1,q/p}(x, b; Q) \\ &\quad = e^{-(1/2)S_{\text{pert}}(Q,b_*) - S_{\text{NP}}^{f_{1,q/p}}(Q,b)} \mathscr{F}\left(\alpha_s(Q)\right) \sum_i C_{q\longleftarrow i} \\ &\qquad \otimes f_{1,i/p}(x, \mu_b) \end{aligned} \tag{25}$$

$$\begin{aligned} &\widetilde{f}_{1,q/\pi}(x, b; Q) \\ &\quad = e^{-(1/2)S_{\text{pert}}(Q,b_*) - S_{\text{NP}}^{f_{1,q/\pi}}(Q,b)} \mathscr{F}\left(\alpha_s(Q)\right) \sum_i C_{q\longleftarrow i} \\ &\qquad \otimes f_{1,i/\pi}(x, \mu_b). \end{aligned} \tag{26}$$

If we perform a Fourier transformation on the $\widetilde{f}_{1,q/H}(x, b; Q)$, we can obtain the distribution function in $k_\perp$ space as

$$f_{1,q/p}(x, k_\perp; Q) = \int_0^\infty \frac{dbb}{2\pi} J_0(k_\perp b)\, \widetilde{f}_{1,q/p}(x, b; Q), \tag{27}$$

$$f_{1,q/\pi}(x, k_\perp; Q) = \int_0^\infty \frac{dbb}{2\pi} J_0(k_\perp b)\, \widetilde{f}_{1,q/\pi}(x, b; Q). \tag{28}$$

where J_0 is the Bessel function of the first kind, and $k_\perp = |\mathbf{k}_\perp|$.

Similarly, the evolution formalism of the proton transversity distribution in b space and $k_\perp$-space can be obtained as [75]

$$\begin{aligned} &\widetilde{h}_{1,q/p}(x, b; Q) \\ &\quad = e^{-(1/2)S_{\text{p}}(Q,b_*) - S_{\text{NP}}^{h_1}(Q,b)} \mathscr{H}\left(\alpha_s(Q)\right) \sum_i \delta C_{q\longleftarrow i} \\ &\qquad \otimes h_{1,i/p}(x, \mu_b), \end{aligned} \tag{29}$$

$$h_{1,q/p}(x, k_\perp; Q) = \int_0^\infty \frac{dbb}{2\pi} J_0(k_\perp b)\, \widetilde{h}_{1,q/p}(x, b; Q), \tag{30}$$

where $\mathscr{H}$ is the hard factor, and $\delta C_{q\longleftarrow i}$ is the coefficient convoluted with the transversity. The TMD evolution formalism in (30) has been applied in [75] to extract the transversity distribution from the SIDIS data.

The Sivers function and Boer-Mulders function, which are T-odd, can be expressed as follows in b-space [39]

$$\begin{aligned} &\widetilde{f}_{1T,q/H}^{\perp\alpha(\text{DY})}(x, b; \mu, \zeta_F) \\ &\quad = \int d^2\mathbf{k}_\perp e^{-i\vec{\mathbf{k}}_\perp \cdot \vec{\mathbf{b}}} \frac{k_\perp^\alpha}{M_p} f_{1T,q/H}^{\perp(\text{DY})}(x, \mathbf{k}_\perp; \mu), \end{aligned}$$

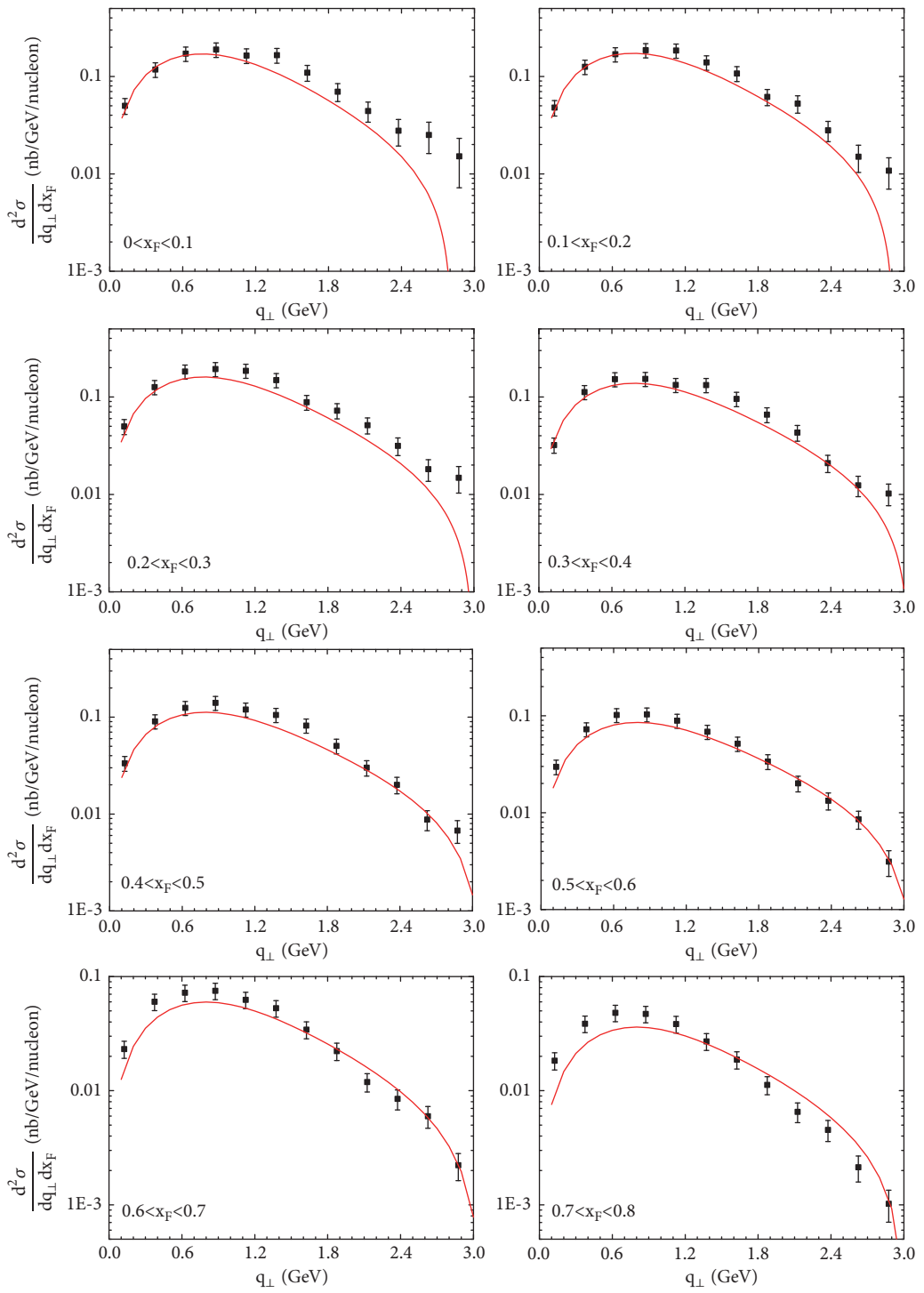

FIGURE 1: The fitted cross section (solid line) of pion-nucleon Drell-Yan as functions of $q_\perp$, compared with the E615 data (full square), for different x_F bins in the range $0 < x_F < 0.8$. The error bars shown here include the statistical error and the 16% systematic error. Figure from [59].

$$\widetilde{h}_{1,q/H}^{\perp\alpha(\mathrm{DY})}(x,b;\mu,\zeta_F) = \int d^2\mathbf{k}_\perp e^{-i\vec{\mathbf{k}}_\perp\cdot\vec{\mathbf{b}}}\frac{k_\perp^\alpha}{M_p}h_{1,q/H}^{\perp(\mathrm{DY})}(x,\mathbf{k}_\perp;\mu). \tag{31}$$

Here, the superscript "DY" represents the distributions in the Drell-Yan process. Since QCD predicts that the sign of the distributions changes in the SIDIS process and Drell-Yan process, for the distributions in SIDIS process, there has to be an extra minus sign regard to $f_{1T,q/H}^{\perp(\mathrm{DY})}$ and $h_{1,q/H}^{\perp(\mathrm{DY})}$.

Similar to what has been done to the unpolarized distribution function and transversity distribution function, in the low b region, the Sivers function $\widetilde{f}_{1T,q/H}^{\perp\alpha(\mathrm{DY})}$ can also be expressed as the convolution of perturbatively calculable hard coefficients and the corresponding collinear correlation functions as [69, 88]

$$\widetilde{f}_{1T,q/H}^{\perp\alpha(\mathrm{DY})}(x,b;\mu) = \left(\frac{-ib^{\alpha}}{2}\right)\sum_{i}\Delta C_{q\longleftarrow i}^{T}\otimes f_{i/p}^{(3)}\left(x',x'';\mu\right). \tag{32}$$

Here, $f_{i/p}^{(3)}(x',x'')$ denotes the twist-three quark-gluon-quark or trigluon correlation functions, among which the transverse spin-dependent Qiu-Sterman matrix element $T_{q,F}(x',x'')$ [89–91] is the most relevant one. Assuming that the Qiu-Sterman function $T_{q,F}(x,x)$ is the main contribution, the Sivers function in b-space becomes

$$\widetilde{f}_{1T,q/H}^{\perp\alpha(\mathrm{DY})}(x,b;Q) = \left(\frac{-ib^{\alpha}}{2}\right)\mathscr{F}_{\mathrm{Siv}}\left(\alpha_s(Q)\right)\sum_{i}\Delta C_{q\longleftarrow i}^{T} \otimes T_{i/H,F}(x,x;\mu_b)\, e^{-S_{\mathrm{NP}}^{\mathrm{siv}}-(1/2)S_{\mathrm{P}}}, \tag{33}$$

where $\mathscr{F}_{\mathrm{Siv}}$ is the factor related to the hard scattering. The Boer-Mulders function in b-space follows the similar result for the Sivers function as:

$$\widetilde{h}_{1,q/H}^{\alpha\perp(\mathrm{DY})}(x,b;Q) = \left(\frac{-ib^{\alpha}}{2}\right)\mathscr{H}_{\mathrm{BM}}\left(\alpha_s(Q)\right)\sum_{i}C_{q\longleftarrow i}^{\mathrm{BM}} \otimes T_{i/H,F}^{(\sigma)}(x,x;\mu_b)\, e^{-S_{\mathrm{NP}}^{\mathrm{BM}}-(1/2)S_{\mathrm{P}}}, \tag{34}$$

Here, $C_{q\longleftarrow i}^{\mathrm{BM}}$ stands for the flavor-dependent hard coefficients convoluted with $T_{i/H,F}^{(\sigma)}$, $\mathscr{H}_{\mathrm{BM}}$ the hard scattering factor and $T_{i/H,F}^{(\sigma)}(x,x;\mu_b)$ denotes the chiral-odd twist-3 collinear correlation function. After performing the Fourier transformation back to the transverse momentum space, one can get the Sivers function and the Boer-Mulders function as

$$\frac{k_{\perp}}{M_H}f_{1T,q/H}^{\perp}(x,k_{\perp};Q) = \int_0^{\infty}db\left(\frac{b^2}{2\pi}\right)J_1(k_{\perp}b)\,\mathscr{F}_{\mathrm{Siv}}\left(\alpha_s(Q)\right)\sum_{i}\Delta C_{q\longleftarrow i}^{T} \otimes f_{1T,i/H}^{\perp(1)}(x,\mu_b)\, e^{-S_{\mathrm{NP}}^{\mathrm{siv}}-(1/2)S_{\mathrm{P}}}, \tag{35}$$

$$\frac{k_{\perp}}{M_H}h_{1,q/H}^{\perp}(x,k_{\perp};Q) = \int_0^{\infty}db\left(\frac{b^2}{2\pi}\right)J_1(k_{\perp}b)\,\mathscr{H}_{\mathrm{BM}}\left(\alpha_s(Q)\right)\sum_{i}C_{q\longleftarrow i}^{\mathrm{BM}} \otimes h_{1,i/H}^{\perp(1)}(x;\mu_b)\, e^{-S_{\mathrm{NP}}^{\mathrm{BM}}-(1/2)S_{\mathrm{P}}}, \tag{36}$$

and $T_{q,F}(x,x;\mu_b)$ and $T_{i/H,F}^{(\sigma)}(x,x;\mu_b)$ are related to Sivers function and Boer-Mulders function as [69, 88]

$$T_{q/H,F}(x,x) = \int d^2k_{\perp}\frac{\left|k_{\perp}^2\right|}{M_H}f_{1T,q/H}^{\perp(\mathrm{DY})}(x,k_{\perp}) = 2M_H f_{1T,q/H}^{\perp(1)(\mathrm{DY})}(x), \tag{37}$$

$$T_{q/H,F}^{(\sigma)}(x,x) = \int d^2k_{\perp}\frac{\left|k_{\perp}^2\right|}{M_H}h_{1,q/H}^{\perp(\mathrm{DY})}(x,k_{\perp}) = 2M_H h_{1,q/H}^{\perp(1)(\mathrm{DY})}(x). \tag{38}$$

The TMD evolution formalism in (35) has been applied to extract [39, 70, 81, 92, 93] the Sivers function. The similar formalism in (36) could be used to improve the previous extractions of the proton Boer-Mulders function [62, 94–96] and future extraction of the pion Boer-Mulders function.

3. Physical Observables in πN Drell-Yan Process within TMD Factorization

In this section we will set up the necessary framework for physical observables in π-N Drell-Yan process within TMD factorization by considering the evolution effects of the TMD distributions, following the procedure developed in [15].

In Drell-Yan process

$$H_A(P_{\pi}) + H_B(P_N) \longrightarrow \gamma^*(q) + X \longrightarrow l^+(\ell) + l^-\left(\ell'\right) + X, \tag{39}$$

$P_{\pi/N}$ and q denote the momenta of the incoming hadron π/N and the virtual photon, respectively; q is a time-like vector, namely, $Q^2 = q^2 > 0$, which is the invariant mass square of the final-state lepton pair. One can define the following useful kinematical variables to express the cross section:

$$s = \left(P_{\pi} + P_N\right)^2, \quad x_{\pi/N} = \frac{Q^2}{2P_{\pi/N}\cdot q}, \quad x_F = \frac{2q_L}{s} = x_{\pi} - x_N, \quad \tau = \frac{Q^2}{s} = x_{\pi}x_N, \quad y = \frac{1}{2}\ln\frac{q^+}{q^-} = \frac{1}{2}\ln\frac{x_{\pi}}{x_N}, \tag{40}$$

where s is the center-of-mass energy squared; $x_{\pi/N}$ is the light-front momentum fraction carried by the annihilating quark/antiquark in the incoming hadron π/N; q_L is the longitudinal momentum of the virtual photon in the c.m. frame of the incident hadrons; x_F is the Feynman x variable,

which corresponds to the longitudinal momentum fraction carried by the lepton pair; and y is the rapidity of the lepton pair. Thus, $x_{\pi/N}$ is expressed as the function of x_F, τ and of y, τ

$$x_{\pi/N} = \frac{\pm x_F + \sqrt{x_F^2 + 4\tau}}{2}, \qquad x_{\pi/N} = \sqrt{\tau} e^{\pm y}. \tag{41}$$

3.1. Differential Cross Section for Unpolarized Drell-Yan Process. The differential cross section formulated in TMD factorization is usually expressed in the b-space to guarantee conservation of the transverse momenta of the emitted soft gluons. Later on it can be transformed back to the transverse momentum space to represent the experimental observables. We will introduce the physical observables in the following part of this section.

The general differential cross section for the unpolarized Drell-Yan process can be written as [12]

$$\frac{d^4\sigma_{UU}}{dQ^2 dy d^2\mathbf{q}_\perp} = \sigma_0 \int \frac{d^2b}{(2\pi)^2} e^{i\vec{\mathbf{q}}_\perp \cdot \vec{\mathbf{b}}} \widetilde{W}_{UU}(Q;b) + Y_{UU}(Q, q_\perp) \tag{42}$$

where $\sigma_0 = 4\pi\alpha_{em}^2/3N_C s Q^2$ is the cross section at tree level with α_{em} the fine-structure constant, $\widetilde{W}(Q;b)$ is the structure function in the b-space which contains all-order resummation results and dominates in the low $q_\perp$ region ($q_\perp \ll Q$); and the Y term provides necessary correction at $q_\perp \sim Q$. In this work we will neglect the Y-term, which means that we will only consider the first term on the r.h.s of (42).

In general, TMD factorization [15] aims at separating well-defined TMD distributions such that they can be used in different processes through a universal way and expressing the scheme/process dependence in the corresponding hard factors. Thus, $\widetilde{W}(Q;b)$ can be expressed as [97]

$$\widetilde{W}_{UU}(Q;b) = H_{UU}(Q;\mu) \cdot \sum_{q,\overline{q}} e_q^2 \tilde{f}^{\text{sub}}_{q/\pi}(x_\pi, b; \mu, \zeta_F)\, \tilde{f}^{\text{sub}}_{q/p}(x_p, b; \mu, \zeta_F), \tag{43}$$

where $\tilde{f}^{\text{sub}}_{q/H}$ is the subtracted distribution function in the b space and $H_{UU}(Q;\mu)$ is the factor associated with hard scattering. The superscript "sub" represents the distribution function with the soft factor subtracted. The subtraction guarantees the absence of light-cone singularities in the TMDs and the self-energy divergencies of the soft factors [15, 22]. However, the way to subtract the soft factor in the distribution function and the hard factor $H_{UU}(Q;\mu)$ depends on the scheme to regulate the light-cone singularity in the TMD definition [12, 14, 15, 22, 98–103], leading to the scheme dependence in the TMD factorization. In literature, several different schemes are used [97]: the CSS scheme [12, 22], the Collins-11 (JCC) scheme [15], the Ji-Ma-Yuan (JMY) scheme [13, 14], and the lattice scheme [103]. Although different schemes are adopted, the final results of the structure functions $\widetilde{W}(Q;b)$ as well as the differential cross section should not depend on a specific scheme. In the following we will apply the JCC and JMY schemes to display the scheme-independence of the unpolarized differential cross section.

The hard $H_{UU}(Q;\mu)$ have different forms in the JCC and JMY schemes:

$$H^{\text{JCC}}(Q;\mu) = 1 + \frac{\alpha_s(\mu)}{2\pi} C_F \left(3\ln\frac{Q^2}{\mu^2} - \ln^2\frac{Q^2}{\mu^2} + \pi^2 - 8 \right), \tag{44}$$

$$H^{\text{JMY}}(Q;\mu,\rho) = 1 + \frac{\alpha_s(\mu)}{2\pi} C_F \left(\left(1 + \ln\rho^2\right)\ln\frac{Q^2}{\mu^2} - \ln\rho^2 + \ln^2\rho + 2\pi^2 - 4 \right). \tag{45}$$

Like ζ_F, here ρ is another variable to regulate the light-cone singularity of TMD distributions. The scheme dependence of the distribution function is manifested in the hard factor $\mathscr{F}(\alpha_s(Q))$, which has the following forms in different schemes:

$$\widetilde{\mathscr{F}}^{\text{JCC}}(\alpha_s(Q)) = 1 + \mathcal{O}\left(\alpha_s^2\right), \tag{46}$$

$$\widetilde{\mathscr{F}}^{\text{JMY}}(\alpha_s(Q), \rho) = 1 + \frac{\alpha_s}{2\pi} C_F \left[\ln\rho - \frac{1}{2}\ln^2\rho - \frac{\pi^2}{2} - 2 \right], \tag{47}$$

The C coefficients in (25) and (26) do not depend on the types of initial hadrons and are calculated for the parton-target case [23, 68] with the results presented in [67] (see also Appendix A of [23])

$$C_{q\leftarrow q'}(x, b; \mu, \zeta_F) = \delta_{qq'} \left[\delta(1-x) + \frac{\alpha_s}{\pi} \left(\frac{C_F}{2}(1-x) \right) \right], \tag{48}$$

$$C_{q\leftarrow g}(x, b; \mu, \zeta_F) = \frac{\alpha_s}{\pi} T_R x(1-x), \tag{49}$$

where $C_F = (N_C^2 - 1)/(2N_C)$, $T_R = 1/2$.

One can absorb the scheme-dependent hard factors $H_{UU}(Q;\mu)$ and $\mathscr{F}$ of the TMD distributions into the C-functions using

$$C'_{j\leftarrow i} = C_{j\leftarrow i} \times \mathscr{F} \times \sqrt{H_{UU}(Q;\mu = Q)}. \tag{50}$$

The results for the splitting to quark are

$$C'_{q\leftarrow q'}(x, b; \mu_b) = \delta_{qq'} \left[\delta(1-x) + \frac{\alpha_s}{\pi} \left(\frac{C_F}{2}(1-x) + \frac{C_F}{4}\left(\pi^2 - 8\right)\delta(1-x) \right) \right], \tag{51}$$

$$C'_{q\leftarrow g}(x, b; \mu_b) = \frac{\alpha_s}{\pi} T_R x(1-x). \tag{52}$$

The new C-coefficients turn out to be scheme independent (independent on ρ) [104] but process dependent [105, 106].

With the new C-coefficients in hand, one can obtain the structure functions $\widetilde{W}_{UU}(Q;b)$ in b-space as

$$\widetilde{W}_{UU}(Q;b) = e^{-S_{\rm pert}(Q^2,b)-S_{\rm NP}^{f_1^{q/\pi}}(Q^2,b)-S_{\rm NP}^{f_1^{q/p}}(Q^2,b)} \times \sum_{q,\overline{q}} e_q^2 C'_{q\leftarrow i} \otimes f_{i/\pi^-}(x_1,\mu_b)\, C'_{\overline{q}\leftarrow j} \otimes f_{j/p}(x_2,\mu_b). \quad (53)$$

After performing the Fourier transformation, we can get the differential cross section as

$$\frac{d^4\sigma}{dQ^2 dy d^2\mathbf{q}_\perp} = \sigma_0 \int_0^\infty \frac{dbb}{2\pi} J_0(q_\perp b) \times \widetilde{W}_{UU}(Q;b), \quad (54)$$

where J_0 is the zeroth order Bessel function of the first kind.

3.2. The Sivers Asymmetry. In the Drell-Yan process with a π beam colliding on the transversely polarized nucleon target, an important physical observable is the Sivers asymmetry, as it can test the sign change of the Sivers function between SIDIS and Drell-Yan processes, a fundamental prediction in QCD. The future precise measurement of the Sivers asymmetry in πN Drell-Yan in a wide kinematical region can be also used to extract the Sivers function. The Sivers asymmetry is usually defined as [39]

$$A_{UT} = \frac{d^4\Delta\sigma/dQ^2 dy d^2\mathbf{q}_\perp}{d^4\sigma/dQ^2 dy d^2\mathbf{q}_\perp}, \quad (55)$$

where $d^4\sigma/dQ^2 dy d^2\mathbf{q}_\perp$ and $d^4\Delta\sigma/dQ^2 dy d^2\mathbf{q}_\perp$ are the spin-averaged (unpolarized) and spin-dependent differential cross section, respectively. The latter one has the general form in the TMD factorization [39, 69, 88]

$$\frac{d^4\Delta\sigma}{dQ^2 dy d^2\mathbf{q}_\perp} = \sigma_0 \epsilon_\perp^{\alpha\beta} S_\perp^\alpha \int \frac{d^2b}{(2\pi)^2} e^{i\vec{\mathbf{q}}_\perp\cdot\vec{\mathbf{b}}} \widetilde{W}_{UT}^\beta(Q;b) + Y_{UT}^\beta(Q,q_\perp). \quad (56)$$

Similar to (42), $\widetilde{W}_{UT}(Q,b)$ denotes the spin-dependent structure function in the b-space and dominates at $q_\perp \ll Q$, and Y_{UT}^β provides correction for the single-polarized process at $q_\perp \sim Q$. The antisymmetric tensor $\epsilon_\perp^{\alpha\beta}$ is defined as $\epsilon^{\alpha\beta\mu\nu}P_\pi^\mu P_p^\nu/P_\pi\cdot P_p$, and $S_\perp$ is the transverse-polarization vector of the proton target.

The structure function $\widetilde{W}_{UT}(Q,b)$ can be written in terms of the unpolarized distribution function of pion and Sivers function of proton as

$$\widetilde{W}_{UT}^\alpha(Q;b) = H_{UT}(Q;\mu) \cdot \sum_{q,\overline{q}} e_q^2 \widetilde{f}_{1\overline{q}/\pi}(x_\pi,b;\mu,\zeta_F)\, \widetilde{f}_{1Tq/p}^{\perp\alpha({\rm DY})}(x_p,b;\mu,\zeta_F), \quad (57)$$

with $\widetilde{f}_{1Tq/p}^{\perp\alpha({\rm DY})}(x_p,b;\mu,\zeta_F)$ given in (33). Similar to the unpolarized case, the scheme-dependent hard factors can be absorbed into the C-coefficients, leading to [69, 88]

$$\Delta C_{q'\leftarrow q}^T(x,b;\mu_b) = \delta_{qq'}\left[\delta(1-x) + \frac{\alpha_s}{\pi}\left(-\frac{1}{4N_c}(1-x) + \frac{C_F}{4}\left(\pi^2-8\right)\delta(1-x)\right)\right]. \quad (58)$$

The spin-dependent differential cross section in (56) thus has the form

$$\frac{d^4\Delta\sigma}{dQ^2 dy d^2\mathbf{q}_\perp} = \frac{\sigma_0}{4\pi}\int_0^\infty dbb^2 J_1(q_\perp b) \sum_{q,i,j} e_q^2 \Delta C_{q\leftarrow i}^T \otimes T_{i,F}(x_p,x_p;\mu_b)\, C_{\overline{q}\leftarrow j} \otimes f_{1,j/\pi}(x_\pi,\mu_b)\, e^{-(S_{\rm NP}^{\rm Siv}+S_{\rm NP}^{f_{1q/\pi}}+S_{\rm P})}. \quad (59)$$

Combing (55), (54), (59), one can get the Sivers asymmetry in the Drell-Yan process with a π beam colliding on a transversely polarized proton target.

3.3. The $\cos 2\phi$ Asymmetry in the Unpolarized Drell-Yan from Double Boer-Mulders Effect. The angular differential cross section for unpolarized Drell-Yan process has the following general form

$$\frac{1}{\sigma}\frac{d\sigma}{d\Omega} = \frac{3}{4\pi}\frac{1}{\lambda+3}\left(1+\lambda\cos^2\theta+\mu\sin 2\theta\cos\phi + \frac{\nu}{2}\sin^2\theta\cos 2\phi\right), \quad (60)$$

where θ is the polar angle and ϕ is the azimuthal angle of the hadron plane with respect to the dilepton plane in the Collins-Soper (CS) frame [107]. The coefficients λ, μ, ν in (60) describe the sizes of different angular dependencies. Particularly, ν stands for the asymmetry of the $\cos 2\phi$ azimuthal angular distribution of the dilepton.

The coefficients λ, μ, ν have been measured in the process $\pi^- N \longrightarrow \mu^+\mu^- X$ by the NA10 Collaboration [5, 6] and the E615 Collaboration [7] for a π^- beam with energies of 140, 194, 286 GeV, and 252 GeV, with N denoting a nucleon in the deuterium or tungsten target. The experimental data showed a large value of ν, near 30% in the region $Q_T \sim 3$ GeV. This demonstrates a clear violation of the Lam-Tung relation [47]. In the last decade the angular coefficients were also measured in the pN Drell-Yan processes in both the fixed-target mode [108, 109] and collider mode [48, 49]. The origin of large $\cos 2\phi$ asymmetry–or the violation of the Lam-Tung relation–observed in Drell-Yan process has been studied extensively in literature [30, 50–57, 110–114]. Here we will only consider the contribution from the coupling of two Boer-Mulders functions from each hadron, denoted by $\nu_{\rm BM}$. It might be measured through the combination $2\nu_{\rm BM} \approx 2\nu + \lambda - 1$, in which the perturbative contribution is largely subtracted.

The $\cos 2\phi$ asymmetry coefficient $\nu_{\rm BM}$ contributed by the Boer-Mulders function can be written as

$$\nu_{\rm BM} = \frac{2\sum_q \mathcal{F}\left[\left(2\hat{\mathbf{h}}\cdot\mathbf{k}_\perp\hat{\mathbf{h}}\cdot\mathbf{p}_\perp - \mathbf{k}_\perp\cdot\mathbf{p}_\perp\right)\left(h_{1,q/\pi}^\perp h_{1,\overline{q}/p}^\perp/M_\pi M_p\right)\right]}{\sum_q \mathcal{F}\left[f_{1,q/\pi}f_{1,\overline{q}/p}\right]}, \quad (61)$$

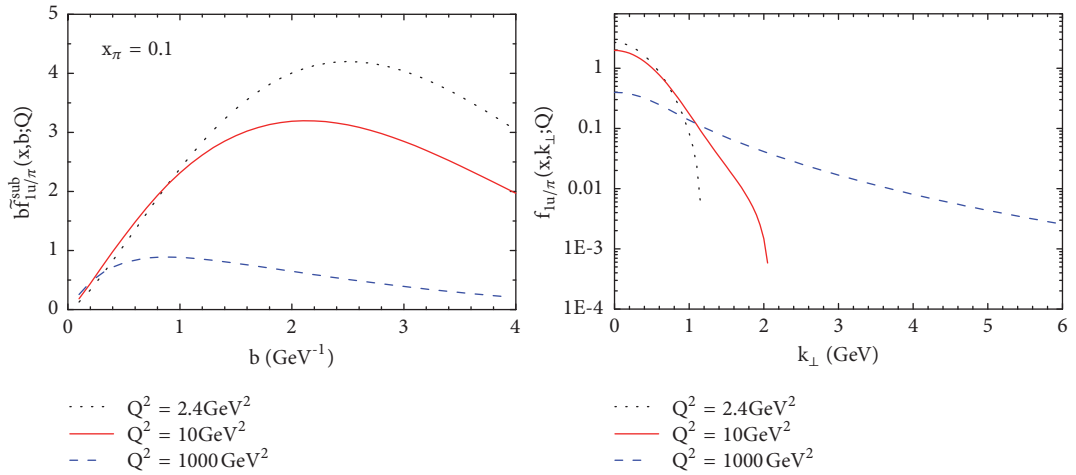

FIGURE 2: Subtracted unpolarized TMD distribution of the pion meson for valence quarks in b-space (left panel) and $k_\perp$-space (right panel), at energies: $Q^2 = 2.4$ GeV^2 (dotted lines), $Q^2 = 10$ GeV^2 (solid lines), and $Q^2 = 1000$ GeV^2 (dashed lines). From [59].

where the notation

$$\mathscr{F}\left[\omega f \overline{f}\right] = e_q^2 \int d^2\mathbf{k}_\perp d^2\mathbf{p}_\perp \delta^2\left(\mathbf{k}_\perp + \mathbf{p}_\perp - \mathbf{q}_\perp\right) \cdot \omega f\left(x_\pi, \mathbf{k}_\perp^2\right) \overline{f}\left(x_p, \mathbf{p}_\perp^2\right) \tag{62}$$

has been adopted to express the convolution of transverse momenta. $\mathbf{q}_\perp$, $\mathbf{k}_\perp$ and $\mathbf{p}_\perp$ are the transverse momenta of the lepton pair, quark, and antiquark in the initial hadrons, respectively. $\hat{\mathbf{h}}$ is a unit vector defined as $\hat{\mathbf{h}} = \mathbf{q}_\perp/|\mathbf{q}_\perp| = \mathbf{q}_\perp/q_\perp$. One can perform the Fourier transformation from $\mathbf{q}_\perp$ space to $\mathbf{b}$ space on the delta function in the notation of (62) to obtain the denominator in (61) as

$$\begin{aligned}\mathscr{F}\left[f_{1,q/\pi} f_{1,\overline{q}/p}\right] &= \sum_q e_q^2 \int \frac{d^2b}{(2\pi)^2} \\ &\cdot \int d^2\mathbf{k}_\perp d^2\mathbf{p}_\perp e^{i(\mathbf{q}_T - \mathbf{k}_\perp - \mathbf{p}_\perp)\cdot\mathbf{b}} f_{1,q/\pi}\left(x_\pi, \mathbf{k}_\perp^2\right) \\ &\cdot f_{1,\overline{q}/p}\left(x_p, \mathbf{p}_\perp^2\right) = \sum_q e_q^2 \\ &\cdot \int \frac{d^2b}{(2\pi)^2} e^{i\mathbf{q}_\perp\cdot\mathbf{b}} \tilde{f}_{1,q/\pi}\left(x_\pi, b; Q\right) \tilde{f}_{1,\overline{q}/p}\left(x_p, b; Q\right)\end{aligned} \tag{63}$$

where the unpolarized distribution function in b space is given in (25) and (26). Similar to the treatment of the denominator, using the expression of the Boer-Mulders function in (34) the numerator can be obtained as

$$\begin{aligned}&\mathscr{F}\left[\left(2\hat{\mathbf{h}}\cdot\mathbf{k}_\perp\hat{\mathbf{h}}\cdot\mathbf{p}_\perp - \mathbf{k}_\perp\cdot\mathbf{p}_\perp\right)\frac{h_{1,q/\pi}^\perp h_{1,\overline{q}/p}^\perp}{M_\pi M_p}\right] = \sum_q e_q^2 \\ &\cdot \int \frac{d^2b}{(2\pi)^2}\int d^2\mathbf{k}_\perp d^2\mathbf{p}_\perp e^{i(\mathbf{q}_T - \mathbf{k}_\perp - \mathbf{p}_\perp)\cdot b}\left[\left(2\hat{\mathbf{h}}\cdot\mathbf{k}_\perp\hat{\mathbf{h}}\right.\right. \\ &\left.\left.\cdot\mathbf{p}_\perp - \mathbf{k}_\perp\cdot\mathbf{p}_\perp\right)\frac{h_{1,q/\pi}^\perp h_{1,\overline{q}/p}^\perp}{M_\pi M_p}\right] = \sum_q e_q^2 \\ &\cdot \int \frac{d^2b}{(2\pi)^2} e^{i\mathbf{q}_\perp\cdot\mathbf{b}}\left(2\hat{h}_\alpha\hat{h}_\beta - g_{\alpha\beta}^\perp\right)\tilde{h}_{1,q/\pi}^{\alpha\perp}\left(x_\pi, b; Q\right) \\ &\cdot \tilde{h}_{1,\overline{q}/p}^{\beta\perp}\left(x_p, b; Q\right) = \sum_q e_q^2 \int_0^\infty \frac{dbb^3}{8\pi} J_2\left(q_\perp b\right) \\ &\cdot T_{q/\pi,F}^{(\sigma)}\left(x_\pi, x_\pi; \mu_b\right) T_{\overline{q}/p,F}^{(\sigma)}\left(x_p, x_p; \mu_b\right) \\ &\cdot e^{-\left(S_{\text{NP}}^{f_{1,q/p}} + S_{\text{NP}}^{f_{1,q/\pi}} + S_{\text{P}}\right)}.\end{aligned} \tag{64}$$

Different from the previous two cases, the hard coefficients C_i^{BM} and $\mathscr{H}_{\text{BM}}$ for the Boer-Mulders function have not been calculated up to next-to-leading order (NLO), and still remain in leading order (LO) as $C_{q\longleftarrow i} = \delta_{qi}\delta(1-x)$ and $\mathscr{H} = 1$.

4. Numerical Estimate for the TMD Distributions

Based on the TMD evolution formalism for the distributions set up in Section 2, we will show the numerical results for the TMD distributions. Particularly attention will be paid on those of the pion meson, as those of the proton have been studied numerically in [23, 71, 77].

4.1. The Unpolarized TMD Distribution of the Pion Meson. In [59], the authors applied (26) and the extracted parameters g_1^π and g_2^π to quantitatively study the scale dependence of the unpolarized TMD distributions of the pion meson with the JCC Scheme. For the collinear unpolarized distribution function of the pion meson, the NLO SMRS parameterization [115] was chosen. The results are plotted in Figure 2, with the left and right panels showing the subtracted distribution in b space and $k_\perp$ space, for fixed $x_\pi = 0.1$, at three different energy scales: $Q^2 = 2.4$ GeV^2 (dotted line), 10 GeV^2 (solid line), 1000 GeV^2 (dashed line). From the b-dependent plots,

one can see that at the highest energy scale $Q^2 = 1000\ \mathrm{GeV}^2$, the peak of the curve is in the low b region where $b < b_{\max}$, since in this case the perturbative part of the Sudakov form factor dominates. However, at lower energy scales, e.g., $Q^2 = 10\ \mathrm{GeV}^2$ and $Q^2 = 2.4\ \mathrm{GeV}^2$, the peak of the b-dependent distribution function moves towards the higher b region, indicating that the nonperturbative part of the TMD evolution becomes important at lower energy scales. For the distribution in $k_\perp$ space, at higher energy scale the distribution has a tail falling off slowly at large $k_\perp$, while at lower energy scales the distribution function falls off rapidly with increasing $k_\perp$. It is interesting to point out that the shapes of the pion TMD distribution at different scales are similar to those of the proton, namely, Fig. 8 in [77].

4.2. The Sivers Function of the Proton. The scale dependence of the T-odd distributions, such as the Sivers function and the Boer-Mulders function, is more involved than that of the T-even distributions. This is because their collinear counterparts are the twist-3 multiparton correlation functions [39, 60, 61, 69, 88], for which the exact evolution equations are far more complicated than those for the unpolarized distribution function. In numerical calculation, some approximations on the evolution kernels are usually adopted.

In [39], the Qiu-Sterman function was assumed to be proportional to f_1, namely, it follows the same evolution kernel as that for f_1. A different choice was adopted in [60], where the homogenous terms of the exact evolution kernel for the Qiu-Sterman function [88, 116–124] were included to deal with the scale dependence of Qiu-Sterman function:

$$P_{qq}^{\mathrm{QS}} \approx P_{qq}^{f_1} - \frac{N_c}{2}\frac{1+z^2}{1-z} - N_c\delta(1-z), \tag{65}$$

with $P_{qq}^{f_1}$ the evolution kernel of the unpolarized PDF

$$P_{qq}^{f_1} = \frac{4}{3}\left(\frac{1+z^2}{(1-z)_+} + \frac{3}{2}\delta(1-z)\right). \tag{66}$$

To solve the QCD evolution numerically, we resort to the QCD evolution package HOPPET [125] and we custom the code to include the splitting function in (65). For a comparison, in Figure 3 we plot the TMD evolution of the Sivers function for proton in b space and the $k_\perp$ space using the above-mentioned two approaches [60]. In this estimate, the next leading order C-coefficients $\Delta C_{q\leftarrow i}^{T}$ was adopted from [69, 88] and the nonperturbative Sudakov form factor for the Sivers function of proton was adopted as the form in (17). The Sivers functions are presented at three different energy scales: $Q^2 = 2.4\ \mathrm{GeV}^2$, $Q^2 = 10\ \mathrm{GeV}^2$ and $Q^2 = 100\ \mathrm{GeV}^2$. Similar to the result for f_1, one can conclude from the curves that the perturbative Sudakov form factor dominated in the low b region at higher energy scales and the nonperturbative part of the TMD evolution became more important at lower energy scales. However, the $k_\perp$ tendency of the Sivers function in the two approaches is different, which indicates that the scale dependence of the Qiu-Sterman function may play a role in the TMD evolution.

4.3. The Boer-Mulders Function of the Pion Meson. The evolution of the Boer-Mulders function for the valence quark inside π meson has been calculated from (34) and (36) in [61], in which the collinear twist-3 correlation function $T_{q,F}^{(\sigma)}$ at the initial energy scale was obtained by adopting a model result of the Boer-Mulders function of the pion meson calculated from the light-cone wave functions [126]. For the scale evolution of $T_{q,F}^{(\sigma)}$, the exact evolution effect has been studied in [116]. For our purpose, we only consider the homogenous term in the evolution kernel

$$P_{qq}^{T_{q,F}^{(\sigma)}}(x) \approx \Delta_T P_{qq}(x) - N_C\delta(1-x), \tag{67}$$

with $\Delta_T P_{qq}(x) = C_F[2z/(1-z)_+ + (3/2)\delta(1-x)]$ being the evolution kernel for the transversity distribution function $h_1(x)$. We customize the original code of QCDNUM [127] to include the approximate kernel in (67). For the nonperturbative part of the Sudakov form factor associated with Boer-Mulders function, the information still remains unknown. The assumption that S_{NP} for Boer-Mulders function is same as that for f_1 can be a practical way to access the information of TMD evolution for Boer-Mulders function.

We plot the b-dependent and k_T-dependent Boer-Mulders function at $x = 0.1$ in the left and right panels of Figure 4, respectively. In calculating $\widetilde{h}_{1,q/\pi}^{\perp}(x,b;Q)$ in Figure 4, we have rewritten the Boer-Mulders function in b space as

$$\widetilde{h}_{1,q/\pi}^{\perp}(x,b;Q) = \frac{ib_\alpha}{\pi}\widetilde{h}_{1,q/\pi}^{\alpha\perp}(x,b;Q). \tag{68}$$

The three curves in each panel correspond to three different energy scales: $Q^2 = 0.25\mathrm{GeV}^2$ (solid lines), $Q^2 = 10\mathrm{GeV}^2$ (dashed lines), $Q^2 = 1000\mathrm{GeV}^2$ (dotted lines). From the curves, we find that the TMD evolution effect of the Boer-Mulders function is significant and should be considered in phenomenological analysis. The result also indicates that the perturbative Sudakov form factor dominates in the low b region at higher energy scales and the nonperturbative part of the TMD evolution becomes more important at lower energy scales.

In conclusion, we find that the tendency of the distributions is similar: the distribution is dominated by perturbative region in b space at large Q^2, while at lower Q^2 the distribution shifts to the large b region, indicating that the nonperturbative effects of TMD evolution become important. For the distributions in $k_\perp$ space, as the value of Q^2 increases, the distributions become wider with a perturbative tail, while at low values of Q^2, the distributions resemble Gaussian-type parameterization. However, the widths of the transverse momentum differ among different distributions.

5. Numerical Estimate for the Physical Observables in π-N Drell-Yan Process

Based on the general TMD factorization framework provided in Section 3, we present several physical observables in π-N Drell-Yan process in this section.

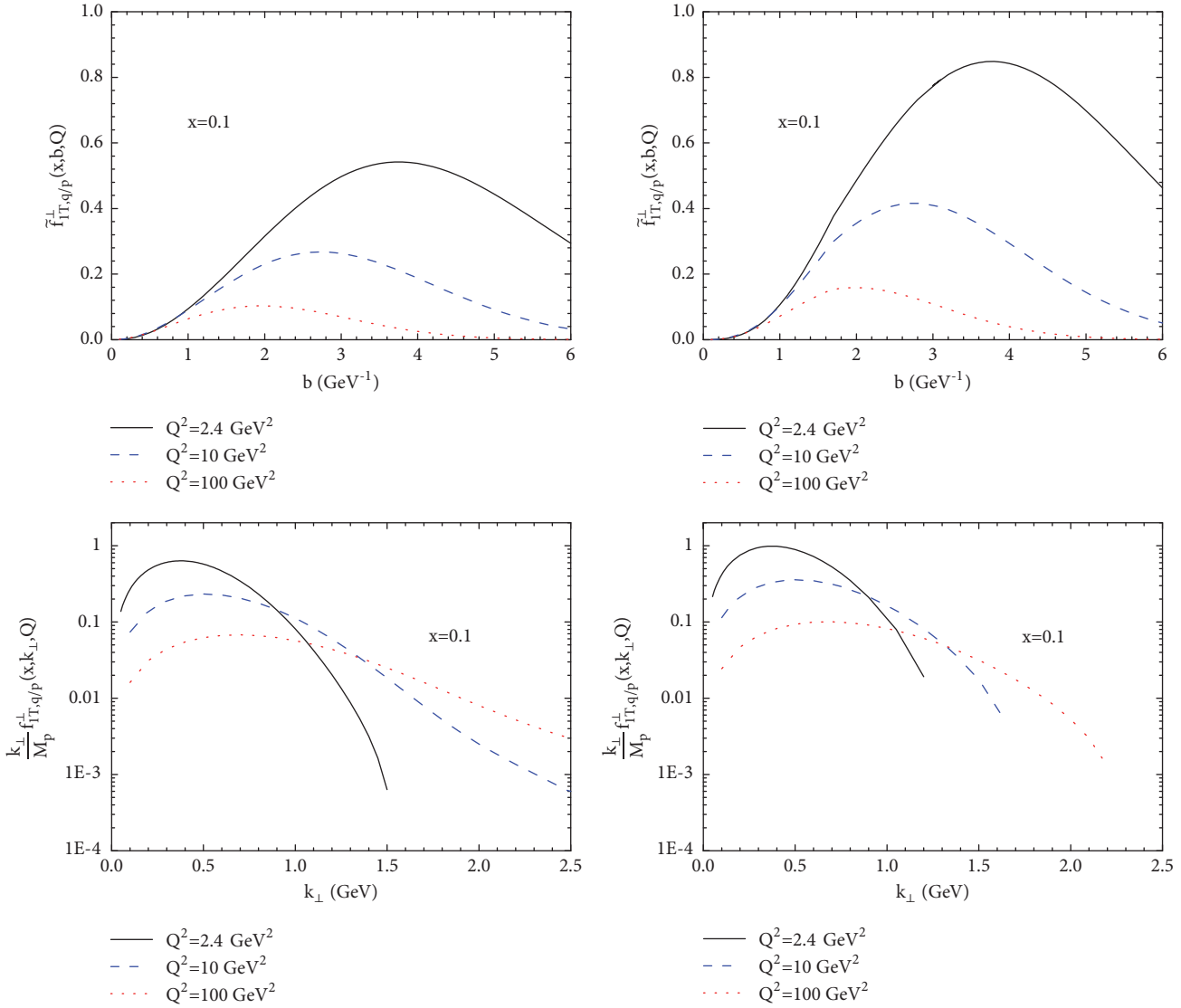

FIGURE 3: Subtracted Sivers function for the up quarks in Drell-Yan in b-space (upper panels) and $k_\perp$-space (lower panels), at energies: Q^2 = 2.4 GeV^2 (solid lines), Q^2 = 10 GeV^2 (dashed lines), and Q^2 = 100 GeV^2 (dotted lines). The left panel shows the result from the same evolution kernel as that for f_1 in (66); the right panel shows the result from an approximate evolution kernel for the Qiu-Sterman function in (65), respectively. Figure from [60].

QCD predicts that the T-odd PDFs present generalized universality, i.e., the sign of the Sivers function measured in Drell-Yan process should be opposite to its sign measured in SIDIS [16, 34, 35] process. The verification of this sign change [36–41] is one of the most fundamental tests of our understanding of the QCD dynamics and the factorization scheme, and it is also the main pursue of the existing and future Drell-Yan facilities [10, 11, 42–45]. The COMPASS Collaboration has reported the first measurement of the Sivers asymmetry in the pion-induced Drell-Yan process, in which a π^- beam was scattered off the transversely polarized NH_3 target [11]. The polarized Drell-Yan data from COMPASS together with the previous measurement of the Sivers effect in the W- and Z-boson production from $p^\uparrow p$ collision at RHIC [45] will provide the first evidence of the sign change of the Sivers function. As COMPASS experiment has almost the same setup [11, 46] for SIDIS and Drell-Yan process, it will provide the unique chance to explore the sign change since the uncertainties in the extraction of the Sivers function from the two kinds of measurements can be reduced.

5.1. The Normalized Cross Section for Unpolarized π-N Drell-Yan Process. The very first step to understand the Sivers asymmetry in the π-N Drell-Yan process is to quantitatively estimate the differential cross section in the same process for unpolarized nucleon target with high accuracy, since it always appears in the denominator of the asymmetry definition. The differential cross section for unpolarized Drell-Yan process has been given in (54). Applying the extracted nonperturbative Sudakov form factor for pion

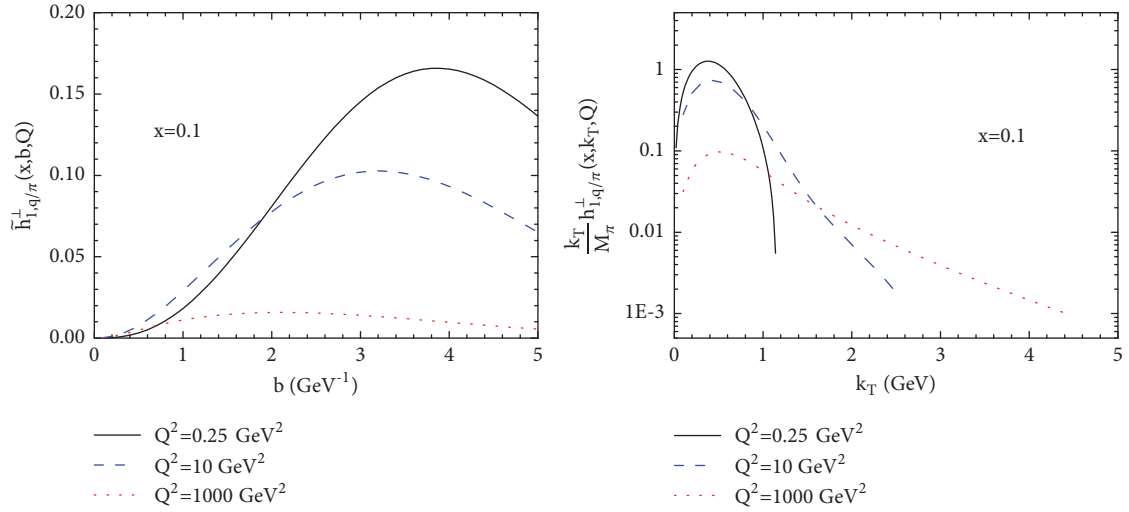

FIGURE 4: The Boer-Mulders function for u-quark in b space (left panel) and k_T space (right panel) considering three different energy scales: $Q^2 = 2.4\text{GeV}^2$ (solid lines), $Q^2 = 10\text{GeV}^2$ (dashed lines), and $Q^2 = 1000\text{GeV}^2$ (dotted lines). Figures from [61].

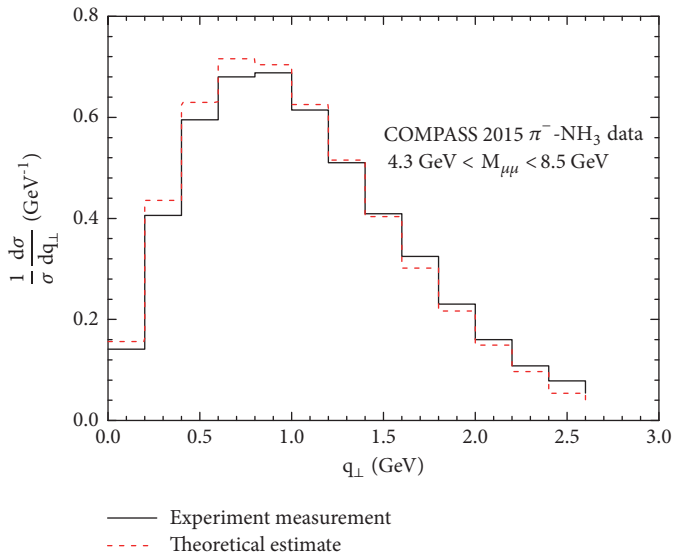

FIGURE 5: The transverse spectrum of lepton pair production in the unpolarized pion-nucleon Drell-Yan process, with an NH_3 target at COMPASS. The dashed line represents the theoretical calculation in [59]. The solid line shows the experimental measurement at COMPASS [11]. Figure from [59].

meson in [59] and the extracted S_{NP} for nucleon in [77], we estimated the normalized transverse momentum spectrum of the dimuon production in the pion-nucleon Drell-Yan process at COMPASS for different $q_\perp$ bins with an interval of 0.2 GeV. The result is plotted in Figure 5. From the curves, one can find the theoretical estimate on the $q_\perp$ distribution of the dimuon agreed with the COMPASS data fairly well in the small $q_\perp$ region where the TMD factorization is supposed to hold. The comparison somehow confirms the validity of extraction of the nonperturbative Sudakov form factor for the unpolarized distribution $f_{1\pi}$ of pion meson, within the TMD factorization. This may indicate that the framework can also be extended to the study of the azimuthal asymmetries in the πN Drell-Yan process, such as the Sivers asymmetry and Boer-Mulders asymmetry. We should point out that at larger $q_\perp$, the numerical estimate in [59] cannot describe the data, indicating that the perturbative correction from the Y_{UU} term may play an important role in the region $q_\perp \sim Q$. Further study on the Y term is needed to provide a complete picture of the $q_\perp$ distribution of lepton pairs from πN Drell-Yan in the whole $q_\perp$ range.

5.2. The Sivers Asymmetry. In [39], the authors adopted the Gaussian form of the nonperturbative Sudakov form factor S_{NP} in (17) and the leading order C coefficients to perform a global fit on the Sivers function from the experimental data at HERMES [128], COMPASS [129, 130], and Jefferson Lab (JLab) [131]. With the extracted Sivers function from

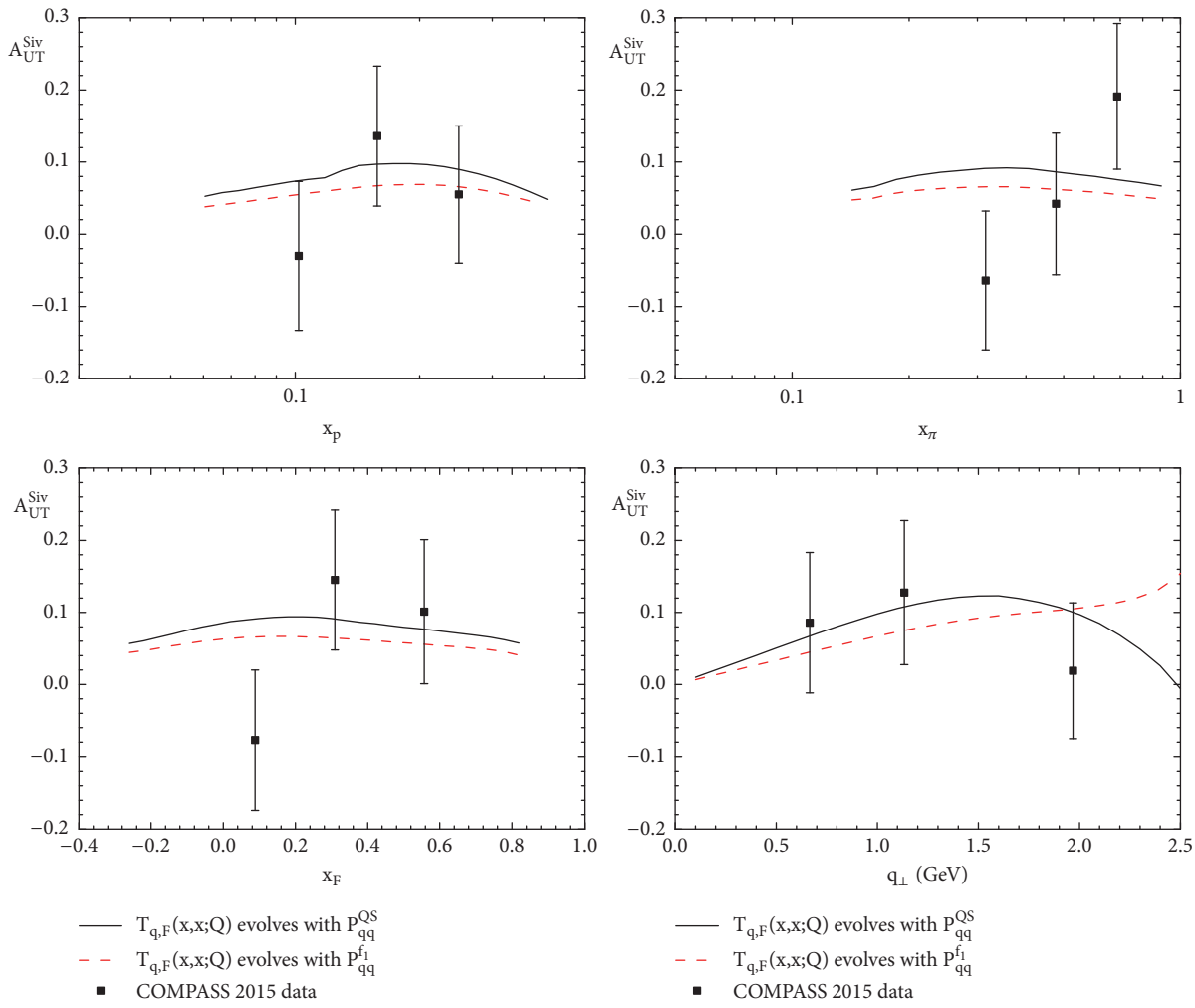

FIGURE 6: The Sivers asymmetry within TMD factorization for a π^- scattering off transversely polarized proton Drell-Yan process as functions of x_p (upper left), x_π (upper right), x_F (lower left), and $q_\perp$ (lower right), compared with the COMPASS data [11]. Figure from [60].

SIDIS process at hand, they made predictions for the Sivers asymmetry in Drell-Yan lepton pair and W production at future planned Drell-Yan facilities at COMPASS [10], Fermilab [42, 43], and RHIC [44, 132], which can be compared to the future experimental measurements to test the sign change of the Sivers functions between SIDIS and Drell-Yan processes. The predictions were presented in Fig. 12 and 13 of [39].

The TMD evolution effect of the Sivers asymmetry in SIDIS and pp Drell-Yan at low transverse momentum has also been studied in [88], in which a framework was built to match SIDIS and Drell-Yan and cover the TMD physics with Q^2 from several GeV^2 to 10^4GeV^2 (for W/Z boson production). It has shown that the evolution equations derived by a direct integral of the CSS evolution kernel from low to high Q can describe well the transverse momentum distribution of the unpolarized cross sections in the Q^2 range from 2 to 100 GeV^2. With this approach, the transverse moment of the quark Sivers functions can be constrained from the combined analysis of the HERMES and COMPASS data on the Sivers asymmetries in SIDIS. Based on this result, [88] provided the predictions for the Sivers asymmetries in pp Drell-Yan, as well as in $\pi^- p$ Drell-Yan. The latter one has been measured by the COMPASS Collaboration, and the comparison showed that the theoretical result is consistent with data (Fig. 6 in [11]) within the error bar.

With the numerical results of the TMD distributions in (57), the Sivers asymmetry A_{UT}^{Siv} as function of x_p, x_π, x_F, and $q_\perp$ in $\pi^- p^\uparrow \longrightarrow \mu^+\mu^- + X$ in the kinematics of COMPASS Collaboration was calculated in [60], as shown in Figure 6. The magnitude of the asymmetry is around $0.05 \div 0.10$, which is consistent with the COMPASS measurement (full squares in Figure 6) [11] within the uncertainties of the asymmetry. The different approaches dealing with the energy dependence of Qiu-Sterman function lead to different shapes of the asymmetry. Furthermore, the asymmetry from the approximate evolution kernel has a fall at larger $q_\perp$, which is more compatible to the shape of $q_\perp$-dependent asymmetry of measured by the COMPASS Collaboration. The study may indicate that, besides the TMD evolution effect, the scale

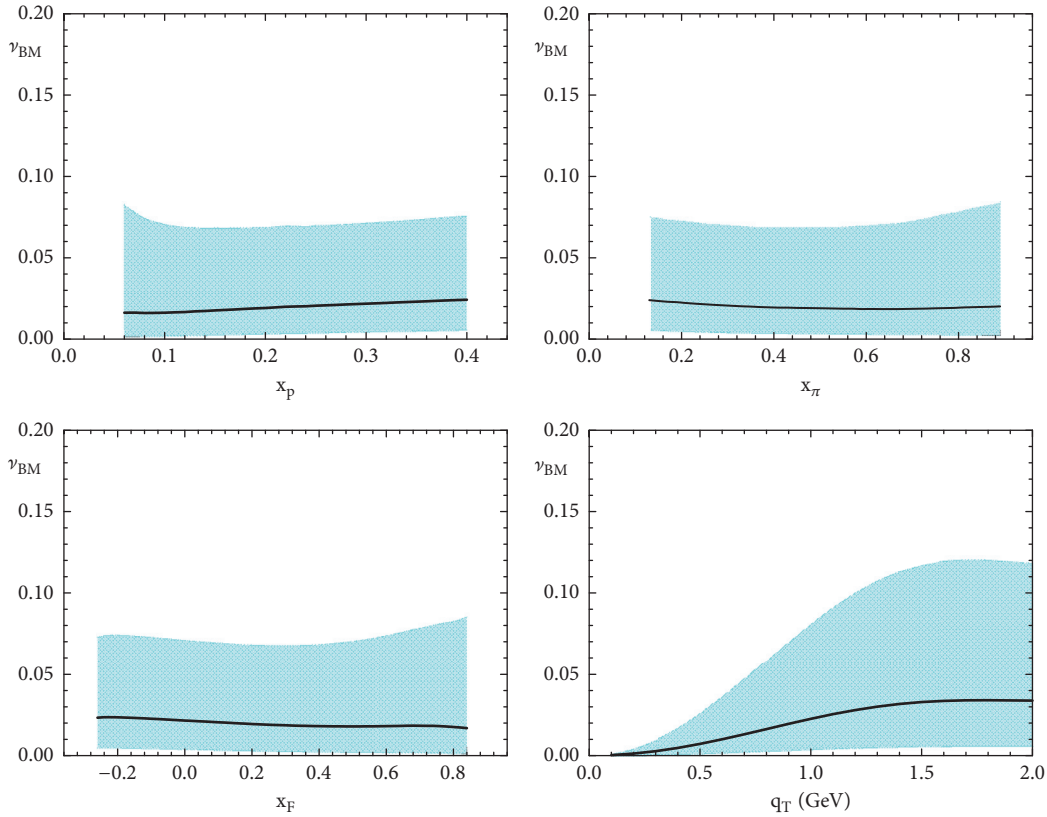

FIGURE 7: The cos 2ϕ azimuthal asymmetries ν_{BM} as the functions of x_p (upper left), x_π (upper right), x_F (lower left), and $q_\perp$ (lower right) for the unpolarized πp Drell-Yan process considering the TMD evolution in the kinematical region of COMPASS. The shadow areas correspond to the uncertainty of the parameters in the parameterization of the Boer-Mulders function for proton in [62]. Figures from [61].

dependence of the Qiu-Sterman function will also play a role in the interpretation of the experimental data.

5.3. The cos 2ϕ *Azimuthal Asymmetry.* Using (64), the cos 2ϕ azimuthal asymmetry contributed by the double Boer-Mulders effect in the πN Drell-Yan process was analyzed in [61], in which the TMD evolution of the Boer-Mulders function was included. In this calculation, the Boer-Mulders function of the proton was chosen from the parameterization in [62] at the initial energy $Q_0^2 = 1\text{GeV}^2$. As mentioned in Section 4.3, the Boer-Mulders function of the pion was adopted from the model calculation in [126]. Here we plot the estimated asymmetry ν_{BM} as function of x_p, x_π, x_F and $q_\perp$ in the kinematical region of COMPASS in Figure 7. The bands correspond to the uncertainty of the parameterization of the Boer-Mulders function of the proton [62]. We find from the plots that, in the TMD formalism, the cos 2ϕ azimuthal asymmetry in the unpolarized $\pi^- p$ Drell-Yan process contributed by the Boer-Mulders functions is around several percent. Although the uncertainty from the proton Boer-Mulders functions is rather large, the asymmetry is firmly positive in the entire kinematical region. The asymmetries as the functions of x_p, x_π, x_F show slight dependence on the variables, while the $q_\perp$ dependent asymmetry shows increasing tendency along with the increasing $q_\perp$ in the small $q_\perp$ range where the TMD formalism is valid. The result in Figure 7 indicates that precise measurements on the Boer-Mulders asymmetry ν_{BM} as functions of x_p, x_π, x_F, and $q_\perp$ can provide an opportunity to access the Boer-Mulders function of the pion meson. Furthermore, the work may also shed light on the proton Boer-Mulders function since the previous extractions on it were mostly performed without TMD evolution.

6. Summary and Prospects

It has been a broad consensus that the study on the TMD observables will provide information on the partons' intrinsic transverse motions inside a hadron. In the previous sections we have tried to substantiate this statement mainly focusing on the unpolarized and single-polarized πp Drell-Yan process within the TMD factorization. In particular, we reviewed the extraction of the nonperturbative function from the Drell-Yan and SIDIS data in the evolution formalism of the TMD distributions. We also discussed the further applications of the TMD factorization in the phenomenology of unpolarized cross section, the Sivers asymmetry, and the cos 2ϕ azimuthal asymmetry in the πp Drell-Yan process. In summary, we have the following understanding on the πN Drell-Yan from the viewpoint of the TMD factorization:

(i) The extraction of nonperturbative Sudakov form factor from the πN Drell-Yan may shed light on the

evolution (scale dependence) of the pion TMD distribution. The prediction on transverse momentum distribution of the dilepton in the small $q_\perp$ region is compatible with the COMPASS measurement and may serve as a first step to study the spin/azimuthal asymmetry in the πN Drell-Yan process at COMPASS.

(ii) The precise measurement on the single-spin asymmetry in the kinematical region of COMPASS can provide great opportunity to access the Sivers function. Besides the TMD evolution effect, the choice of the scale dependence of the Qiu-Sterman function can affect the shape of the asymmetry and should be considered in the future extraction of the Sivers function.

(iii) Sizable $\cos 2\phi$ asymmetry contributed by the convolution of the Boer-Mulders functions of the pion meson and the proton can still be observed at COMPASS after the TMD evolution effect is considered. Future data with higher accuracy may provide further constraint on the Boer-Mulders function of the pion meson as well as that of the proton.

Although a lot of progress on the theoretical framework of the TMD factorization and TMD evolution has been made, the improvement is still necessary both from the perturbative and nonperturbative aspects. In the future, the study of S_{NP} based on more precise experimental data is needed, such as including the flavor dependence and hadron dependence on the functional form for S_{NP}. From the viewpoint of the perturbative region, higher-order calculation of the hard factors and coefficients will improve the accuracy of the theoretical framework. Moreover, most of the numerical calculations are based on the approximation that the Y-term correction is negligible in the small transverse momentum region; the inclusion of this term in the future estimate could be done to test the magnitude of the term. In addition, the TMD factorization is suitable to describe the small transverse momentum physics, while the collinear factorization is suitable for the large transverse momentum or the integrated transverse momentum. The matching between the two factorization schemes to study the unpolarized and polarized process over the whole transverse momentum region may be also necessary [65, 133].

Conflicts of Interest

The authors declare that they have no conflicts of interest.

Acknowledgments

This work is partially supported by the NSFC (China) Grant 11575043 and by the Fundamental Research Funds for the Central Universities of China. X. Wang is supported by the NSFC (China) Grant 11847217 and the China Postdoctoral Science Foundation under Grant no. 2018M640680.

References

[1] J. H. Christenson, G. S. Hicks, L. M. Lederman, P. J. Limon, B. G. Pope, and E. Zavattini, "Observation of massive muon pairs in hadron collisions," *Physical Review Letters*, vol. 25, no. 21, pp. 1523–1526, 1970.

[2] S. D. Drell and T. Yan, "Massive Lepton-Pair Production in Hadron-Hadron Collisions at High Energies," *Physical Review Letters*, vol. 25, no. 13, p. 316, 1970, Erratum: [Physical Review Letters, vol. 25, pp. 902, 1970].

[3] P. Bordalo, P. Busson, L. Kluberg et al., "Nuclear effects on the nucleon structure functions in hadronic high-mass dimuon production," *Physics Letters B*, vol. 193, p. 368, 1987.

[4] B. Betev, J. J. Blaising, P. Bordalo et al., "Differential cross-section of high-mass muon pairs produced by a 194 GeV/c$\pi-$ beam on a tungsten target," *Zeitschrift für Physik C*, vol. 28, p. 9, 1985.

[5] S. Falciano, M. Guanziroli, H. Hofer et al., "Angular distributions of muon pairs produced by 194 GeV/c negative pions," *Zeitschrift für Physik C*, vol. 31, p. 513, 1986.

[6] M. Guanziroli, D. A. Jensen, P. Le Coultre et al., "Angular distributions of muon pairs produced by negative pions on deuterium and tungsten," *Zeitschrift für Physik C*, vol. 37, p. 545, 1988.

[7] J. S. Conway, C. E. Adolphsen, J. P. Alexander et al., "Experimental study of muon pairs produced by 252-GeV pions on tungsten," *Physical Review D*, vol. 39, p. 92, 1989.

[8] S. Palestini, C. Biino, J. F. Greenhalgh et al., "Pion Structure as Observed in the Reaction $\pi-\mathrm{N}\longrightarrow\ \mu+\mu-\mathrm{X}$ at 80 GeV/c," *Physical Review Letters*, vol. 55, p. 2649, 1985.

[9] E. Anassontzis, S. Katsanevas, E. Kiritsis et al., "High-mass dimuon production in pN and πN interactions at 125 GeV/c," *Physical Review D*, vol. 38, p. 1377, 1988.

[10] COMPASS Collaboration, F. Gautheron et al., "COMPASS-II proposal," SPSC-P-340, CERN-SPSC-2010-014, 2010.

[11] M. Aghasyan, R. Akhunzyanov, G. D. Alexeev et al., "First Measurement of Transverse-Spin-Dependent Azimuthal Asymmetries in the Drell-Yan Process," *Physical Review Letters*, vol. 119, Article ID 112002, 2017.

[12] J. C. Collins, D. E. Soper, and G. F. Sterman, "Transverse momentum distribution in Drell-Yan pair and W and Z boson production," *Nuclear Physics B*, vol. B250, p. 199, 1985.

[13] X. D. Ji, J. P. Ma, and F. Yuan, "QCD factorization for spin-dependent cross sections in DIS and Drell–Yan processes at low transverse momentum," *Physics Letters B*, vol. 597, p. 299, 2004.

[14] X. D. Ji, J. P. Ma, and F. Yuan, "QCD factorization for semi-inclusive deep-inelastic scattering at low transverse momentum," *Physical Review D*, vol. 71, Article ID 034005, 2005.

[15] J. Collins, *Foundations of Perturbative QCD*, vol. 32 of *Cambridge Monographs on Particle Physics, Nuclear Physics and Cosmology*, Cambridge University Press, Cambridge, UK, 2011.

[16] J. C. Collins, "Leading-twist single-transverse-spin asymmetries: Drell–Yan and deep-inelastic scattering," *Physics Letters B*, vol. 536, p. 43, 2002.

[17] X. D. Ji and F. Yuan, "Parton distributions in light-cone gauge: where are the final-state interactions?" *Physics Letters B*, vol. 543, p. 66, 2002.

[18] A. V. Belitsky, X. Ji, and F. Yuan, "Final state interactions and gauge invariant parton distributions," *Nuclear Physics B*, vol. 656, p. 165, 2003.

[19] D. Boer, P. J. Mulders, and F. Pijlman, "Universality of T-odd effects in single spin and azimuthal asymmetries," *Nuclear Physics B*, vol. 667, p. 201, 2003.

[20] P. J. Mulders and R. D. Tangerman, "The complete tree-level result up to order 1/Q for polarized deep-inelastic leptoproduction," *Nuclear Physics B*, vol. 461, p. 197, 1996, Erratum: [Nuclear Physics B, vol. 484, pp. 538, 1997].

[21] A. Bacchetta, M. Diehl, K. Goeke, A. Metz, P. J. Mulders, and M. Schlegel, "Semi-inclusive deep inelastic scattering at small transverse momentum," *Journal of High Energy Physics*, vol. 2007, no. 02, pp. 093-093, 2007.

[22] J. C. Collins and D. E. Soper, "Back-to-back jets in QCD," *Nuclear Physics B*, vol. 193, no. 2, pp. 381–443, 1981, Erratum: [Nuclear Physics B, vol. 213, pp. 545, 1983].

[23] S. M. Aybat and T. C. Rogers, "Transverse momentum dependent parton distribution and fragmentation functions with QCD evolution," *Physical Review D*, vol. 83, Article ID 114042, 2011.

[24] J. C. Collins and F. Hautmann, "Infrared divergences and non-lightlike eikonal lines in Sudakov processes," *Physics Letters B*, vol. 472, p. 129, 2000.

[25] J. C. Collins and T. C. Rogers, "Equality of two definitions for transverse momentum dependent parton distribution functions," *Physical Review D*, vol. 87, Article ID 034018, 2013.

[26] M. G. Echevarria, A. Idilbi, A. Schäfer, and I. Scimemi, "Model independent evolution of transverse momentum dependent distribution functions (TMDs) at NNLL," *European Physical Journal C*, vol. 73, p. 2636, 2013.

[27] D. Pitonyak, M. Schlegel, and A. Metz, "Polarized hadron pair production from electron-positron annihilation," *Physical Review D: Particles, Fields, Gravitation and Cosmology*, vol. 89, no. 5, Article ID 054032, 2014.

[28] D. Boer, "Angular dependences in inclusive two-hadron production at BELLE," *Nuclear Physics B*, vol. 806, p. 23, 2009.

[29] S. Arnold, A. Metz, and M. Schlegel, "Dilepton production from polarized hadron hadron collisions," *Physical Review D: Particles, Fields, Gravitation and Cosmology*, vol. 79, no. 3, Article ID 034005, 2009.

[30] M. Lambertsen and W. Vogelsang, "Drell-Yan lepton angular distributions in perturbative QCD," *Physical Review D*, vol. 93, Article ID 114013, 2016.

[31] X. Ji, J. W. Qiu, W. Vogelsang, and F. Yuan, "Unified picture for single transverse-spin asymmetries in hard-scattering processes," *Physical Review Letters*, vol. 97, Article ID 082002, 2006.

[32] X. Ji, J. W. Qiu, W. Vogelsang, and F. Yuan, "Single transverse-spin asymmetry in Drell-Yan production at large and moderate transverse momentum," *Physical Review D: Particles, Fields, Gravitation and Cosmology*, vol. 73, Article ID 094017, 2006.

[33] D. W. Sivers, "Single-spin production asymmetries from the hard scattering of pointlike constituents," *Physical Review D: Particles, Fields, Gravitation and Cosmology*, vol. 41, no. 1, pp. 83–90, 1990.

[34] S. J. Brodsky, D. S. Hwang, and I. Schmidt, "Final-state interactions and single-spin asymmetries in semi-inclusive deep inelastic scattering," *Physics Letters B*, vol. 530, p. 99, 2002.

[35] S. J. Brodsky, D. S. Hwang, and I. Schmidt, "Initial-State Interactions and Single-Spin Asymmetries in Drell-Yan Processes," *Nuclear Physics B*, vol. 642, p. 344, 2002.

[36] M. Anselmino, M. Boglione, U. D'Alesio, S. Melis, F. Murgia, and A. Prokudin, "Sivers effect in Drell-Yan processes," *Physical Review D: Particles, Fields, Gravitation and Cosmology*, vol. 79, no. 5, Article ID 054010, 2009.

[37] Z. B. Kang and J. W. Qiu, "Testing the Time-Reversal Modified Universality of the Sivers Function," *Physical Review Letters*, vol. 103, Article ID 172001, 2009.

[38] J. C. Peng and J. W. Qiu, "Novel phenomenology of parton distributions from the Drell–Yan process," *Progress in Particle and Nuclear Physics*, vol. 76, p. 43, 2014.

[39] M. G. Echevarría, A. Idilbi, Z. B. Kang, and I. Vitev, "QCD evolution of the Sivers asymmetry," *Physical Review D: Particles, Fields, Gravitation and Cosmology*, vol. 89, no. 7, Article ID 074013, 2014.

[40] J. Huang, Z. B. Kang, I. Vitev, and H. Xing, "Spin asymmetries for vector boson production in polarized p + p collisions," *Physical Review D*, vol. 93, Article ID 014036, 2016.

[41] M. Anselmino, M. Boglione, U. D'Alesio, F. Murgia, and A. Prokudin, "Study of the sign change of the Sivers function from STAR collaboration W/Z production data," *Journal of High Energy Physics*, vol. 04, p. 046, 2017.

[42] L. D. Isenhower, T. Hague, R. Towell et al., *Polarized Drell-Yan Measurements with the Fermilab Main Injector*, 2012, http://www.fnal.gov/directorate/program_planning/June2012Public/P-1027_Pol-Drell-Yan-proposal.pdf.

[43] D. Geesaman, P. Reimer, C. Brown et al., *Letter of Intent for a Drell-Yan experiment with a polarized proton target*, 2014, http://www.fnal.gov/directorate/program_planning/June2013PACPublic/P-1039_LOI_polarized_DY.pdf.

[44] E. C. Aschenauer, A. Bazilevsky, L. C. Bland et al., *Large Rapidity Drell Yan Production at RHIC*, 2011, https://www.bnl.gov/npp/docs/pac0611/DY_pro_110516_final.2.pdf.

[45] L. Adamczyk, J. K. Adkins, G. Agakishiev et al., "Measurement of the Transverse Single-Spin Asymmetry in $p^{\uparrow}+p \longrightarrow W^{\pm}/Z^{0}$ at RHIC," *Physical Review Letters*, vol. 116, Article ID 132301, 2016.

[46] C. Adolph, M. Aghasyan, R. Akhunzyanov et al., "Sivers asymmetry extracted in SIDIS at the hard scales of the Drell–Yan process at COMPASS," *Physics Letters B*, vol. 770, p. 138, 2017.

[47] C. S. Lam and W. K. Tung, "Systematic approach to inclusive lepton pair production in hadronic collisions," *Physical Review D*, vol. 18, p. 2447, 1978.

[48] T. Aaltonen et al., "First Measurement of the Angular Coefficients of Drell-Yan e+e− Pairs in the Z Mass Region from pp Collisions at $\sqrt{s}$=1.96 TeV," *Physical Review Letters*, vol. 106, Article ID 241801, 2011.

[49] CMS Collaboration, V. Khachatryan, A. M. Sirunyan, A. Tumasyan et al., "Angular coefficients of Z bosons produced in pp collisions at sqrt(s) = 8 TeV and decaying to mu+mu- as a function of transverse momentum and rapidity," *Physics Letters B*, vol. 750, p. 154, 2015.

[50] A. Brandenburg, O. Nachtmann, and E. Mirkes, "Spin effects and factorization in the Drell-Yan process," *Zeitschrift für Physik C Particles and Fields*, vol. 60, no. 4, pp. 697–709, 1993.

[51] A. Brandenburg, S. J. Brodsky, V. V. Khoze, and D. Müller, "Angular Distributions in the Drell-Yan Process: A Closer Look at Higher Twist Effects," *Physical Review Letters*, vol. 73, no. 7, pp. 939–942, 1994.

[52] K. J. Eskola, P. Hoyer, M. Väntinnen, and R. Vogt, "Higher-twist effects in the Drell-Yan angular distribution," *Physics Letters B*, vol. 333, p. 526, 1994.

[53] J. G. Heinrich, C. Biino, J. F. Greenhalgh et al., "Higher-twist effects in the reaction π−N$\longrightarrow$ μ+μ−X at 253 GeV/c," *Physical Review D: Particles, Fields, Gravitation and Cosmology*, vol. 44, Article ID 1909, 1991.

[54] J.-C. Peng, W.-C. Chang, R. E. McClellan, and O. Teryaev, "Interpretation of angular distributions of Z-boson production at colliders," *Physics Letters B*, vol. 758, pp. 384–388, 2016.

[55] D. Boer and W. Vogelsang, "Drell-Yan lepton angular distribution at small transverse momentum," *Physical Review D*, vol. 74, Article ID 014004, 2006.

[56] W. C. Chang, R. E. McClellan, J. C. Peng, and O. Teryaev, "Lepton Angular Distributions of Fixed-target Drell-Yan Experiments in Perturbative QCD and a Geometric Approach," https://arxiv.org/abs/1811.03256.

[57] D. Boer, "Investigating the origins of transverse spin asymmetries at BNL RHIC," *Physical Review D*, vol. 60, Article ID 014012, 1999.

[58] D. Boer and P. J. Mulders, "Time-reversal odd distribution functions in leptoproduction," *Physical Review D: Particles, Fields, Gravitation and Cosmology*, vol. 57, pp. 5780–5786, 1998.

[59] X. Wang, Z. Lu, and I. Schmidt, "Transverse momentum spectrum of dilepton pair in the unpolarized $\pi-$ N Drell-Yan process within TMD factorization," *Journal of High Energy Physics*, vol. 08, p. 137, 2017.

[60] X. Wang and Z. Lu, "Sivers asymmetry in the pion induced Drell-Yan process at COMPASS within transverse momentum dependent factorization," *Physical Review D: Particles, Fields, Gravitation and Cosmology*, vol. 97, Article ID 054005, 2018.

[61] X. Wang, W. Mao, and Z. Lu, "Boer-Mulders effect in the unpolarized pion induced Drell–Yan process at COMPASS within TMD factorization," *The European Physical Journal C*, vol. 78, p. 643, 2018.

[62] Z. Lu and I. Schmidt, "Updating Boer-Mulders functions from unpolarized pd and pp Drell-Yan data," *Physical Review D*, vol. 81, Article ID 034023, 2010.

[63] A. Idilbi, X. Ji, J. Ma, and F. Yuan, "Collins-Soper equation for the energy evolution of transverse-momentum and spin dependent parton distributions," *Physical Review D: Particles, Fields, Gravitation and Cosmology*, vol. 70, no. 7, Article ID 074021, 2004.

[64] J. Collins and T. Rogers, "Understanding the large-distance behavior of transverse-momentum-dependent parton densities and the Collins-Soper evolution kernel," *Physical Review D*, vol. 91, Article ID 074020, 2015.

[65] J. Collins, L. Gamberg, A. Prokudin, T. Rogers, N. Sato, and B. Wang, "Relating transverse-momentum-dependent and collinear factorization theorems in a generalized formalism," *Physical Review D: Particles, Fields, Gravitation and Cosmology*, vol. 94, no. 3, Article ID 034014, 2016.

[66] A. Bacchetta, F. Delcarro, C. Pisano, M. Radici, and A. Signori, "Extraction of partonic transverse momentum distributions from semi-inclusive deep-inelastic scattering, Drell-Yan and Z-boson production," *Journal of High Energy Physics*, vol. 06, p. 081, 2017.

[67] A. Bacchetta and A. Prokudin, "Evolution of the helicity and transversity: Transverse-momentum-dependent parton distributions," *Nuclear Physics B*, vol. 875, p. 536, 2013.

[68] J. C. Collins and D. E. Soper, "Parton distribution and decay functions," *Nuclear Physics B*, vol. 194, p. 445, 1982.

[69] Z. B. Kang, B. W. Xiao, and F. Yuan, "QCD resummation for single spin asymmetries," *Physical Review Letters*, vol. 107, Article ID 152002, 2011.

[70] S. M. Aybat, J. C. Collins, J. W. Qiu, and T. C. Rogers, "QCD evolution of the Sivers function," *Physical Review D: Particles, Fields, Gravitation and Cosmology*, vol. 85, no. 3, Article ID 034043, 2012.

[71] M. G. Echevarria, A. Idilbi, and I. Scimemi, "Unified treatment of the QCD evolution of all (un-)polarized transverse momentum dependent functions: Collins function as a study case," *Physical Review D: Particles, Fields, Gravitation and Cosmology*, vol. 90, no. 1, Article ID 014003, 2014.

[72] F. Landry, R. Brock, P. M. Nadolsky, and C. Yuan, "Fermilab Tevatron run-1," *Physical Review D: Particles, Fields, Gravitation and Cosmology*, vol. 67, no. 7, Article ID 073016, 2003.

[73] J. Qiu and X. Zhang, "QCD Prediction for Heavy Boson Transverse Momentum Distributions," *Physical Review Letters*, vol. 86, no. 13, pp. 2724–2727, 2001.

[74] G. P. Korchemsky and G. F. Sterman, "Nonperturbative Corrections in Resummed Cross Sections," *Nuclear Physics B*, vol. 437, p. 415, 1995.

[75] Z. B. Kang, A. Prokudin, P. Sun, and F. Yuan, "Extraction of quark transversity distribution and Collins fragmentation functions with QCD evolution," *Physical Review D*, vol. 93, Article ID 014009, 2016.

[76] P. Sun and F. Yuan, "Energy evolution for the Sivers asymmetries in hard processes," *Physical Review D*, vol. 88, Article ID 034016, 2013.

[77] P. Sun, J. Isaacson, C.-P. Yuan, and F. Yuan, "Nonperturbative functions for SIDIS and Drell–Yan processes," *International Journal of Modern Physics A*, vol. 33, no. 11, Article ID 1841006, 2018.

[78] A. V. Konychev and P. M. Nadolsky, "Universality of the Collins–Soper–Sterman nonperturbative function in vector boson production," *Physics Letters B*, vol. 633, p. 710, 2006.

[79] C. T. H. Davies, B. R. Webber, and W. J. Stirling, "Drell-Yan cross sections at small transverse momentum," *Nuclear Physics B*, vol. 256, p. 413, 1985.

[80] R. K. Ellis, D. A. Ross, and S. Veseli, "Vector boson production in hadronic collisions," *Nuclear Physics B*, vol. 503, p. 309, 1997.

[81] M. Anselmino, M. Boglione, and S. Melis, "Strategy towards the extraction of the Sivers function with transverse momentum dependent evolution," *Physical Review D*, vol. 86, Article ID 014028, 2012.

[82] C. A. Aidala, B. Field, L. P. Gamberg, and T. C. Rogers, "Limits on TMD Evolution From Semi-Inclusive Deep Inelastic Scattering at Moderate," *Physical Review D*, vol. 89, Article ID 094002, 2014.

[83] J. C. Collins and D. E. Soper, "The two-particle-inclusive cross section in e+e- annihilation at PETRA, PEP and LEP energies," *Nuclear Physics B*, vol. 284, p. 253, 1987.

[84] W. J. Stirling and M. R. Whalley, "A compilation of Drell-Yan cross sections," *Journal of Physics G*, vol. 19, p. D1, 1993.

[85] F. James and M. Roos, "Minuit - a system for function minimization and analysis of the parameter errors and correlations," *Computer Physics Communications*, vol. 10, no. 6, pp. 343–367, 1975.

[86] F. James, "MINUIT—Function Minimization and Error Analysis," CERN Program Library Long Writeup D506, 1994.

[87] F. A. Ceccopieri, A. Courtoy, S. Noguera, and S. Scopetta, "Pion nucleus Drell–Yan process and parton transverse momentum in the pion," *The European Physical Journal C*, vol. 78, p. 644, 2018.

[88] P. Sun and F. Yuan, "Transverse momentum dependent evolution: Matching semi-inclusive deep inelastic scattering processes to Drell-Yan and W/Z boson production," *Physical Review D*, vol. 88, Article ID 114012, 2013.

[89] J.-W. Qiu and G. F. Sterman, "Single transverse spin asymmetries," *Physical Review Letters*, vol. 67, no. 17, pp. 2264–2267, 1991.

[90] J. W. Qiu and G. F. Sterman, "Single transverse spin asymmetries in direct photon production," *Nuclear Physics B*, vol. 378, p. 52, 1992.

[91] J. W. Qiu and G. F. Sterman, "Single Transverse-Spin Asymmetries in Hadronic Pion Production," *Physical Review D*, vol. 59, Article ID 014004, 1999.

[92] M. Anselmino, M. Boglione, and S. Melis, "Phenomenology of Sivers Effect with TMD Evolution," *International Journal of Modern Physics: Conference Series*, vol. 20, pp. 145–152, 2012.

[93] M. Boglione, U. D'Alesio, C. Flore, and J. O. Gonzalez-Hernandez, "Assessing signals of TMD physics in SIDIS azimuthal asymmetries and in the extraction of the Sivers function," *Journal of High Energy Physics*, vol. 07, p. 148, 2018.

[94] B. Zhang, Z. Lu, B. Q. Ma, and I. Schmidt, "Extracting Boer-Mulders functions from p+D Drell-Yan processes," *Physical Review D*, vol. 77, Article ID 054011, 2008.

[95] V. Barone, S. Melis, and A. Prokudin, "Boer-Mulders effect in unpolarized SIDIS: An analysis of the COMPASS and HERMES data on the," *Physical Review D: Particles, Fields, Gravitation and Cosmology*, vol. 81, no. 11, Article ID 114026, 2010.

[96] V. Barone, S. Melis, and A. Prokudin, "Azimuthal asymmetries in unpolarized Drell-Yan processes and the Boer-Mulders distributions of antiquarks," *Physical Review D: Particles, Fields, Gravitation and Cosmology*, vol. 82, no. 11, Article ID 114025, 2010.

[97] A. Prokudin, P. Sun, and F. Yuan, "Scheme dependence and transverse momentum distribution interpretation of Collins–Soper–Sterman resummation," *Physics Letters B*, vol. 750, p. 533, 2015.

[98] J. C. Collins and A. Metz, "Universality of Soft and Collinear Factors in Hard-Scattering Factorization," *Physical Review Letters*, vol. 93, Article ID 252001, 2004.

[99] S. Mantry and F. Petriello, "Factorization and resummation of Higgs boson differential distributions in soft-collinear effective theory," *Physical Review D*, vol. 81, Article ID 093007, 2010.

[100] T. Becher and M. Neubert, "Drell–Yan production at small q_T , transverse parton distributions and the collinear anomaly," *European Physical Journal C*, vol. 71, p. 1665, 2011.

[101] M. G. Echevarria, A. Idilbi, and I. Scimemi, "Factorization theorem for Drell-Yan at low q_T and transverse-momentum distributions on-the-light-cone," *Journal of High Energy Physics*, vol. 07, p. 002, 2012.

[102] J. Y. Chiu, A. Jain, D. Neill, and I. Z. Rothstein, "A Formalism for the Systematic Treatment of Rapidity Logarithms in Quantum Field Theory," *Journal of High Energy Physics*, vol. 05, p. 084, 2012.

[103] X. Ji, P. Sun, X. Xiong, and F. Yuan, "Soft factor subtraction and transverse momentum dependent parton distributions on the lattice," *Physical Review D*, vol. 91, Article ID 074009, 2015.

[104] S. Catani, D. de Florian, and M. Grazzini, "Universality of non-leading logarithmic contributions in transverse-momentum distributions," *Nuclear Physics B*, vol. 596, p. 299, 2001.

[105] P. Nadolsky, D. R. Stump, and C. Yuan, "Erratum: Semi-inclusive hadron production at DESY HERA: The effect of QCD gluon resummation," *Physical Review D: Particles, Fields, Gravitation and Cosmology*, vol. 64, no. 5, Article ID 059903, 2001, Erratum: [Physical Review D, vol. 64, article 059903, 2001].

[106] Y. Koike, J. Nagashima, and W. Vogelsang, "Resummation for Polarized Semi-Inclusive Deep-Inelastic Scattering at Small Transverse Momentum," *Nuclear Physics B*, vol. 744, p. 59, 2006.

[107] J. C. Collins and D. E. Soper, "Angular distribution of dileptons in high-energy hadron collisions," *Physical Review D: Particles, Fields, Gravitation and Cosmology*, vol. 16, no. 7, pp. 2219–2225, 1977.

[108] L. Y. Zhu, J. C. Peng, P. E. Reimer et al., "Measurement of Angular Distributions of Drell-Yan Dimuons in p+d Interactions at 800 GeV/c," *Physical Review Letters*, vol. 99, Article ID 082301, 2007.

[109] L. Y. Zhu, J. C. Peng, P. E. Reimer et al., "Measurement of Angular Distributions of Drell-Yan Dimuons in p+p Interactions at 800 GeV/c," *Physical Review Letters*, vol. 102, Article ID 182001, 2009.

[110] J. C. Collins, "Simple Prediction of Quantum Chromodynamics for Angular Distribution of Dileptons in Hadron Collisions," *Physical Review Letters*, vol. 42, p. 291, 1979.

[111] P. Chiappetta and M. Le Bellac, "Angular distribution of lepton pairs in Drell-Yan-like processes," *Zeitschrift für Physik C Particles and Fields*, vol. 32, no. 4, pp. 521–526, 1986.

[112] M. Blazek, M. Biyajima, and N. Suzuki, "Angular distribution of muon pairs produced by negative pions on deuterium and tungsten in terms of coherent states," *Zeitschrift für Physik C Particles and Fields*, vol. 43, p. 447, 1989.

[113] J. Zhou, F. Yuan, and Z. T. Liang, "Drell–Yan lepton pair azimuthal asymmetry in hadronic processes," *Physics Letters B*, vol. 678, p. 264, 2009.

[114] Z. Lu, "Spin physics through unpolarized processes," *Frontiers of Physics (Beijing)*, vol. 11, no. 1, Article ID 111204, 2016.

[115] P. J. Sutton, A. D. Martin, R. G. Roberts, and W. J. Stirling, "Parton distributions for the pion extracted from Drell-Yan and prompt photon experiments," *Physical Review D: Particles, Fields, Gravitation and Cosmology*, vol. 45, no. 7, pp. 2349–2359, 1992.

[116] Z. B. Kang and J. W. Qiu, "QCD evolution of naive-time-reversal-odd parton distribution functions," *Physics Letters B*, vol. 713, p. 273, 2012.

[117] Z. B. Kang and J. W. Qiu, "Evolution of twist-3 multi-parton correlation functions relevant to single transverse-spin asymmetry," *Physical Review D*, vol. 79, Article ID 016003, 2009.

[118] J. Zhou, F. Yuan, and Z. T. Liang, "QCD Evolution of the Transverse Momentum Dependent Correlations," *Physical Review D*, vol. 79, Article ID 114022, 2009.

[119] W. Vogelsang and F. Yuan, "Next-to-leading order calculation of the single transverse spin asymmetry in the Drell-Yan process," *Physical Review D*, vol. 79, Article ID 094010, 2009.

[120] V. M. Braun, A. N. Manashov, and B. Pirnay, "Scale dependence of twist-three contributions to single spin asymmetries," *Physical Review D: Particles, Fields, Gravitation and Cosmology*, vol. 80, Article ID 114002, 2009, Erratum: [Physical Review D, vol. 86, pp. 119902, 2012].

[121] J. P. Ma and H. Z. Sang, "Soft-gluon-pole contribution in single transverse-spin asymmetries of Drell-Yan processes," *Journal of High Energy Physics*, vol. 04, p. 062, 2011.

[122] A. Schafer and J. Zhou, "Note on the scale evolution of the Efremov-Teryaev-Qiu-Sterman function $T_F(x,x)$," *Physical Review D*, vol. 85, Article ID 117501, 2012.

[123] J. P. Ma and Q. Wang, "Scale dependence of twist-3 quark–gluon operators for single spin asymmetries," *Physics Letters B*, vol. 715, p. 157, 2012.

[124] J. Zhou, "Note on the scale dependence of the Burkardt sum rule," *Physical Review D: Particles, Fields, Gravitation and Cosmology*, vol. 92, no. 7, Article ID 074016, 2015.

[125] G. P. Salam and J. Rojo, "A Higher Order Perturbative Parton Evolution Toolkit (HOPPET)," *Computer Physics Communications*, vol. 180, no. 1, pp. 120–156, 2009.

[126] Z. Wang, X. Wang, and Z. Lu, "Boer-Mulders function of the pion and the qT-weighted cos2φ asymmetry in the unpolarized π−p Drell-Yan process at COMPASS," *Physical Review D*, vol. 95, Article ID 094004, 2017.

[127] M. Botje, "QCDNUM: Fast QCD evolution and convolution," *Computer Physics Communications*, vol. 182, no. 2, pp. 490–532, 2011.

[128] A. Airapetian, N. Akopov, Z. Akopov et al., "Observation of the Naive-T-Odd Sivers Effect in Deep-Inelastic Scattering," *Physical Review Letters*, vol. 103, Article ID 152002, 2009.

[129] M. Alekseev, V. Y. Alexakhin, Y. Alexandrov et al., "Collins and Sivers asymmetries for pions and kaons in muon–deuteron DIS," *Physics Letters B*, vol. 673, p. 127, 2009.

[130] C. Adolph, M. G. Alekseev, V. Y. Alexakhin et al., "II – Experimental investigation of transverse spin asymmetries in μ-p SIDIS processes: Sivers asymmetries," *Physics Letters B*, vol. 717, p. 383, 2012.

[131] X. Qian, K. Allada, C. Dutta et al., "Single Spin Asymmetries in Charged Pion Production from Semi-Inclusive Deep Inelastic Scattering on a Transversely Polarized ^{3}He Target at Q^2=1.4–2.7 GeV^2," *Physical Review Letters*, vol. 107, Article ID 072003, 2011.

[132] E. C. Aschenauer, A. Bazilevsky, K. Boyle et al., "The RHIC Spin Program: Achievements and Future Opportunities," https://arxiv.org/abs/1304.0079.

[133] L. Gamberg, A. Metz, D. Pitonyak, and A. Prokudin, "Connections between collinear and transverse-momentum-dependent polarized observables within the Collins–Soper–Sterman formalism," *Physics Letters B*, vol. 781, p. 443, 2018.